2013 Chino Basin Groundwater Model Update and Recalculation of Safe Yield Pursuant to the Peace Agreement

Final Report

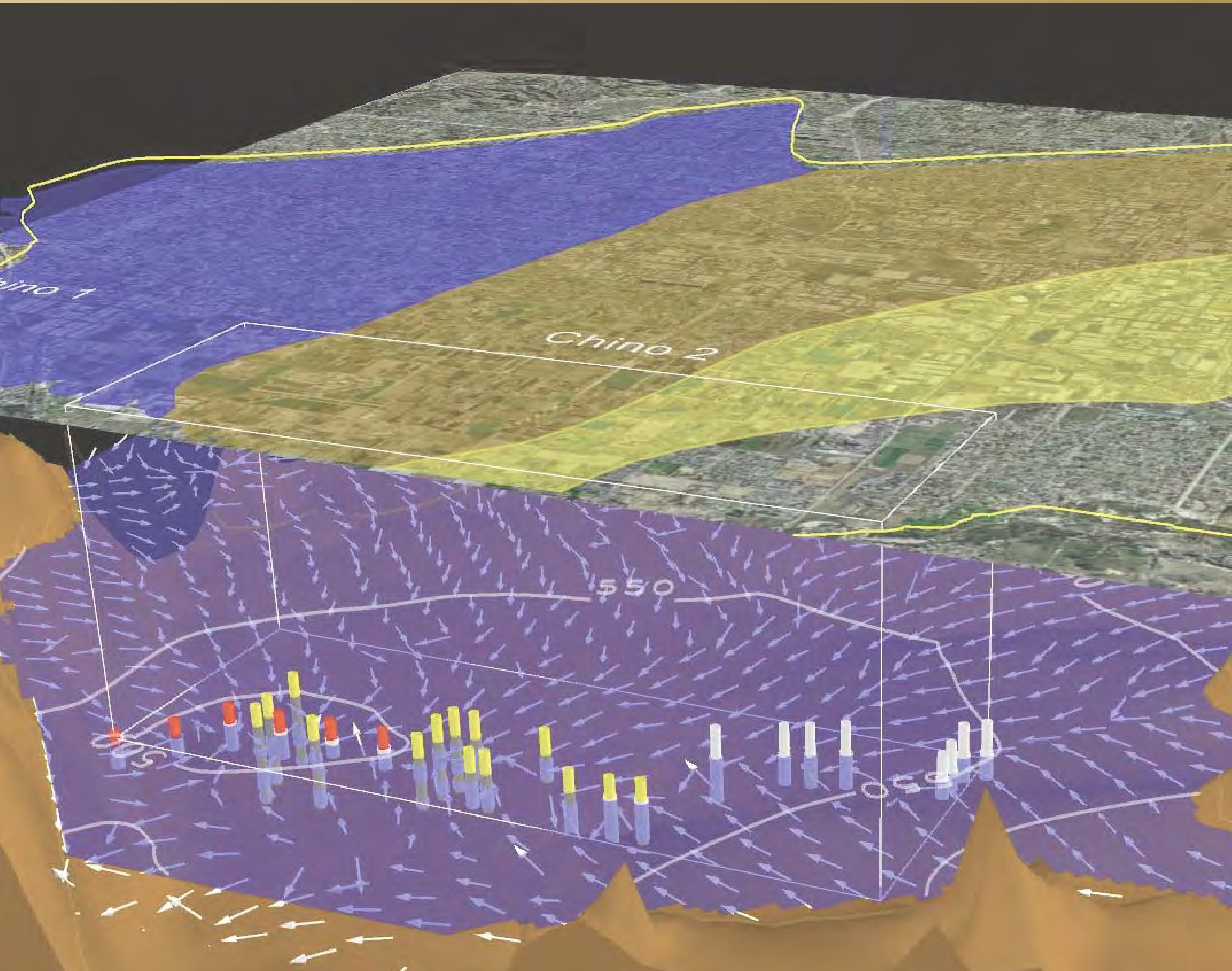

Prepared for

Chino Basin Watermaster

October 2015

Prepared by

Wildermuth Environmental Inc.

2013 Chino Basin Groundwater Model Update and Recalculation of Safe Yield Pursuant to the Peace Agreement

Prepared for

Chino Basin Watermaster

Prepared by

Wildermuth Environmental, Inc.

October 2015

Table of Contents

Section 1 – Introduction 1-1

1.1 Background 1-1
1.2 Project Objectives 1-1
1.2.1 Model Recalibration 1-1
1.2.2 Safe Yield and the Balance of Recharge and Discharge 1-2
1.2.3 New Yield from Desalters and Reoperation 1-2
1.3 Report Organization 1-2

Section 2 – Hydrogeologic Setting 2-1

2.1 Geologic Setting 2-1
2.2 Stratigraphy 2-1
2.2.1 Consolidated Bedrock 2-2
2.2.1.1 Basement Complex 2-2
2.2.1.2 Undifferentiated Pre-Pliocene Formations 2-2
2.2.1.3 Plio-Pleistocene Formations 2-2
2.2.2 Water-Bearing Sediments 2-3
2.2.2.1 Older Alluvium 2-3
2.2.2.2 Younger Alluvium 2-3
2.2.3 Effective Base of the Freshwater Aquifer 2-3
2.2.3.1 Eastern Chino Basin 2-4
2.2.3.2 Western Chino Basin 2-4
2.2.3.3 Bedrock Fault 2-5
2.3 Occurrence and Movement of Groundwater 2-6
2.3.1 Chino Basin Boundaries 2-6
2.3.2 Groundwater Recharge, Flow, and Discharge 2-7
2.3.3 Internal Faults 2-8
2.4 Aquifer Systems 2-8
2.5 Hydrostratigraphy 2-10
2.5.1 Layer 1 2-11
2.5.2 Layer 2 2-11
2.5.3 Layer 3 2-12
2.5.4 Creation of a Three-Dimensional Hydrostratigraphic Model 2-12
2.6 Aquifer Properties 2-13
2.6.1 Compilation of Existing Well Data 2-13
2.6.2 Classification of Texture and Reference Hydraulic Values for Aquifer Sediments 2-13
2.6.3 Geostatistical Model Approach 2-14
2.6.4 Specific Yield 2-15
2.6.5 Horizontal Hydraulic Conductivity 2-15
2.6.6 Vertical Hydraulic Conductivity 2-16

Section 3 – Water Balance 3-1

3.1 Introduction 3-1
3.2 Recharge Stresses 3-1
3.2.1 Subsurface Inflow 3-1
3.2.2 Streambed and Storm Water Recharge 3-2
3.2.3 Areal Recharge 3-3
3.2.3.1 Deep Infiltration of Precipitation and Applied Water 3-3
3.2.3.2 Deep Infiltration of Onsite Wastewater System Discharge 3-3

3.2.3.3 Deep infiltration of Leaks from Municipal Water Systems ... 3-4
3.2.3.4 Areal Recharge Calibration ... 3-4
3.2.4 Supplemental Water Recharge ... 3-4
3.3 Discharge ... 3-4
3.3.1 Subsurface Outflow ... 3-4
3.3.2 Rising Groundwater ... 3-5
3.3.3 Evapotranspiration ... 3-5
3.3.4 Groundwater Production ... 3-5
3.3.4.1 Overlying Agricultural Production ... 3-6
3.3.4.2 Overlying Non-Agricultural Production and Appropriator Production ... 3-6
3.3.4.3 Desalter Production ... 3-7
3.3.4.4 Temescal Basin Production ... 3-7
3.4 Change in Storage ... 3-7
Section 4 – Computer Codes ... 4-1
4.1 MODFLOW ... 4-1
4.2 R4 Surface Water Simulation Model ... 4-2
4.3 HYDRUS-2D ... 4-3
4.4 PEST and SENSAN ... 4-3
Section 5 – Model Construction ... 5-1
5.1 Model Domain and Grid ... 5-1
5.2 Time Discretization ... 5-1
5.3 Hydraulic Properties and Zonation ... 5-1
5.4 Initial Condition ... 5-3
5.5 Boundary Conditions ... 5-3
5.5.1 MODFLOW Packages for Boundary Conditions ... 5-4
5.5.1.1 Recharge Package ... 5-4
5.5.1.2 Flow and Head Boundary Package (FHB) ... 5-4
5.5.1.3 Evapotranspiration Package (EVT) ... 5-4
5.5.1.4 Well Package (WEL) ... 5-5
5.5.1.5 Stream Package (STR) ... 5-5
5.5.2 Other MODFLOW Packages ... 5-6
5.5.2.1 Geometric Multigrid Solver Package (GMG) ... 5-6
5.5.2.2 Head-Observation Package (HOB) ... 5-6
5.5.2.3 Sensitivity Process Package (SEN) ... 5-6
Section 6 Model Calibration ... 6-1
6.1 Model Calibration Procedure ... 6-1
6.2 Sensitivity Analysis and Covariance Matrix ... 6-2
6.3 Selection of Calibration Data ... 6-3
6.4 PEST Settings and Calibration Results ... 6-3
6.4.1 PEST Settings ... 6-4
6.4.2 Calibration Results ... 6-5
6.4.3 Residual Analysis ... 6-7
6.4.4 Validation ... 6-8
Section 7 - Safe Yield and Future Basin Conditions ... 7-1
7.1 Safe Yield ... 7-1

7.1.1 Definition and Theory of Net Recharge and Safe Yield 7-1
7.1.2 Safe Yield Criteria 7-3
7.1.2.1 Base Period 7-3
7.1.2.2 Storage 7-3
7.1.2.3 Basin Area 7-3
7.1.2.4 Land Use 7-4
7.1.2.5 Changes in Drainage 7-5
7.1.2.6 Groundwater Production 7-5
7.1.3 Estimate of the Safe Yield Included in the 1978 Chino Basin Judgment 7-6
7.2 Present and Projected Future Cultural Conditions 7-7
7.2.1 Planning Scenarios 7-8
7.2.1.1 Future Projections of Groundwater Production 7-8
7.2.1.2 Replenishment Obligation Projections 7-11
7.2.2 Planning Period Hydrology 7-12
7.2.2.1 Recharge Components 7-12
7.2.2.2 Discharge Components 7-13
7.3 Projected Basin Response 7-13
7.3.1 Projected Future Water Budget 7-14
7.3.1.1 Model-Estimated Recharge Components 7-14
7.3.1.2 Model-Estimated Discharge Components 7-14
7.3.2 Net Recharge 7-15
7.3.3 Projected Changes in Groundwater Level 7-15
7.3.4 Projected Changes in Groundwater Storage 7-16
7.3.5 Projected State of Hydraulic Control 7-16
7.3.6 Storage Loss Rate Post Attainment of Hydraulic Control 7-17
7.3.7 New Yield Created by the Desalters and Reoperation 7-18
7.4 Recommendations Regarding Net Recharge and the Redetermining of Safe Yield.. 7-19
Section 8 – References 8-1
Appendix B – Hydrologic Appendix 1

Appendix A Hydrostratigraphic Cross Sections
Appendix B Hydrologic Appendix
Appendix C1 Time-History Plots of Simulated and Measured Groundwater Elevations in the Wells Used in Model Calibration 1961 - 2011
Appendix C2 Time-History Plots of Simulated and Measured Groundwater Elevations in the Wells Used in Model Validation 1961 – 2011
Appendix D Time-History Plots of Projected Groundwater Elevations in Select Wells for Scenario 5A

List of Tables

3-1	Annual Water Budget for the Calibration Period, 1961-2011
5-1	Model Parameters, Zonation and Initial Estimates
5-2	Boundary Conditions
6-1	Model Parameter Sensitivity in Initial Optimization
6-2	Calibration Wells
6-3	Model Parameter Base Value, Calibrated Value and Range of Parameter Values in PEST
6-4	Residual General Statistics
6-5	Residual Error Classification
7-1	Historical and projected Land Uses in the Chino Basin Area
7-2	Imperviousness and Irrigation Assumptions for Land Uses in the Chino Basin
7-3	William J Carroll's Estimation of Safe Yield Adopted in the Chino Basin Judgment
7-4	Scenario 5A - Projected Groundwater Production for the Chino Basin
7-5	Scenario 5A - Projected Groundwater Production and End of Year Storage Account Balance
7-6	Water Budget for Chino Basin (2011-2050) – Scenario 5A
7-7	Summary of Projected Groundwater Elevation Changes by Water Service Area – Scenario 5A
7-8	CDA Desalter Well Production Schedule for Scenario 5G
7-9	Subsurface Discharge through the CCWF for Scenarios 5A and 5G
7-10	Santa Ana River Underflow New Yield Created by the CDA Chino Desalter Well Production and Reoperation

List of Figures

1-1	Study Area Map
2-1	Geologic Map and Boundaries of the Chino Basin
2-2	Effective Base of the Freshwater Aquifer
2-3	Bouguer Gravity Map
2-4	Depth-Dependent Piezometric Response to Pumping – Southwestern Chino Basin
2-5	Map View of Hydrostratigraphic Cross-Sections
2-6a	Cross-Section A-A’
2-6b	Cross-Section G-G’
2-6c	Cross-Section J-J’
2-7	Groundwater Elevation Contours Spring 2012 – Chino Basin
2-8	Areas of Subsidence and Historical Artesian Conditions
2-9	Water Level Time Histories (Non-Pumping) – City of Chino Wells 1A and 1B
2-10a	Layer 1 Bottom Elevation Contours
2-10b	Layer 2 Bottom Elevation Contours
2-11a	Kriging-Estimated Specific Yield of Layer 1
2-11b	Kriging-Estimated Specific Yield of Layer 2
2-11c	Kriging-Estimated Specific Yield of Layer 3
2-12a	Kriging-Estimated Horizontal Hydraulic Conductivity of Layer 1
2-12b	Kriging-Estimated Horizontal Hydraulic Conductivity of Layer 2
2-12c	Kriging-Estimated Horizontal Hydraulic Conductivity of Layer 3
2-13a	Kriging-Estimated Vertical Hydraulic Conductivity of Layer 1
2-13b	Kriging-Estimated Vertical Hydraulic Conductivity of Layer 2
2-13c	Kriging-Estimated Vertical Hydraulic Conductivity of Layer 3
3-1	Calibration Period Water Balance for the Entire Model Area
3-2	Groundwater Model Boundary Conditions
3-3	Hydrologic Sub-areas, Channel Lining Timeframe and Recharge Facilities
3-4	Streambed Infiltration for the Santa Ana River Tributaries for the Calibration Period, Fiscal 1961 - 2011
3-5	Infiltration at the Root Zone and Recharge at the Water Table
3-6	Groundwater Production For the Calibration Period, Fiscal 1960 - 2011
5-1	Map of Model Domain and Model Grid
5-2a	Model Parameter Zonation, Base Value and Heterogeneity Map: Horizontal Hydraulic Conductivity-- Layer 1
5-2b	Model Parameter Zonation, Base Value and Heterogeneity Map: Horizontal Hydraulic Conductivity-- Layer 2

List of Figures

5-2c	Model Parameter Zonation, Base Value and Heterogeneity Map: Horizontal Hydraulic Conductivity-- Layer 3
5-3	Groundwater Elevation Contours Initial Condition Water Level Map - June 1960
5-4	Groundwater Model Boundary Conditions
5-5	Location of Wells With Historical Water Level Records – Bloomington Divide Area
5-6	Comparison of Water Levels Across the Rialto-Colton Fault near the Bloomington Divide
5-7	Comparison of Water Levels Across Bloomington Divide
5-8	STR Package of Channel Segments where Simulation of Groundwater and Surface Water Interaction Occur
6-1	Location of Calibration Wells - Chino Basin
6-2a	Comparison of Simulated and Measured Water Levels in the Calibration Wells of Chino Basin
6-2b	Comparison of Simulated and Measured Water Levels in the Wells of Chino Basin Management Zone 1
6-2c	Comparison of Simulated and Measured Water Levels in the Wells of Chino Basin Management Zone 2
6-2d	Comparison of Simulated and Measured Water Levels in the Wells of Chino Basin Management Zone 3
6-2e	Comparison of Simulated and Measured Water Levels in the Wells of MZ-4, MZ-5 and the Prado Basin MZ
6-2f	Comparison of Simulated and Measured Water Levels in the Wells around Chino City Area
6-3a	MODFLOW Estimated Santa Ana River Discharge into Prado Dam Reservoir versus Total Santa Ana River Discharge Estimated by US Army Corps of Engineers
6-3b	Model-Estimated Stream Flow to Prado versus Prado Inflow Estimated by US Army Corps of Engineers
6-4	Residual Relative Frequency Histogram in Chino-Temescal Basin
6-5a	Residual Relative Frequency Histogram in Chino Basin
6-5b	Residual Relative Frequency Histogram in MZ1 of Chino Basin
6-5c	Residual Relative Frequency Histogram in MZ2 of Chino Basin
6-5d	Residual Relative Frequency Histogram in MZ3 of Chino Basin
6-6	Mean Residual Error of Calibration Wells
7-1	Historical and Projected Distribution of Land Use in the Chino Basin
7-2	Historical and Projected Chino Basin Groundwater Production
7-3	Comparison of Historical and Projected Net Recharge to Overlying Ag and CDA Production
7-4a	Groundwater Elevation Contours – Layer 1, Scenario 5A Initial Condition – 2011

List of Figures

7-4b	Projected Groundwater Elevation Contours – Layer 1, Scenario 5A – 2020
7-4c	Projected Groundwater Elevation Contours – Layer 1, Scenario 5A – 2030
7-4d	Projected Groundwater Elevation Contours – Layer 1, Scenario 5A – 2040
7-4e	Projected Groundwater Elevation Contours – Layer 1, Scenario 5A – 2050
7-5a	Projected Groundwater Elevation Change – Layer 1, Scenario 5A –2011 to 2020
7-5b	Projected Groundwater Elevation Change – Layer 1, Scenario 5A –2011 to 2030
7-5c	Projected Groundwater Elevation Change – Layer 1, Scenario 5A –2011 to 2040
7-5d	Projected Groundwater Elevation Change – Layer 1, Scenario 5A –2011 to 2050
7-6	Projected Aggregate Water in Storage Accounts and Change in Storage for Scenario 5A
7-7	Estimated Storage in the Chino Basin, 1922 through 2050
7-8a	Projected State of Hydraulic Control in 2020 – Scenario 5G
7-8b	Projected State of Hydraulic Control in 2025 – Scenario 5G
7-9	Relationship of Discharge through the CCWF from the Chino North Management Zone to the Prado Basin Management Zone to the Aggregate Volume of Stored Water and Carryover

1.1 Background

The Chino Basin consists of about 235 square miles of the upper Santa Ana River watershed. The basin is bounded by the Cucamonga Basin and the San Gabriel Mountains to the north; the Rialto-Colton Basin to the northeast; the chain of Jurupa, Pedley, and La Sierra Hills to the southeast; the Temescal Basin to the south; the Chino and Puente Hills to the southwest; and the San Jose Hills and the Pomona and Claremont Basins to the northwest as shown on Figure 1-1. The basin lies within the Counties of San Bernardino and Riverside and includes the Cities of Chino, Ontario, Chino Hills, Norco, and several other communities.

The Chino Basin is an integral part of the regional and statewide water supply system. One of the largest groundwater basins in Southern California, the Chino Basin contains about 5,000,000 acre-ft (ac-ft) of water and has an unused storage capacity of about 1,000,000 acre-ft. Cities and other water supply entities produce groundwater for all or part of their municipal and industrial supplies. Agricultural users also produce groundwater from the basin, but irrigated agriculture has declined substantially in recent years and is projected to be almost nonexistent by 2020 [Ref. 1].

The boundary of the Chino Basin is legally defined in the Stipulated Judgment (Judgment) issued in 1978 (Chino Basin Municipal Water District vs. the City of Chino et al. [SBSC Case No. RCV 51010]). Since that time, the basin has been operated, as described in the Judgment, under the direction of a court-appointed Watermaster. The OBMP is being implemented pursuant to the Judgment and a 1998 ruling of the court in its exercise of continuing jurisdiction.

1.2 Project Objectives

The objectives of this investigation were to update the Watermaster's groundwater model and to use the model to make certain assessments as required by the Judgment, the Peace Agreements, Watermaster Rules and Regulations, and the October 2010 court order regarding implementation of the 2010 Recharge Master Plan Update. These efforts include:

- Completion of the safe yield redetermination,
- Evaluation New Yield created by the desalters and reoperation
- Evaluation of the state of hydraulic control,
- Evaluation of the balance of recharge and discharge,

The required technical activities and their nexus to their requirements are described below.

1.2.1 Model Recalibration

The 2007 Chino Basin Watermaster Model was updated and recalibrated by extending its calibration period from 1960-2006 to 1960 through June 30, 2011, making improvements to the model structure and hydrology, and recalibrating the updated model. The update included revisions to the conceptual model, improvements in other model features and update of the recharge and discharge stresses for the calibration and planning periods.

1.2.2 Safe Yield and the Balance of Recharge and Discharge

The updated model will be used to estimate the safe yield for the 2011 through 2020 period. (R&R, 6.5; September 2010 Court Order) The model will be used to fine tune supplemental water recharge (done for replenishment and other purposes) to revise the balance of recharge and discharge as required by the Peace Agreement and the Watermaster Rules and Regulations Sections 7.1b (iii) and (iv).

1.2.3 New Yield from Desalters and Reoperation

The updated Watermaster Model was used to estimate Santa Ana River underflow new yield (SARUNY) from the desalters and reoperation from both the calibration and planning periods. SARUNY means the same thing as the term *Desalter Induced Recharge* that is used in the 2015 Safe Yield Reset Agreement.

1.3 Report Organization

The bulk of this report (Sections 2 through 7, and Appendices) describes the careful scientific work performed to update Watermaster's groundwater model. Section 7 contains an analysis of safe yield and an assessment of projected groundwater levels and hydraulic control based on projected groundwater production and replenishment.

Section 1 Introduction: This section describes the general setting, presents the overall project objectives and the purpose and use of the groundwater-flow model.

Section 2 Hydrogeologic Setting: This section describes the hydrogeologic conditions of the Chino Basin. The topics covered include geologic setting, hydrostratigraphy, the occurrence and movement of groundwater, aquifer properties, groundwater levels, and groundwater quality. These data were used to construct a hydrogeologic conceptual model of the Chino Basin for input to the groundwater-flow model.

Section 3 Water Balance: This section presents a description of the recharge and discharge components to the groundwater system of the Chino Basin.

Section 4 Computer Code: This section presents a description of the computer codes used in the groundwater-flow model.

Section 5 Model Construction: This section describes how the hydrogeologic conceptual model was translated into a numerical model. The model domain, initial conditions, boundary conditions, and hydraulic conditions are defined in this section.

Section 6 Model Calibration: This section discusses the model calibration procedures. The simulated results over the calibration period (Fiscal year 1960-2011) are quantitatively compared to observed data in this section.

Section 7 Safe *Yield and Future Basin Conditions:* This section describes an analysis of safe yield and an assessment of projected groundwater levels and hydraulic control based on projected groundwater production and replenishment.

Section 8 References: This section lists the references for data, computer codes, and modeling procedures used in the modeling effort.

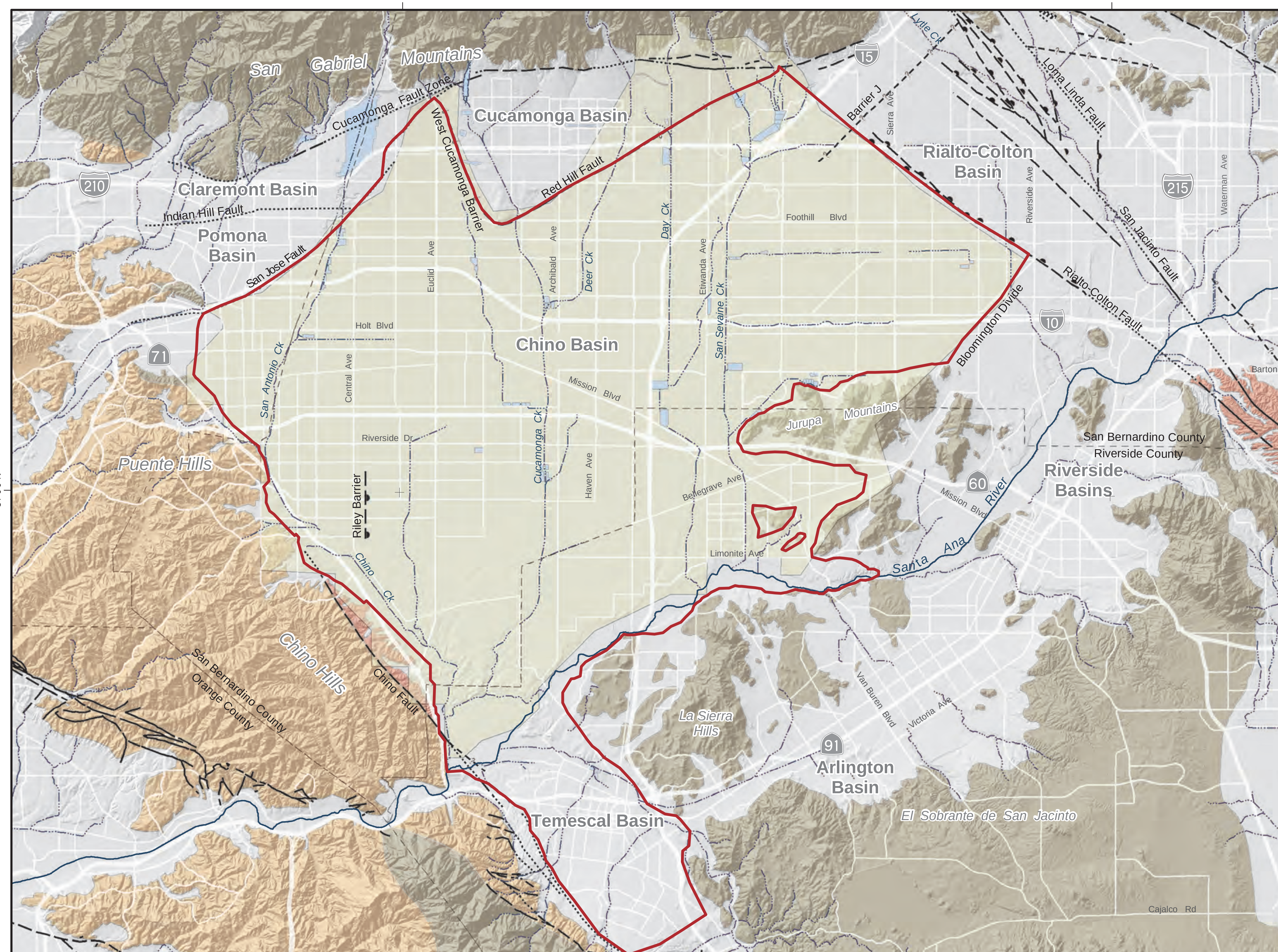

117°40'0"W 117°20'0"W

MODFLOW Groundwater Flow Model Boundary

Chino Basin Adjudicated Boundary

Streams & Flood Control Channels

Flood Control & Conservation Basins

Geology

Water-Bearing Sediments

Quaternary Alluvium

Consolidated Bedrock

Plio-Pleistocene Sedimentary Rocks

Cretaceous to Miocene Sedimentary Rocks

Pre-Tertiary Igneous and Metamorphic Rocks

Faults

Location Certain

Location Approximate

Approximate Location of Groundwater Barrier

Location Concealed

Location Uncertain

Produced by:

WEI
WILDERMUTH ENVIRONMENTAL, INC.

Author: MJC
Date: 10/1/2015
Document Name: Figure_1-1_20131230

0 1 2 3 4 5 Miles
0 2 4 6 8 KM

2013 Chino Basin Groundwater Model Update
and Analysis of Safe Yield

Study Area

Figure 1-1

Section 2 – Hydrogeologic Setting

In 2000/01, a numerical computer-simulation groundwater flow model was constructed to simulate the effects of a proposed conjunctive use storage program (WEI, 2003), hereafter referred to as the "2003 model." The hydrogeologic conceptual model, which was used as an input to the 2003 model, was based on Watermaster's understanding of Chino Basin hydrogeology at that time. Since then, Watermaster and others have conducted hydrogeologic investigations and collected new hydrogeologic data. These new data have been utilized to update the hydrogeologic conceptual model of the Chino Basin for the 2007 Model and subsequently for the new 2013 Watermaster model described in this report.

The purpose of this section is to describe the geology and hydrogeology of Chino Basin based on the most current information available. The topics covered include the geologic setting, geologic stratigraphy, the occurrence and movement of groundwater, hydrostratigraphy, and aquifer properties. This information was used to update the hydrogeologic conceptual model of the Chino Basin for input to the groundwater-flow model.

2.1 Geologic Setting

Figure 2-1 is a generalized geologic map of the Chino Basin. The Chino Basin was formed as a result of tectonic activity along major fault zones during the Quaternary Period[1]. It is part of a large, broad, alluvial-filled plain located between the San Gabriel Mountains to the north (Transverse Ranges) and the elevated Perris Block to the south (Peninsular Ranges), which is sometimes referred to as the Chino Plain. The Santa Ana River is the main tributary draining the area.

The major faults in the Chino Basin area—the Cucamonga Fault Zone, the Rialto-Colton Fault, the Red Hill Fault, the San Jose Fault, and the Chino Fault—are at least partly responsible for the uplift of the surrounding mountains and the depression of the Chino Basin. The bottom of the basin, the effective base of the freshwater aquifer, consists of impermeable sedimentary and igneous bedrock formations that are exposed at the surface in the surrounding mountains and hills. Sediments that were eroded and washed out from the surrounding mountains filled the Chino Basin to form its groundwater reservoirs. In the deepest portions of the Chino Basin, these sediments are greater than 1,000 feet thick.

The major faults are also significant in that they are known barriers to groundwater flow within the aquifer sediments and, hence, define some of the external boundaries of the basin by influencing the magnitude and direction of groundwater flow. The locations of these major faults are shown in Figure 2-1. These faults, their effects on groundwater movement, and the hydrogeology of the Chino Basin area have been documented by various entities and authors (Eckis, 1934; Gleason, 1947; Burnham, 1953; MacRostie and Dolcini, 1959; Dutcher & Garrett, 1963; Gosling, 1966; DWR, 1970; Woolfenden and Kadhim, 1997).

2.2 Stratigraphy

In this report, the stratigraphy of the Chino Basin is divided into two natural divisions: (1) the permeable formations that comprise the primary groundwater reservoirs are termed "water-bearing sediments," and (2) the less permeable formations that enclose the groundwater reservoirs are termed

[1] Approximately 2 million ago to the present.

"consolidated bedrock." Consolidated bedrock is further differentiated as the metamorphic and igneous rocks of the "basement complex," which are overlain in places by consolidated sedimentary rocks. The water-bearing sediments overlie the consolidated bedrock. The bedrock formations come to the surface in the surrounding hills and highlands. These geologic formations are described below in stratigraphic order, starting with the oldest formations first.

The terms used in this report to describe the bedrock formations—such as "consolidated," "non-water-bearing," and "impermeable"—are used in a relative sense. The water content and permeability of these bedrock formations, in fact, is not zero. Pervious strata or fracture zones in bedrock formations may yield water to wells locally; however, the storage and transmissive properties are typically inadequate for sustained production. The primary point is that the permeability of the geologic formations in the areas flanking the basin is much less than the aquifers in the groundwater basin.

2.2.1 Consolidated Bedrock

The consolidated bedrock formations of the Chino Basin area include the basement complex; consolidated, marine, sedimentary and volcanic strata; and more recent, semi-consolidated, continental sedimentary deposits. Figure 2-1 shows the surface outcrops of the consolidated bedrock formations that surround the Chino Basin. Note that the basement complex is the exposed bedrock to the north and southeast of the Chino Basin. The sedimentary bedrock is exposed to the west of the Chino Basin. The general character of the consolidated bedrock is known from drillers' logs and surface outcrops.

2.2.1.1 Basement Complex

The basement complex consists of deformed and re-crystallized metamorphic rocks that have been invaded in places by masses of granitic and related igneous rocks. The intrusive granitic rocks, which make up most of the basement complex, were emplaced about 110 million years ago in the late Middle Cretaceous (Larsen, 1958). These rocks were subsequently uplifted and exposed by erosion, as presently seen in the San Gabriel Mountains and in the uplands of the Perris Block (Jurupa Mountains and La Sierra Hills). They have been the major source of detritus to the younger sedimentary formations and, in particular, the water-bearing sediments of the Chino Basin.

2.2.1.2 Undifferentiated Pre-Pliocene Formations

Consolidated sedimentary and volcanic rocks that unconformably overlie the basement complex outcrop along the western margin of the Chino Basin in the Chino Hills and Puente Hills. They consist of well-stratified marine sandstones, conglomerates, shales, and interlayered lava flows that range in age from late Cretaceous to Miocene. According to Durham and Yerkes (1964), this sequence reaches a total stratigraphic thickness of more than 24,000 feet in the Puente Hills and is down-warped more than 8,000 feet below sea level in the Prado Dam area. Wherever mapped, these strata are folded and faulted and, in most places, dip from 20 to 60 degrees.

2.2.1.3 Plio-Pleistocene Formations

A thick series of semi-consolidated clays, sands, and gravels of marine and non-marine origin overly the older consolidated bedrock formations. These sediments have been named the Fernando Group (Eckis, 1934) and outcrop in two general locations of the study area: the Chino Hills on the western margin of the Chino Basin and the San Timoteo Badlands southeast of the Chino Basin. In this study, the entire group is considered consolidated bedrock, and is likely the first bedrock penetrated in the southwestern portion of the Chino Basin. The upper portion of the Fernando Group is more permeable than the lower portion and thus represents a gradual transition from non-water-bearing consolidated rocks to water-bearing sediments. The upper Fernando sediments are similar in texture and composition to the overlying water-bearing sediments, which make the distinction between the formations difficult to identify in borehole data.

2.2.2 Water-Bearing Sediments

Beginning in the Pleistocene and continuing to the present, an intense episode of faulting depressed the Chino Basin area and uplifted the surrounding mountains and hills. Detritus eroded from the mountains were transported and deposited in the Chino Basin atop the bedrock formations as interbedded, discontinuous layers of gravel, sand, silt, and clay to form the water-bearing sediments.

Eckis (1934) speculated that the contact between consolidated bedrock and water-bearing sediments in the Chino Basin is unconformable, as indicated by an ever-present weathered zone in the consolidated bedrock directly underlying the contact with the water-bearing sediments. This observed relationship suggests that the consolidated bedrock in the Chino Basin area was undergoing erosion prior to the deposition of water-bearing sediments.

In this study, the water-bearing sediments are differentiated into Older Alluvium of the Pleistocene age and Younger Alluvium of the Holocene age. The general character of these formations is known from driller's logs and surface outcrops.

2.2.2.1 Older Alluvium

The Older Alluvium varies in thickness from about 200 feet near the southwestern end of the Chino Basin to over 1,100 feet southwest of Fontana. It is commonly distinguishable in surface outcrop by its red-brown or brick-red color and is generally more weathered than the overlying Younger Alluvium. The pumping capacities of wells completed in the Older Alluvium generally range between 500 and 1,500 gallons per minute (gpm). Capacities exceeding 1,000 gpm are common, and some modern production wells test-pumped at over 4,000 gpm (*e.g.* Ontario Wells 30 and 31 in southeastern Ontario). In the southern part of the basin where the water-bearding sediments tend to be more clay rich, the wells generally yield less than 1,000 gpm.

2.2.2.2 Younger Alluvium

The Younger Alluvium occupies streambeds, washes, and other areas of recent sedimentation. Oxidized particles tend to be flushed out of the sediments during transport, and the Younger Alluvium is commonly light yellow, brown, or gray. It consists of rounded fragments derived from the erosion of bedrock, reworked Older Alluvium, and the mechanical breakdown of larger fragments within the Younger Alluvium itself. The Younger Alluvium varies in thickness from over 100 feet near the mountains to a just few feet south of Interstate 10 and generally covers most of the north half of the basin. The Younger Alluvium is not saturated and, thus, does not yield water directly to wells. Water percolates readily in the Younger Alluvium, and most of the large spreading basins in Chino Basin are located in the Younger Alluvium.

2.2.3 Effective Base of the Freshwater Aquifer

Figure 2-2 shows Watermaster's current interpretation of the effective base of the freshwater aquifer in Chino Basin, herein referred to as the "bottom of the aquifer." The bottom of the aquifer is depicted in Figure 2-2 by equal elevation contour lines. These contours were first drawn by the California Department of Water Resources (DWR, 1970). New data and interpretations by Watermaster were used to modify the DWR contours during model updates in 2003 (WEI, 2003) and 2007 (WEI, 2007).

The bottom of the aquifer contours were not modified during this model update.

2.2.3.1 Eastern Chino Basin

On the east side of Chino Basin (east of Archibald Avenue), the contours of the bottom of the aquifer are based on depth to the basement complex. Figure 2-2 shows borehole locations in eastern Chino Basin where the basement complex was penetrated at depths ranging from 35 to 1,100 feet below ground surface (ft-bgs). Since 2000, several new wells were drilled in the southeastern portion of Chino Basin that penetrated crystalline bedrock, including several HCMP monitoring wells and the production wells of the Chino Basin Desalter Authority, and were used to refine the contours of the bottom of the aquifer in the southeastern portion of Chino Basin.

2.2.3.2 Western Chino Basin

On the west side of the Chino Basin (west of Archibald Avenue) and in the Temescal Basin, the determination of the bottom of the aquifer is not as straightforward. Figure 2-2 shows the locations of boreholes of depths 1,000 to 1,400 ft-bgs that did not penetrate the basement complex, but terminated in highly-weathered and consolidated sediments that may be formations of the sedimentary bedrock formations. These deep sedimentary bedrock formations are similar in texture and composition to the overlying water-bearing sediments, which make the contact between the formations difficult to identify in borehole data. In addition, there is evidence to suggest that the upper portions of the sedimentary bedrock formations have a useful porosity and permeability, and that these formations contribute water to deep production wells. For these reasons:

1. It is now believed that the bottom of the aquifer in the western Chino Basin includes the upper portion of the sedimentary bedrock, where present.
2. Other data (as opposed to a simple delineation based on the contact between bedrock and unconsolidated sediments) is used to estimate the geometry of the bottom of the aquifer in the western Chino Basin.

Gravity Data. The basement complex presumably underlies sedimentary bedrock in the western Chino Basin, but at depths too great to play a factor in the shallow freshwater aquifers. Durham and Yerkes (1964) estimated a depth to the basement complex of several thousand ft-bgs and a contact of angular unconformity with the overlying sedimentary bedrock. Geophysical data supports this conceptualization. Figure 2-3 shows regional gravity data plotted and contoured as Bouguer anomalies with a contour interval of 5 milligals (MGal). The gravity data was collected in May 2007 from GEONET at the United States Gravity Data Repository System. The Bouguer anomalies in the Chino Basin area range between -80 MGal in the western Chino Basin to about -55 MGal in the granitic Jurupa Mountains and La Sierra Hills. Gravity lows can be attributed to a greater thickness of low-density rock formations, such as loose sediments and sedimentary rocks. Note how the Bouguer anomaly contours have a similar shape to the contours of the bottom of the aquifer in Figure 2-2 with a trough of low values in western Chino Basin. These gravity data are consistent with a deep sedimentary trough in the western Chino Basin with progressively shallower crystalline bedrock to the east and southeast toward the granitic Jurupa Mountains and La Sierra Hills.

Hydrogeologic Data. Figure 2-2 shows deep wells in the western Chino Basin and the Temescal Basin with screens deeper than 1,000 ft-bgs. All of the well boreholes penetrated a similar sequence of sediments that include sands, gravels, silts, and clays. At some of these wells, spinner tests were performed after well development. The spinner tests generally demonstrate that the pumped groundwater enters a well primarily from shallower sediments (probably from the higher-permeability sediments of the Older Alluvium) with a much smaller contribution from deeper sediments (probably from the lower-permeability sediments of the sedimentary bedrock formations). The deepest production wells in the western Chino Basin are about 1,200 ft-bgs.

Figure 2-2 shows two well locations along Central Avenue in the westernmost portion of Chino Basin. At one location, there is a deep production well (CH-19), which is screened from 340-1,000 ft-bgs. At the other location, there is a subsidence monitoring facility that contains multiple piezometers—two of which are highlighted here (PA-7, which is screened from 438-448 ft-bgs, and PB-2, which is screened from 1,086-1,096 ft-bgs). Note that PB-2 is screened about 100 feet below the deepest screens of CH-19. Both PA-7 and PB-2 are completed in sand and gravel units. Slug test data from PA-7 and PB-2 have indicated that the hydraulic conductivity of PA-7 (48 ft/day) is much greater than that of PB-2 (0.5 ft/day).

Figure 2-4 is a water-level time-series chart that shows the water level responses at PA-7 and PB-2 to pumping at CH-19. Note the immediate drawdown of water levels at PA-7 to the initiation of pumping at CH-19. Also note the relatively delayed and muted drawdown of water levels at PB-2.

The above observations indicate that pumping of the aquifer system in the western Chino Basin above 1,000 ft-bgs causes:

1. The horizontal flow of groundwater to pumping wells within the high-permeability sand and gravel units of the Older Alluvium, like those screened in PA-7 at 438-448 ft-bgs.
2. The oblique and upward flow of groundwater to pumping wells within the deeper low-permeability sands and gravels of the sedimentary bedrock formations, like those screened in PB-2 at 1,086-1,096 ft-bgs.

Based on the above information, Watermaster has set the bottom of the aquifer at approximately 1,300 ft-bgs across most of the western portion of the Chino Basin and in the Temescal Basin as shown in Figure 2-2.

2.2.3.3 Bedrock Fault

Another major feature of the bottom of the aquifer in the Chino Basin is the assumed bedrock fault that underlies Archibald Avenue. This bedrock fault has uplifted the crystalline bedrock of the basement complex in the eastern Chino Basin relative to the sedimentary bedrock and water-bearing sediments in the western Chino Basin. The evidence for this bedrock fault comes from well borehole data.

Figure 2-5 displays the map that shows the location of several hydrogeologic cross-sections that have been drawn across Chino Basin, and Figures 2-6a-c show three of these sections[2]. Figure 2-6a is a profile view of hydrogeologic cross-section A-A' that crosses the bedrock fault in the southern Chino Basin. Note that the borehole of well CD1-13 terminates in crystalline bedrock at a depth of 320 ft-bgs. Also, note that just 4,500 ft to the west, the borehole of well CD1-7 was drilled to a depth of 680 ft-bgs without penetrating crystalline bedrock. This information and other similar observations were used to define the location and orientation of the assumed bedrock fault. The location and orientation of the bedrock fault and the existence of deep, low-permeability aquifers in the western Chino Basin are entirely consistent with past work in this area (French, 1972).

[2] All the cross-sections are shown in Appendix A as Adobe PDF files.

2.3 Occurrence and Movement of Groundwater

The physical nature of the Chino Basin as a groundwater reservoir is described below with regard to basin boundaries, recharge, groundwater flow, internal barriers to groundwater flow, and discharge. In short, this section describes (i) where groundwater occurs in the Chino Basin, (ii) how groundwater recharges and moves through the Chino Basin, and (iii) where groundwater discharges from the Chino Basin.

2.3.1 Chino Basin Boundaries

The physical boundaries of the Chino Basin are shown in Figure 2-1 and include:

- **Red Hill Fault to the north.** The Red Hill Fault is a recently active fault, evidenced by recognizable fault scarps such as Red Hill at the extreme southern extent of the fault near Foothill Boulevard. The fault is a known barrier to groundwater flow, and groundwater elevation differences on the order of several hundred feet on opposite sides of the fault are typical (Eckis, 1934; DWR, 1970). Groundwater seeps across the Red Hill Fault as underflow from the Cucamonga Basin to the Chino Basin, especially during periods of high groundwater elevations within the Cucamonga Basin.
- **San Jose Fault to the northwest.** The San Jose Fault is known as an effective barrier to groundwater flow with groundwater elevation differences on the order of several hundred feet on opposite sides of the fault (Eckis, 1934; DWR, 1970). Groundwater seeps across the San Jose Fault as underflow from the Claremont Heights and Pomona Basins to the Chino Basin, especially during periods of high groundwater elevations within the Claremont Heights and Pomona Basins.
- **Groundwater divide to the west.** A natural groundwater divide near Pomona separates the Chino Basin from the Spadra Basin in the west. The divide, which extends from the eastern tip of the San Jose Hills southward to the Puente Hills, is produced by groundwater seepage from the Pomona Basin across the southern portion of the San Jose Fault (Eckis, 1934).
- **Puente Hills/Chino Hills to the southwest.** The Chino Fault extends from the northwest to the southeast along the western boundary of the Chino Basin. It is, in part, responsible for uplift of the Puente Hills and Chino Hills, which form a continuous belt of low hills west of the fault. The Chino and Puente Hills, which are primarily composed of consolidated sedimentary rocks, form a low permeability barrier to groundwater flow.
- **Flow system boundary with Temescal Basin to the south.** A comparison of groundwater elevation contour maps over time suggests a consistent distinction between flow systems within the lower Chino Basin and Temescal Basin. As groundwater within Chino Basin flows southwest into the Prado Basin area, it converges with groundwater flowing northwest out of the Temescal Valley (Temescal Basin). These groundwaters commingle and flow southwest toward Prado Dam and can rise to become surface water in Prado Basin. This area of convergence of Chino and Temescal groundwater is indistinct and probably varies with changes in climate and production patterns. As a result, the boundary that separates Chino Basin from Temescal Basin was drawn along the legal boundary of the Chino Basin (Chino Basin Municipal Water District v. City of Chino, *et al.*, San Bernardino Superior Court, No. 164327).
- **La Sierra Hills to the south.** The La Sierra Hills outcrop south of the Santa Ana River, are primarily composed of impermeable crystalline bedrock, and form a barrier to groundwater flow between the Chino Basin and the Arlington and Riverside Basins.

- **Shallow bedrock at the Riverside Narrows to the southeast.** Between the communities of Pedley and Rubidoux, the impermeable bedrock that outcrops on either side of the Santa Ana River narrows considerably. In addition, the alluvial thickness underlying the Santa Ana River thins to approximately 100 feet or less (*i.e.*, shallow bedrock). This area of narrow and shallow bedrock along the Santa Ana River is commonly referred to as the Riverside Narrows. Groundwater upgradient of the Riverside Narrows within the Riverside Basins is forced to the surface and becomes rising water within the Santa Ana River (Eckis, 1934). Downstream of the Riverside Narrows, the bedrock configuration widens and deepens, and surface water within the Santa Ana River can infiltrate to become groundwater in the Chino Basin.
- **Jurupa Mountains and Pedley Hills to the southeast.** The Jurupa Mountains and Pedley Hills are primarily composed of impermeable bedrock and form a barrier to groundwater flow that separates the Chino Basin from the Riverside Basins.
- **Bloomington Divide to the east.** A flattened mound of groundwater exists beneath the Bloomington area as a likely result of groundwater flow from the Rialto-Colton Basin through a gap in the Rialto-Colton Fault north of Slover Mountain (Dutcher and Moyle, 1963; Gosling, 1966; DWR, 1970). This mound of groundwater extends from the gap in the Rialto-Colton Fault southwest towards the northeast tip of the Jurupa Mountains. Groundwater to the northwest of this divide recharges the Chino Basin and flows westward staying north of the Jurupa Mountains. Groundwater southeast of the divide recharges the Riverside Basins and flows southwest towards the Santa Ana River.
- **Rialto-Colton Fault to the northeast.** The Rialto-Colton Fault separates the Rialto-Colton Basin from the Chino and Riverside Basins. This fault is a known barrier to groundwater flow along much of its length—especially in its northern reaches (south of Barrier J) where groundwater elevations can be hundreds of feet higher within the Rialto-Colton Basin (Dutcher and Garrett, 1963; DWR, 1970; Woolfenden and Kadhim, 1997). The disparity in groundwater elevations across the fault decreases to the south. To the north of Slover Mountain, a gap in the Rialto-Colton Fault exists. Groundwater within the Rialto-Colton Basin passes through this gap to form a broad groundwater mound (divide) in the vicinity of Bloomington and, hence, is called the Bloomington Divide (Dutcher and Moyle, 1963; Gosling, 1966; DWR, 1970).
- **Extension of the Rialto-Colton Fault north of Barrier J.** Little well data exist to support the extension of the Rialto-Colton Fault north of Barrier J (although hydraulic gradients are steep through this area). Groundwater flowing south out of Lytle Creek Canyon, in part, is deflected by Barrier J and likely flows across the extension of the Rialto-Colton Fault north of Barrier J and into the Chino Basin.

2.3.2 Groundwater Recharge, Flow, and Discharge

The predominant source of recharge to Chino Basin groundwater reservoirs is the percolation of direct precipitation and returns from applied water. The following is a list of all potential sources of recharge in Chino Basin:

- Infiltration of flow within unlined stream channels overlying the basin
- Infiltration of stormwater flow and municipal wastewater discharges within the channel of the Santa Ana River
- Underflow from the saturated sediments and fractures within the bounding mountains and hills
- Artificial recharge of storm water, imported water, and recycled water at spreading grounds

- Underflow from seepage across the bounding faults, including the Red Hill Fault (from Cucamonga Basin), the San Jose Fault (from the Claremont Heights and Pomona Basins), and the Rialto-Colton Fault (from the Rialto-Colton Basin)
- Intermittent underflow from the Temescal Basin
- Deep percolation of precipitation and returns from use

In general, groundwater flow mimics surface drainage patterns: from the forebay areas of high elevation in the north and east flanking the San Gabriel and Jurupa Mountains, towards areas of discharge near the Santa Ana River within Prado Basin. Figure 2-7 is a groundwater-elevation contour map for spring 2012 that shows this general groundwater flow pattern (perpendicular to the contours). A comparison of this contour map to groundwater-elevation contour maps from other periods shows similar flow paths, indicating consistent flow systems within the Chino Basin (WEI, 2000).

While considered one basin from geologic and legal perspectives, the Chino Basin can be hydrologically subdivided into at least five groundwater-flow systems that act as separate and distinct hydrologic units. Each flow system has a unique hydrology. Water resource management activities that occur in one unit will have limited impacts on the other units. For this reason, the five district hydrologic units have been termed "management zones."

Figure 2-7 shows the five management zones in Chino Basin that were developed during the TIN/TDS Study (WEI, 2000) of which Watermaster, the Chino Basin Water Conservation District (CBWCD), and the Inland Empire Utilities Agency (IEUA) were study participants. Nearing the southwestern (lowest) portion of the basin, these flows systems become less distinct as all groundwater flow within Chino Basin converges and rises beneath the Prado Basin.

In general, groundwater discharge occurs in Chino Basin via:

- Groundwater production
- Rising water within Prado Basin (and potentially other locations along the Santa Ana River depending on climate and season)
- Evapotranspiration within Prado Basin (and potentially other locations along the Santa Ana River depending on climate and season) where groundwater is near or at the ground surface
- Intermittent underflow to the Temescal Basin

2.3.3 Internal Faults

There is only one documented barrier to groundwater flow within the aquifer system of the Chino Basin. This barrier exists only within deep aquifer system of the western Chino Basin and was discovered during the land subsidence investigation in MZ-1. The location of the barrier is shown on Figure 2-2, and has been named the "Riley Barrier" by Watermaster to recognize Francis Riley (a retired USGS hydrogeologist) for his invaluable contributions to the design and implementation of the subsidence management program in MZ-1. A more extensive discussion of the Riley Barrier can be found in the MZ-1 Summary Report (WEI, 2006a).

2.4 Aquifer Systems

The saturated sediments within Chino Basin comprise one groundwater reservoir, but the reservoir can be sub-divided into distinct aquifer systems based on the physical and hydraulic characteristics of the aquifer-system sediments and the contained groundwater. These aquifer systems include a shallow aquifer system and at least one deep aquifer system.

The sediments that comprise the shallow aquifer system are almost fully saturated in the southern portion of the Chino Basin. Depth to groundwater increases to the north to provide a thick vadose zone for percolating groundwater in the forebay regions of the Chino Basin. The sediments that comprise the deep aquifer system are always fully saturated.

The shallow aquifer system is generally characterized by unconfined to semi-confined groundwater conditions, high permeability within its sand and gravel units, and high concentrations of dissolved solids and nitrate (especially in the southern portions of the Chino Basin). The deep aquifer system is generally characterized by confined groundwater conditions, lower permeability within its sand and gravel units, and lower concentrations of dissolved solids and nitrate. Where depth-specific data are available, piezometric head tends to be higher in the shallow aquifer system, indicating a downward vertical hydraulic gradient.

To illustrate the above generalizations, Figure 2-8 shows the location of Well 1A and Well 1B, which are owned by the City of Chino Hills. These two wells are physically located within 30 feet of each other on the west side of the Chino Basin, but their non-pumping water-level time histories are distinctly different. Figure 2-9 displays the water-level time series of Well 1A (perforated within the shallow aquifer system), which maintains a relatively stable water level that fluctuates annually by about 20-30 feet, which is probably in response to seasonal production and recharge. Depth to water averages about 80 feet-bgs. Comparatively, Well 1B (perforated within the deep aquifer system) displays a wildly fluctuating piezometric level that can vary seasonally by as much as 250 feet. Depth to water in Well 1B averages about 220 feet-bgs. The water level fluctuations observed in the deep aquifer system are typical of confined groundwater conditions where small changes in storage (caused by pumping in this case) can generate large changes in piezometric levels.

Wells 1A and 1B also have significant differences in water quality. Nitrate concentrations in 1A and 1B averaged 7 mg/L and 1 mg/L, respectively, from 1997 to 2002. Total dissolved solids (TDS) concentrations in 1A and 1B averaged 288 mg/L and 175 mg/L, respectively, from 1997 to 2002. Arsenic concentrations are relatively high in the deep aquifer system (averaging 66 micrograms per liter [μg/L] in Well 1B from 1997 to 2002 compared to non-detectable in Well 1A). Similar vertical water quality gradients have been noted between deep and shallow groundwater in the area of the Chino Desalter well fields (see Figure 2-8) (GSS, 2001; Dennis Williams, GSS, pers. comm., 2003).

At the Ayala Park Extensometer Facility (location shown in Figure 2-8), there are 11 piezometers with screens of 5-20 feet in length that were completed at various depths, ranging from 139-1,229 ft-bgs. Slug tests were performed at a number of these piezometers to determine, among other objectives, the permeabilities of the sediments at various depths within the total aquifer system. Figure 2-6b is a cross-section that includes the deep borehole at Ayala Park and some of the slug test results at the piezometers. In general, the piezometers in the shallow aquifer system (less than about 350 ft-bgs) display relatively high hydraulic conductivities of 20 to 27 ft/day. The piezometers within the deep aquifer system display relatively low hydraulic conductivities of 1.6 to 0.5 ft/day. A notable exception is a piezometer that was completed in a gravelly sand in the uppermost portion of the deep aquifer system (438-448 ft-bgs), which displays a relatively high hydraulic conductivity of 48 ft/day, indicating the existence of some higher permeability zones within the deep aquifer system.

The distinction between aquifer systems is most pronounced within the west-southwest portions of the Chino Basin. This is likely because of the relative abundance of fine-grained sediments in the southwest (multiple layers of clays and silts). Groundwater flowing from high-elevation forebay areas in the north and east become confined beneath these fine-grained sediments in the west-southwest, and these sediments effectively isolate the shallow aquifer system from the deep aquifer system(s).

The three-dimensional extent of these fine-grained sedimentary units and their effectiveness as confining layers has never been mapped in detail across the Chino Basin. However, the following data, shown on Figure 2-8, can be used to estimate the lateral extent of these units:

- Historical flowing artesian conditions were mapped in the early 1900s in the southwest portion of the Chino Basin (Mendenhall, 1905, 1908; Fife *et al.*, 1976), which indicates the existence of confining layers in these areas.
- Remote sensing studies were conducted to analyze land subsidence in Chino Basin (Peltzer, 1999a, 1999b). These studies employed InSAR, which utilizes radar imagery from an Earth-orbiting spacecraft to map ground surface deformation. InSAR has indicated the occurrence of persistent subsidence across the western portion of Chino Basin from 1992 to 2000. It is likely that this subsidence is due to the compaction of fine-grained sediments, resulting from lower pore pressures within the aquifer system (WEI, 2002). The southern extent of persistent subsidence is currently unknown because InSAR data is difficult to obtain in areas of agricultural land uses, but it may extend southward to encompass the historical artesian area.

North and east of these areas, the distinction between aquifer systems is less pronounced because the fine-grained layers in the west-southwest thin and/or pinch-out to the north and east, and much of the shallow aquifer system sediments are unsaturated in the forebay regions of Chino Basin.

Geologic descriptions from well completion reports in the Chino Basin confirm the predominance of fine-grained sediments in the west-southwest portion of the Chino Basin and the predominance of coarser-grained sediments in the north and east portions of Chino Basin.

2.5 Hydrostratigraphy

The analysis and documentation of Chino Basin stratigraphy, occurrence and movement of groundwater, and aquifer system characteristics has allowed Watermaster to create a hydrostratigraphic conceptual model of the basin. Watermaster created a hydrostratigraphic model in 2003, which was subsequently updated for the 2007 model update. In the 2007 model update nine hydrogeologic cross-sections were constructed across the Chino Basin (WEI, 2007). For the 2013 model update two additional hydrogeologic cross-sections were prepared and the other nine were revised based on new data and hydrogeologic interpretations.

The plan-view locations of these cross-sections are shown in Figure 2-5, and the profile-view cross-sections are shown in Appendix A. Three representative cross-sections A-A', G-G' and J-J' are shown in Figures 2-6a through 2-6c. Plotted on these cross-sections are selected well and borehole data, including borehole lithology, short-normal resistivity logs, well casing perforations, specific capacities, slug test and spinner test results, water quality, and piezometric levels.

Through the analyses of these cross-sections and other hydrogeologic data, the aquifer systems of Chino Basin were generalized into three hydrostratigraphic units—herein referred to as Layer 1, Layer 2, and Layer 3. In the descriptions of each layer below, specific examples from individual wells and cross-sections are discussed to highlight certain characteristics of the hydrostratigraphic units, but the delineation of these layers in three dimensions was drawn from a holistic analysis of the entire data set. In other words, the layer boundaries do not always and exactly match specific observations at every well on every cross-section, but do honor the general patterns of Chino Basin hydrostratigraphy.

2.5.1 Layer 1

Layer 1 consists of the upper 150-950 feet of sediments and is generally representative of the shallow aquifer system. Layer 1 sediments are typically coarse-grained (sand and gravel layers) and, where saturated, transmit large quantities of groundwater to wells due to high hydraulic conductivities. On the west side of Chino Basin, Layer 1 sediments are composed of a greater fraction of finer-grained sediments (silt and clay layers), especially in the uppermost 100 feet. Layer 1 water quality is generally poor in the southern portion of the Chino Basin with relatively high concentrations of TDS and nitrate. Water quality is generally excellent in the northern portions of the Chino Basin.

Figure 2-6c displays the profile view of cross-section J-J', which is aligned southwest-northeast and illustrates the thickening of Layer 1 in the northeastern direction at the expense of Layer 2. The thickening of Layer 1 is supported by the observation that the silt and clay layers, which are typical of Layer 2 sediments in the southwestern Chino Basin, become thinner and less abundant in the eastern and northeastern portions of the Chino Basin.

Figure 2-6b displays the profile view of cross-section G-G', which is aligned southeast-northwest and bisects Management Zone 1. This cross-section displays three of the newly-installed HCMP monitoring wells (HCMP-3, 4, and 6) and the piezometers at Ayala Park (AP Piezometer), which were used to refine the layer geometries in the southern Chino Basin. The monitoring wells are nested piezometers that allow for depth-specific monitoring of the aquifer system. Note the vertical stratification of the groundwater quality in Figure 2-6b (and other cross-sections with vertically distinct groundwater quality data). The relatively high TDS and nitrate concentrations in the shallow aquifer system (Layer 1) decrease significantly with depth (Layers 2 and 3), especially in the southern portions of the Chino Basin.

Figure 2-6a displays the profile view of cross-section A-A', which is aligned west-east and bisects the southern portion of the Chino Basin through the Chino 1 Desalter well field. Note the depth of the well screens relative to the water quality and specific capacity data. The wells with shallow well screens (at least partly in Layer 1) have relatively high TDS and nitrate concentrations while the wells screen exclusively in Layers 2 and 3 have relatively low TDS and nitrate concentrations. The same pattern can be observed in the specific capacity data: wells with shallow well screens have relatively high specific capacities, indicating relatively high permeability in the shallow aquifer system; wells with screens exclusively in Layers 2 and 3 have relatively low specific capacities, indicating relatively low permeability in the deep aquifer system.

2.5.2 Layer 2

Layer 2, where present, consists of 0-500 feet of sediments underlying Layer 1 and is representative of the upper portion of the deep aquifer system. Layer 2 is generally characterized by an abundance of fine-grained sediments (silt and clay layers), confined groundwater conditions, and lower permeabilities and better water quality than in Layer 1 (relatively low TDS and nitrate concentrations—especially in the southern Chino Basin).

Figure 2-6c displays the profile view of cross-section J-J', and illustrates that Layer 2 is spatially restricted to the western portion of Chino Basin and "pinches out" to the northeast as Layer 1 thickens. This pinching out is supported by the observation that the silt and clay layers, which are typical of Layer 2 sediments in the southwestern Chino Basin, become thinner and less abundant in the eastern and northeastern portions of the Chino Basin.

The confined groundwater conditions of Layer 2 and the low concentrations of TDS and nitrate are best illustrated in Figures 2-6a and 2-6b (cross-sections A-A' and G-G') and in Figure 2-9. Figure 2-6a shows well CH-1B located in southwestern Chino Basin and screened across Layers 2 and 3. The water-level time series for CH-1B (shown in Figure 2-9) displays a wildly fluctuating piezometric level that varies seasonally by as much as 250 feet, mainly in response to nearby pumping. These water-level fluctuations observed in CH-1B are typical of confined groundwater conditions where small changes in storage (caused by pumping in this case) can generate large changes in piezometric levels. This is a consistent observation that can be seen in all wells screened exclusively in the deep aquifer system in southwestern Chino Basin and indicates the existence of an effective upper confining layer separating the deep and shallow aquifer systems. The silt and clay layers above the well screens in CH-1B were correlated to other wells in the southwestern Chino Basin (see Figures 2-6a and 2-6b), which assisted in the delineation of the boundary between Layers 1 and 2.

Figure 2-6a also shows wells with shallow well screens have relatively high TDS/nitrate concentrations and relatively high specific capacities, and wells with screens exclusively in Layers 2 and 3 have relatively low TDS/nitrate concentrations and relatively low specific capacities.

2.5.3 Layer 3

Layer 3 consists of up to 800 feet of sediments underlying Layers 1 and 2 within the deep aquifer system. Layer 3 is generally characterized by an abundance of coarse-grained sediments (sand and gravel layers), but due to their greater age, consolidation, and state of weathering, these sediments have lower permeability than the coarse-grained sediments of Layers 1 and 2. In the western Chino Basin, Layer 3 sediments underlie Layer 2 and represent the lower portion of the deep aquifer system. Layer 3 is likely composed of the sedimentary bedrock formations in the western Chino Basin. In the eastern Chino Basin, Layer 3 sediments underlie Layer 1 and represent the deep aquifer system. In this area, Layer 3 sediments are likely composed of the lower portion of the Older Alluvium. In the southeastern Chino Basin, Layer 3 does not extend east of the assumed Bedrock Fault toward the Jurupa Mountains and La Sierra Hills.

The best example of Layer 3 characteristics are observed at the Ayala Park Extensometer Facility. In Figure 2-6b, note the coarse-grained nature of the deep sediments, the very low concentrations of TDS and nitrate, and the very low hydraulic conductivity at PB-2 as estimated from slug tests. In other regions of the Chino Basin, some of these same observations for Layer 3 can be seen in the lithologic data, geophysical logs, and the spinner test results. For example, in Figure A-6, note how the top of Layer 3 is drawn in Well MP-2 at the transition from the relatively fine-grained sediments of Layer 2 to the relatively coarse-grained sediments of Layer 3. Also note in this figure how the spinner test analysis for Well FWC-17C indicates that only 30 percent of the total well discharge comes from Layer 3 despite the fact that most of the screened interval resides in it. Wherever possible, these types of observations assisted in the delineation of Layer 3.

2.5.4 Creation of a Three-Dimensional Hydrostratigraphic Model

At each well on each cross-section, the bottom elevations of all the three layers were plotted on maps and hand-contoured. The elevation contours for the bottom of Layer 1 and Layer 2 are shown in Figures 2-10a and 2-10b. The elevation contours for the bottom of Layer 3 are shown in Figure 2-2. These contours were digitized, brought into ArcGIS, converted to point values, and combined with the bottom elevation point values at the wells into a single point shapefile. The Geostatistical Analyst extension of ArcGIS was used to interpolate between the point values to create three-dimensional rasters (grids) of the layer bottom elevations. These rasters are the updated hydrostratigraphic model of the Chino Basin, and were used as input files for the hydrostratigraphic geometry for the 2013 model update.

2.6 Aquifer Properties

Hydraulic conductivity is the measure of a fluid's ability to flow through a medium. The value relates to fluid density (ρ), dynamic viscosity (μ), and the effective grain size (d_{10}) in unconsolidated deposits, as depicted in the following equation:

$$K = \frac{C{d_{10}}^2 \rho g}{\mu}$$

Where, C is a constant of proportionality.

This definition of hydraulic conductivity suggests that its value increases with the median grain size. This same relationship applies to specific yield (McCuen et al., 1981). We employed a method of sediment texture analysis to develop initial estimates of horizontal and vertical hydraulic conductivity and storage properties within the study area.

2.6.1 Compilation of Existing Well Data

Textural analysis in this study relied on lithological data from well driller's logs. Our study on geologic setting and stratigraphy show that driller's logs can provide valid textural information and help to configure the basin stratigraphy. WEI collected 1,083 drillers' logs in the Chino and Temescal Basins. All of the drillers' logs were located, if possible, and the lithologic descriptions were assigned a model layer based on depth interval.

2.6.2 Classification of Texture and Reference Hydraulic Values for Aquifer Sediments

Hydraulic properties are closely related to the lithology of aquifers. In other words, each textural class has its own hydraulic properties. This allows one to find appropriate values of hydraulic parameters based on textural class. Several databases have been developed for this purpose, including RAWLS (Rawls et al., 1982), ROSETTA (Schaap and Leij, 1998), and CARSEL (Carsel and Parrish, 1988).

Many authors (Bouwer, 1978; Prudic, 1991; Reese and Cunningham, 2000; Kuniansky and Hamrick, 1998; Domenico and Schwartz, 1990; Freeze and Cherry, 1979, Johnson, 1967) relate material grain-size class texture to hydraulic property values. WEI has conducted various pumping tests in the Chino and Temescal Basins, as well as in various other basins that are located in Santa Ana River watershed. Based on above published information and local data, a reference table was developed, which relates 80 lithological descriptions to the values of specific yield and saturated hydraulic conductivity. These 80 lithological descriptions cover a wide range of sediments: from boulders/cobbles, to gravels and sands, to clays and silts, and to lava flows, granites, and shales.

With the reference table and lithologic descriptions on the well drillers' logs, the following procedure is used to determine the hydraulic properties at well locations and within each layer:

- Determine the historical highest or potential highest water table in the Chino Basin.
- Define the model layer bottom elevation for layer 1, layer 2, and layer 3, respectively.

- Determine the thickness for each sediment texture in a layer.
- Use the reference table to assign the hydraulic properties based on the lithologic descriptions.
- Calculate the thickness-weighted horizontal and vertical hydraulic conductivity and specific yield at each valid well in each layer using the formulas below:

$$K_h = \sum_{i=1}^{n} \frac{K_i b_i}{b}$$

$$K_v = b / \sum_{i=1}^{n} \frac{b_i}{K_i}$$

$$S_y = \sum_{i=1}^{n} \frac{S_{yi} b_i}{b}$$

where K_h is the average horizontal conductivity in the layer, K_i is the hydraulic conductivity of *i* bed, b_i is the thickness of *i* bed, b is the total thickness of aquifer in a layer, K_v is average vertical hydraulic conductivity in a layer, S_y is average specific yield in a layer, and S_{yi} is the specific yield for *i* bed.

By using above method, the values of specific yield, horizontal hydraulic conductivity, and vertical hydraulic conductivity were computed for each layer at each well location.

2.6.3 Geostatistical Model Approach

Geostatistics is a set of applications and statistical techniques used to analyze spatial and temporal correlations of variables distributed in space and time. Applications include modeling geological heterogeneities such as the heterogeneity and distribution of hydraulic properties.

We used a geostatistical method termed the best linear unbiased estimation (BLUE) to estimate the spatial distribution of hydraulic conductivity and specific yield. "Best" means the estimates with minimal variance or estimation error. "Unbiased" means the average value of the estimates in repeated sampling equals the true parameter. Like other simple spatial interpolation methods, such as inverse-distance method, BLUE is a linear estimator but takes the observed spatial correlation structure into account. Because of this, BLUE not only has the capability of producing a prediction field, but also provides some measure of the certainty or accuracy of the predictions. The method can also integrate physical constraints and combine multiple data sources.

The core of the BLUE method, or Kriging method, is to configure the data spatial structure by using a semi-variogram model. The underlying principle of semi-variogram model is that on average two observations closer together are more similar than two observations farther apart. Because the underlying data have preferred orientations, values may change more quickly in one direction than another. As such, the semi-variogram is a function of direction.

The procedure used to generate Kriging-estimated hydraulic properties was as follows:

1. Compute each hydraulic parameter's value in each layer at each well.
2. Conduct semi-variogram analyses of hydraulic properties, determine their spatial variation structure, and obtain the best-fitted semi-variogram spatial structure model and parameters.

3. Conduct the Kriging computation based on the hydraulic property value at each well location. During the processes, the best-fit semi-variogram model and parameters are used to generate hydraulic property grids in each layer in the model domain.

4. Check the uncertainty of estimated hydraulic properties.

2.6.4 Specific Yield

The spatial data distribution of specific yield was the first property estimated. A semi-variogram model was generated for specific yield based on the lithologic descriptions from about 1,000 representative well logs. The Kriging method that implemented the semi-variogram model was used to make a prediction for specific yield across the model domain in each layer. The specific yield rasters are limited to the spatial extent of their respective layers and are shown in Figures 2-11a through 2-11c.

Figure 2-11a displays the spatial distribution of specific yield for Layer 1. Specific yield is highest (up to 20 percent) in the northern and eastern portions of the Chino Basin. A belt of similarly high specific yield runs north of the Jurupa Mountains from Fontana toward Prado Basin. This belt may represent coarse-grained sediments deposited by an ancestral Santa Ana River or Lytle Creek. The lowest specific yields in Layer 1 (8 to 10 percent) are on the west side of the Chino Basin. This area overlaps the historical artesian area, and likely represents the shallow fine-grained sediments that historically acted as confining layers.

Figure 2-11b displays the spatial distribution of specific yield for Layer 2. Specific yield is highest, ranging up to 15 percent, in the central portions of the Chino Basin. Specific yield is lowest, ranging down to 5 percent, on the west side of the Chino Basin. The areas of relatively low specific yield overlap the historical artesian area and the areas of historical subsidence as indicated by InSAR, and may represent the fine-grained sediments that have experienced compaction due to reduced pore pressures.

Figure 2-11c displays spatial distribution of specific yield for Layer 3. The primary observation in Layer 3 is a generally higher specific yield in the Fontana area relative to a lower specific yield in the western Chino Basin. This observation is consistent with Watermaster's current hydrostratigraphic conceptual model where the deep aquifer sediments of the western Chino Basin represent the highly-weathered and partially-consolidated sedimentary bedrock formations, and the deep sediments of the northern Chino Basin represent the more recent coarse-grained sediments of the Older Alluvium.

2.6.5 Horizontal Hydraulic Conductivity

The horizontal hydraulic conductivity of water-bearing sediments is a measure of their capacity to transmit water. Generally, sands and gravels have high hydraulic conductivities while clays and silts have low hydraulic conductivities. A semi-variogram model was generated for horizontal hydraulic conductivity based on lithologic descriptions from about 1,000 representative well logs. The Kriging method that implemented the semi-variogram model was used to make a prediction for horizontal hydraulic conductivity across the model domain in each layer. The horizontal hydraulic conductivity rasters are limited to the spatial extent of their respective layers and are shown in Figures 2-12a through 2-12c.

Figure 2-12a displays spatial distribution of horizontal hydraulic conductivity for Layer 1. Horizontal hydraulic conductivities are highest in the northern (70-100 ft/day) and eastern (60-80 feet/day) portions of the Chino Basin. A belt of similarly high horizontal hydraulic conductivity runs north of the Jurupa Mountains from Fontana toward the Prado Flood Control Basin. This belt may represent coarse-grained sediments deposited by an ancestral Santa Ana River or Lytle Creek. Horizontal hydraulic conductivity in Layer 1 is the lowest on the west side of the Chino Basin.

Figure 2-12b displays spatial distribution of horizontal hydraulic conductivity for Layer 2. Horizontal hydraulic conductivities are highest, ranging up to 120 feet/day, in the central portions of the Chino Basin. Horizontal hydraulic conductivities are lowest on the west side of the Chino Basin.

Figure 2-12c displays spatial distribution of horizontal hydraulic conductivity for Layer 3. Horizontal hydraulic conductivities are generally higher in the Fontana area relative to lower values in the western Chino Basin.

There is reason to believe that hydraulic conductivities and specific yield decrease with depth due to the greater age, weathering, and consolidation of the aquifer sediments. However, our methods that rely on borehole lithology may not take this into account. We will leave this problem to be solved in model calibration, that is, a model parameter acting as a zonation coefficient will take the effect of age, weathering, and consolidation into account.

2.6.6 Vertical Hydraulic Conductivity

The average vertical hydraulic conductivity in a layer will be very low when a clay bed is present. This can also be observed from the equation that is used to compute average or equivalent vertical hydraulic conductivity for a stratified material. A semi-variogram model was generated for vertical hydraulic conductivity based on lithologic descriptions from about 1,000 representative well logs. The Kriging method that implemented the semi-variogram model was used to make a prediction for vertical hydraulic conductivity across the model domain in each layer. The vertical hydraulic conductivity rasters are limited to the spatial extent of their respective layers and are shown in Figures 2-13a through 2-13c.

Figure 2-13a displays the spatial distribution of vertical hydraulic conductivity for Layer 1. Vertical hydraulic conductivities are high in the northern (15-28 ft/day) and eastern (22-35 feet/day) portions of the Chino Basin. A belt of relatively high vertical hydraulic conductivity (15-28 feet/day) runs north of the Jurupa Mountains from Fontana toward Prado Basin. This belt is similar to those of specific yield and horizontal hydraulic conductivity. Vertical hydraulic conductivity in Layer 1 is the lowest on the west side of the Chino Basin. This area contains many interbedded clays in Layer 1.

Figure 2-13b displays the spatial distribution of vertical hydraulic conductivity for Layer 2. Vertical hydraulic conductivities are highest in the central and in eastern portions of the Chino Basin. Vertical hydraulic conductivities are very low on the west side of the Chino Basin. This area overlaps the historical artesian area and the area of historical subsidence as indicated by InSAR.

Figure 2-13c displays spatial distribution of vertical hydraulic conductivity for Layer 3. Vertical hydraulic conductivities are high in the north and are lower in the western and southern portions of the Chino Basin.

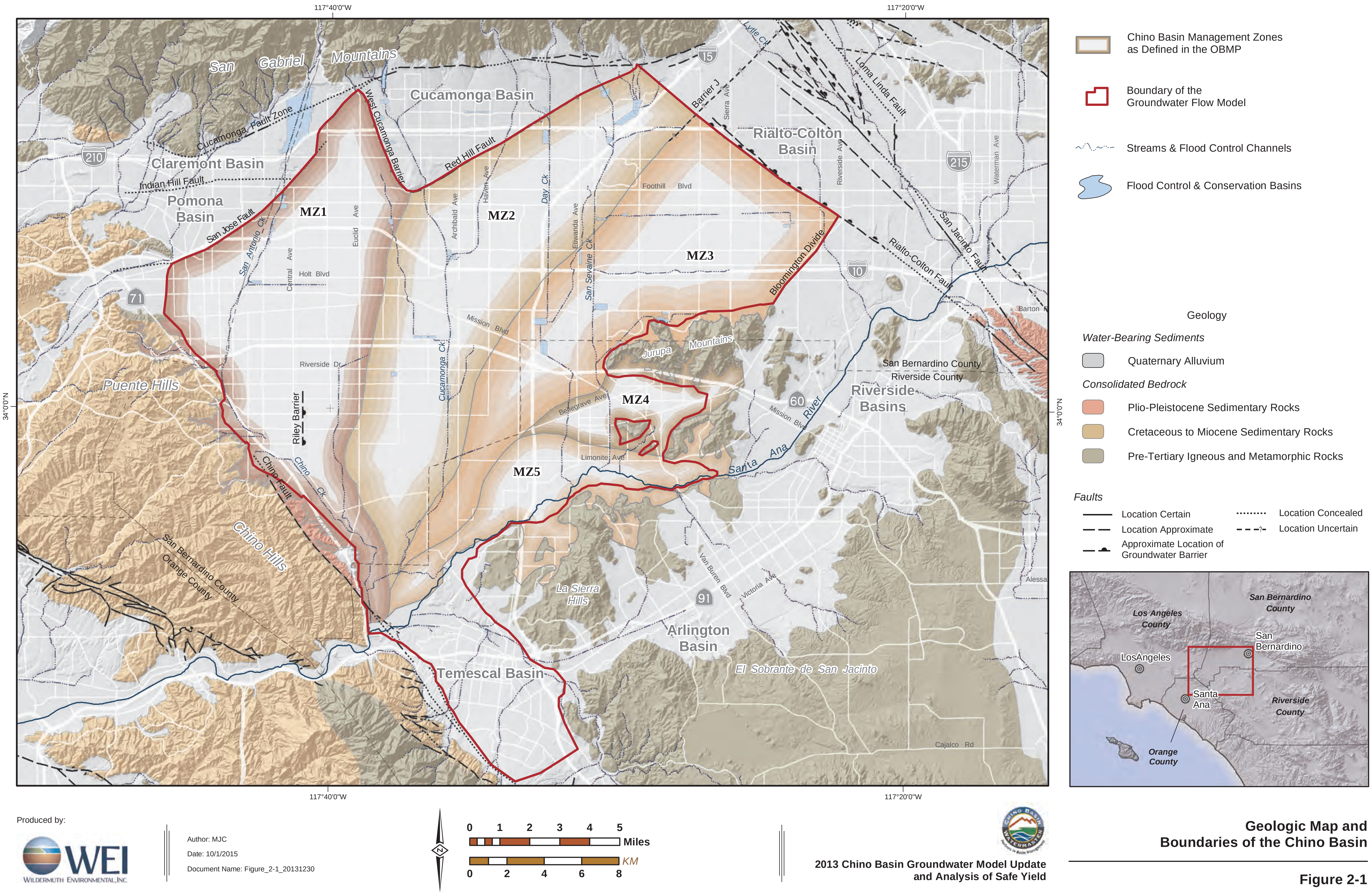

Produced by:

WEI
Wildermuth Environmental, Inc.

Author: MJC
Date: 10/1/2015
Document Name: Figure_2-1_20131230

2013 Chino Basin Groundwater Model Update and Analysis of Safe Yield

Geologic Map and Boundaries of the Chino Basin

Figure 2-1

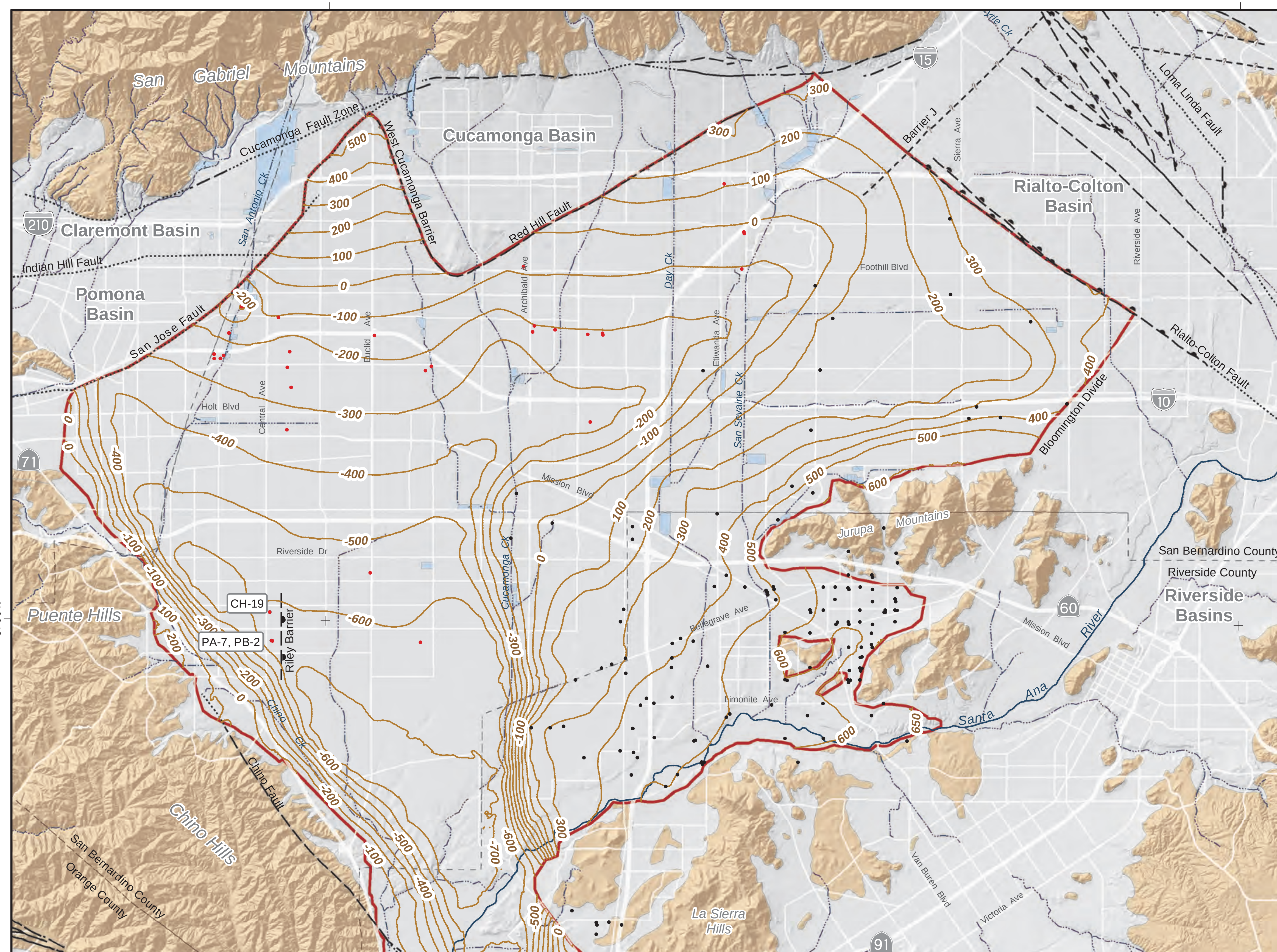

−600− Equal Elevation Contour of the Effective Base of Freshwater Aquifer (ft-above msl)

• Borehole Location Deeper than 1,000 ft and did not Penetrate Crystalline Bedrock

• Borehole Location which Penetrated Crystalline Bedrock

Geology

Water-Bearing Sediments

Quaternary Alluvium

Consolidated Bedrock

Undifferentiated Pre-Tertiary to Early Pleistocene Igneous, Metamorphic, and Sedimentary Rocks

Faults

Location Certain

Location Approximate

Approximate Location of Groundwater Barrier

Location Concealed

Location Uncertain

Produced by:

WEI
Wildermuth Environmental, Inc.

Author: MJC

Date: 10/1/2015

Document Name: Figure_2-2_20140128

0 1 2 3 4 5 Miles

0 2 4 6 8 KM

2013 Chino Basin Groundwater Model Update and Analysis of Safe Yield

Effective Base of the Freshwater Aquifer

Figure 2-2

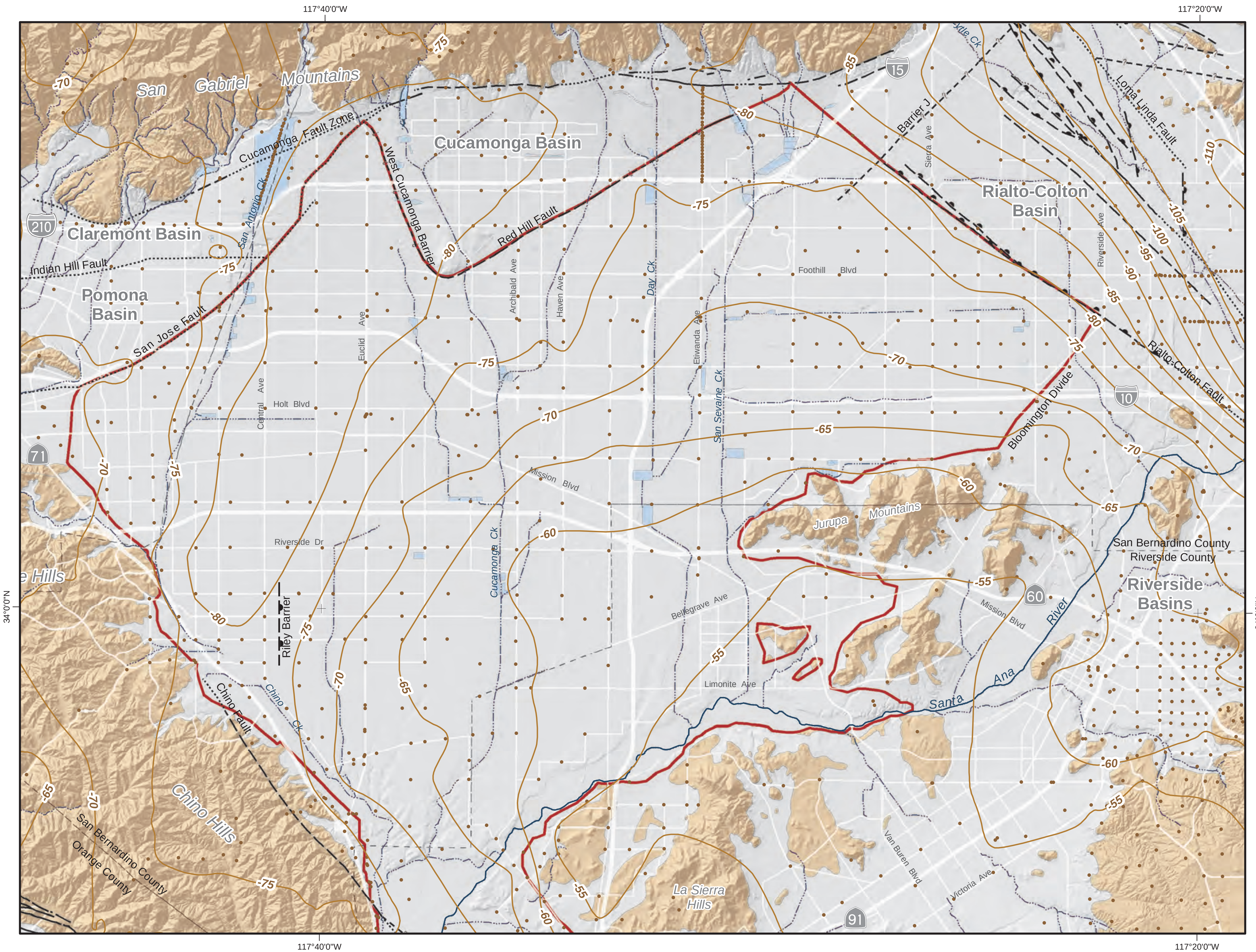

-50 Lines of Equal Bouguer Gravity Anomalies (milligals)

• Gravity Station

Geology

Water-Bearing Sediments

Quaternary Alluvium

Consolidated Bedrock

Undifferentiated Pre-Tertiary to Early Pleistocene Igneous, Metamorphic, and Sedimentary Rocks

Faults

- Location Certain
- Location Approximate
- Approximate Location of Groundwater Barrier
- Location Concealed
- Location Uncertain

Produced by:

WEI
Wildermuth Environmental, Inc.

Author: MJC

Date: 10/1/2015

Document Name: Figure_2-3_20131230

0 1 2 3 4 5 Miles

0 2 4 6 8 KM

2013 Chino Basin Groundwater Model Update and Analysis of Safe Yield

Bouguer Gravity Map

Figure 2-3

Figure 2-4
Depth-Dependent Piezometric Response to Pumping
Southwestern Chino Basin

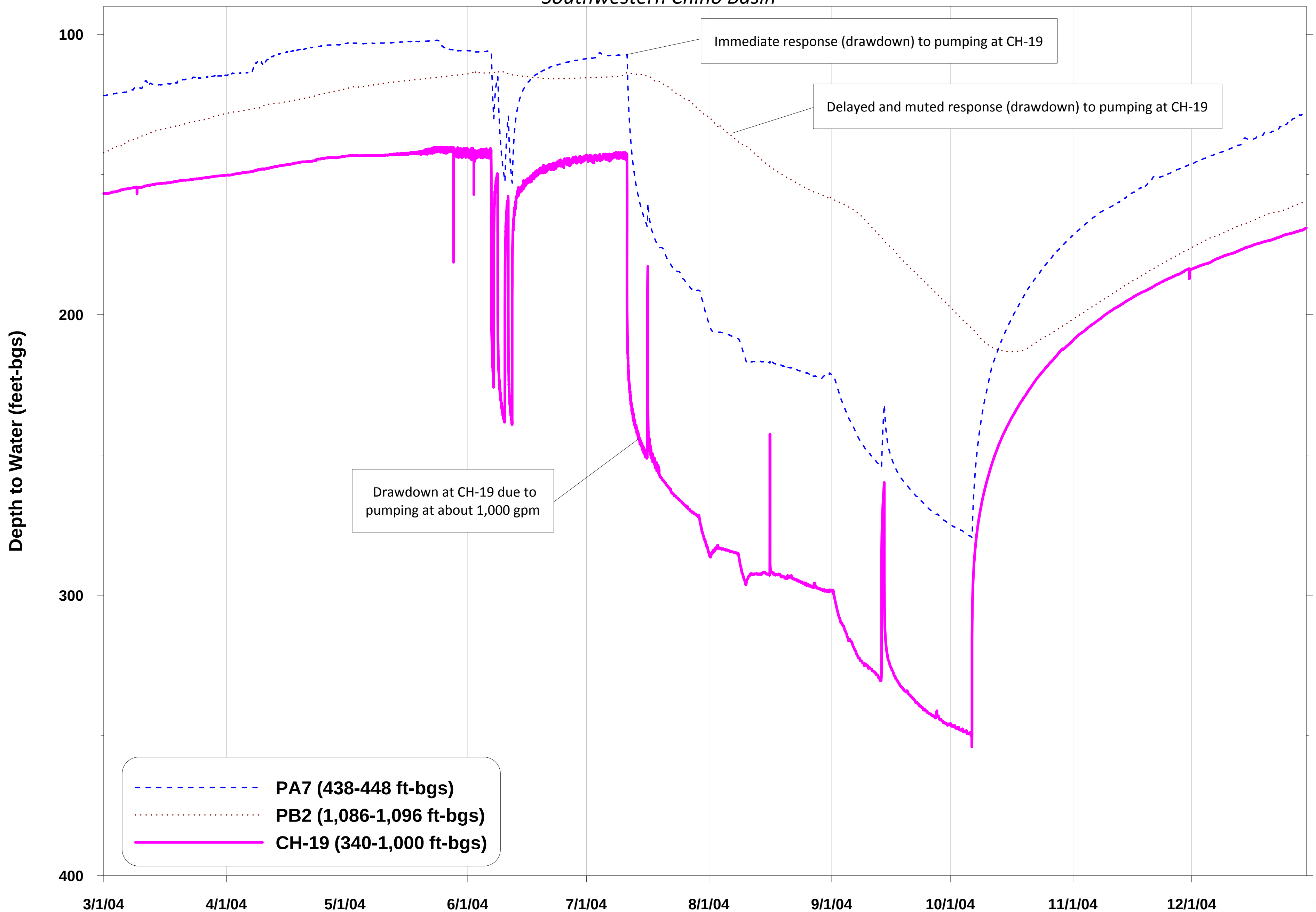

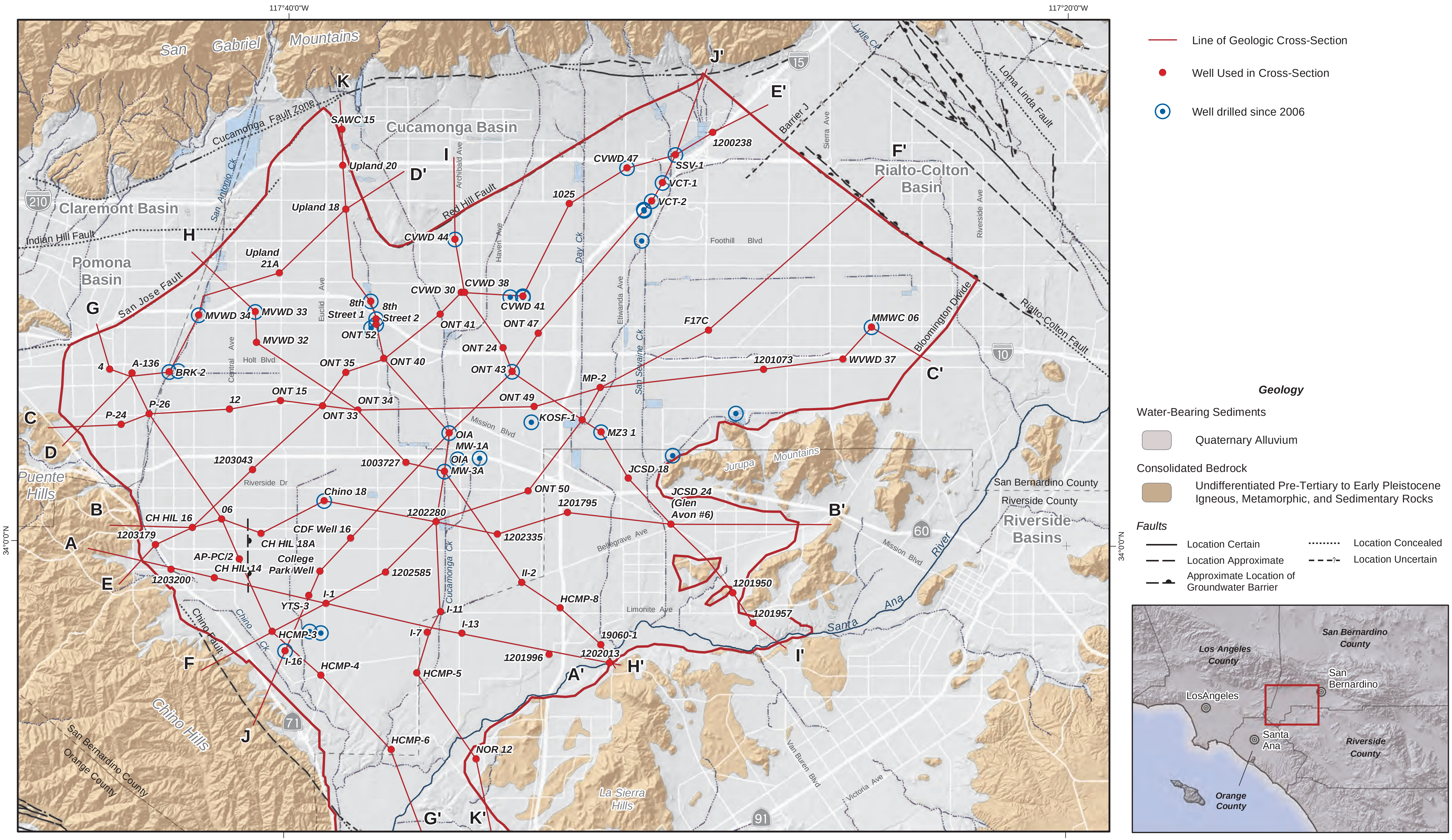

Produced by:

WEI
WILDERMUTH ENVIRONMENTAL, INC.

Author: MJC

Date: 10/1/2015

Document Name: Figure_2-5_20131230

0 1 2 3 4 5 Miles

0 2 4 6 8 KM

2013 Chino Basin Groundwater Model Update and Analysis of Safe Yield

Map View of Hydrostratigraphic Cross Sections

Figure 2-5

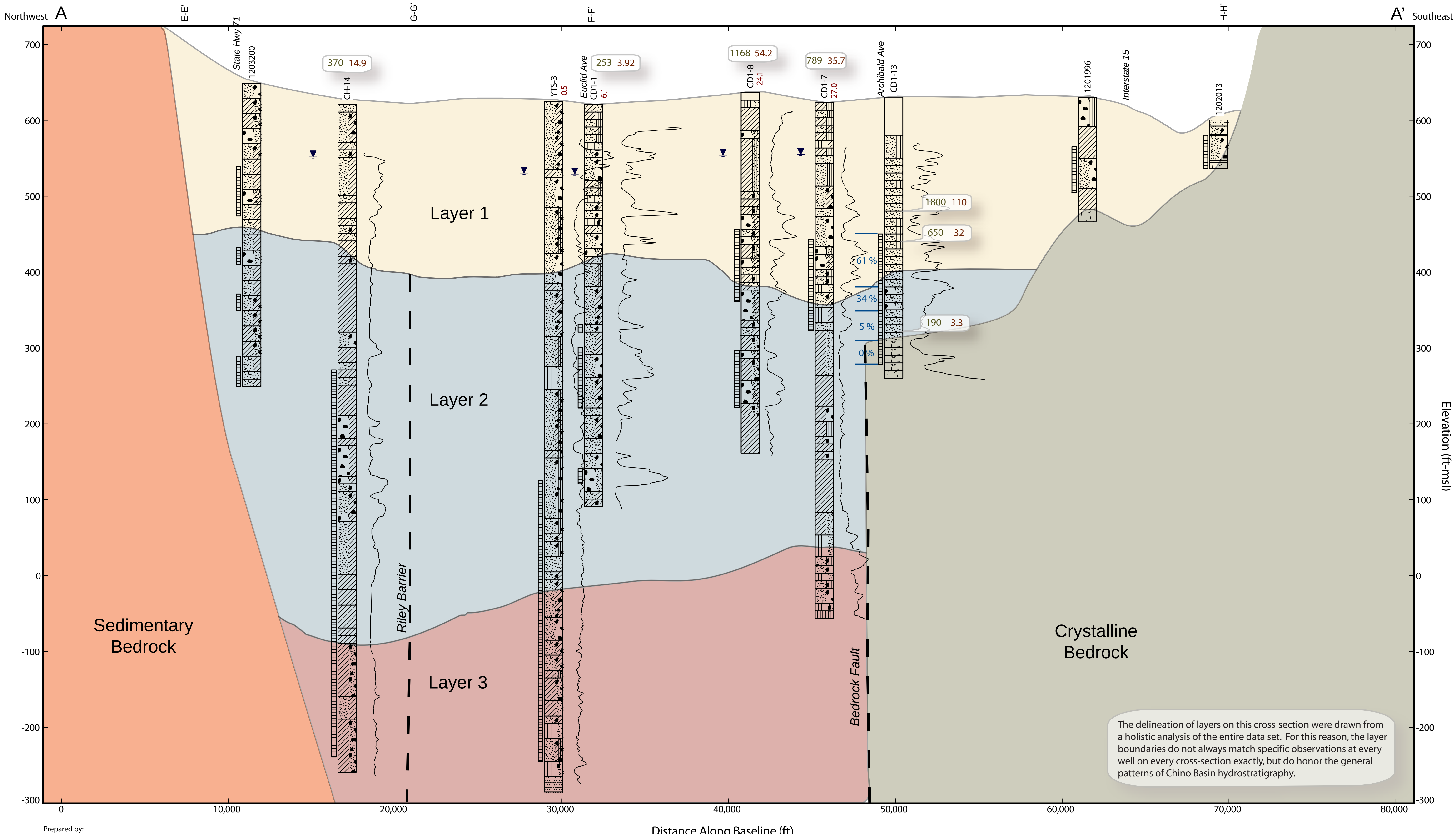

Prepared by:

WEI

Vertical Scale: 1" = 120'
Horizontal Scale: 1" = 5500'
Vertical Exaggeration: 46:1

Author: MJC
Date: 201510
File: a-a.pdf

Lithologic Graphics

Gravel	Granite
Sand	Decomposed Granite
Silt	Topsoil
Clay	Interbedded Sandstone\ Siltstone

Where the lithologic graphic column is split, the primary component is on the left side of the column;secondary component(s) are on the right.

Well Screen Interval

Water Level (Fall 2006)

16" Short Normal Geophysical Log

50 % Spinner Log Analysis (% of flow from depth interval)

27.2 Specific Capacity (gpm/ft)

Average Water Quality (1999- 2006; mg/L)

TDS NO_3-N Well Discharge Sample

TDS NO_3-N Depth Specific Sample

2013 Chino Basin Groundwater Model Update and Analysis of Safe Yield

Cross-Section A-A'

Figure 2-6a

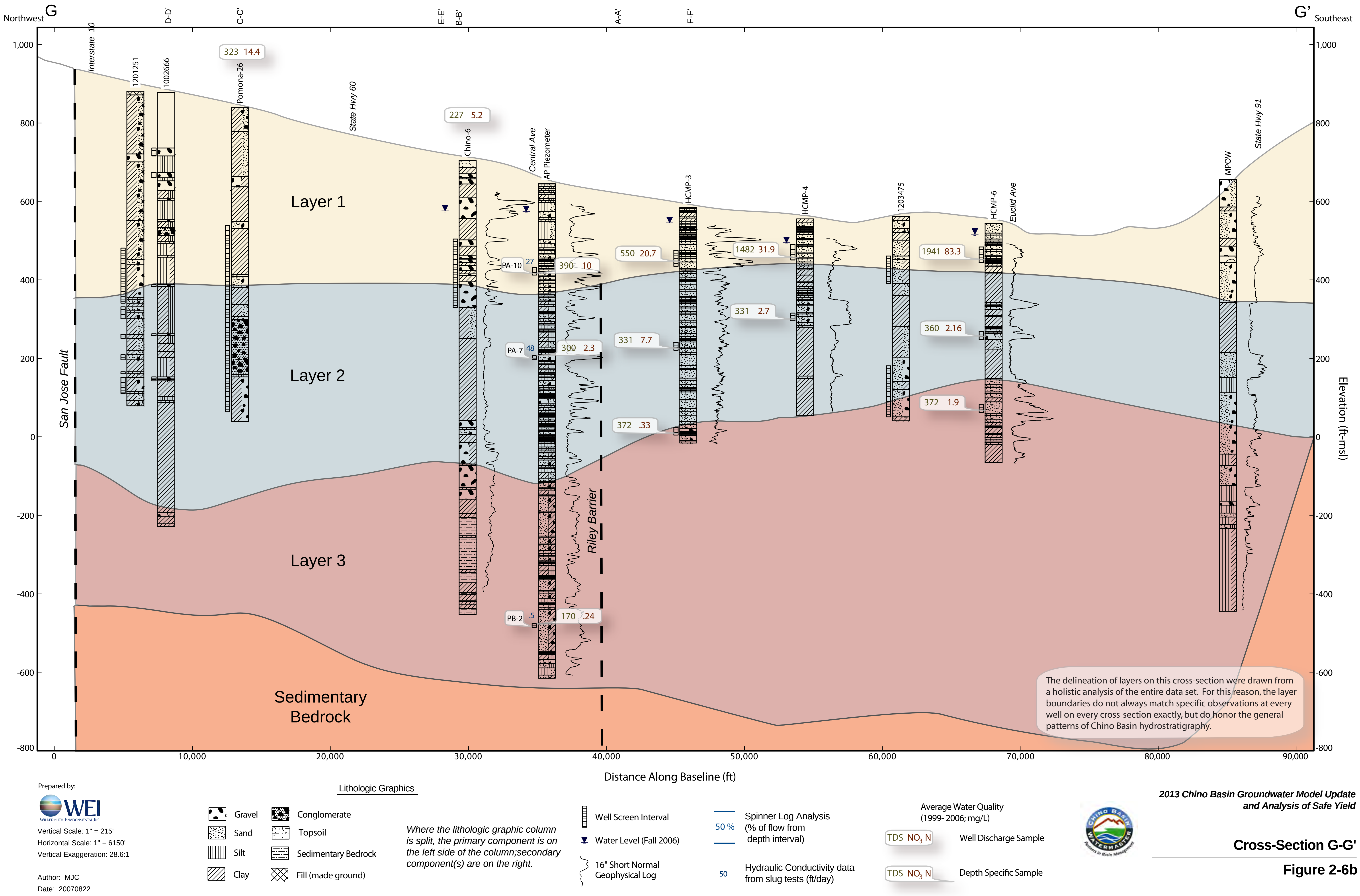

Cross-Section G-G'

Figure 2-6b

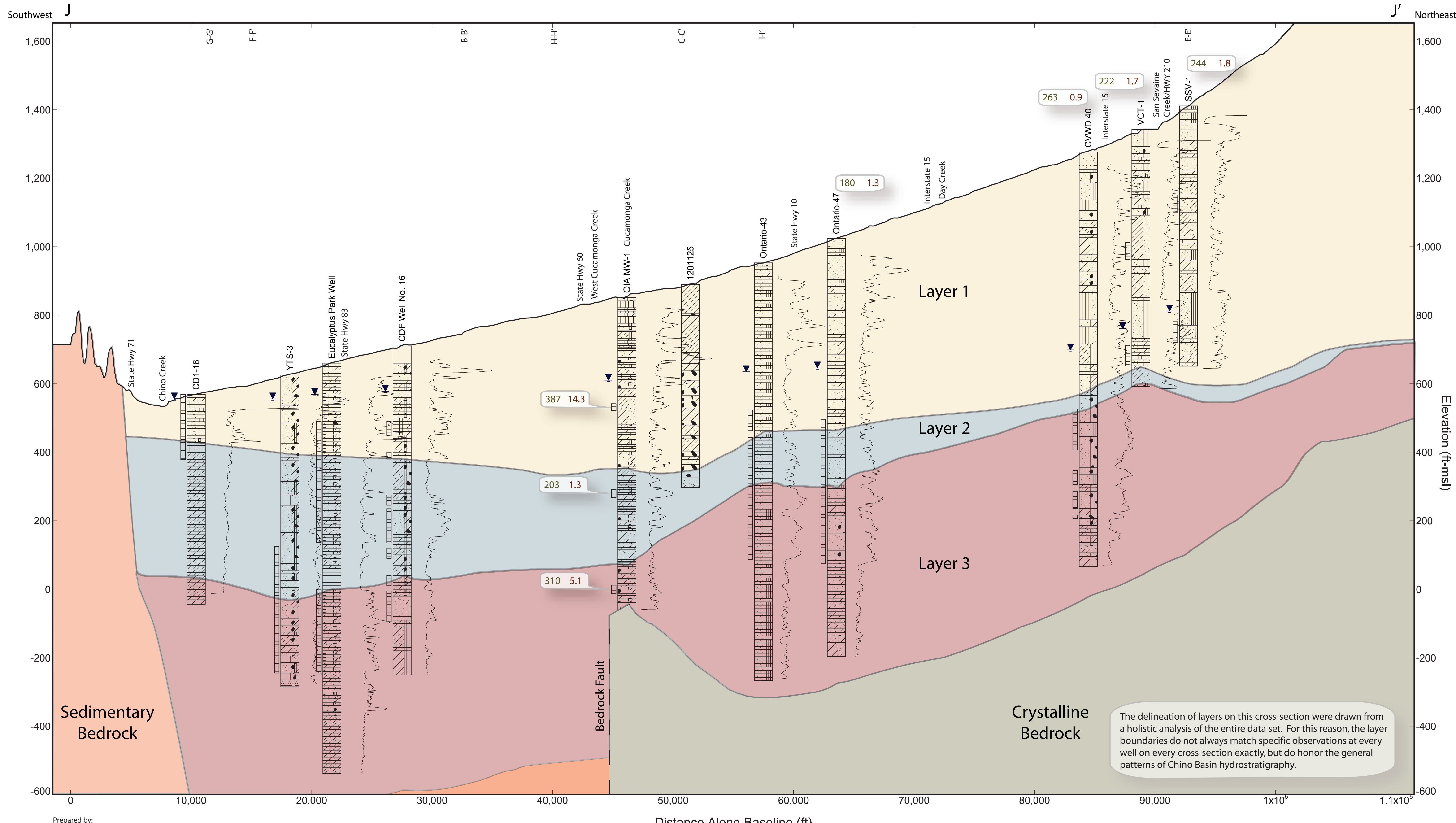

Report: STRAT+GEOPHYSICAL_11X17; File: 2011_CBWM_MODEL RECALIBRATION.GPJ; 7/2/2013

Prepared by:

WEI

Vertical Scale: 1" = 264'
Horizontal Scale: 1" = 7539'
Vertical Exaggeration: 29:1

Author: MJC
Date: 20130702
File: 2-5c.pdf

Lithologic Graphics

Gravel
Sand
Silt
Clay
Granite
Decomposed Granite
Topsoil
Interbedded Sandstone\ Siltstone

Where the lithologic graphic column is split, the primary component is on the left side of the column; secondary component(s) are on the right.

Well Screen Interval
Water Level (Fall 2011)
16" Short Normal Geophysical Log

Average Water Quality (2006 - 2011; mg/L)

TDS NO_3-N Well Discharge Sample

TDS NO_3-N Depth Specific Sample

2013 Chino Basin Groundwater Model Update and Analysis of Safe Yield

Cross-Section J-J'

Figure 2-6c

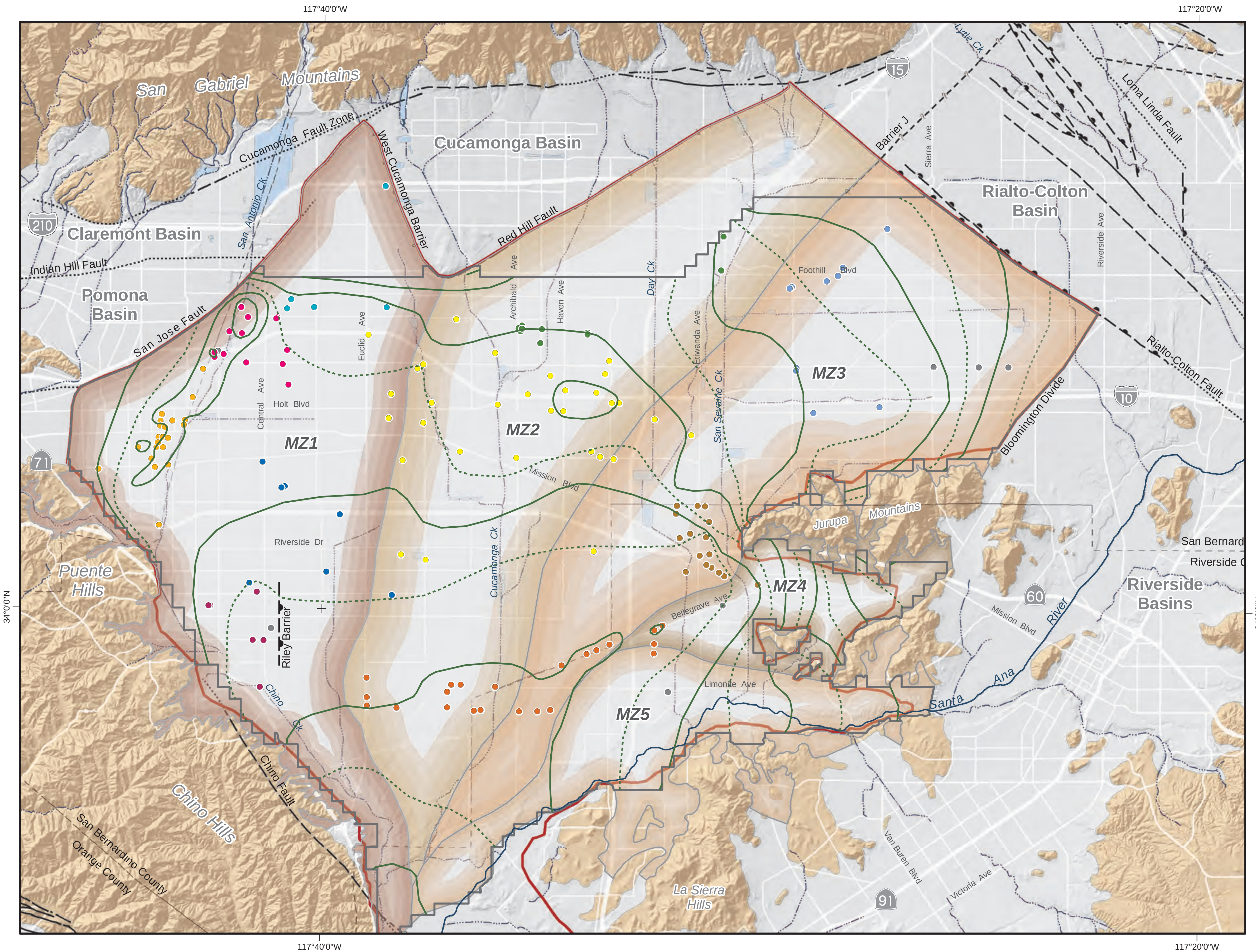

Groundwater Elevation Contours (feet above mean sea-level)

800

775

Boundry of Contoured Area (contours are not shown outside of this boundary due to lack of water level data)

Production Wells

- Chino Desalter Authority
- City of Chino
- City of Chino Hills
- City of Ontario
- City of Pomona
- City of Upland
- Cucamonga Valley Water District
- Fontana Water Company
- Jurupa Community Services District
- Monte Vista Water District
- Other Appropriators

Geology

Water-Bearing Sediments

Quaternary Alluvium

Consolidated Bedrock

Undifferentiated Pre-Tertiary to Early Pleistocene Igneous, Metamorphic, and Sedimentary Rocks

Faults

- Location Certain
- Location Approximate
- Approximate Location of Groundwater Barrier
- Location Concealed
- Location Uncertain

Produced by:

WEI
Wildermuth Environmental, Inc.

Author: MJC

Date: 10/1/2015

Document Name: Figure_2-7_20131230

0 1 2 3 4 5 Miles

0 2 4 6 8 KM

2013 Chino Basin Groundwater Model Update and Analysis of Safe Yield

Groundwater Elevation Contours

Spring 2012 -- Chino Basin

Figure 2-7

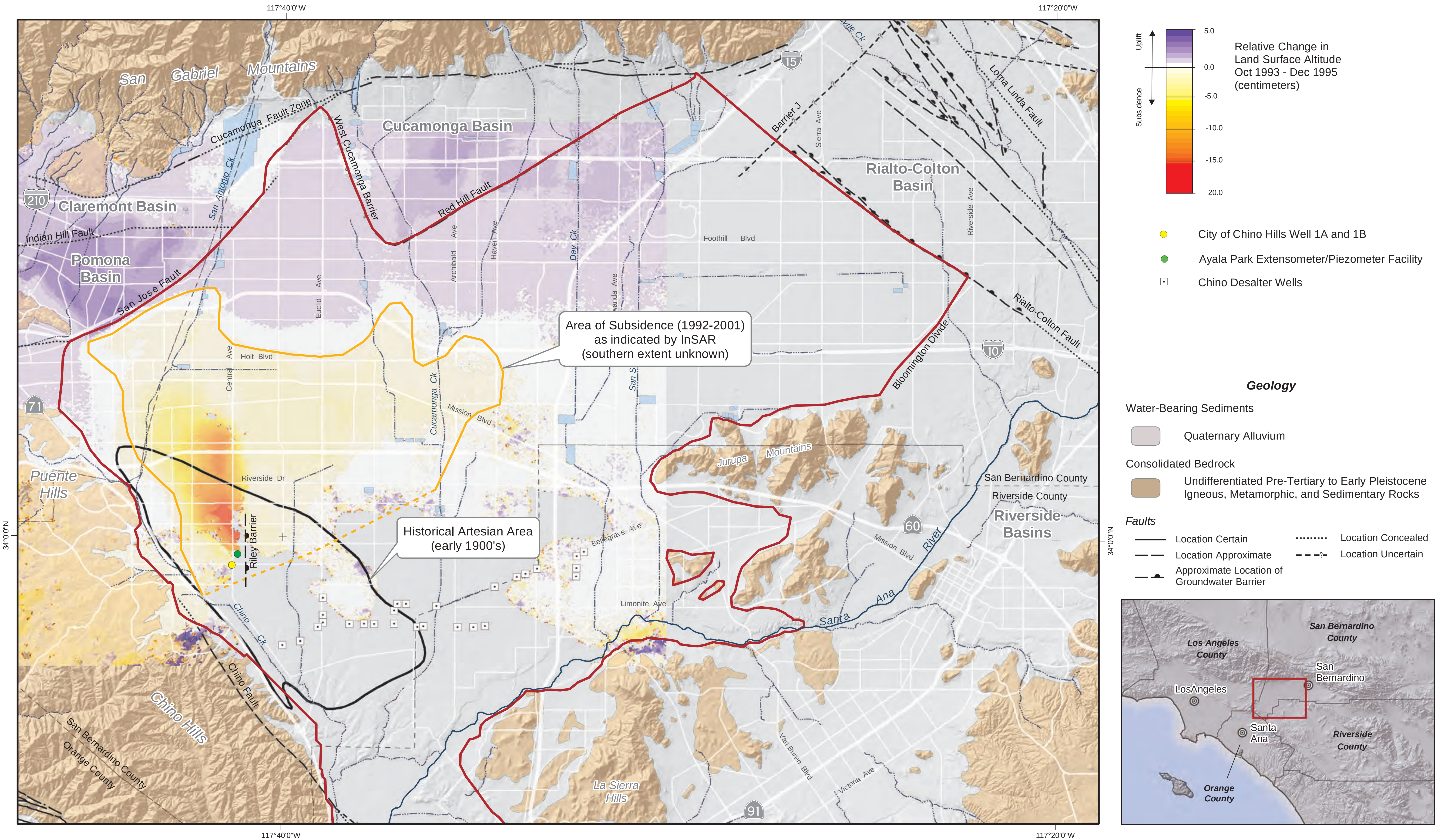

Produced by:

WEI
WILDERMUTH ENVIRONMENTAL, INC.

Author: MJC

Date: 10/1/2015

Document Name: Figure_2-8_subsidence_20131230

0 1 2 3 4 5 Miles

0 2 4 6 8 KM

2013 Chino Basin Groundwater Model Update
and Analysis of Safe Yield

**Areas of Subsidence and
Historical Artesian Conditions**

Figure 2-8

Figure 2-9
Water Level Time Histories (Non-Pumping) City of Chino Hills Wells 1A and 1B

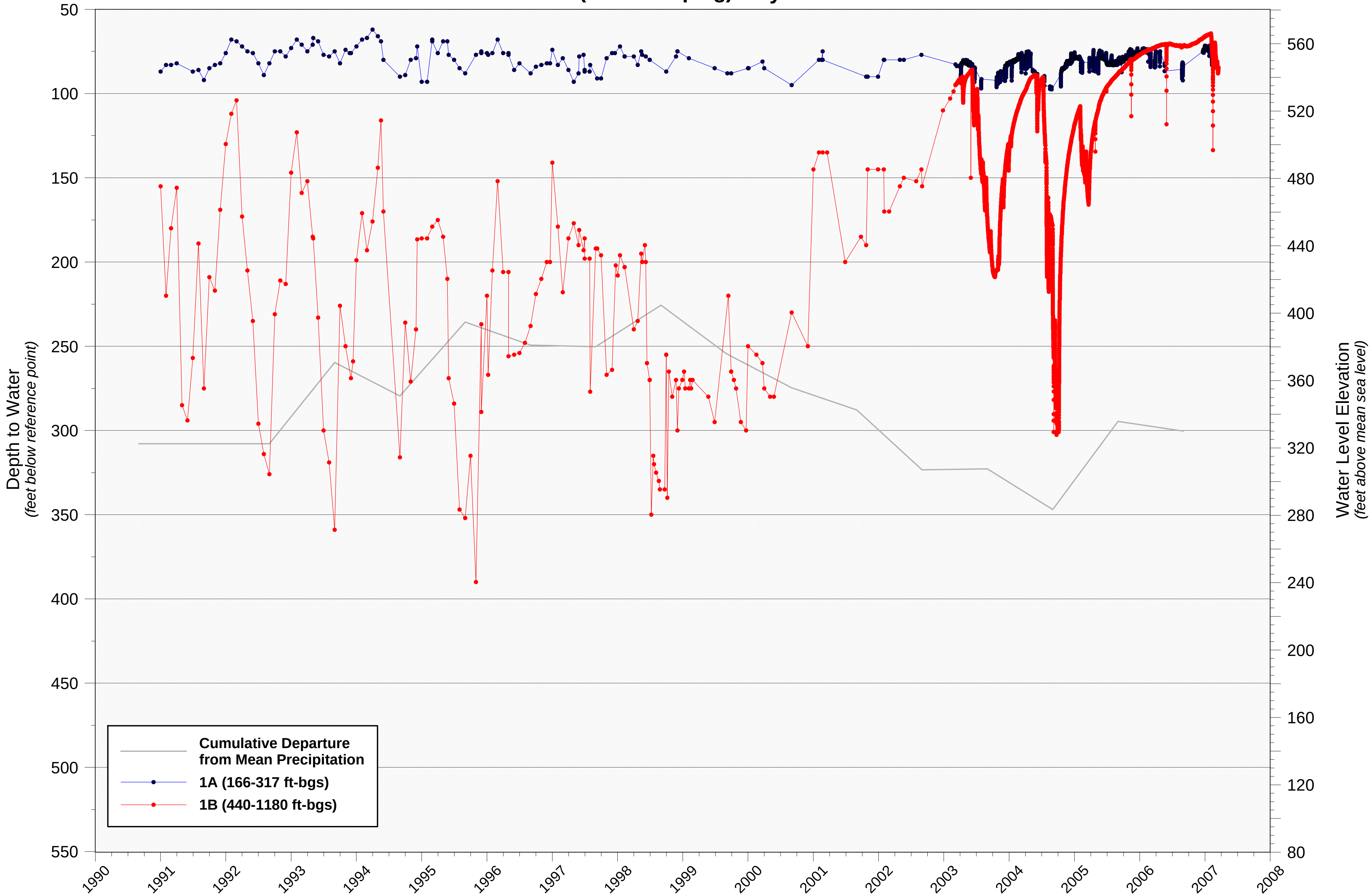

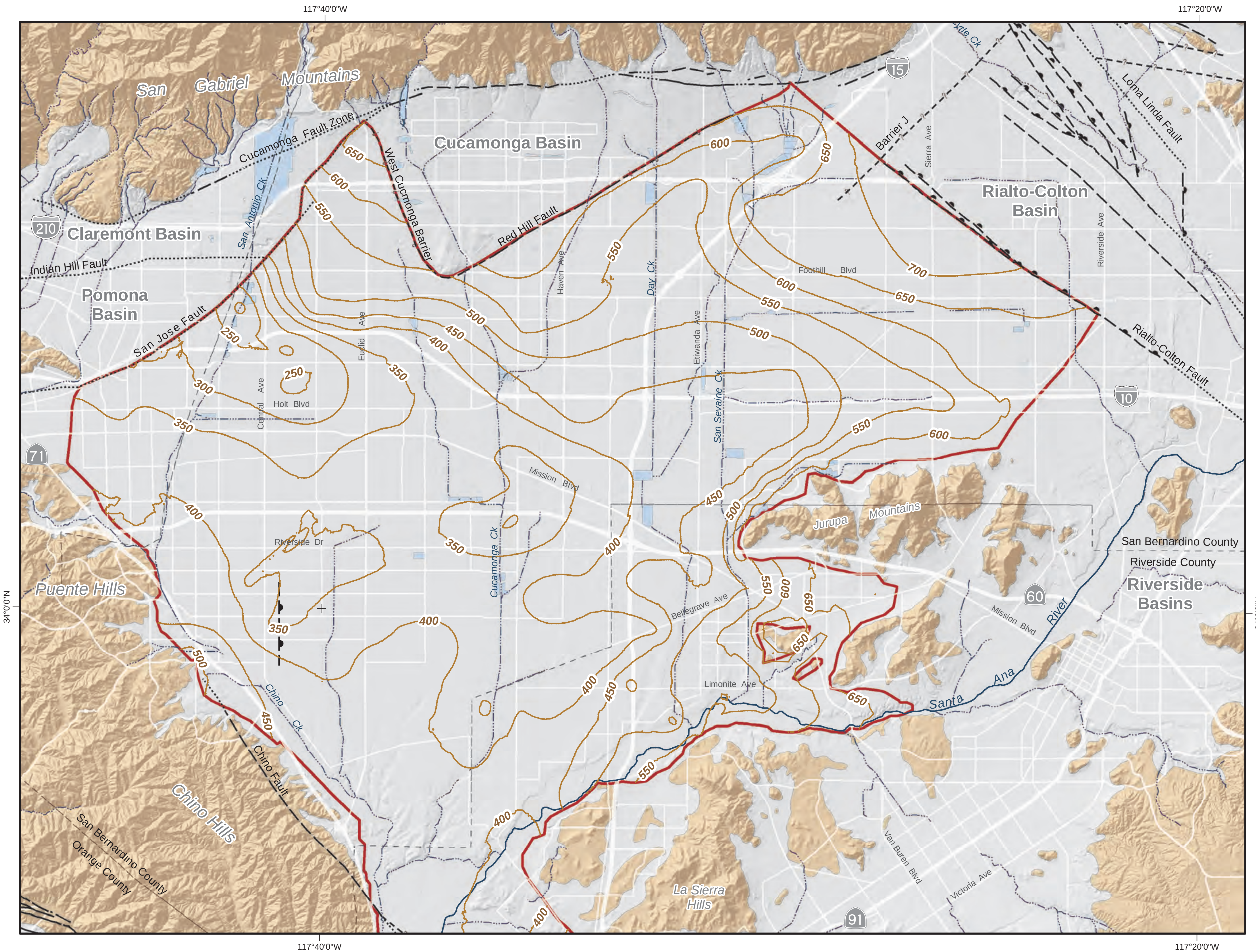

-600- Bottom Elevation Contour of the Model Layer 1 (ft-above msl)

Geology

Water-Bearing Sediments

Quaternary Alluvium

Consolidated Bedrock

Undifferentiated Pre-Tertiary to Early Pleistocene Igneous, Metamorphic, and Sedimentary Rocks

Faults

- Location Certain
- Location Approximate
- Approximate Location of Groundwater Barrier
- Location Concealed
- Location Uncertain

Produced by:

WEI
WILDERMUTH ENVIRONMENTAL, INC.

Author: MJC
Date: 10/1/2015
Document Name: Figure_2-10a_20131230

0 1 2 3 4 5 Miles
0 2 4 6 8 KM

2013 Chino Basin Groundwater Model Update and Analysis of Safe Yield

Layer 1 Bottom Elevation Contours

Figure 2-10a

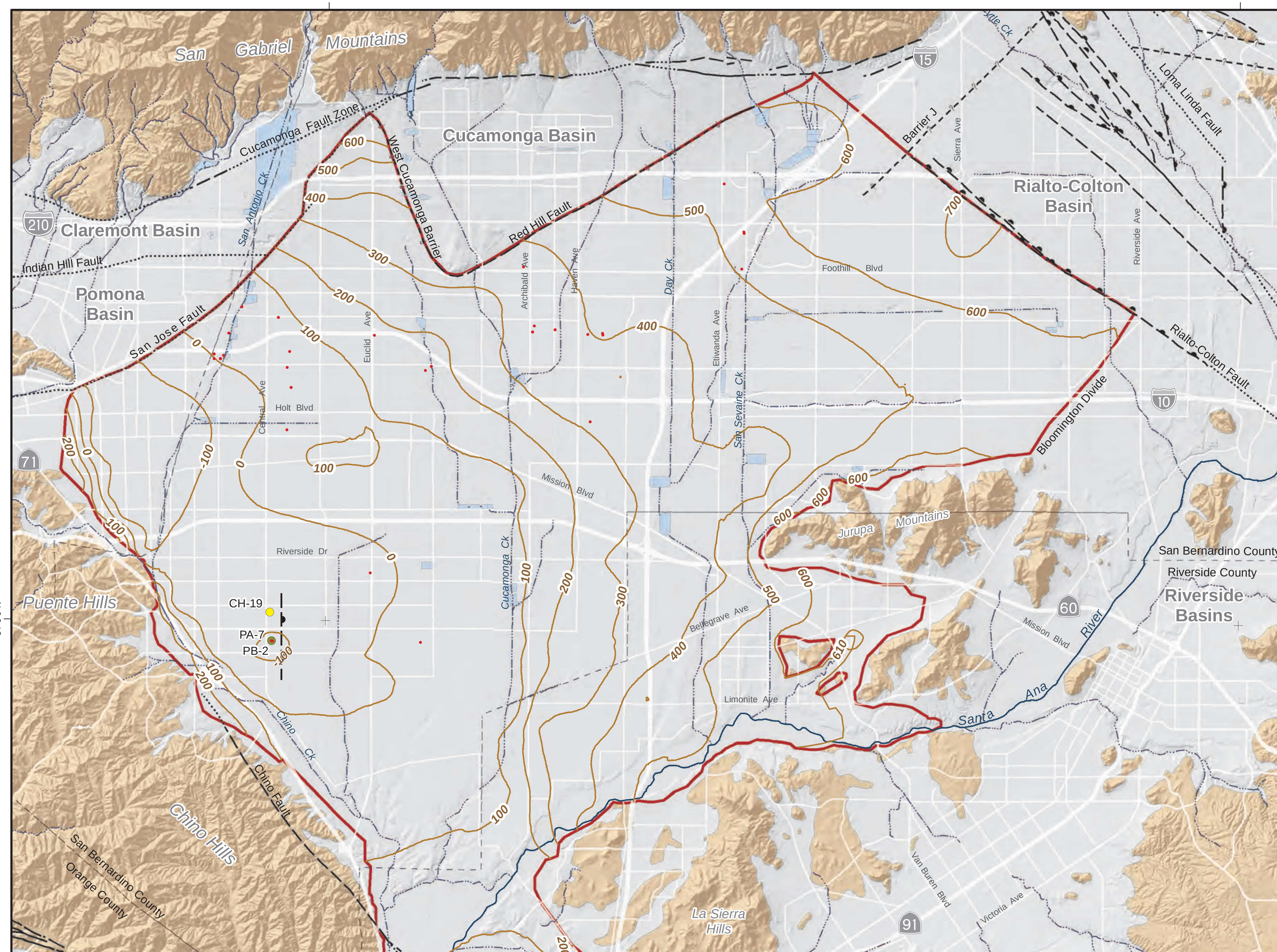

−600− Bottom Elevation Contour of the Model Layer 2 (ft-above msl)

Well Owned by City of Chino Hills

Ayala Park Extensometer/Piezometer Facility

Well Location Where Well Perforations are Deeper than 1,000 feet

Well Location Where Borehole Penetrated Crystalline Bedrock

Geology

Water-Bearing Sediments

Quaternary Alluvium

Consolidated Bedrock

Undifferentiated Pre-Tertiary to Early Pleistocene Igneous, Metamorphic, and Sedimentary Rocks

Faults

Location Certain

Location Approximate

Approximate Location of Groundwater Barrier

Location Concealed

Location Uncertain

0 1 2 3 4 5 Miles

0 2 4 6 8 KM

Produced by:

WEI
Wildermuth Environmental, Inc.

Author: MJC
Date: 10/1/2015
Document Name: Figure_2-10b_20131230

2013 Chino Basin Groundwater Model Update and Analysis of Safe Yield

Layer 2 Bottom Elevation Contours

Figure 2-10b

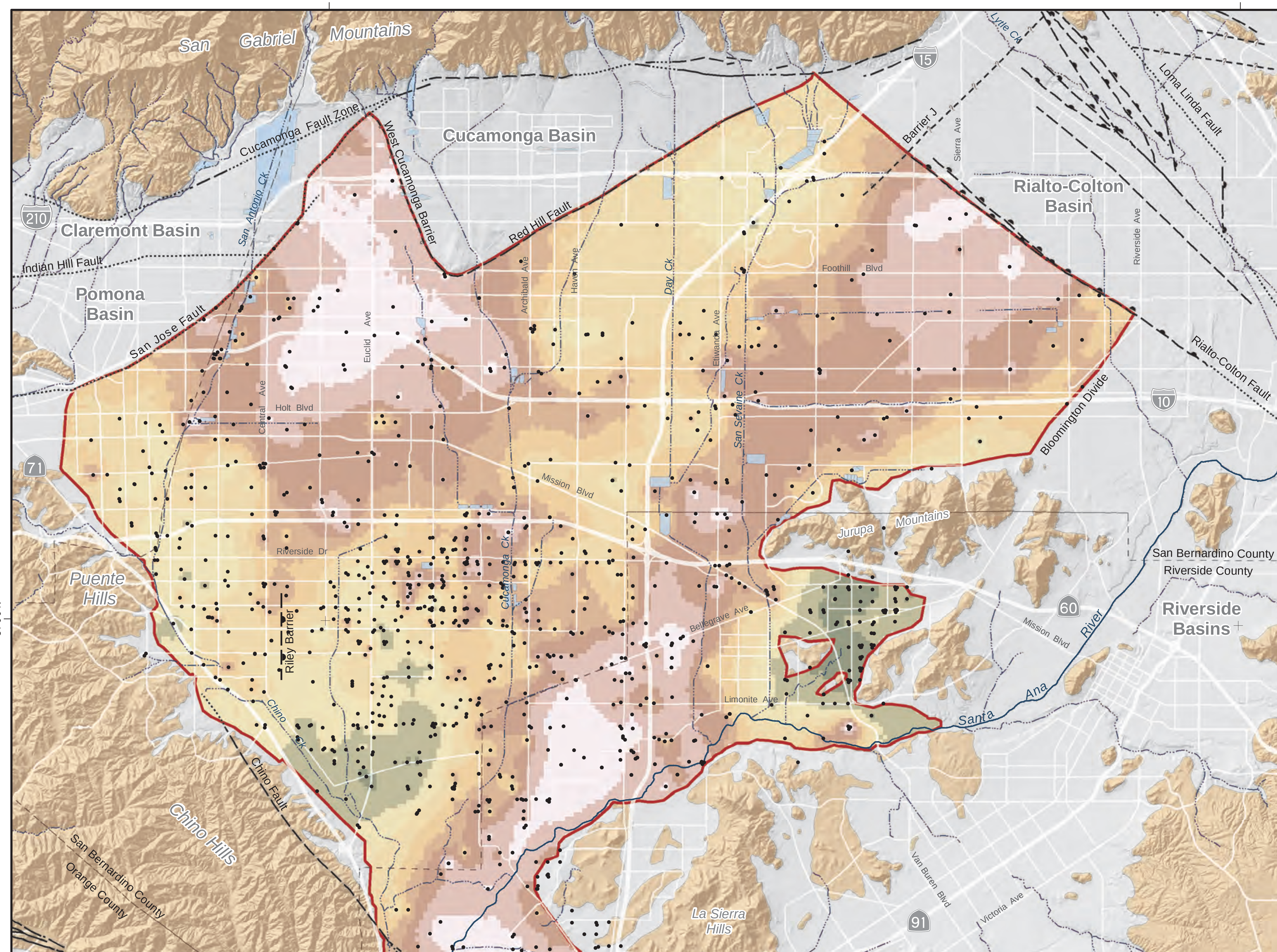

Initial Estimated Specific Yield
Layer 1

- 0.045- 0.074
- 0.075 - 0.093
- 0.094 - 0.11
- 0.110 - 0.116
- 0.117 - 0.123
- 0.124 - 0.129
- 0.13 - 0.139
- 0.14 - 0.152
- 0.153 - 0.171
- 0.172 - 0.199

• Borehole with Lithologic Data used to Estimate Specific Yield

Geology

Water-Bearing Sediments

- Quaternary Alluvium

Consolidated Bedrock

- Undifferentiated Pre-Tertiary to Early Pleistocene Igneous, Metamorphic, and Sedimentary Rocks

Faults

- Location Certain
- Location Approximate
- Approximate Location of Groundwater Barrier
- Location Concealed
- Location Uncertain

Produced by:

WEI
WILDERMUTH ENVIRONMENTAL, INC.

Author: MJC
Date: 10/1/2015
Document Name: Figure_2-11a_20131230

0 1 2 3 4 5 Miles
0 2 4 6 8 KM

2013 Chino Basin Groundwater Model Update and Analysis of Safe Yield

Kriging-Estimated Specific Yield of Layer 1

Figure 2-11a

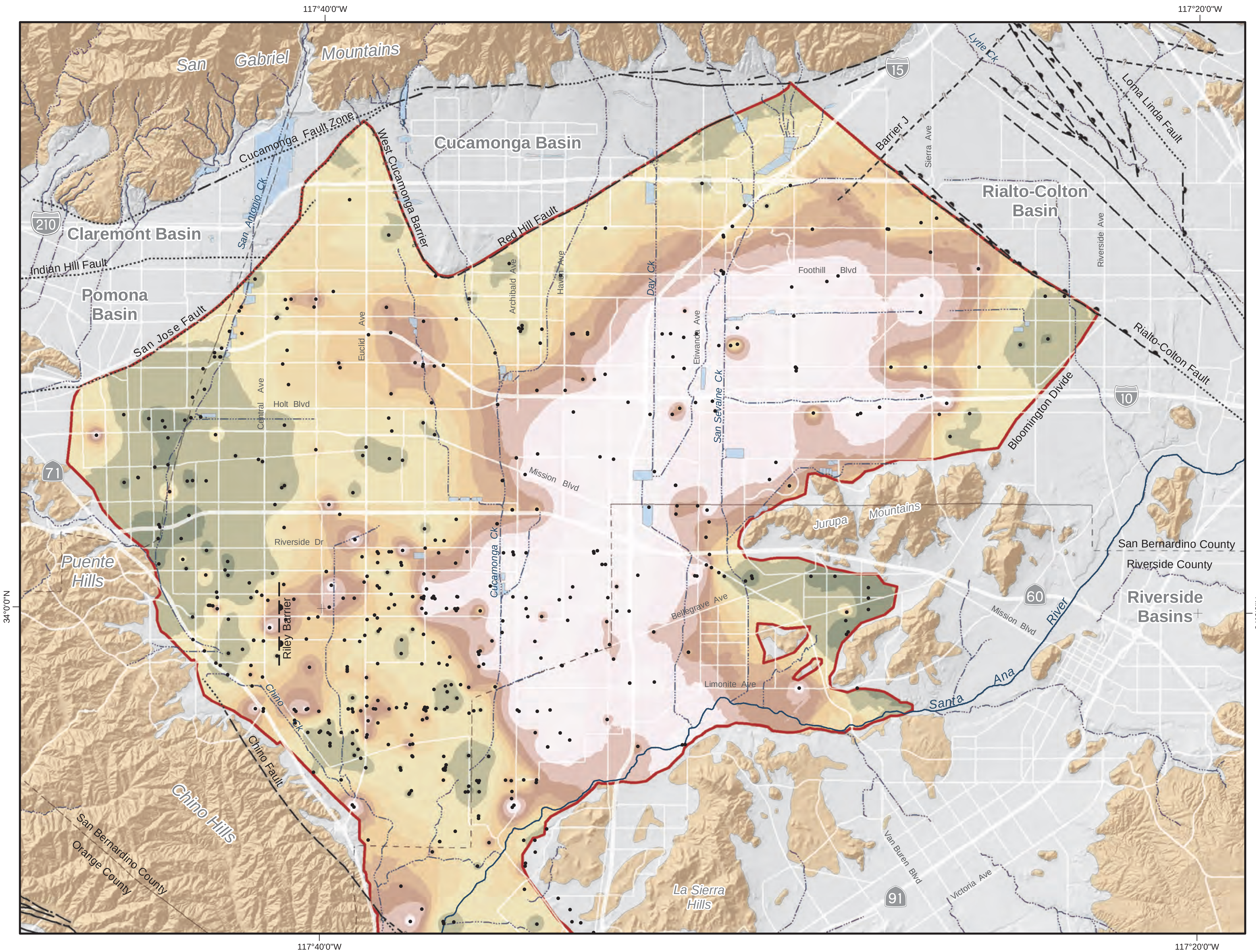

Initial Estimated Specific Yield
Layer 2

- 0.045- 0.074
- 0.075 - 0.093
- 0.094 - 0.11
- 0.110 - 0.116
- 0.117 - 0.123
- 0.124 - 0.129
- 0.13 - 0.139
- 0.14 - 0.152
- 0.153 - 0.171
- 0.172 - 0.199

• Borehole with Lithologic Data used to Estimate Specific Yield

Geology

Water-Bearing Sediments

Quaternary Alluvium

Consolidated Bedrock

Undifferentiated Pre-Tertiary to Early Pleistocene Igneous, Metamorphic, and Sedimentary Rocks

Faults

- Location Certain
- Location Approximate
- Approximate Location of Groundwater Barrier
- Location Concealed
- Location Uncertain

Produced by:

WEI
Wildermuth Environmental, Inc.

Author: MJC
Date: 10/1/2015
Document Name: Figure_2-11b_20131230

0 1 2 3 4 5 Miles
0 2 4 6 8 KM

2013 Chino Basin Groundwater Model Update and Analysis of Safe Yield

Kriging-Estimated Specific Yield of Layer 2

Figure 2-11b

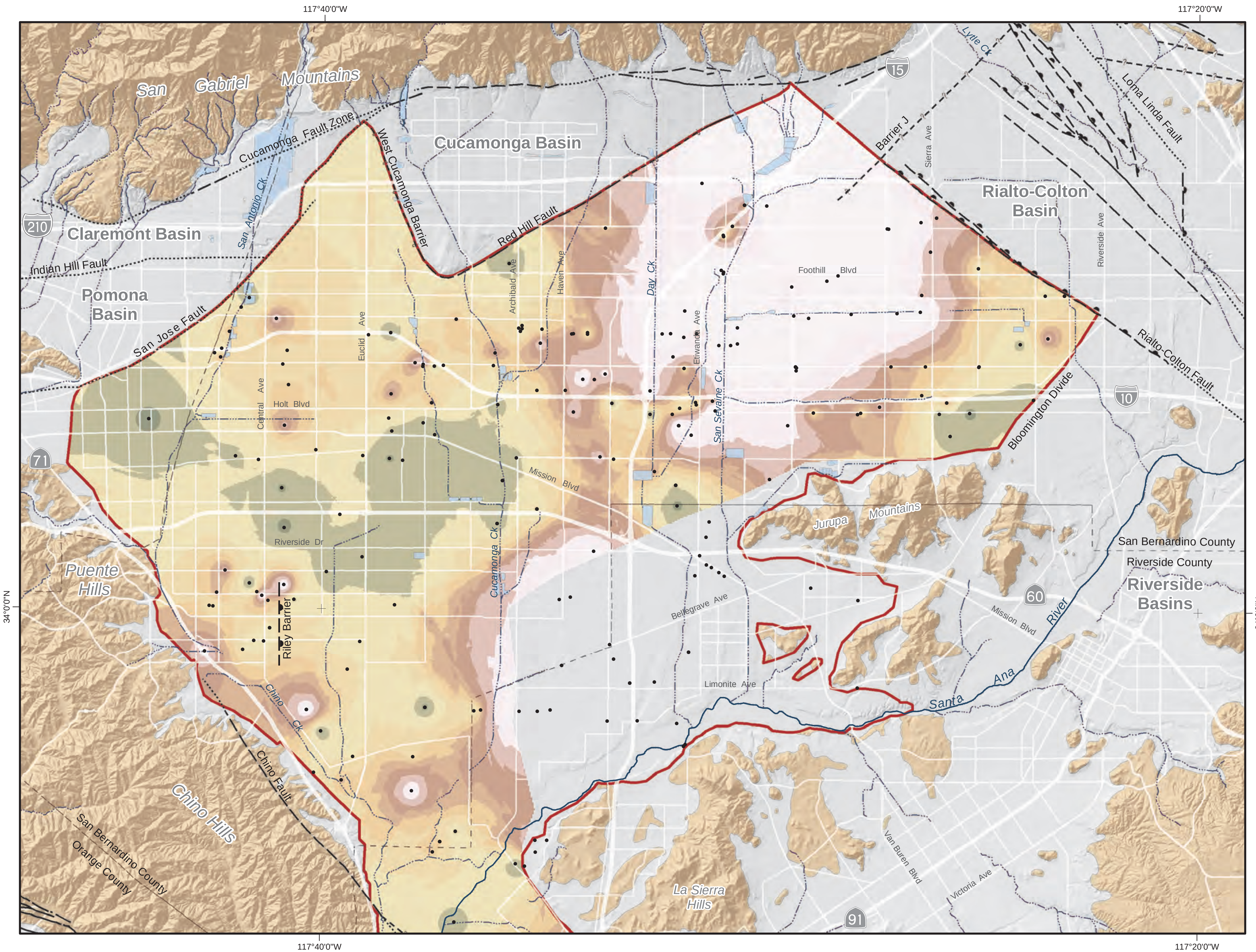

Initial Estimated Specific Yield Layer 3

- 0.045- 0.074
- 0.075 - 0.093
- 0.094 - 0.11
- 0.110 - 0.116
- 0.117 - 0.123
- 0.124 - 0.129
- 0.13 - 0.139
- 0.14 - 0.152
- 0.153 - 0.171
- 0.172 - 0.199

• Borehole with Lithologic Data used to Estimate Specific Yield

Geology

Water-Bearing Sediments

- Quaternary Alluvium

Consolidated Bedrock

- Undifferentiated Pre-Tertiary to Early Pleistocene Igneous, Metamorphic, and Sedimentary Rocks

Faults

- Location Certain
- Location Approximate
- Approximate Location of Groundwater Barrier
- Location Concealed
- Location Uncertain

Produced by:

WEI
Wildermuth Environmental, Inc.

Author: MJC
Date: 10/1/2015
Document Name: Figure_2-11c_20131230

0 1 2 3 4 5 Miles
0 2 4 6 8 KM

2013 Chino Basin Groundwater Model Update and Analysis of Safe Yield

Kriging-Estimated Specific Yield of Layer 3

Figure 2-11c

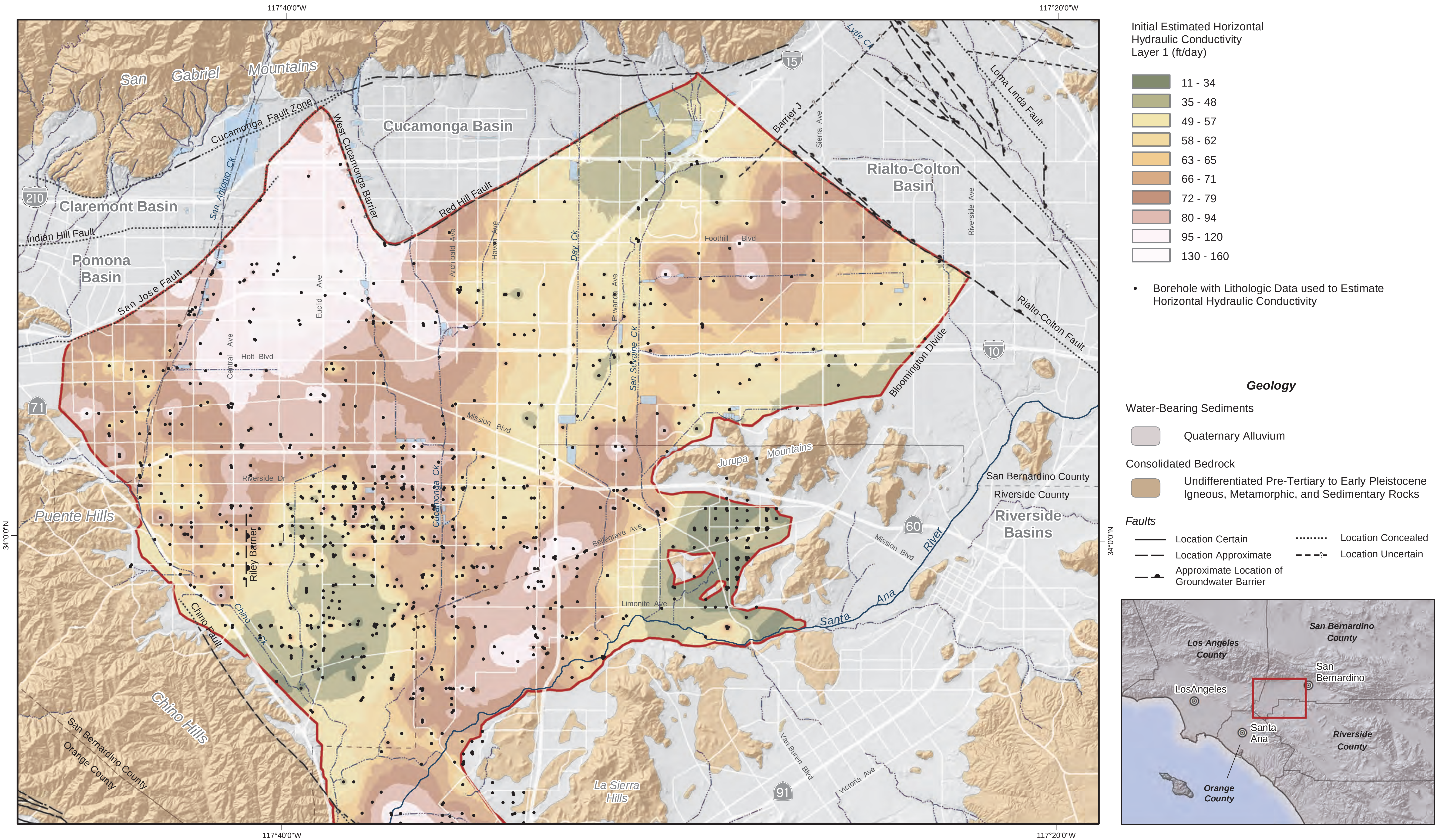

Produced by:

WEI
Wildermuth Environmental, Inc.

Author: MJC

Date: 10/1/2015

Document Name: Figure_2-12a_20131230

2013 Chino Basin Groundwater Model Update and Analysis of Safe Yield

Kriging-Estimated Horizontal Hydraulic Conductivity of Layer 1

Figure 2-12a

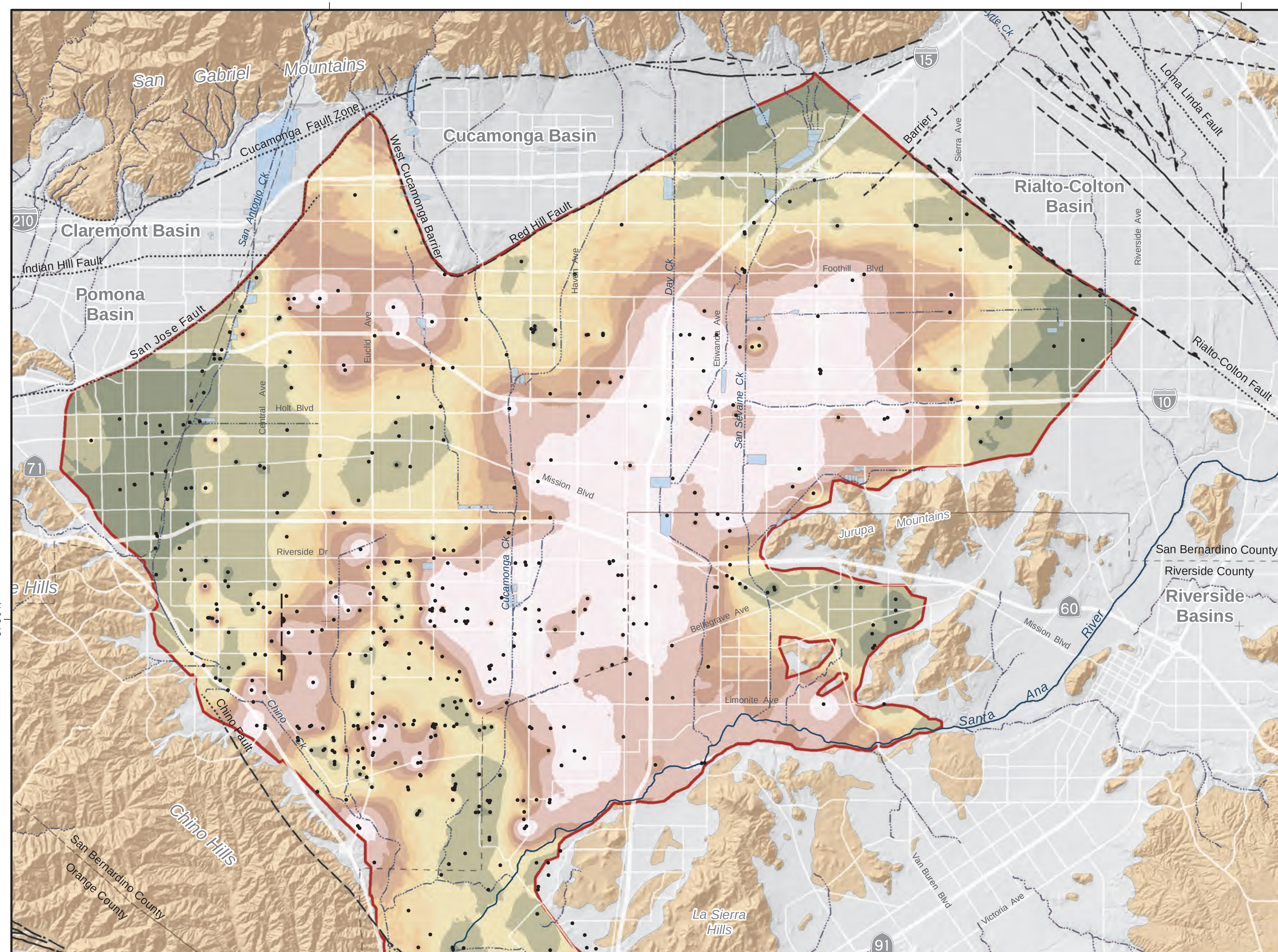

Initial Estimated Horizontal Hydraulic Conductivity Layer 2 (ft/day)

- 11 - 34
- 35 - 48
- 49 - 57
- 58 - 62
- 63 - 65
- 66 - 71
- 72 - 79
- 80 - 94
- 95 - 120
- 130 - 160

• Borehole with Lithologic Data used to Estimate Horizontal Hydraulic Conductivity

Geology

Water-Bearing Sediments

Quaternary Alluvium

Consolidated Bedrock

Undifferentiated Pre-Tertiary to Early Pleistocene Igneous, Metamorphic, and Sedimentary Rocks

Faults

- Location Certain
- Location Approximate
- Approximate Location of Groundwater Barrier
- Location Concealed
- Location Uncertain

Produced by:

WEI
Wildermuth Environmental, Inc.

Author: MJC

Date: 10/1/2015

Document Name: Figure_2-12b_20131230

0 1 2 3 4 5 Miles

0 2 4 6 8 KM

2013 Chino Basin Groundwater Model Update and Analysis of Safe Yield

Kriging-Estimated Horizontal Hydraulic Conductivity of Layer 2

Figure 2-12b

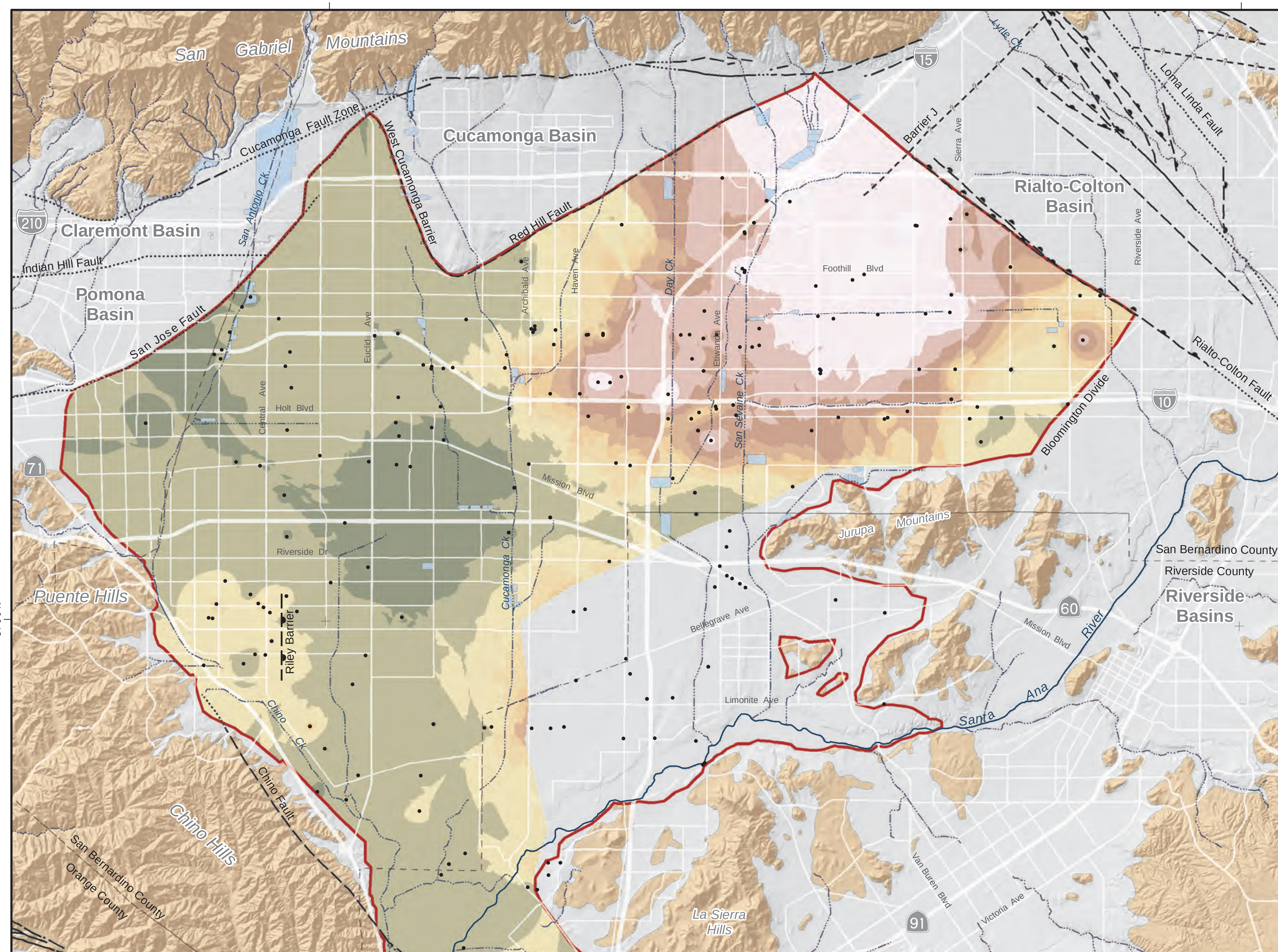

Initial Estimated Horizontal Hydraulic Conductivity Layer 3 (ft/day)

- 11 - 34
- 35 - 48
- 49 - 57
- 58 - 62
- 63 - 65
- 66 - 71
- 72 - 79
- 80 - 94
- 95 - 120
- 130 - 160

• Borehole with Lithologic Data used to Estimate Horizontal Hydraulic Conductivity

Geology

Water-Bearing Sediments

- Quaternary Alluvium

Consolidated Bedrock

- Undifferentiated Pre-Tertiary to Early Pleistocene Igneous, Metamorphic, and Sedimentary Rocks

Faults

- Location Certain
- Location Approximate
- Approximate Location of Groundwater Barrier
- Location Concealed
- Location Uncertain

Produced by:

WEI
Wildermuth Environmental, Inc.

Author: MJC
Date: 10/1/2015
Document Name: Figure_2-12c_20131230

0 1 2 3 4 5 Miles
0 2 4 6 8 KM

2013 Chino Basin Groundwater Model Update and Analysis of Safe Yield

Kriging-Estimated Horizontal Hydraulic Conductivity of Layer 3

Figure 2-12c

117°40'0"W
117°20'0"W

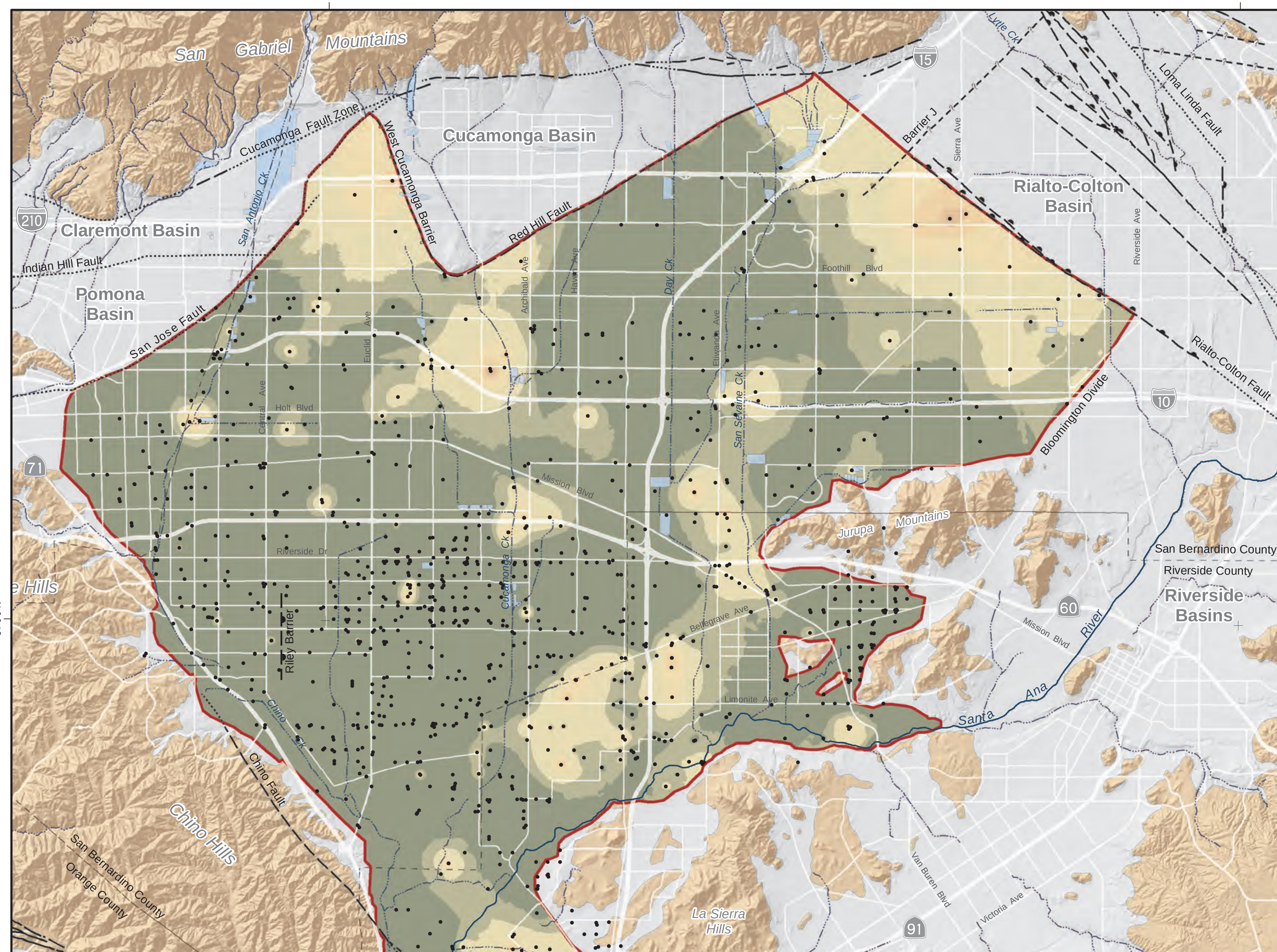

117°40'0"W
117°20'0"W
34°0'0"N
34°0'0"N

Initial Estimated Vertical Hydraulic Conductivity Layer 1 (ft/day)

- 0.0015 - 7
- 7.1 - 14
- 15 - 21
- 22 - 28
- 29 - 35
- 36 - 42
- 43 - 49
- 50 - 56
- 57 - 63
- 64 - 70

• Borehole with Lithologic Data used to Estimate Vertical Hydraulic Conductivity

Geology

Water-Bearing Sediments

Quaternary Alluvium

Consolidated Bedrock

Undifferentiated Pre-Tertiary to Early Pleistocene Igneous, Metamorphic, and Sedimentary Rocks

Faults

- Location Certain
- Location Approximate
- Approximate Location of Groundwater Barrier
- Location Concealed
- Location Uncertain

Produced by:

WEI
Wildermuth Environmental, Inc.

Author: MJC

Date: 10/1/2015

Document Name: Figure_2-13a_20131230

0 1 2 3 4 5 Miles

0 2 4 6 8 KM

2013 Chino Basin Groundwater Model Update and Analysis of Safe Yield

Kriging-Estimated Vertical Hydraulic Conductivity of Layer 1

Figure 2-13a

117°40'0"W 117°20'0"W

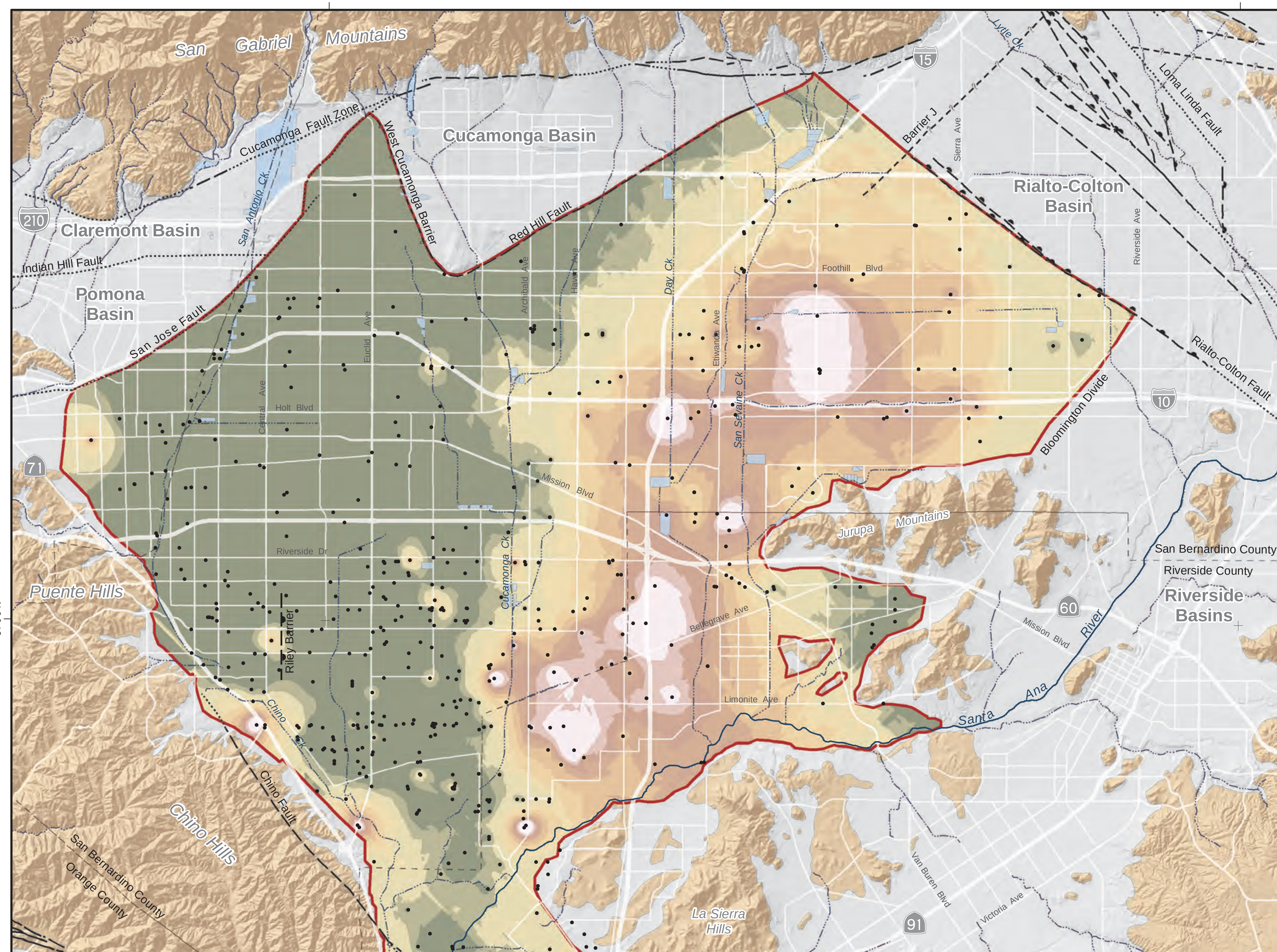

117°40'0"W 117°20'0"W

Initial Estimated Vertical Hydraulic Conductivity Layer 2 (ft/day)

- 0.0015 - 7
- 7.1 - 14
- 15 - 21
- 22 - 28
- 29 - 35
- 36 - 42
- 43 - 49
- 50 - 56
- 57 - 63
- 64 - 70

• Borehole with Lithologic Data used to Estimate Vertical Hydraulic Conductivity

Geology

Water-Bearing Sediments

Quaternary Alluvium

Consolidated Bedrock

Undifferentiated Pre-Tertiary to Early Pleistocene Igneous, Metamorphic, and Sedimentary Rocks

Faults

- Location Certain
- Location Approximate
- Approximate Location of Groundwater Barrier
- Location Concealed
- Location Uncertain

Produced by:

WEI
Wildermuth Environmental, Inc.

Author: MJC
Date: 10/1/2015
Document Name: Figure_2-13b_20131230

0 1 2 3 4 5 Miles
0 2 4 6 8 KM

2013 Chino Basin Groundwater Model Update and Analysis of Safe Yield

Kriging-Estimated Vertical Hydraulic Conductivity of Layer 2

Figure 2-13b

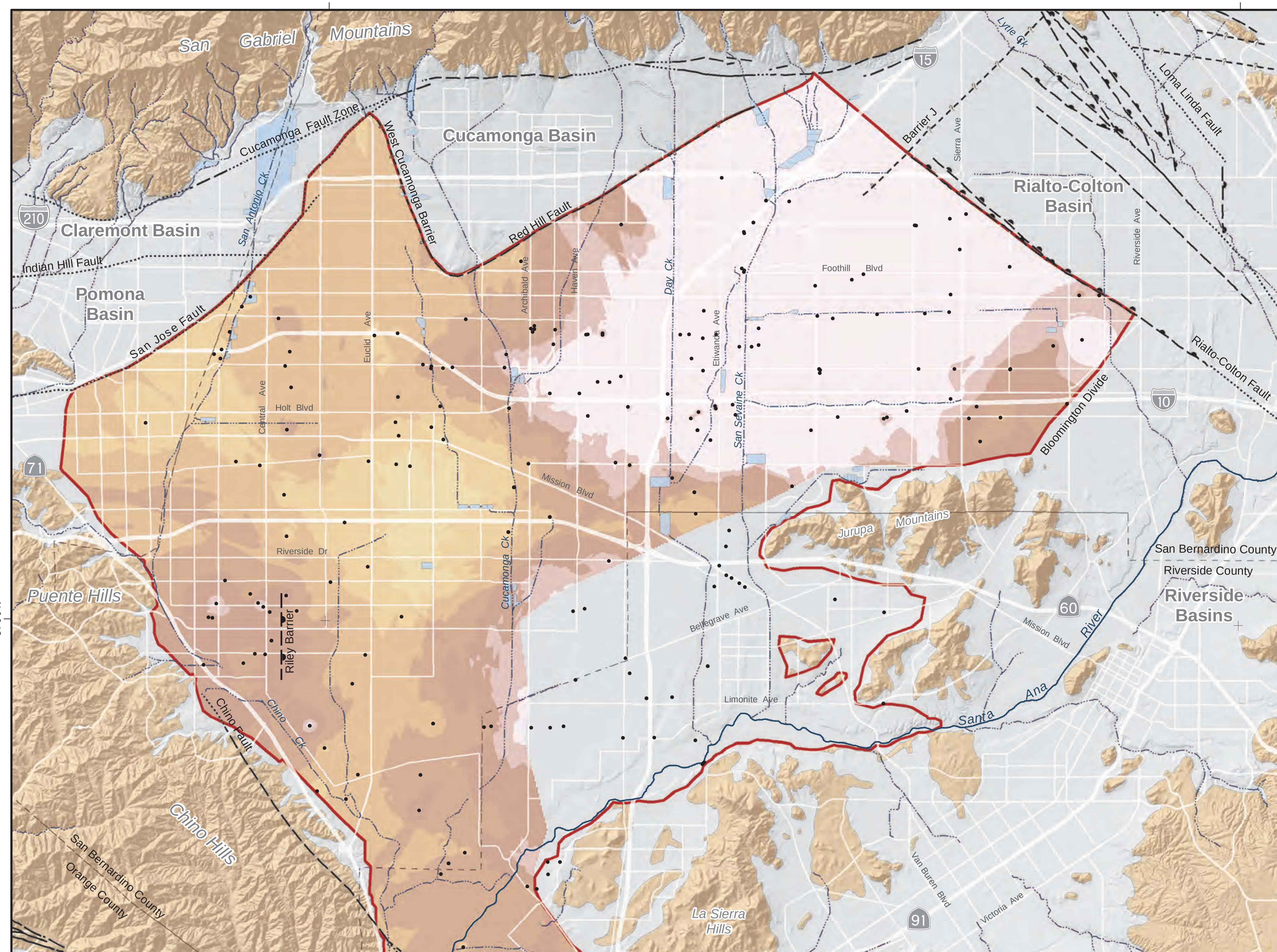

Initial Estimated Vertical Hydraulic Conductivity Layer 3 (ft/day)

- 0.0015 - 7
- 7.1 - 14
- 15 - 21
- 22 - 28
- 29 - 35
- 36 - 42
- 43 - 49
- 50 - 56
- 57 - 63
- 64 - 70

• Borehole with Lithologic Data used to Estimate Vertical Hydraulic Conductivity

Geology

Water-Bearing Sediments

Quaternary Alluvium

Consolidated Bedrock

Undifferentiated Pre-Tertiary to Early Pleistocene Igneous, Metamorphic, and Sedimentary Rocks

Faults

Location Certain

Location Approximate

Approximate Location of Groundwater Barrier

Location Concealed

Location Uncertain

Produced by:

WEI
Wildermuth Environmental, Inc.

Author: MJC

Date: 10/1/2015

Document Name: Figure_2-13c_20131230

0 1 2 3 4 5 Miles

0 2 4 6 8 KM

2013 Chino Basin Groundwater Model Update and Analysis of Safe Yield

Kriging-Estimated Vertical Hydraulic Conductivity of Layer 3

Figure 2-13c

3.1 Introduction

Recharge and discharge are defined as the contributions of water to a groundwater system (recharge stress or component) and the loss of water from the groundwater system (discharge stress or component), respectively. The recharge stresses consist of subsurface boundary inflows, recharge from streams or creeks, supplemental (imported or recycled water) recharge, storm water recharge, and areal recharge. Areal recharge consists of the deep infiltration of precipitation and applied water, onsite wastewater disposal systems (septic tank leach fields and cesspools), and the deep infiltration of leaks from municipal water systems. Discharge stresses consist of evapotranspiration, groundwater discharge to streams, subsurface outflows to the Temescal Basin, and groundwater pumping. For the calibration period, the total inflow was less than the total outflow; in other words, water was removed from storage to meet the discharge. This section reviews the components of recharge and discharge for the calibration and planning periods.

This section discusses the Chino Basin hydrology during the calibration period, which is defined as fiscal year 1961 through 2011 (July 1960 through June 30, 2011). The annual recharge and discharge stresses after model calibration are listed in Table 3-1 and are illustrated graphically in Figure 3-1.

3.2 Recharge Stresses

Recharge stresses include subsurface inflow from adjacent mountain areas and groundwater basins, storm water recharge in natural channels and recharge works, deep infiltration of precipitation and applied water, artificial recharge of imported and recycled water, and onsite wastewater treatment system (septic tank and cesspool) discharge. These recharge stresses were estimated from basic data, hydrologic model computations, and were finalized in during the 2013 Model calibration.

3.2.1 Subsurface Inflow

Subsurface inflows from adjacent groundwater basins were estimated during the 2013 Model calibration process and are listed in Table 3-1. The locations of subsurface inflow on the model boundary are shown in Figure 3-2. The initial estimates for subsurface inflows from mountain front areas were estimated from the Rainfall, Runoff, Router, and Root Zone Model (R4) developed by WEI3. The R4 model was used to calculate surface and subsurface discharge from the mountain front watersheds tributary to the model domain. Subsurface inflow from the Cucamonga Basin through the Red Hill Fault and from the Rialto Basin through the Rialto Fault were estimated in calibration and assumed to be constant over the calibration period. Subsurface inflows from the Cucamonga Basin through the West Cucamonga Barrier and from the Six Basins area through the San Jose Fault were estimated during calibration and were found to be related to the head difference across the barrier faults.4 Subsurface inflow from the Riverside Basin into the Chino Basin was also based on the head difference across the so-called Bloomington Divide.

There is no subsurface barrier between the Temescal and Chino Basins and subsurface flow between the Temescal Basin and Chino Basin can occur in both directions at the same time at different points

[3] The R4 model description is included as an Appendix A to the 2007 CBWM Model Documentation and Evaluation of the Peace II Project Description (WEI, 2007)

[4] This variable flux boundary is an improvement over that constant flux boundary assumed in the 2007 Model

along the boundary. The Temescal Basin is included in the 2013 Model. The subsurface inflow shown in Table 3-1 was estimated in the calibration of the 2013 Model. Table 3-1 shows the time history of subsurface inflow for the calibration period for the Bloomington Divide, Temescal Basin and an aggregate of the remaining subsurface inflows. Total subsurface inflow ranges from a low of 22,000 acre-ft/yr in fiscal 1962 to a high of 47,700 acre-ft/yr in fiscal 2003 and averaged about 36,900 acre-ft/yr. The increase in subsurface inflow from the Six Basins area and the Riverside Basin at the Bloomington Divide through the calibration period is due to declining groundwater production in the Pomona and Riverside Basins and increases in Santa Ana River recharge in the Riverside Basin.

3.2.2 Streambed and Storm Water Recharge

Streambed recharge occurs in unlined stream channels and in flood control and water conservation basins. Most of the major stream channels in the Chino Basin were concrete-lined as of March 2003 (WEI, 2003). Figures 3-3a-f shows the location of and time history of channel lining over the Chino Basin.

The R4 Model was used to estimate the storm water recharge in stream channels and in flood control and recharge basins. The R4 Model was developed from the Chino Basin Watermaster Recharge Model (Wildermuth, 1998; WEI, 2001) and the Wasteload Allocation Model (WEI, 2002). It has subsequently used in the 2007 Chino Basin Model, the Arlington Basin Model and is being currently used to build new groundwater models for the Cucamonga Basin and Six Basins area. R4 contains three modules: Runoff, Router, and Root Zone. The Runoff module estimates daily runoff from discrete drainage areas. The Router module routes runoff from each drainage area and non-tributary discharges (recycled and imported water) through the drainage system and calculates, among other things, discharge and recharge in channels and in flood control and conservation basins. The Root Zone module is used to estimate the amount of water that recharges to the aquifer out of the root zone. Data that were used in the R4 model include precipitation data, Soil Conservation Service (SCS) hydrologic soil types, land use, and the physical properties of the drainage system (channel geometry, slope, lining, etc.). A description of the R4 model and its application to the study area is provided in Appendix A for the 2007 CBWM Model Documentation and Evaluation of the Peace II Project Description (WEI, 2007).

Figure 3-4 is a stacked bar chart that illustrates the stormwater recharge over the calibration period excluding the Santa Ana River. The streambed recharge is greatest in wet years (such as 1969and 1978) and lowest in dry years (such as 1961 and 1976), and drops to essentially zero with the complete lining of stream channels. The average streambed recharge, excluding Santa Ana River recharge over the calibration period is 7,300 acre-ft/yr for the Chino Basins. After 1988, when most of the channels lining projects were completed, streambed recharge, excluding the Santa Ana River, dropped to an average of 2,300 acre-ft/yr. The maximum streambed recharge for the study area is 32,600 acre-ft/yr, which occurred in 1969. The second largest streambed recharge in the Chino Basin occurred in 1978 and was 24,700 acre-ft. Figure 3-9a shows how streambed recharge has decreased over time for all creeks in the study area, excluding the Santa Ana River.

Stormwater recharge in flood control and conservation basins was estimated with the R4 model throughout the calibration period except when IEUA could provide estimates of stormwater recharge for flood control and water conservation facilities monitored by IEUA. Storm water recharge in flood control and conservation facilities ranged from a low of about 700 acre-ft/yr in 1961 to a high of about 17,600 acre-ft/yr in 2005 and averaged about 6,000 acre-ft/yr.

Streambed recharge in the Santa Ana River has increased due to the increase recycled water and storm water discharges to the Santa Ana River. Santa Ana River recharge was initially estimated with the R4 model and finally in calibration with the 2013 model. Figure 3-9c illustrates the calibrated Santa Ana River recharge time series. Urbanization in the Santa Ana River watershed has lead to increases in recycled water production and discharge. Urbanization has also increased the amount of storm and dry-weather discharge to the River and its tributaries. Recharge from the Santa Ana River has increased throughout most of the calibration period ranging from a low of about 22,700 acre-ft/yr in 22,400 acre-ft/yr to a high of about 36,800 acre-ft/yr in 1978 and averaged about 29,600 acre-ft/yr.

3.2.3 Areal Recharge

Areal recharge consists of three components: deep infiltration of precipitation and applied water, onsite wastewater treatment system discharges and discharge from leaky municipal systems. Table 3-1 contains the annual estimate of the aggregate of these recharge stresses.

3.2.3.1 Deep Infiltration of Precipitation and Applied Water

WEI estimated deep infiltration of precipitation and applied water (DIPAW) with the R4 model and routed this recharge through the vadose zone with a simplified routing model based on results from the HYDRUS-2D model. DIPAW was assumed to occur when soil moisture exceeded field capacity. Field capacity is the maximum volume of water that can be stored in the soil zone against the force of gravity. Soil moisture in excess of field capacity is assumed to infiltrate beyond the root zone and migrate through the vadose zone to the saturated zone.

For urban areas DIPAW estimates were based on land use, soil type, irrigable area, evapotranspiration, precipitation and applied water. The initial estimate of applied water for urban areas was estimated from reports prepared by the IEUA.[5] These reports show the monthly volume of water produced by each water purveyor by source in the IEUA service areas and the volume of sewage produced by each purveyor. The difference was assumed to be equal to initial estimate of applied water. The final estimate of water applied for irrigation is equal to the trial estimate minus the dry weather discharge in Cucamonga and Chino Creek. The final applied water estimates were developed at the retail water purveyor level.

DIPAW for agricultural, native and undeveloped areas (land in transition from agricultural uses and urban uses) were based on vegetation type and associated root zone depth, soil type, permeable area, irrigable area, evapotranspiration and precipitation.

Evapotranspiration was estimated for various vegetation types based on published unit consumptive use rates and California Irrigation Management Information System (CIMIS) data.

3.2.3.2 Deep Infiltration of Onsite Wastewater System Discharge

Areal recharge from onsite wastewater disposal systems was estimated based on data collected from the Counties and the Cities, which showed by year which land parcels were developed and not sewered. The discharge rates associated with the onsite wastewater disposal systems is based on estimates developed on unit sewage generation developed from IEUA data. Appendix B summarizes some of this information used to prepare this estimate.

[5] These are reports prepared by IEUA to determine the total dissolved solids increment in water use and wastewater treatment. These reports are filed with the Santa Ana Regional Board.

3.2.3.3 Deep infiltration of Leaks from Municipal Water Systems

Areal recharge from leaks in municipal water systems was estimated at 2 percent of water production. Appendix B summarizes some the information used to prepare this estimate.

3.2.3.4 Areal Recharge Calibration

All three of these recharges were aggregated into the term deep infiltration of precipitation and applied water and abbreviated as DIPAW. Within the Chino Basin, the travel time from these sources to the water table varies depending on water application rate, thickness of the vadose zone, lithology of the vadose zone, and land use. For example, in the northern Chino Basin the vadose zone is over 600 feet thick; whereas near the Prado Basin, the vadose zone may be less than 20 feet thick. The HYDRUS-2D model was used to estimate the time required for DIPAW to transit the vadose zone. For a detailed discussion of this process, refer to Appendix B in the 2007 CBWM Model Documentation and Evaluation of the Peace II project Description (WEI, 2007). The annual DIPAW was refined in model calibration. Figure 3-5 shows the calibration time history of DIPAW near the ground surface and DIPAW reaching the water table.

3.2.4 Supplemental Water Recharge

Supplemental water consists of water imported from outside the Chino and Temescal Basins and recycled water. Imported water is recharged in the Chino Basin by the Chino Basin Watermaster pursuant to the 1978 Chino Basin Judgment and the Peace Agreements. Prior to the 1978 Judgment the Chino Basin Water Conservation District recharged some imported water. IEUA and its predecessor entities recharge recycled water in during the calibration period. Table 3-1 lists the annual time history of imported and recycled water recharge during the calibration period. Imported water recharge ranged from a low of zero throughout in several years to a high of about 34,600 acre-ft/yr in 2006.

Recycled water is recharged in the numerous recharge basins in the Chino and Temescal Basins. During the period of 1961-1973 IEUA recharged recycled water at its regional plants RP-1, RP-2, and RP-3. After 1973 recharge at RP1 and RP2 ceased. Recharge at RP4 continued through 1984. During the period of 1999-2004, recycled water was recharged to the Ely basins. Thereafter IEUA has expanded recycled water to several recharge facilities. Recycled water recharge ranged from a low of zero in 1990 to a high of about 16,900 acre-ft/yr in 1969 and averaged about 4,600 acre-ft/yr.

The city of Corona has recharged recycled water in the Temescal Basin throughout the calibration period at its Airport ponds and later at the Lincoln and Cota ponds. Recycled water recharge in the Temescal Basin affects the subsurface flow between the Chino and Temescal Basin and Santa Ana River recharge in Prado Basin.

3.3 Discharge

3.3.1 Subsurface Outflow

In the Chino Basin, subsurface outflow can only occur to the Temescal Basin and as underflow at Prado Dam. Historical groundwater levels in the Temescal Basin have caused groundwater outflow into the Chino Basin. However, it is possible for groundwater levels in the Temescal Basin to drop to levels where groundwater outflow from Chino to Temescal Basin could occur. The subsurface outflow from Chino to Temescal, or vice versa, is included in the water budget shown in Table 3-1 because the boundary between the basins is internal to the study area. The subsurface outflow across this boundary is computed in the model calibration and in the planning simulations and can be estimated from an analysis of cell-by-cell flow.

The Army Corps of Engineers constructed a grout curtain under Prado Dam. As is such, the subsurface outflow from Chino Basin at Prado Dam is assumed to be zero. Subsurface outflow from the model domain area was assumed to be zero.

3.3.2 Rising Groundwater

Rising groundwater can occur in the Santa Ana River and its tributaries in the southern Chino and Temescal Basins when the piezometric level of groundwater under the river exceeds the elevation of the streambed. The magnitude of rising groundwater varies seasonally, being greater in the winter and lesser in the summer. Rising groundwater cannot be directly calculated from existing monitoring programs. The available data consist of surface water discharge monitoring stations on the Santa Ana River at the Metropolitan Water District of Southern California (MWD) pipeline crossing located in the City of Riverside, and at below Prado Dam as well as stations on the following tributaries: Chino Creek, Cucamonga Creek, and Temescal Creek. Other measured non-tributary discharges include recycled water discharges from the Cities of Corona and Riverside, the IEUA, the Western Riverside Regional JPA plant, Arlington Desalter discharge, and State Project water discharges to San Antonio Creek in Upland. Between the MWD Crossing and Prado Dam, there are few measurements of surface water discharge that can be used to define reaches of rising groundwater or streambed recharge. The great stands of riparian vegetation along the Santa Ana River and the Prado Reservoir area are likely to contribute to the seasonal variation of base flow in the Santa Ana River and may impact rising groundwater in the Prado Reservoir area. Rising groundwater discharge estimates were made during model calibration and are listed in Table 3-1. For the calibration period, the rising groundwater discharge ranges from a low of about 13,400 acre-ft/yr 1976 to a high of 29,300 acre-ft/yr in 2004 and averaged about 19,400 acre-ft/yr.

3.3.3 Evapotranspiration

Evapotranspiration (ET) is the combination of water loss due to evaporation from the soil and transpiration from plants. In the majority of the study area, ET occurs from the unsaturated zone and is not accounted for by the groundwater model. Within the Prado Basin area and along the Santa Ana Stream in the south of Chino Basin, however, ET occurs from the saturated zone and is explicitly computed by groundwater model. Appendix B contains information used to estimate the time history of the spatial extent of riparian vegetation and the unit ET. For the calibration period the ET ranged from a low of 7,000 acre-ft/yr in 1961 to a high of 18,800 acre-ft/yr and averaged about 15,800 acre-ft/yr. The time history of increasing riparian ET estimated by the model corresponds to the increases in discharge to the Santa Ana River and its tributaries from urbanization and change in vegetation management in Prado Basin and the Santa Ana River.

3.3.4 Groundwater Production

Estimates of groundwater production were developed from the records of the Chino Basin Watermaster for the Chino Basin, production records compiled by the WMWD for the Temescal Basin, previous modeling reports, crop transpiration requirements, and diary operation records. Watermaster determined the physical locations of wells in the Chino Basin using Global Positioning System (GPS) technology. The locations of wells in the Temescal Basin were digitized from well location maps prepared by the WMWD and the City of Corona. Figure 3-6 shows and Table 3-1 lists the groundwater production time history that occurred during the calibration period by water use type.

Groundwater production was categorized into four groups in the Chino Basin based on water use. Agricultural production includes water pumped by dairymen, farmers, and the State of California. Overlying non-agricultural water users include industrial and other non-agricultural users. Appropriative users include local cities, public water districts, and private water companies. Chino Desalter Authority (CDA) production occurs in the southern Chino Basin and after treatment most of the produced groundwater is served to Appropriators.

3.3.4.1 Overlying Agricultural Production

Over the calibration period, agricultural production averaged 90,781 acre-ft/yr. The maximum agricultural production during the calibration period was 160,702 acre-ft/yr, in the year of 1960/1961, and the minimum during this period was 21,021 acre-ft/yr, which occurred in the year 2011. The trend for agricultural production is decreasing over the calibration period. Agricultural production was estimated during the period from 1961 to 2001 because reliable historical records were not available. After the year 2001, the historical records of agriculture production were used in the model and the record data are quite similar to the estimates from land use.

Two approaches were used to estimate agricultural production. For the period of fiscal 1961 through fiscal 2001 a water duty method was used because a significant amount of the agricultural production was unmetered. Thereafter Watermaster records were used Watermaster started its metering program for agricultural production.

Agricultural production was divided into two categories: irrigation and dairy. This production was estimated on a daily step with the R4 model and aggregated to quarterly time step used in the groundwater model. Agricultural production was determined by estimating the crop demand (after precipitation) and diary demands and then subtracting any non-groundwater source of water, such as water in the soil profile, surface water, or dairy wash water. R4 uses a grid-based method to incorporate hydrological processes, agricultural practices, and land use properties. Land use data from 1957, 1963, 1975, 1984, 1990, 2000, and 2006 were used in the spatial calculation of production. A linear interpolation method was used to estimate groundwater production between each published land use.

Irrigation demands can be satisfied by rainfall, groundwater production, and other sources. Groundwater production for irrigation is estimated as the water needed by the crops minus the water supplied through non-groundwater sources. The study area was divided into Hydrologic Sub-Areas (HSA). HSAs are primarily sub-drainage areas and are the primary level of discretization used in the R4 model. The R4 Model accounts for the hydrologic processes and agricultural activities of the land surface and is used to calculate applied water for each HSA. The quarterly applied irrigation water (water needed by the crops minus the water supplied through non-groundwater sources) is then assigned as the production rate at the centroid of each cell.

Diary production before fiscal 2002 was estimated based on cow counts from the RWQCB and the USDA and metered dairy production from fiscal 2002 through 2010. Appendix B contains information used to estimate the time history of the groundwater production by dairies and the fate of dairy wash water.

3.3.4.2 Overlying Non-Agricultural Production and Appropriator Production

Estimates of overlying non-agricultural and appropriator production prior to 1978 were obtained from (JMM, 1992; and Carroll, 1974) which were based on IEUA estimates developed for the Chino Basin adjudication. Thereafter production estimates were obtained from the Watermaster. The combined production by both user groups ranged from a low of 47,700 acre-ft/yr in 1963 to a high of 136,500 acre-ft/yr in 2009 and averaged about 100,400 acre-ft/yr.

3.3.4.3 Desalter Production

Chino Basin Desalter Authority (CDA) groundwater production started in fiscal 2000, and reached a maximum production of 30,100 acre-ft/yr in 2008 and produced slightly less thereafter.

3.3.4.4 Temescal Basin Production

Over the calibration period, the well production in the Temescal Basin, including appropriate production, desalter production, agriculture production, and non-agricultural production, ranged from about 6,700 acre-ft/yr to about 22,200 acre-ft/yr and averaged 13,220 acre-ft/yr. This data is not shown in Table 3-1, as Table 3-1 is the water budget for Chino Basin only.

3.4 Change in Storage

Table 3-1 lists the annual recharge and discharge stresses, annual change in storage and cumulative change in storage based on the calibrated 2013 Chino Basin model. Since the Chino Basin Judgment became effective in 1978, the storage in the Basin has declined about 550,000 acre-ft and since the Peace Agreement became effective in 2001 the groundwater storage has decline about 286,000 acre-ft.

Table 3-1
Water Budget for Chino Basin
Scenario 1 Calibration Period 1961 through 2011
(acre-ft)

Year	Recharge										Discharges							Change in Storage = Recharge minus Discharge	Cumulative Change in Storage	
	Subsurface Boundary Inflow, Chino Hills, Six Basins, Cucamonga Basin and Rialto Basin	Subsurface Boundary Inflow from Bloomington Divide	Subsurface Inflow From Temescal Basin	Deep Infiltration of Precipitation and Applied Water[1]	Streambed Infiltration from Santa Ana River Tributaries	Storm Water Recharge in Basins	Recycled Water Recharge	Imported Water Recharge	Streambed Infiltration in the Santa Ana River	Subtotal Recharge	CDA Pumping	Pool 2 and 3 Pumping	Pool 1 Pumping	ET	GW Discharge to Streams	Subsurface Discharge to Temescal Basin	Subtotal Discharge		Since 1977	Since 2000
1961	14,475	7,595	1,868	120,415	6,192	694	11,561	0	24,088	186,888	0	53,154	160,702	6,979	20,414	1,647	242,896	-56,009		
1962	14,016	6,677	1,291	117,266	17,751	2,926	10,785	0	25,751	196,462	0	49,119	151,486	7,839	20,392	3,064	231,901	-35,439		
1963	14,124	6,669	1,615	117,217	7,698	1,623	12,466	0	23,628	185,040	0	47,744	155,542	8,469	18,488	2,142	232,385	-47,345		
1964	13,815	6,979	2,079	115,475	10,278	2,068	13,959	0	28,425	193,077	0	53,087	147,770	9,252	20,705	3,442	234,255	-41,178		
1965	13,491	6,652	2,019	113,070	11,841	2,664	10,900	0	28,724	189,360	0	57,063	148,293	9,857	18,203	2,450	235,866	-46,506		
1966	14,186	6,531	2,530	113,396	17,380	4,158	14,362	0	28,400	200,944	0	52,282	154,903	10,414	18,656	3,017	239,271	-38,328		
1967	15,000	7,214	2,925	113,550	22,755	5,021	14,810	0	34,215	215,491	0	48,477	139,984	11,171	17,318	3,623	220,572	-5,082		
1968	15,656	7,817	3,393	108,679	12,692	3,463	12,390	0	29,268	193,357	0	57,342	149,236	11,793	17,412	2,862	238,645	-45,288		
1969	16,383	7,900	3,400	108,745	32,599	7,507	16,927	0	31,978	225,439	0	59,672	113,262	12,503	15,602	2,446	203,486	21,953		
1970	17,429	8,555	3,492	109,118	10,165	3,218	15,059	0	27,759	194,795	0	58,491	134,624	13,089	17,178	1,873	225,255	-30,460		
1971	17,127	8,989	3,788	109,264	11,301	2,967	16,179	0	28,869	198,484	0	61,522	134,658	13,616	17,568	1,697	229,061	-30,577		
1972	16,595	9,463	3,558	107,214	6,293	1,976	14,000	0	28,396	187,494	0	61,345	150,534	14,117	15,703	1,500	243,199	-55,705		
1973	16,657	9,050	3,797	111,835	20,936	6,189	3,028	0	31,412	202,903	0	58,428	119,331	14,907	19,489	2,149	214,304	-11,401		
1974	17,347	9,334	3,815	104,184	11,168	3,746	2,600	0	31,090	183,284	0	62,542	123,791	15,585	15,771	2,023	219,713	-36,429		
1975	17,140	9,838	4,128	104,122	12,879	4,142	2,600	0	31,998	186,847	0	74,093	113,842	16,297	16,687	2,508	223,428	-36,581		
1976	16,413	10,144	4,369	100,305	6,480	2,111	3,000	0	32,529	175,351	0	77,891	135,455	16,165	13,442	1,827	244,781	-69,430		
1977	15,857	10,145	4,503	109,299	8,710	4,198	3,100	0	34,120	189,932	0	69,412	110,767	16,807	17,461	2,491	216,938	-27,006		
1978	16,571	10,220	5,234	107,520	24,697	10,741	8,506	6,978	36,777	227,244	0	71,336	117,554	17,107	19,265	3,555	228,816	-1,573	-1,573	
1979	17,561	10,270	6,388	103,354	15,750	6,952	5,718	28,395	32,342	226,729	0	67,892	116,394	16,924	17,537	2,592	221,339	5,391	3,818	
1980	18,091	11,794	6,518	100,461	20,312	10,268	3,300	16,428	34,902	222,073	0	72,114	108,338	16,606	14,729	1,670	213,456	8,617	12,436	
1981	18,310	12,595	6,693	99,078	7,717	3,378	3,500	20,890	30,304	202,465	0	76,888	113,506	16,290	14,348	1,380	222,412	-19,947	-7,511	
1982	18,069	12,927	6,815	109,767	11,217	6,126	3,800	21,656	33,571	223,948	0	72,174	99,313	16,664	17,851	2,148	208,150	15,798	8,288	
1983	18,722	13,142	7,555	107,741	18,133	11,889	3,900	27,588	31,293	239,963	0	65,755	92,248	17,168	20,822	2,041	198,034	41,930	50,217	
1984	19,518	14,528	8,339	116,193	8,674	5,302	0	22,237	27,609	222,401	0	73,647	105,405	17,262	20,476	1,005	217,795	4,605	54,822	
1985	20,156	14,242	8,643	106,568	6,271	4,256	0	20,897	29,413	210,446	0	79,148	103,218	16,835	18,608	1,357	219,165	-8,719	46,104	
1986	21,892	13,119	8,836	105,053	6,103	5,752	0	18,427	31,024	210,206	0	84,033	103,384	16,980	20,438	1,501	226,336	-16,130	29,974	
1987	22,614	12,632	8,942	108,395	2,893	3,598	0	20,007	31,720	210,800	0	87,358	102,568	17,228	18,640	1,223	227,017	-16,217	13,757	
1988	21,453	11,957	8,836	105,703	2,919	5,169	173	2,494	31,357	190,061	0	94,597	93,360	17,141	19,872	1,539	226,510	-36,449	-22,691	
1989	21,560	11,856	8,445	107,042	1,428	4,260	0	7,407	27,756	189,754	0	97,309	87,080	16,998	18,803	1,306	221,495	-31,741	-54,433	
1990	20,667	11,856	8,345	105,309	437	2,936	0	0	30,588	180,139	0	106,271	81,631	16,930	16,953	1,173	222,959	-42,820	-97,253	
1991	20,015	12,233	8,973	107,770	722	4,094	0	3,607	27,161	184,575	0	91,992	80,536	16,855	16,509	1,089	206,981	-22,406	-119,659	
1992	20,645	12,606	8,981	110,778	1,032	6,349	0	5,551	30,444	196,386	0	96,632	75,192	17,063	17,926	1,316	208,130	-11,745	-131,403	
1993	22,018	12,740	8,430	104,591	2,263	11,615	0	14,212	36,701	212,570	0	91,806	80,747	17,199	16,228	1,787	207,768	4,803	-126,600	
1994	21,761	12,827	8,619	104,825	656	3,574	0	16,493	31,273	200,028	0	85,254	69,971	17,238	17,983	1,437	191,884	8,144	-118,456	
1995	22,200	12,730	7,924	102,615	1,555	8,419	0	10,300	31,525	197,268	0	97,733	59,634	17,616	21,078	1,910	197,970	-702	-119,158	
1996	19,868	12,797	7,978	98,001	710	4,516	0	82	28,950	172,903	0	106,964	69,076	17,673	20,527	1,185	215,425	-42,522	-161,680	
1997	21,235	12,768	8,259	106,542	1,011	6,062	0	17	28,782	184,676	0	116,299	66,431	17,865	21,707	1,569	223,871	-39,195	-200,875	
1998	23,120	12,815	8,271	101,964	1,655	10,346	0	8,323	28,869	195,364	0	103,021	43,158	18,186	23,167	2,253	189,784	5,579	-195,296	
1999	24,513	12,969	8,836	103,634	522	2,879	0	5,796	24,269	183,418	0	114,718	44,193	18,331	25,379	1,985	204,606	-21,188	-216,483	
2000	21,718	13,392	9,518	99,331	500	3,619	507	1,001	23,358	172,944	0	134,423	44,394	18,432	25,511	1,909	224,669	-51,725	-268,208	
2001	22,794	13,404	10,331	98,288	607	4,638	500	6,530	24,478	181,570	7,989	121,151	36,521	18,551	26,438	2,343	212,994	-31,424	-299,632	-31,424
2002	22,543	13,771	10,808	98,820	231	1,818	505	6,500	24,451	179,448	9,458	127,044	38,194	18,577	26,597	2,310	222,179	-42,731	-342,364	-74,155
2003	22,683	14,168	10,829	95,569	865	8,328	185	6,499	23,864	182,990	10,439	124,995	35,167	18,676	27,405	2,589	219,271	-36,280	-378,644	-110,435
2004	21,791	14,125	10,778	101,648	537	5,137	49	7,582	22,669	184,315	10,605	126,609	38,190	18,804	29,274	2,954	226,436	-42,121	-420,765	-152,557
2005	22,138	12,575	7,461	90,538	1,715	17,648	158	12,259	27,956	192,446	9,854	119,393	31,502	18,719	24,581	4,402	208,449	-16,003	-436,768	-168,560
2006	20,865	12,423	7,117	90,327	712	12,940	1,303	34,567	28,982	209,237	16,542	109,125	30,250	18,533	19,319	3,035	196,803	12,434	-424,334	-156,125
2007	20,569	13,234	6,498	88,836	157	4,745	2,993	32,960	26,680	196,673	27,077	121,861	29,649	18,201	18,266	2,141	217,195	-20,522	-444,856	-176,647
2008	20,865	13,285	5,534	87,410	791	10,205	2,340	0	31,965	172,394	30,121	124,030	23,530	18,090	17,223	2,772	215,767	-43,373	-488,229	-220,021
2009	21,992	13,359	5,797	91,650	605	7,543	2,684	0	30,938	174,569	29,012	136,528	23,268	18,140	18,436	2,793	228,178	-53,609	-541,838	-273,629
2010	21,940	13,486	6,117	87,817	1,046	14,139	7,210	5,001	33,008	189,764	28,857	119,036	21,034	18,230	17,848	3,044	208,048	-18,284	-560,122	-291,914
2011	23,077	13,726	6,744	81,096	1,308	16,985	7,743	9,466	33,110	193,255	29,043	98,922	21,021	18,186	17,492	2,890	187,555	5,700	-554,422	-286,213
Statistics for the Post Judgment Period Period 1978 through 2011																				
Total	713,535	436,571	273,395	3,434,235	145,753	246,226	55,073	400,148	1,008,090	6,713,025	208,996	3,416,055	2,285,656	599,297	687,238	70,205	7,267,447	-554,422		
Total (%)	11%	7%	4%	51%	2%	4%	1%	6%	15%	100%	3%	47%	31%	8%	9%	1%	100%	na		
Average	20,986	12,840	8,041	101,007	4,287	7,242	1,620	11,769	29,650	197,442	6,147	100,472	67,225	17,626	20,213	2,065	213,748	-16,307		
Median	21,507	12,821	8,305	102,984	1,177	5,907	166	7,952	30,374	194,309	0	98,327	69,524	17,439	19,034	1,948	216,481	-17,250		
Maximum	24,513	14,528	10,829	116,193	24,697	17,648	8,506	34,567	36,777	239,963	30,121	136,528	117,554	18,804	29,274	4,402	228,816	41,930		
Minimum	16,571	10,220	5,234	81,096	157	1,818	0	0	22,669	172,394	0	65,755	21,021	16,290	14,348	1,005	187,555	-53,609		
Statistics for the Post Peace Agreement Period 2001 through 2011																				
Total	218,180	133,829	81,271	930,904	7,266	87,141	17,926	111,898	274,991	1,863,406	179,953	1,229,771	307,304	184,521	225,387	28,384	2,155,320	-291,914		
Total (%)	12%	7%	4%	50%	0%	5%	1%	6%	15%	100%	8%	57%	14%	9%	10%	1%	100%	na		
Average	21,818	13,383	8,127	93,090	727	8,714	1,793	11,190	27,499	186,341	17,995	122,977	30,730	18,452	22,539	2,838	215,532	-29,191		
Median	21,966	13,382	7,289	91,094	659	7,936	904	6,515	27,318	183,653	13,573	122,946	30,876	18,542	21,950	2,783	216,481	-33,852		
Maximum	22,794	14,168	10,829	101,648	1,715	17,648	7,210	34,567	33,008	209,237	30,121	136,528	38,194	18,804	29,274	4,402	228,178	12,434		
Minimum	20,569	12,423	5,534	87,410	157	1,818	49	0	22,669	172,394	7,989	109,125	21,034	18,090	17,223	2,141	196,803	-53,609		

[1] Includes recharge from onsite wastewater disposal systems and leaks from municpal water systems.

Figure 3-1
Calibration Period Water Balance for the Entire Model Area

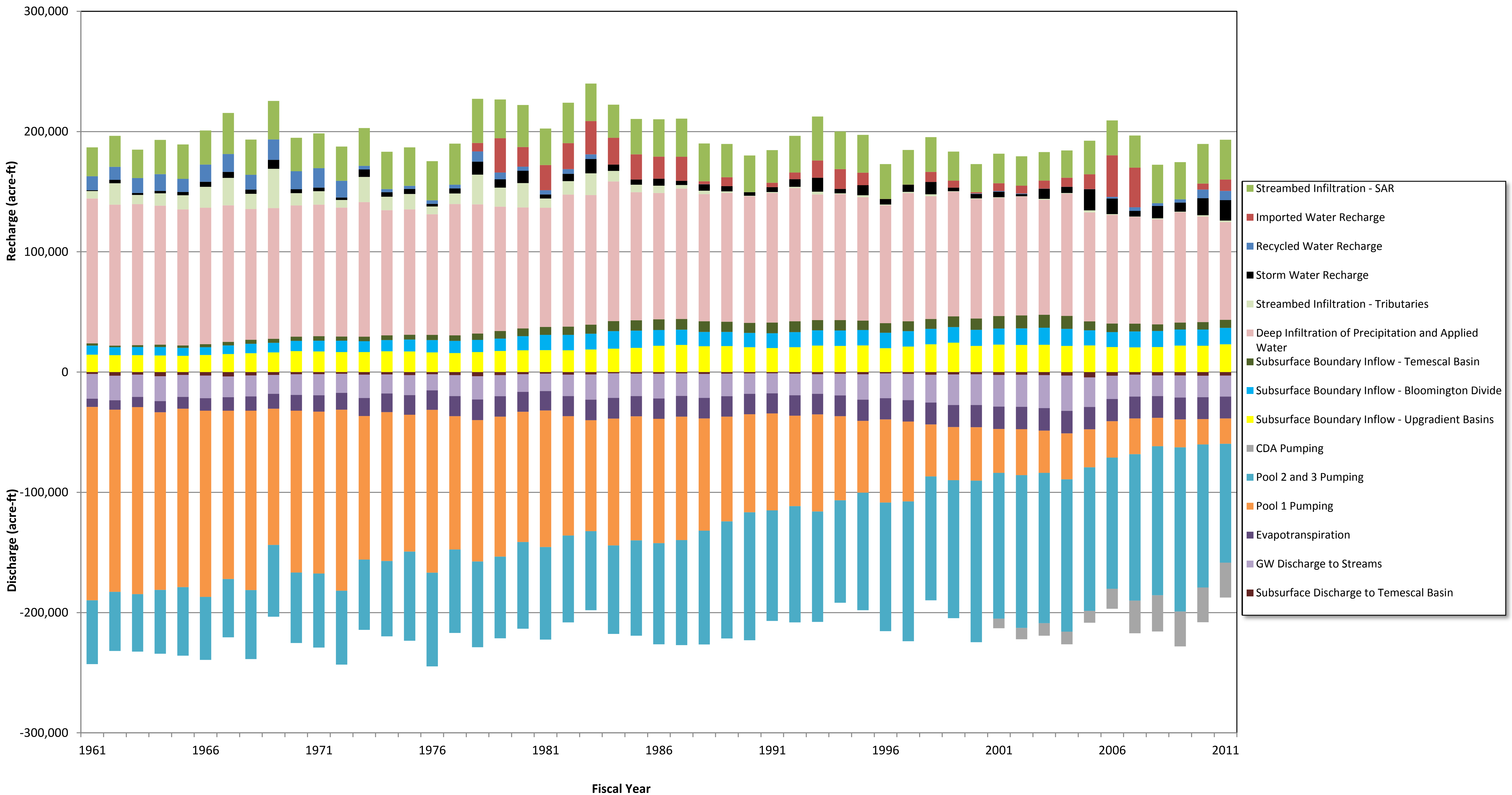

Figure 3-1 Recharge Discharge stresses .xlsx
Revised 10/2/2015

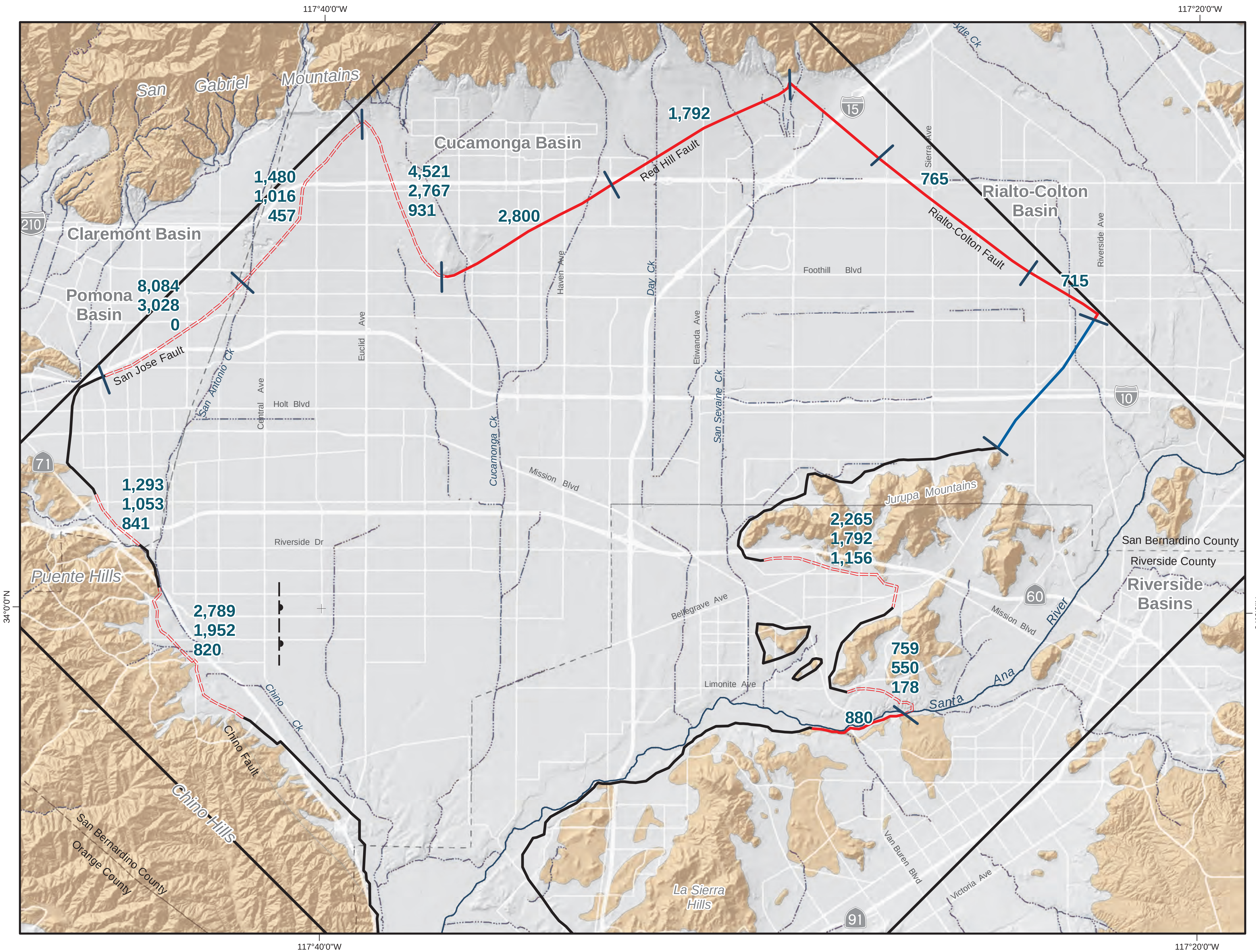

General Head Boundary

Variable Influx Boundary

Constant Influx Boundary

No Flow Boundary

Constant Influx Term

765 Constant Annual Inflow (acre-feet)

Variable Influx Term

2,265 Maximum Inflow (acre-feet)

1,792 Average Inflow (acre-feet)

1,156 Minimum Inflow (acre-feet)

Model Grid Boundary

Geology

Water-Bearing Sediments

Quaternary Alluvium

Consolidated Bedrock

Undifferentiated Pre-Tertiary to Early Pleistocene Igneous, Metamorphic, and Sedimentary Rocks

Faults

Location Certain

Location Approximate

Approximate Location of Groundwater Barrier

Location Concealed

Location Uncertain

Produced by:

WEI
Wildermuth Environmental, Inc.

Author: MJC

Date: 10/1/2015

Document Name: Figure_3-2

0 1 2 3 4 5 Miles

0 2 4 6 8 KM

2013 Chino Basin Groundwater Model Update and Analysis of Safe Yield

Groundwater Model Boundary Conditions

Figure 3-2

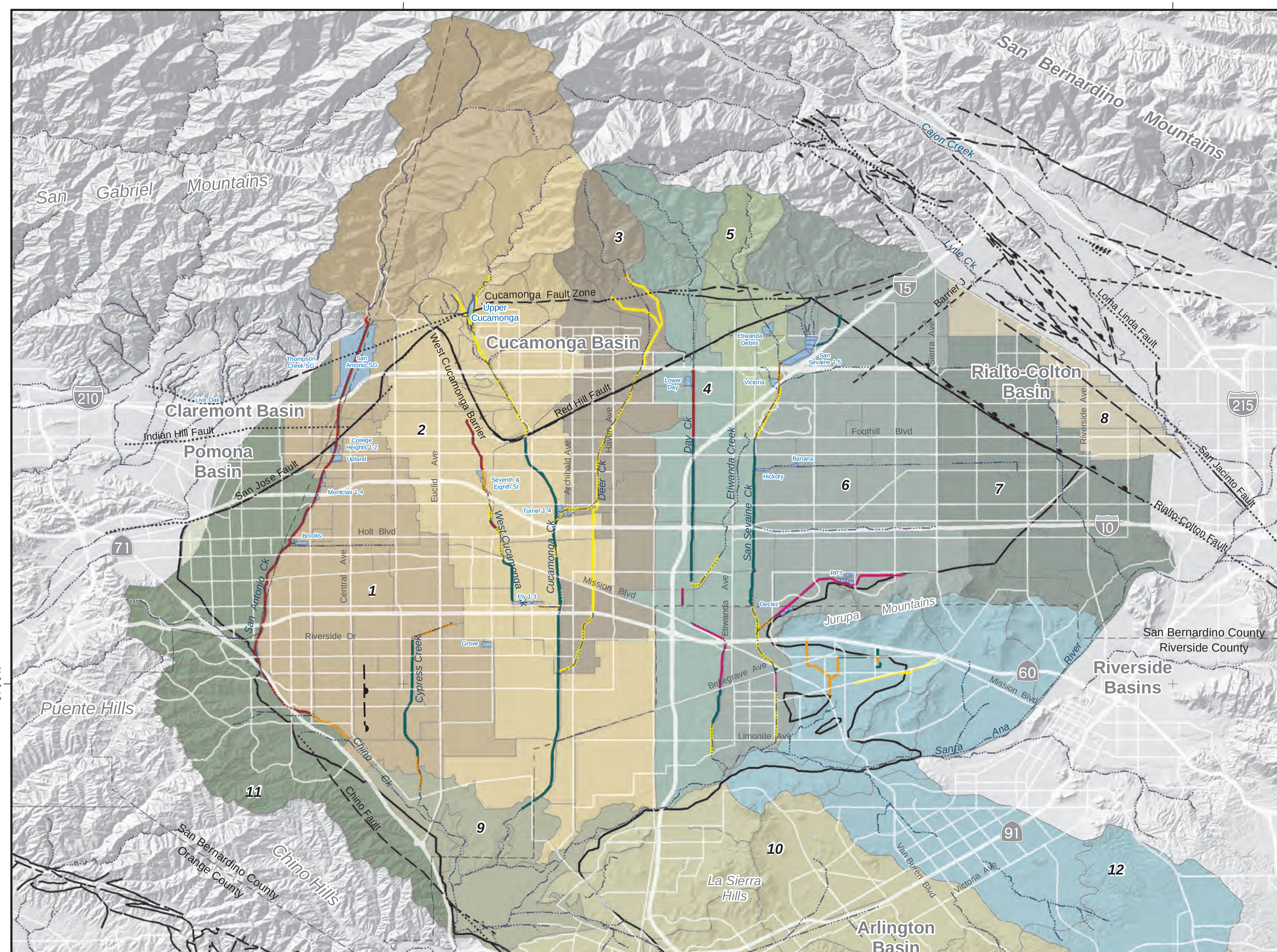

Time Periods in Which Channel Segments Were Lined (years)

- 1950 - 1959
- 1960 - 1969
- 1970 - 1979
- 1980 - 1989
- 1990 - 1999

Hydrologic Sub-Areas

1	San Antonio Creek	7	Fontana
2	Cucamonga Creek	8	Rialto/Colton
3	Deer Creek	9	Prado
4	Day Creek	10	Temescal Creek
5	Etiwanda Creek	11	Chino Creek
6	San Sevaine Creek	12	Riverside

MODFLOW Groundwater Flow Model Boundary

Flood Control and Conservation Basins

Unlined Streams, Rivers, and Flood Control Channels

Faults

- Location Certain
- Location Approximate
- Approximate Location of Groundwater Barrier
- Location Concealed
- Location Uncertain

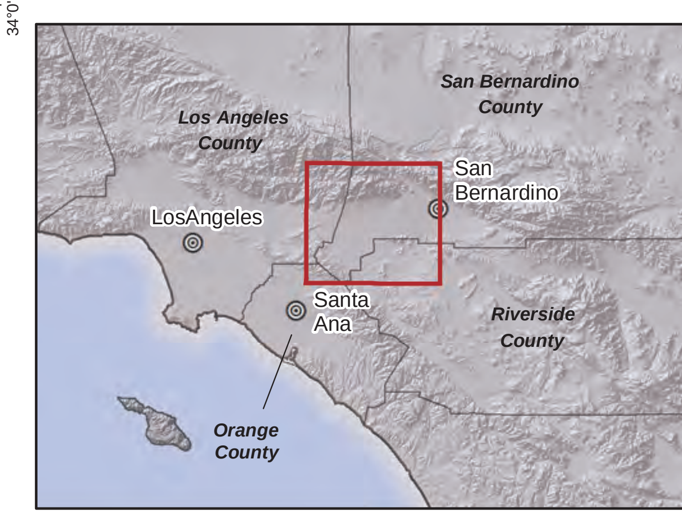

Produced by:

WEI
WILDERMUTH ENVIRONMENTAL, INC.

Author: MJC

Date: 10/1/2015

Document Name: Figure_3-3 channel linings 20140128

0 1 2 3 4 5 Miles

0 2 4 6 8 KM

2013 Chino Basin Groundwater Model Update and Analysis of Safe Yield

Hydrologic Sub-areas, Channel Lining Timeframe and Recharge Facilities

Figure 3-3

Figure 3-4 Streambed Infiltration for the Santa Ana River Tributaries for the Calibration Period, Fiscal 1961 - 2011

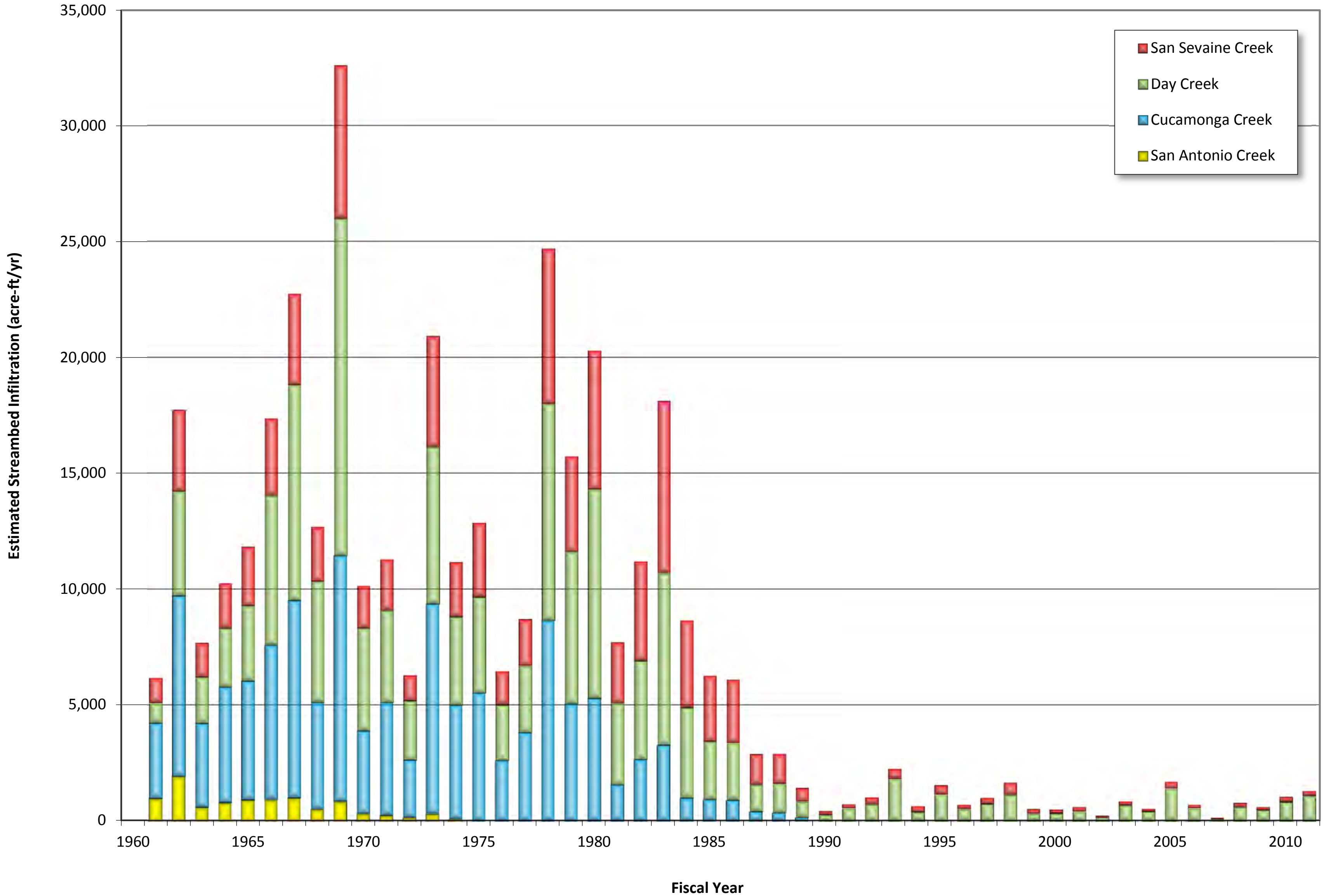

Figure 3-4 Stormwater Recharge .xlsx
Revised 10/2/2015

Figure 3-5
Infiltration at the Root Zone and Recharge at the Water Table

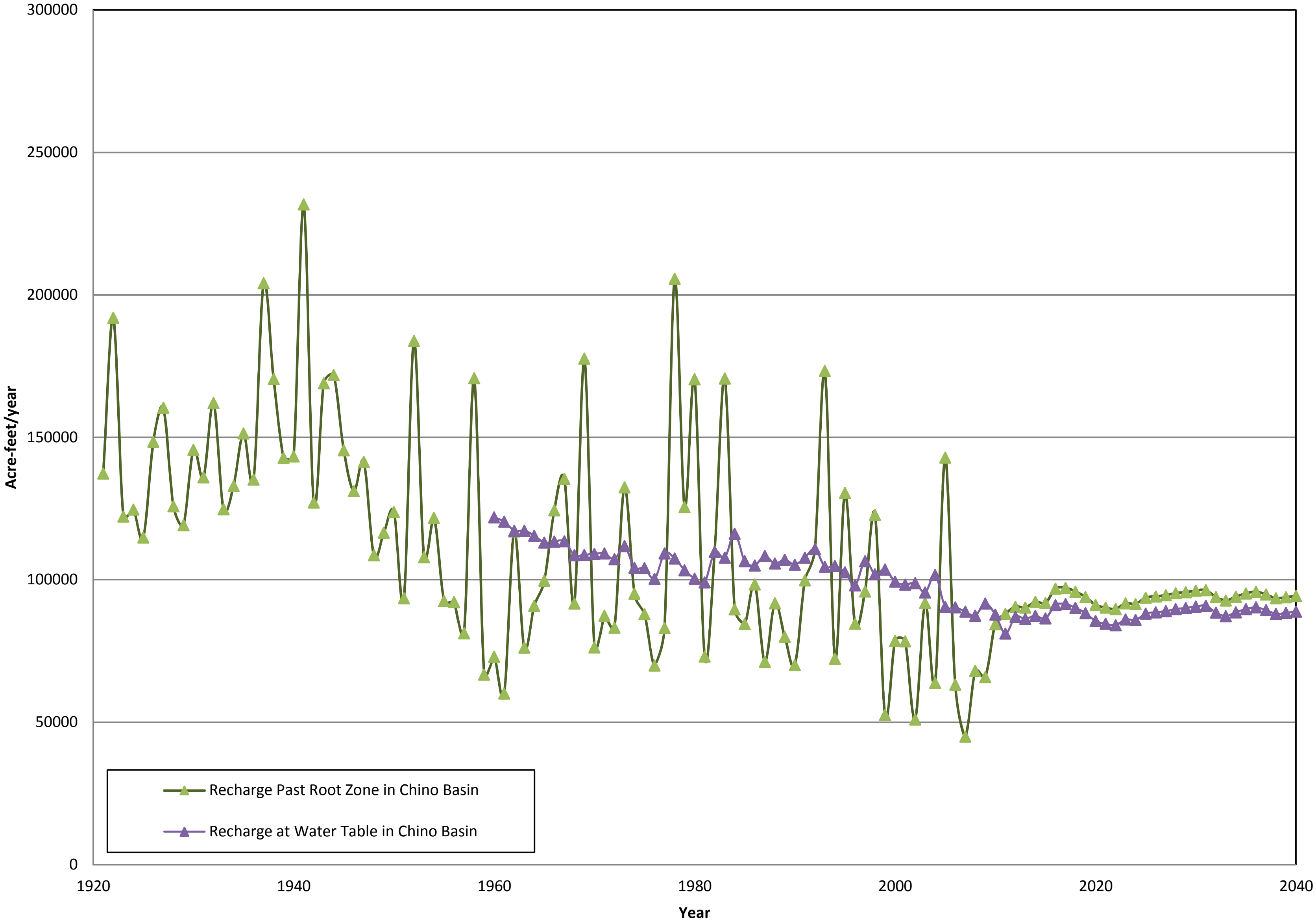

Figure 3-5_DIPAW infiltration.xlsx
Revised 10/2/2015

Figure 3-6
Groundwater Production For the Calibration Period, Fiscal 1960 - 2011

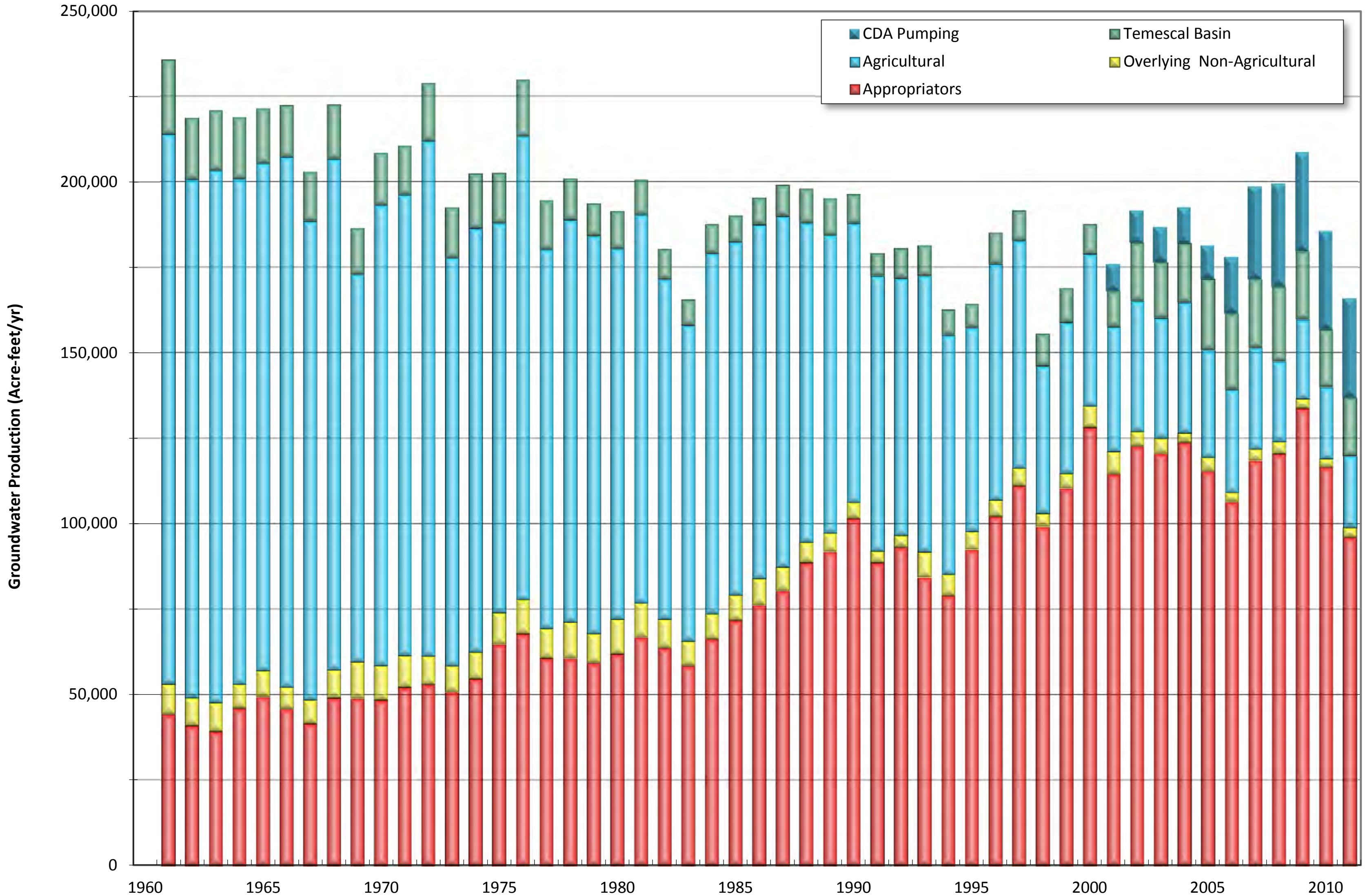

Figure 3-6_20140128.xlsx
Revised 10/2/2015

This section describes the computer codes used in this project and addresses the selection criteria, assumptions, limitations, and governing equations relative to each computer code.

A groundwater flow model was prepared to represent the physical properties of the Chino Basin aquifer system and test conceptual management decisions. This model employed four model codes for the purposes listed below:

- Groundwater flow: MODFLOW (McDonald and Harbaugh, 1988)
- Surface flow, recharge, runoff, and routing: R4 (WEI, 2007)
- Unsaturated flow and transport: HYDRUS-2D (Simunek et al., 1999)
- Parameter estimation and calibration: PEST and SENSAN (Doherty, 2004)

4.1 MODFLOW

The USGS has developed a wide range of computer models to simulate saturated and unsaturated subsurface flow, solute transport, and chemical reactions. The most widely used of these models is MODFLOW (McDonald and Harbaugh, 1988), which simulates three-dimensional groundwater flow using the finite-difference method (Harbaugh, 2005). Although it was conceived solely as a groundwater flow model in 1984, MODFLOW's modular structure has provided a robust framework for the integration of additional simulation capabilities that build on and enhance its original scope. The family of MODFLOW-related models now includes capabilities for simulating coupled groundwater/surface water systems and solute transport.

MODFLOW-2000 (Harbaugh et al, 2000) was chosen for this project because 1) it has extensive publicly available documentation, 2) it has sustained rigorous USGS and academic peer review, 3) it has a long history of development and use, 4) it is widely used around the world in public and private sectors, and 5) it can easily operate with additional simulation tools published by others due to its availability and robust framework.

MODFLOW requires several general assumptions to approximate the partial differential equations that represent flow in a system. The groundwater system must be divided up into a series of finite difference cells, each with uniform hydraulic properties. Boundary conditions must be simplified to constant head, head dependent, or specified flux estimates. Transmissivity is calculated based on the saturated thickness of layers, but it is constant for the entire saturated thickness of each layer. Time must be simplified into a consistent series of discrete time units for the estimation of partial differential equations—the higher the frequency, the longer the processing time. MODFLOW also assumes all groundwater flow is laminar.

There are some limitations to the MODFLOW codes. The limitations of MODLFOW are provided below:

- MODFLOW is only capable of simulating fully saturated groundwater flow and lacks the ability to model groundwater percolating through the unsaturated zone. This limitation was mitigated by combining MODFLOW with HYDRUS-2D.
- There are limitations associated with representing a system as a finite-difference grid. This is not exclusive to MODFLOW. This was mitigated in the approach by using small grid cells.
- The MODFLOW code has a steep learning curve and requires an experienced user to obtain

reliable results.

4.2 R4 Surface Water Simulation Model

TheR4 Model is a comprehensive suite of hydrologic simulation modules that were developed by WEI to support hydrologic decision support processes and groundwater modeling. R4 was used in this investigation to calculate areal recharge from precipitation and irrigation, and storm water recharge that occurs along pervious stream bottoms and in stormwater management basins.[6]

The origin of this model can be traced to the Chino Basin Water Conservation District and Watermaster. These agencies wanted to estimate the volume of stormwater recharge that occurred in recharge basins, flood retention basins, and unlined streams in the Chino Basin. WEI developed a daily simulation model that estimates runoff from daily precipitation, routes the runoff through the Chino Basin drainage system, calculates recharge on a daily basis, and produces reports that summarize recharge performance. This model was initially developed in 1994 for the western portion of the Chino Basin (Mark J. Wildermuth, 1995) and expanded to the entire Chino Basin in 1996 (WEI, 1998). Subsequently, it was used in the Chino Basin to estimate the recharge performance of new basins and the recharge benefits of improved basin maintenance (Black and Veatch, 2001). The model was then expanded to include water quality simulations and applied to the Wasteload Allocation Investigation for the Santa Ana Watershed (WEI, 2002). With the root zone simulation module is capable of estimating all surface water components for the groundwater model: areal recharge from precipitation, returns from urban and agricultural applied water, and stormwater infiltration in the basins and channel systems. The model has been used for several groundwater models developed by WEI, including models of the Chino Basin (WEI, 2003) the Beaumont Basin (WEI, 2005) the Arlington Basin (WEI, 2007) and the six Basins are and the Cucamonga Basin[7].

The rainfall module consists of several procedures that prepare the hydrologic data, which include precipitation, evaporation, evapotranspiration, and geographic data, such as land use, soil type, vegetation, etc. The study area is subdivided based on land use, soil, vegetation, natural drainage, and urban stormwater management plans.

The runoff module calculates daily runoff and abstractions from precipitation data for each drainage area using a modified Soil Conservation Service (SCS) method. The runoff module summarizes data and prepares two files: runoff for the router module and soil zone infiltration for the root zone module.

The router module collects stormwater runoff from sub-drainage areas, point discharge data, and boundary inflow data from mountain watersheds, and routes the combined water through drainage systems and retention/recharge basins. This module calculates infiltration through pervious stream bottoms, simulates retention/recharge basins using a modified pulse method, and calculates the infiltration of water through pervious bottoms and basin sides as and evaporation from the free surface.

---

[6] Documentation for the R4 Model is included as Appendix A in the report entitled: " 2007 CBWM Model Documentation and Evaluation of the Peace II project Description (WEI, 2007).

[7] The R4 Model is being used in the Six Basins area and the Cucamonga Basin is as of the date of this draft report (January 28, 2014) to estimate areal recharge for use in new groundwater models. These new groundwater models are being developed to evaluate proposed groundwater management plans and to estimate safe yield.

The root zone module is a soil moisture accounting model. It estimates the evapotranspiration requirement for the vegetation type on pervious area and uses the estimated precipitation infiltration provided by runoff module to estimate estimates the irrigation water requirement. Precipitation infiltration and applied irrigation water are then routed through the root zone on a daily time step. When the volume of water in the root zone exceeds the storage capacity of the root zone the excess precipitation and or irrigation water passes the soil zone and percolates to the groundwater basin. The model summarizes the irrigation water requirement and deep percolation on monthly basis and is imported to the groundwater model.

4.3 HYDRUS-2D

The HYDRUS-2D software package is a major upgrade and extension of the HYDRUS-2D/MESHGEN-2D software package that was originally developed and released by the U.S. Salinity Laboratory, PC-Progress, and the International Ground Water Modeling Center. HYDRUS-2D is a Microsoft Windows-based modeling environment for the analysis of water flow and solute and heat transport in variably saturated porous media.

The HYDRUS-2D (Simunek et al., 1999) computer model was used to simulate unsaturated flow and solute transport in the Chino Basin. This program numerically solves the Richards equation for saturated-unsaturated flow and the Fickian-based advection-dispersion equations for heat and solute transport. This program can be used to analyze water and solute movement in unsaturated, partially saturated, or fully saturated porous media.

HYDRUS-2D has been updated numerous times since its development. It is currently used worldwide and is arguably considered a standard in unsaturated flow modeling. The program continues to be updated and supported. The specific application of HYDRUS-2D for this model is to estimate the travel time of areal recharge from the root zone to the water table.[8]

4.4 PEST and SENSAN

PEST (Doherty, 2004), an acronym for Parameter ESTimation, is a computer code for model calibration and predictive analysis. During the calibration process, parameters are adjusted until model generated results fit a set of observations as closely as possible. PEST adjusts model parameters until the fit between model outputs and field observations are optimized in terms of the weighted least squares. PEST is not unique to groundwater flow models or MODFLOW. PEST is a public domain code that applies the Gauss-Marquardt-Levenberg algorithm. The mathematics of PEST is further described in Section 6 of this report. PEST has been successfully applied in many fields of the geophysical sciences, including groundwater modeling. It has been proven to be a robust tool and was therefore applied to the Chino Basin groundwater model.

SENSAN (Doherty, 2004), an acronym for SENSitivity ANalysis, is a command-line program that provides the ability to carry out multiple model runs in parallel. WEI is able to operate 24 systems in parallel with key model output from each run being recorded for later analysis. This allows for very complex multiple parameter sensitivity analyses to be completed in a much shorter time period.

[8] Documentation for the use and application of HYDRUS for the 2007 CBWM Model and the 2013 Watermaster Model is included as Appendix B in the report entitled: " 2007 CBWM Model Documentation and Evaluation of the Peace II project Description (WEI, 2007).

PEST and SENSAN are prepared by Watermark Consulting and distributed as standalone packages as well as with numerous groundwater modeling packages (e.g. Groundwater Vistas and Groundwater Modeling System). The PEST software bundle was first distributed in 1994 and has since been updated five times.

PEST and SENSAN were chosen for this project because 1) they reduce modeling time and significantly increase the value of the results, 2) the software has extensive publicly available documentation, 3) it has a strong history of development, and 4) it is considered a standard in the groundwater industry and has been incorporated into most MODFLOW model processors.

This section describes how the conceptual model of the groundwater system, as described in Section 2, was translated into a numerical model. The topics discussed in this section include the model domain and grid, the assignment of hydraulic properties to the model grid, the initial conditions, and the boundary conditions.

5.1 Model Domain and Grid

The model domain and the model grid within the domain are shown in Figure 5-1. The model grid consists of 577 rows, 562 columns, and three layers. Horizontally, each cell has a dimension of 60 by 60 meters (196 by 196 feet). This fine cell size was selected to model the curvature of drawdown near the desalter wells and to provide a model that is flexible for potential future needs. The grid cells are designated as "inactive" outside the model domain and as "active" inside the domain. There are a total of 494,634 active cells.

The spatial extent of the model domain was determined by the saturated extent and thickness of the aquifer system; the extent was limited to regions where the saturated thickness was greater than about 40 feet. The saturated thickness was determined based on initial condition water levels and the effective base of the aquifer.

The vertical extent of the model is comprised of three layers, representing three hydrostratigraphic layers. The discretization of these layers is discussed in Section 2.5. Layer 1 represents the unconfined system, is classified as an unconfined aquifer within the MODFLOW model, and has a minimum thickness of 75 feet and maximum thickness of 1,300 feet. Layer 2 is classified as a confined aquifer within the MODFLOW model. Layer 2 has a minimum thickness of 30 feet and a maximum thickness of 600 feet. Layer 3 is also classified as a confined aquifer within the MODFLOW model. Layer 3 has a minimum thickness of 75 feet and maximum thickness of 925 feet.

As discussed in Section 2, there is no layer 3 in the Chino East and Chino South area, in where numerical model has only two active layers.

5.2 Time Discretization

The discretization of time is a critical step in model construction because the resolution of model results is related to the stress period of the model. The temporal discretization in MODFLOW 2000 includes stress periods and time steps. The transient stress period of the model is three months or one-quarter year, based primarily on the availability of historic pumping and the distinct seasonal features of water recharge, such as precipitation, irrigation return flow, and stream flow.

5.3 Hydraulic Properties and Zonation

The hydraulic properties used in the model include horizontal hydraulic conductivity, vertical hydraulic conductivity, the specific yield for an unconfined aquifer, and the specific storage for confined aquifers. Although the hydrogeologic systems in the Chino Basin are inherently heterogeneous on many scales, site-scale hydrogeologic heterogeneity was incorporated into this revised model.

In general, the values of hydraulic parameters vary systematically with sediment texture classes (McCuen, et al., 1981). The definition of hydraulic conductivity suggests that its value increases with the median grain size. For a given median grain size, hydraulic conductivity is lower in a poorly sorted medium than in well-sorted medium because poorly sorted mediums have a smaller effective grain size. In section 2.6, hydraulic properties of aquifers and their distribution fields in the Chino and Temescal Basins were shown in the cell basis based only on lithological model. However, other factors, such as sorting and compaction, can also significantly affect the values of hydraulic properties. For example, well-sorted sand or gravel in the river channel characterizes higher porosity and hydraulic conductivity than glacial deposit, and compaction reduces the pore space of sediment deposit, resulting lower porosity and hydraulic conductivity.

Sorting is the process by which sediment grains are selected and separated according to the grain size by the agents of transportation. Sediment sorting is directly related to the environment of deposition. In the Chino Basin, the environments of deposition include alluvial fan, river channel, floodplain, and lake. The purpose of hydraulic parameter zonation is to take sorting or environment of deposition into account. Compaction is in general related to the depth of sediment deposit. In another words, layering is necessary for the identification of hydraulic parameters.

In an attempt to reduce the number of parameters to a manageable level, the model domain was subdivided into a number of zones of assumed similar parameter values. Zonation is a way to reduce the number of estimated parameters and thus make inverse modeling possible. The hydraulic parameter zonation in the basin is based on 1) geologic and geomorphologic condition, 2) hydrogeological condition, 3) the location of final selected calibration wells, and 4) the capability and flexibility of selected numerical tool and computer resources to handle zone parameters. Figures 5-2 through 5-4 show the parameter zonation, composite zonation, and its base parameters of horizontal hydraulic conductivity in each layer, respectively. Vertical hydraulic conductivity, specific yield in unconfined layer, and specific storage in confined aquifer layers display the same or similar parameter zonation and composite zonation. Composite zonation described here is consisted of several parameter zones with similar environments of deposition, such as alluvial fan, river channels, floodplain, or lake deposit. The purpose of composite zonation is to further reduce the number of calibration parameters in the inverse modeling.

The hydraulic property values in each cell of the model domain were then calculated using MODFLOW 2000 based on the following equations:

$$K_h(i,j,k) = XK_h(zone) \times KH(i,j,k)$$
$$K_v(i,j,k) = XK_v(zone) \times KV(i,j,k)$$
$$S_y(i,j,k) = XS_y(zone) \times SY(i,j,k)$$

Where *i, j, and k* represent row, column, and layer in the model domain; and, $XK_h(zone)$, $XK_v(zone)$, and $XS_y(zone)$ are the model base parameter of horizontal hydraulic conductivity, vertical hydraulic conductivity, and specific yield or specific storage in each zonation. KH, KV, and SY are the estimates of horizontal hydraulic conductivity, vertical hydraulic conductivity, and specific yield from lithological model at the location of row, column, and layer. Simply put, the calculated parameter value is the product of the zonation base value and the hydraulic parameter value in an individual cell. This allows for the model to have a heterogeneous K_h, K_v, S_y, and S_s. The model parameters XK_h(zone), XK_v(zone), and XS_y(zone) will be adjusted in the calibration processes.

A total of 31 zones comprise layer 1 of the model domain, 20 zones comprise layer 2 and 15 zones comprise layer 3. As shown in Figure 5-2 through Figure 5-4, there are 11 composite zones in layer 1, 7 composite zones in layer 2, and 9 composite zones in layer 3. Table 5-1 lists all of the model initial estimated parameter values by composite zone and layer. These initial estimates were indirectly derived from the earlier version Chino groundwater model with the knowledge of the new Kriging-estimated KH, KV, and SY. Generally, hydraulic conductivities decrease with depth because deeper sediments typically have experienced compaction.

5.4 Initial Condition

An initial condition is required to solve numerical groundwater flow problems. The initial condition for the Chino Basin flow model was the water level distribution at the beginning of the transient simulation period. The calibration period starts in fiscal year 1960/61 and ends fiscal year 2005/06. The model's initial condition was based on published water level maps (JMM, 1992) and historic water level records. The initial condition or water level contour map was further adjusted in areas lacking water level data, using the estimated hydraulic parameters to extrapolate reasonable hydraulic gradients. Figure 5-6 is the final water level elevation contour map, representing the initial condition of groundwater flow for layers 1, 2, and 3. All layers started with the same initial head for the following reasons: 1) there was limited deep pumping before the 1960s, and 2) the deep pumping that occurred before 1960 was located in areas of high vertical hydraulic conductivity, which made the water level in the different layers very similar.

5.5 Boundary Conditions

Boundary conditions are necessary in solving numerical groundwater flow problems. Ideally, in groundwater investigations, the study area is bound by identifiable hydrogeologic features that can be quantified relative to the groundwater system. These boundaries can also occur within the active model domain (*e.g.* a creek). For the study area, the numerous faults and groundwater divides required calculations of inflow from these boundaries. Boundary conditions from creeks were developed outside of the groundwater model and were input as a given flux for a model stress period. Boundary inflows across fault zones (*e.g.* the San Jose Fault and Red Hill Fault) were determined during the calibration process.

Table 5-2 lists the boundary conditions by geographic name, the type of boundary, and the MODFLOW package utilized to simulate the boundary. Figure 5-7 shows the boundary condition inflows in the calibration period.

The boundary condition along Bloomington Divide was carefully specified. The Bloomington Divide is regarded as a groundwater divide (USGS, 1967); however, more recent studies (WEI, 2003, 2006) have postulated that a certain amount of water recharges from the east side across the north part of the divide. Figure 5-8 shows the locations of wells with historical water level measurements. Figure 5-9 shows that the water levels in wells located on the north side of Rialto-Colton Fault, near Bloomington, are about 50 to 100 feet higher than those on the south side. Figure 5-10 shows that the water levels on the east side of the "divide" are about 20 feet higher than the water levels on the west side and that the water levels in the north along the "divide" are higher than those in the south. This similar groundwater level fluctuation indicates a hydraulic connection from the north of the fault, through the east of the divide, to the west of the divide. Based on relatively detailed water level data along the divide (historical groundwater measurements), the boundary condition during the calibration period was set as a variable head boundary. The hydraulic conductivity of layers 1 and 3 in the divide area was then calibrated using local historical water level measurements. The boundary inflow was therefore computed using calibrated hydraulic conductivity and boundary heads or water levels during the calibration.

5.5.1 MODFLOW Packages for Boundary Conditions

5.5.1.1 Recharge Package

The Recharge Package (McDonald and Harbaugh, 1988) was used to simulate the deep percolation (areal recharge) from precipitation and applied water (*e.g.* agricultural and landscape irrigation). This package was used to assign a constant flux for each stress period. The flux rates were determined using the R4 Model. The following factors were used by the model to compute the deep percolation of precipitation and applied water: historical daily rainfall, daily evapotranspiration, soil type, drainage area, and estimated irrigation rates based on land use. The output from the R4 Model is the calculated recharge out of the root zone into the vadose zone. An unsaturated flow and transport model, HYDRUS-2D, calculated the amount of time for recharge to travel from the root zone to the piezometric surface. The Recharge Package applies a constant flux to the piezometric surface. The Recharge Package used the R4 Model results that had been time adjusted (or lagged) based on calculated travel time from the root zone to the piezometric surface.

5.5.1.2 Flow and Head Boundary Package (FHB)

The Flow and Head Boundary Package (Leake and Lilly, 1997) was used to specify subsurface inflows to the study area aquifer system and to specify streambed percolation along unlined channels of upper Santa Ana River tributaries that cross the model domain, storm water recharge, and supplemental recharge. The Flow and Head Boundary Package allows MODFLOW users to specify flow or head boundary conditions that vary at times other than the starting and ending times of stress periods and associated time steps.

5.5.1.3 Evapotranspiration Package (EVT)

The MODFLOW ET Package was used in the model to simulate the discharge of water to evaporation and transpiration in the Prado Basin. For the remainder of the study area, it was assumed that ET does not occur from the saturated zone.

The ET Package simulates ET with a relationship between the ET rate and hydraulic head. In the ET Package, the relation of the ET rate to the hydraulic head is conceptualized as a piece-wise linear curve relating the ET surface, defined as the elevation where the evapotranspiration rate reaches a maximum, and an elevation located at an extinction depth below the evaporation surface where the evapotranspiration rate reaches zero (Banta, 2000).

The ET rate for a model cell is calculated for each stress period based on its calculated head, the ET Surface value, the Extinction Depth, and the maximum ET flux rate. If the elevation of the calculated head in the cell is at or above the ET surface value, the ET rate is the maximum evapotranspiration rate (high groundwater condition). If the calculated head is equal to or below the extinction depth, the evapotranspiration rate is zero (low groundwater dry condition). When the head is between the ET Surface and the Extinction Depth, the ET rate is a linear function of the head below the ET Surface. This relation is defined by the equation below:

$$Q_{ET} = Q_{ETMax}\left(1 - \frac{D}{X}\right)$$

Where Q is the volumetric evapotranspiration rate for the cell, Q_{ETMAX} is the maximum evapotranspiration flux rate times the area of the cell, D is the depth of the head below the ET surface, and X is the extinction depth.

5.5.1.4 Well Package (WEL)

The Well Package was used to simulate the withdrawal of water from aquifers by wells. The Well Package can also be used to simulate any other source of withdrawal or recharge that occurs at a known rate, including specified flow boundaries. This package uses a constant flow rate for each stress period.

5.5.1.5 Stream Package (STR)

The Stream Package was used to simulate the Santa Ana River and the lower reaches of some of its tributaries in the Prado Basin. The Stream Package (Prudic, 1998) was used to simulate stream aquifer interactions. The Stream Package routes surface flow and calculates flow to and from the aquifer based on the elevation of a stream, water level in the stream, piezometric surface of the aquifer, and conductance of the stream bottom. The shift from recharge of the aquifer to discharge to the stream occurs at the point where the head in the aquifer equals the head in the stream.

Streams were divided into segments and reaches with each reach corresponding to a single cell in MODFLOW. Reaches were grouped into segments. Each segment consists of a series of contiguous reaches where flows can be routed.

Flow between a stream and an aquifer is computed using the streambed's conductance, the head in the stream, and the calculated head of the aquifer in each cell. Volumetric flow between the streambed and groundwater system is computed as:

$$Q_{STR} = C_{STR}\ (h_{STR} - h(i,j,k))$$

Where Q_{STR} is the flow rate across the streambed, C_{STR} is the conductance of the riverbed, h_{STR} is the head in stream stage, and $h(i,j,k)$ is the hydraulic head in the cell of row i, column j, and layer k underlying the streambed.

The conductance of the riverbed is given by:

$$C_{STR} = (K_v LW)/M$$

Where K_v is the vertical hydraulic conductivity of the riverbed sediment, W is the width of the river reach, L is the length of the river reach, and M is the thickness of riverbed sediment.

However, K, W, L, and M are not individually specified. Instead, conductance of the riverbed (C_{STR}) is specified. The stream segment is specified such that the conductance of the riverbed in each segment remains constant but varies from one segment to another segment.

Figure 5-11 shows the stream segments and reaches in the Chino and Temescal Basins. The streambed elevations along creeks and channels were extracted from the USGS 10-meter digital elevation model (DEM) cell by cell. The assigned streambed elevations are about 3-10 feet below the DEM elevation, depending on location, because the center of a model stream cell is not exactly located in the middle of a stream.

The stream stage in each reach was computed using Manning's equation prior to calculating leakage to or from the aquifer. The stage for each reach was calculated using the specified inflow into the stream segment. The initial slope of the stream channel was computed based on the 10-meter DEM. The stream channel slopes were further adjusted as needed to ensure a decreasing slope.. The estimates of Manning's roughness coefficient were based on the streambed characteristics of the Santa Ana River and its tributaries; the values range from 0.025 to 0.04. If no stream flow is specified into a segment, the stage for all reaches in the segment will equal the top of the streambed. Leakage was iteratively computed on the basis of the computed stream stage, streambed conductance, and head for each model cell.

5.5.2 Other MODFLOW Packages

5.5.2.1 Geometric Multigrid Solver Package (GMG)

The Geometric Multigrid Solver Package (GMG) was selected as a numerical solver in the MODFLOW 2000 model. When calibration was initiated, the convergence criteria were set with a head change criterion for convergence (HCLOSE) of 0.01 feet and a residual criterion for convergence (RCLOSE) of 100. However, these strict criteria provided only a limited improvement of the solution at the cost of a longer computation time. Considering the long computing time required with PEST inverse modeling, the MODFLOW 2000 closure criteria were relaxed to reduce computation time during the calibration without reducing the precision of solution. Head change criterion for convergence was set to 0.1 feet (HCLOSE) and residual criterion for convergence was set to 1000 (RCLOSE). To be consistent, the criteria remained the same as in calibration model for all future flow simulations.

5.5.2.2 Head-Observation Package (HOB)

The Head-Observation Package (HOB) was used to specify observations of head for use in the observation process. More than 11,000 observation points from 67 calibration wells in the calibration period were read. HOB package generates model-calculated values for comparison with measured ones.

5.5.2.3 Sensitivity Process Package (SEN)

The Sensitivity Process Package (SEN) was used to calculate the sensitivity of hydraulic heads throughout the model with respect to specified parameters using the accurate sensitivity-equation method.

Table 5-1. Model Parameters, Zonation, and Initial Estimates

Model Parameter name	Parameter Type	Layer	Zone	Initial Value
hk1z1	XKh(zone)	1	1-2-3-4	2.50E+00
hk1z5	XKh(zone)	1	5	1.25E+00
hk1z6	XKh(zone)	1	6-7-8-10	6.80E-01
hk1z11	XKh(zone)	1	11-12	1.40E+00
hk1z13	XKh(zone)	1	13-14-15-23-24	7.50E-01
hk1z16	XKh(zone)	1	9-16	4.70E-01
hk1z17	XKh(zone)	1	17-18-27-28	1.61E+00
hk1z19	XKh(zone)	1	19-20-21	1.20E+00
hk1z22	XKh(zone)	1	22-25-26	3.40E-01
hk1z29	XKh(zone)	1	29-31	8.50E-01
hk1z31	XKh(zone)	1	30-32	4.90E-01
sy1z1	XSY(Zone)	1	1-2-3-4-5	1.01E+00
sy1z3	XSY(Zone)	1	6-7-8-10-11-12	5.10E-01
sy1z13	XSY(Zone)	1	13-14-15-9-16-23-24	7.10E-01
sy1z17	XSY(Zone)	1	17-18-19-27-28-20-21	6.40E-01
sy1z22	XSY(Zone)	1	22-25-26	5.60E-01
sy1z29	XSY(Zone)	1	29-31	6.10E-01
sy1z30	XSY(Zone)	1	30-32	1.01E+00
vk1z1	XVk(Zone)	1	1-2-3-4-5-6-7-8-10-11	3.27E+01
vk1z9	XVk(Zone)	1	9-13-15-16-17-22-24-25-26-27	1.87E+00
vk1z14	XVk(Zone)	1	14-23	1.80E-04
vk1z17	XVk(Zone)	1	18-19-20-21-12-28-29-30-31-32	3.40E+01
hk2z1	XKh(zone)	2	1-2-3-4	3.40E-01
hk2z8	XKh(zone)	2	9-10-11-18	5.00E-01
hk2z5	XKh(zone)	2	5-7-8	1.10E-01
hk2z13	XKh(zone)	2	6-13	2.20E-01
hk2z12	XKh(zone)	2	12-15-16-17-14	1.90E-01
hk2z19	XKh(zone)	2	19	1.60E-01
hk2z20	XKh(zone)	2	20-21	1.60E-01
ss2z1	XSS(Zone)	2	1-2-3-4	1.43E-04

Table 5-1. Model Parameters, Zonation, and Initial Estimates

Model Parameter name	Parameter Type	Layer	Zone	Initial Value
ss2z5	XSS(Zone)	2	5-6-7-8-13-14-16	1.43E-04
ss2z9	XSS(Zone)	2	9-10-11-12-15-17-18	1.43E-04
ss2z19	XSS(Zone)	2	19	1.43E-04
ss2z20	XSS(Zone)	2	20-21	1.43E-04
vk2z1	XVk(Zone)	2	1-2-3-4-9-10-11-18	7.01E+00
vk2z5	XVk(Zone)	2	5-7-8-14-16-12-15-16-17	5.00E-01
vk2z6	XVk(Zone)	2	6-13	1.40E-04
vk2z17	XVk(Zone)	2	19-20-21	1.40E+01
hk3z1	XKh(zone)	3	1-2	1.80E-01
hk3z3	XKh(zone)	3	3	2.40E-01
hk3z4	XKh(zone)	3	4-5-	1.30E-01
hk3z6	XKh(zone)	3	6-7	2.80E-01
hk3z9	XKh(zone)	3	9-11	1.90E-01
hk3z10	XKh(zone)	3	8-10	1.80E-01
hk3z12	XKh(zone)	3	12-13	2.80E-01
hk3z14	XKh(zone)	3	14	2.20E-01
hk3z15	XKh(zone)	3	15-16	3.00E-01
ss3z1	XSS(Zone)	3	1-2-3	1.43E-04
ss3z4	XSS(Zone)	3	4-5-	1.43E-04
ss3z6	XSS(Zone)	3	6-7-9-11	1.43E-04
ss3z8	XSS(Zone)	3	8-10	1.43E-04
ss3z12	XSS(Zone)	3	12-13-	1.43E-04
ss3z14	XSS(Zone)	3	14-	1.43E-04
ss3z15	XSS(Zone)	3	15-16	1.43E-04
vk3z1	XVk(Zone)	3	1-2-	1.08E+00
vk3z3	XVk(Zone)	3	3	3.40E+01
vk3z4	XVk(Zone)	3	4-5-	1.70E+01
vk3z6	XVk(Zone)	3	6-7	3.60E-01
vk3z9	XVk(Zone)	3	9-11	4.30E-02
vk3z10	XVk(Zone)	3	8-10	1.00E-04
vk3z12	XVk(Zone)	3	12-13	1.03E+01
vk3z14	XVk(Zone)	3	14	2.95E+00
vk3z15	XVk(Zone)	3	15-16	6.40E+00
hfb1	HFB	2, 3		1.43E-03

Table 5-2
Boundary Conditions

Geographic Name	Boundary Condition	MODFLOW Package Applied for Condition
Red Hill Fault	Constant Flux	FHB[1]
Red Hill Fault	Variable Flux	FHB[1]
San Jose Fault	Variable Flux	FHB[1]
Groundwater divide (Chino Basin from the Spadra Basin)	No Flow	NA
Puente Hills/Chino Hills	Variable Flux	FHB[1]
La Sierra Hills	Variable Flux	FHB[1]
Riverside Narrows	Variable Flux	FHB[2]
Jurupa Mountains and Pedley Hills	Variable Flux	FHB[1]
Bloomington Divide	Variable Head	FHB[2]
Rialto-Colton Fault	Constant Flux	FHB[1]
Extension of the Rialto-Colton Fault north of Barrier J	Constant Flux	FHB[1]
Santa Ana Mountains	Variable Flux	FHB[2]
Arlington Narrows	Variable Flux	FHB[2]
Areal Recharge	Variable Flux	RCH[3]
Wells	Variable Flux	WEL[4]
Santa Ana River	Variable Flux	STR[5]
Cucamonga Creek	Variable Flux	FHB[1]
Chino Creek	Variable Flux	FHB[1]
Day Creek	Variable Flux	FHB[1]
Artificial Recharge Basins	Variable Flux	FHB[1]
Stormwater Recharge	Variable Flux	FHB[1]
Evapotranspiration	Variable Flux	EVT[6]
Calculated Stream Recharge for Upper Tributaries (calibration only)	Variable Flux	FHB[1]

1. FHB - Flow Head Boundary Package - constant and variable flux
2. FHB - Flow Head Boundary Package - variable head for calibration period and constant flux for planning alternatives
3. RCH - Recharge Package
4. WEL - Well Package
5. STR - Stream Package
6. EVT - Evapotranspiration Package

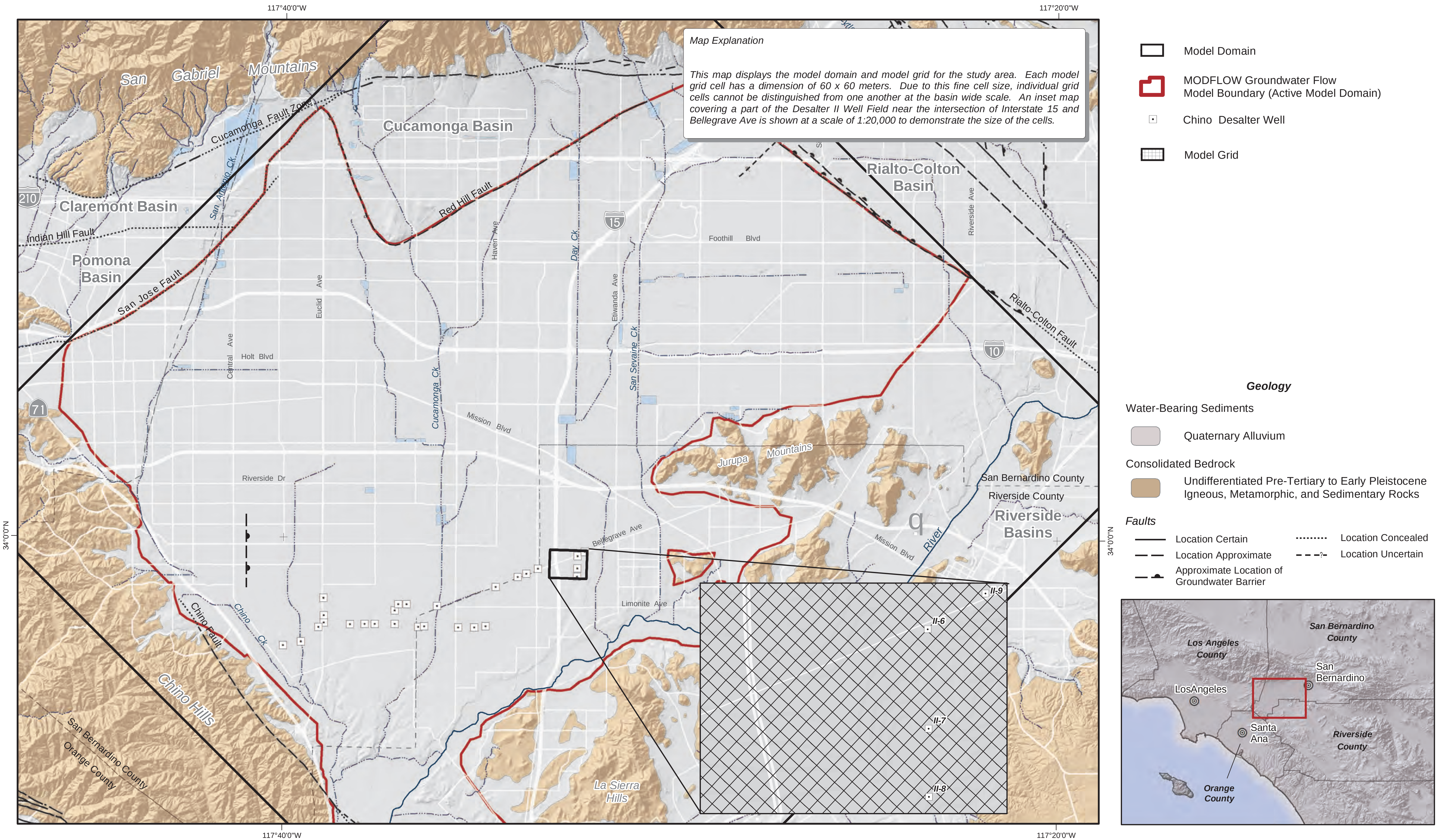

Produced by:

WEI
Wildermuth Environmental, Inc.

Author: MJC
Date: 10/1/2015
Document Name: Figure_5-1

2013 Chino Basin Groundwater Model Update and Analysis of Safe Yield

Map of Model Domain and Model Grid

Figure 5-1

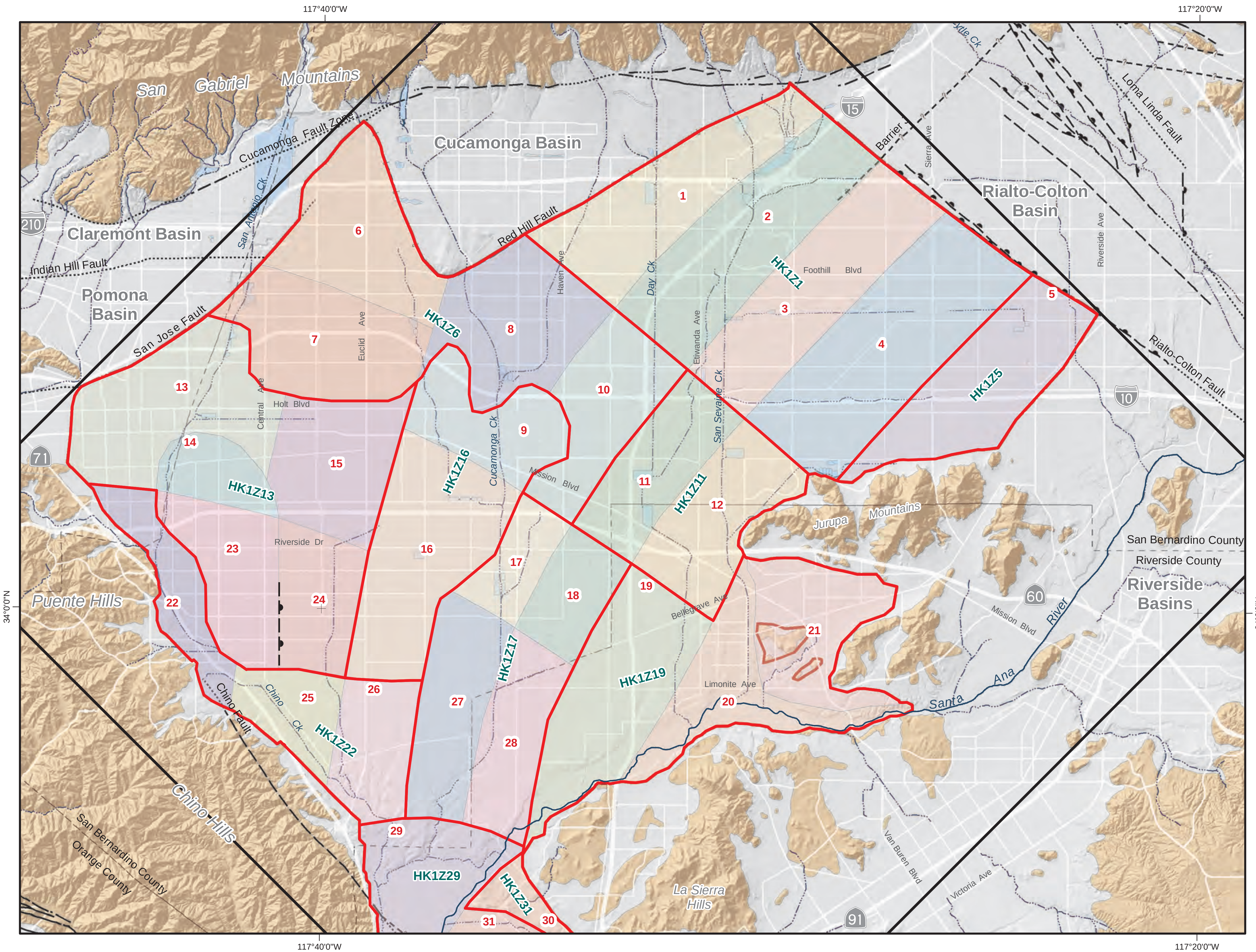

Calibration Zonation and Parameter

Calibration Composite Zone and Parameter Name

Zone and Number

Model Grid Boundary

Geology

Water-Bearing Sediments

Quaternary Alluvium

Consolidated Bedrock

Undifferentiated Pre-Tertiary to Early Pleistocene Igneous, Metamorphic, and Sedimentary Rocks

Faults

Location Certain

Location Approximate

Approximate Location of Groundwater Barrier

Location Concealed

Location Uncertain

Produced by:

WEI
Wildermuth Environmental, Inc.

Author: MJC

Date: 10/1/2015

Document Name: Figure_5-2a_20130801

0 1 2 3 4 5 Miles

0 2 4 6 8 KM

2013 Chino Basin Groundwater Model Update and Analysis of Safe Yield

Model Zonation and Calibrated Parameters
Horizontal Hydraulic Conductivity -- Layer 1

Figure 5-2a

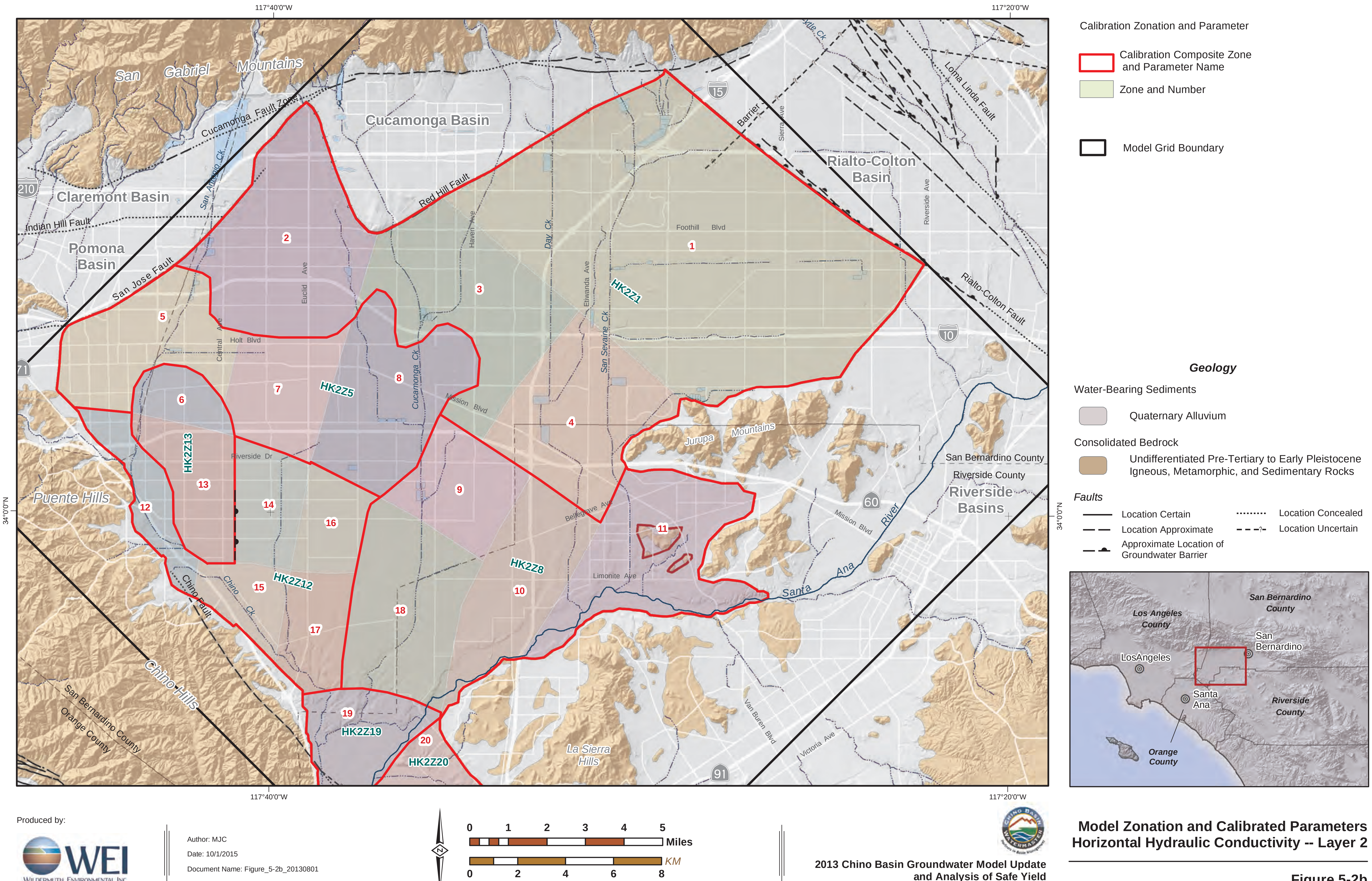

Produced by:

WEI
Wildermuth Environmental, Inc.

Author: MJC
Date: 10/1/2015
Document Name: Figure_5-2b_20130801

2013 Chino Basin Groundwater Model Update and Analysis of Safe Yield

Model Zonation and Calibrated Parameters Horizontal Hydraulic Conductivity -- Layer 2

Figure 5-2b

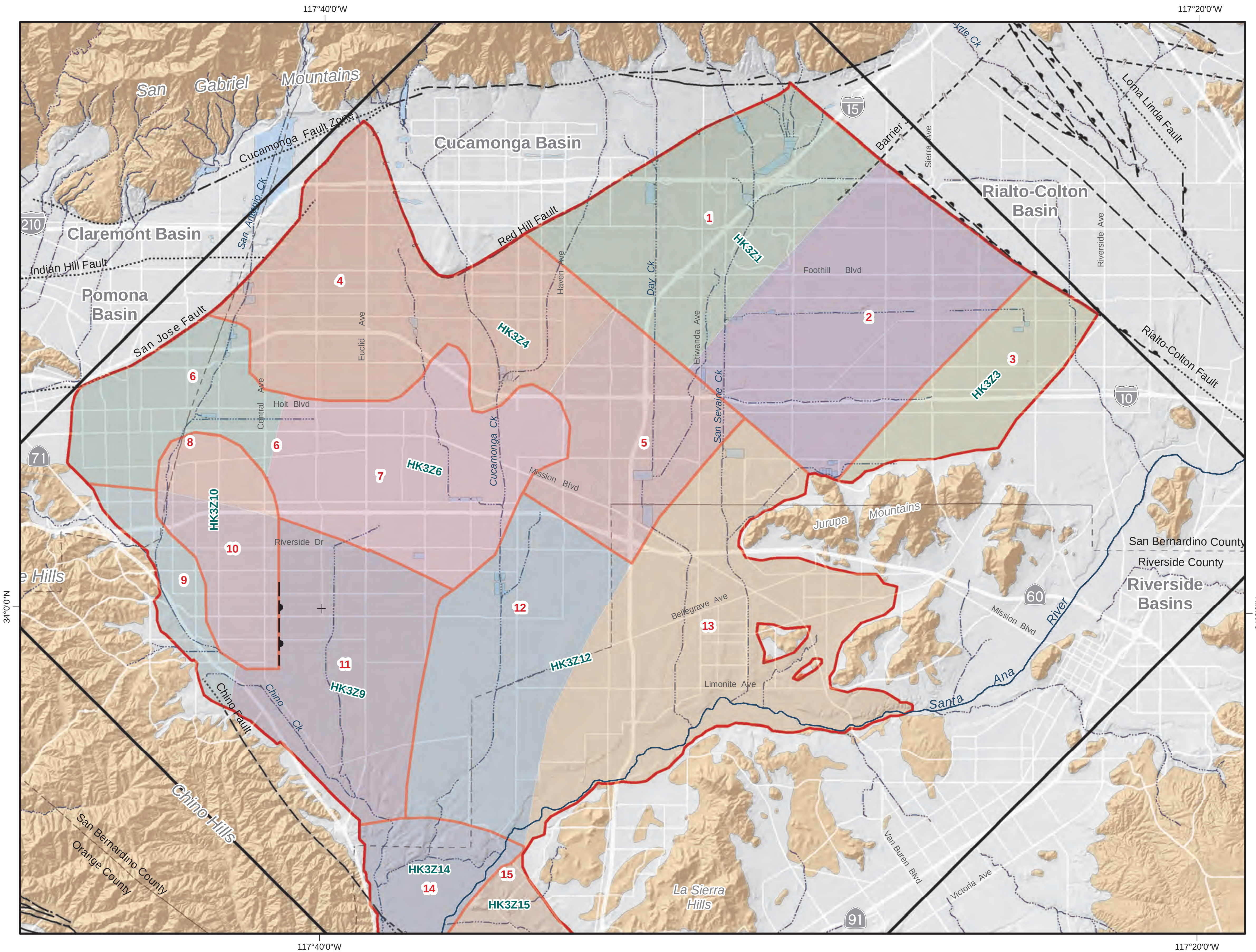

Calibration Zonation and Parameter

- Calibration Composite Zone and Parameter Name
- Zone and Number
- Model Grid Boundary

Geology

Water-Bearing Sediments

- Quaternary Alluvium

Consolidated Bedrock

- Undifferentiated Pre-Tertiary to Early Pleistocene Igneous, Metamorphic, and Sedimentary Rocks

Faults

- Location Certain
- Location Approximate
- Approximate Location of Groundwater Barrier
- Location Concealed
- Location Uncertain

Produced by:

WEI
Wildermuth Environmental, Inc.

Author: MJC

Date: 10/1/2015

Document Name: Figure_5-2c_20130801

0 1 2 3 4 5 Miles

0 2 4 6 8 KM

2013 Chino Basin Groundwater Model Update and Analysis of Safe Yield

Model Zonation and Calibrated Parameters Horizontal Hydraulic Conductivity -- Layer 3

Figure 5-2c

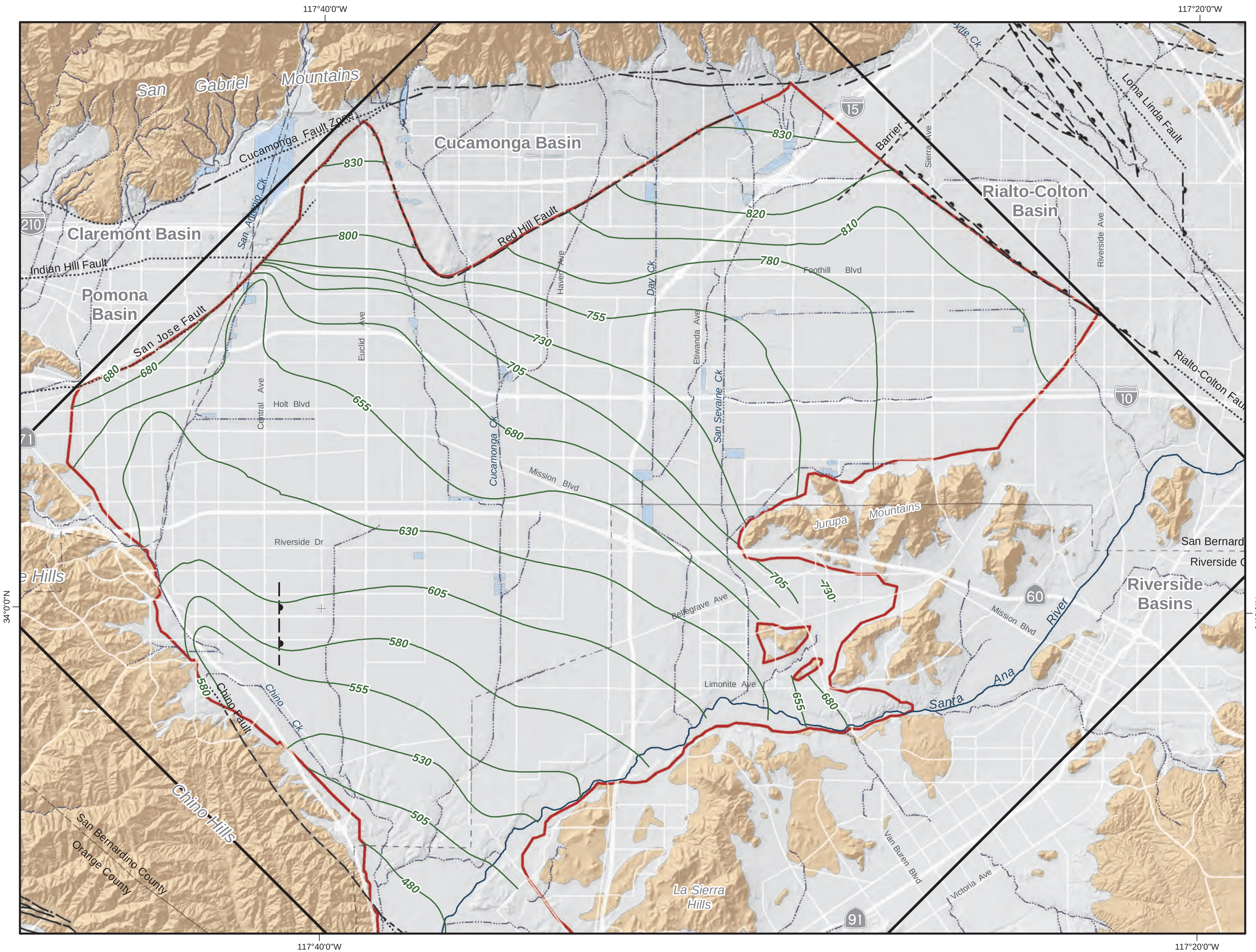

Measured Groundwater Elevation Contours (feet above mean sea-level)

Model Grid Boundary

Geology

Water-Bearing Sediments

Quaternary Alluvium

Consolidated Bedrock

Undifferentiated Pre-Tertiary to Early Pleistocene Igneous, Metamorphic, and Sedimentary Rocks

Faults

Location Certain

Location Approximate

Approximate Location of Groundwater Barrier

Location Concealed

Location Uncertain

Produced by:

WEI
Wildermuth Environmental, Inc.

Author: MJC

Date: 10/1/2015

Document Name: Figure_5-3

0 1 2 3 4 5 Miles

0 2 4 6 8 KM

2013 Chino Basin Groundwater Model Update and Analysis of Safe Yield

Groundwater Elevation Contours

Intitial Condition Water Level Map -- June 1960

Figure 5-3

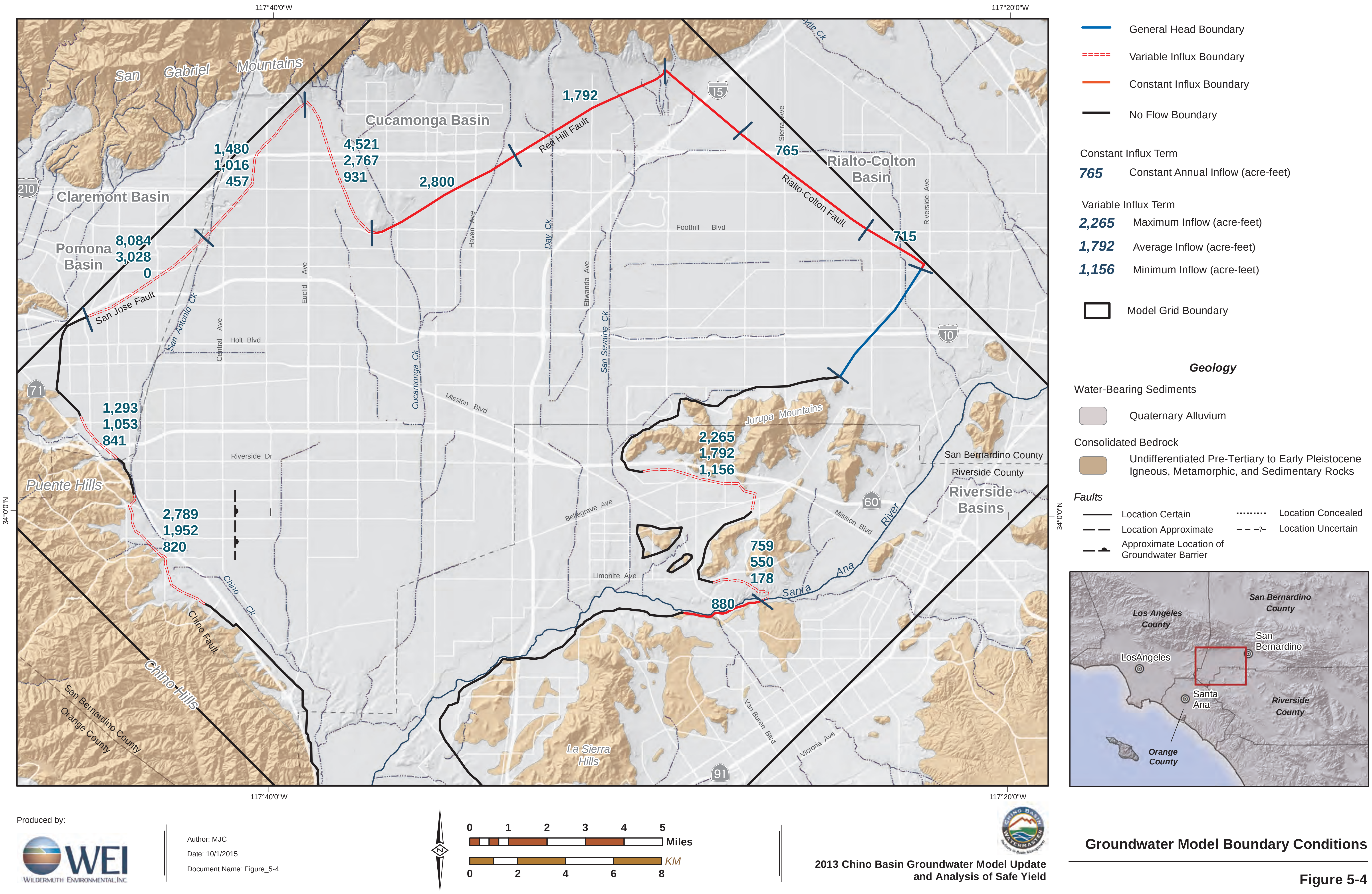

Produced by:

WEI
Wildermuth Environmental, Inc.

Author: MJC
Date: 10/1/2015
Document Name: Figure_5-4

2013 Chino Basin Groundwater Model Update and Analysis of Safe Yield

Groundwater Model Boundary Conditions

Figure 5-4

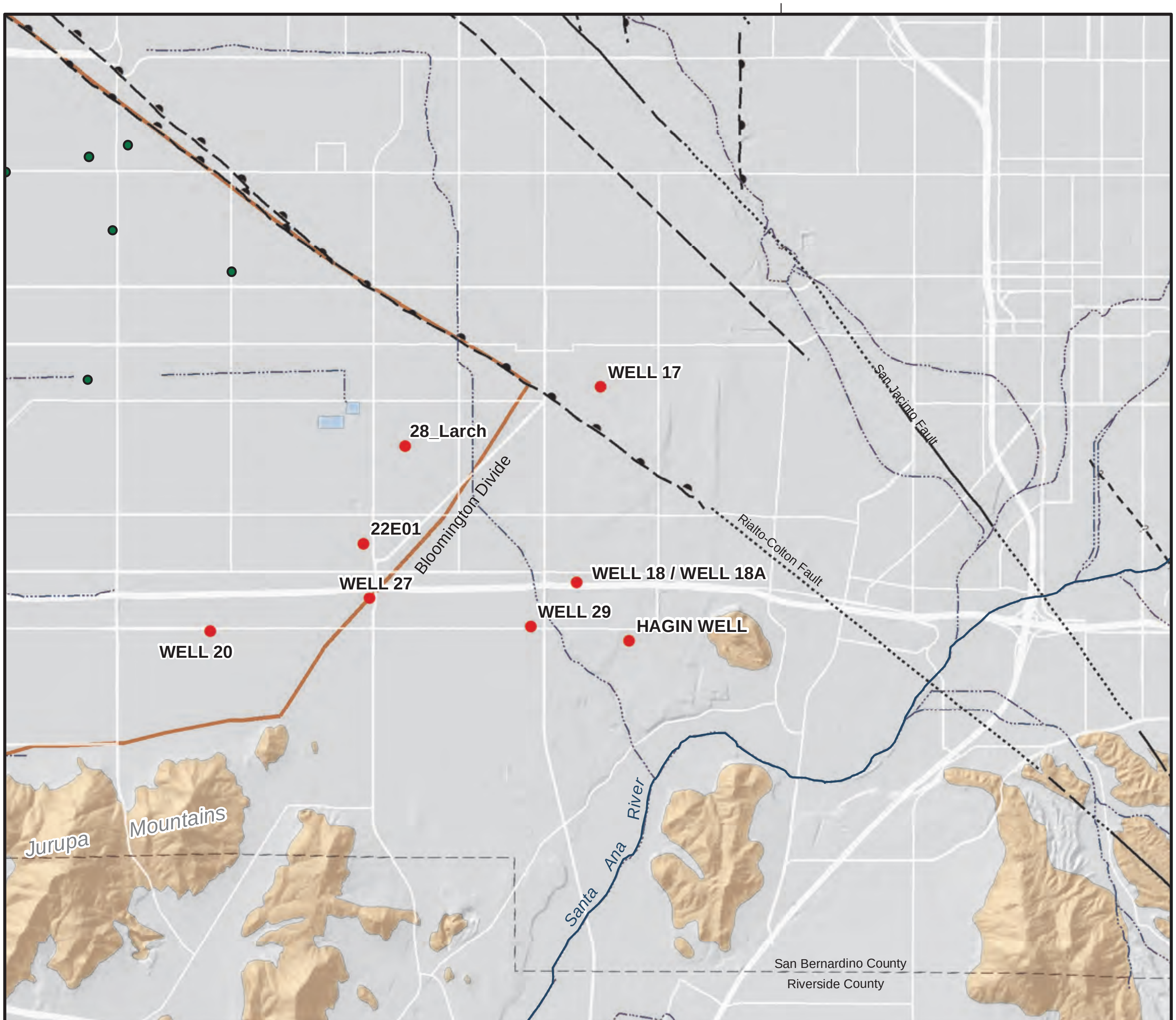

MODFLOW Groundwater Flow Model Boundary

WELL 17
Well with Historical Water Levels

Geology

Water-Bearing Sediments

Quaternary Alluvium

Consolidated Bedrock

Undifferentiated Pre-Tertiary to Early Pleistocene Igneous, Metamorphic, and Sedimentary Rocks

Faults

Location Certain
Location Approximate
Approximate Location of Groundwater Barrier
Location Concealed
Location Uncertain

Other Features

Groundwater Divides
Flood Control/Conservation Basins
Streams, Rivers, and Channels

Location of Wells With Historical Water Level Records
Bloomington Divide Area

Produced by:
WEI
Wildermuth Environmental, Inc.

Author: MJC
Date: 20071112
File: Figure_5-8a.mxd

0 1 Miles
0 2 KM

2013 Chino Basin Groundwater Model Update and Analysis of Safe Yield

Figure 5-5

Figure 5-6
Comparison of Groundwater Level Across the Rialto-Colton Fault near the Bloomington Divide

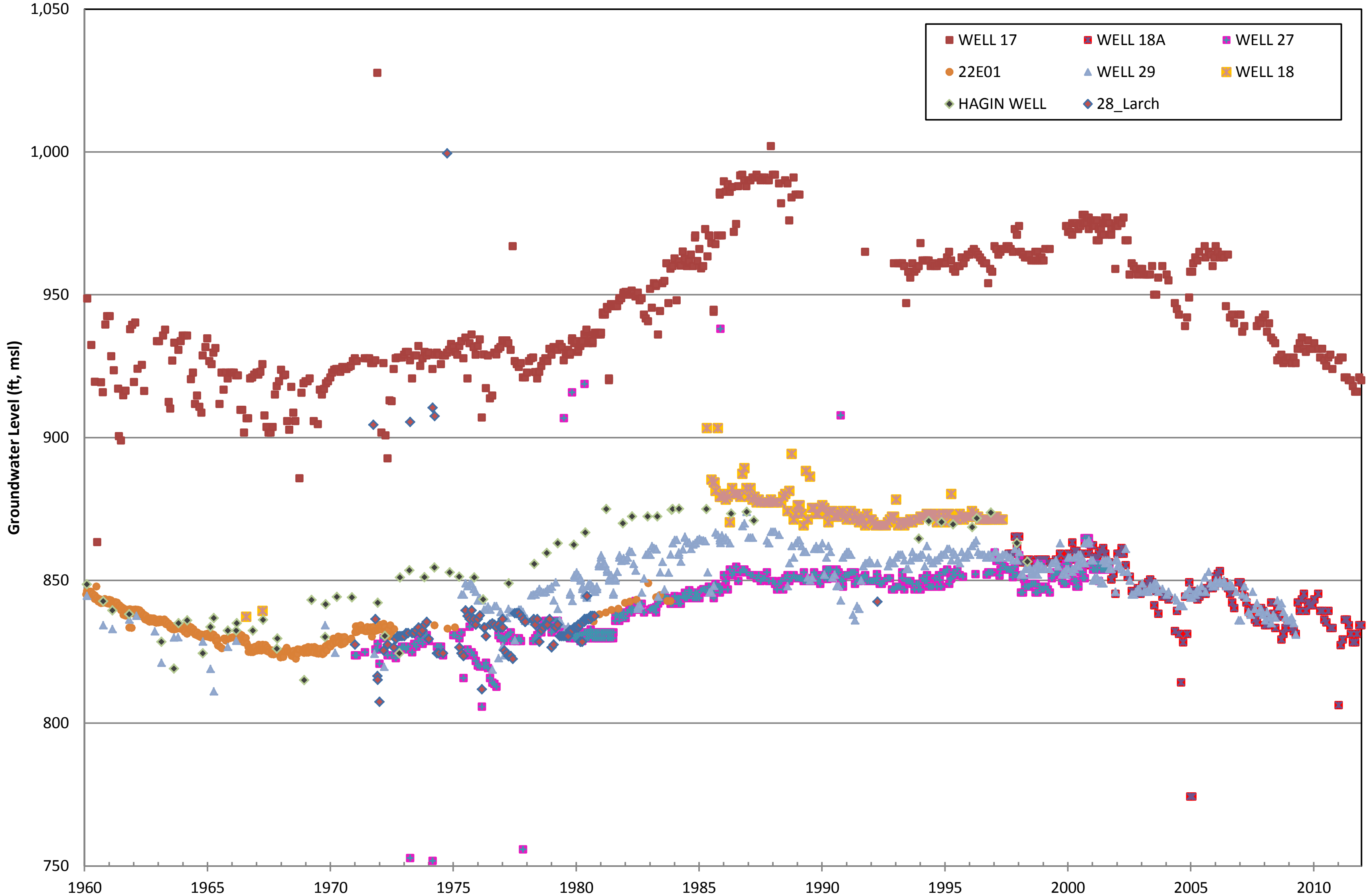

Figure 5-7
Comparison of Groundwater Level Across the Bloomington Divide

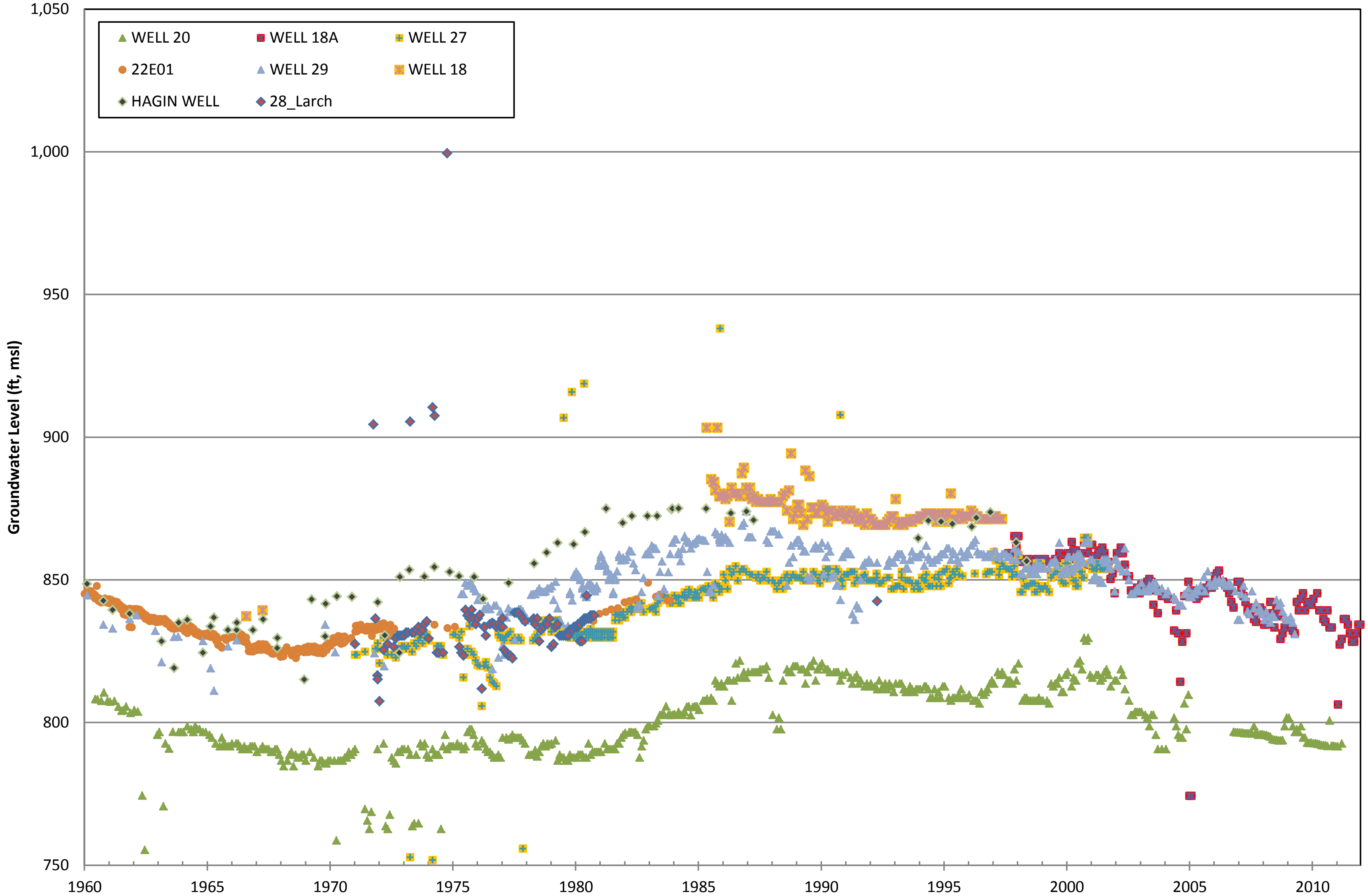

Figure 5-7_20131230.xlsx
Revised 10/2/2015

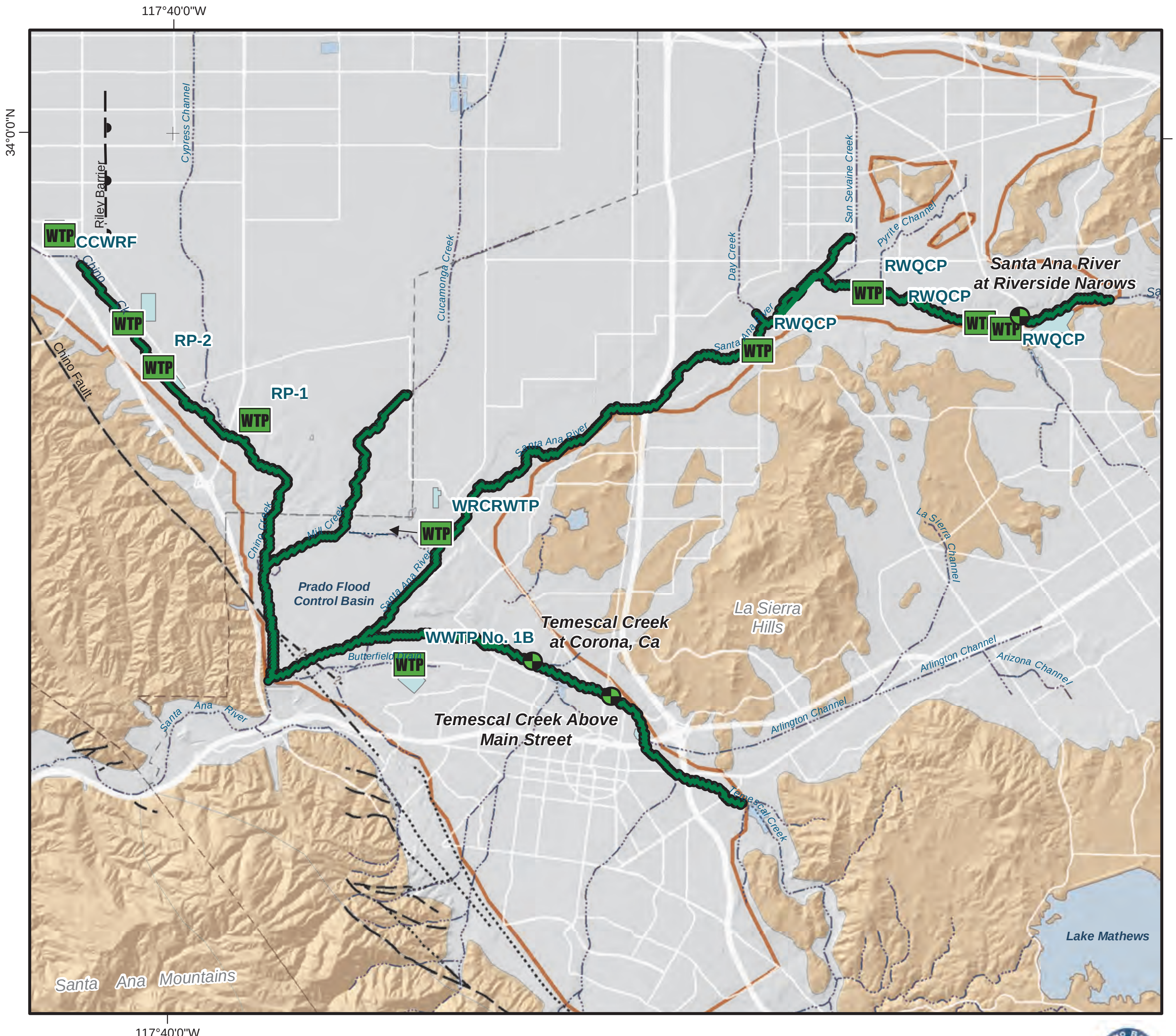

MODFLOW Groundwater Flow Model Boundary

Stream Channels Where MODFLOW Stream Package Was Used

Streams, Rivers, and Channels

Recycled Water Discharge Locations

Recycled Water Treatment Plant

Surface Water Gaging Station

Geology

Water-Bearing Sediments

Quaternary Alluvium

Consolidated Bedrock

Undifferentiated Pre-Tertiary to Early Pleistocene Igneous, Metamorphic, and Sedimentary Rocks

Faults

Location Certain

Location Approximate

Approximate Location of Groundwater Barrier

Location Concealed

Location Uncertain

Other Features

Groundwater Divides

Flood Control/Conservation Basins

Streams, Rivers, and Channels

STR Package of Channel Segments Where Simulation of Groundwater and Surface Water Interaction Occur

Produced by:

WEI
Wildermuth Environmental, Inc.

Author: MJC

Date: 20130715

File: Figure_5-8a.mxd

0 1 Miles

0 2 KM

2013 Chino Basin Groundwater Model Update and Analysis of Safe Yield

Figure 5-8

Section 6 Model Calibration

Reliability is vital for a groundwater model. Model reliability increases as model errors decrease. The main sources of modeling errors or uncertainty are from inconsistencies in the model conceptualization processes, such as inappropriate model structure or inaccuracy of water balance. Once a model's structure has been appropriately set up (Section 2) and some water recharge and discharge input files are ready, model uncertainty mainly comes from the uncertainty of model parameters, including unknown boundary inflows and outflows, which can be organized as model parameters.

The purpose of model calibration is to estimate the best set of model parameters in the given model structure for a numerical groundwater flow model. Calibration is the process of adjusting model parameters to produce the best match between simulated and observed groundwater system responses, such as water levels at wells. During the process of calibration, model parameters are adjusted (subject to reasonable bounds) with manual methods or automatic parameter estimation techniques to match observed water levels at wells. Automatic parameter estimation is also termed inverse modeling. Numerical inverse methods are widely used in hydrology and are discussed in numerous scientific publications and books. Milestone papers include those of Neuman (1973), Yeh (1986), and Carrera and Neuman (1986a, b, and c). Inverse modeling was utilized for the calibration of the 2013 Watermaster model.

MODFLOW-2000 (Harbaugh et al, 2000), UCODE_2005 (Hill, 2006), and PEST (Doherty, 2004) all provide a means to automate parameter estimation and further evaluate a model. PEST was selected due to its robust calibration capabilities. This section describes the procedure for calibrating the 2013 Chino Basin groundwater flow model; defines the objective function, minimization algorithm, and sensitivity analysis; and discusses calibration data selection, the residual analysis, and model validation.

6.1 Model Calibration Procedure

The parameter estimation program PEST Version 12 (Doherty, 2004) was used to calibrate the Chino Basin groundwater flow model. The major steps in the model calibration process include:

1. **Numerical Formulation of Developed Conceptual Model:** Calibration starts with the development of model conceptualization and mathematical-numerical descriptions of relevant physical processes. First, a developed conceptual model is converted to a numerical model. The numerical conversion includes the definition of the model aquifer geometry, the assignment of initial and boundary conditions, discretization in space and time, and the selection of hydraulic parameter zonation and heterogeneity. Next, forward modeling is conducted to check the water balance and for possible errors caused in the process of conversion. Finally, modeling results are checked to see whether the developed numerical model is capable of simulating the groundwater system's behavior under specifically measured conditions. All of the model parameters, including the model inputs that can be parameterized, are then fixed at their best estimates. Forward modeling is solved by the MODFLOW-2000 groundwater model.
2. **Sensitivity Analysis:** The next step is to determine which model parameters should be calibrated. Model parameters include the hydraulic properties of the aquifer, boundary conditions, as well as any other features of the model that can be parameterized. It is unnecessary to adjust all of the model parameters in the calibration process, and not all of the parameters should be subjected to each iterative optimization process. In general, reducing the number of estimated parameters can significantly simplify inverse modeling, but this comes at a cost: it might sacrifice the model's reliability. The selection criterion for deciding which

parameters should be subjected to inverse modeling should not be subjective. It should depend on the importance of the parameters, which can be measured by parameter sensitivity. The model parameters with high sensitivity coefficients should be determined as accurately as possible. For this reason, a sensitivity analysis is conducted to examine the importance of model parameters before inverse modeling commences. Because parameter sensitivities vary in each iterative optimization process, sensitivity analyses should be conducted in all steps of the calibration process.

3. **Selection of Calibration Data:** These data points are a key element to the success or failure of model development. Information about the model parameters is drawn from measurements of the groundwater system. Model output and measured data are compared only at discrete points in space and time—the calibration data points. The differences between the measured and computed system responses at the calibration points are termed residual. Calibration is the process of minimizing the sum of the squared-weighted residuals by updating model parameters.
4. **Forward Modeling:** A MODFLOW-2000 simulation is performed with current parameter values to obtain the simulated water levels that correspond to measured water levels.
5. **Parameter Estimation:** The calculated and measured system responses (water levels) are compared using the sum of the squared-weighted residuals—also known as the objective function. PEST uses the Marquardt-Levenberg method to minimize the objective function. Details of this method are given in the PEST user's manual (Doherty, 2004). The purpose of the minimization algorithm is to find the minimum of the objective function by iteratively updating the model parameters. There are a number of strategies for updating model parameters, as discussed in papers by Neuman (1973, 1986a, 1986b, 1986c), Finsterle and Najita (1998), and Sun and Yeh (1990). The value of the objective function decreases iteratively with the progress of calibration. The simulation is repeated (Step 4) with updated parameters, from the minimization algorithm.
6. **Analysis of Residuals:** If the measured data are not properly reproduced by the model (i.e. if the final residuals are large or exhibit systematic errors), the resulting parameters are likely to be inaccurate and or highly biased. Another possibility is that inconsistencies and/or errors exist in a developed conceptual model. And, a good match does not imply that all of the parameter estimates are reasonable.

6.2 Sensitivity Analysis and Covariance Matrix

Parameter sensitivity measures the impact of a small parameter change on the calculated system response. If a small model parameter change results in a large change in the simulated water levels of the model domain, the parameter is regarded as highly sensitive. PEST calculates sensitivities for values of hydraulic head throughout the model using the Jacobian matrix. Certain parameter values, such as those parameters related to storage coefficients and hydraulic conductivity differ greatly in orders of magnitude and therefore incomparable for parameter sensitivities are therefore not directly comparable. PEST scales the elements of the Jacobian matrix by the magnitude of the parameter value to make parameter sensitivities comparable with one another. This feature allows for measuring the sensitivity of a calibration point and measuring the importance of the parameters.

The sensitivity analysis was conducted in two steps. At the beginning, all model parameters were selected to compute their sensitivity. This is called the primal sensitivity analysis. The purpose is to exclude insensitive parameters from the final adjusted parameter set. During this processes, the covariance matrix from the sensitivity analysis was checked. The covariance matrix of model parameters describes the statistical correlations between pairs of parameters. If two parameters show a strong correlation, they cannot be determined independently. For example, if two parameters are negatively (inversely) correlated, a similar system response is obtained by concurrently increasing one and decreasing the other parameter. These kind of strong correlations exist in the Chino Basin. For example, the vertical hydraulic conductivity in layer 1 in the so-called "big shoe" area is negatively correlated to the vertical hydraulic conductivity in layer 2. After the primal sensitivity analysis, insensitive parameters and one of the paired correlated parameters are excluded from the list of calibration parameters. In another words, these parameters will not be adjusted in calibration. In general, the primal sensitivity analysis was useful for determining which parameters should be updated while providing direction for the most efficient use of computer processing time.

Forty two parameters were selected through the primal sensitivity analysis. Table 6-1 lists these model parameter sensitivities, their relative sensitivities, and their sensitivity rankings at the start of parameter optimization. The model parameters hk1z1 and hk1z5, which relate to the horizontal hydraulic conductivities of zones 1, 2, 3, 4, and 5, and model parameter sy1z13, which relates to the specific yield in zones 13, 14, 15, 9, 16, 23, and 24, are very sensitive, while the specific storage in zones 20 and 21 of layer 2 are the least sensitive. These results were used to initially determine which parameters were to be estimated with PEST. These results can also be used to determine future data collection sites, areas with high uncertainty, and/or tests in order to refine the model.

6.3 Selection of Calibration Data

The transient calibration period is July 1, 1960 through June 30, 2011 or fiscal year 1960/61 through fiscal year 2010/11. This period was chosen primarily based on the availability of continuous groundwater level records.

The model was calibrated by comparing measured and model estimated groundwater-level and total historic surface water discharge into Prado Dam reservoir. Groundwater-level measurements were selected based on the following criteria:

- Measurement locations with time-series data should have sufficient sensitivities.
- Calibration wells should be geographically distributed.
- Calibration wells should vertically distributed vertically in model layers if possible.
- Measurements should be relatively evenly distributed over time if possible.

In the 2007 model, over 2,436 water-level measurements from 47 wells were used in calibration. For the 2013 model, over 10,466 water-level measurements from 67 wells were used in calibration.

Surface water discharge at Santa Ana River below Prado Dam and stage observations for the Prado Dam reservoir pool were used by the Army Corps of Engineers to estimate the total discharge into Prado Dam reservoir. This reconstructed daily inflow hydrograph was used as a calibration target for 2013 Watermaster model.

Figure 6-1 shows selected calibration well locations. Table 6-2 lists the owners, local names, and screen positions of these wells. For calibration wells that span multiple layers, a weight was assigned to the water levels of each layer to derive a final value for comparison to the observed data. Weights were assigned to layers based on the thickness of the aquifer and the estimated hydraulic conductivity.

6.4 PEST Settings and Calibration Results

All of the efforts taken within a calibration process are ultimately evaluated on the success or failure of meeting three conditions: (1) the groundwater system processes and geometry are adequately represented and simulated, (2) weighted true errors are independent, and (3) errors in the observation data used for calibration are independent (Hill and Tiedeman 2007). As to condition 3, it was assumed that the water level measurements were taken by numerous personnel, representing numerous agencies, and that these measurements would therefore have random errors. It was also assumed that there are no natural processes that might make these observations biased. In this report, only conditions 1 and 2 are addressed.

6.4.1 PEST Settings

Forward simulation of the flow model for the calibration period requires 45 to 55 minutes of computational time. Since the model output, as it corresponds to the calibration points, depends on the estimation of parameters and the fit can be improved by appropriately changing model parameters, a number of strategies were used to find a parameter set that iteratively yields smaller values of the objective function. These strategies resulted in good matches between simulated and measured data and reasonable parameter estimates, not only in their values but also in comparison to other parameters in space. The major steps used in PEST inverse modeling are described below.

The initial model parameter values were derived and estimated based on the parameter estimates of the 2007 model.

The Levenberg-Marquardt algorithm was used to minimize the objective function. Details of this method are given in the PEST user's manual (Doherty, 2004) and in numerous inverse modeling papers and text books. It is necessary to note how to make the best choice for the Marquardt parameter (λ), as it is referred to in PEST (some other books and papers refer to it as Levenberg parameter [i.e. Levenberg, 1944, and Finsterle, 1999]). The choices for this value depend on how well-scaled the initial problem is. Marquardt recommends starting with a value λ and a factor $\nu > 1$ (1963). When λ becomes large, this algorithm acts as the steepest-descent algorithm. When λ is zero, it is reduced to the Gauss-Newton method, which is better suited for small residuals. During iteration, the algorithm decreases or increases the parameter λ value through multiplication or division by ν so as to accelerate convergence. Based on theoretical study of the algorithm as well as trial and error, the initial λ value was set to 10.0 and ν was fixed at 2.0.

The parameter-updated step size was limited in PEST's settings. During any optimization iteration, the objective function reduction rate was set to be less than 30 percent. This setting prevented the minimization algorithm from moving too far beyond the region in which the linearity assumption is justified. The parameter maximum relative and factor change limits were also set to prevent the parameter adjustment from overshooting.

Upper and lower parameter bounds were set to limit the parameters to a reasonable range. These bounds were carefully chosen based on pumping tests and published literature (Table 6-3). The upper and lower bounds, combined with the step size limitation and parameter selection technology (discussed in detail below), makes calibration process stable and the results reasonable.

Error analyses for several trial inverse modeling runs revealed that some of the hydraulic parameters are highly correlated with others. For example, the hydraulic conductivity of layer 1 in zone 29 is highly correlated with many hydraulic parameters. This finding was not surprising because zone 29 is located in the Prado Basin, which controls the surface and subsurface flow of the lower Chino Basin and Temescal area. However, PEST does not provide a function that can automatically select the most independent parameters for each optimization process. To settle this correlation problem, the correlation coefficients among parameters were examined, using the trial inverse modeling runs, and then some of the parameters that strongly correlated to others from the optimization process were excluded (e.g. the hydraulic conductivity of layer 1 in zone 29). In addition, prior information was incorporated into the estimation process. Using a combination of methods described above, PEST was able to adjust a large number of parameters, avoiding unnecessary numerical difficulties.

Inverse modeling was guided by sensitivity and error analysis. Although 42 model parameters were selected to be adjusted, all of these parameters were not subjected to inverse modeling in each iterative-optimization process. In general, reducing the number of estimated parameters can significantly simplify inverse modeling, but this comes at a cost; that is, it might sacrifice the model's reliability. The selection criterion for deciding which parameters should be subjected to inverse modeling should not be subjective: it should depend on the parameters' importance, which can be measured by parameter sensitivity. Because parameter sensitivity varies in each iterative optimization process, sensitivity analyses were conducted in all steps of the calibration processes. Only the most important and independent parameters were adjusted in each model optimization iteration. After examining the model parameter sensitivities, up to eight parameters were allowed to be adjusted in each optimization iteration process.

Automatic User Intervention was activated in the PEST settings and used to guide model parameter updates. PEST was forced to compute the Jacobian matrix in each optimization iteration. The Jacobian matrix revealed the sensitivity of model parameters. During each iteration, PEST was forced to hold a model parameter value if the ratio of the highest sensitivity of any given parameter to the sensitivity of said parameter was lower than 4.0. Only highly sensitive parameters were subjected to the minimization algorithm, while relatively insensitive and troublesome parameters were temporarily held at their then current values. The selection of adjustable parameters was reviewed after each optimization iteration; the calibration process was guided by sensitivity analyses. This methodology requires additional computational time. For example, to compute the Jacobian matrix, one parameter requires 50 minutes of computational time. For this regional flow model, which has more than several dozen adjustable parameters, several days could be required to calculate the Jacobian matrix. To address this time constraint, a 26-processor computer system was used; this is discussed in greater detail below.

Each model calibration simulation takes about 50 minutes to complete. Since inverse modeling needs to check the sensitivity of all 42 parameters, this requires approximately 42 times 50 minutes, totaling about 2,100 minutes of computational time for the Jacobian matrix calculation process. The same amount of time is needed to find the optimal Marquardt λ. Thus, the total computing time on a single processor computer would be at least 4,200 minutes to conduct one optimization iteration. To meet the computing time demand, parallel PEST simulations for Chino-Temescal groundwater model were conducted on a 26-processor computing platform with one processor acting as the "master" machine and 25 processors functioning as "slave" machines For the Chino-Temescal Basin, each processor had to be run twice to finish the Jacobian matrix calculation or to find the optimal Marquardt λ.

6.4.2 Calibration Results

Calibration concluded when the objective function could no longer be practically minimized. Figure 6-2a shows the modeled versus measured heads for all calibration wells. All of the points are distributed closely around the diagonal line except for some of the groundwater elevations that are less than 500 feet, indicating good inverse modeling performance and a robust calibration. Figures 6-2b through 6-2d compare simulated and measured water levels in MZ1, MZ2, MZ3 wells, respectively. Figure 6-2e compares simulated and measured water levels in MZ4, MZ5 and the Prado Basin MZ.

Further exploration of the model results indicates that the poor matches in the City of Chino area occur at deep wells screened in layers 2 and of the so-called "big shoe" area. Figure 6-2f shows the measured groundwater elevations versus model-estimated groundwater elevations for wells in the City of Chino area. This scatter plot shows that these poor correlations occur at Chino Hills Wells 07C, 15B, and 19. Pumping events at these wells were short, lasting maybe a couple of weeks or a month. And, groundwater levels fluctuated significantly when pumping started and stopped. Groundwater elevation data at these wells does not correlate temporarily with the stress periods used in the model which contributes to the lack of correlation.

Appendix C1 contains time-history plots of simulated and measured water levels for the calibration wells during the calibration period. The time-history plots are useful indicators for success as they show transient calculated water levels compared to measured water levels at a single location. Overall, the time-history plots in Appendix C1 show a good match between the simulated and measured values, indicating that trends within the aquifer are being simulated well.

One estimate of the goodness of fit for model calibration is the coefficient of determination (R^2 or R-square) statistic. In words the coefficient of determination is the fraction of the observed variance that is explained by the model. Using the entire calibration dataset, the coefficient of determination is about 93 percent, that is, the model can explain 93 percent of the variance observed in groundwater level observations. If the problematic groundwater elevations in the City of Chino were eliminated from analysis the coefficient of determination would be 0.94. By this criterion the calibration is considered very good.

The Nash-Sutcliffe efficiency (NSE) index is a normalized statistic that determines the relative magnitude of the residual variance ("noise") compared to the measured data variance ("information") (Nash and Sutcliffe, 1970). The NSE index indicates how well the plot of observed versus simulated data fits the "perfect-fit" line. The NSE index is computed as shown below:

$$NSE = 1 - [\Sigma\, (Y_i^{\,obs} - Y_i^{\,sim})^2 / \Sigma(\,Y_i^{\,obs} - Y^{mean})^2]$$

Where $Y_i^{\,obs}$ is the i^{th} observed groundwater level, $Y_i^{\,sim}$ is the i^{th} simulated groundwater level, and Y^{mean} is the mean of observed groundwater level,. The NSE index ranges between $-\infty$ and 1.0 (1 inclusive), with the NSE index equal to1 being the optimal value. Values between 0.0 and 1.0 are generally viewed as acceptable levels of performance, whereas values <0.0 indicate that the mean observed value is a better predictor than the simulated value, which indicates unacceptable performance. The value of NSE index from the groundwater model calibration were 0.93 and 0.94 for all the calibration wells and all the calibration wells less the problematic wells, respectively. The characterization of the calibration performance using the NSE index is reported (Moriasi, et. al., 2007) as follows: negative infinity to 0.5 as unsatisfactory; 0.5 to 0.65 as satisfactory; 0.65 to 0.75 as good; 0.75 to 1.0 as very good. Using this criterion the groundwater model calibration is characterized as very good. The NSE index was used for two major reasons: (1) it is recommended for use by ASCE (1993) and Legates and McCabe (1999), and (2) it is commonly used, which provides extensive information on reported values. (Sevat and Dezetter, 1991) also found the NSE index to be the best objective function for reflecting the overall fit of a hydrograph.

Table 6-3 compares the initial and final mean model parameter values by zone. The final estimates are within a reasonable range of expected values for texture and depth.

The final calibrated model also resulted in a good fit to the total observed stream discharge into the Prado Dam reservoir. Figure 6-3a is a time-history plot of the model-estimated stream inflow to Prado versus the total Prado inflow estimated by US Army Corps of Engineers based on adjusted measurements. Figure 6-3b is a scatter plot of model-estimated discharge into the Prado Dam reservoir versus the ACOE-estimated inflow; the diagonal red line on the plot indicates a perfect match between model-estimated and ACOE-estimated discharge. The coefficient of determination is 0.92. The standard for goodness of fit for surface water models as characterized by the coefficient of determination and as promulgated by the Environmental Protection Agency[9] for surface water models is as follows: 0.65 or less as poor, 0.65 to 0.75 as fair, 0.75 to 0.85 as good, and greater than 0.85 as very good. The NSE index is about 0.9. Using these criteria the surface water calibration is characterized as very good.

The high coefficient of determination and NSE index for the groundwater levels and surface water discharge into the Prado Dam reservoir indicate that the overall water budget for the new 2013 Chino Basin groundwater model is accurate: it would not be possible to achieve good calibration in the groundwater basin and the surface water system, as indicated by the high coefficient of determination and NSE index, if the water budget was not accurate.

6.4.3 Residual Analysis

Residual analysis is critical in evaluating the performance of inverse modeling and calibration. Minimizing the objective function using the Levenberg-Marquardt algorithm may lead to the best-estimate parameters for a given groundwater flow model. However, this does not imply that a real groundwater system is properly represented by a model. If a conceptual model fails to reproduce the salient features of a system, the given calibrated model may not be able to match the observed data as expected. Residual analysis can reveal potential trends in residuals, indicating a systematic error in a model or the data, and can point out aspects of a model that require modification.

Statistics on hydraulic head residuals aid in the evaluation of model calibration. The mean of the residuals is expected to be close to zero. A large positive or negative mean indicates that data are systematically under-predicted or over-predicted by the model. The standard error in a regression is the square root of the calculated error variance. If a model fits the observations consistent with the assigned weighting, the calculated standard error of the regression will equal 1.0. Smaller values indicate that the model fits the observations better than indicated by the assigned weighting. A large variance or standard deviation either indicates that the data were nosier than expected or that there is a trend in the residuals. The skewness of the residuals characterizes the degree of asymmetry in the distribution. Kurtosis compares the peakedness or flatness of the distribution relative to the Gaussian distribution—a distribution with Kurtosis greater than 3 is relatively peaked and less than 3 is relatively flat. A large difference between the mean and the median is indicative of a robustness problem; that is, the distribution is likely to be heavy-tailed and asymmetric.

Figure 6-4 shows the frequency residual distribution in the model domain with a mean of 0.502 and a residual standard deviation of 25.3. Figure 6-5a shows the frequency residual distribution with a residual mean of 3.34 and a standard distribution of 26.5. Figures 6-5b through 6-5d show the frequency distribution in Chino Basin Management Zones 1 through 3. Table 6-4 lists the hydraulic-head residual statistics. These data illustrate that the mean of the residuals is around 0.50, which is very near the zero, with a standard deviation of about 25 feet. The value of skewness of close to zero indicates that the residual is almost symmetrically distributed. And, the Kurtosis was greater than 3, which means that there are more residuals around zero.

[9] See Watershed Model calibration and Validation: the HSPF Experience (Donigian,2002) and Basins/HSPF: Model Use, Calibration and Validation (Duda, et al., 2012)

The residual distribution is statistically random and shows little geographical trend when observed on the map. Figure 6-6 shows each calibration well and their mean residuals. Some wells in the western portion of the basin have a mean residual greater than 20 feet, which is attributed to historical data collection in the Monte Vista Water District and City of Pomona areas. These wells are next to wells with very small mean residuals, indicating little spatial trending.

Table 6-5 lists the residual errors, classified by percentage group. This table indicates that 98 percent of the residual errors are less than 60 feet, 83 percent of the residual errors are less than 30 feet, and that 66 percent are less than 30.

6.4.4 Validation

Validation checks the accuracy of the model's representation of the real system. Model validation is defined as the "substantiation that a computerized model within its domain of applicability possesses a satisfactory range of accuracy consistent with the intended application of the model" (Schlesinger, S. 1979). For the Chino Basin Model, model-projected groundwater elevations were compared to observed groundwater elevations at wells that were not used in the calibration process. The wells selected for validation and the associated time histories of the model-projected and corresponding groundwater elevations are included in Appendix C2. The wells selected for validation were located in the JCSD and CDA wells fields. A total of 3,500 observed static groundwater elevations were used. The mean of the residuals for the validation process was about -8.64 feet.

Table 6-1
Model Parameter Sensitivity in Initial Optimization

Parameter name	Parameter Type	Layer	Zone	Value	Relative Sensitivity	Ranking
hk1z1	XKh(zone)	1	1-2-3-4	2.50E+00	0.211	3
hk1z5	XKh(zone)	1	5	1.25E+00	0.213	2
hk1z6	XKh(zone)	1	6-7-8-10	6.80E-01	0.129	13
hk1z11	XKh(zone)	1	11-12	1.40E+00	0.122	14
hk1z13	XKh(zone)	1	13-14-15-23-24	7.50E-01	0.147	10
hk1z16	XKh(zone)	1	9-16	4.70E-01	0.136	11
hk1z17	XKh(zone)	1	17-18-27-28	1.61E+00	0.154	9
hk1z19	XKh(zone)	1	19-20-21	1.20E+00	0.200	5
hk1z22	XKh(zone)	1	22-25-26	3.40E-01	0.110	17
hk1z29	XKh(zone)	1	29-31	8.50E-01	0.122	15
hk1z31	XKh(zone)	1	30-32	4.90E-01	0.183	6
sy1z3	XSY(Zone)	1	6-7-8-10-11-12	4.74E-01	0.104	20
sy1z13	XSY(Zone)	1	13-14-15-9-16-23-24	5.10E-01	0.233	1
sy1z17	XSY(Zone)	1	17-18-19-27-28-20-21	7.10E-01	0.115	16
sy1z22	XSY(Zone)	1	22-25-26	5.60E-01	0.135	12
sy1z29	XSY(Zone)	1	29-31	6.10E-01	0.061	26
sy1z30	XSY(Zone)	1	30-32	1.01E+00	0.180	7
vk1z1	XVk(Zone)	1	1-2-3-4-5-6-7-8-10-11	3.27E+01	0.018	37
vk1z9	XVk(Zone)	1	9-13-15-16-17-22-24-25-26-27	1.87E+00	0.010	40
vk1z17	XVk(Zone)	1	18-19-20-21-12-28-29-30-31-32	3.40E+01	0.032	33
hk2z1	XKh(zone)	2	1-2-3-4	3.49E-01	0.107	19
hk2z5	XKh(zone)	2	5-7-8	1.10E-01	0.082	22
hk2z13	XKh(zone)	2	6-13	2.20E-01	0.174	8
hk2z12	XKh(zone)	2	12-15-16-17-14	1.90E-01	0.072	24
hk2z19	XKh(zone)	2	19	1.60E-01	0.037	31
hk2z20	XKh(zone)	2	20-21	1.60E-01	0.205	4
ss2z5	XSS(Zone)	2	5-6-7-8-13-14-16	1.43E-04	0.036	32
ss2z20	XSS(Zone)	2	20-21	1.43E-04	0.000	42
vk2z1	XVk(Zone)	2	1-2-3-4-9-10-11-18	7.01E+00	0.030	34
vk2z5	XVk(Zone)	2	5-7-8-14-16-12-15-16-17	5.00E-02	0.081	23
vk2z6	XVk(Zone)	2	6-13	1.40E-05	0.005	41
hk3z1	XKh(zone)	3	1-2	1.80E-01	0.104	21
hk3z3	XKh(zone)	3	3	2.40E-01	0.056	27
hk3z6	XKh(zone)	3	6-7	2.80E-01	0.038	30
hk3z9	XKh(zone)	3	9-11	1.90E-01	0.041	29
hk3z10	XKh(zone)	3	8-10	1.80E-01	0.022	36
hk3z12	XKh(zone)	3	12-13	2.80E-01	0.070	25
hk3z14	XKh(zone)	3	14	2.20E-01	0.023	35
hk3z15	XKh(zone)	3	15-16	3.00E-01	0.110	18
ss3z1	XSS(Zone)	3	1-2-3	1.43E-05	0.011	39
ss3z4	XSS(Zone)	3	4-5	1.43E-05	0.050	28
hfb1	HFB	2, 3		1.43E-05	0.017	38

abbriviations:

XHK	Model base parameter of Horizontal Hydraulic Conductivity
XSS	Model base parameter of Specific Storage
XSy	Model base parameter of Specific Yield
XVK	Model base parameter of Vertical Hydraulic Conductivity
HFB	Horizontal flow barrier

Table 6-2
Calibration Wells

WellId	WellName	Screened Layer	Model Location		UTMX	UTMY	Owner
			Row	Column			
1206952	AP-PA/7	2	474	181	436641.00	761478.00	Chino Basin Watermaster
1206955	AP-PA/10	1	474	181	436641.00	761478.00	Chino Basin Watermaster
1002743	C 09	1	411	127	437046.00	766408.00	City of Chino
1004185	C 13	1	428	181	438612.00	763452.00	City of Chino
1206674	C 15	12	469	138	435047.12	763518.63	City of Chino
1206686	YMCA	1	464	184	437230.74	761769.76	City of Chino
1004179	CH HIL 17	12	465	160	436162.52	762761.20	City of Chino Hills
1004217	CH HIL 07C	2	489	148	434621.00	762264.00	City of Chino Hills
1203149	CH HIL 18A	2	453	178	437467.00	762490.00	City of Chino Hills
1203158	CH HIL 19	2	464	168	436556.00	762454.00	City of Chino Hills
1203214	CH HIL 15B	2	486	179	436058.00	761042.00	City of Chino Hills
1203215	CH HIL 15A	12	486	179	436063.93	761049.67	City of Chino Hills
1002319	ONT 09	12	312	100	440085.02	771772.38	City of Ontario
1002654	P 16	1	435	54	432941.00	768526.00	City of Pomona
1002685	P 24 (OLD)	1	467	63	431989.66	766766.24	City of Pomona
1203062	P 29	1	478	92	432727.00	765099.00	City of Pomona
1207026	GE MW-11	1	350	149	440548.64	768089.84	General Electric Corporation
1002554	GSWC Margarita 1	1	381	44	434803.33	771208.95	Golden State Water Company
1002321	SAWC 18	1	336	99	439046.67	770776.13	San Antonio Water Company
1004299	CIM 09	1	477	226	438440.67	759455.99	State of California, California Institution for Men
1206765	CIM MW 24I	1	486	193	436669.31	760429.81	State of California, California Institution for Men
1206766	CIM MW 24S	1	486	193	436672.70	760451.86	State of California, California Institution for Men
1002536	WECWC 1	1	327	66	438035.17	772611.38	West End Consolidated Water Co.
1206514	PW 1	1	350	260	445289.73	763365.09	Archibald Ranch Community Church
1206512	PW 2	1	393	229	442131.73	762861.73	Basque American Dairy
1206682	CDA I-10	1	419	283	443331.00	759491.00	Chino Basin Desalter Authority
1002305	ONT 20	1	224	210	448539.89	770852.76	City of Ontario
1002328	ONT 04	12	300	137	442191.58	770716.13	City of Ontario
1002343	ONT 07	1	299	178	443933.02	769030.13	City of Ontario
1002346	ONT 11	12	326	169	442417.36	768263.88	City of Ontario
1002371	ONT 08	1	304	212	445164.00	767374.00	City of Ontario
1002372	ONT 36	12	302	212	445285.52	767449.51	City of Ontario
1002205	CVWD 35	1	140	222	452547.20	773907.86	Cucamonga Valley Water District
1002312	CVWD 3	12	245	174	446117.71	771480.88	Cucamonga Valley Water District
1206630	PW 3	1	469	290	441516.50	757057.14	H & R Barthelemy Dairy
1202872	IEUA MW-2	1	478	300	441585.32	756253.14	Inland Empire Utilities Agency
1202809	PW 4	1	453	268	441243.79	758646.30	Stark, Everett
1002219	Cal Speedway 1	1	157	250	453043.14	772014.82	California Speedway
1002254	ONT 31	123	220	275	451415.39	768242.01	City of Ontario
1201166	MIL M-03	1	283	265	448342.30	765980.80	County of San Bernardino
1002081	F31A	23	54	271	458311.30	775488.57	Fontana Water Company
1002085	F35A	23	75	319	459471.52	772554.76	Fontana Water Company
1002101	FU28	1	46	355	462215.56	772243.25	Fontana Water Company
1002153	FU6	1	131	365	459033.92	768226.95	Fontana Water Company
1002213	F30A	1	101	267	456181.32	773647.15	Fontana Water Company
1002242	F21A	1	161	316	455716.33	769023.63	Fontana Water Company
1003502	JCSD 16	1	268	335	451949.21	763694.26	Jurupa Community Services District
1004058	PW 5	1	421	331	445253.71	757370.08	Michel, Louise
1002150	WVWD 20	1	96	381	461197.81	769001.95	West Valley Water District
1207215	FC-936A2	1	229	410	456790.09	762140.69	State of California, Department of Toxic Substances Control
1003613	NOR 11	1	345	336	448699.14	760390.51	City of Norco
1003630	SARWC 07	1	308	376	451968.36	760257.88	Santa Ana River Water Company
1003682	PW 6	1	356	377	449996.00	758199.00	Unknown
1202861	PW 7	1	478	274	440441.94	757354.76	Lizzaraga, Frank
1004843	PW 8	1	540	380	442335.00	750232.00	Santa Ana River Dev. Co.
1207088	USGS Archibald 1	1	458	364	445086.00	754390.00	United States, Geological Survey (USGS)
1004010	PW 9	1	488	283	440395.00	756575.00	Unknown
1004787	PW 10	1	528	350	441563.00	752007.00	Unknown
1206507	PW 11	1	500	251	438508.40	757397.23	Van Leeuwen, John
1004636	COR 06	12	491	480	448600.16	748058.35	City of Corona
1004907	COR 08	2	490	469	448230.00	748584.01	City of Corona
1004914	COR 15	2	507	437	446094.00	749340.00	City of Corona
1004920	COR 11	2	528	418	444441.52	749155.82	City of Corona
1004949	COR 14	2	525	447	445730.00	748240.00	City of Corona
1222093	Corona CG-1	1	480	509	450351.28	747312.60	Riverside County Waste Management Department
1004876	COR 10	1	497	423	445978.00	750225.00	Unknown

Table 6-3
Model Parameter Base Value, Calibrated Value and Range of Parameter Values in PEST

Parameter Name	Parameter Type	Parameter Activity	Zone	Base Value	Calibrated Value	Lower Bound	Upper Bound
HK1Z1	HK	1	1-2-3-4	2.50E+00	2.72E+00	2.57E-01	2.57E+01
HK1Z5	HK	1	5	1.25E+00	1.23E+00	1.18E-01	1.18E+01
HK1Z6	HK	1	6-7-8-10	6.80E-01	5.81E-01	6.50E-02	6.50E+00
HK1Z11	HK	1	11-12	1.40E+00	1.50E+00	1.44E-01	1.44E+01
HK1Z13	HK	1	13-14-15-23-24	7.50E-01	8.87E-01	8.47E-02	8.47E+00
HK1Z16	HK	1	9-16	4.70E-01	4.75E-01	4.09E-02	4.09E+00
HK1Z17	HK	1	17-18-27-28	1.61E+00	1.53E+00	1.58E-01	1.58E+01
HK1Z19	HK	1	19-20-21	1.20E+00	1.20E+00	1.17E-01	1.17E+01
HK1Z22	HK	1	22-25-26	3.40E-01	7.98E-01	7.54E-02	7.54E+00
HK1Z29	HK	1	29-31	8.50E-01	8.06E-01	7.02E-02	7.02E+00
HK1Z31	HK	1	30-32	4.90E-01	4.78E-01	5.04E-02	5.04E+00
SY1Z1	SY	1	1-2-3-4-5	1.01E+00	1.04E+00	5.18E-01	2.07E+00
SY1Z3	SY	1	6-7-8-10-11-12	5.10E-01	4.59E-01	2.45E-01	9.82E-01
SY1Z13	SY	1	13-14-15-9-16-23-24	7.10E-01	7.27E-01	3.74E-01	1.49E+00
SY1Z17	SY	1	17-18-19-27-28-20-21	6.40E-01	7.61E-01	3.27E-01	1.31E+00
SY1Z20	SY	1	22-25-26	5.60E-01	6.21E-01	3.37E-01	1.35E+00
SY1Z29	SY	1	29-31	6.10E-01	7.87E-01	4.52E-01	1.81E+00
SY1Z30	SY	1	30-32	1.01E+00	1.09E+00	5.04E-01	2.02E+00
VK1Z1	VK	1	1-2-3-4-5-6-7-8-10-11	3.27E+01	5.01E-01	5.16E-02	1.03E+02
VK1Z9	VK	1	9-13-15-16-17-22-24-25-26-27	1.87E+00	1.82E-02	1.30E-03	2.60E+00
VK1Z14	VK	1	14-23-24	1.80E-03	1.80E-04	9.00E-06	3.60E-02
VK1Z17	VK	1	18-19-20-21-12-28-29-30-31-32	3.40E+01	1.46E-01	1.90E-02	3.80E+01
HK2Z1	HK	1	1-2-3-4	3.40E-01	3.96E-01	2.99E-02	2.99E+00
HK2Z8	HK	1	9-10-11-18	5.00E-01	3.47E-01	3.47E-02	3.47E+00
HK2Z5	HK	1	5-7-8	1.10E-01	1.74E-01	1.33E-02	1.33E+00
HK2Z13	HK	1	6-13	2.20E-01	4.32E-02	4.00E-03	4.00E-01
HK2Z12	HK	1	12-15-16-17-14	1.90E-01	8.97E-02	1.62E-02	1.62E+00
HK2Z19	HK	1	19	1.60E-01	1.25E-02	1.25E-02	1.25E+00
HK2Z20	HK	1	20-21	1.60E-01	1.97E-01	1.70E-02	1.70E+00
SS2Z1	SS	0	1-2-3-4	1.43E-04	6.00E-04	6.00E-05	6.00E-03
SS2Z5	SS	1	5-6-7-8-13-14-16	1.43E-04	4.32E-06	2.00E-07	2.00E-04
SS2Z9	SS	0	9-10-11-12-15-17-18	1.43E-04	2.00E-06	2.00E-07	2.00E-04
SS2Z19	SS	0	19	1.43E-04	6.00E-06	6.00E-07	6.00E-04
SS2Z20	SS	1	20-21	1.43E-04	2.00E-06	4.00E-07	4.00E-04
VK2Z1	VK	1	1-2-3-4-9-10-11-18	7.01E+00	3.82E-01	3.00E-02	1.50E+01
VK2Z5	VK	1	5-7-8-14-16-12-15-16-17	5.00E-02	2.57E-04	1.49E-05	5.96E-02
VK2Z6	VK	1	6-13	1.40E-05	2.43E-05	1.22E-07	1.22E-04
VK2Z17	VK	0	19-20-21	1.40E+01	3.00E-01	3.00E-02	1.50E+01
HK3Z1	HK	1	1-2	1.80E-01	1.60E-01	3.56E-02	8.90E-01
HK3Z3	HK	1	3	2.40E-01	2.96E-01	4.70E-02	1.17E+00
HK3Z4	HK	1	4-5	1.30E-01	1.39E-01	2.78E-02	6.96E-01
HK3Z6	HK	1	6-7	2.80E-01	3.23E-02	8.00E-03	5.00E-01
HK3Z9	HK	1	9-11	1.90E-01	1.12E-01	3.70E-02	9.26E-01
HK3Z10	HK	1	8-10	1.80E-01	2.25E-01	2.35E-02	5.89E-01
HK3Z12	HK	1	12-13	2.80E-01	3.49E-01	8.43E-02	2.11E+00
HK3Z14	HK	1	14	2.20E-01	3.40E-01	4.55E-02	1.14E+00
HK3Z15	HK	1	15-16	3.00E-01	4.12E-01	6.30E-02	1.58E+00
SS3Z1	SS	1	1-2-3	1.43E-05	1.33E-06	6.34E-07	1.13E-04
SS3Z4	SS	1	4-5	1.43E-05	1.13E-04	7.55E-06	1.13E-04
SS3Z6	SS	0	6-7-9-11	1.43E-05	1.63E-05	3.26E-06	1.13E-04
SS3Z8	SS	0	8-10	1.43E-05	9.35E-06	1.87E-06	1.13E-04
SS3Z12	SS	0	12-13	1.43E-05	9.15E-06	1.87E-06	1.13E-04
SS3Z14	SS	0	14	1.43E-05	7.94E-06	1.87E-06	1.13E-04
SS3Z15	SS	0	15-16	1.43E-05	5.27E-04	1.87E-06	7.13E-04
VK3Z1	VK	0	1	1.84E-01	1.84E-01	3.68E-02	9.20E-01
VK3Z3	VK	1	2-3	3.37E-01	3.37E-01	6.74E-02	1.69E+00
VK3Z4	VK	0	4-5	2.44E-01	2.44E-01	4.88E-02	1.22E+00
VK3Z6	VK	0	6-7	1.54E-02	1.54E-02	3.08E-03	7.70E-02
VK3Z9	VK	0	9-11	3.50E-04	3.50E-04	7.00E-05	1.75E-03
VK3Z10	VK	0	8-10	3.50E-06	3.50E-06	7.00E-07	1.75E-05
VK3Z12	VK	0	12-13	1.53E-01	1.53E-01	3.06E-02	7.65E-01
VK3Z14	VK	0	14	3.85E-02	3.85E-02	7.70E-03	1.93E-01
VK3Z15	VK	0	15	6.71E-02	6.71E-02	1.34E-02	3.36E-01
HFB1	HFB	1		1.43E-05	8.47E-06	1.00E-07	1.00E-04

abbriviations:

HK	Horizontal Hydraulic Conductivity
SS	Specific Storage
SY	Specific Yield
VK	Vertical Hydraulic Conductivity
HFB	Horizontal flow barrier
Parameter Activity	1 represents active and 0 inactive in the PEST

Table 6-4
Residual General Statistics

Statistic	Value
Mean	0.50
Standard Error	0.25
Median	2.68
Mode	-2.72
Standard Deviation	25.38
Kurtosis	6.46
Skewness	-0.85
Range	392.41
Minimum	-238.56
Maximum	153.85
Confidence Level(95.0%)	0.49

Table 6-5
Residual Error Classification

Residual Error	Percent of Residuals within the Corresponding Residual Error
±10	37%
±20	66%
±30	83%
±40	91%
±50	96%
±60	98%
±70	98%

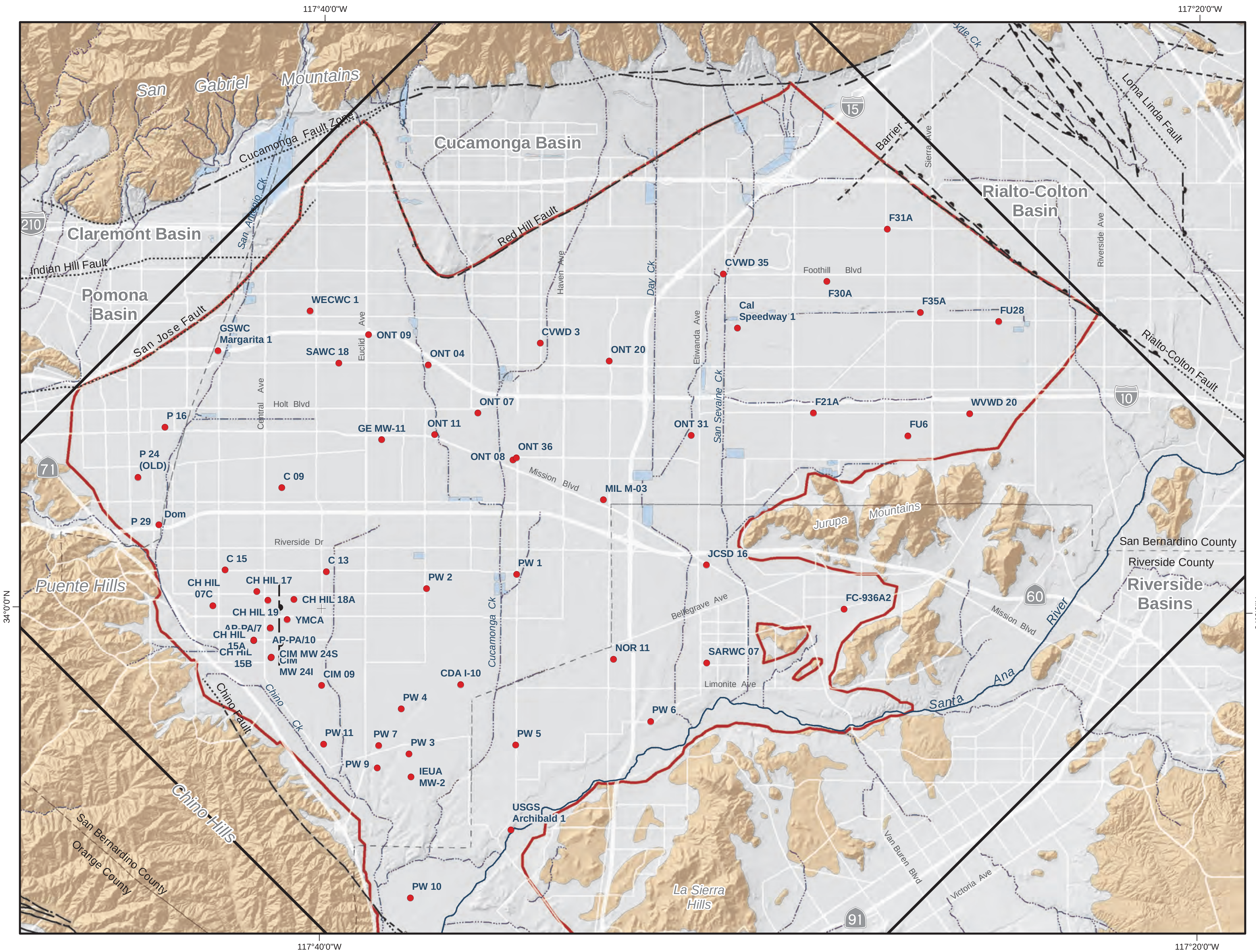

Calibration Wells

Model Grid Boundary

Streams, Rivers, and Flood Control Channels

Flood Control and Conservation Basins

Geology

Water-Bearing Sediments

Quaternary Alluvium

Consolidated Bedrock

Undifferentiated Pre-Tertiary to Early Pleistocene Igneous, Metamorphic, and Sedimentary Rocks

Faults

Location Certain

Location Approximate

Approximate Location of Groundwater Barrier

Location Concealed

Location Uncertain

Produced by:

WEI
Wildermuth Environmental, Inc.

Author: MJC
Date: 10/1/2015
Document Name: Figure_6-1

0 1 2 3 4 5 Miles
0 2 4 6 8 KM

2013 Chino Basin Groundwater Model Update and Analysis of Safe Yield

Location of Calibration Wells

Chino Basin

Figure 6-1

Figure 6-2a
Comparison of Simulated and Measured Water Levels in the Calibration Wells of Chino Basin

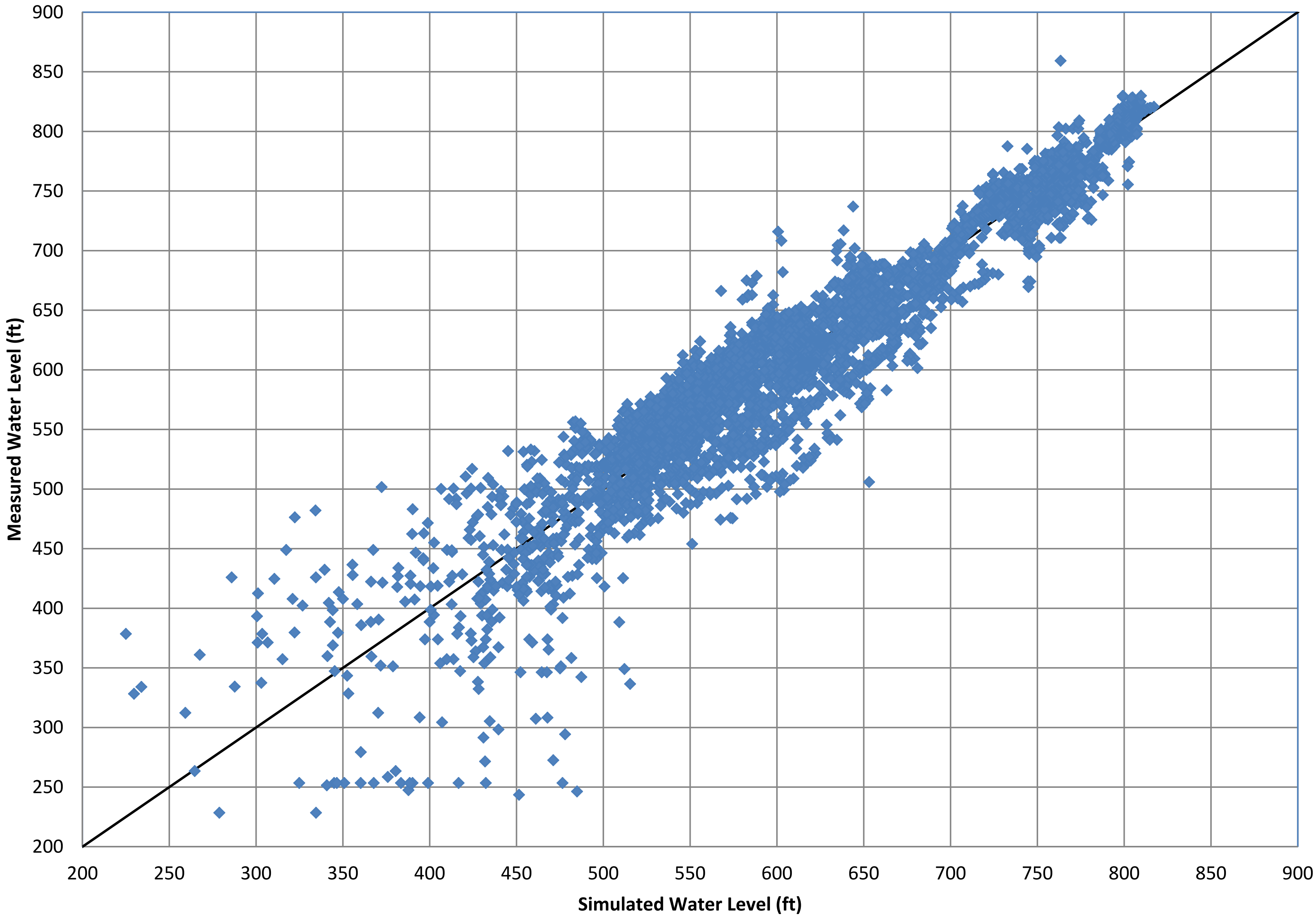

Figure 6_2abcdef_Scatter_plot_group 20131230.xlsx

Revised 10/2/2015

Figure 6-2b
Comparison of Simulated and Measured Water Levels in the Wells of Chino Basin Management Zone 1

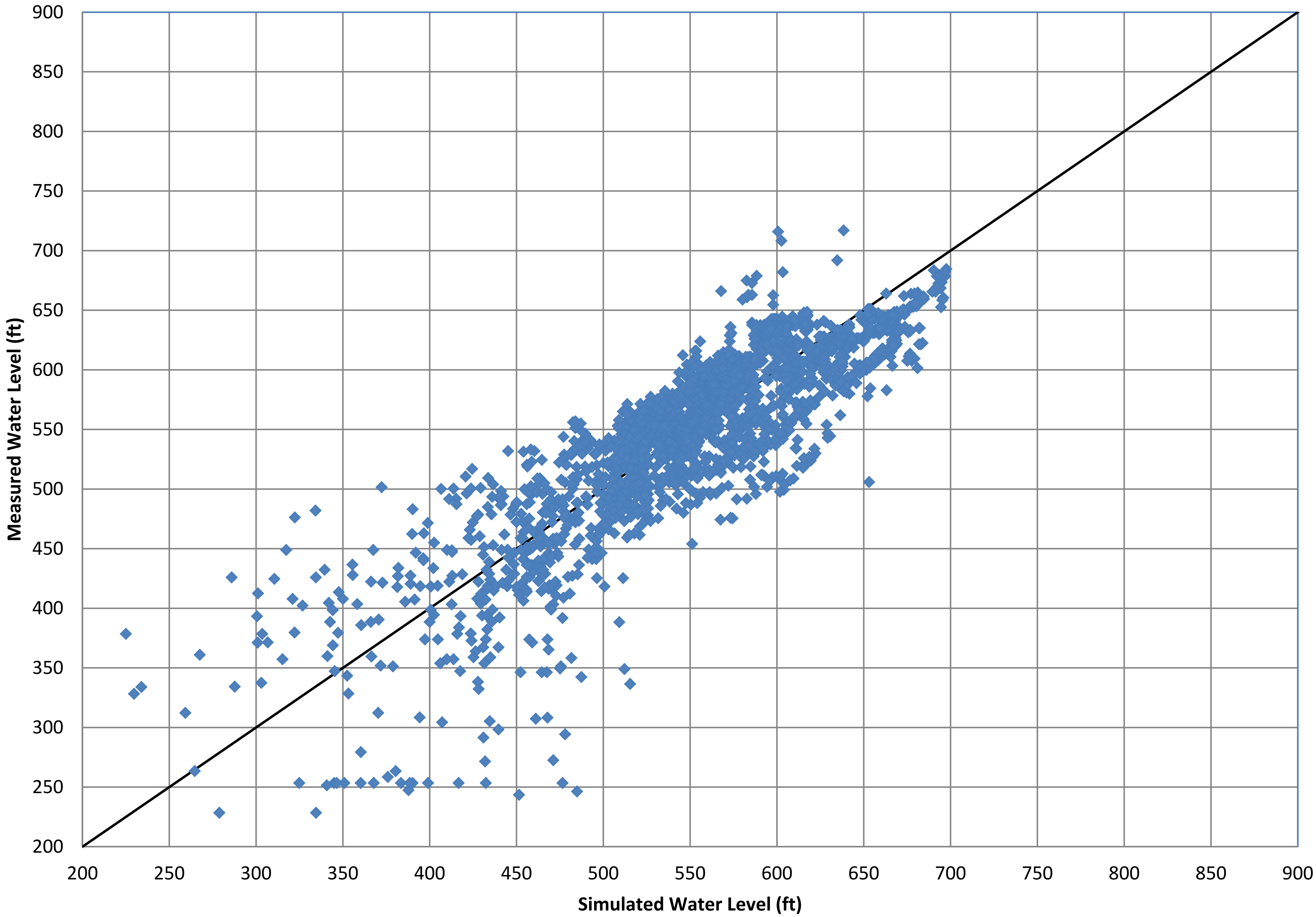

Figure 6_2abcdef_Scatter_plot_group 20131230.xlsx

Revised 10/2/2015

Figure 6-2c
Comparison of Simulated and Measured Water Levels in the Wells of Chino Basin Management Zone 2

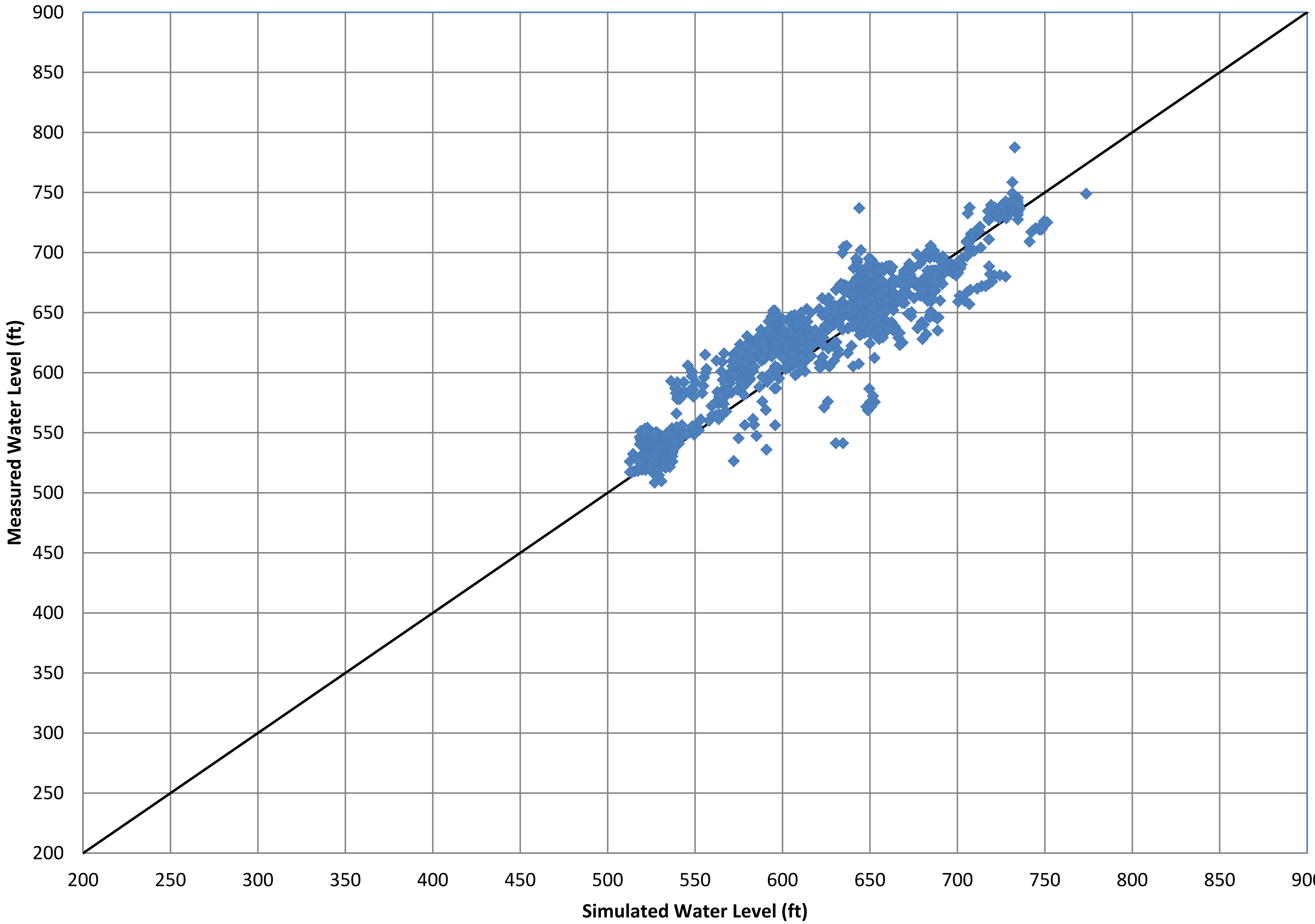

Figure 6_2abcdef_Scatter_plot_group 20131230.xlsx

Revised 10/2/2015

Figure 6-2d
Comparison of Simulated and Measured Water Levels in the Wells of Chino Basin Management Zone 3

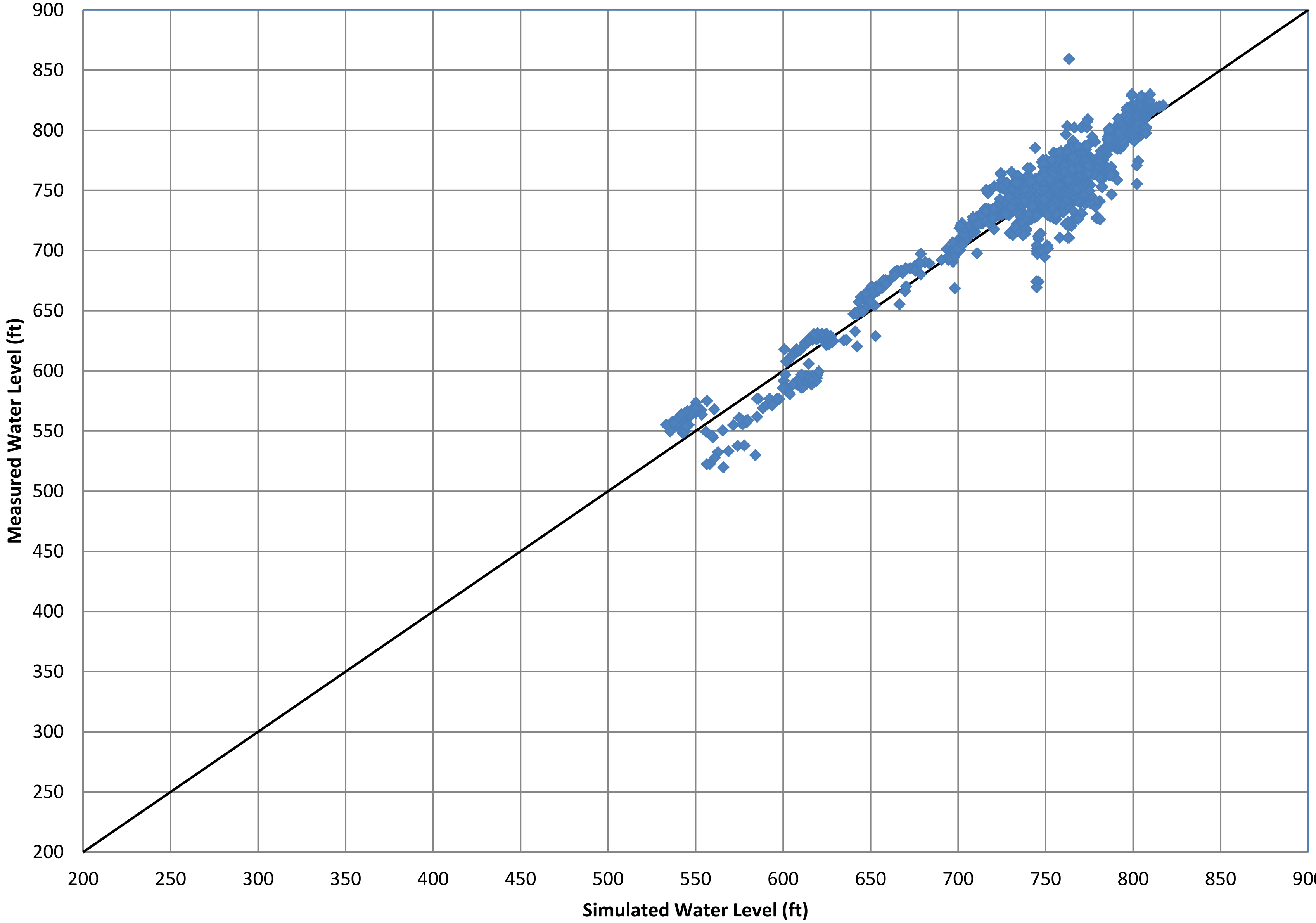

Figure 6_2abcdef_Scatter_plot_group 20131230.xlsx

Revised 10/2/2015

Figure 6-2e

Comparison of Simulated and Measured Water Levels in the Wells of MZ-4, MZ-5 and the Prado Basin MZ

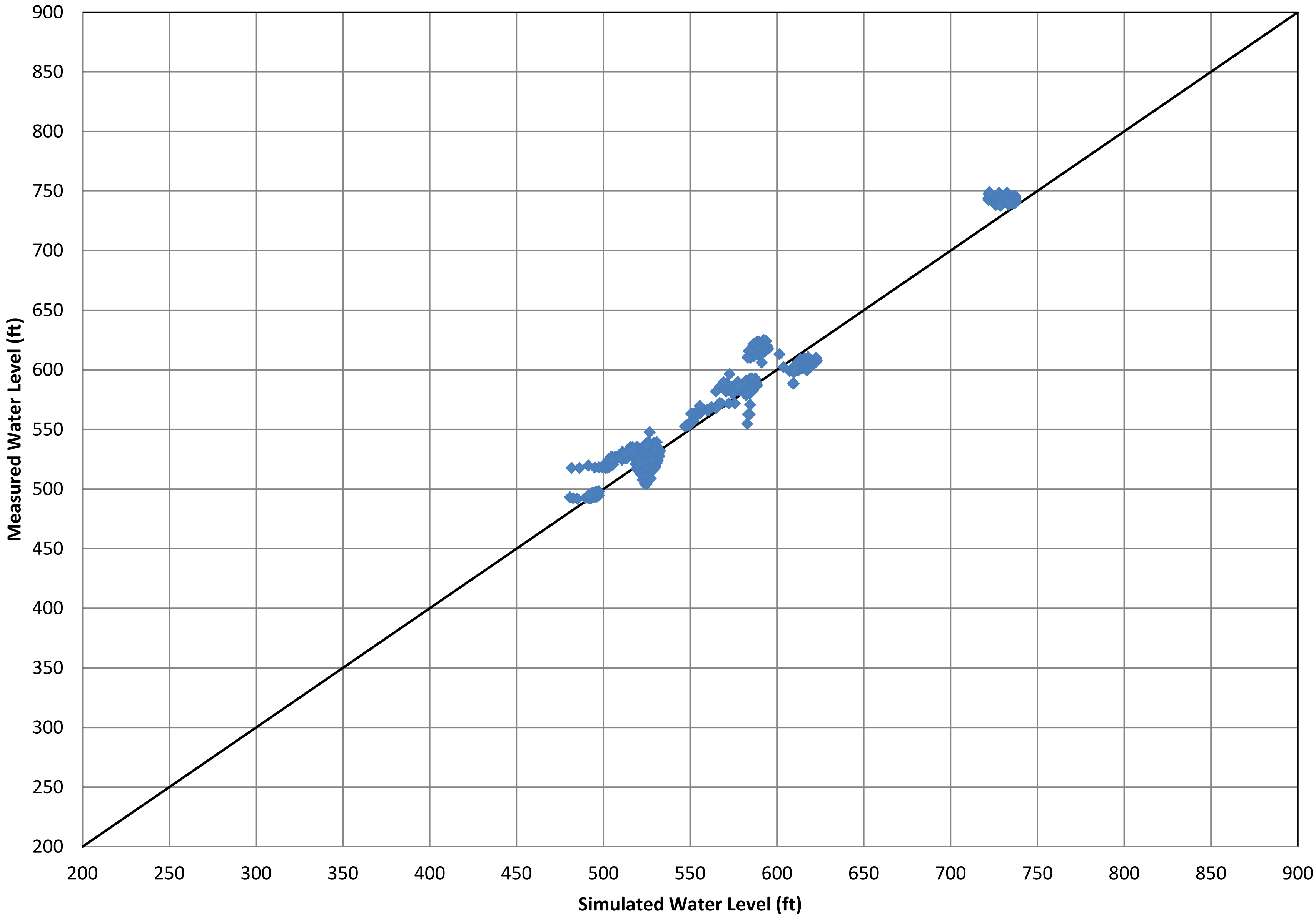

Figure 6_2abcdef_Scatter_plot_group 20131230.xlsx

Revised 10/2/2015

Figure 6-3a. MODFLOW Estimated Santa Ana River Discharge into Prado Dam Reservoir versus Total Santa Ana River Discharge Estimated by US Army Corps of Engineers

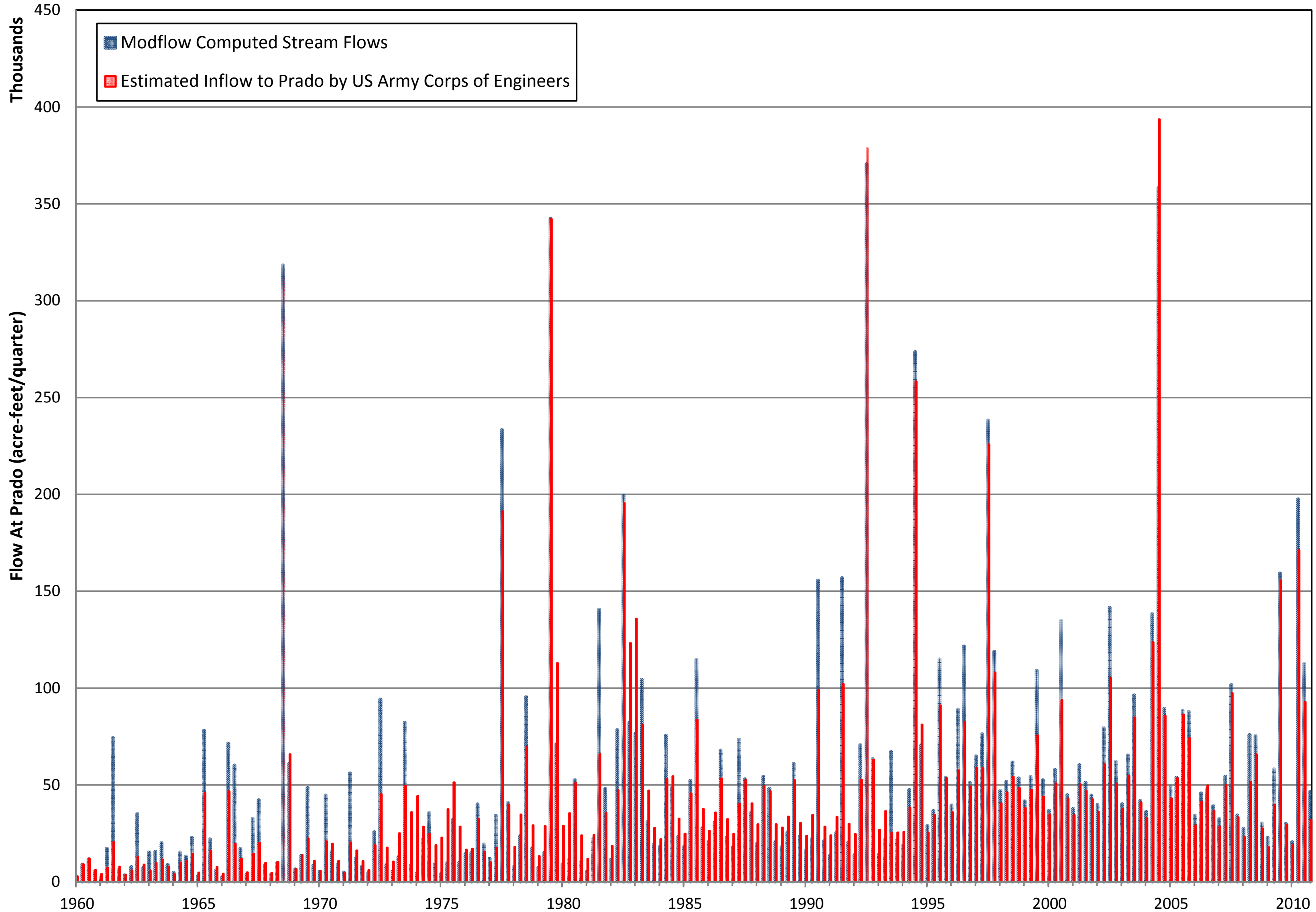

Figure 6-3ab_20131230.xlsx

Revised 10/2/2015

Figure 6-3b Model-Estimated Stream Flow to Prado versus Prado Inflow Estimated by US Army Corps of Engineers

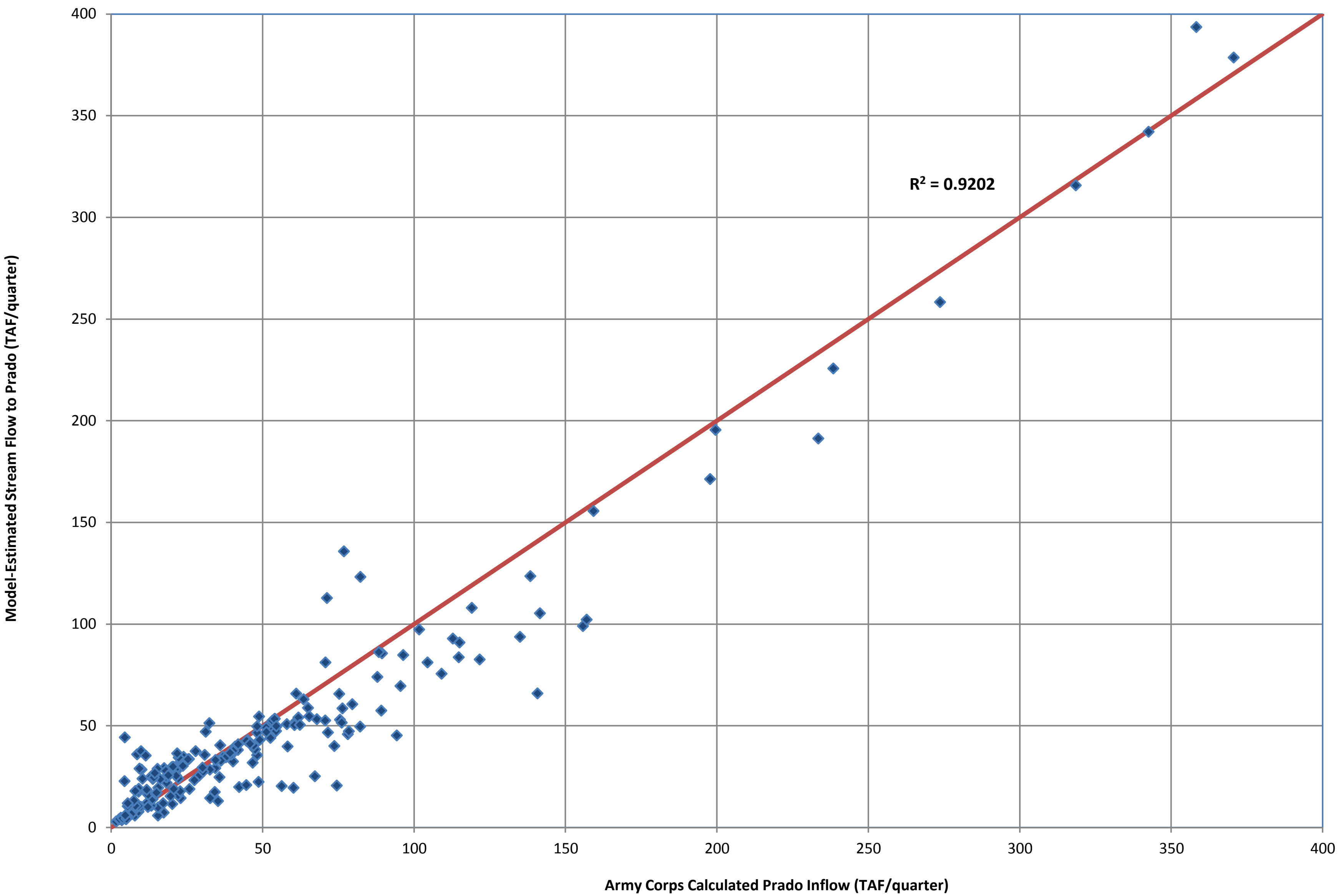

Figure 6-3ab_20131230.xlsx
Revised 10/2/2015

Figure 6-4
Residual Relative Freqency Histogram in Chino-Temescal Basin

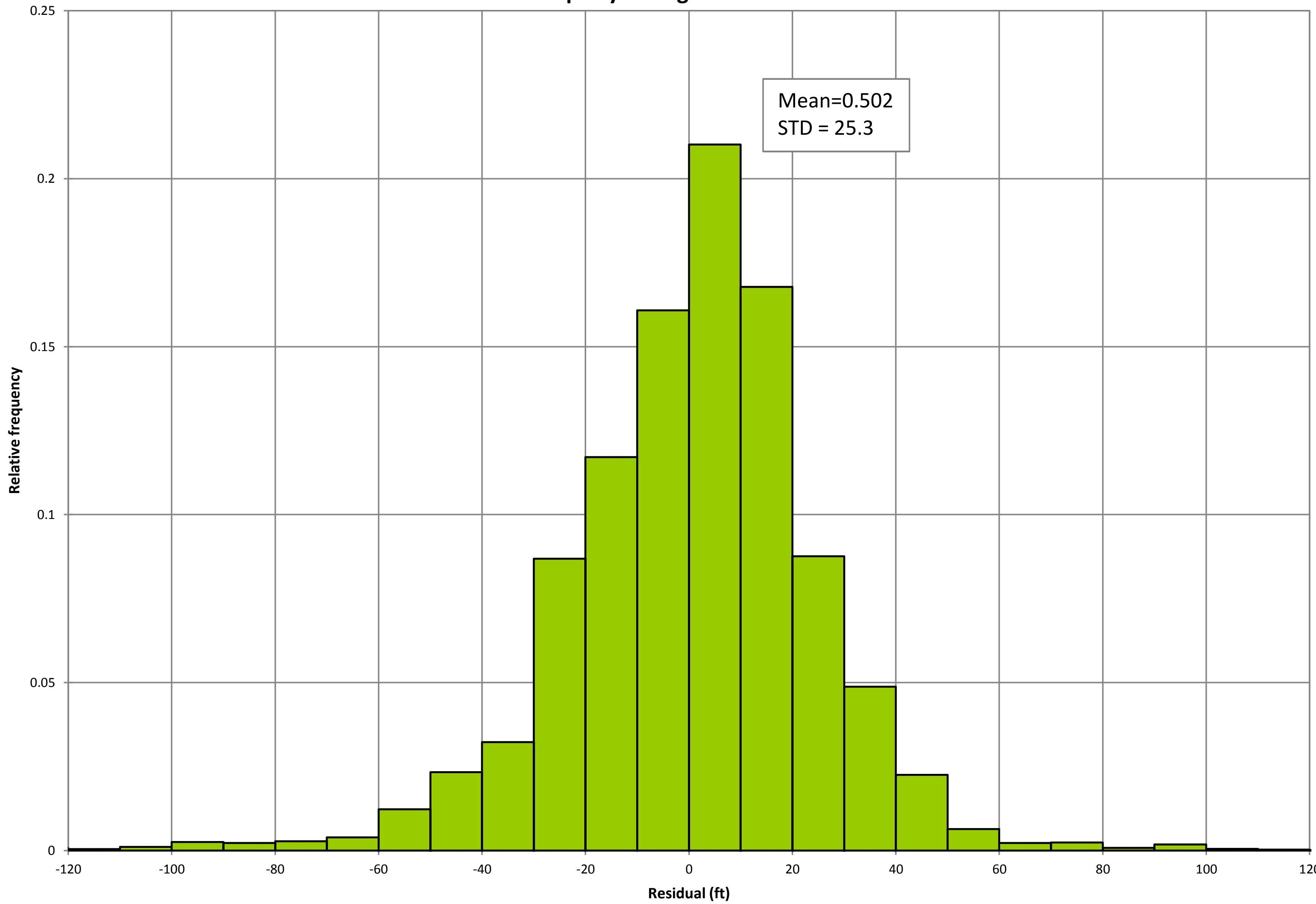

Figure 6_4_20131230.xlsx

Revised 10/2/2015

Figure 6-5a
Residual Relative Freqency Histogram in Chino Basin

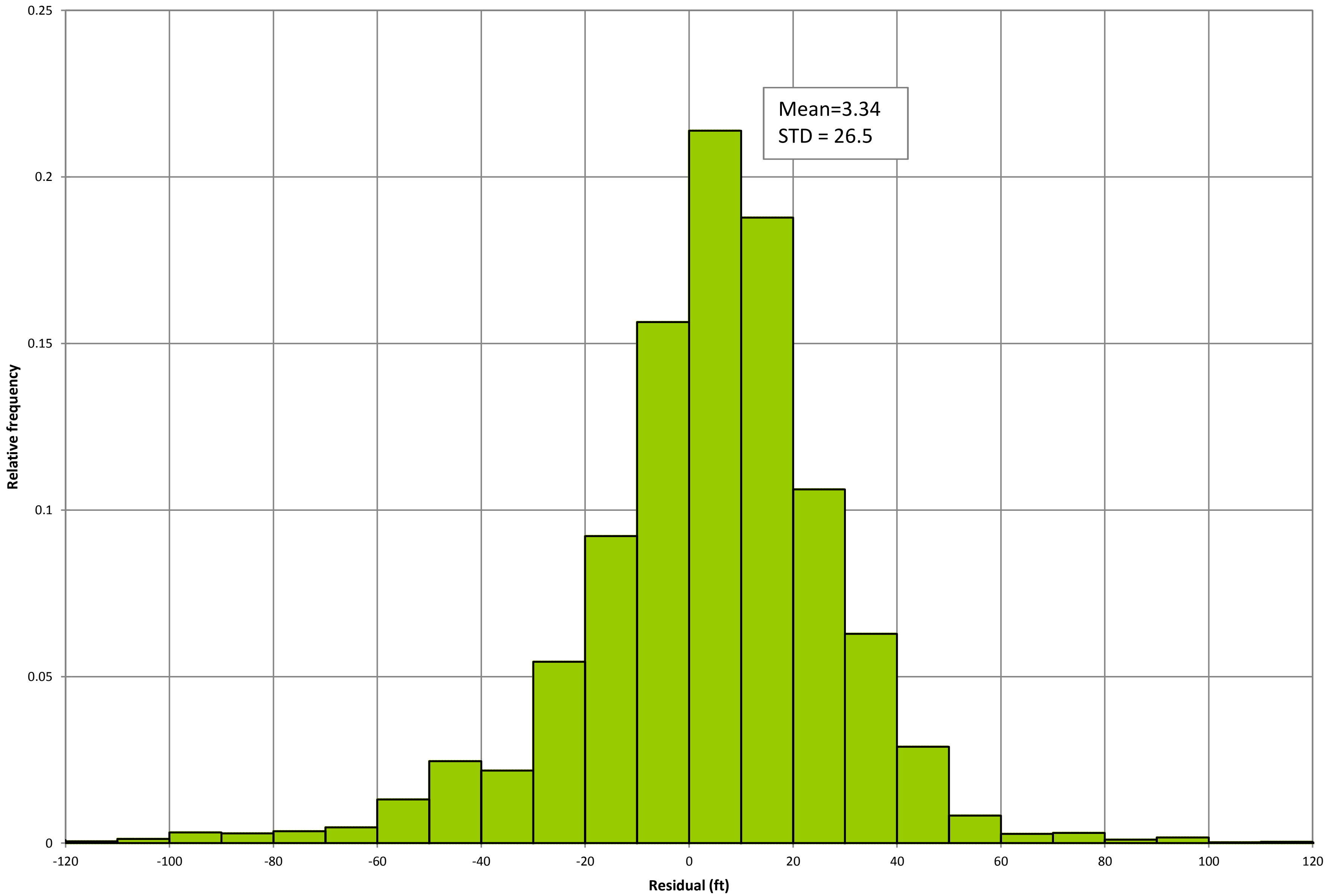

Figure 6_5abcd_20131230.xlsx

Revised 10/2/2015

Figure 6-5b
Residual Relative Freqency Histogram in MZ1 of Chino Basin

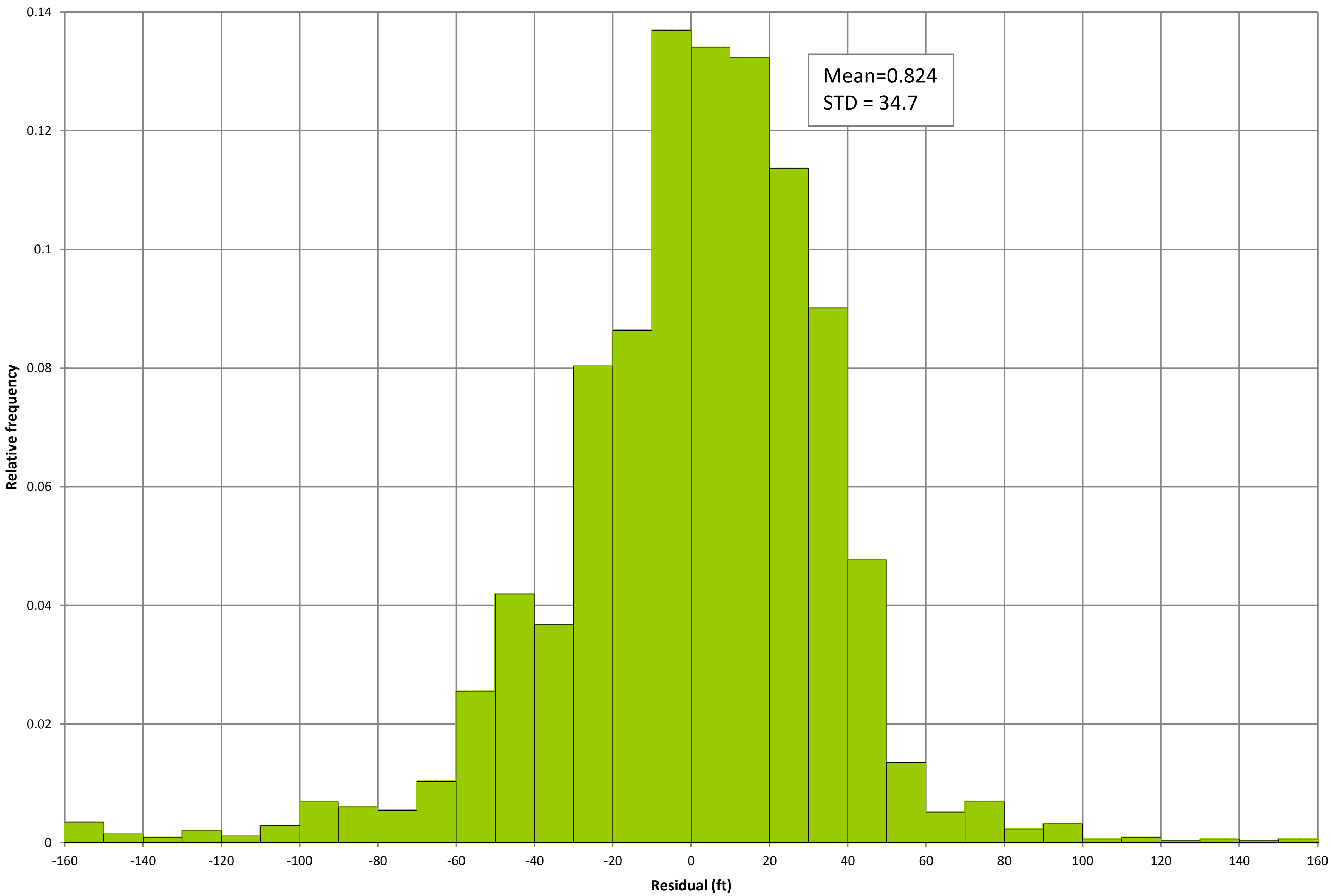

Figure 6_5abcd_20131230.xlsx

Revised 10/2/2015

Figure 6-5c
Residual Relative Freqency Histogram in MZ2 of Chino Basin

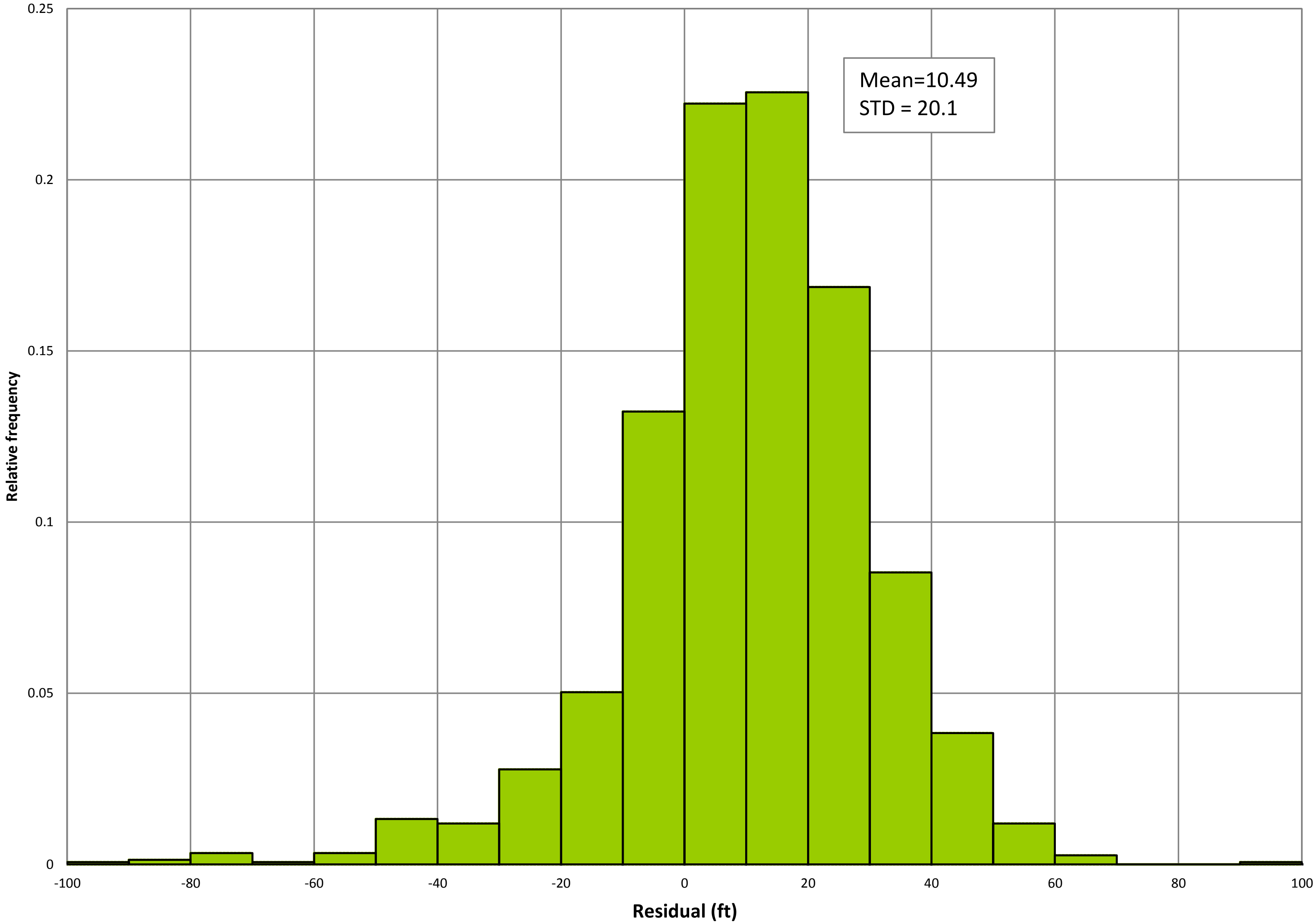

Figure 6_5abcd_20131230.xlsx

Revised 10/2/2015

Figure 6-5d
Residual Relative Freqency Histogram in MZ3 of Chino Basin

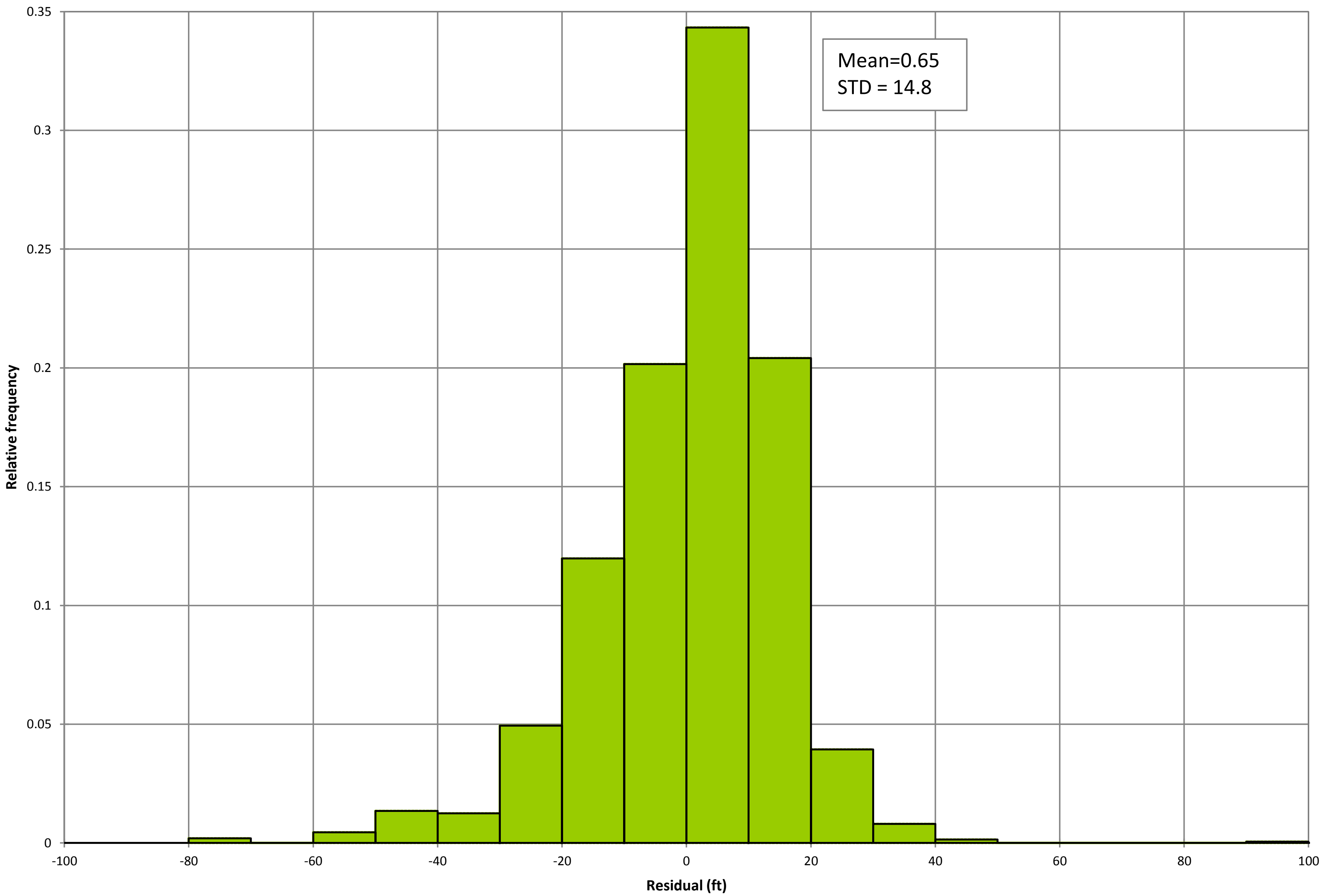

Figure 6_5abcd_20131230.xlsx

Revised 10/2/2015

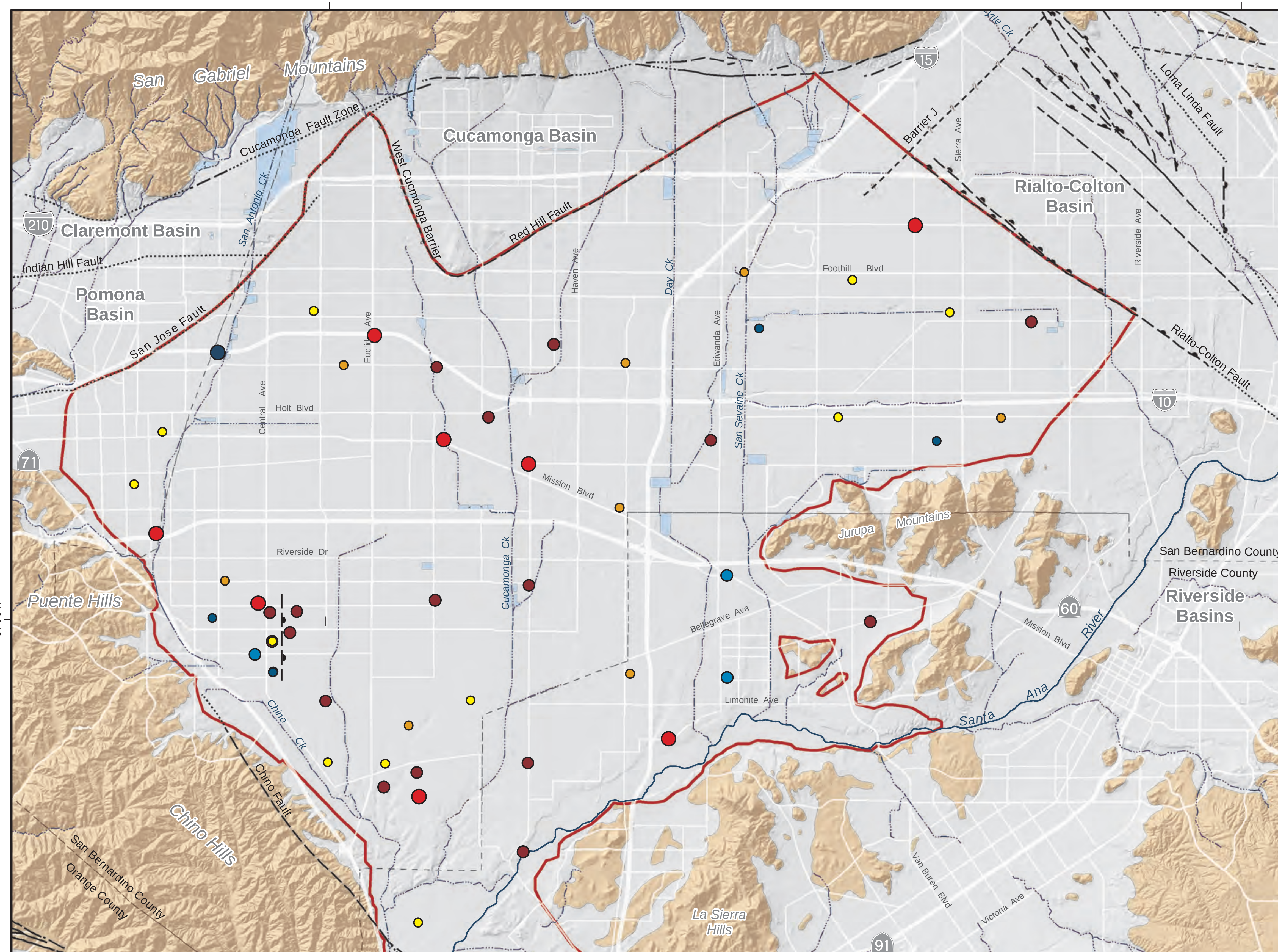

Mean Residual Error

- -23 to -20
- -20 to -10
- -10 to -5
- -5 to 5
- 5 to 10
- 10 to 20
- 20 to 30

Geology

Water-Bearing Sediments

Quaternary Alluvium

Consolidated Bedrock

Undifferentiated Pre-Tertiary to Early Pleistocene Igneous, Metamorphic, and Sedimentary Rocks

Faults

- Location Certain
- Location Approximate
- Approximate Location of Groundwater Barrier
- Location Concealed
- Location Uncertain

Produced by:

WEI
WILDERMUTH ENVIRONMENTAL, INC.

Author: MJC
Date: 10/1/2015
Document Name: Figure_6-6_20140124

0 1 2 3 4 5 Miles
0 2 4 6 8 KM

2013 Chino Basin Groundwater Model Update and Analysis of Safe Yield

Mean Residual Error of Calibration Wells

Figure 6-6

Section 7 - Safe Yield and Future Basin Conditions

This section discusses: the commonly accepted definition of safe yield; the criteria used to establish safe yield; the historical hydrology and cultural conditions assumed in the safe yield included in the 1978 Chino Basin Judgment; current and future projected cultural conditions; current and future projected net recharge; and the basin's response to projected future groundwater production, storage management, and replenishment plans. This section concludes with the recommended approach to estimate current and future projected net recharge and safe yield.

7.1 Safe Yield

7.1.1 Definition and Theory of Net Recharge and Safe Yield

Net recharge, as used herein, is the exploitable inflow to a groundwater basin over a specified period, either under historical conditions or in a future projection under prescribed operating conditions, and it is a result of the hydrology, cultural conditions, and water management practices of the time period.

The most common definition of safe yield is attributed to Todd (1959):

> "[T]he rate at which groundwater can be withdrawn perennially under specified operating conditions without producing an undesirable result."

Most modern groundwater adjudications use some form of this definition. The Stipulated Agreement for the Chino Basin defines safe yield as:

> "[T]he long-term average annual quantity of groundwater (excluding replenishment or stored water but including return flow to the basin from the use of replenishment or stored water) which can be produced from the Basin under cultural conditions of a particular year without causing an undesirable result."[10]

This definition ties the safe yield to the cultural conditions of a specific year, presumably a near current or representative year if cultural conditions are changing. The Judgment declares the Chino Basin safe yield to be 140,000 acre-ft.[11]

Undesirable results commonly listed in published literature include: the depletion of groundwater reserves, the intrusion of water of undesirable quality, contravention of existing water rights, excessive increases in production costs, streamflow depletions, and subsidence (Freeze & Cherry, 1979). Avoiding the depletion of groundwater reserves was the primary undesirable result that the Chino Basin Judgment sought to protect. The physical solution provided in the Judgment and the groundwater management plan in the OBMP limit the undesirable results listed above through the implementation of localized management programs. The Judgment requires Watermaster to offset production in excess of the safe yield by Replenishment. Watermaster assesses the parties that produce groundwater in excess of their safe yield allocation to fund the purchase of replenishment water. The OBMP requires that Watermaster use its discretion when recharging Supplemental Water to balance recharge and discharge in every area and subarea.

[10] Judgment, Section I Introduction, Paragraph 4 Definitions.

[11] Judgment, Section II Declaration of Rights, Part A Hydrology, Paragraph 6 Safe Yield.

Common engineering practice is to estimate net recharge and safe yield based on hydrologic principles. The following discussion describes the basic methodology used to estimate net recharge and safe yield from hydrologic principles.

Net recharge is estimated as the average net inflow to the basin, excluding the direct recharge of supplemental water. Supplemental water, as used herein, refers to water not tributary to the basin and includes imported and recycled waters. Returns from agricultural uses and on-site wastewater disposal systems (e.g. septic tanks, cesspools, etc.) that overlie the basin are included in net recharge. There are two ways to compute net recharge under this concept, both of which can be derived from the continuity equation. The continuity equation is:

$$\text{Change in Storage } (\Delta S) = [\text{Inflow (I)} - \text{Outflow (O)}] * \Delta t \tag{1}$$

Where:

- S^t is the storage at time t,
- ΔS is the change in storage calculated as S^{t+1} minus S^t,
- I is the total inflow to the basin over the period t to $t+1$ and is equal to the sum of Streambed Recharge (I_{sr}) + Deep Infiltration of Precipitation (I_p) + Subsurface Inflow (I_{ssi}) + Artificial Recharge of Supplemental Water (I_{ar}) + Deep Infiltration of Irrigation Return Flows ($I_{rf.}$),
- O is the total outflow from the basin over the period t to $t+1$ and is equal to the sum of Groundwater Pumping (O_p) + Subsurface Outflow (O_{ss}) + Groundwater Discharge to Surface Water (Q_{rw}) + Evapotranspiration (Q_{et}), and
- Δt is the length of the time period used to compute the balance.

The inflow and outflow terms listed above have dimensions of L^3/T.[12] If expanded using the hydrologic terms listed above, the continuity equation becomes:

$$\Delta S = [I_{sr} + I_p + I_{ssi} + I_{ar} + I_{rf.} - O_p - O_{ss} - O_{rw} - O_{et}] * \Delta t \tag{2}$$

The net recharge (net inflow) to a basin for a single year is:

$$\text{Net recharge} = I_{sr} + I_p + I_{ssi} + I_{rf.} - O_{ss} - O_{rw} - O_{et} = S^{t+1} - S^t + O_p - I_{ar} \tag{3}$$

The net recharge over a multiple-year period can be estimated from:

$$\text{Net recharge} = [\, \Sigma I_{sr} + \Sigma I_p + \Sigma I_{ssi} + \Sigma I_{rf.} - \Sigma O_{ss} - \Sigma O_{rw} - \Sigma O_{et}] \,/\, \Delta t \tag{4}$$

$$= [\, \Delta S + \Sigma O_p - \Sigma I_{ar}]/\Delta t$$

The summation symbol (Σ) in equation 4 for each term aggregates the contiguous time series over multiple years that comprise a base period or period of interest.

In modern practice, the most pragmatic way to estimate net recharge is to rigorously apply numerical models and evaluate equation (4):

$$\text{Net recharge} = \Delta S/\Delta t + O_p - I_{ar} \tag{5}$$

[12] L means length, and T means time.

Where O_p and I_{ar} are the average groundwater pumping and average supplemental water recharge over the base period, respectively.

7.1.2 Safe Yield Criteria

The net recharge from a groundwater basin, estimated using equations 4 or 5 above, corresponds to the net inflow to a groundwater basin over a specified period of time. If the period includes representative long-term hydrology and meets other safe yield related criteria, then the net recharge for that period can be assumed to be the safe yield.

7.1.2.1 Base Period

In safe yield determinations, it is common engineering practice to select a base period from precipitation records that span a reasonably long period of time, which contains wet periods and dry periods, and for which the annual average precipitation equals the long-term average annual precipitation. The availability of data for estimating the inflow, outflow, and storage terms can also factor into the ultimate base period selection.

The watershed surface that is tributary to and overlies the Chino Basin and water management practices over the basin have changed dramatically over the last 70 years. The land use, water management, and drainage conditions that are tributary to and overlie the Basin at a specific time are herein referred to collectively as the cultural condition of the basin. The types of land uses that overlie a groundwater basin have a profound impact on recharge. The land use transition from natural use to agricultural uses and subsequently to developed urban uses radically changes the amount of recharge to the basin. Furthermore, irrigation practices change over time in response to agricultural economics (e.g. demand for various agricultural products, commodity prices, production costs, etc.), the availability of water, regulatory requirements, technology, and the cost of water. Urbanization increases the amount of imperviousness, decreasing the irrigable and permeable areas, which allow irrigation return flows and precipitation to infiltrate through the soil, and conversely increases the amount of stormwater produced on the land surface. Drainage improvements associated with the transition from natural and agricultural uses to urban uses reduce the recharge of stormwater: channels and streams are concrete-lined to move stormwater efficiently through the watershed overlying the groundwater basin.

Changes in land use, water management, and drainage over time produce groundwater recharge and discharge time histories that are not stationary: the relationship of the inflow and outflow terms to precipitation and other hydrologic and management drivers change over time. Thus, the selection of a representative base period that satisfies the traditional criteria for a determination of safe yield that is representative of current and near-future cultural conditions is not possible using the actual historical record.

7.1.2.2 Storage

The availability of water in storage at the beginning of the base period and the availability of operational storage space during the base period must be such that production at the estimated safe yield can be sustained. There must be enough storage space (operational storage) available to store recharge in excess of the safe yield during wet years so that it can be available in years when recharge is less than the safe yield.

7.1.2.3 Basin Area

The safe yield is determined for a geographically defined groundwater basin. The recharge and discharge to the basin occur within or on the boundaries of the basin. The Chino Basin has two boundaries: the legal boundary, as defined in the 1978 Judgment, and the hydrologic boundary, which more accurately reflects the locations of physical barriers to groundwater movement and basin recharge. Figure 1-1 shows the locations of these boundaries. The primary differences in these boundaries can be observed in the northern part of the basin and its boundary with the Cucamonga Basin. The net recharge computed in this investigation is based on the hydrologic boundary; the net recharge applies to the legal boundary.

7.1.2.4 Land Use

Land use is key component of the cultural conditions for a specific point in time. Table 7-1 summarizes the land use history in the hydrologically defined Chino Basin for the historical period of 1933 through 2010 and projected land use through assumed build-out in 2030.[13] The land use characterizations for:

- 1933 through 1984 are based on land use maps that were prepared by the DWR,
- 1990 and 2000 are based on land use maps that were obtained from SAWPA,
- 2005 are based on data provided by the Southern California Association of Governments (SCAG), and
- 2010 and 2030 are based on the 2005 SCAG land use characterization updated with a 2010 aerial photo and general plan land use maps, respectively.

Table 7-2 summarizes, by land use category, the estimated imperviousness, crop evapotranspiration, irrigation efficiency, applied water, and irrigation return properties.

With few exceptions, as land is converted from natural undeveloped conditions to human uses, it becomes more impervious and produces more stormwater runoff. Historically, when land use has converted from natural and agricultural uses to urban uses, imperviousness has increased from near zero to between 60 and almost 100 percent, depending on the specific land use. Table 7-1 lists thirteen land use classifications in the Chino Basin model domain and their area totals for years 1933, 1949, 1957, 1963, 1975, 1984, 1990, 2000, 2010, and 2030. Figure 7-1 illustrates the time series of land use and imperviousness in the Chino Basin from 1933 through 2010 and the relationship of imperviousness to urban land uses. The land use was predominantly in an agricultural and undeveloped state until 1984: urban uses accounted for about 10 percent from 1933 through 1957, grew steadily thereafter to about 26 percent in 1975, and reached about 66 percent in 2010. And, the fraction of the Chino Basin model domain that was impervious was about 10 percent between 1933 and 1957, grew steadily to about 21 percent in 1975, and reached about 51 percent in 2010. At build-out, the fraction of the Chino Basin model domain that is projected to be impervious is about 70 percent.

In an undeveloped state, most of the precipitation that fell on the watershed tributary to and over the Chino Basin was intercepted by vegetation or absorbed into the soils overlying the Basin. This water would have either been consumed by native vegetation or lost to evaporation. The overlying soils would become wet near the surface and completely dry before the next winter. Infrequent large storms produced significant runoff, some of which recharged the underlying groundwater basin through streambed infiltration.

[13] Table 7-1 is a revised version of Table 3-1 in the 2010 Recharge Master Plan Update (WEI, 2010), reflects an increase in model area in the Jurupa area, and includes all of the Prado Basin Management Zone.

Most of the precipitation that falls on paved areas and roofs becomes runoff. In the urban landscape, permeable areas are covered with vegetation that is irrigated and cultivated or left unplanted and not irrigated. The soil underlying irrigated vegetation is maintained in a moist state and never completely dries out—the significance being that when soil is continuously moist, some of the irrigation water and precipitation can infiltrate beyond the root zone and recharge the underlying groundwater basin.

Agricultural irrigation is never 100-percent efficient. Flood and furrow irrigation practices have irrigation efficiencies typically ranging from 40 to 60 percent and sprinkler irrigation from 70 to 80 percent. Irrigation return flows were a major source of recharge to the basin when irrigated agriculture dominated the land use. Figure 3-5 shows the time history of the deep infiltration of precipitation and applied water (DIPAW). DIPAW was about 140,000 acre-ft/yr in the period 1930 through 1940 and declined to less than 100,000 acre-ft/yr by and after 2000.

7.1.2.5 Changes in Drainage

Drainage improvements that were incorporated into the urban landscape were designed to convey stormwater rapidly, safely, and efficiently from the land surface through urban developments, and to discharge stormwater away from urbanized areas. Until the late 1990s there was little or no thought as to the value of the stormwater that discharged out of the Chino Basin.

Figure 3-3 shows the stream systems that start in the San Gabriel Mountains and flow from the north to the south, crossing the Cucamonga, Chino, and Six Basins. From about 1957 to present, the drainage areas overlying the valley floor have been almost completely converted to urban uses, and almost all of the streams have been converted from unlined to lined channels. The lining of these channels almost completely eliminated stormwater recharge in the Chino and Cucamonga Basins after 1984. Figure 3-4 shows the time history of streambed infiltration for the Santa Ana River tributaries that cross the Chino Basin and formerly recharged it. Figure 3-4 is a stacked bar chart that illustrates the stormwater recharge over the calibration period excluding the Santa Ana River. Streambed recharge is greatest in wet years (such as 1969 and 1978) and lowest in dry years (such as 1961 and 1976), and it drops to about 900 acre-ft/yr after 1990 with the almost complete lining of stream channels.

7.1.2.6 Groundwater Production

Figure 7-2 shows historical groundwater production for 1961 through 2013. Groundwater production for the Overlying Non Ag and Appropriator Parties was estimated from data provided by them. The Overlying Agricultural Parties' groundwater production was estimated using WEI's R4 model[14] for the period of 1961 through 2002 and subsequently from Watermaster records through 2013. Total groundwater production was just over 200,000 acre-ft/yr through 1968 and generally declined thereafter reaching about 148,000 acre-ft/yr in 2012. Groundwater production exceeded the 1978 Judgment safe yield each year from 1978 through 1998. The Overlying Agricultural Pool Parties' aggregate production exceeded their production right of 82,800 acre-ft/yr each year from 1978 through the 1989.

[14] The R4 model is described in Appendix A. The land use and water use data used in R4 are summarized in Tables 7-1 and 7-2.

7.1.3 Estimate of the Safe Yield Included in the 1978 Chino Basin Judgment

In the 1978 Judgment, the safe yield of the Chino Basin was established to be 140,000 acre-ft/yr. The basis for this estimate was described by William J. Carroll in his testimony on December 19 and 20, 1977, during the Chino Basin adjudication process. Table 7-3 lists the hydrologic components developed by Carroll to estimate the safe yield of the Chino Basin. These components were developed for the 1965 to 1974 period, a period that Carroll referred to as the base period. The hydrologic components listed in Table 7-3 are described below.

- Deep Percolation of Precipitation and Surface Inflow – consists of the deep percolation of precipitation and streamflow. Carroll developed an estimate of 47,500 acre-ft/yr, based on Chino Basin modeling results from the DWR.
- Deep Percolation of Artificial Recharge – consists of the percolation of local runoff in spreading basins. Carroll estimated the local runoff recharged in San Bernardino County facilities to be about 2,800 acre-ft/yr during the base period. The Etiwanda Water Company also recharged about 1,000 acre-ft/yr of water to the Chino Basin from Deer and Day Creeks during the base period.
- Deep Percolation of Chino Basin Groundwater Used for Irrigation (Domestic and Agricultural) – defined as the fraction of water applied for irrigation that percolates through the soil and recharges underlying groundwater. Carroll estimated that about 15 percent of the water used for domestic irrigation would percolate to groundwater and about 45 percent of the water used for agricultural irrigation would percolate to groundwater. Carroll estimated the volume of percolation of Chino Basin groundwater used for irrigation over the base period to be about 61,700 acre-ft/yr.
- Deep Percolation of Imported Water Used for Irrigation (Domestic and Agricultural) – same as deep percolation of Chino Basin groundwater except the water used for irrigation is imported to and used over the Chino Basin. Carroll estimated the volume of percolation of imported water used for irrigation over the base period to be about 7,000 acre-ft/yr.
- Recharge of Sewage – defined as the percolation in ponds of wastewater discharged by municipal wastewater treatment plants. This component ceased almost completely at the end of the base period and was known to be eliminated as a recharge source when the safe yield was estimated. The volume of sewage recharge over the base period was about 18,200 acre-ft/yr. The inclusion of sewage recharge as a component of the safe yield in the stipulated Judgment was therefore not hydrologically consistent with how the Basin was to be operated post-Judgment.
- Subsurface Inflow – defined as groundwater inflow to the Chino Basin from adjacent groundwater basins and mountain fronts, totaling 7,000 acre-ft/yr.
- Subsurface Outflow – defined as groundwater that rises to the ground surface in the Prado Basin to become Santa Ana River flow. Estimates of subsurface outflow were based on studies by the DWR, the United States Geological Survey (USGS), and Carroll. Carroll estimated subsurface outflow to average about 7,200 acre-ft/yr over the base period.
- Extractions – defined as groundwater extractions from the Chino Basin. Carroll estimated groundwater extractions to average about 180,000 acre-ft/yr during the base period.

In addition to these components, Carroll estimated the change in storage over the base period to be about -40,000 acre-ft/yr, which equates to a decline in the volume of groundwater in storage of about 400,000 acre-ft during the base period. Carroll estimated the safe yield to equal the average production over the base period plus the average change in storage during the base period:

$$\begin{aligned} \text{Safe Yield} &= \text{Production} + \text{Change in Storage} \\ &= 180{,}000 - 40{,}000 \\ &= 140{,}000 \text{ acre-ft/yr} \end{aligned} \tag{6}$$

This safe yield estimate is approximately equal to the total average inflow to the basin (145,500 acre-ft/yr) minus the non-production outflow (7,200 acre-ft/yr). This 140,000 acre-ft/yr safe yield estimate was incorporated into the Judgment and is the current Safe Yield used by Watermaster. Note that Carroll's equation is similar to equation 5, with Carroll omitting the artificial recharge of supplemental water term. Seemingly, Carroll and the Watermaster Parties ignored the actual recharge of supplemental water that occurred during Carroll's base period and that ceased almost immediately after the base period. During the Carroll base period, about 120,300 acre-ft of recycled water was recharged by the IEUA and its member agencies, averaging about 12,000 acre-ft/yr. If Carroll had strictly applied equation 5 with his estimates of production and change in storage and the historical estimates of recycled water recharge, his estimate of safe yield would have been about 128,000 acre-ft/yr. Carroll's safe yield estimate is a net recharge estimate that was assumed by the Court to be the safe yield of the basin.

The hydrology and cultural conditions of Carroll's base period do not comport with the definition of safe yield in the Judgment or with the current accepted and common engineering practice for a safe yield determination. Carroll's ten-year base period is far too short to be hydrologically representative of the hydrology of the Chino Basin. And, the cultural conditions that occurred in Carroll's base period are not representative of the period in which the safe yield would be used, specifically:

- The impervious cover during the Carroll base period was about 18 percent[15] compared to 32 percent in 1984, 39 percent in 1990, and about 51 percent in 2010;
- The lining of the major streams that cross the Chino Basin, most of which occurred after 1974; and
- The decline in agricultural production with the attendant shift in location of groundwater from the south to the north.[16]

Figure 7-3 shows the annual agricultural groundwater production in the Chino Basin for the historical period of 1961 through 2013, projected production through 2050, and the net recharge in the basin. Clearly, changes in agricultural groundwater production and cultural conditions have contributed to changes in net recharge. The net recharge during Carroll's base period was about 155,000 acre-ft/yr. The estimated net recharge declines with the conversion of agricultural land use to urban uses and the reduction in agricultural groundwater production.

7.2 Present and Projected Future Cultural Conditions

The 2013 Watermaster model was used to evaluate net recharge, groundwater levels, the state of hydraulic control, and losses from storage for the 2012 through 2050 period. Planning scenarios were created based on the water resource plans provided by the Watermaster Parties, planning hydrology, and assumptions regarding cultural conditions and future replenishment. The information and assumptions included in the planning scenarios are described in this section.

[15] From Table 7-1, the average of 15 percent in 1963 and 21 percent in 1975.

[16] See the OBMP Phase 1 Report, August 1999.

7.2.1 Planning Scenarios

In addition to Scenario 1 – Historical Calibration Period through June 2011, other planning scenarios were developed to test the model hydrology (Scenario 2), to provide preliminary evaluations of future planning scenarios (Scenario 3), and to provide specific planning information to Watermaster, including projected future net recharge, expected changes in groundwater levels and storage from future groundwater production and replenishment plans, and losses from stored water (Scenario 5). Scenario 5A represents the Watermaster Parties' best estimate of current and projected future groundwater production and artificial recharge. The following discussion will focus on a description of Scenario 5A.

Planning Scenario 5A includes cultural conditions representative of the period of 2012 through 2050 and uses a 92-year hydrologic period from 1921 through 2012. Planning Scenario 5A assumed a gradual increase in groundwater production, based on groundwater production projections developed in the 2013 Amendment of the 2010 Recharge Master Plan Update (WEI, 2013), and that replenishment and recharge operations would be conducted by Watermaster pursuant to the Judgment and Peace Agreement. Planning Scenario 5A assumes the following:

- Planning period runs from 2012 through 2050.
- The economy will expand with the build-out of undeveloped land occurring by 2030.
- The CDA expansion would occur based on an approved schedule, and re-operation will occur based on the current approved schedule through 2030.
- The 6,500 acre-ft/yr supplemental water recharge obligation for MZ1 will terminate in 2030.
- Projected future recycled water recharge estimates were provided by the IEUA.
- Projected future stormwater recharge estimates were based on average historical stormwater recharge estimates.
- There will be no increase in future stormwater recharge capacity.
- The 5,000 acre-ft/yr of controlled overdraft pursuant to the Judgment will cease after 2017.
- Production rights will be based on the current and projected future safe yield.
- Groundwater production estimates for fiscal years 2012 and 2013 were actual production estimates, and groundwater production estimates for 2014 through 2050 were provided by the Parties or developed by Watermaster staff and approved by the Parties.
- The annual replenishment obligation was estimated using the efficient market assumption, which includes:
  - On a go-forward (post 2013) basis, under-producers will transfer un-pumped rights to over-producers each year; that is, there is an efficient market that moves unused production rights from under-producers to over-producers.
  - Water in storage accounts will be used to meet future replenishment obligations prior to the purchase of supplemental water for wet-water for recharge.
  - All transfers among the parties and depletion from storage accounts will not cause an MPI.

7.2.1.1 Future Projections of Groundwater Production

The 2010 RMPU (WEI et al., 2010) contained a recommendation to update the groundwater production and replenishment obligations to reflect the water purveyor plans being developed to comply with SBX7-7 (20 percent reduction in per capita potable demands by 2020) and the 2010 Urban Water Management Plans (UWMPs) that were due in June 2011. Some stakeholders in the 2010 RMPU process noted that water purveyors may have overestimated groundwater production projections, which would lead to an overestimate of future replenishment obligations and potentially investments in new recharge facilities that may not be required if more recent future groundwater production estimates were used. The Court accepted this recommendation and included it in its October 8, 2010 Court Order, directing Watermaster and the IEUA to prepare updated groundwater production and replenishment obligation projections and to submit them to the Court by December 17, 2011.

Watermaster staff collected available UWMPs from the Chino Basin Parties, including the Cities of Chino, Chino Hills, Ontario, Pomona, and Upland; the Golden State Water Company; the San Antonio Water Company; the Monte Vista Water District; the Cucamonga Valley Water District; the Fontana Water Company; the Jurupa Community Services District; the Chino Desalter Authority; the Inland Empire Utilities Agency; the Three Valleys Municipal Water District; the Western Municipal Water District; and the Metropolitan Water District of Southern California (Metropolitan). For those retail water agencies that are not required to prepare UWMPs, Watermaster staff conducted interviews or reviewed other planning information to estimate water demands and to establish water supply plans. Metropolitan indicated that it will discontinue Replenishment Service water deliveries and replace those deliveries with some other program that will be developed in the future. Seemingly, Watermaster will likely be required to purchase untreated water from Metropolitan at Tier 1 or Tier 2 rates for future replenishment. Some Appropriators expressed that, given increased replenishment, power, and Watermaster assessment costs, it is currently or will soon be more economical to purchase Metropolitan water directly than to produce groundwater in excess of their production rights.

Watermaster staff reviewed this planning information. Where the Parties' water supply plans showed more water supply than demand, Watermaster staff conducted additional discussions to distinguish their Chino Basin groundwater production projections and was able to establish priorities of the various supplies and adjust their water supply plans. The resulting groundwater production projection for the Chino Basin is listed in Table 7-4 and shown graphically in Figure 7-2.

The production projection for agricultural producers has not changed in concept from the 2010 RMPU. Agricultural groundwater production was assumed to decrease linearly from about 24,000 acre-ft/yr in 2013 to about 5,000 acre-ft/yr by 2020. In the last few years, recycled water has been supplied for agricultural uses and has resulted in a decline in agricultural groundwater use. The land remaining in agricultural land use is mostly within the sphere of influence of the Cities of Chino and Ontario.

The production projections for individual Overlying Non-Agricultural producers were based on the following:

- For active producers where planning information was unavailable, production was assumed to be their maximum annual production from the five prior years (2006-07 through 2010-11).
- For General Electric (GE), production was assumed to be zero; GE now injects all of its produced groundwater back into the Chino Basin.
- For all other producers, planning estimates were provided.

Table 7-4 shows the projected time history of appropriator production for the 2015 through 2035 period, based on the information collected from the water supply agencies. "Normal" water supply conditions were used from the 2010 UWMPs. Under normal supply conditions, total annual groundwater production is projected to be about 158,000 acre-ft/yr in 2015, 159,000 acre-ft/yr in 2020, and then gradually increases to about 191,000 acre-ft/yr by 2035. Projected annual groundwater production is shown below.

Summary of Projected Groundwater Production by Pool and the CDA (acre-ft/yr)

Planning Year	Agricultural Pool Production	Overlying Non-Agricultural Pool Production	Appropriative Pool and CDA Projection	Total Production
2015	19,125	3,387	135,876	158,388
2020	5,000	3,667	150,723	159,390
2025	5,000	3,667	161,723	170,390
2030	5,000	3,667	172,336	181,003
2035	5,000	3,667	182,242	190,909

The table below contains aggregate water supply projections, based on the UWMPs and other information obtained for this investigation.

Aggregate Water Supply Plan for Watermaster Parties and the CDA (acre-ft/yr)

Water Source	2015	2020	2025	2030	2035
Chino Basin Groundwater	158,388	159,390	170,390	181,003	190,909
Non-Chino Basin Groundwater[17]	57,463	57,463	57,463	57,463	57,463
Local Surface Water	18,869	18,869	18,869	18,869	18,869
Imported Water From Metropolitan	87,558	95,521	98,448	101,327	105,768
Other Imported Water	3,500	3,500	3,500	3,500	3,500
Recycled Water for Direct Reuse	21,393	26,393	30,993	35,593	40,694
Total	347,171	361,136	379,663	397,755	417,203

The total water demand is projected to grow from about 347,000 acre-ft/yr in 2015 to about 417,000 acre-ft/yr by 2035. Recycled water for direct reuse is projected to increase from about 14,000 acre-ft/yr in 2010 to about 41,000 acre-ft/yr by 2035. The amount of imported water supplied by Metropolitan is projected to increase from about 88,000 acre-ft/yr in 2015 to about 106,000 acre-ft/yr by 2035.

[17] Non-Chino Basin groundwater includes groundwater from the Six Basins area, the Cucamonga Basin, the Rialto-Colton Basin, the Lytle Creek Basin, the No-Man's Land area, and the Riverside Basin.

7.2.1.2 Replenishment Obligation Projections

Watermaster recharges supplemental water into the Chino Basin pursuant to the Judgment and the Peace Agreement. Total annual replenishment is calculated herein based on projected groundwater production and production rights. Production rights are based on the following assumptions:

- The safe yield is 140,000 acre-ft/yr through 2014; thereafter, the safe yield is replaced with an estimate of safe yield based on net recharge. The annual net recharge is projected to be about 135,000 acre-ft/yr from 2015 through 2020, 134,000 for 2021 through 2030, 140,000 acre-ft/yr from 2031 to 2040, and 142,000 acre-ft /yr from 2041 to 2050.
- The Judgment allows for 5,000 acre-ft/yr of controlled overdraft of the Chino Basin through 2017.
- Reoperation[18] water is allocated to the replenishment of CDA desalter production, as provided for in the Peace II Agreement, as updated in the report prepared to satisfy Condition Subsequent No. 7 (WEI, 2008), and as updated thereafter based on actual CDA production. Reoperation water is completely used up by 2030.[19]
- The 6,500 acre-ft/yr supplemental water recharge commitment to Management Zone 1 (MZ1) occurs pursuant to the Peace II Agreement through 2030.
- Recycled water recharge was assumed to occur as projected by the IEUA in its February 10, 2012 email to interim Watermaster CEO Ken Jeske.

Recycled water recharge is used in MZ1 to partially meet the 6,500 acre-ft/yr supplemental water recharge obligation. Therefore, some of the recycled water recharge that has historically occurred in MZ1 and is planned to occur in the future is credited to meet the 6,500 acre-ft/yr supplemental water recharge obligation.

Table 7-5 contains the projected groundwater production from Table 7-4, the various components of production rights and total production rights, the projected aggregate replenishment obligation, and the end of year total of water in storage accounts and carryover. The decrease in production rights over the period of 2018 through 2035, due to the elimination of 5,000 acre-ft/yr of controlled overdraft after 2017, is partially offset by the increase in recycled water recharge. The sudden decrease in production rights that occurs in 2031 is due to the assumed ending of the 6,500 acre-ft/yr recharge obligation in MZ1 and ending the use of the second tranche of reoperation water. The aggregate replenishment obligation was estimated using the following assumptions:

- On a go-forward basis, under-producers will transfer un-pumped rights to over-producers each year; that is, there is an efficient market that moves unused production rights from under-producers to over-producers (the efficient market assumption).
- Water in storage accounts will be used to meet future replenishment obligations prior to the purchase of wet-water for recharge.

The annual aggregate replenishment obligation is projected to be negative through 2023, meaning that, in aggregate, water is going into storage accounts through 2023. Thereafter, the aggregate

[18] Reoperation means the controlled overdraft of the basin by the managed withdrawal of groundwater production for the desalters and the potential increase in the cumulative un-replenished production from the 200,000 acre-ft authorized by paragraph 3 of the Engineering Appendix to the Judgment to 600,000 acre-ft for the express purpose of securing and maintaining hydraulic control as a component of the physical solution.

[19] The Peace Agreement was assumed to be not renewed after 2030.

replenishment obligation is projected to be positive reaching about 32,000 acre-ft/yr in 2035 and declining slightly to 30,000 acre-ft/yr after 2040. The "wet-water" replenishment obligation—assuming normal water supply years—is projected to be zero through 2043 and reach 30,000 acre-ft/yr in 2045 and thereafter. As noted above, this assumes that under-producers will transfer unused production rights to over-producers each year; there is an efficient market that moves unexercised rights from under-producers to over-producers. This assumption may underestimate the replenishment obligation for some parties in some years if water cannot be acquired in those years. Over the long term, this assumption is valid because the Appropriator Parties cannot store unused production rights indefinitely, and the demand for replenishment water will provide financial incentives for unused production rights to be sold to over-producers.

In this investigation, it was assumed that when the net annual replenishment obligation became positive in 2024, the replenishment obligation would be satisfied with water from storage accounts. The aggregate water in storage accounts and carryover for the Parties in the Overlying Non-Ag and Appropriative Pools at the end of fiscal 2013 was about 403,405 acre-ft. Given the groundwater production and production right projections in Table 7-5, the aggregate water in storage accounts is projected to grow to about 457,000 acre-ft by 2023 and then steadily decline to zero in 2044.

The combination of the efficient market assumption and the use of storage to meet replenishment obligations means that the only imported water recharge scheduled to occur in the basin through 2043 will be about 3,300 acre-ft/yr, occurring in Management Zone 1 as required to meet the 6,500 acre-ft/yr supplemental water recharge requirement through 2030 with no imported water recharge from 2031 through 2043.

7.2.2 Planning Period Hydrology

Table 7-6 shows the recharge and discharge components for the planning period for Scenario 5A. Some of the recharge and discharge components come directly from the planning projections described above or were abstracted from the planning period hydrology that was input to the model (shown in Table 7-6 with a column heading of "I"). The remaining recharge and discharge components are computational results from simulating Scenario 5A and, hence, are groundwater basin responses to the assumed planning projections and other assumptions (shown in Table 7-6 with a column heading of "R"). The recharge and discharge components that come directly from the planning projections or from the planning period hydrology are characterized below for the period of 2011 through 2050. The recharge and discharge components estimated by the model are described in Section 7.3.1 *Projected Future Water Budget Net Recharge*.

7.2.2.1 Recharge Components

Subsurface Boundary Inflow from the Chino Hills, Six Basins, Cucamonga Basin, Rialto Basin, and Riverside Basin (Bloomington Divide). The annual estimate of subsurface boundary inflow to the Chino Basin from the Chino Hills, Six Basins, Cucamonga Basin, Rialto Basin, and Riverside Basin are listed in columns 2 and 3 in Table 7-6. This recharge component was assumed to be 27,500 acre-ft/yr. This is less than the boundary inflows near the end of the calibration period, which were about 37,000 acre-ft/yr in 2011. These boundary flows were reduced to reflect anticipated future improvements in the management of the Six Basins, Cucamonga Basin, and Riverside Basin (through the Bloomington Divide). The subsurface boundary flows from the Chino, Puente, and Jurupa Hills were estimated with the R4 model and are based on the daily precipitation record for 1921 through 2012 and the land use and drainage conditions in those watersheds. The management strategies considered in the adjacent basins include increased production, reduced groundwater elevations, and subsequently reduced inflow to the Chino Basin.

Deep Infiltration of Precipitation and Applied Water (DIPAW). The annual estimate of DIPAW is listed in column 5 of Table 7-6. The expected value for DIPAW was computed for 2010, the last year for which land use data were readily available, and planning year 2030, using the R4 model, which was calibrated with the 2013 Watermaster Model. For the 2010 and 2030 DIPAW estimates, daily precipitation data for the period of 1921 to 2012 were used (a 92-year period) to estimate the long-term average DIPAW corresponding to the cultural conditions on the land surface. The 2012 DIPAW expected value was assumed to be the same as the 2010 value. And, the DIPAW expected values for the years between 2012 and 2030 were interpolated annually from the 2012 and 2030 values and assumed to be equal to the 2030 value thereafter. After being routed through the unsaturated zone, the DIPAW that reached the saturated zone ranged from a low of about 81,000 acre-ft/yr to a high of about 97,000 acre-ft/yr and averaged about 94,000 acre-ft/yr.

Streambed Infiltration from Santa Ana River Tributaries. The annual estimate of streambed infiltration from Santa Ana River tributaries that cross the Chino Basin is listed in column 6 of Table 7-6. This component was estimated with the R4 model in a manner identical to the DIPAW term and was fairly constant at about 1,100 acre-ft/yr.

Storm Water Recharge in Basins. The annual estimate of stormwater recharged in stormwater management basins is listed in column 7 of Table 7-6. Total stormwater recharge in the recharge basins was estimated to be about 12,000 acre-ft/yr, based on the historical performance of these facilities between 2004 and 2011.

Recycled and Imported Water Recharge. The annual estimates of recycled and imported water recharge are listed in columns 8 and 9 of Table 7-6, respectively. These components were described in the section above entitled Replenishment Obligation Projections, and when combined, they range from 10,500 acre-ft/yr to 49,000 acre-ft/yr. After 2044, imported water recharge increases from zero (2044) to 30,300 acre-ft/yr in 2046[20].

7.2.2.2 Discharge Components

Groundwater Pumping. The annual estimate of groundwater production by the CDA, the aggregated Appropriative and Overlying Non-Ag pools, and the Overlying Ag Pool are listed in columns 12, 13, and 14 of Table 7-6, respectively. These are planning projections that were described in Section 7.2.2 *Groundwater Production Projections* (above). In aggregate, they range from about 148,000 to 191,000 acre-ft/yr and average about 178,000 acre-ft/yr.

7.3 Projected Basin Response

This section describes the projected basin response to Scenario 5A and includes a description of the water budget components that are estimated by the model, net recharge, groundwater levels, storage, the state of hydraulic control, and storage losses.

[20] Note that the imported water recharge estimates in Table 7-6 lag the wet-water replenishment obligation listed in Table 7-5 by one year. Actual replenishment occurs following the production year in which replenishment obligation was created.

7.3.1 Projected Future Water Budget

Table 7-6 contains the complete water budget for the period of 2011 through 2050. The table is divided into annual estimates of recharge components and discharge components, change in storage, and net recharge. Individual recharge and discharge components with a column heading of "I" were discussed in Section 7.2.4 above. Recharge and discharge with a column heading of "R" are computational results produced by the model and are discussed below.

7.3.1.1 Model-Estimated Recharge Components

Subsurface Inflow from the Temescal Basin. The annual estimate of subsurface inflow to the Chino Basin from the Temescal Basin is listed in column 4 of Table 7-6. The Temescal Basin is included in the 2013 Chino Basin Model, and the groundwater exchange between the basins is derived by aggregating cell-by-cell groundwater discharge along the boundary that separates the basins. Both subsurface inflow from and subsurface outflow to the Temescal Basin occur. This is due to the irregular boundary between the Chino and Temescal Basins and hydrologic conditions on each side of the boundary. The subsurface inflow from the Temescal Basin ranges from a low of 4,900 acre-ft/yr to a high of 6,800 acre-ft/yr and averages about 6,200 acre-ft/yr.

Streambed Infiltration in the Santa Ana River. The annual estimate of streambed infiltration in the Santa Ana River and lower reaches of Chino and Mill Creeks is listed in column 10 of Table 7-6. This recharge term includes the recharge of surface water discharge in the Santa Ana River and the lower reaches of Chino and Mill Creeks where surface and ground water can interact directly. Both recharge to groundwater and rising groundwater discharge to the surface water can occur in these streams. Recharge generally occurs in the Santa Ana River in the reach that starts below the Riverside Narrows downstream to the Prado Basin area. Groundwater discharges into the Santa Ana River in the Prado Basin area. Streambed recharge in the Santa Ana River and lower reaches of Chino and Mill Creek's ranges from a low of 34,300 acre-ft/yr to a high of 41,500 acre-ft/yr and averages about 37,600 acre-ft/yr.

Subtotal of All Recharge Components. The sum of all recharge components ranges from about 179,000 to 228,000 acre-ft/yr and averages about 202,000 acre-ft/yr.

7.3.1.2 Model-Estimated Discharge Components

Evapotranspiration by Riparian Vegetation. The annual estimate of groundwater discharge to ET is listed in column 15 of Table 7-6. Discharge to ET was computed by the model and ranges from a low of 17,800 acre-ft/yr to a high of 18,400 acre-ft/yr and averages about 18,100 acre-ft/yr. The annual ET generally declines through the projection period in response to declines in groundwater levels along the Santa Ana River and in the Prado Basin. The decline in groundwater levels is relative to the initial groundwater levels in July 2011 and is caused by the expansion of the desalters, reoperation, and the use of stored groundwater for replenishment.

Groundwater Discharge to the Santa Ana River and Chino and Mill Creeks. The annual estimate of groundwater discharge to the Santa Ana River and Chino and Mill Creeks is listed in column 16 of Table 7-6. Discharge to the Santa Ana River and Chino and Mill Creek's ranges from a low of 15,400 acre-ft/yr to a high of about 20,200 acre-ft/yr and averages about 17,800 acre-ft/yr.

During the period of 2011 through 2050, streambed infiltration in the Santa Ana River is always greater than groundwater discharge to the Santa Ana River. Net streambed recharge is computed by taking the difference between streambed infiltration in the Santa Ana River minus groundwater discharge to the Santa Ana River (column 10 minus column 16 in Table 7-6). The net streambed recharge ranges from a low of about 19,000 acre-ft/yr to high of about 21,300 acre-ft/yr and averages about 19,800 acre-ft/yr.

Subsurface Outflow to the Temescal Basin. The annual estimate of subsurface outflow to the Temescal Basin is listed in column 17 of Table 7-6. The subsurface outflow to the Temescal Basin ranges from a low of 2,900 acre-ft/yr to a high of 4,100 acre-ft/yr and averages about 3,900 acre-ft/yr.

The subsurface inflow from the Temescal Basin is always greater than the subsurface outflow to the Temescal Basin. The net subsurface inflow from the Temescal Basin is computed by taking the difference between the inflow from Temescal Basin minus the outflow to the Temescal Basin (column 4 minus column 17 in Table 7-6). The net subsurface inflow from the Temescal Basin is relatively small and varies from a about 1,000 to about 3,900 acre-ft/yr and averages about 2,300 acre-ft/yr.

Subtotal All Discharge Components. The sum of all discharge components ranges from about 187,000 to 230,000 acre-ft/yr and averages about 217,000 acre-ft/yr.

7.3.2 Net Recharge

Net recharge is estimated using equation 5 in Section 7.1 and is equal to groundwater production plus the change in storage minus supplemental water recharge. Figure 7-3 shows the annual net recharge for the Chino Basin for both the calibration and projection periods and spans 1961 through 2050.

Net recharge is estimated to have been greater than the 140,000 acre-ft/yr safe yield from 1978 through 1998 and then to have dropped below 140,000 acre-ft/yr through the end of the calibration period (June 2011). The decline in net recharge is attributable to changes in cultural conditions and specifically the change in land use from irrigated agricultural to urban use, reductions in groundwater production in the southern part of the basin associated with the land use change from irrigated agricultural uses to dairy and urban uses, and the concrete lining of channels.

The net recharge is projected to subsequently rebound due to the construction and operation of the CDA desalter wells, reoperation, and projected withdrawals of stored water after 2023. The projected net recharge for the period of 2011 through 2030 is about 135,000 acre-ft/yr and about 134,000 acre-ft/yr for 2021 through 2030.

7.3.3 Projected Changes in Groundwater Level

Groundwater elevation maps were prepared for July 2011 (initial condition for the planning period), 2020, 2030, 2040, and 2050, shown in Figures 7-4a through 7-4e, respectively. The changes in groundwater elevations over the periods of 2011 to 2020, 2011 to 2030, 2011 to 2040, and 2011 to 2050 are shown in Figures 7-5a through 7-5d, respectively. In general, relative to 2011 conditions, groundwater levels are projected to decrease slightly through 2020, to decrease at slightly higher rate from 2020 through 2030, and to decline at greater rate thereafter through 2050.

Table 7-7 characterizes, by Appropriator Party service area, the projected groundwater elevation change for Scenario 5A. Table 7-7 summarizes an analysis that compares the groundwater elevations at each model cell in the Appropriator Party service areas from 2011 to 2020, 2011 to 2030, 2011 to 2040, and 2011 to 2050, and reports the minimum and maximum change for model cells in the Appropriator Party service areas and the average change across all model cells in the Appropriator Party service areas. Negative values indicate a decline, and positive values indicate an increase. For example, the values -20, 20, and -3 for the JCSD service area for the min, max, and average columns in the 2011 through 2020 period mean that there is at least one model cell where the groundwater elevation declines by 20 feet by 2020, there is at least one model cell where the groundwater elevation increases by 20 feet by 2020, and the average change in the groundwater elevation across the JCSD service area was a decline of 3 feet by 2020.

The groundwater level changes shown in Figures 7-5a to 7-5d and Table 7-7 indicate that groundwater levels are generally constant with local exceptions through about 2030 and then decline sharply thereafter. Recall from Table 7-5 that the volume of water in storage accounts is projected to increase to about 457,000 acre-ft in 2023, slightly decline to about 402,000 acre-ft in 2030, and then decline sharply to zero by 2044. The change in groundwater levels reflected in Figures 7-5a to 7-5d and Table 7-7 tracks the storage change shown in Table 7-5. The declining groundwater level changes in the Cities of Ontario, Pomona, and Upland, and the MVWD services area are not sustainable sometime after 2030 as they will likely exacerbate land subsidence. The declining groundwater levels in the JCSD area may contribute to production sustainability challenges for the JCSD and the CDA.

Appendix D contains projected groundwater elevation time histories at most of the Appropriator Party wells. If provided by the Appropriator, these time history plots include a production sustainability metric. The term sustainability, as used herein, refers specifically to the ability to produce water from a specific well at a desired production rate, given the groundwater level at that well and its specific well construction and current equipment details. It has no nexus to the Judgment or Peace Agreements. Sustainability metrics are defined for each well by well owner. Groundwater production at a well is presumed to be sustainable if the groundwater level at that well is greater than the sustainability metric. If the groundwater level falls below the sustainability metric, the owner will either lower the pumping equipment in their well or reduce production.

7.3.4 Projected Changes in Groundwater Storage

Figure 7-6 shows the projected change in storage relative to July 2011 for the period through June 2050 and the aggregate volume of stored water and carryover water. The volume of water in storage accounts and carryover is projected to increase to about 457,000 acre-ft in 2023 and decline thereafter to zero by 2044. Groundwater storage in the basin is projected to decline gradually while the volume of water in storage accounts is increasing and then more steeply as the water in storage accounts is used to meet replenishment obligations. The total decline in water stored in the basin is about 603,000 acre-ft through 2050.

Figure 7-7 shows the estimated change in storage for the historical period of 1922 through 2011 and the projection period of 2012 through 2050, a period that spans 129 years. This information is provided herein to provide context to projected change in storage through 2050. The change in storage for selected periods is listed below.

- -1,560,000 acre-ft – pre Judgment period 1922 through 1977
- -573,000 acre-ft – post Judgment period through 2015
- -2,134,000 acre-ft – period from 1922 through 2015
- -165,000 acre-ft – remaining Peace Agreement period 2015 though 2030
- -426,000 acre-ft – period of 2031 through 2050
- -2,725,000 acre-ft – period of 1922 through 2050

7.3.5 Projected State of Hydraulic Control

The projected state of hydraulic control was estimated with the 2013 Groundwater Model by simulating the Chino Basin's response to Watermaster planning Scenarios 5A and 5G. Scenarios 5A and 5G are identical except for the location of the future CDA II-12 well and when its production commences. And, the model-projected groundwater responses to Scenarios 5A and 5G are identical except in the immediate vicinity of the proposed CDA well II-12 locations. Scenario 5G is representative of the actual well location for CDA well II-12. Table 7-8 lists existing and proposed CDA wells, nominal production capacities in gallons per minute (gpm), use factors (fraction of time well is in use), effective production capacities (gpm), and annual production expressed in acre-ft/yr.

The attainment of hydraulic control is measured by demonstrating, from groundwater elevation data, either that all groundwater north of the desalter well fields cannot pass through the desalter well fields (total hydraulic containment standard) or that groundwater discharge through the desalter well fields is, in aggregate, less than 1,000 acre-ft/yr (de minimis standard). The Regional Board has agreed that compliance with the de minimis standard will be determined from the results of periodic calibrations of the Watermaster groundwater model and interpretations of the calibration results.

Figures 7-8a and 7-8b illustrate the state of hydraulic control for Scenario 5G for 2020 and 2025, respectively. These maps include groundwater-elevation contours and arrows that depict groundwater-flow directions in the southern part of the Chino Basin in the vicinity of the CDA well field and the Santa Ana River. Hydraulic containment is attained at and east of CDA well I-20 by 2020 for both scenarios.

Groundwater discharge from the Chino North Management Zone to the Prado Basin Management Zone and the Santa Ana River is projected to not be fully contained by the CCWF in the area between the Chino Hills and CDA well I-20. Groundwater discharge through the CCWF was estimated through the analysis of 2013 Groundwater Model projected cell-by-cell discharges through the CCWF. Table 7-9 lists the projected annual time series of this discharge through the CCWF for Scenario 5G (as reported in the May 29, 2014 report to the Regional Board) and comparable time series, taking into account an updated schedule to bring the CCWF online. Using the de minimis discharge threshold of 1,000 acre-ft/yr or less of groundwater discharge from the Chino North Management Zone to the Santa Ana River, hydraulic control is achieved in 2016 and maintained thereafter. Thus, hydraulic control will likely be established in 2016.

7.3.6 Storage Loss Rate Post Attainment of Hydraulic Control

Surface water discharge in the Santa Ana River consists of storm flow and base flow. Base flow is divided into two components: wastewater discharged from publicly owned treatment works and rising groundwater. Section 2 of the Optimum Basin Management Program, Phase 1 Report (Wildermuth, 2003) contains a description of the relationship of groundwater discharge from the Chino Basin to the Santa Ana River due to storing water in the Chino Basin. The discussion below describes the theoretical background for the storage loss rate and its application using the modeling results from the hydraulic control investigation described above.

In the absence of complete hydraulic containment, the aggregate volume of water held in storage accounts and carryover will increase groundwater discharge and a subsequent increase in Santa Ana River base flow. The physics of the groundwater storage-base flow relationship can be represented by the linear reservoir theory, where discharge is directly proportional to storage:

$$Q = K * S$$

Where:

Q	is the discharge from storage (acre-ft/yr)
S	is the volume of water in storage (acre-ft)
K	is the linear reservoir coefficient (y^{-1})

This formula can be calibrated to a specific range of storage and groundwater management conditions. Figure 7-9 shows the relationship of total groundwater discharge through the CCWF to the projected future aggregate volume of water held in storage accounts and carryover; this relationship is shown by the dark blue curve. This curve is divided into two parts, corresponding to the period of projected future increases in the aggregate volume of water in storage accounts and carryover (2015 through 2023) and the subsequent period of decline in the aggregate volume of water in storage accounts and carryover (2024 through 2043). Inspection of the curve indicates the following:

- The decreasing storage limb of the curve has a slope of about 0.07 percent for a range of storage of 0 to 450,000 acre-ft and is where the slope is the storage loss rate (K).
- The increasing storage limb of the curve is too short to interpret except to conclude that it is suggestive of a comparable storage loss rate.
- The increasing limb of the curve does not include the full hydraulic effect of the CCWF well field as it was assumed to come online in 2014, and the production trough created by it will take a few years to reach its maximum effectiveness.
- There is a minimum groundwater discharge through the CCWF of about 500 acre-ft/yr regardless of amount of water in storage: when the aggregate volume of water in storage accounts and carryover is 0 acre-ft, the groundwater discharge is about 500 acre-ft/yr.

Watermaster should use the slope of the decreasing limb of the curve to estimate the storage loss rate.

The second (green) curve shown in Figure 7-9 represents the estimated discharge through the CCWF attributable to the aggregate volume of water in storage accounts and carryover. It is identical to the total discharge through the CCWF curve plotted above minus 500 acre-ft/yr. Based on the modeling work described herein, there will be about 500 acre-ft/yr of discharge through the CCWF regardless of the volume of water in storage accounts and carryover. This base 500 acre-ft/yr discharge is an artifact of the CCWF design and projected operation. This base 500 acre-ft/yr of discharge is accounted for in the net recharge calculation and could be eliminated through additional production wells in the CCWF.

7.3.7 New Yield Created by the Desalters and Reoperation

In the Peace Agreement, new yield is defined as:

> "New Yield means proven increases in yield in quantities greater than historical amounts from sources of supply including, but not limited to, capture of rising water, capture of available storm flow, operation of the Desalters (including the Chino I Desalter), induced Recharge and other management activities implemented and operational after June 1, 2000."[21]

The new yield created by the desalters and reoperation, hereafter Santa Ana River Underflow New Yield or SARUNY, is estimated to be the change in net Santa Ana River recharge to the Chino Basin since July 2000. SARUNY means the same thing as the term *Desalter Induced Recharge* that is used in the

[21] Peace Agreement, Definitions, page 8.

2015 Safe Yield Reset Agreement. The net Santa Ana River recharge in the fiscal year spanning July 1999 through June 2000 is the baseline from which to measure SARUNY, which was estimated to be -2,153 acre-ft/yr, indicating that the Chino Basin discharged to the Santa Ana River 2,153 acre-ft/yr more water than was recharged by the River into the Basin. Table 7-10 compares Chino Desalter production and SARUNY over the period of July 2000 through June 2030. Specifically, Table 7-10 shows annual and cumulative CDA production, annual and cumulative SARUNY, the ratio of annual SARUNY to annual CDA production, and the ratio of cumulative SARUNY to cumulative CDA production. The effect of the Chino Desalters and reoperation becomes clear in 2005 when SARUNY reaches about 50 percent of CDA production. The New Yield results from the implementation of the Chino Desalters and reoperation and is consistent with the planning estimates that were assumed during the development of the Peace Agreements.

7.4 Recommendations Regarding Net Recharge and the Redetermining of Safe Yield

The safe yield of the Chino Basin is defined by the Judgment as:

> "The long-term average annual quantity of ground water (excluding replenishment or stored water but including return flow to the Basin from use of replenishment or stored water) which can be produced from the Basin under *cultural conditions* of a particular year without causing an undesirable result."[22] (emphasis added)

The "long-term average annual quantity of ground water which can be produced from the Basin" is directly related to the long-term average hydrologic conditions, including precipitation. "Cultural conditions" refers to overlying land uses and water-management practices that affect the net recharge to the basin, including, but not limited to, impervious cover, channel lining, land use, the installation and operation of the Chino Desalter well fields, the construction of recharge basins, the location and magnitude of groundwater pumping, etc.

The Judgment additionally provides for a Physical Solution to provide maximum flexibility and adaptability such that Watermaster and the Court may be free to use existing and future technological, social, institutional, and economic options to maximize the beneficial use of the waters of Chino Basin.[23]

Subject to these requirements, Watermaster developed an Optimum Basin Management Program [OBMP] that both preserved the quantity of the basin's waters and maximized their beneficial use.[24]

Watermaster's OBMP Implementation Plan called for an initial redetermination of basin's safe yield in 2011, using monitoring data that would be gathered for the first time during the period of 2001 through 2010.[25] This requirement is also carried forward in Section 6.5 of Watermaster's Rules and Regulations, which states that the "Safe Yield shall be recalculated in year 2011 based upon data from the ten-year period 2001 to 2010." The cultural conditions during the period of 2001 through 2010 are not representative of present and future cultural conditions; therefore, this period should not be used

---

[22] Restated Judgment, ¶ 4 (x)

[23] Restated Judgment, ¶ 40

[24] Restated Judgment, ¶ 41

[25] OBMP Implementation Plan, pages 44-45, Program Element 8 – Develop and Implement Groundwater Storage Management Program, Program Element 9 – Develop and Implement Storage and Recovery Programs

to estimate safe yield. And, the hydrology of the 2001 through 2010 period is not representative of the long-term hydrology of the Chino Basin.

The cultural conditions included in Scenario 5A are representative of the present and future projected cultural conditions. Furthermore, the hydrology assumed in Scenario 5A is based on 92-years of daily precipitation data and is representative of the long-term hydrology of the Chino Basin. Thus, the projected net recharge for Scenario 5A should be used as a starting point for the safe yield determination for the period of 2011 through 2020.

The recommended methodology to redetermine the safe yield for the period of 2011 through 2020 and the recommended methodology for future safe yield evaluations is listed below. This methodology is consistent with professional custom, standard practice, and the definition of safe yield in the Judgment and the Physical Solution.

1. Use the data collected during 2001 to 2010 (and in the case of subsequent resets newly collected data) in the re-calibration process for Watermaster's groundwater-flow model.
2. Use a long-term historical record of precipitation falling on current and projected future land uses to estimate the long-term average net recharge to the basin.
3. Describe current and projected future cultural conditions, including, but not limited to, plans for pumping, stormwater recharge, and supplemental-water recharge.
4. With the information generated in [1] through [3] above, use the groundwater-flow model to redetermine the net recharge to the Chino Basin, taking into account then existing current and projected future cultural conditions.
5. Qualitatively evaluate whether groundwater production at the net recharge rate estimated in [4] above will cause or threaten to cause undesirable results or Material Physical Injury. If groundwater production at the net recharge rate estimated in [4] above will cause or threaten to cause undesirable results or Material Physical Injury, Watermaster will identify and implement the prudent measures necessary to mitigate undesirable results or Material Physical Injury, set the value of safe yield to ensure there is no undesirable results or Material Physical Injury, or implement a combination of mitigation measures and a changed safe yield.

Using this methodology, the net recharge for the period of 2001 through 2030 is about 135,000 acre-ft/yr and increases slightly thereafter. Watermaster should use the net recharge of 135,000 acre-ft/yr and apply step 5 above to set the value of safe yield.

In future planning investigations Watermaster should reevaluate the use of the efficient market assumption to estimate the wet-water replenishment that was used in Scenario 5A to project future groundwater conditions and net recharge. The use of the efficient market assumption prioritizes the use of stored water to meet replenishment obligations and minimizes the recharge of supplemental water. The projected decline in groundwater levels and storage through 2044 would be less if a combination of stored water and wet-water recharge were used to meet future replenishment obligations.

Table 7-1
Historical and Projected Land Use in the Chino Basin Area
(acres unless indicated otherwise)

Land Use Type	1933	1949	1957	1963	1975	1984	1990	2000	2010	2030
Non-Irrigated Field Crops, Pasture, Fruits and Nuts	41,872	41,872	4,023	707	2,294	945	782	553	177	0
Irrigated Field Crops, Pasture, Fruits and Nuts	41,345	41,345	36,335	34,543	28,262	23,845	20,544	16,220	12,447	4,900
Irrigated and Non-Irrigated Citrus	19,669	19,669	11,292	5,521	2,652	1,259	4,487	1,838	1,615	101
Irrigated Vineyard	1,669	1,669	13,029	22,045	14,657	9,936	0	0	0	0
Non-Irrigated Vineyard	132	132	233	12	31	8	198	157	103	0
Dairies and Feedlots	546	546	2,686	5,503	7,351	8,301	8,646	8,029	6,551	0
Medium and High Density Urban Residential	7,511	7,511	8,746	15,333	19,898	26,210	35,349	40,018	44,642	77,326
Special Impervious	1,750	1,750	1,389	1,730	4,411	4,612	6,706	8,361	8,230	11,349
Native Vegetation	4	4	9	9	9	4	5	7	6	6
Low Density Urban Residential	2,583	2,583	1,287	4,517	5,372	8,149	12,122	12,379	12,908	13,924
Commercial	2,182	2,182	1,696	2,999	4,165	7,555	9,430	16,190	19,140	19,708
Industrial	2,444	2,444	1,828	2,116	3,573	11,203	9,663	10,756	10,770	10,960
Undeveloped	18,292	17,983	59,214	46,745	47,184	37,605	31,424	25,151	23,068	1,602
Phreatophyte	4,466	4,466	2,859	2,985	4,543	4,825	4,884	4,573	4,573	4,573
Totals (acres)	144,464	144,155	144,626	144,764	144,403	144,456	144,239	144,230	144,230	144,449
Total Imperviousness	10%	10%	10%	15%	21%	32%	39%	47%	51%	70%
Aggregated Area by Landuse Group (acres)										
Agricultural	105,233	105,233	67,598	68,331	55,247	44,293	34,657	26,796	20,893	5,001
Urban	16,470	16,470	14,946	26,694	37,420	57,729	73,269	87,704	95,690	133,267
Undeveloped + Native Vegetation	22,762	22,452	62,082	49,739	51,736	42,434	36,313	29,731	27,648	6,181
Total	144,464	144,155	144,626	144,764	144,403	144,456	144,239	144,230	144,230	144,449
Aggregated Area by Landuse Group (percent of total)										
Agricultural	73%	73%	47%	47%	38%	31%	24%	19%	14%	3%
Urban	11%	11%	10%	18%	26%	40%	51%	61%	66%	92%
Undeveloped + Native Vegetation	16%	16%	43%	34%	36%	29%	25%	21%	19%	4%
Total	100%	100%	100%	100%	100%	100%	100%	100%	100%	100%
Aggregated Imperviousness by Landuse Group										
Agricultural	1%	1%	1%	1%	1%	1%	1%	1%	1%	0%
Urban	8%	8%	8%	13%	19%	30%	37%	46%	50%	70%
Undeveloped + Native Vegetation	0%	0%	1%	1%	1%	1%	0%	0%	0%	0%
Total	10%	10%	10%	15%	21%	32%	39%	47%	51%	70%

Table 7-2
Imperviousness and Irrigation Assumptions for Land Uses in the Chino Basin

Land Use Type	Total Imperviousness (%)	Crop Evapotranspiration (ft/yr)	Irrigation Efficiency[1] (%)	Applied Water (ft/yr)	Irrigation Return (ft/yr)
Non-Irrigated Field Crops, Pasture, Fruits and Nuts	2	2.38	na	na	na
Irrigated Field Crops, Pasture, Fruits and Nuts	2	2.38	55 - 75	4.33 3.18	1.95 0.79
Irrigated and Non-Irrigated Citrus	2	2.53	60 - 80	4.22 3.16	1.69 0.63
Irrigated Vineyard	2	2.07	60 - 75	3.45 2.76	1.38 0.69
Non-Irrigated Vineyard	2	1.75	na	na	na
Dairies and Feedlots	10	na	na	na	na
Medium and High Density Urban Residential	75	3.06	75 - 75	4.08 4.08	1.02 1.02
Low Density Urban Residential	30	3.06	75 - 75	4.08 4.08	1.02 1.02
Commercial	90	3.50	75 - 75	4.67 4.67	1.17 1.17
Industrial	90	3.06	75 - 75	4.08 4.08	1.02 1.02
Special Impervious	95	na	na	na	na
Native Vegetation	2	0.74 to 3.50	na	na	na
Undeveloped	2	1.44	na	na	na

[1] Irrigation efficiency corresponds to the current period for urban uses and to the period of time in which crops were principally grown. For example, citrus was flood irrigated when it was cultivated in the northern part of the Chino Basin area and, thus, has a low irrigation efficiency, whereas modern citrus cultivation utilizes drip irrigation with a much greater irrigation efficiency. Irrigation of turf and ornamental plants is assumed to occur by sprinkler irrigation, which is assumed to have an irrigation efficiency of 75 percent.

Table 7-3
William J Carroll's Estimation of Safe Yield Adopted in the Chino Basin Judgment[1]
(acre-ft)

Hydrologic Component	Annual Average (acre-ft/yr)	Annual Average (%)
Inflows to the Chino Basin		
Deep Percolation		
Precipitation and Surface Inflow	47,500	33%
Imported Water Used for Irrigation	7,000	5%
Groundwater Used for Irrigation	61,700	42%
Artificial Recharge	3,900	3%
Recharge of Sewage	18,200	13%
Subsurface Inflow	7,000	5%
Total Inflow	145,300	100%
Outflows from the Chino Basin		
Subsurface Outflow	7,200	4%
Extractions	180,000	96%
Total Outflow	187,200	100%
Hydrologic Balance		
Estimated Annual Average Change in Storage 1965-1974	-40,000	
Safe Yield (equal to average annual extraction plus annual average change in storage)	140,000	

[1] Trial exhibit No. 6

Table 7-4
Scenario 5A - Projected Groundwater Production for the Chino Basin
(acre-ft)

Producer	Historical Production by Fiscal Year 2010	2011	2012	2013	Scenario 5A Production Projection[1] 2015	2020	2025	2030	2035
Overlying Agricultural Pool									
Aggregate Agricultural Pool Production [2]	*21,034*	*21,021*	*22,407*	*23,950*	*19,125*	*5,000*	*5,000*	*5,000*	*5,000*
Overlying Non-Agricultural Pool									
Ameron	28	28	-	-	28	28	28	28	28
Angelica Textile Service[3]	41	54	46	48	54	54	54	54	54
Auto Club Speedway	496	449	447	509	621	621	621	621	621
California Steel Industries Inc.[5]	1,059	1,085	1,362	1,303	2,170	2,450	2,450	2,450	2,450
General Electric Company[6]	287	31	1,115	1,285	-	-	-	-	-
GenOn West, LP (Formerly RRI Etiwanda)[7]	138	323	131	346	500	500	500	500	500
San Antonio Winery	12	11	10	10	13	13	13	13	13
Subtotal Overlying Non-Agricultural Pool Production	*2,061*	*1,981*	*3,111*	*3,501*	*3,387*	*3,667*	*3,667*	*3,667*	*3,667*
Appropriative Pool									
Arrowhead Mountain Spring Water Company	374	408	369	413	378	378	378	378	378
City of Chino	7,808	7,304	7,856	7,010	8,574	9,526	11,278	12,563	13,796
City of Chino Hills	1,446	1,986	3,137	3,039	2,900	2,900	2,900	2,900	2,900
City of Norco	0	0	0	0	-	-	-	-	-
City of Ontario	25,269	19,010	19,268	21,089	20,373	24,242	29,631	35,049	39,383
City of Pomona	11,404	10,528	12,040	12,833	13,103	14,300	14,300	14,300	15,000
City of Upland[4]	3,410	734	525	492	250	250	250	250	250
Cucamonga Valley Water District	19,263	20,318	14,949	18,740	17,931	16,331	17,931	19,631	21,231
Fontana Union Water Company	0	0	0	0	-	-	-	-	-
Fontana Water Company	13,557	8,348	5,694	11,752	5,319	6,413	8,372	10,332	12,041
Jurupa Community Services District	15,979	14,642	16,322	17,469	16,900	18,800	18,800	18,800	18,800
Inland Empire Utilities Agency	0	0	0	0	-	-	-	-	-
Marygold Mutual Water Company	346	1,107	1,175	1,250	2,200	2,200	2,200	2,200	2,200
Monte Vista Irrigation Company	0	0	0	0	-	-	-	-	-
Monte Vista Water District	15,803	12,264	10,616	10,324	12,191	11,231	11,531	11,781	12,111
Niagara	1,298	1,345	729	394	1,210	1,210	1,210	1,210	1,210
San Antonio Water Company	966	716	172	1,540	1,507	1,507	1,507	1,507	1,507
San Bernardino County (Olympic Facility)	16	18	15	12	22	22	22	22	22
Santa Ana River Water Company	0	0	0	0	318	335	335	335	335
Golden State Water Company	359	444	746	1,059	411	411	411	411	411
West End Consolidated Water Company	0	0	0	0	-	-	-	-	-
West Valley Water District	0	0	0	0	-	900	900	900	900
Subtotal Appropriative Pool Production	*117,299*	*99,172*	*93,615*	*107,416*	*103,587*	*110,956*	*121,956*	*132,569*	*142,475*
Chino Desalter Authority									
Total Desalter Production	*28,940*	*28,940*	*28,411*	*27,098*	*32,289*	*39,767*	*39,767*	*39,767*	*39,767*
Total Basin Production	169,334	151,114	147,543	161,965	158,388	159,390	170,390	181,003	190,909

1 -- The production projection for the Overlying Ag Pool is based on prior OBMP planning investigations. The production projection for the Appropriative Pool Parties is based on their UWMPs and the resulting projections refined based on subsequent discussions. The production projection for the Overlying Non-ag Pool was estimated based on discussions with individual Parties or from historical data.

2 -- The ramp down in projected Overlying Ag Pool production mirrors the increase in total water demand projected by the Cities of Chino and Ontario.

3 -- Projected production is based on maximum annual production for the period of 2006-07 through 2010-11. Brian Geye confirmed for the Auto Club Speedway.

4 -- Updated on February 1, 2012 by Rosemary Hoerning

5 -- Projection provided by Ken Jeske via email on October 21, 2011.

6 -- Projection provided by Ken Jeske via email on October 21, 2011.

7 -- Confirmed by Len Moore at Genon

Table 7-5

Scenario 5A - Projected Groundwater Production and End of Year Storage Account Balance

Fiscal Year	Projected Groundwater Production per 2010 UWMP for Normal Year	Production Rights							Aggregate Replenishment Obligation[2]	Wet Water Replenishment	End of year Balance of Water in Storage Accounts and Carryover
		Safe Yield[1]	Controlled Overdraft Pursuant to Judgment	Reoperation Water Offset to Desalter Production	6,500 acre-ft/yr Supplemental Water Recharge in MZ1 per Peace II	Mid-Range Recycled Water Recharge	Debit Against 6,500 acre-ft/yr Obligation from Recycled Water Recharged in MZ1	Total			
(1)	(2)	(3)	(4)	(5)	(6)	(7)	(8)	(9) = (3)+(4)+(5)+(6)+(7)+(8)	(10) = (2)-(9)	(11)	$(12)_t = [(2)_t-(9)_t]+(10)_t+(12)_{t-1}$
2015	158,388	135,169	5,000	10,000	6,500	14,500	-2,504	168,665	-10,277	0	421,349
2016	162,303	135,169	5,000	10,000	6,500	14,500	-2,504	168,665	-6,362	0	427,711
2017	163,275	135,169	5,000	10,000	6,500	14,500	-2,504	168,665	-5,390	0	433,101
2018	161,980	135,169	0	10,000	6,500	16,900	-2,504	166,065	-4,085	0	437,186
2019	160,685	135,169	0	10,000	6,500	16,900	-2,504	166,065	-5,380	0	442,565
2020	159,390	135,169	0	10,000	6,500	16,900	-2,504	166,065	-6,675	0	449,240
2021	161,590	134,309	0	10,000	6,500	16,900	-2,504	165,205	-3,616	0	452,856
2022	163,790	134,309	0	10,000	6,500	18,700	-2,504	167,005	-3,216	0	456,072
2023	165,990	134,309	0	10,000	6,500	18,700	-2,504	167,005	-1,016	0	457,088
2024	168,190	134,309	0	10,000	6,500	18,700	-2,504	167,005	1,184	0	455,903
2025	170,390	134,309	0	10,000	6,500	18,700	-2,504	167,005	3,384	0	452,519
2026	172,512	134,309	0	10,000	6,500	18,700	-2,504	167,005	5,507	0	447,012
2027	174,635	134,309	0	10,000	6,500	18,700	-2,504	167,005	7,629	0	439,383
2028	176,758	134,309	0	10,000	6,500	18,700	-2,504	167,005	9,752	0	429,630
2029	178,880	134,309	0	10,000	6,500	18,700	-2,504	167,005	11,875	0	417,756
2030	181,003	134,309	0	10,000	6,500	18,700	-2,504	167,005	13,997	0	403,759
2031	182,984	140,441	0	0	0	18,700	0	159,141	23,843	0	379,916
2032	184,965	140,441	0	0	0	18,700	0	159,141	25,824	0	354,091
2033	186,946	140,441	0	0	0	18,700	0	159,141	27,805	0	326,286
2034	188,928	140,441	0	0	0	18,700	0	159,141	29,787	0	296,500
2035	190,909	140,441	0	0	0	18,700	0	159,141	31,768	0	264,732
2036	190,909	140,441	0	0	0	18,700	0	159,141	31,768	0	232,964
2037	190,909	140,441	0	0	0	18,700	0	159,141	31,768	0	201,196
2038	190,909	140,441	0	0	0	18,700	0	159,141	31,768	0	169,429
2039	190,909	140,441	0	0	0	18,700	0	159,141	31,768	0	137,661
2040	190,909	140,441	0	0	0	18,700	0	159,141	31,768	0	105,893
2041	190,909	141,918	0	0	0	18,700	0	160,618	30,291	0	75,602
2042	190,909	141,918	0	0	0	18,700	0	160,618	30,291	0	45,311
2043	190,909	141,918	0	0	0	18,700	0	160,618	30,291	0	15,020
2044	190,909	141,918	0	0	0	18,700	0	160,618	30,291	15,271	0
2045	190,909	141,918	0	0	0	18,700	0	160,618	30,291	30,291	0
2046	190,909	141,918	0	0	0	18,700	0	160,618	30,291	30,291	0
2047	190,909	141,918	0	0	0	18,700	0	160,618	30,291	30,291	0
2048	190,909	141,918	0	0	0	18,700	0	160,618	30,291	30,291	0
2049	190,909	141,918	0	0	0	18,700	0	160,618	30,291	30,291	0
2050	190,909	141,918	0	0	0	18,700	0	160,618	30,291	30,291	0

1 -- Safe yield estimate from net recharge estimated in Scenario 5A

2 -- This is the net replenishment obligation based on the assumptions described in the text; negative values mean underproduction and an increase in stored water accounts.

Table 7-6
Water Budget for Chino Basin (2011-2050)
Scenario 5A
(acre-ft)

End of Fiscal Year	Recharge										Discharge							Recharge minus Discharge	Annual Net Recharge	Ten-Year Average net Recharge
	I*	I	R	I	I	I	I	I	R		I	I	I	R	R	R				
	Subsurface Boundary Inflow, Chino Hills, Six Basins, Cucamonga Basin and Rialto Basin	Subsurface Boundary Inflow from Bloomington Divide	Subsurface Inflow From Temescal Basin	Deep Infiltration of Precipitation and Applied Water	Streambed Infiltration from Santa Ana River Tributaries	Storm Water Recharge in Basins	Recycled Water Recharge	Imported Water Recharge	Streambed Infiltration in the Santa Ana River	Subtotal Recharge	CDA Pumping	Overlying Non Ag and Appropriative Pools Production	Overlying Agricultural Pool Production	ET	GW Discharge to Streams	Subsurface Discharge to Temescal Basin	Subtotal Discharge			
(1)	(2)	(3)	(4)	(5)	(6)	(7)	(8)	(9)	(10)	(11)	(12)	(13)	(14)	(15)	(16)	(17)	(18)	(19)	(20)	(21)
2011	23,077	13,658	6,750	81,096	1,308	16,985	7,743	9,466	34,347	194,431	29,043	98,922	21,021	18,190	18,358	2,899	188,433	5,997	137,775	130,286
2012	19,106	8,153	5,892	91,059	1,081	9,271	8,634	22,560	38,444	204,199	28,411	96,725	22,407	18,060	17,440	3,520	186,563	17,636	133,985	131,408
2013	19,106	8,153	4,949	90,236	1,084	5,271	10,479	0	39,746	179,023	27,098	110,918	23,950	18,024	17,260	3,946	201,196	-22,173	129,314	131,440
2014	19,106	8,153	5,432	91,466	1,087	12,000	9,300	3,996	38,934	189,473	31,440	105,212	21,950	18,118	17,987	4,070	198,778	-9,304	136,002	132,514
2015	19,106	8,153	5,953	91,550	1,089	12,000	14,500	3,996	37,760	194,108	32,289	106,595	19,125	18,214	18,715	4,013	198,951	-4,843	134,670	132,791
2016	19,106	8,153	6,122	95,445	1,092	12,000	14,500	3,996	36,855	197,270	37,500	108,125	16,300	18,266	19,272	3,924	203,387	-6,117	137,312	133,255
2017	19,106	8,153	6,233	96,220	1,095	12,000	14,500	3,996	36,776	198,079	39,767	109,655	13,475	18,267	19,231	3,881	204,275	-6,196	138,205	134,798
2018	19,106	8,153	6,310	96,705	1,098	12,000	16,900	3,996	36,048	200,316	39,767	111,184	10,650	18,287	19,428	3,862	203,178	-2,862	137,844	135,414
2019	19,106	8,153	6,365	95,553	1,101	12,000	16,900	3,996	35,467	198,641	39,767	112,714	7,825	18,323	19,760	3,855	202,244	-3,603	135,808	135,749
2020	19,106	8,153	6,405	94,200	1,104	12,000	16,900	3,996	34,878	196,741	39,767	114,244	5,000	18,358	20,120	3,851	201,341	-4,600	133,516	135,443
2021	19,106	8,153	6,410	92,631	1,106	12,000	16,900	3,996	34,770	195,073	39,767	116,444	5,000	18,357	20,189	3,854	203,612	-8,540	131,776	134,843
2022	19,106	8,153	6,403	91,884	1,109	12,000	18,700	3,996	34,787	196,139	39,767	118,644	5,000	18,342	20,133	3,860	205,746	-9,608	131,108	134,555
2023	19,106	8,153	6,393	93,273	1,112	12,000	18,700	3,996	34,671	197,404	39,767	120,844	5,000	18,316	19,872	3,869	207,668	-10,264	132,651	134,889
2024	19,106	8,153	6,378	93,509	1,115	12,000	18,700	3,996	34,824	197,781	39,767	123,044	5,000	18,303	19,717	3,878	209,709	-11,928	133,187	134,608
2025	19,106	8,153	6,361	94,353	1,118	12,000	18,700	3,996	34,992	198,778	39,767	125,244	5,000	18,290	19,564	3,887	211,752	-12,974	134,341	134,575
2026	19,106	8,153	6,345	94,889	1,121	12,000	18,700	3,996	35,164	199,475	39,767	127,367	5,000	18,276	19,405	3,896	213,711	-14,236	135,202	134,364
2027	19,106	8,153	6,329	94,717	1,124	12,000	18,700	3,996	35,355	199,479	39,767	129,489	5,000	18,262	19,234	3,905	215,658	-16,179	135,381	134,081
2028	19,106	8,153	6,315	94,652	1,126	12,000	18,700	3,996	35,523	199,571	39,767	131,612	5,000	18,247	19,079	3,912	217,618	-18,047	135,637	133,861
2029	19,106	8,153	6,301	95,291	1,129	12,000	18,700	3,996	35,727	200,403	39,767	133,735	5,000	18,231	18,898	3,920	219,550	-19,147	136,659	133,946
2030	19,106	8,153	6,286	95,381	1,132	12,000	18,700	3,996	35,961	200,715	39,767	135,857	5,000	18,213	18,699	3,929	221,465	-20,750	137,179	134,312
2031	19,106	8,153	6,274	96,029	1,132	12,000	18,700	0	36,203	197,597	39,767	137,838	5,000	18,193	18,482	3,934	223,215	-25,618	138,288	134,963
2032	19,106	8,153	6,263	94,944	1,132	12,000	18,700	0	36,428	196,726	39,767	139,820	5,000	18,172	18,269	3,938	224,967	-28,241	137,646	135,617
2033	19,106	8,153	6,252	95,236	1,132	12,000	18,700	0	36,700	197,279	39,767	141,801	5,000	18,149	18,015	3,944	226,676	-29,397	138,471	136,199
2034	19,106	8,153	6,242	96,292	1,132	12,000	18,700	0	36,996	198,621	39,767	143,782	5,000	18,124	17,746	3,948	228,367	-29,746	140,103	136,891
2035	19,106	8,153	6,232	96,476	1,132	12,000	18,700	0	37,318	199,117	39,767	145,763	5,000	18,097	17,492	3,953	230,072	-30,954	140,876	137,544
2036	19,106	8,153	6,222	96,794	1,132	12,000	18,700	0	37,700	199,807	39,767	145,763	5,000	18,069	17,248	3,957	229,805	-29,997	141,833	138,207
2037	19,106	8,153	6,215	96,137	1,132	12,000	18,700	0	38,080	199,523	39,767	145,763	5,000	18,041	17,027	3,960	229,559	-30,036	141,795	138,849
2038	19,106	8,153	6,205	95,400	1,132	12,000	18,700	0	38,468	199,164	39,767	145,763	5,000	18,014	16,808	3,966	229,318	-30,154	141,676	139,453
2039	19,106	8,153	6,197	95,022	1,132	12,000	18,700	0	38,850	199,159	39,767	145,763	5,000	17,987	16,605	3,970	229,092	-29,933	141,898	139,977
2040	19,106	8,153	6,191	94,503	1,132	12,000	18,700	0	39,207	198,993	39,767	145,763	5,000	17,962	16,431	3,972	228,895	-29,902	141,928	140,451
2041	19,106	8,153	6,185	94,044	1,132	12,000	18,700	0	39,547	198,867	39,767	145,763	5,000	17,938	16,275	3,975	228,719	-29,852	141,978	140,821
2042	19,106	8,153	6,179	93,678	1,132	12,000	18,700	0	39,911	198,859	39,767	145,763	5,000	17,914	16,099	3,978	228,522	-29,662	142,168	141,273
2043	19,106	8,153	6,174	93,144	1,132	12,000	18,700	0	40,232	198,641	39,767	145,763	5,000	17,892	15,948	3,981	228,351	-29,710	142,120	141,638
2044	19,106	8,153	6,168	92,707	1,132	12,000	18,700	0	40,494	198,461	39,767	145,763	5,000	17,873	15,827	3,984	228,214	-29,753	142,077	141,835
2045	19,106	8,153	6,164	92,038	1,132	12,000	18,700	15,271	40,727	213,291	39,767	145,763	5,000	17,856	15,728	3,985	228,100	-14,809	141,751	141,923
2046	19,106	8,153	6,159	91,738	1,132	12,000	18,700	30,291	40,962	228,241	39,767	145,763	5,000	17,840	15,625	3,988	227,984	258	141,797	141,919
2047	19,106	8,153	6,155	91,657	1,132	12,000	18,700	30,291	41,149	228,343	39,767	145,763	5,000	17,827	15,551	3,990	227,899	444	141,984	141,938
2048	19,106	8,153	6,150	91,506	1,132	12,000	18,700	30,291	41,305	228,343	39,767	145,763	5,000	17,816	15,490	3,992	227,828	515	142,055	141,976
2049	19,106	8,153	6,147	91,385	1,132	12,000	18,700	30,291	41,421	228,335	39,767	145,763	5,000	17,808	15,442	3,993	227,774	561	142,101	141,996
2050	19,106	8,153	6,143	91,158	1,132	12,000	18,700	30,291	41,495	228,177	39,767	145,763	5,000	17,803	15,411	3,995	227,739	438	141,978	142,001
Statistics for the Period 2011 through 2050																				
Total	768,211	331,625	247,849	3,743,997	44,973	475,527	689,556	266,683	1,504,224	8,072,646	1,537,873	5,232,026	311,703	724,318	713,882	156,131	8,675,933	-603,287	5,522,076	5,472,600
Total (%)	10%	4%	3%	46%	1%	6%	9%	3%	19%	100%	18%	60%	4%	8%	8%	2%	100%			
Average	19,205	8,291	6,196	93,600	1,124	11,888	17,239	6,667	37,606	201,816	38,447	130,801	7,793	18,108	17,847	3,903	216,898	-15,082	138,052	136,815
Median	19,106	8,153	6,227	94,276	1,132	12,000	18,700	3,996	37,157	198,863	39,767	136,848	5,000	18,137	18,001	3,945	222,340	-14,523	138,024	135,530
Maximum	23,077	13,658	6,750	96,794	1,308	16,985	18,700	30,291	41,495	228,343	39,767	145,763	23,950	18,358	20,189	4,070	230,072	17,636	142,168	142,001
Minimum	19,106	8,153	4,949	81,096	1,081	5,271	7,743	0	34,347	179,023	27,098	96,725	5,000	17,803	15,411	2,899	186,563	-30,954	129,314	130,286

Table 7-7
Summary of Projected Groundwater Elevation Changes by Water Service Area - Scenario 5A
(feet)

Agency Service Area	Initial Groundwater Elevation 2011			Projected Groundwater Elevation 2020			Projected Change in Groundwater Elevation 2020-2011			Projected Groundwater Elevation 2030			Projected Change in Groundwater Elevation 2030-2011			Projected Groundwater Elevation 2040			Projected Change in Groundwater Elevation 2040-2011			Projected Groundwater Elevation 2050			Projected Change in Groundwater Elevation 2050-2011		
	Min	Max	Avg	Min	Max	Avg	Min	Max	Avg	Min	Max	Avg	Min	Max	Avg	Min	Max	Avg	Min	Max	Avg	Min	Max	Avg	Min	Max	Avg
City of Chino	490	584	547	491	591	554	-12	25	8	491	583	547	-17	18	1	491	567	532	-42	5	-15	482	555	522	-67	2	-27
City of Chino Hills	524	586	562	526	593	569	2	14	7	526	584	565	-2	8	2	525	568	555	-23	2	-7	525	559	547	-43	1	-16
City of Ontario	528	661	582	515	673	587	-20	34	5	508	669	576	-27	22	-6	491	653	552	-48	3	-30	482	648	543	-68	-3	-43
City of Pomona	562	597	580	563	591	578	-10	5	-2	551	580	567	-22	-5	-13	511	551	534	-62	-31	-47	504	554	525	-94	-54	-74
City of Upland	588	696	624	601	689	631	-14	19	7	589	685	620	-22	7	-4	544	631	584	-47	-30	-39	562	598	584	-74	-53	-63
Cucamonga Valley Water District	585	735	678	610	746	689	4	27	11	592	751	686	-6	21	8	565	741	668	-36	11	-10	563	774	669	-57	77	3
Fontana Water Company	608	811	722	622	800	729	-11	18	7	617	798	728	-13	19	5	599	795	718	-16	9	-5	593	788	716	-22	72	1
Jurupa Community Services District	506	751	589	507	757	586	-20	20	-3	506	757	583	-28	18	-6	493	757	574	-50	6	-15	485	756	570	-57	14	-18
Monte Vista Water District	573	600	583	573	606	589	-3	18	6	561	594	577	-15	6	-6	523	555	542	-57	-25	-41	517	583	543	-81	-46	-63
Santa Ana River Water Co.	577	638	606	572	639	604	-6	1	-2	569	639	602	-10	1	-4	558	638	596	-25	1	-9	552	637	594	-29	0	-11
West Valley Water District	734	835	803	744	825	792	-22	11	-11	749	822	791	-23	16	-12	739	820	787	-27	6	-17	743	813	780	-33	53	-21

Table 7-8

CDA Desalter Well Production Schedule for Scenario 5G

Well	Operational Assumptions		Model-Assumed Production			Well in Service
	Current Capacity (gpm)	Operating Factor (% used)	Average Capacity (gpm)	Annual Capacity (acre-ft/yr)	*acre-ft/quarter*	
(1)	(2)	(3)	(4) = (2) * (3)	(5) = (4) * 1.631		(6)
CDA I-1	399	95%	379	611	153	Now
CDA I-2	210	95%	200	322	80	Now
CDA I-3	555	95%	527	850	213	Now
CDA I-4	170	95%	162	260	65	Now
CDA I-5	1,327	70%	932	1,504	376	Now
CDA I-6	297	70%	209	337	84	Now
CDA I-7	302	70%	212	342	86	Now
CDA I-8	1,098	70%	771	1,244	311	Now
CDA I-9	1,096	70%	770	1,242	310	Now
CDA I-10	1,304	70%	916	1,478	369	Now
CDA I-11	789	70%	554	894	224	Now
CDA I-13	1,185	70%	833	1,343	336	Now
CDA I-14	2,103	70%	1,477	2,383	596	Now
CDA I-15	2,496	70%	1,754	2,828	707	Now
CDA I-16	250	70%	176	283	71	5/1/2014
CDA I-17	300	70%	211	340	85	5/1/2014
CDA I-18	0	0%	0	0	0	Not Used
CDA I-19	0	0%	0	0	0	Abandoned
CDA I-20	400	70%	281	453	113	9/1/2015
CDA I-21	400	70%	281	453	113	9/1/2015
CDA II-1	2,162	70%	1,519	2,450	612	Now
CDA II-2	1,791	70%	1,258	2,029	507	Now
CDA II-3	1,848	70%	1,298	2,094	524	Now
CDA II-4	2,030	70%	1,426	2,300	575	Now
CDA II-6	1,758	70%	1,235	1,992	498	Now
CDA II-7	1,089	70%	765	1,234	308	Now
CDA II-8	1,287	70%	904	1,458	365	Now
CDA II-9A	1,980	70%	1,391	2,244	561	Now
CDA II-10	2,000	70%	1,405	2,266	567	1/1/2016
CDA II-11	2,000	70%	1,405	2,266	567	1/1/2016
CDA II-12 Opt 1					0	Not Used
CDA II-12 Opt 2						Not Used
CDA II-12 Opt 3	2,000	70%	1,405	2,266		6/1/2016
Totals	**34,626**	**71%**	**24,656**	**39,768**	**9,375**	
CCWF Sub-totals	1,350		948	1,530	382	

Table 7-9
Subsurface Discharge through the CCWF for Scenarios 5A and 5G
(acre-ft/yr)

Year	Per May 29, 2014 Report Scenario 5A Including CDA II Option 1	Scenario 5A	Scenario 5G
2015	910	1,061	1,061
2016	910	910	910
2017	916	910	910
2018	916	916	916
2019	911	916	917
2020	905	911	911
2021	904	905	905
2022	899	904	904
2023	890	899	898
2024	878	890	888
2025	865	878	876
2026	852	865	863
2027	839	852	850
2028	827	839	837
2029	814	827	824
2030	800	814	811
2040	589	567	562
2050	422	421	416

Table 7-10
Santa Ana River Underflow New Yield[1] Created by the CDA Chino Desalter Well Production and Reoperation
(acre-ft)

Year	CDA Production		New Yield[2]		Ratio of New Yield to CDA Production	
	Annual	Cumulative	Annual	Cumulative	Annual	Cumulative
2001	7,989	7,989	192	192	2%	2%
2002	9,458	17,447	7	199	0%	1%
2003	10,439	27,885	-1,388	-1,189	-13%	-4%
2004	10,605	38,490	-4,453	-5,642	-42%	-15%
2005	9,854	48,344	5,528	-114	56%	0%
2006	16,542	64,886	11,816	11,702	71%	18%
2007	27,077	91,962	10,567	22,269	39%	24%
2008	30,121	122,084	16,895	39,164	56%	32%
2009	29,012	151,096	14,655	53,819	51%	36%
2010	28,857	179,953	17,313	71,132	60%	40%
2011	29,043	208,996	17,771	88,903	61%	43%
2012	28,411	237,407	23,157	112,059	82%	47%
2013	27,098	264,505	24,639	136,698	91%	52%
2014	31,440	295,945	23,099	159,798	73%	54%
2015	32,289	328,234	21,198	180,995	66%	55%
2016	37,500	365,734	19,736	200,731	53%	55%
2017	39,767	405,501	19,698	220,429	50%	54%
2018	39,767	445,269	18,773	239,203	47%	54%
2019	39,767	485,036	17,859	257,062	45%	53%
2020	39,767	524,804	16,910	273,972	43%	52%
2021	39,767	564,571	16,734	290,706	42%	51%
2022	39,767	604,338	16,807	307,513	42%	51%
2023	39,767	644,106	16,952	324,465	43%	50%
2024	39,767	683,873	17,260	341,724	43%	50%
2025	39,767	723,641	17,580	359,304	44%	50%
2026	39,767	763,408	17,912	377,216	45%	49%
2027	39,767	803,175	18,273	395,489	46%	49%
2028	39,767	842,943	18,597	414,086	47%	49%
2029	39,767	882,710	18,982	433,067	48%	49%
2030	39,767	922,478	19,415	452,482	49%	49%

[1]SAR Underflow New Yield is estimated as the increase in net Santa Ana River (SAR) Recharge to the Chino Basin.

[2] Annual relative to the 2000 SAR Underflow baseline of -2,153 acre-ft/yr

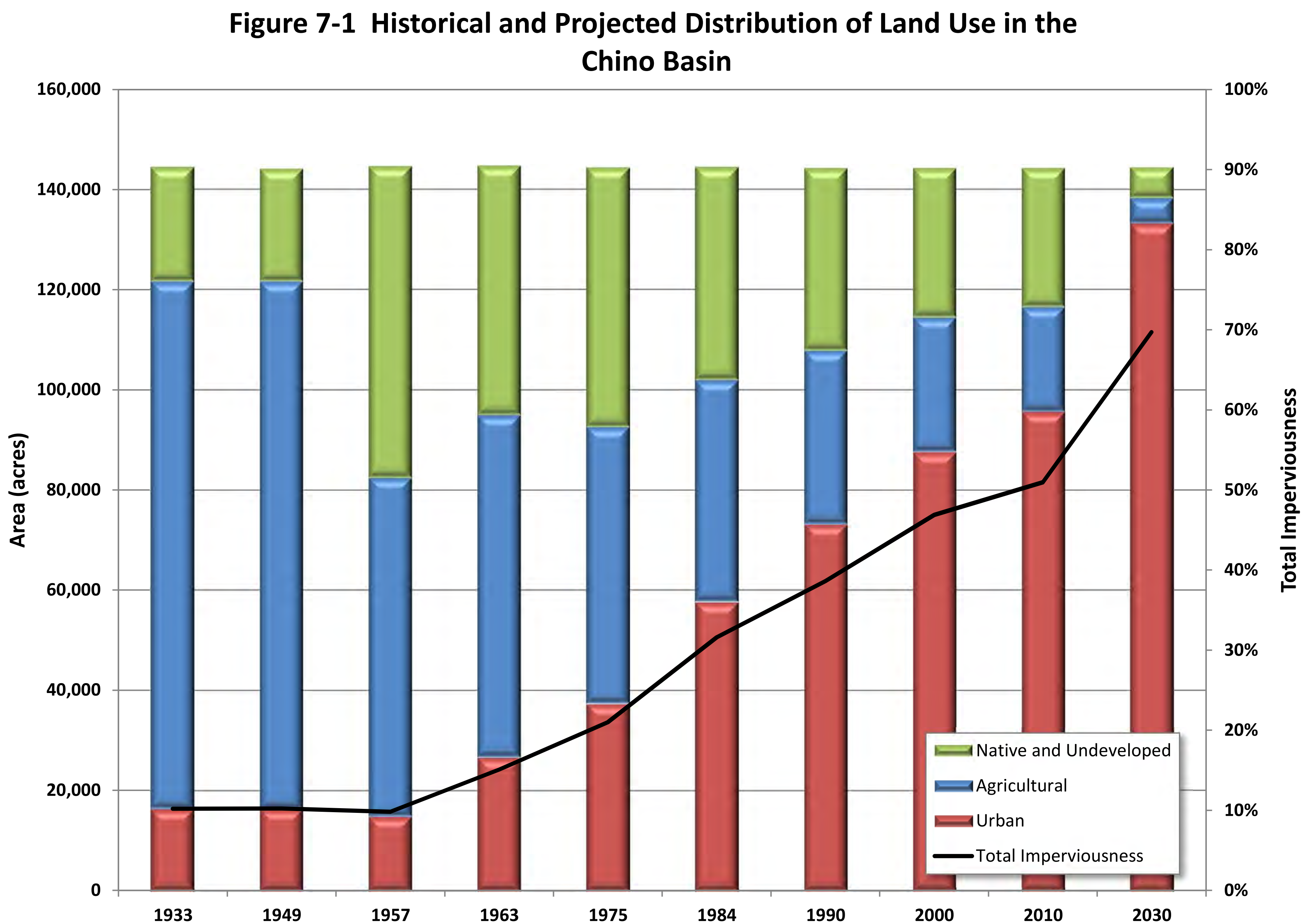

20150930 Final Fig 7-1 Tabs 7-1 and 7-2.xlsx

Revised 10/1/2015

Figure 7-2 Historical and Projected Chino Basin Groundwater Production

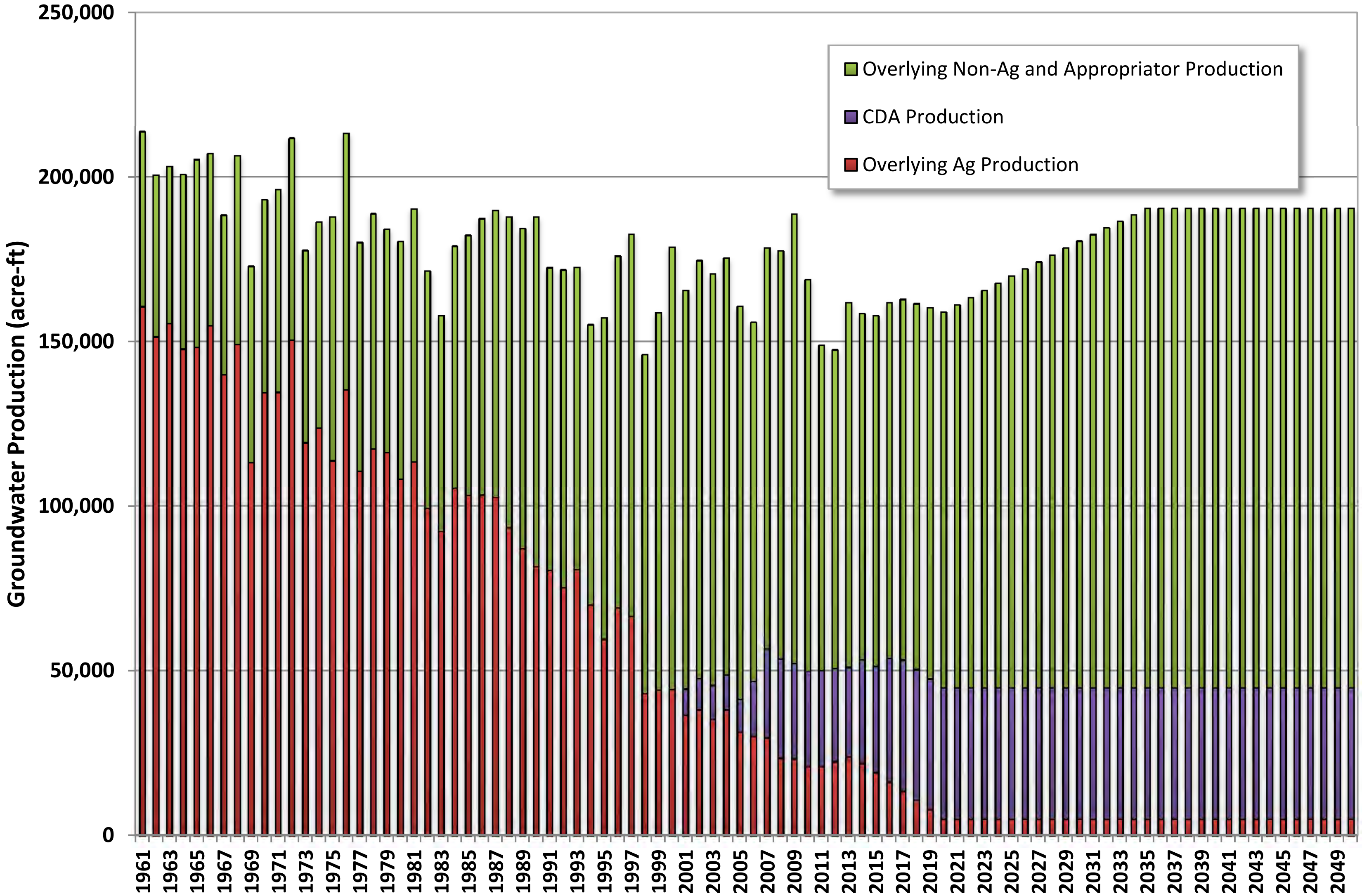

20150930 Final Tab 7-6 and 7-10 and Fig 7-2.xlsx -- Figure 7-2
Created 09/13/2015
Printed 10/1/2015

Figure 7-3 Comparison of Historical and Projected Net Recharge to Overlying Ag and CDA Production

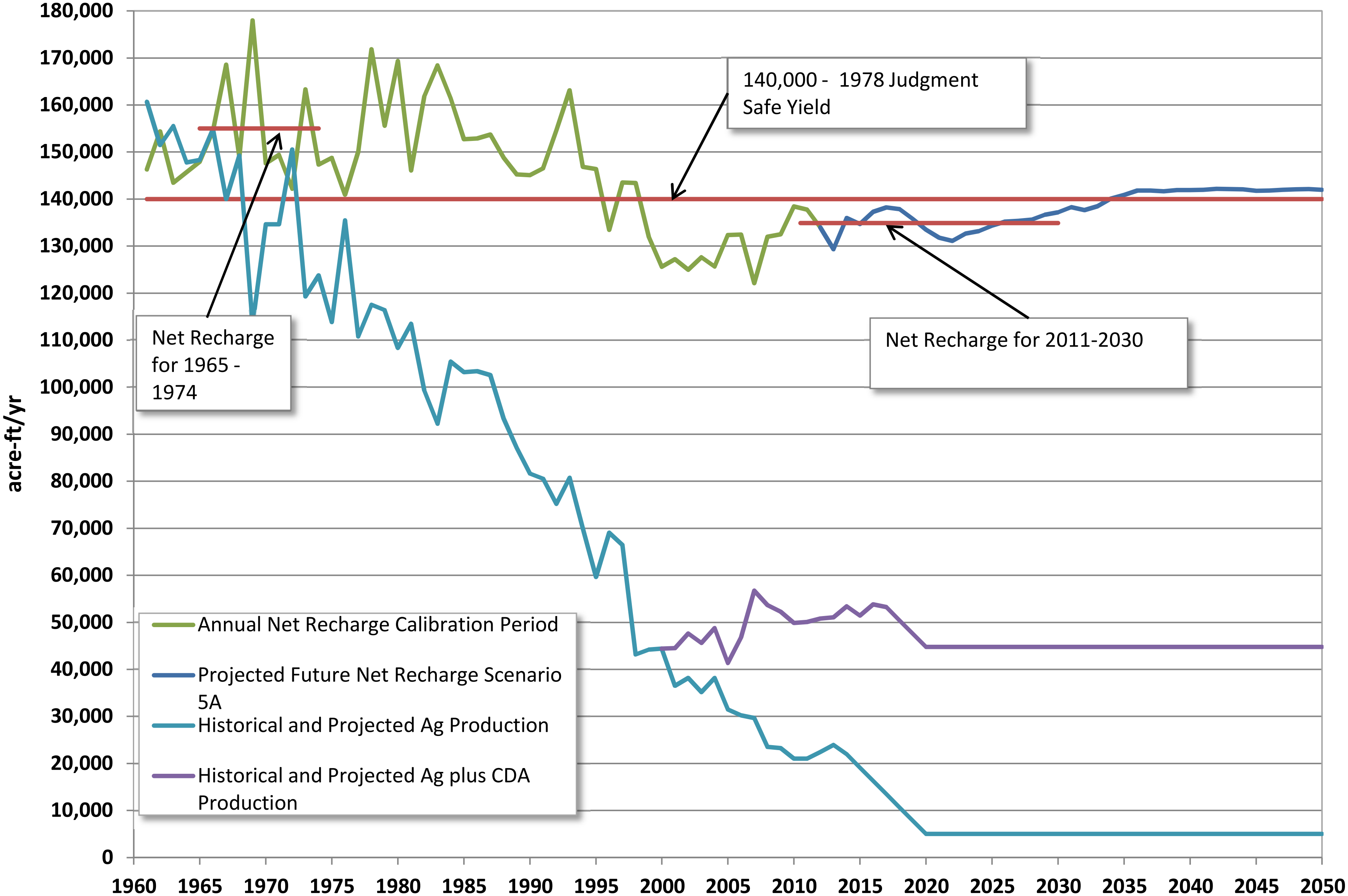

20150930 Final Fig 7-3.xlsx -- Figure 7-3
Created 09/10/2014
Printed 10/1/2015

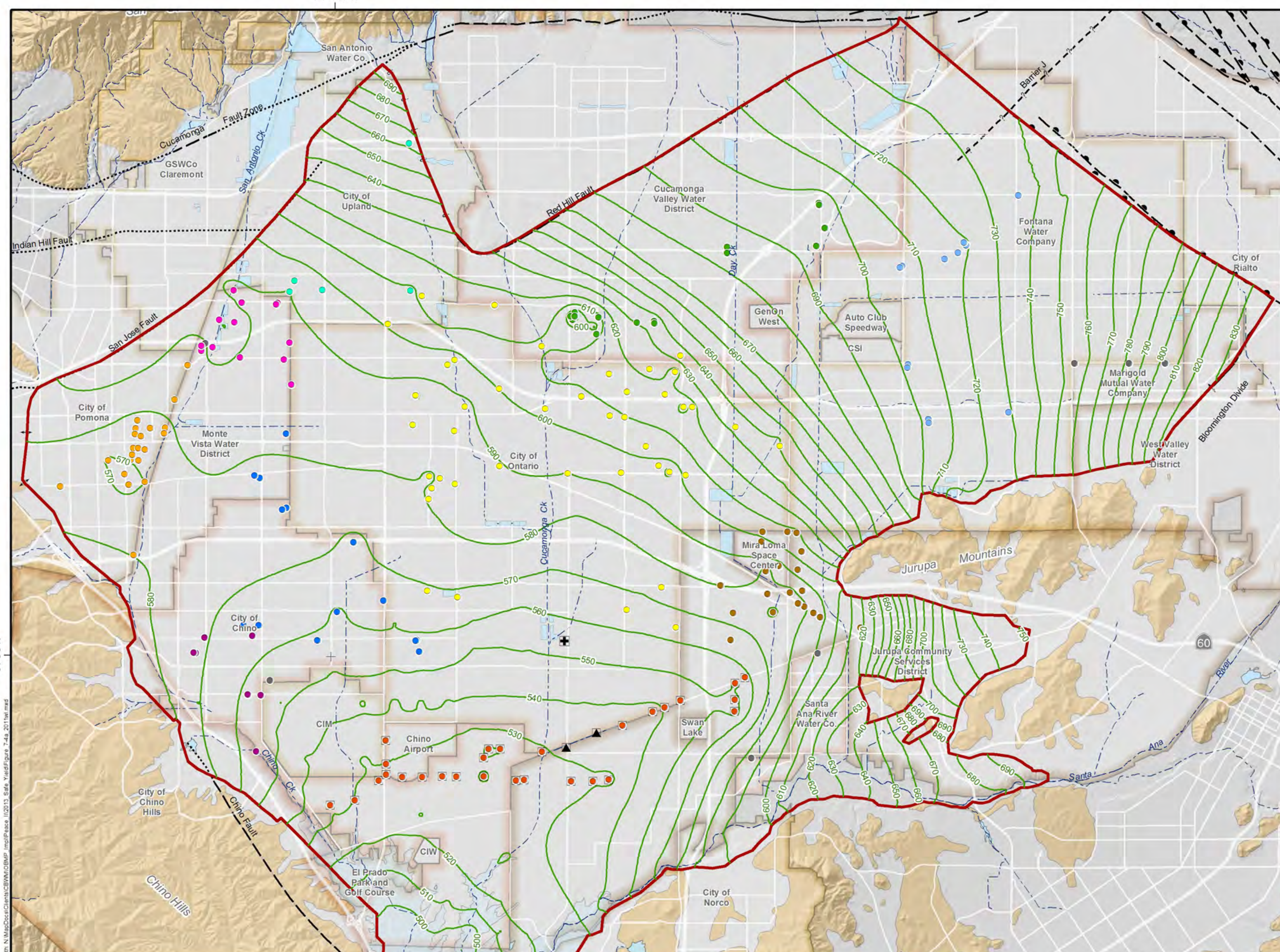

2011 Groundwater Elevation Contours (Secnario 5A) *(feet above mean sea-level)*

Water Service Area Boundaries

CDA & Appropriator Production Wells

- Chino Desalter Authority
- City of Chino
- City of Chino Hills
- City of Ontario
- City of Pomona
- City of Upland
- Cucamonga Valley Water District
- Fontana Water Company
- Jurupa Community Services District
- Monte Vista Water District
- Other Appropriators

- Chino Desalter Well
- New Chino II Desalter Well (January 2016)
- Third New Chino II Desalter Well (June 2016)

Other Features

- Groundwater Flow Model Boundary
- Flood Control and Conservation Basins

Produced by: WEI Wildermuth Environmental, Inc.

Author: LBB
Date: 9/16/2015

0 1 2 Miles
0 2 4 Kilometers

2013 Chino Basin Groundwater Model Update and Analysis of Safe Yield

Groundwater Elevation Contours -- Layer 1
Scenario 5A Initial Condition - 2011

Figure 7-4a

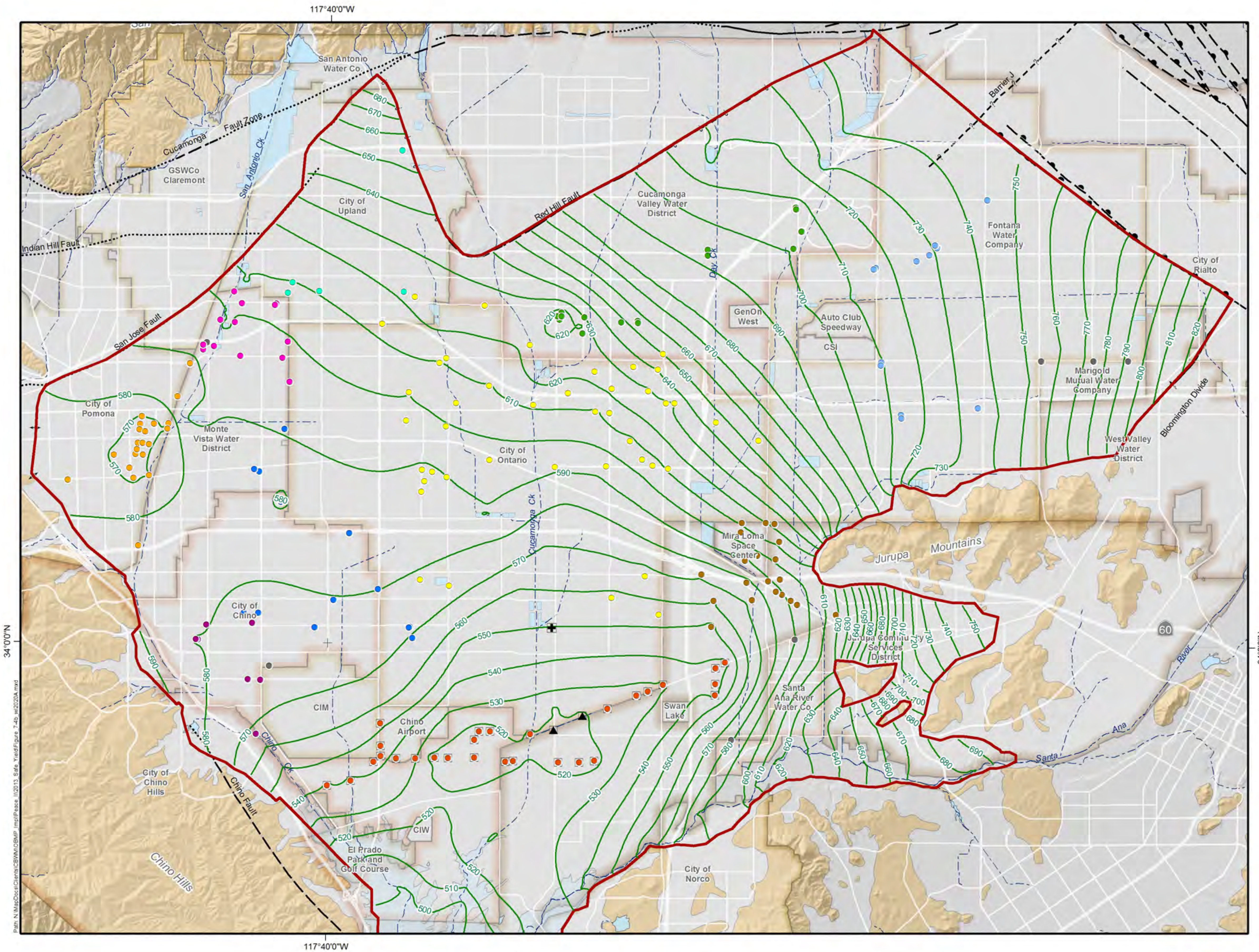

2020 Groundwater Elevation Contours (Secnario 5A) *(feet above mean sea-level)*

Water Service Area Boundaries

CDA & Appropriator Production Wells

- Chino Desalter Authority
- City of Chino
- City of Chino Hills
- City of Ontario
- City of Pomona
- City of Upland
- Cucamonga Valley Water District
- Fontana Water Company
- Jurupa Community Services District
- Monte Vista Water District
- Other Appropriators

- Chino Desalter Well
- New Chino II Desalter Well (January 2016)
- Third New Chino II Desalter Well (June 2016)

Other Features

- Groundwater Flow Model Boundary
- Flood Control and Conservation Basins

Produced by:

WEI
Wildermuth Environmental, Inc.

Author: LBB
Date: 9/16/2015

0 1 2 Miles
0 2 4 Kilometers

2013 Chino Basin Groundwater Model Update and Analysis of Safe Yield

Projected Groundwater Elevation Contours -- Layer 1
Scenario 5A - 2020

Figure 7-4b

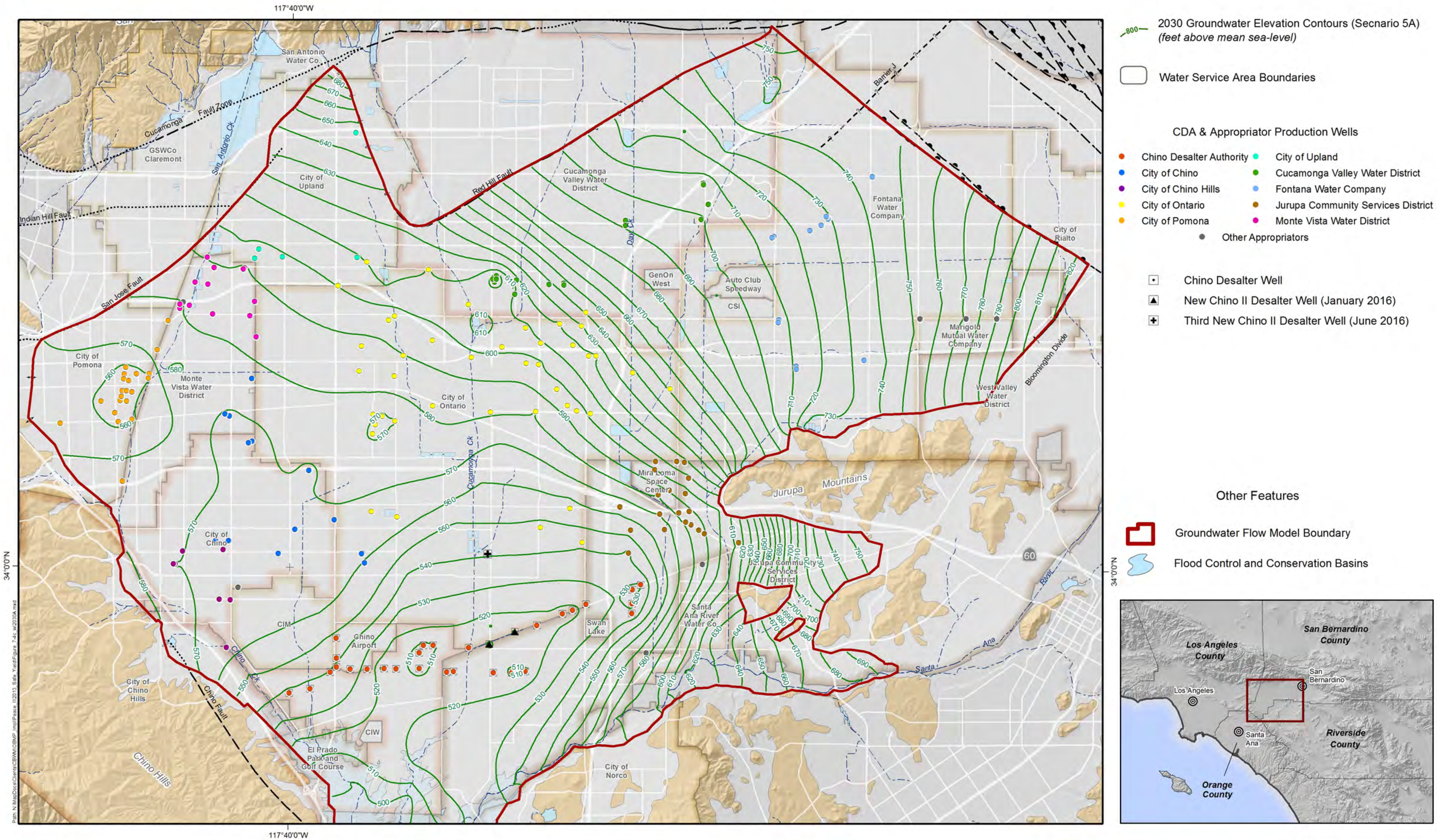

Produced by:

WEI
Wildermuth Environmental, Inc.

Author: LBB
Date: 9/16/2015

2013 Chino Basin Groundwater Model Update and Analysis of Safe Yield

Projected Groundwater Elevation Contours -- Layer 1
Scenario 5A - 2030

Figure 7-4c

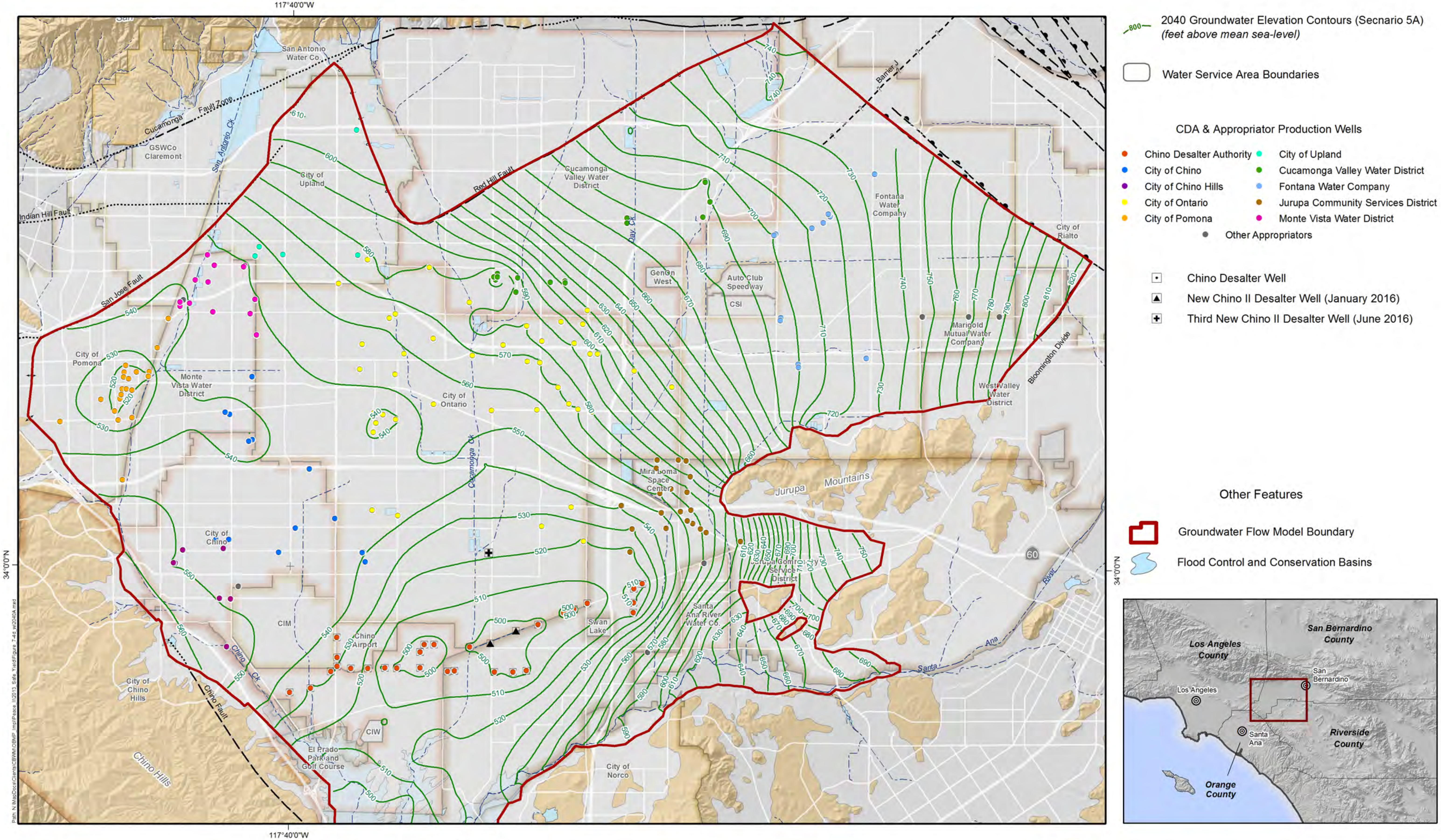

Produced by:

WEI Wildermuth Environmental, Inc.

Author: LBB
Date: 9/16/2015

0 1 2 Miles

0 2 4 Kilometers

2013 Chino Basin Groundwater Model Update and Analysis of Safe Yield

Projected Groundwater Elevation Contours -- Layer 1
Scenario 5A - 2040

Figure 7-4d

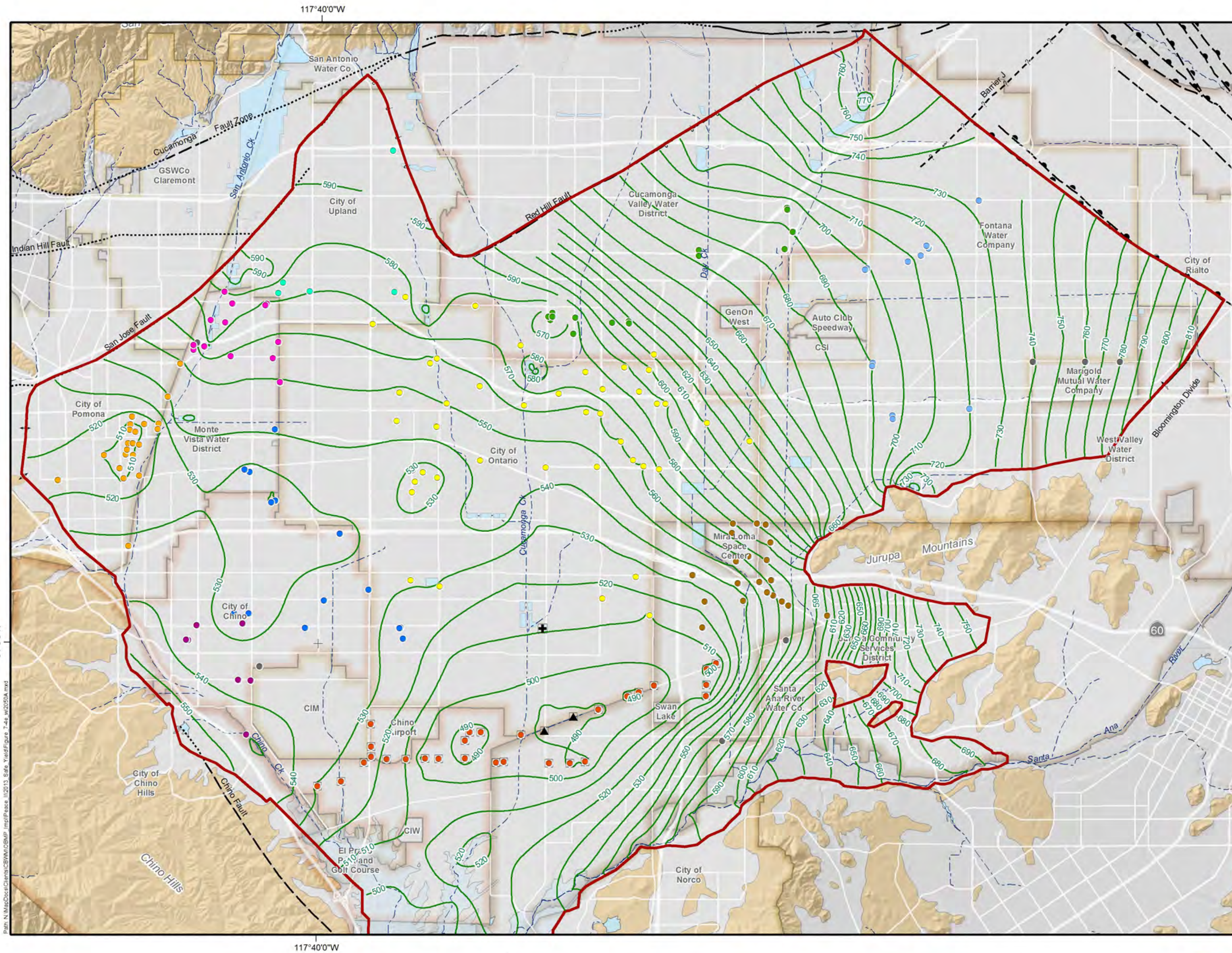

2050 Groundwater Elevation Contours (Secnario 5A) *(feet above mean sea-level)*

Water Service Area Boundaries

CDA & Appropriator Production Wells

- Chino Desalter Authority
- City of Chino
- City of Chino Hills
- City of Ontario
- City of Pomona
- City of Upland
- Cucamonga Valley Water District
- Fontana Water Company
- Jurupa Community Services District
- Monte Vista Water District
- Other Appropriators

- Chino Desalter Well
- New Chino II Desalter Well (January 2016)
- Third New Chino II Desalter Well (June 2016)

Other Features

- Groundwater Flow Model Boundary
- Flood Control and Conservation Basins

Produced by: WEI Wildermuth Environmental, Inc.

Author: LBB
Date: 9/16/2015

0 1 2 Miles
0 2 4 Kilometers

Chino Basin Watermaster

2013 Chino Basin Groundwater Model Update and Analysis of Safe Yield

Projected Groundwater Elevation Contours -- Layer 1
Scenario 5A - 2050

Figure 7-4e

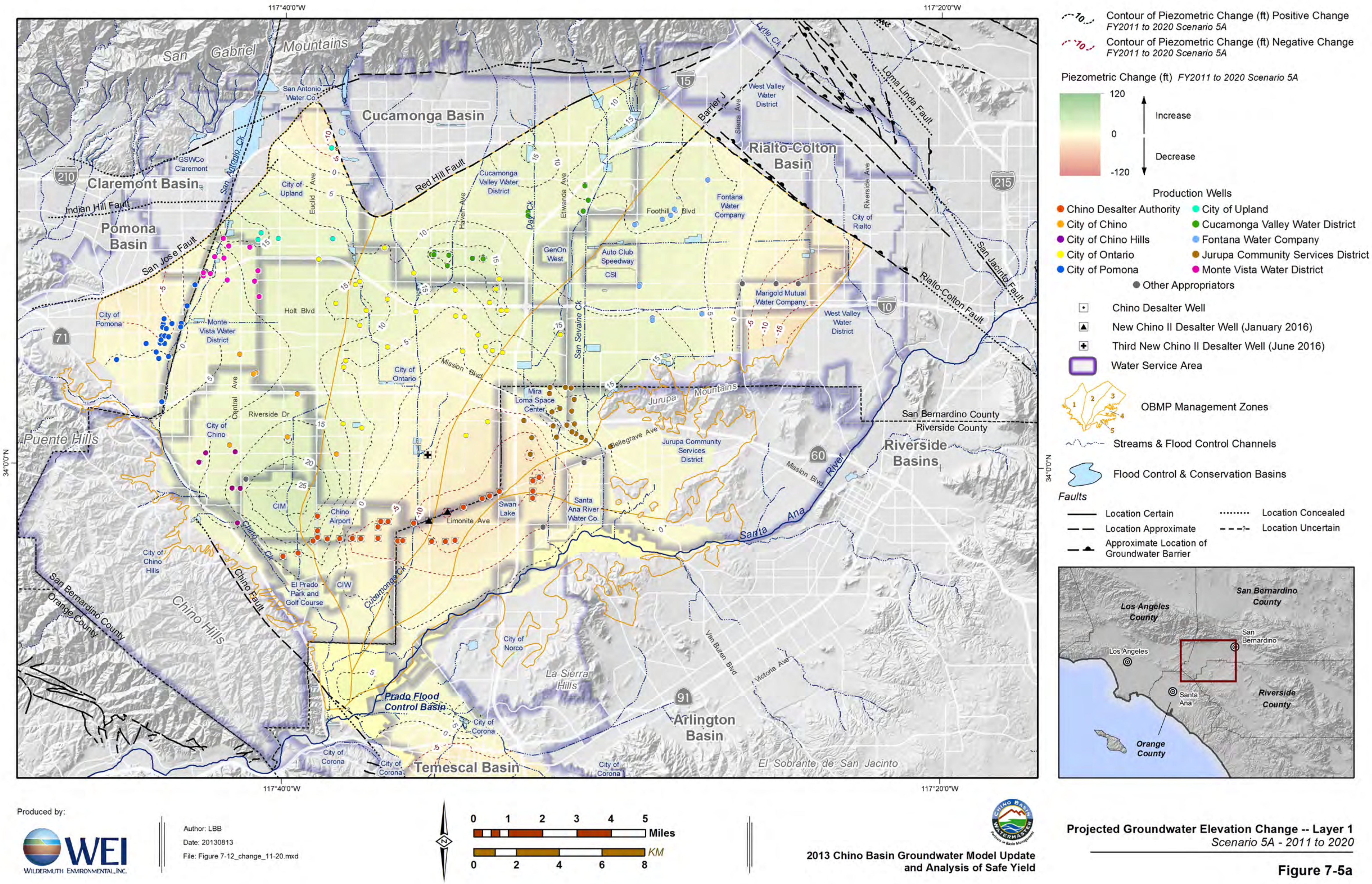

Produced by:

WEI
WILDERMUTH ENVIRONMENTAL, INC.

Author: LBB

Date: 20130813

File: Figure 7-12_change_11-20.mxd

2013 Chino Basin Groundwater Model Update and Analysis of Safe Yield

Projected Groundwater Elevation Change -- Layer 1
Scenario 5A - 2011 to 2020

Figure 7-5a

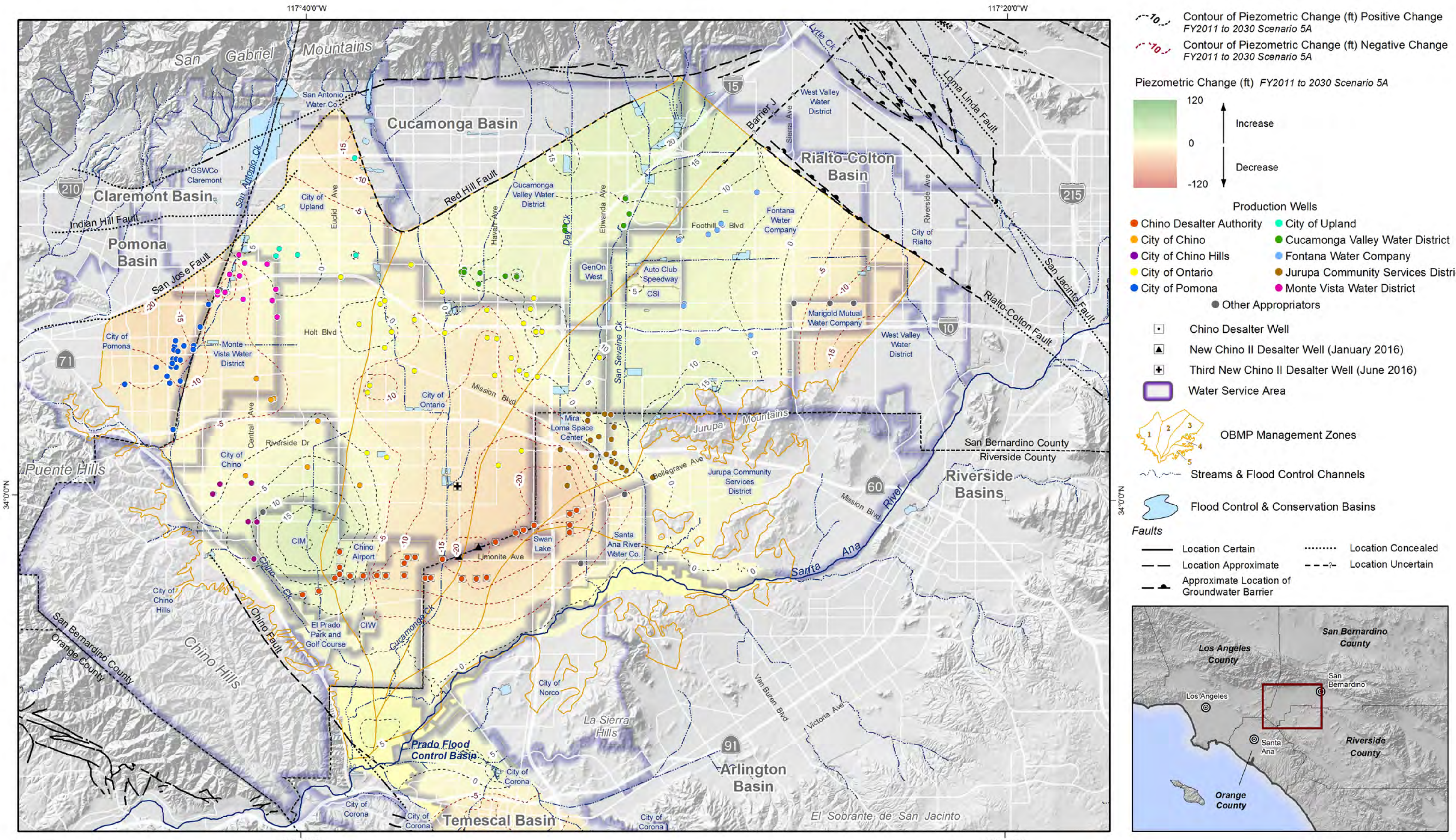

Produced by:
WEI
Wildermuth Environmental, Inc.

Author: LBB
Date: 20130813
File: Figure 7-12_change_11-20.mxd

2013 Chino Basin Groundwater Model Update and Analysis of Safe Yield

Projected Groundwater Elevation Change -- Layer 1
Scenario 5A - 2011 to 2030

Figure 7-5b

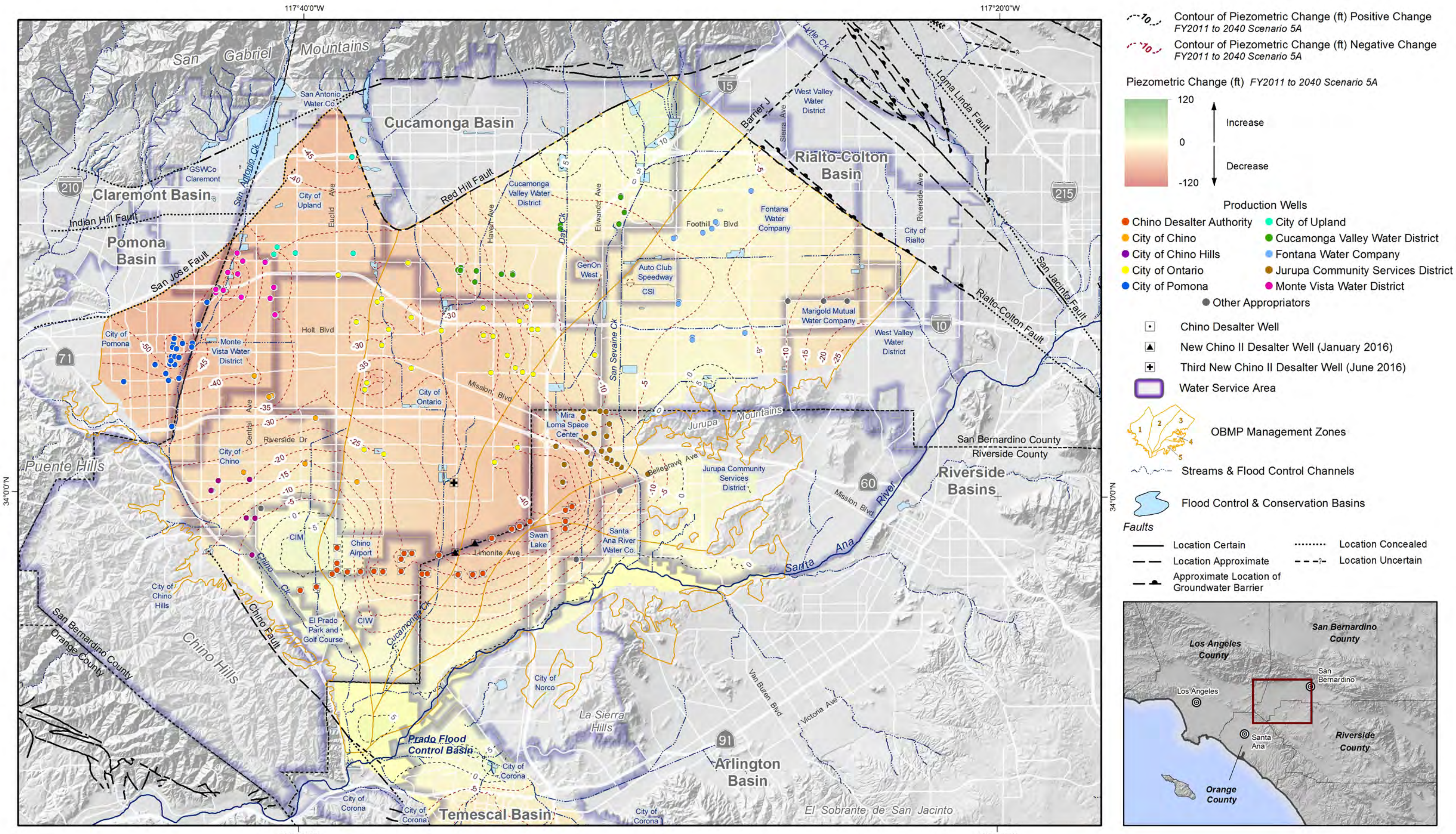

Produced by:

WEI
WILDERMUTH ENVIRONMENTAL, INC.

Author: LBB
Date: 20130813
File: Figure 7-12_change_11-20.mxd

0 1 2 3 4 5 Miles
0 2 4 6 8 KM

2013 Chino Basin Groundwater Model Update and Analysis of Safe Yield

Projected Groundwater Elevation Change -- Layer 1
Scenario 5A - 2011 to 2040

Figure 7-5c

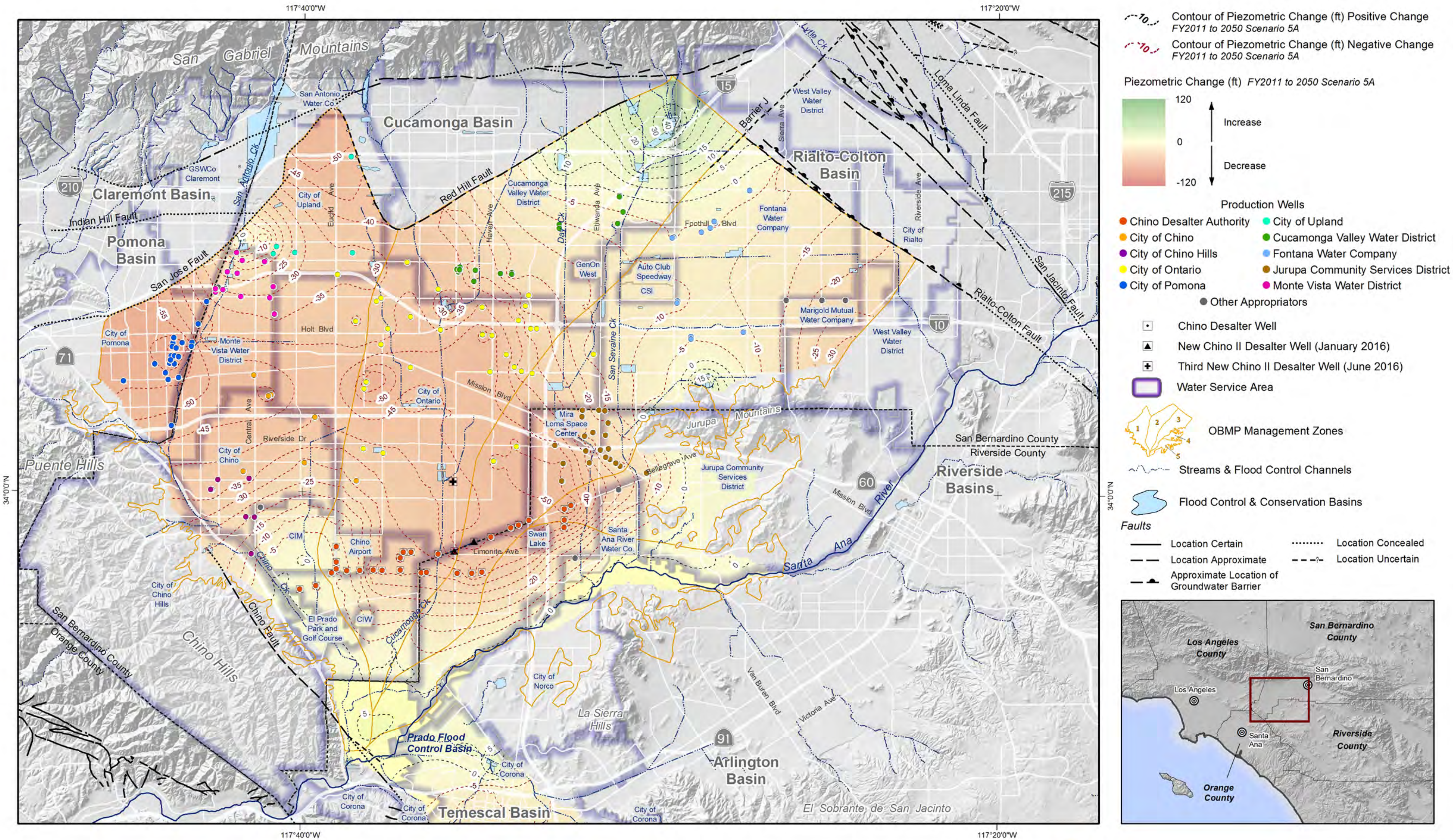

Produced by:

WEI
WILDERMUTH ENVIRONMENTAL, INC.

Author: LBB
Date: 20130813
File: Figure 7-12_change_11-20.mxd

0 1 2 3 4 5 Miles
0 2 4 6 8 KM

2013 Chino Basin Groundwater Model Update and Analysis of Safe Yield

Projected Groundwater Elevation Change -- Layer 1
Scenario 5A - 2011 to 2050

Figure 7-5d

Figure 7-6 Projected Aggregate Water in Storage Accounts and Change in Basin Storage for Scenario 5A

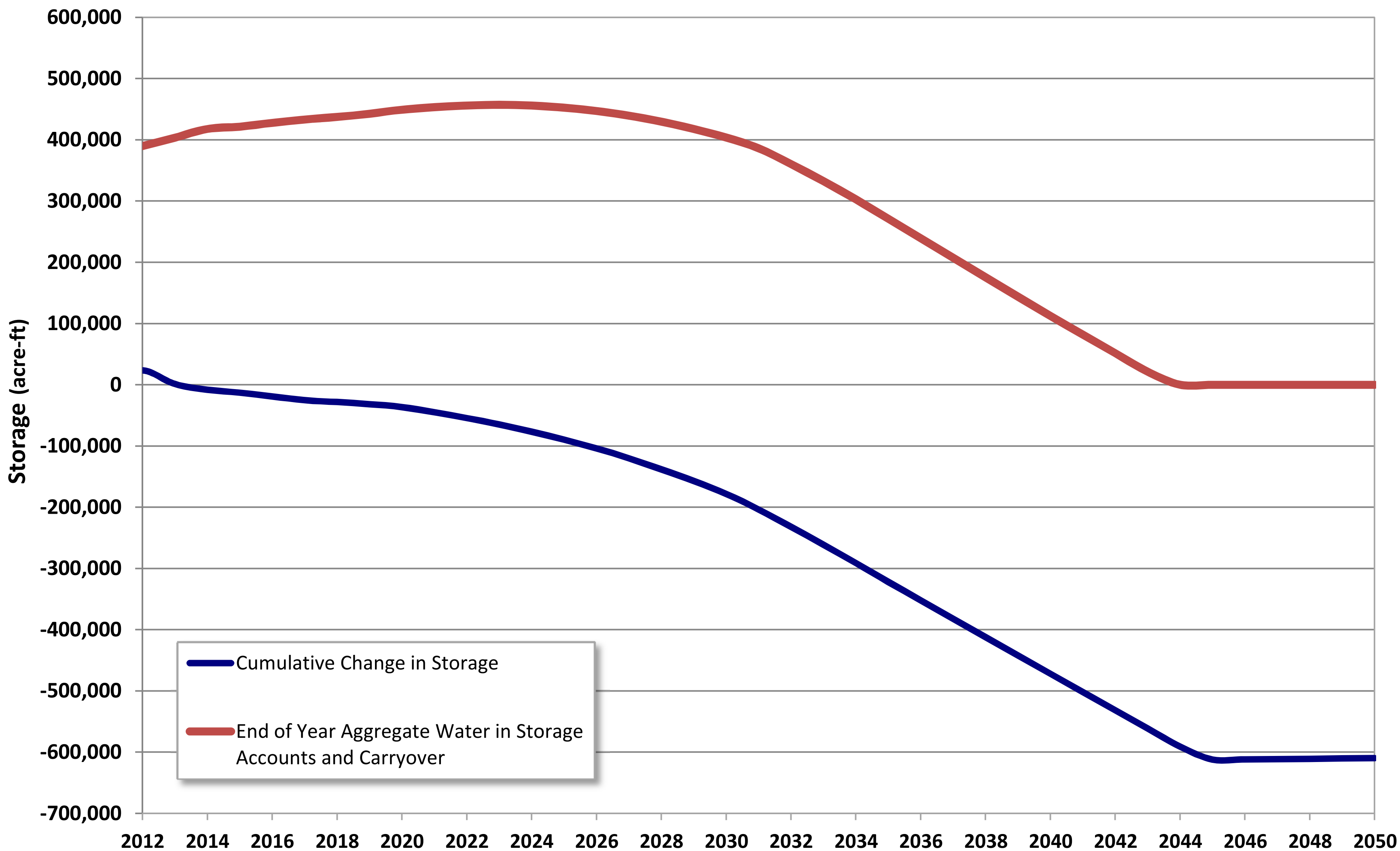

20150930 Final Fig 7-6 Storage change.xlsx -- Figure 7-6
Created 07/23/2015
Printed 10/2/2015

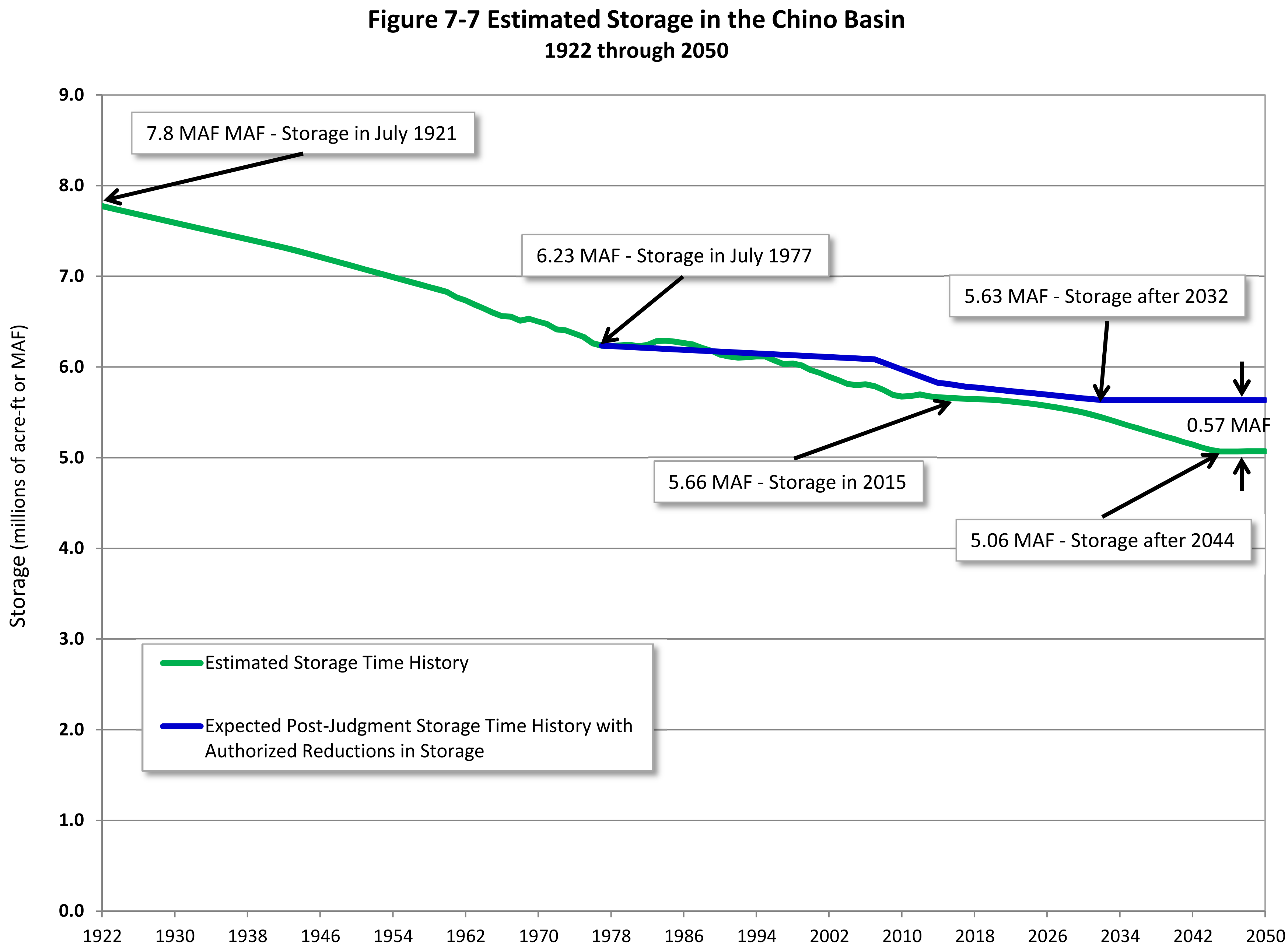

20151001 Final Fig 7-7 Storage Time History.xlsx -- Figure 7- 7
Created 09/10/2014
Printed 10/2/2015

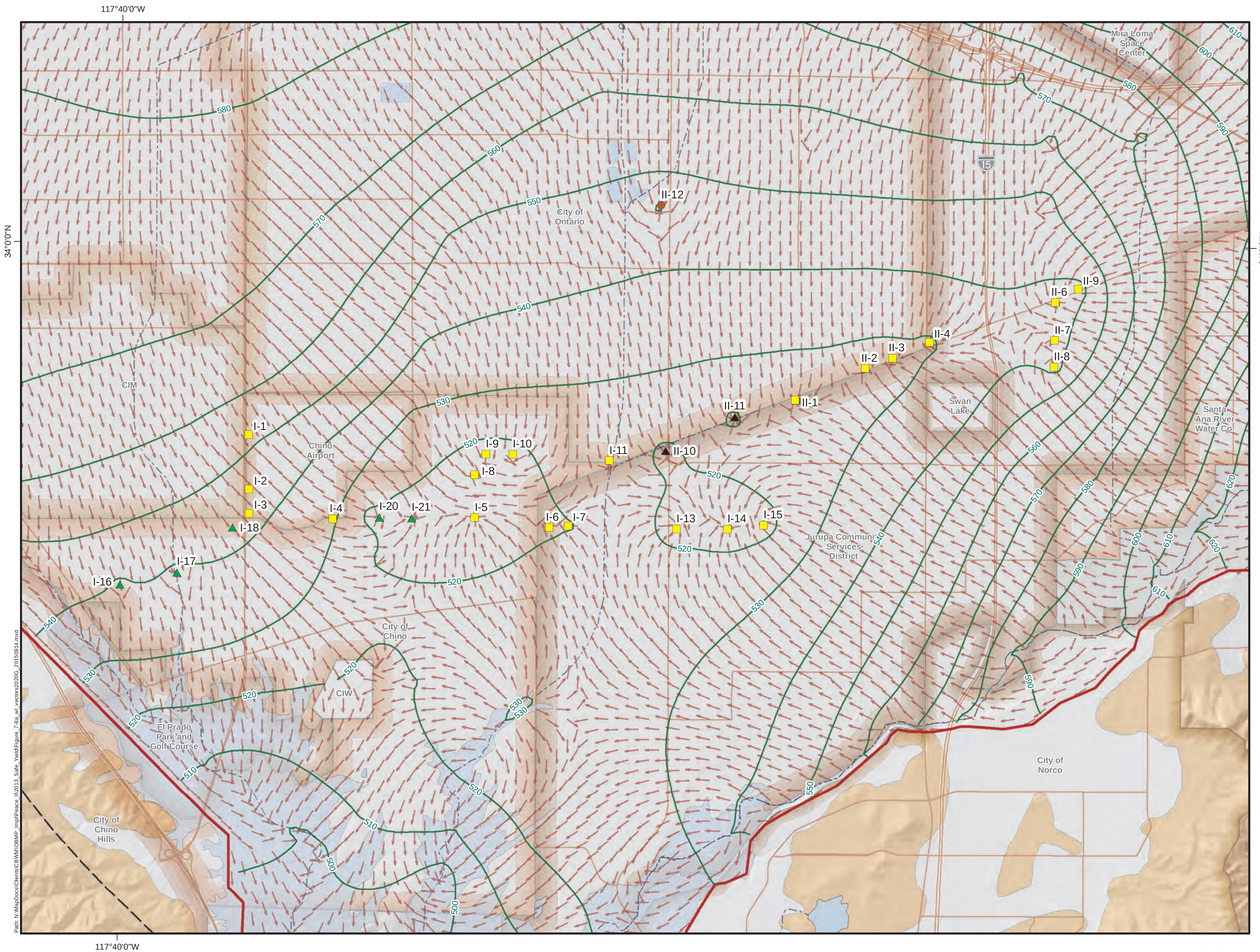

2020 Groundwater Flow Vectors
Model Layer 1 - Scenario 5G

2020 Groundwater Elevation Contours (Secnario 5G)
(feet above mean sea-level)

Water Service Area Boundaries

Existing Chino Desalter Wells

New Chino Creek Well Field Wells

Future Chino II Desalter Wells (January 2016)

Location of Third
New Chino II Desalter Well (June 2016)

Other Features

Groundwater Flow Model Boundary

Flood Control and Conservation Basins

Path: N:\MapDocs\Clients\CBWM\OBMP_Imp\Peace_II\2013_Safe_Yield\Figure_7-8a_wl_vectors2020G_20150914.mxd

117°40'0"W

Produced by:

WEI
Wildermuth Environmental, Inc.

Author: LBB
Date: 10/1/2015

0 1 2 Miles
0 0.5 1 1.5 Kilometers

2013 Chino Basin Groundwater Model Update
and Analysis of Safe Yield

State of Hydraulic Control in 2020
Scenario 5G

Figure 7-8a

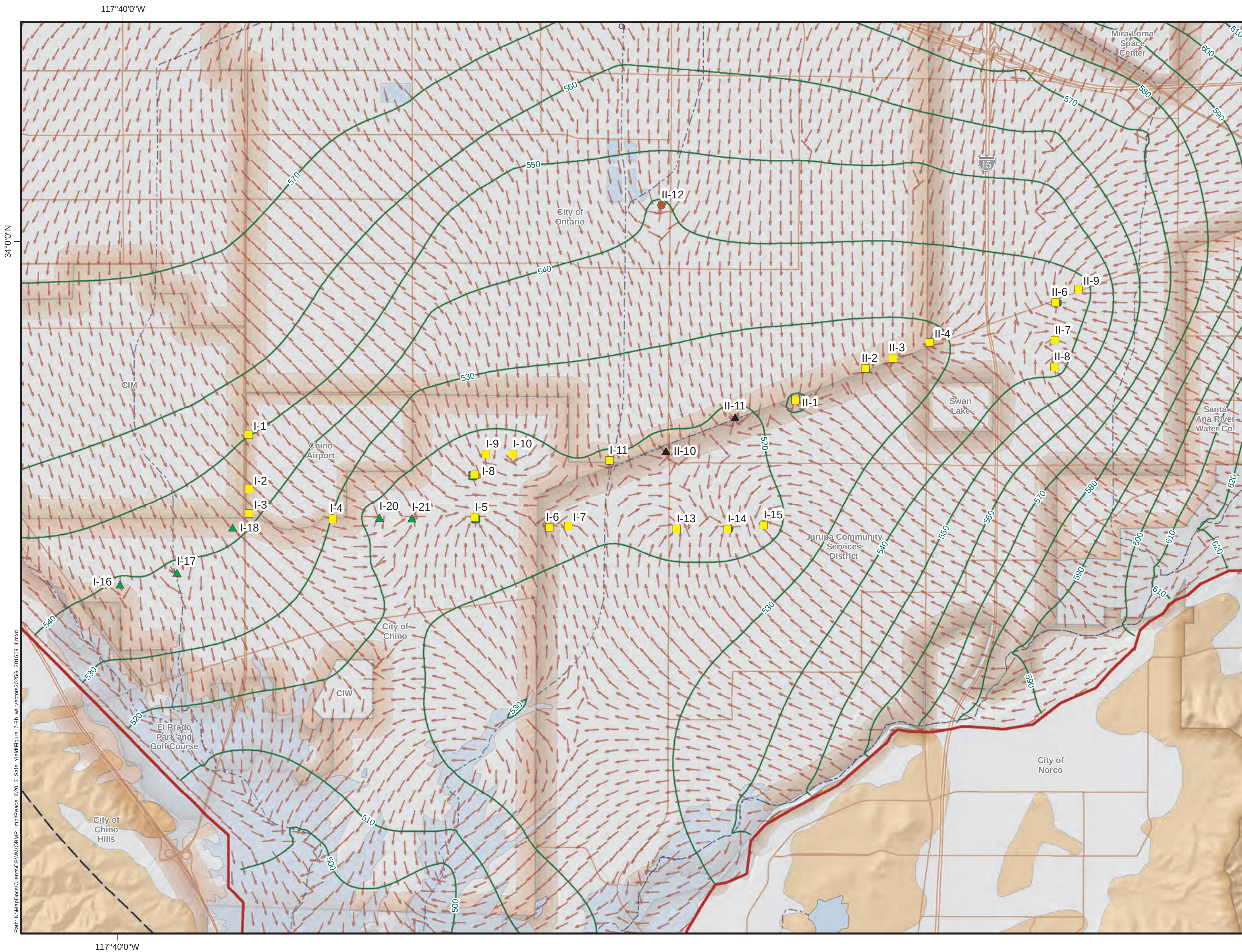

2025 Groundwater Flow Vectors
Model Layer 1 - Scenario 5G

2025 Groundwater Elevation Contours (Secnario 5G)
(feet above mean sea-level)

Water Service Area Boundaries

Existing Chino Desalter Wells

New Chino Creek Well Field Wells

Future Chino II Desalter Wells (January 2016)

Location of Third
New Chino II Desalter Well (June 2016)

Other Features

Groundwater Flow Model Boundary

Flood Control and Conservation Basins

Path: N:\MapDocs\Clients\CBWM\OBMP_Imp\Peace_II\2013_Safe_Yield\Figure_7-8b_wl_vectors2025G_20150914.mxd

Produced by:

WEI
Wildermuth Environmental, Inc.

Author: LBB
Date: 10/1/2015

0 1 2 Miles
0 0.5 1 1.5 Kilometers

2013 Chino Basin Groundwater Model Update
and Analysis of Safe Yield

State of Hydraulic Control in 2025
Scenario 5G

Figure 7-8b

Figure 7-9 Relationship of Discharge through the CCWF from the Chino North Management Zone to the Prado Basin Management Zone to the Aggregate Volume of Stored Water and Carryover

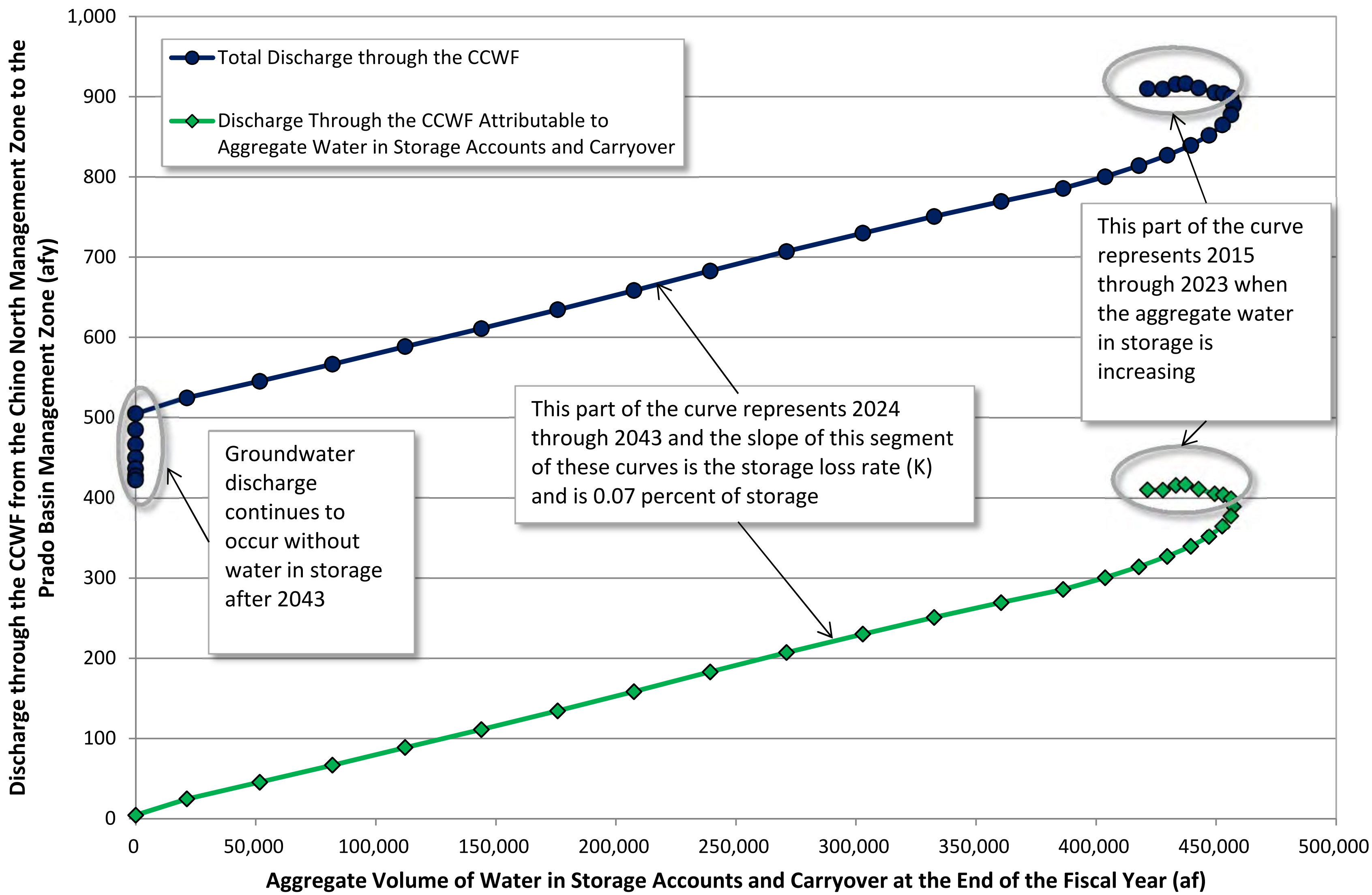

20150930 Final Tabs 7-8_7-9 and Figure 7-9.xlsx -- Figure 7-9
Created 07/27/2015
Printed 10/1/2015

Section 8 – References

Barlow, P.M. and A.W. Harbaugh, 2006, Groundwater, v. 44, no. 6, November-December 2006, pp. 771-774.

Bredehoeft, J.D., S.S. Papadopulis, and H.H. Cooper, 1982, Groundwater: The Water Budget Myth, In: Scientific Basis of Water Resources Management, Studies in Geophysics, National Academy Press, Washington D.C., pp 51-57.

Black and Veatch, 2001, Phase 2 (Chino Basin) Master Plan.

California Department of Water Resources (DWR). 1970. Meeting Water Demands in the Chino-Riverside Area, Appendix A: Water Supply. Bulletin No. 104-3, 108 p.

Carrera, J., and S. P. Neuman, 1986a, Estimation of Aquifer Parameters Under Transient and Steady State Conditions: 1. Maximum Likelihood Method Incorporating Prior Information, Water Resources Research, Vol. 22, No. 2, p 199-210.

Carrera, J., and S. P. Neuman, 1986b, Estimation of aquifer parameters under steady state and transient condition: 2. Uniqueness, stability, and solution algorithms, Water Resources Research, Vol. 22, No. 2, p 211 – 227.

Carrera, J., and S. P. Neuman, 1986c, Estimation of Aquifer Parameters Under Transient and Steady State Conditions: 3. Application to Synthetic and Field Data, Water Resources Research, Vol. 22, No. 2, p 228-242, 1986c.

Carroll, W. J. 1977. Superior Court of California for the County of San Bernardino, "Chino Basin Municipal Water District vs. City of Chino, et al.," Case No. 164327, Reporter's Transcripts of Proceedings, December, 1977.

Doherty, J. 1994, PEST, Watermark Computing, Corinda, Australia, 122p.

Driscoll, F.G., 1986, Groundwater and Wells, Second Edition, Johnson Filtration Systems, Inc.

Eckis, R. 1934. Geology and Ground Water Storage Capacity of Valley Fill, South Coastal Basin Investigation: California Department of Public Works, Division of Water Resources Bulletin No. 45, 273 p.

Finsterle, S., 1999, iTOUGH2 User's Guide, Report LBNL-40040, Lawrence Berkeley National Laboratory, Berkeley, California.

Finsterle, S., and J. Najita, 1998, Robust estimation of hydrogeologic model parameters, Water Resources Research, 34(11), 2939-2947.

Freeze A. and J Cherry, 1979, Groundwater, Prentice-Hall, Inc., Englewood Cliffs, New Jersey.

Harbaugh, A.W., Banta, E.R., Hill, M.C., and McDonald, M.G., 2000, MODFLOW-2000, The U.S. Geological Survey Modular Ground-Water Model—User guide to modularization concepts and the ground-water flow process: U.S. Geological Survey Open-File Report 00-92, 121 p.

Johnson, A. I., 1967, Specific yield--compilation of specific yields for various materials: U.S. Geological Survey Water Supply Paper 1662-D, 74 p.

Larsen, E.S., D.J. Gottfried, H.W. Jaffe, and C.L. Waring. 1958. Lead-alpha ages of the Mesozoic batholiths of western North America: USGS Bull. 1070-B, p. 35-62.

Legates, D. R., and G. J. McCabe. 1999. Evaluating the use of "goodness-of-fit" measures in hydrologic and hydroclimatic model validation. Water Resources Res. 35(1): 233-241.

Levenberg, K., 1944, A method for the solution of certain non-linear problems in least squares, Quarterly Journal of Applied Mathematics, 2, 164–168.

Mark J. Wildermuth, Water Resource Engineers, 1995, Annual Recharge Estimates at the Chino Basin, Water Conservation District Spreading Basins.

Marquardt, D.W., 1963, An Algorithm for Least-Squares Estimation of Nonlinear Parameter, Journal of the Society for Industrial and Applied Mathematics, Vol. 11, No. 2, pp. 431-441.

McDonald, M.G., and Harbaugh, A.W., 1988, A modular three-dimensional finite-difference ground-water flow model: U.S. Geological Survey Techniques of Water-Resources Investigations, book 6, chap. A1, 586 p.

Moriasi, D. N., Arnold, J. G., Van Liew, M. W., Binger, r. l., Harmel, R. D., Veith, T. L. 2007. Model Evaluation Guidelines for Systematic Quantification of Accuracy in Watershed Simulations. Vol. 50(3): 885−900 2007 American Society of Agricultural and Biological Engineers ISSN 0001−2351

Morton, D. M., 2004, Preliminary Digital Geological Map of the 30' X 60' Santa Ana Quadrangle, southern California, version 2.0. USGS Open File Report 99-172, Version 2.0 – 2004, 46 p.

Nash, J. E., and J. V. Sutcliffe. 1970. River flow forecasting through conceptual models: Part 1. A discussion of principles. J. Hydrology 10(3): 282-290. Parker, R., J. G. Arnold,

Neuman, S.P., 1973, Saturated-unsaturated seepage by finite elements. ASCE J. Hydraulics Division, 2233-2251.

Prudic, D.E., 1989, Documentation of a computer program to simulate stream-aquifer relations using a modular, finite-difference groundwater flow model: USGS OFR 88-729, 144p.

Schlesinger, S. 1979 el al. Terminology for model credibility. Simulation 32 (3): 103-104.

Sevat, E., and A. Dezetter. 1991. Selection of calibration objective functions in the context of rainfall-runoff modeling in a Sudanese savannah area. Hydrological Sci. J. 36(4): 307-330.

Simunek, J., M. Sejna, and M. Th. van Genuchten, The HYDRUS-2D software package for simulating two-dimensional movement of water, heat, and multiple solutes in variably saturated media. Version 2.0, IGWMC - TPS - 53, International Ground Water Modeling Center, Colorado School of Mines, Golden, Colorado, 251pp., 1999.

Sun, N.Z., and W.W.G Yeh, 1990, Coupled Inverse Problems in Groundwater Modeling: 1. Sensitivity Analysis and Parameter Identification, Water Resources Research, Vol. 26, No. 10, p 2507-2525.

United States Department of Agriculture, 1986, Urban Hydrology for Small Watersheds, Technical Release 55, 210-VI-TR-55, Second Edition.

Wildermuth Environmental, Inc., 1998, Phase 1 Recharge Master Plan (Chino Basin). Prepared for the

Chino Basin Watermaster and the Chino Basin Water Conservation District.

Wildermuth Environmental, Inc., 2002, TIN/TDS Study, Phase 2B of the Santa Ana Watershed, Wasteload Allocation Investigation. Prepared for the N/TDS Task Force.

Wildermuth Environmental, Inc., 2003, Optimum Basin Management Program, Chino Basin Dry-Year Yield Program, Preliminary Modeling Report, Chino Basin Watermaster.

Wildermuth Environmental, Inc., 2006a. Draft Report, Analysis of Future Replenishment and Desalter Plans Pursuant to the Peace Agreement and Peace II Process, April 2006; prepared for the Chino Basin Watermaster.

Wildermuth Environmental, Inc., 2006b. Draft Report, Addendum to the Draft April 2006 Report, Analysis of Future Replenishment and Desalter Plans Pursuant to the Peace Agreement and Peace II Process, December 2006; prepared for the Chino Basin Watermaster.

Wildermuth Environmental, Inc., 2007. 2007 CBWM Groundwater Model Documentation and Evaluation of the Peace II Project Description.

Wildermuth Environmental, Inc., 2010. 2010 Recharge Master Plan Update. Two volumes. Prepared for the Chino Basin Watermaster.

Wildermuth Environmental, Inc. 2013. 2013 Amendment to the 2010 Recharge Master Plan Update. Prepared for the Chino Basin Watermaster.

Yeh W.W.G., 1986, Review of parameter identification procedures in groundwater hydrology -- The inverse problem, Water Resources Research, v. 22, no. 2, pp. 95-108.

Appendix A

Hydrostratigraphic Cross Sections

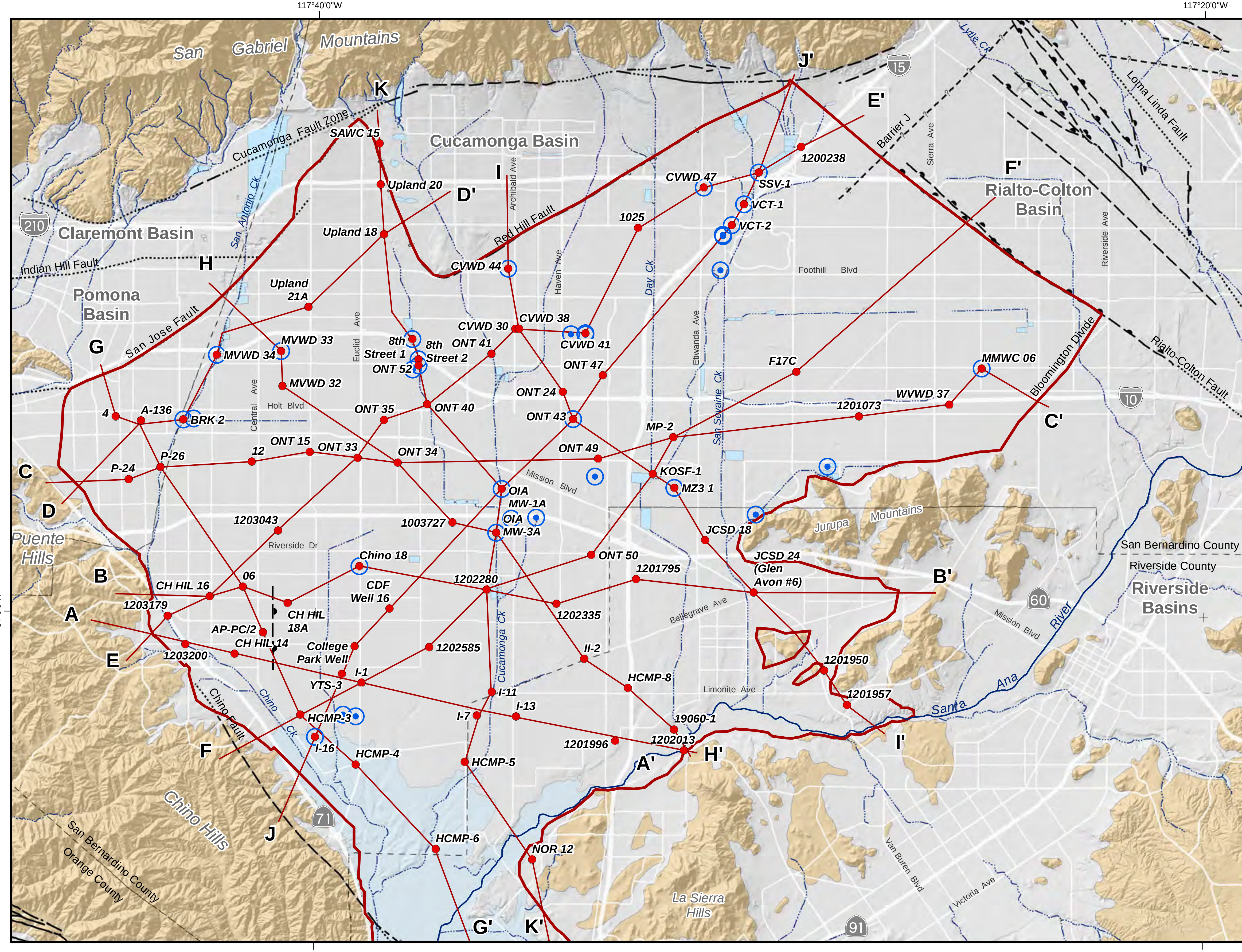

Line of Geologic Cross-Section

Well Used in Cross-Section

Well drilled since 2006

Geology

Water-Bearing Sediments

Quaternary Alluvium

Consolidated Bedrock

Undifferentiated Pre-Tertiary to Early Pleistocene Igneous, Metamorphic, and Sedimentary Rocks

Faults

Location Certain

Location Approximate

Approximate Location of Groundwater Barrier

Location Concealed

Location Uncertain

0 1 2 3 4 5 Miles

0 2 4 6 8 KM

Produced by:

WEI

Wildermuth Environmental, Inc.

Author: MJC

Document Name: Figure_A-1_cross_section_loc

2013 Chino Basin Groundwater Model Update and Analysis of Safe Yield

Map View of Hydrostratigraphic Cross Sections

Figure A-1

2011 CBWM Groundwater Model Recalibration

Cross-Section A-A'

Figure A-2

Prepared by:

WEI
WILDERMUTH ENVIRONMENTAL, INC.

Vertical Scale: 1" = 80'
Horizontal Scale: 1" = 725'
Vertical Exaggeration = 9:1

Sand with Clay
Granite
Gravel with Clay
Clay with Silt
Sand with Silt
Sand
Topsoil
Sedimentary Bedrock
Silt with Clay
Clay with Gravel, Sand and Silt
Sand with Gravel
Silt
Clay with Gravel
Clay with Sand and Silt
Gravel with Sand, Silt and Clay
Clay with Sand
Gravel
Clay with Gravel and Sand
Sand with Gravel, Silt and clay
Gravel with Sand
Clay
Sand with Gravel and Clay
Sand with Silt and Clay

Groundwater Conceptual Model Layer Boundaries
Water Level (year)
Well Screen Interval
Resistivity Short Normal
Resistivity Long Normal

2011 CBWM Groundwater Model Recalibration

Cross-Section B-B'

Figure A-3

Report: FENCE - ELOGS/PERFS/ZONES - D _ILL; File: 2011_CBWM_MODEL RECALIBRATION.GPJ; 10/11/2011

Prepared by:

WEI
Wildermuth Environmental, Inc.

Vertical Scale: 1" = 80'
Horizontal Scale: 1" = 725'
Vertical Exaggeration = 9:1

Sand with Gravel
Clay with Sand
Gravel with Clay
Gravel with Silt
Clay with Sand and Silt
Gravel with Sand
Granite
Clay with Gravel
Conglomerate
Sand with Gravel and Silt
Clay
Sand
Silt with Gravel, Sand and Clay
Silt
Silt with Gravel and Sand
Clay with Gravel and Sand
Gravel
Gravel with Sand and Clay
Sand with Silt
Silt with Clay
Sand with Clay
Sand with Gravel and Clay
Clay with Silt
Topsoil
Silt with Sand

Groundwater Conceptual Model Layer Boundaries
Water Level (year)
Well Screen Interval
Resistivity Short Normal
Resistivity Long Normal

2011 CBWM Groundwater Model Recalibration

Cross-Section C-C'

Figure A-4

Report: FENCE - ELOGSPERFSZONES - D_ALL File: 2011_CBWM_MODEL RECALIBRATION.GPJ 10/7/2011

Prepared by:

WEI
Wildermuth Environmental, Inc.

Vertical Scale: 1" = 80'
Horizontal Scale: 1" = 725'
Vertical Exaggeration = 9:1

Clay
Clay with Sand
Gravel with Sand
Clay with Sand and Silt
Gravel
Silt with Clay
Sand with Gravel
Clay with Gravel and Sand
Sand with Gravel, Silt and clay
Silt
Gravel with Clay
Sand with Gravel and Clay
Sand with Gravel and Silt
Clay with Gravel and Silt
Clay with Silt
Sand
Sand with Silt
Silt with Sand
Sand with Silt and Clay
Conglomerate
Gravel with Sand and Clay
Sand with Clay
Silt with Sand and Clay
Asphalt

Groundwater Conceptual Model Layer Boundaries
Water Level (year)
Well Screen Interval
Resistivity Short Normal
Resistivity Long Normal

2011 CBWM Groundwater Model Recalibration

Cross-Section D-D'

Figure A-5

Report: FENCE - ELOGS/PERFS/ZONES - D _ILL; File: 2011_CBWM_MODEL RECALIBRATION.GPJ; 10/6/2011

Prepared by:

WEI
WILDERMUTH ENVIRONMENTAL, INC.

Vertical Scale: 1" = 80'
Horizontal Scale: 1" = 725'
Vertical Exaggeration = 9:1

Gravel	Gravel with Clay	Sand with Gravel	Gravel with Sand	Clay with Gravel and Sand
Clay with Sand	Clay with Gravel	Clay	Sand with Gravel and Clay	Gravel with Sand and Clay
Sand with Clay	Sand	Silt with Gravel, Sand and Clay	Topsoil	
Gravel with Silt	Sand with Silt	Shale	Sedimentary Bedrock	Sand with Gravel and Silt
Silt	Gravel with Sand and Silt	Silt with Sand	Sand with Silt and Clay	Gravel with Silt and Clay

Groundwater Conceptual Model Layer Boundaries
Water Level (year)
Well Screen Interval
Resistivity Short Normal
Resistivity Long Normal

2011 CBWM Groundwater Model Recalibration

Cross-Section E-E'

Figure A-6

Prepared by:

WEI
WILDERMUTH ENVIRONMENTAL, INC.

Vertical Scale: 1" = 80'
Horizontal Scale: 1" = 725'
Vertical Exaggeration = 9:1

Sand with Gravel
Sand
Sand with Gravel and Clay
Sand with Silt
Gravel with Sand and Clay
Clay with Sand
Sand with Clay
Clay with Gravel and Sand
Sand with Silt and Clay
Aggregate base
Clay with Gravel
Silt
Granite
Silt with Sand
Gravel
Clay
Topsoil
Clay with Sand and Silt
Gravel with Clay
Gravel with Sand
Clay with Silt
Silt with Gravel and Sand

Groundwater Conceptual Model Layer Boundaries
Water Level (year)
Well Screen Interval
Resistivity Short Normal
Resistivity Long Normal

2011 CBWM Groundwater Model Recalibration

Cross-Section F-F'

Figure A-7

Report: FENCE - ELOGS/PERFS/ZONES - D _ILL; File: 2011_CBWM_MODEL RECALIBRATION.GPJ; 10/6/2011

Prepared by:

WEI
WILDERMUTH ENVIRONMENTAL, INC.

Vertical Scale: 1" = 80'
Horizontal Scale: 1" = 725'
Vertical Exaggeration = 9:1

Clay
Sand with Gravel
Sand with Clay
Gravel with Sand
Gravel
Silt with Clay
Clay with Gravel
Fill (made ground)
Silt with Sand
Silt
Gravel with Clay
Topsoil
Sand with Gravel and Clay
Sand with Silt and Clay
Clay with Silt
Clay with Gravel and Sand
Sedimentary Bedrock
Sand with Silt
Clay with Sand and Silt
Conglomerate
Clay with Sand
Sand
Aggregate base
Sand with Gravel, Silt and clay

Groundwater Conceptual Model Layer Boundaries
Water Level (year)
Well Screen Interval
Resistivity Short Normal
Resistivity Long Normal

2011 CBWM Groundwater Model Recalibration

Cross-Section G-G'

Figure A-8

Report: FENCE - ELOGS/PERFS/ZONES - D _ILL; File: 2011_CBWM_MODEL RECALIBRATION.GPJ; 10/11/2011

2011 CBWM Groundwater Model Recalibration

Cross-Section H-H'

Figure A-9

Prepared by:

WEI
Wildermuth Environmental, Inc.

Vertical Scale: 1" = 80'
Horizontal Scale: 1" = 725'
Vertical Exaggeration = 9:1

Sand with Gravel
Sand with Gravel and Clay
Silt with Clay
Sand with Silt
Silt with Sand
Gravel with Sand
Clay
Gravel
Granite
Clay with Silt
Sand
Clay with Gravel and Sand
Gravel with Sand and Clay
Silt
Sand with Gravel and Silt
Sand with Clay
Clay with Gravel
Gravel with Sand, Silt and Clay
Decomposed Granite
Clay with Sand
Gravel with Sand and Silt
Gravel with Clay
Asphalt

Groundwater Conceptual Model Layer Boundaries
Water Level (year)
Well Screen Interval
Resistivity Short Normal
Resistivity Long Normal

2011 CBWM Groundwater Model Recalibration

Cross-Section I-I'

Figure A-10

Cross-Section J-J'

Figure A-11

Prepared by:

WEI — Wildermuth Environmental, Inc.

Vertical Scale: 1" = 80'

Horizontal Scale: 1" = 725'

Vertical Exaggeration = 9:1

Sand; Gravel with Sand and Clay; Clay with Gravel; Clay with Gravel, Sand and Silt; Sand with Silt; Gravel; Clay with Sand; Clay with Gravel and Sand; Clay with Silt; Silt with Clay; Sand with Gravel; Sand with Gravel and Clay; Sand with Silt and Clay; Silt with Sand and Clay; Gravel with Sand and Silt; Sand with Clay; Topsoil; Gravel with Sand; Clay with Sand and Silt; Sand with Gravel and Silt; Granite; Clay; Gravel with Sand, Silt and Clay; Silt with Sand; Silt with Gravel and Sand

Groundwater Conceptual Model Layer Boundaries; Water Level (year); Well Screen Interval; Resistivity Short Normal; Resistivity Long Normal

2011 CBWM Groundwater Model Recalibration

Cross-Section K-K'

Figure A-12

B-1 Recharge from Onsite Wastewater Disposal Systems

The recharge from on-site waste disposal systems (OSWDS) are a component of the deep infiltration of precipitation and applied water that is shown in the water budget tables in Sections 3 and 7 of this report.

In 2011, a data request was made to the Appropriative Pool members, cities and counties in Chino Basin for shapefiles showing the locations of parcels with OSWDS. Shapefiles of known parcels with OSWDS were obtained from Cucamonga Valley Water District, City of Upland, City of Ontario, and Riverside County. The other agencies responded to the request indicating that they did not have a shapefile of parcels with OSWDS, however, some agencies were able to describe areas within their sphere of influence that were not connected to the sewer system. In 2011, approximately 17,000 parcels with septic systems were located within the Chino groundwater model domain.

The unit recharge from septic systems was calculated on an equivalent dwelling unit (EDU) basis. The table below shows the historical returns used in calculating the returns:

Time Period	GPD/EDU	Acre-ft/yr
Pre-1975[1]	335	0.38
1975-2009[2]	270	0.30
2009-2013[3]	206	0.23

[1]CONSOL, 2010, Water Use in the California Residential Home.

[2]IEUA, 1995 Urban Water Management Plan

[3]IEUA, (email correspondence with Lisa Perales from IEUA).

The decrease in discharges is attributed to water conservation efforts in indoor appliances such as showerheads, toilets, dishwashers, clothes washers, etc. In 2011, approximately 4,000 acre-ft of water was recharged to groundwater system as a result of on-site wastewater disposal systems.

The location of historical septic systems has not been precisely documented and only a few of the agencies had shapefiles of parcels on septic systems. To account for the location of historical septic systems the following assumption was made: a parcel that is currently on a septic system in 2011 remained on a septic system as long as the underlying land use remained an urban land use type unless additional information was made available (e.g. parcels in the Eastvale area were sewered in 1998). During the calibration period (1960-2011) the DWR and other agencies conducted land use surveys for the following years: 2005, 2000, 1993, 1990, 1984, 1975, 1963 and 1957. The table below shows the estimated number of parcels on septic by land use year:

Annual Recharge from On-Site Waste Disposal Systems (OSWDS)

Fiscal Year	Number of	Recharge from OSWDS (acre-ft/yr)
1957	1,904	715
1963	5,672	2,129
1975	7,062	2,650
1984	10,546	3,190
1990	13,724	4,156
1993	13,923	4,211
2000	15,021	4,543
2005	15,558	4,706
2011	17,216	3,973

The OSWDS returns were linearly interpreted between land use years. All of the OSWDS discharge was assumed to recharge. Figure B-1 illustrates the OSWDS recharge time history.

B-2 Recharge from Pipe Leaks in Municipal Water Systems

The recharge from pipe leaks in municipal water systems are a component of the deep infiltration of precipitation and applied water that is shown in the water budget tables in Sections 3 and 7 of this report. The total water production by agencies that overlie the Chino Basin was compiled from Chino Basin Watermaster Annual Reports for the time period of 1978-2011. For the portion of the calibration period from 1960-1978, the total water production was estimated based on a correlation between urban land use data and total water consumption. The earliest year that contained both land use and water use data contained in the CBWM Annual reports was 1984. The ratio between urban land use and water consumption within each water service area was calculated for 1984 and applied to 1975, 1963, and 1957 and linearly interpolated between years. Some of the water service areas are located outside of the Chino Basin Groundwater Model domain. The total water consumption was adjusted based on the percentage of the water service area that was located inside the groundwater model domain. The water loss attributed to leaky pipes that manifest itself as recharge was assumed to be 2 percent of the total water production and is shown in Figure B-2. Figure B-2 illustrates the OSWDS recharge time history.

B-3 Detailed Agricultural Land Use Analysis to Improve the Crop Coefficients in the R4 Model

The water requirements for agricultural crops and turf grasses have been established in laboratory and field studies by measuring plant water loss. The total amount of water lost during a specific period of time gives an estimate of the amount that needs to be resupplied by irrigation. This evapotranspiration loss is estimated as follows:

$$ETc = Kc * ETo$$

A crop coefficient (Kc) is used with ETo to estimate the evapotranspiration rate of a specific crop. The crop coefficient is a dimensionless number. Crop coefficients vary by many factors including crop type and the stage of growth. Coefficients for annual crops vary widely through a season: annual crops have small coefficients in their early stages and large coefficients when they are at full cover. Crop coefficient data are available from CIMIS. In a previous study conducted by the California Department of Water Resources (DWR), evapotranspiration data was used to estimate monthly crop coefficients for each land use type.

In an effort to improve the historical crop coefficients for the agricultural land use types (Land Use Type 2 in WEI's model), an area that experienced historical changes in agricultural land uses was digitized using the higher resolution DWR land use codes as shown in Table B-1. A two square mile area in Ontario, bounded to the north by Chino Ave, to the east by Grove Ave, to the south Eucalyptus Ave, and to the west by Euclid Ave, was chosen to be digitized for the years that land use data exists (1957, 1963, 1975, and 1984) and is shown in Figure B-3

The crop coefficients for the agricultural land use types located in the 2 square mile area were compiled from Bulletin No. 113-3, Vegetative Water Use in California, 1974 and are shown in Table B-2. The bottom section of Table B-2 shows the monthly area weighted crop coefficients for land use survey years 1957, 1963, 1975, and 1984 that was applied to root zone module for land use type 2 "Irrigated Field Crops, Pasture, Fruit and Nuts."

B-4 Riparian Vegetation Evapotranspiration

The objective of this work was to improve the riparian vegetation consumptive use estimates that were used in the 2007 Watermaster model. Specifically to delineate the extent and density of the riparian vegetation along the Santa Ana River within the Chino Basin Model Boundary for various years during the model calibration period of fiscal 1961 through 2011 to assist in the estimation of the amount of water consumed by the riparian vegetation annually

The following steps were done to determine the location and spatial density of riparian vegetation in the model domain:

1. Assembled historical aerial photos of the Santa Ana River that covered the entire, or most of the model domain area. Aerial photo sets were obtained for the years 1960, 1977, 1994, and 2006.
2. Geo-referenced aerial photos in Arc Map
3. In ArcMap, imported land use shapefiles that were assembled or digitized for the Chino Basin modeling work and displayed the land use types associated with the riparian vegetation.
4. For each aerial photo year (1960, 1977, 1994, and 2006), the land use shapefile closest to the year of the aerial photo was used as an initial estimate of the extent of the riparian vegetation along the River.
5. Modified the land use shapefiles to match the extent of the riparian vegetation shown in the aerial photos to created riparian vegetation shapefiles for the years 1960, 1977, 1994, and 2006.

6. In Arc Map, the aerial photos and shapefiles of the riparian vegetation for 1960, 1977, 1994, and 2006 were overlain by a 1,320 by 1,320 meter grid, and each grid was assigned a number.
7. For each year, the area of riparian vegetation within each grid cell was calculated in ArcMap.
8. For each year, for each grid cell, the density of the riparian vegetation was evaluated using the aerial photo, and an estimate of the density of the riparian vegetation area for that grid cell was recorded as a percentage.
9. The density estimate analysis described in the bullet above was performed by three different people.
10. The three density estimates were averaged for each year, for each grid cell, to get a final estimate of density for each grid cell.
11. For each year, an area-weighted density was calculated for the entire extent of riparian vegetation. [i.e. $(A_1xD_1 + A_2xD_2 + _{...} A_xxD_x)$ / Total A]. This density was used to determine the ET rate of the riparian vegetation.
12. As determined in the USGS Open File Report 96-4241, the annual consumptive use of groundwater and surface water by riparian vegetation differs based on the aerial density of the vegetation. The density of the riparian vegetation determined for each year (1960, 1977, 1994, and 2006.) was used to determine the ET rate of the riparian vegetation to be used in the model, based on the USGS Open File Report 96-4241 findings.
13. The baseline ET rates used for riparian vegetation in this model are from the evapotranspiration analysis on the Prado Basin prepared by Merkel (2006), for the habitat of a southern Cottonwood Riparian Forest, and southern Willow Scrub, and are in ft/day by calendar year quarter.
14. Below are the ET rates used in the model by year and quarter:

Riparian Vegetation ET ft/day

	Q1	Q2	Q3	Q4
1957	0.002445	0.008855	0.009873	0.002065
1974	0.005640	0.020430	0.022779	0.004764
1994	0.005640	0.020430	0.022779	0.004764
2006	0.005640	0.020430	0.022779	0.004764

Figure B-4 summarizes the spatial distribution riparian and magnitude of its consumptive use.

B-5 Analysis of Historical Diary Related Groundwater Production and Wash Water Disposal

Question: What is the annual groundwater production by dairies in the Chino Basin from 1957-2011?

List of Tables:

- Table B-3: Annual Estimated Number of Dairy Cows in the Chino Basin 1957-2011
- Table B-4: Dairy Cow Water Consumption Requirements
- Table B-5: Summary of Wash Water Use by 18 Dairies Surveyed for the 2011 Chino Basin Model Recalibration
- Table B-6: Estimated Groundwater Production by Dairies in the Chino Basin – Fiscal Year 1957 to 2011

Since the early 2000s, the Chino Basin Watermaster has collected quarterly flow-meter meter reads from privately owned production wells to accurately calculate groundwater production volumes from all known agricultural and dairy wells in the Chino Basin. Prior to this period, only estimates of quarterly or annual groundwater production are available for this user group. To refine the production estimates for the Chino Basin dairies, an analysis of current and historical dairy operations was performed.

The two primary uses of water at a dairy facility are (1) drinking water for the cows and (2) wash water for milking operations, which includes washing the milking cows and washing the milk barn. Therefore, the total annual water use by dairies in the Chino Basin can be estimated with the following data:

- Total number and type of cows in the Chino Basin
- Drinking water consumption requirements, by cow type (gallons/cow)
- Dairy wash water requirements (gallons/cow/day)

Thus, total annual groundwater production by dairies ($\mathbf{P_D}$) can be estimated as follows:

$$\mathbf{P_D} = (\mathbf{C_M} \text{ x } \mathbf{WC_M}) + (\mathbf{C_O} \text{ x } \mathbf{WC_O}) + (\mathbf{WC_M} \text{ x } \mathbf{WW_M})$$

Where,

$\mathbf{C_M}$ = number of milking cows in the Chino Basin
$\mathbf{C_O}$ = number of other dairy cows in the Chino Basin
$\mathbf{WC_M}$ = water consumption requirement of milking cows
$\mathbf{WC_O}$ = water consumption requirement of other dairy cows
$\mathbf{WW_M}$ = average wash water use in the Chino Basin (gallons/cow/day)

Dairy Cows in the Chino Basin

The Santa Ana Regional Water Quality Control Board (Regional Board) and the US Agricultural Census have records of estimated historical cow counts in the Chino Basin. Detailed records of the total number of cows, by type are available for 1997-2010. These data are compiled by the Regional Board as part of its NPDES permitting program. Data prior to 1997 is sparse. Anecdotal information was also obtained from local dairy farmers still living in the Chino Basin. Based on these data sources, the following assumptions were developed to estimate the annual number of cows in the Chino Basin from 1957 to 1996:

- In the early years of dairy development in the Chino Basin, the operations were smaller and there were fewer cows per unit area of dairy.
  - In 1957, the composition of dairy cows is 19 milking cows per acre of dairy and 6 other cows per acre of dairy
  - From 1957-1969 the number of milking cows per acre of dairy increases linearly from 19 to 23
  - From 1957-1969 the number of other cows per acre of dairy increases linearly from 6 to 19
- After the 1970's, almost all dairy operations were concentrated animal feeding operations (CAFOs), in which there were far more dairy cows per unit area of dairy.
  - From 1970-1996 there are 23 milking cows per acre of dairy and 19 other cows per acre of dairy land use
- Based on detailed cow counts from 1997-2010, the composition of other cow types on a dairy is:
  - Calves: 46%
  - Heifers: 36%
  - Dry Cows: 17%

The total acres of dairy land use was calculated in GIS from land use data for 1957, 1963, 1975, 1984, 1990, 1993, 2001, 2005, and 2010. Annual estimates of dairy acreage were calculated by linear interpolation between years with land use data. Finally, annual estimates of dairy cows were then calculated based on the total acreage of dairy land use in each year and estimates for dairy herd composition. Table B-3 shows the total number of estimated dairy cows, by type, in the Chino Basin from 1957 to 2011. The number of dairy cows in the Chino Basin increased from an estimated 94,000 cows in 1957 to a peak of about 356,000 cows in 1984. The dairy cow population remained about the same from 1984 to about 2000 when the population began to rapidly decline. As of 2010, the dairy cow population was about 140,000 cows.

Dairy Cow Drinking Water Requirements

The drinking water requirements of a dairy can be estimated based on industry data. For milking cows, the water consumption requirement is dependent upon both milk production volume and air temperature. Table B-4 shows the water requirements used to calculate drinking water consumption for milk cows and other dairy cows.

Estimates of annual milk production in the Chino Basin were available for 1960-2010 from the US Department of Agriculture. Milk production in the Chino Basin increased from about 27 pounds/cow/day in 1960 to about 60 pounds/cow/day in 2010. Climate data from Oregon State University's PRISM Climate Group was used to develop quarterly temperature estimates for 1957-2011.

These data were used to estimate quarterly groundwater production for satisfying dairy cow drinking water requirements.

Dairy Wash Water Requirements

Given that annual groundwater production for many dairies is known with some certainty for the period since the early 2000's and that drinking water requirements of a dairy were estimated based on industry data, Watermaster's groundwater production data can be used to develop an estimate of typical wash water use at dairies in the Chino Basin. The wash water requirements on any given dairy (WW) can be estimated as follows:

$$\mathbf{WW = P_D - WC_M - WC_O}$$

Where,

WW = volume of wash water used by the dairy
$\mathbf{P_D}$ = annual groundwater production volume
$\mathbf{WC_M}$ = annual water consumption by milking cows
$\mathbf{WC_O}$ = annual water consumption of other cows on the dairy

Although the Watermaster began tracking production meter-reads in the early 2000's, not all operations were set up with groundwater production meters until about 2004. Thus, production records for fiscal year 2004-2011 were surveyed for this analysis.

Land use maps, aerial photographs, dairy cow count records, and groundwater production data were evaluated to select dairies for which wash water use could be estimated for the 2004-2011 period. The criteria for selecting dairies for inclusion in this analysis were:

- The ability to positively match wells to a specific dairy facility
- There are no gaps in the production data record from 2004-2011, and all production values must be based on meter reads
- There were no major changes to the dairy during the time period of interest. Major changes include a significant increase or decrease in the number of milking cows on the dairy or a significant change in the land use footprint of the dairy.

Based on these criteria, 18 dairy operations were selected for developing an estimate of average wash water use in the Chino Basin. The dairies ranged in size from about 375 milking cows to about 1,300 milking cows. Table B-5 is a summary of annual wash water use from 2004-2011, in gallons/cow/day. The average annual wash water use for the 2004-2011 period ranged from 65 gallons/cow/day to 138 gallons/cow/day. The average across all 18 dairies was 92 gallons/cow/day. To account for the range in size of the dairies surveyed, a cow-weighted wash water use was calculated. The cow-weighted average for the 18 dairies surveyed was 90 gallons/cow/day.

Estimated Dairy Groundwater Production

Quarterly groundwater production estimates were developed based on the total number and type of cows in the Chino Basin, industry standard data for drinking water consumption requirements, and estimated wash water use as described above. Table B-6 summarizes total annual groundwater production by dairies for 1957 through 2011. Total groundwater production increased from about 8,900 acre-ft/yr in 1957 to its peak of about 25,000 acre-ft/yr in 1984. Production remained close to 25,000 acre-ft/yr until about 2000. After 2000, production steadily declined to about 8,900 in 2010.

Analysis of Dairy Operations to Calculate the Deep Percolation of Dairy Wash Water Disposed at Ponds and Pastures in the Chino Basin for the 1957-2011 Calibration Period

Question: What is the annual return flow to the Chino Basin from the disposal of wash water used by dairies from 1957-2011?

- Use wash water estimate to calculate the amount of water that must be disposed of by dairies (90 gallons/cow/day)
- Perform land use analysis using GIS to estimate the amount of irrigated land that is watered with dairy wash water. In the early history (History A – the pre-Dutch era), wash water was used to irrigate pasture/crops both on and off of dairy properties. In History B, the Dutch era, all water was disposed of within the boundaries of the dairy properties.
    - History A 1957-1963 - All irrigated land use types within a designated buffer zone of a dairy property were irrigated with wash water. Remainder of wash water was "discharged" to disposal ponds.
    - History B 1975- 2011 –
        - Perform GIS analysis of to delineate the boundaries of dairy properties, and delineate the individual use areas within each property (feed lots, corrals and improved structures vs. disposal areas). For each property, calculate the ratio of disposal land area to total dairy property area of land used by dairies for disposal of dairy wash water to spread wash water for evaporation or percolation. 55 dairies were surveyed. On average, the disposal area makes up 40 percent of the total property area.
        - Based on the area of land use assigned to dairies (land use type 6, which represents the portion of the dairy covered by feed lots, corrals and improved structures), calculate the approximate amount of area used for the disposal of wash water. (Disposal Area = Type 6 Area/0.6 - Type 6 Area).

Appendix C1

Time-History Plots of Simulated and Measured Groundwater Elevations in the Wells Used in Model Calibration 1961 – 2011

Appendix C1
Time-History Plots of Simulated and Measured Groundwater Elevations in the Wells Used in Model Calibration 1961 - 2011

Organization	WellName	Chart Number
Archibald Ranch Community Church	PW 1	C1-1
Basque American Dairy	PW 2	C1-2
California Speedway	Cal Speedway 1	C1-3
Chino Basin Desalter Authority	CDA I-10	C1-4
Chino Basin Watermaster	AP-PA/10	C1-5
	AP-PA/7	C1-6
City of Chino	C 09	C1-7
	C 13	C1-8
	C 15	C1-9
	YMCA	C1-10
City of Chino Hills	CH HIL 07C	C1-11
	CH HIL 15A	C1-12
	CH HIL 15B	C1-13
	CH HIL 17	C1-14
	CH HIL 18A	C1-15
	CH HIL 19	C1-16
City of Corona	COR 06	C1-17
	COR 08	C1-18
	COR 11	C1-19
	COR 14	C1-20
	COR 15	C1-21
City of Norco	NOR 11	C1-22
City of Ontario	ONT 04	C1-23
	ONT 07	C1-24
	ONT 08	C1-25
	ONT 09	C1-26
	ONT 11	C1-27
	ONT 20	C1-28
	ONT 31	C1-29
	ONT 36	C1-30
City of Pomona	P 16	C1-31
	P 24 (OLD)	C1-32
	P 29	C1-33
County of San Bernardino	MIL M-03	C1-34
Cucamonga Valley Water District	CVWD 3	C1-35
	CVWD 35	C1-36
Fontana Water Company	F21A	C1-37
	F30A	C1-38
	F31A	C1-39
	F35A	C1-40
	FU28	C1-41
	FU6	C1-42

Appendix C1
Time-History Plots of Simulated and Measured Groundwater Elevations in the Wells Used in Model Calibration 1961 - 2011

Organization	WellName	Chart Number
General Electric Corporation	GE MW-11	C1-43
Golden State Water Company	GSWC Margarita 1	C1-44
H & R Barthelemy Dairy	PW 3	C1-45
Inland Empire Utilities Agency	IEUA MW-2	C1-46
Jurupa Community Services District	JCSD 16	C1-47
Lizzaraga, Frank	PW 7	C1-48
Michel, Louise	PW 5	C1-49
Riverside County Waste Management Department	Corona CG-1	C1-50
San Antonio Water Company	SAWC 18	C1-51
Santa Ana River Dev. Co.	PW 8	C1-52
Santa Ana River Water Company	SARWC 07	C1-53
Stark, Everett	PW 4	C1-54
State of California, California Institution for Men	CIM 09	C1-55
	CIM MW 24I	C1-56
	CIM MW 24S	C1-57
State of California, Department of Toxic Substances Control	FC-936A2	C1-58
United States, Geological Survey (USGS)	USGS Archibald 1	C1-59
Unknown	COR 10	C1-60
	PW 10	C1-61
	PW 6	C1-62
	PW 9	C1-63
Van Leeuwen, John	PW 11	C1-64
West End Consolidated Water Co.	WECWC 1	C1-65
West Valley Water District	WVWD 20	C1-66

Figure C1-1

Simulated and Measured Groundwater Elevations in the Wells Used in Model Calibration 1961 - 2011

Well PW 1

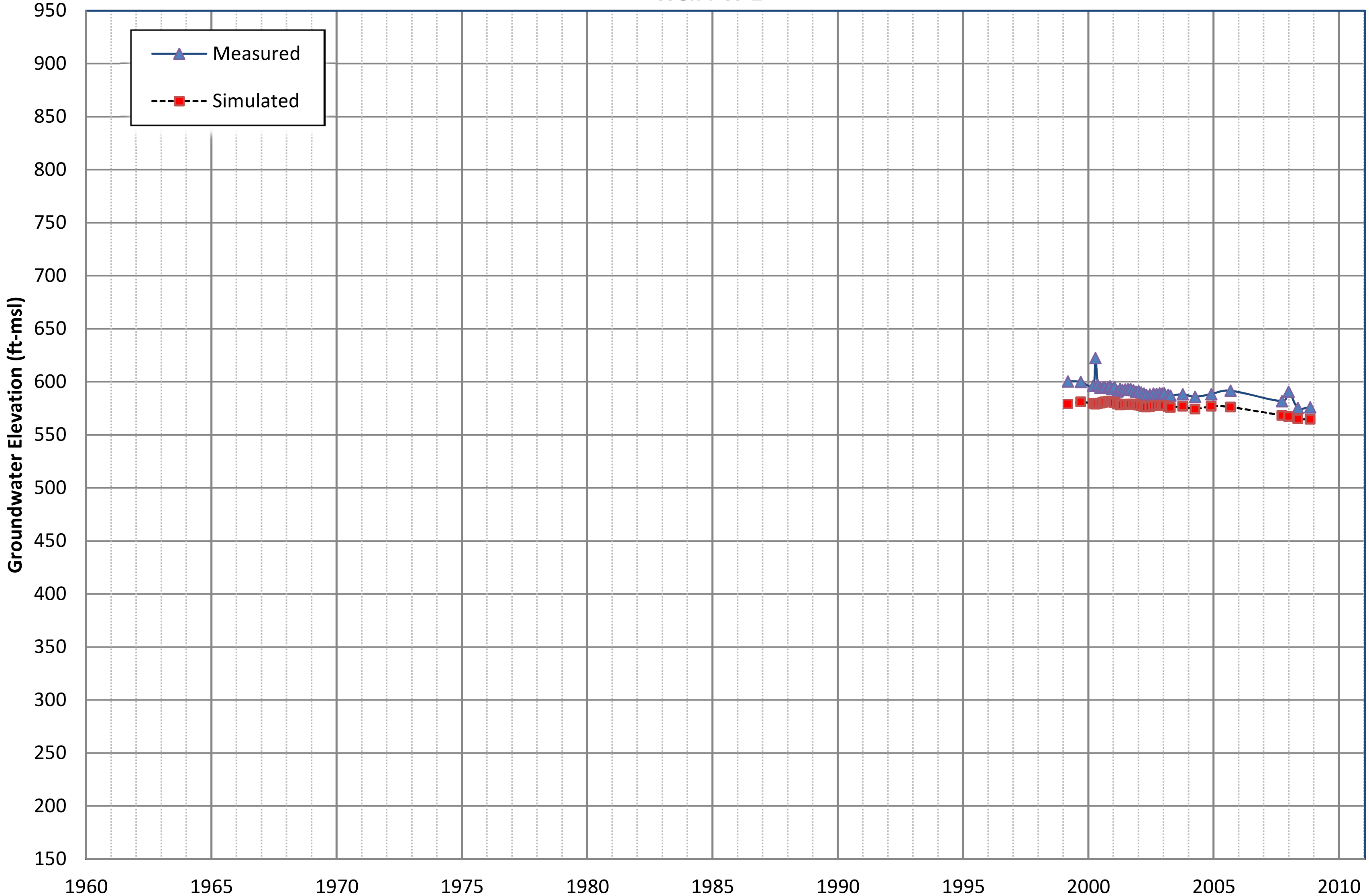

Figure C1-2
Simulated and Measured Groundwater Elevations in the Wells Used in Model Calibration 1961 - 2011
Well PW 2

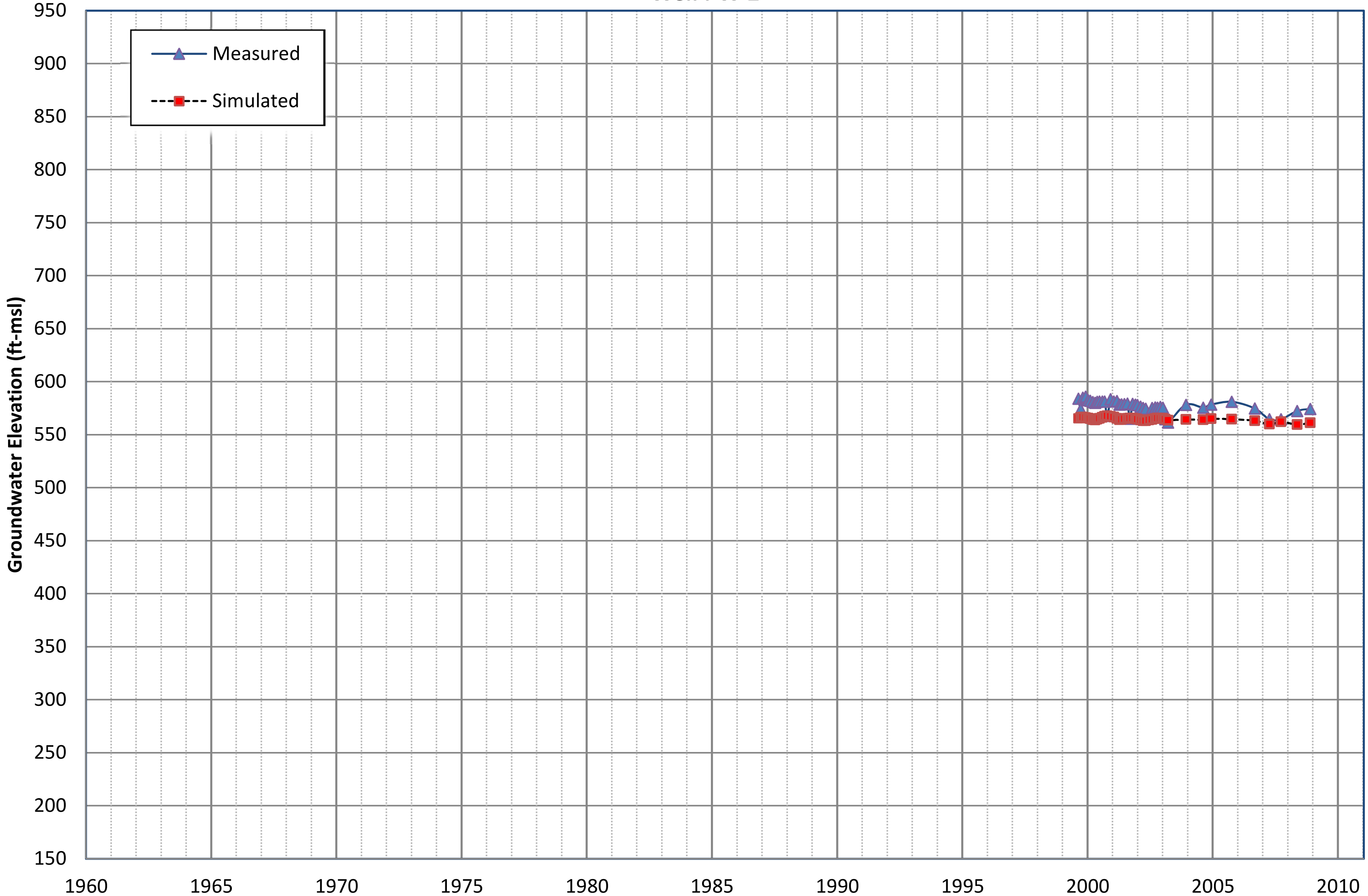

Figure C1-3
Simulated and Measured Groundwater Elevations in the Wells Used in Model Calibration 1961 - 2011
Cal Speedway 1

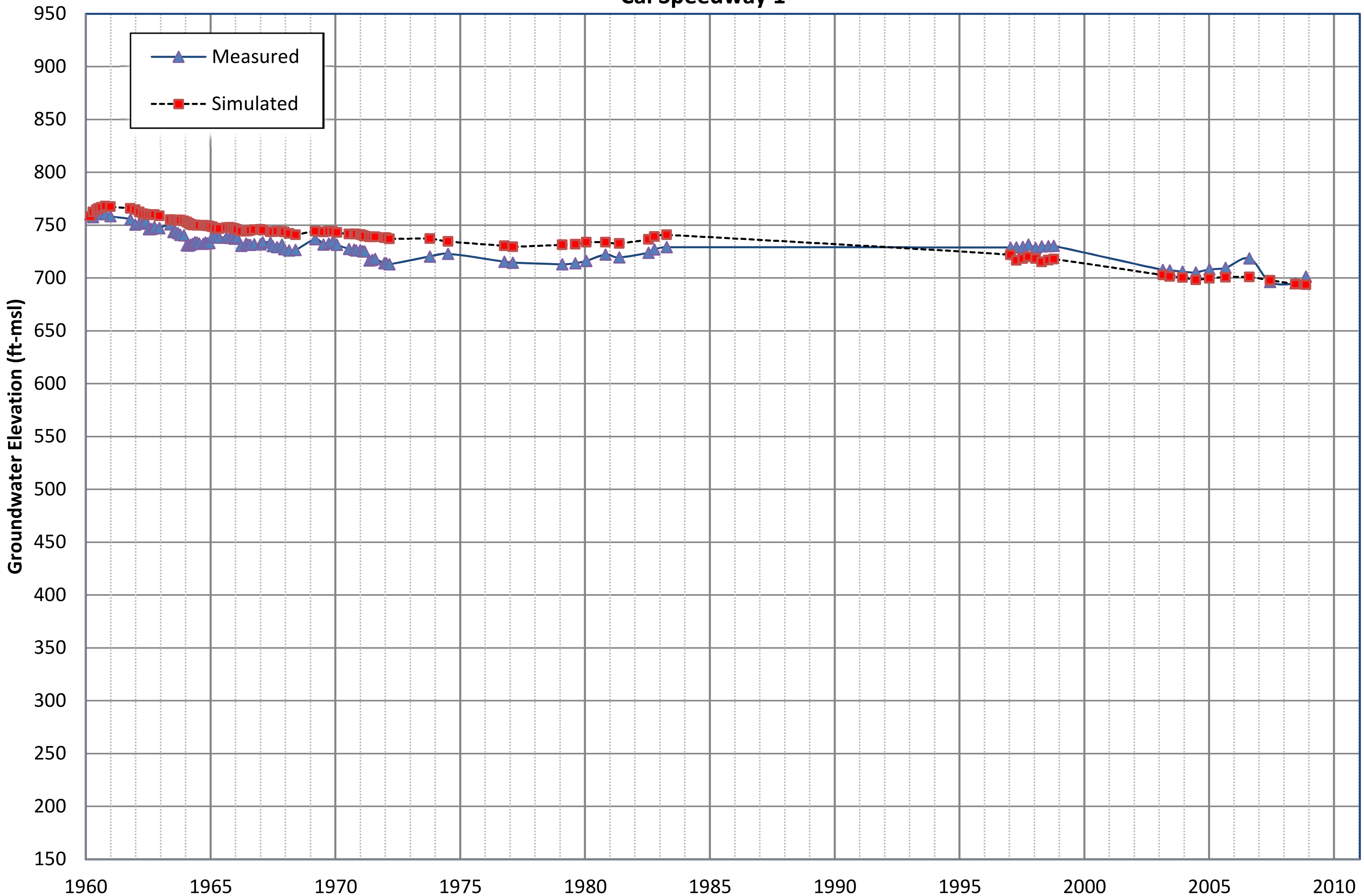

Appendix_C1_20150915_WW_WellHydrograph_calibrationwell_format.xlsm

Figure C1-4
Simulated and Measured Groundwater Elevations in the Wells Used in Model Calibration 1961 - 2011
CDA I-10

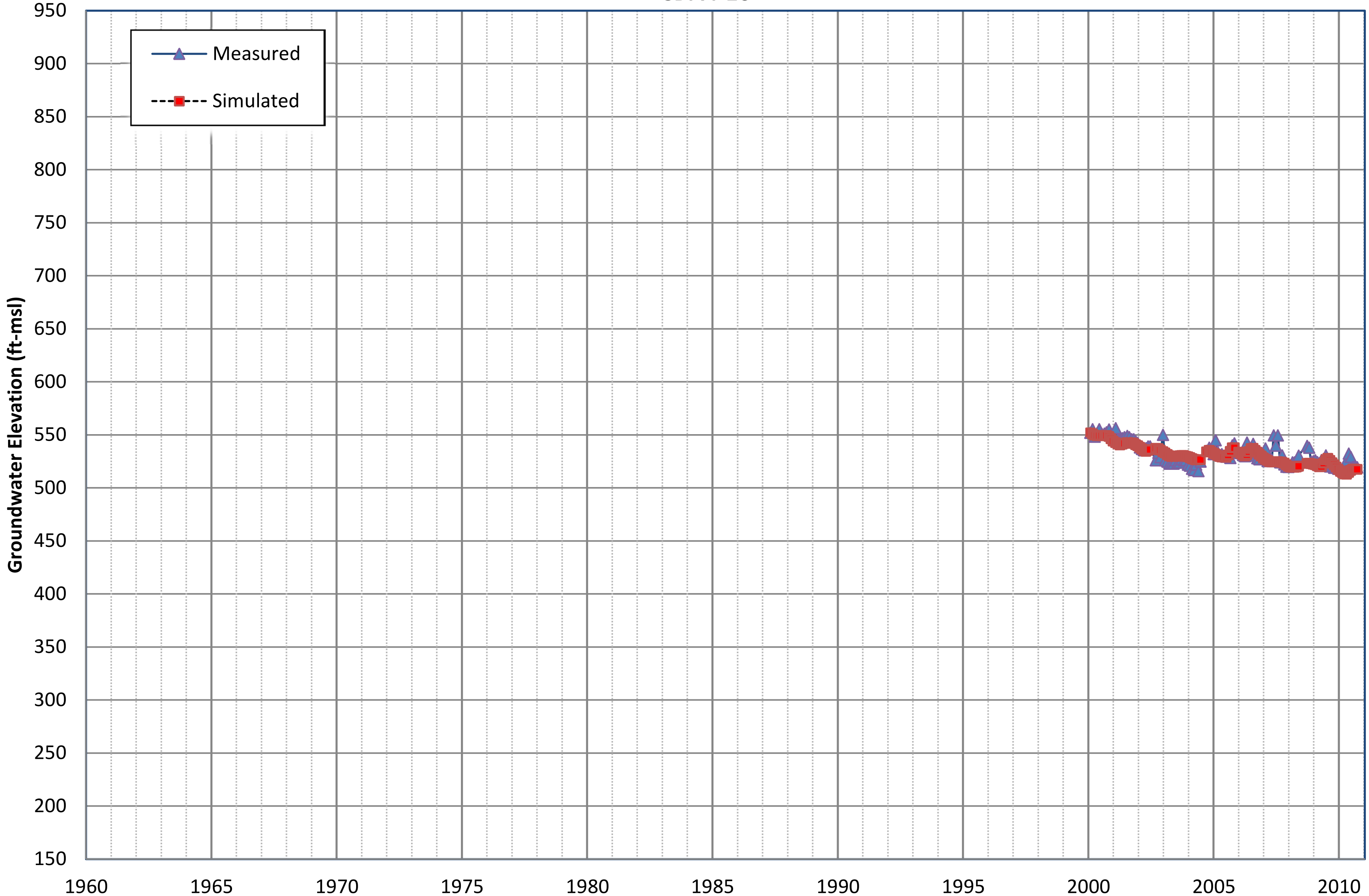

Appendix_C1_20150915_WW_WellHydrograph_calibrationwell_format.xlsm

Figure C1-5
Simulated and Measured Groundwater Elevations in the Wells Used in Model Calibration 1961 - 2011
AP-PA/10

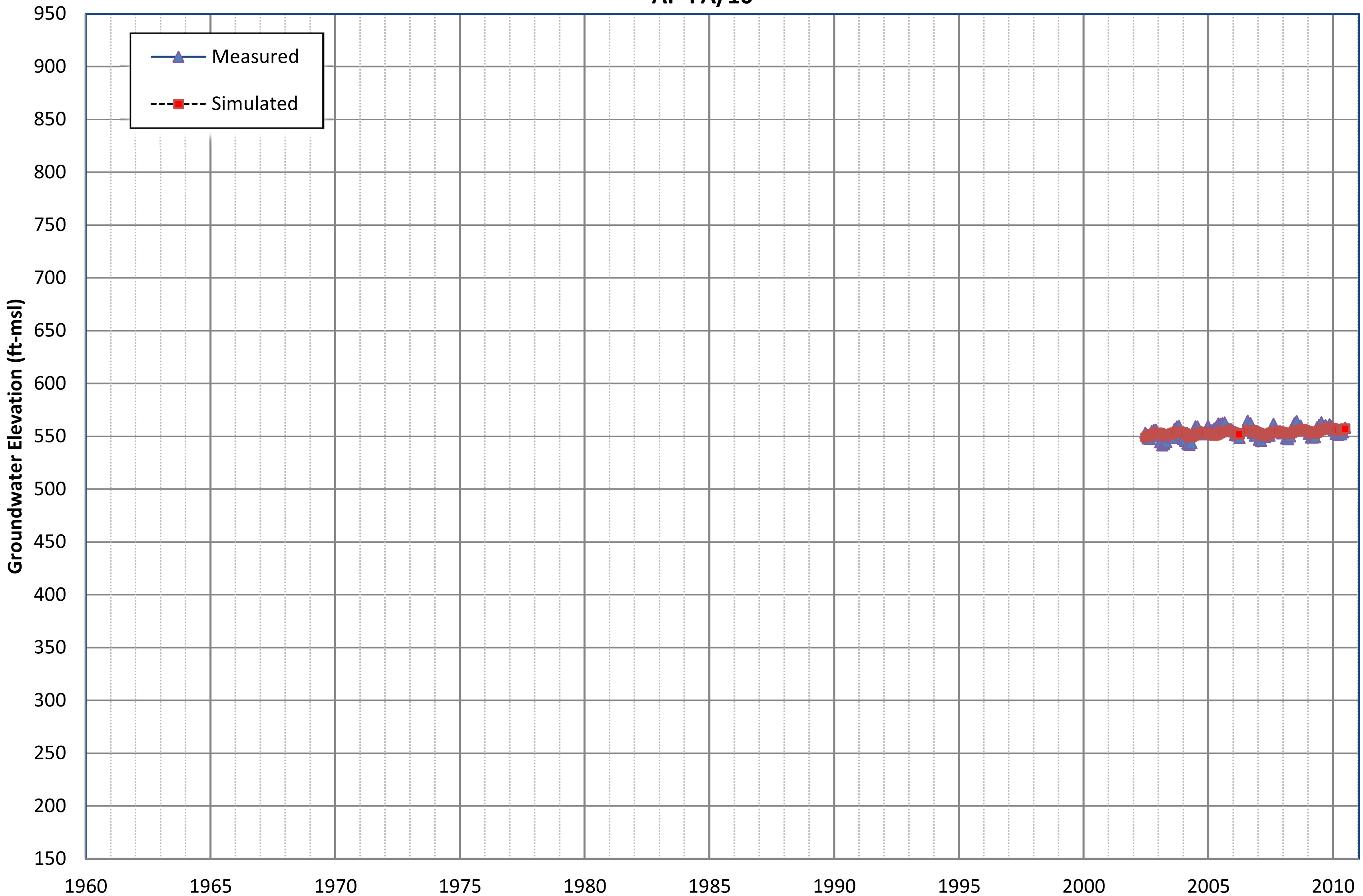

Appendix_C1_20150915_WW_WellHydrograph_calibrationwell_format.xlsm

Figure C1-6
Simulated and Measured Groundwater Elevations in the Wells Used in Model Calibration 1961 - 2011
AP-PA/7

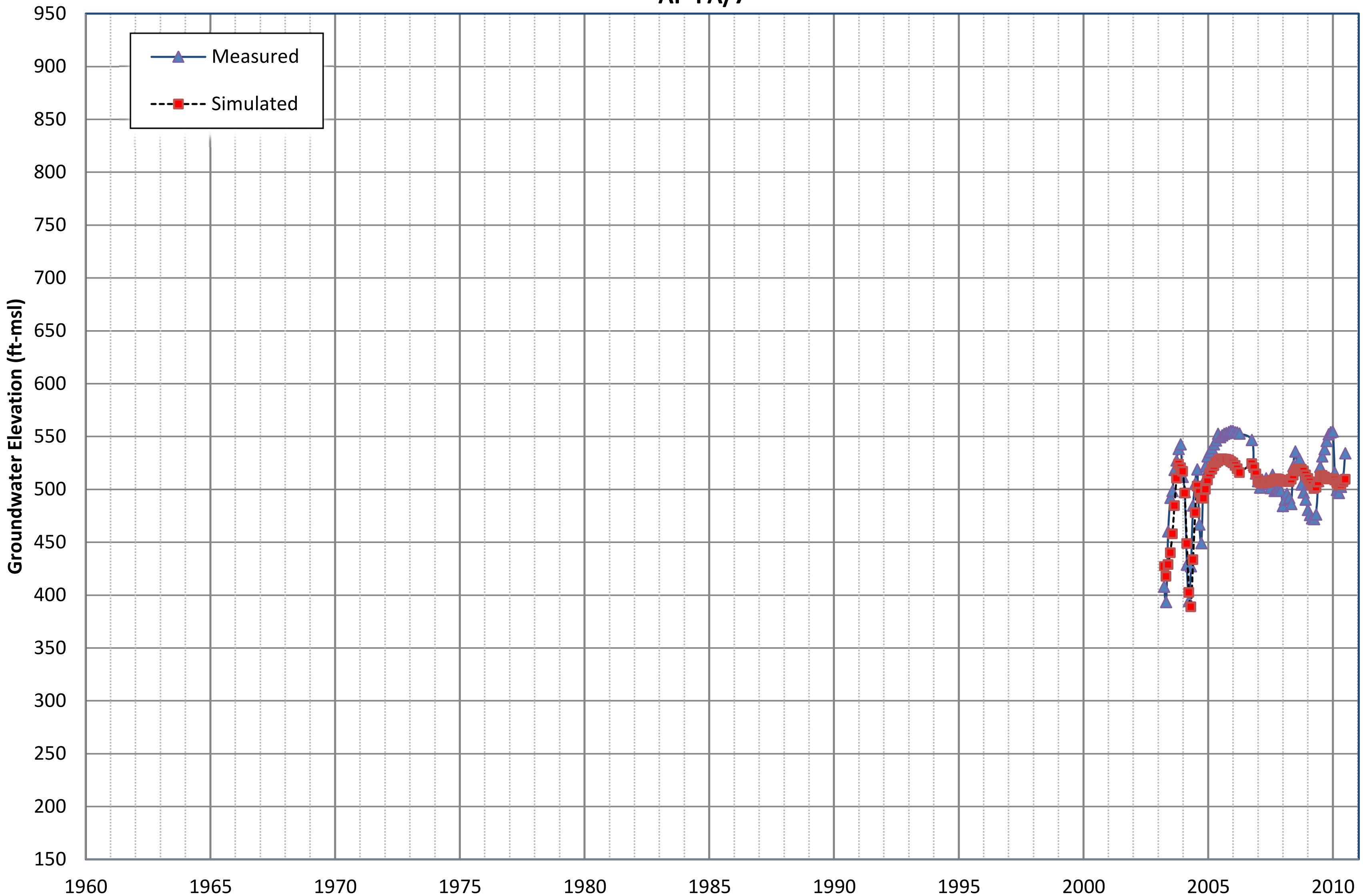

Figure C1-7
Simulated and Measured Groundwater Elevations in the Wells Used in Model Calibration 1961 - 2011
C 09

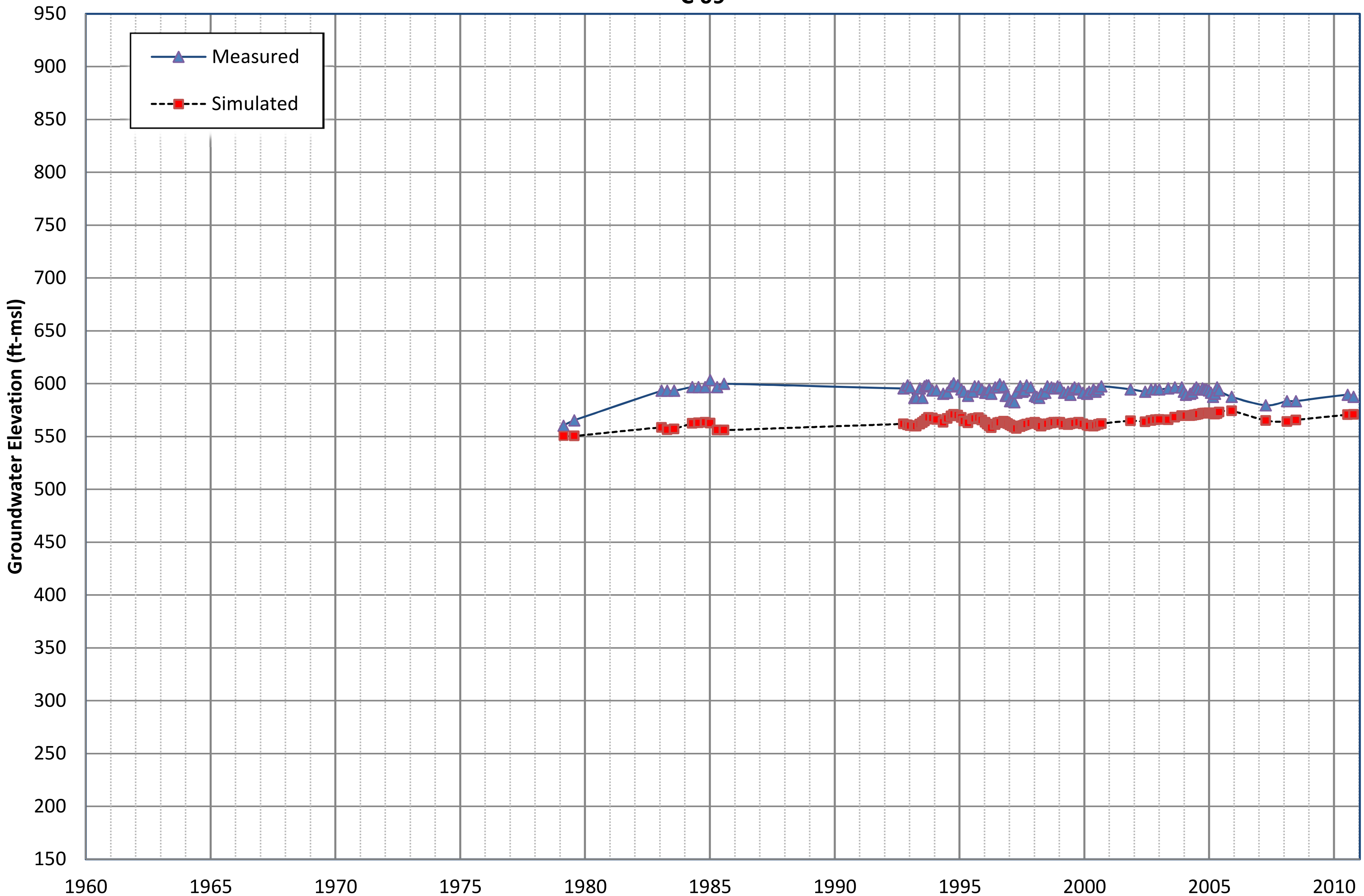

Appendix_C1_20150915_WW_WellHydrograph_calibrationwell_format.xlsm

Figure C1-8
Simulated and Measured Groundwater Elevations in the Wells Used in Model Calibration 1961 - 2011
C 13

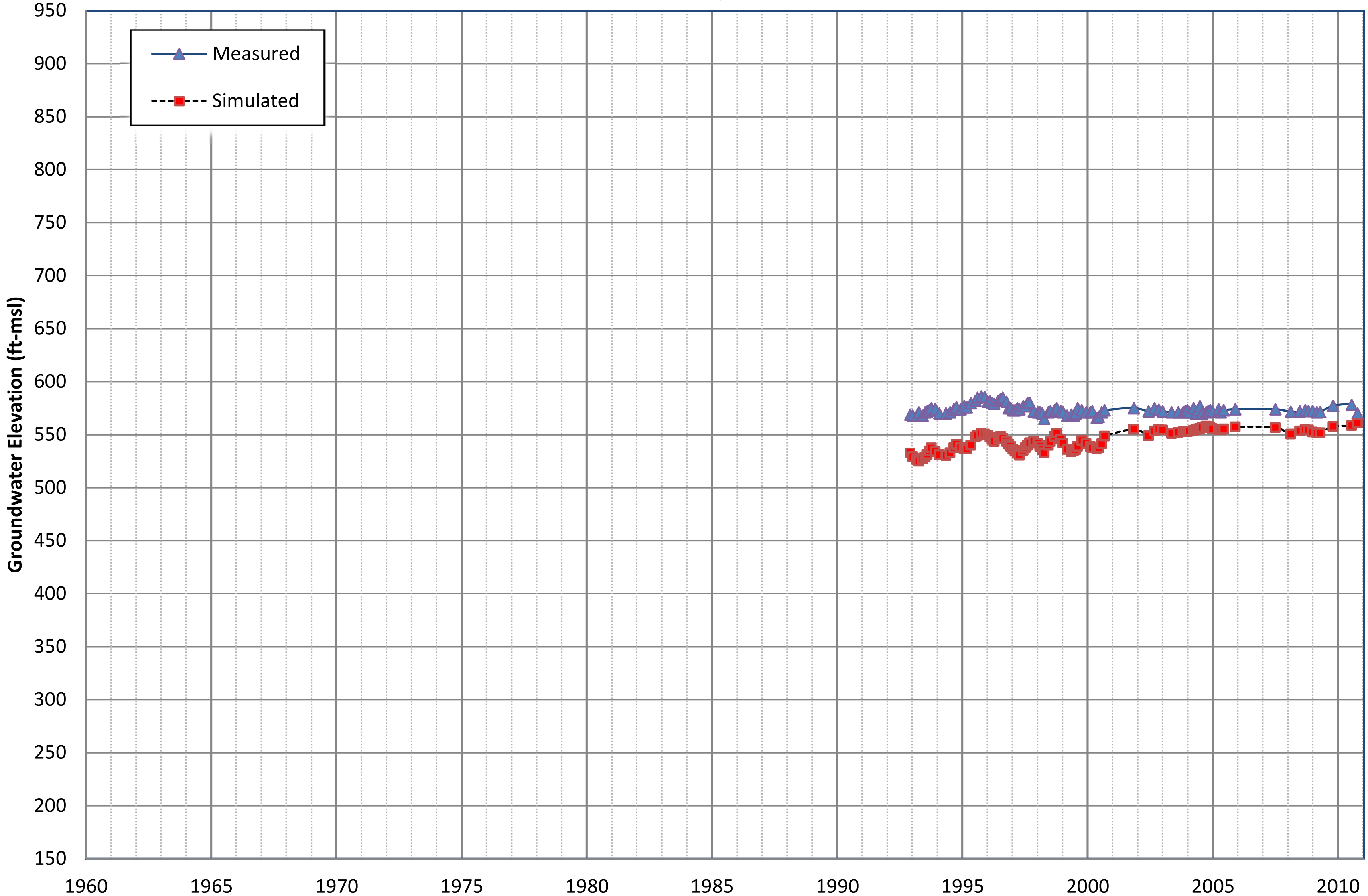

Figure C1-9
Simulated and Measured Groundwater Elevations in the Wells Used in Model Calibration 1961 - 2011
C 15

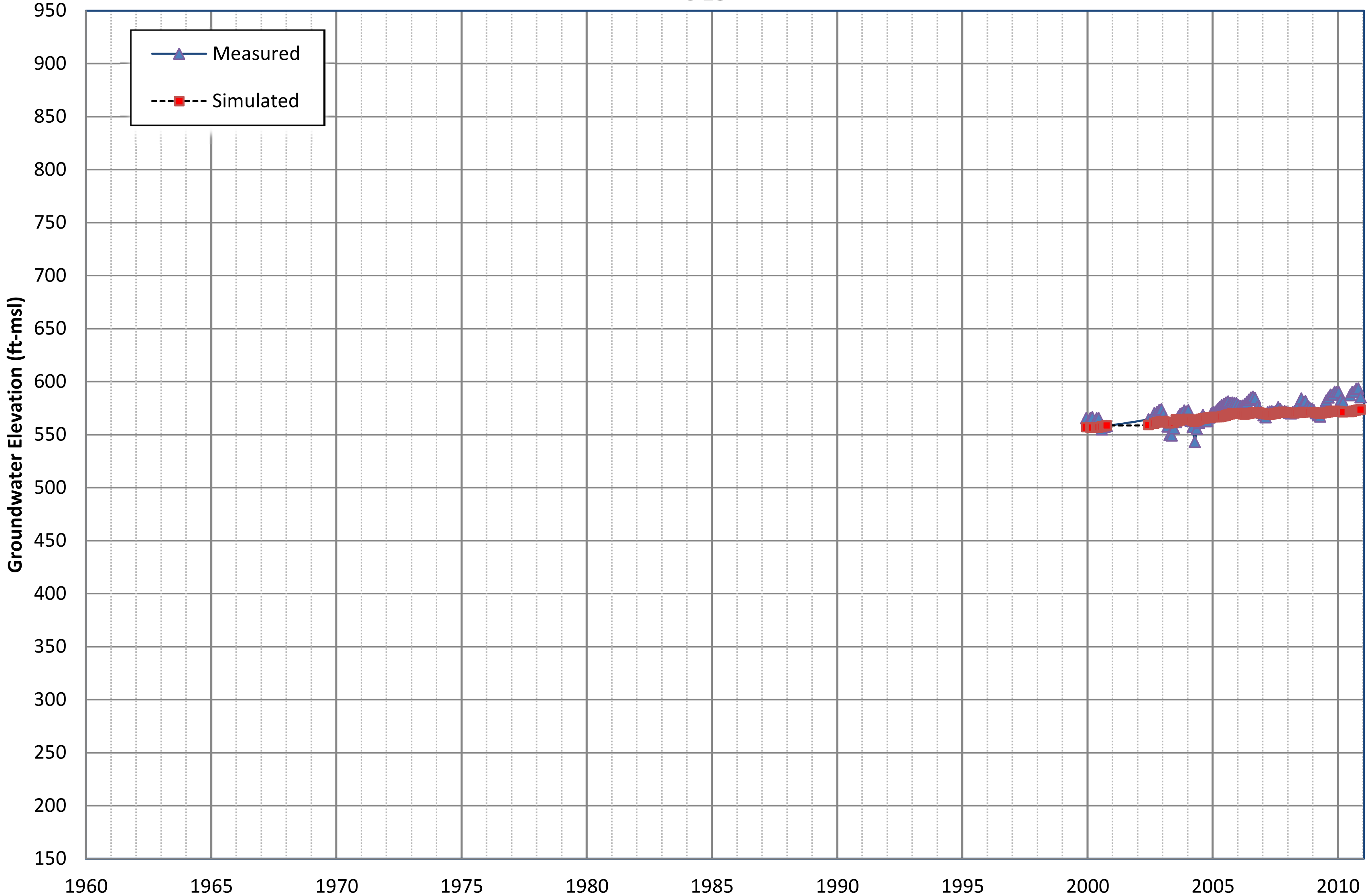

Figure C1-10
Simulated and Measured Groundwater Elevations in the Wells Used in Model Calibration 1961 - 2011
YMCA

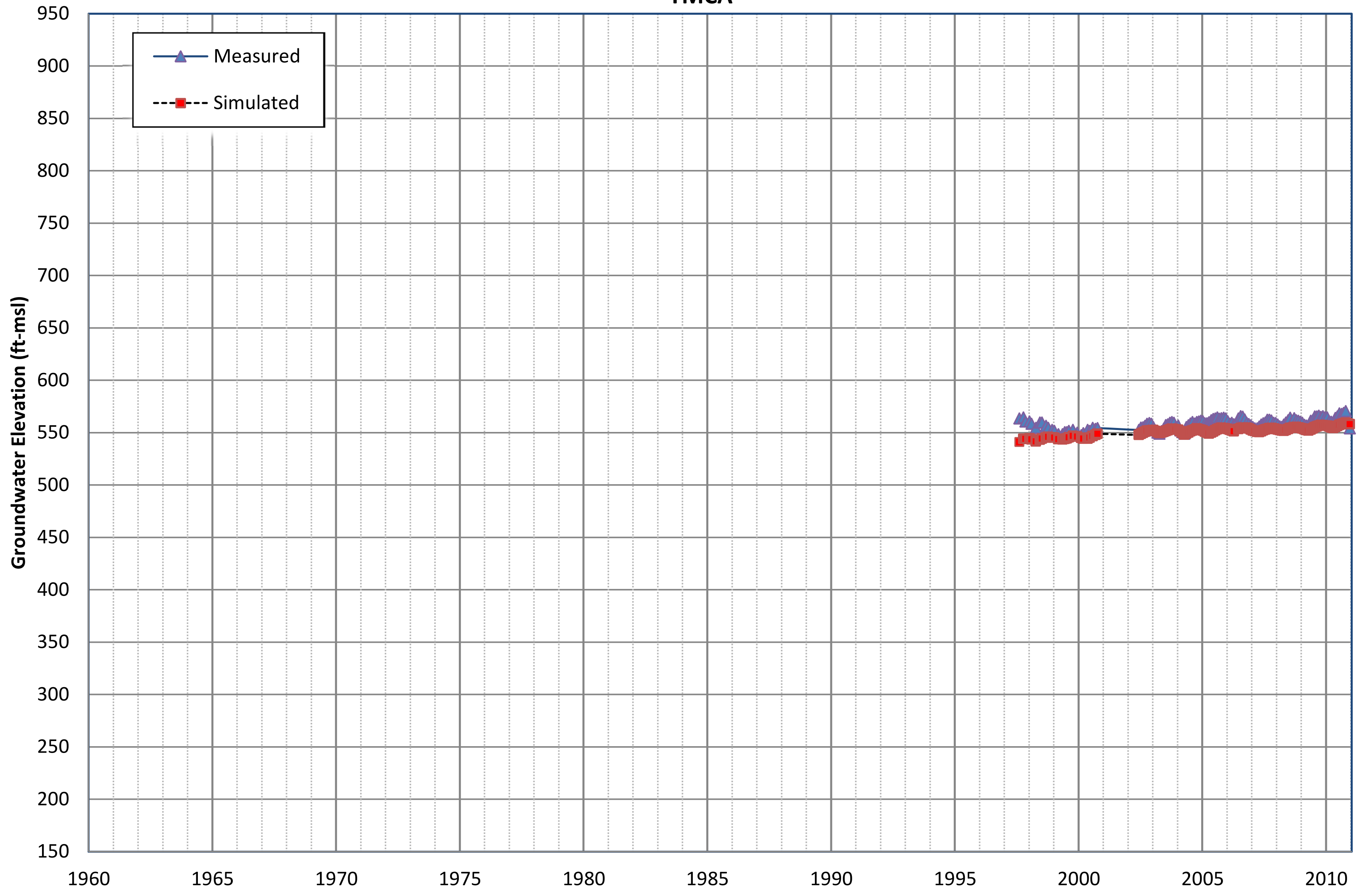

Appendix_C1_20150915_WW_WellHydrograph_calibrationwell_format.xlsm

Figure C1-11
Simulated and Measured Groundwater Elevations in the Wells Used in Model Calibration 1961 - 2011
CH HIL 07C

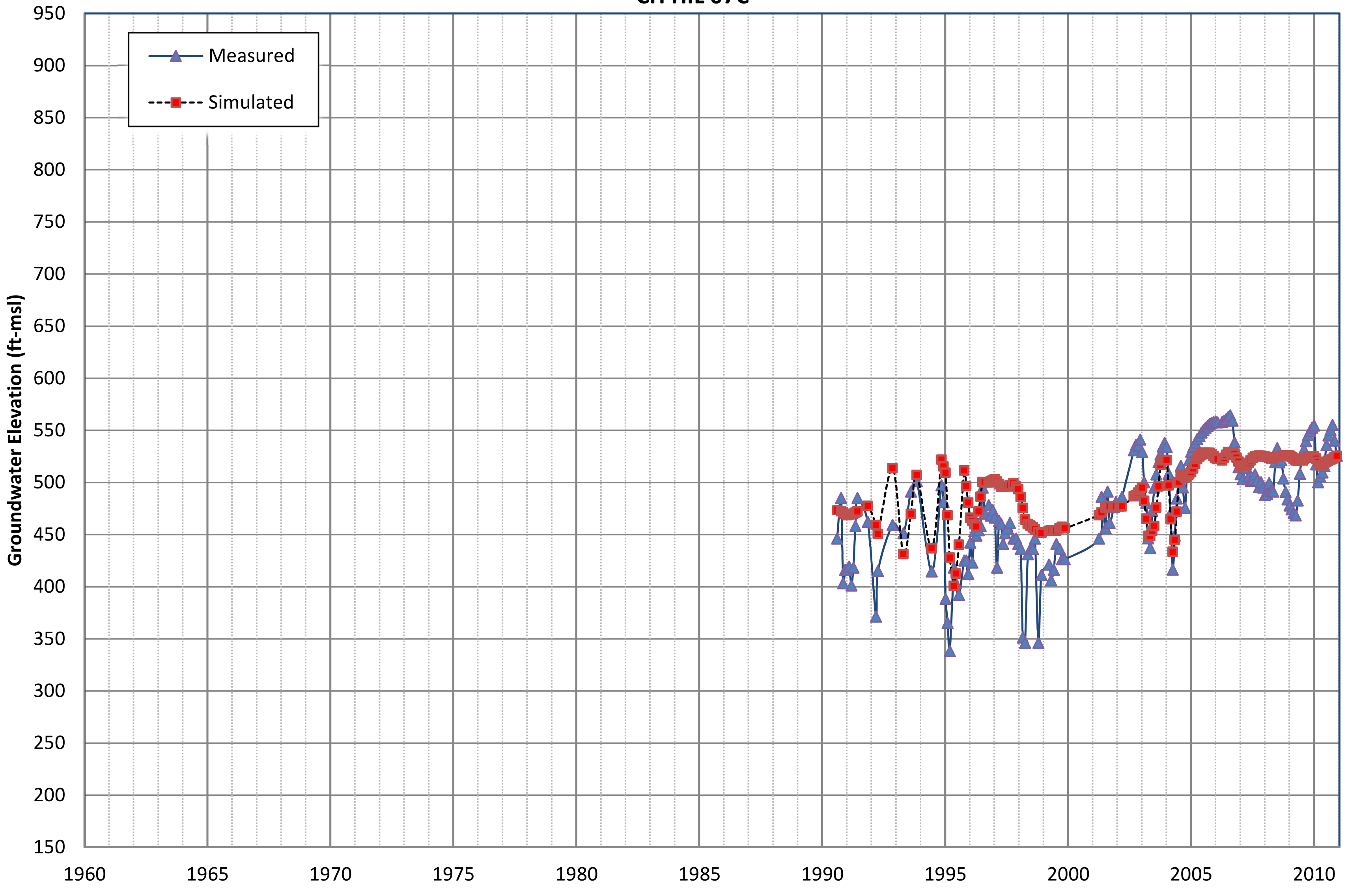

Figure C1-12
Simulated and Measured Groundwater Elevations in the Wells Used in Model Calibration 1961 - 2011
CH HIL 15A

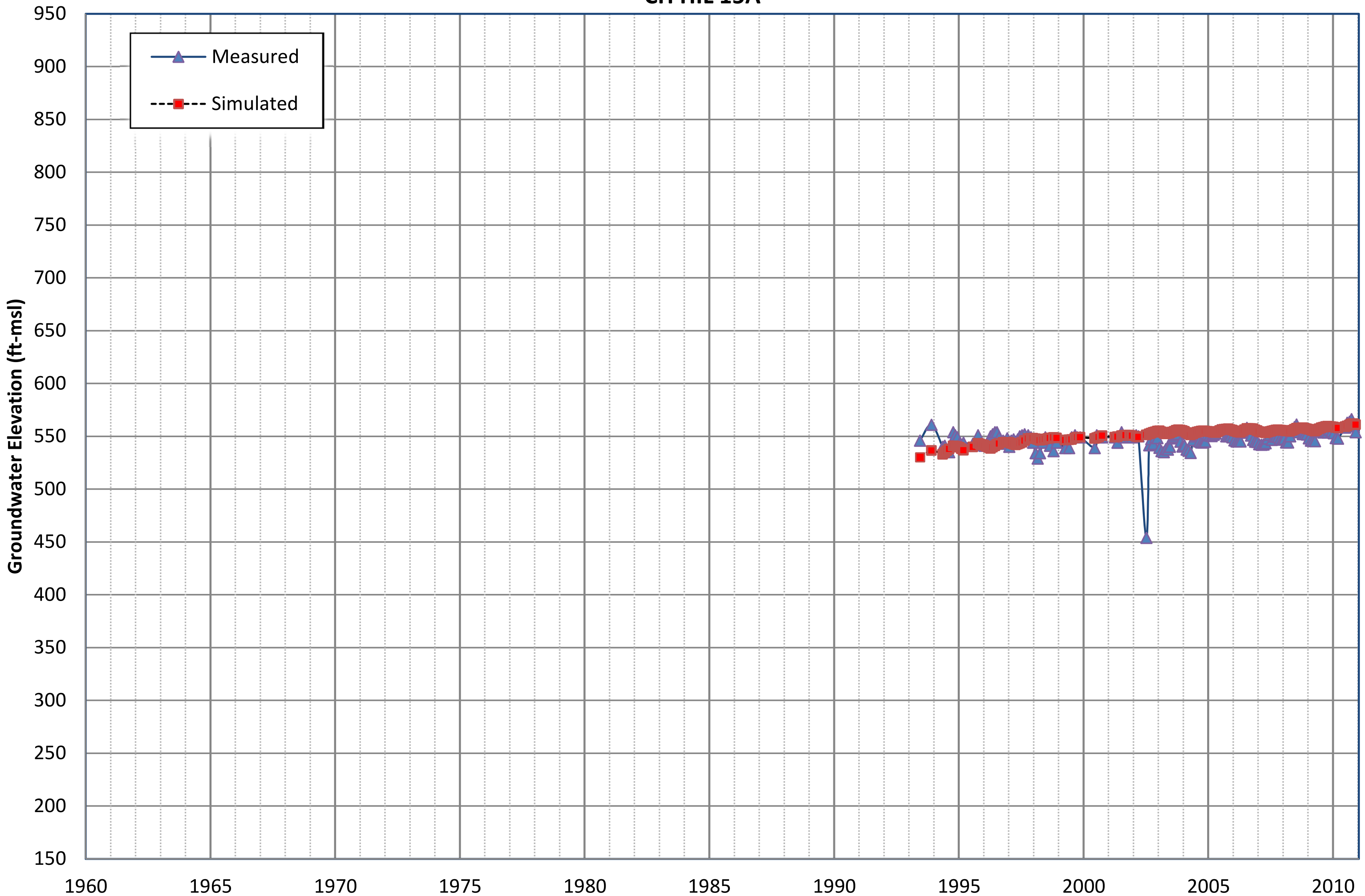

Appendix_C1_20150915_WW_WellHydrograph_calibrationwell_format.xlsm

Figure C1-13
Simulated and Measured Groundwater Elevations in the Wells Used in Model Calibration 1961 - 2011
CH HIL 15B

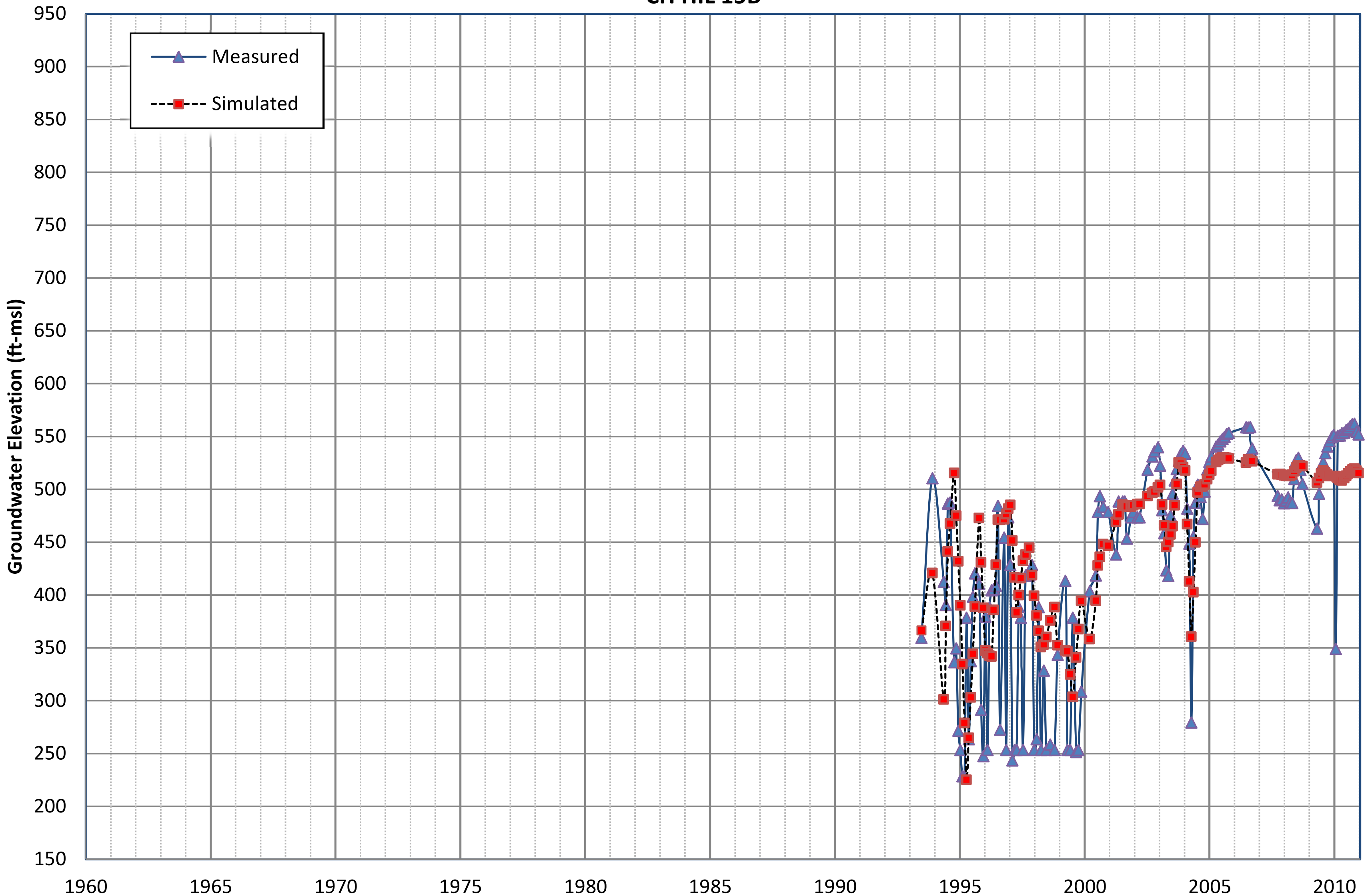

Appendix_C1_20150915_WW_WellHydrograph_calibrationwell_format.xlsm

Figure C1-14
Simulated and Measured Groundwater Elevations in the Wells Used in Model Calibration 1961 - 2011
CH HIL 17

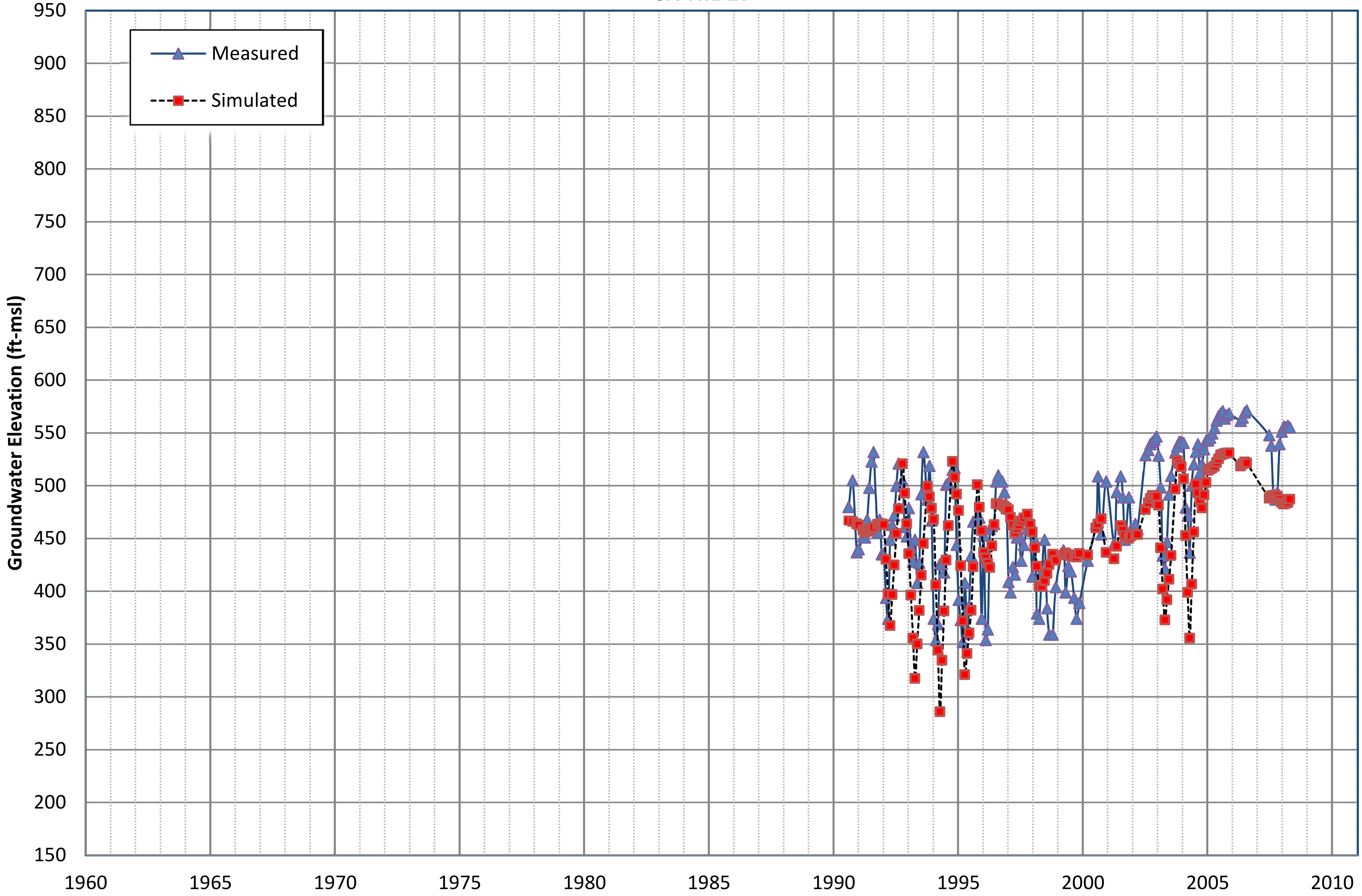

Appendix_C1_20150915_WW_WellHydrograph_calibrationwell_format.xlsm

Figure C1-15
Simulated and Measured Groundwater Elevations in the Wells Used in Model Calibration 1961 - 2011
CH HIL 18A

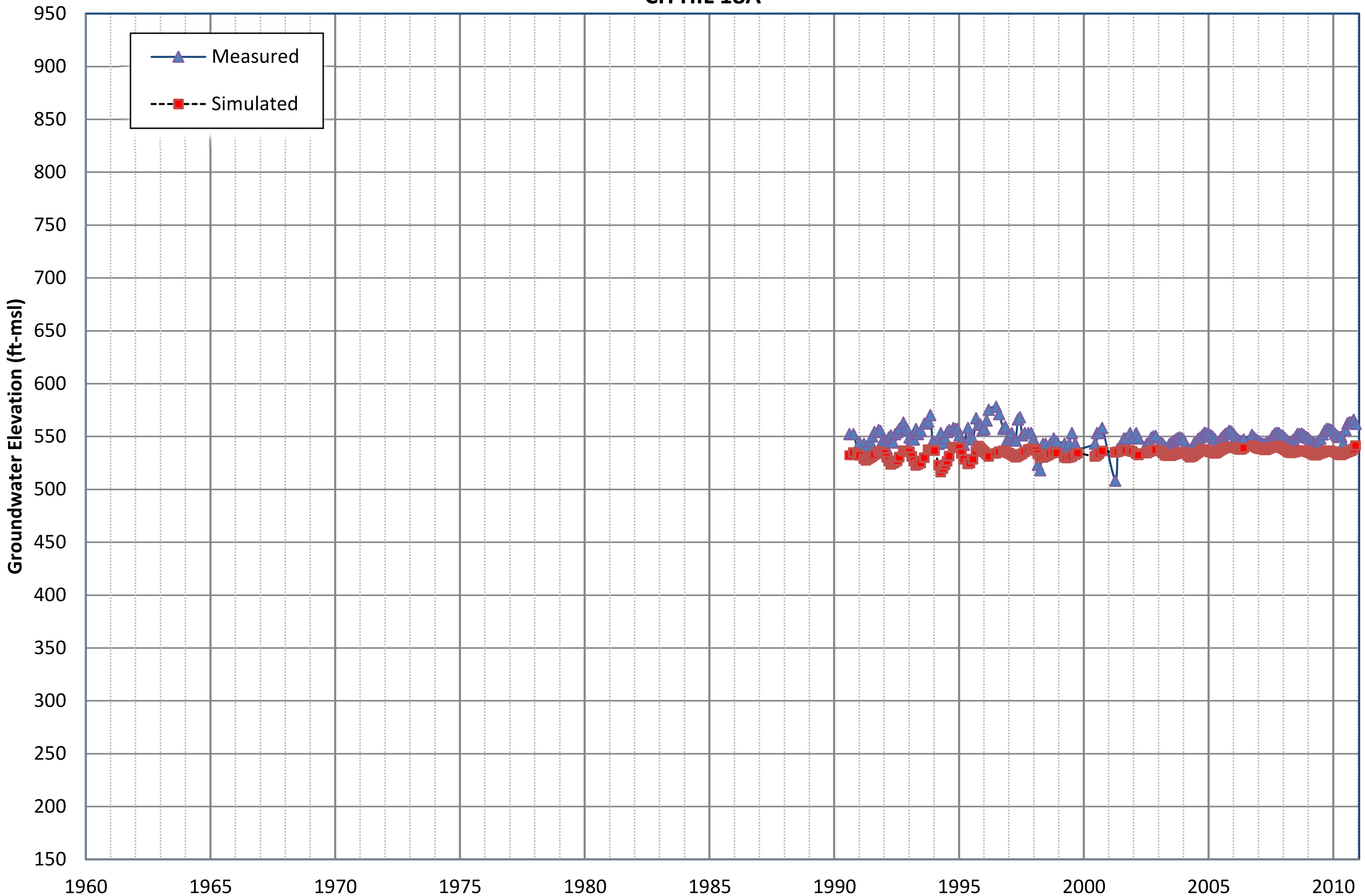

Appendix_C1_20150915_WW_WellHydrograph_calibrationwell_format.xlsm

Figure C1-16
Simulated and Measured Groundwater Elevations in the Wells Used in Model Calibration 1961 - 2011
CH HIL 19

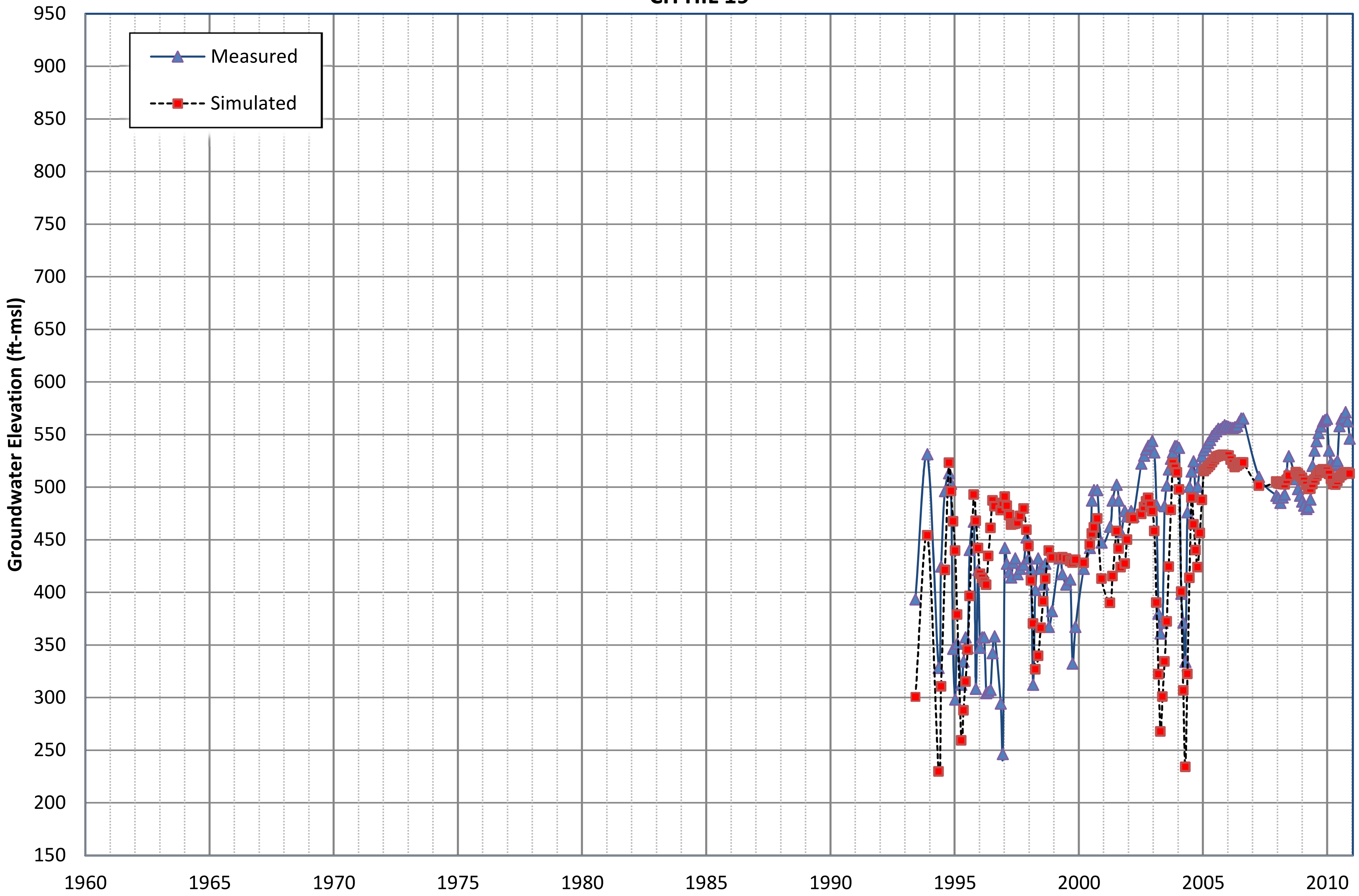

Figure C1-17
Simulated and Measured Groundwater Elevations in the Wells Used in Model Calibration 1961 - 2011
COR 06

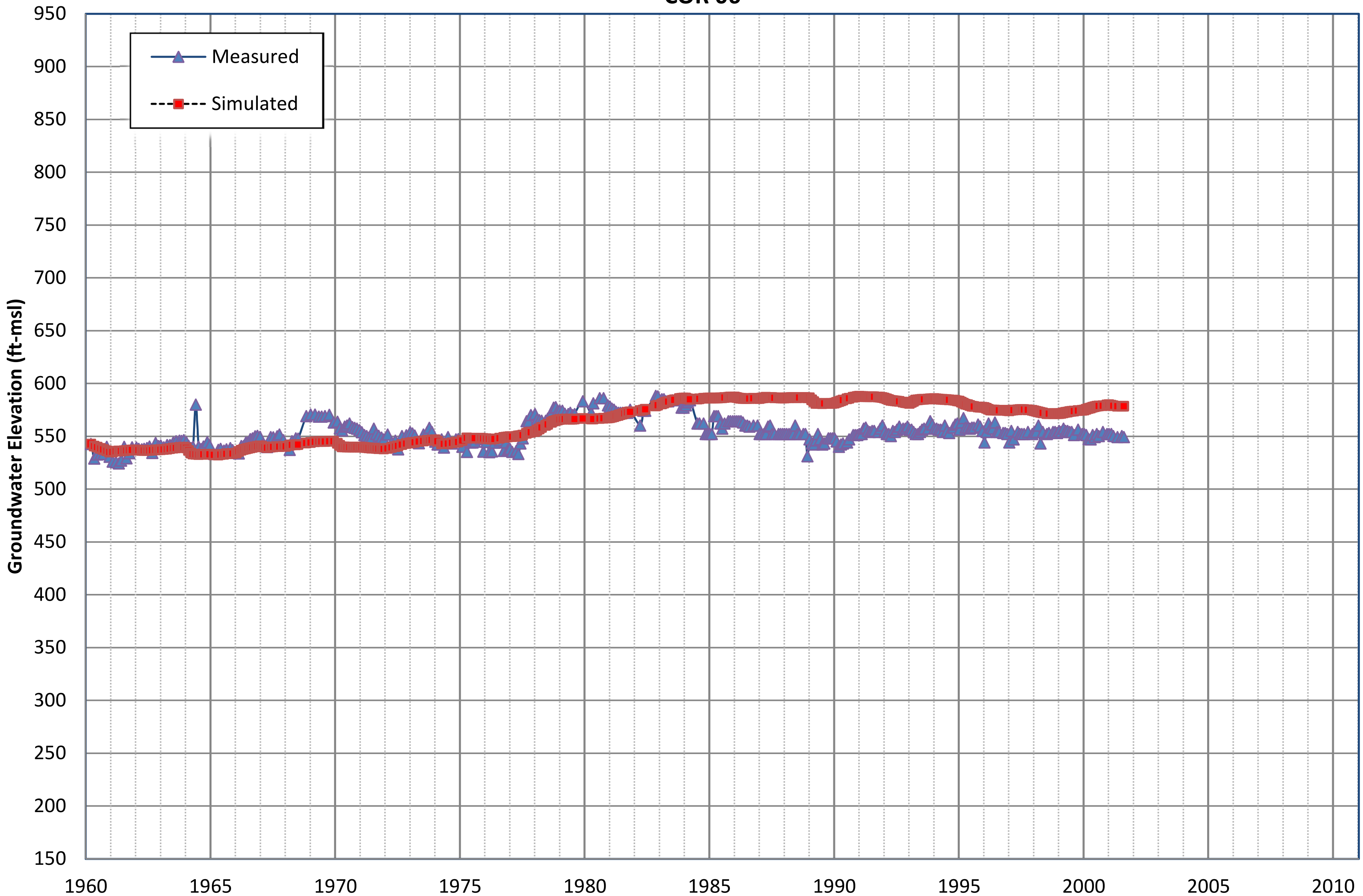

Figure C1-18
Simulated and Measured Groundwater Elevations in the Wells Used in Model Calibration 1961 - 2011
COR 08

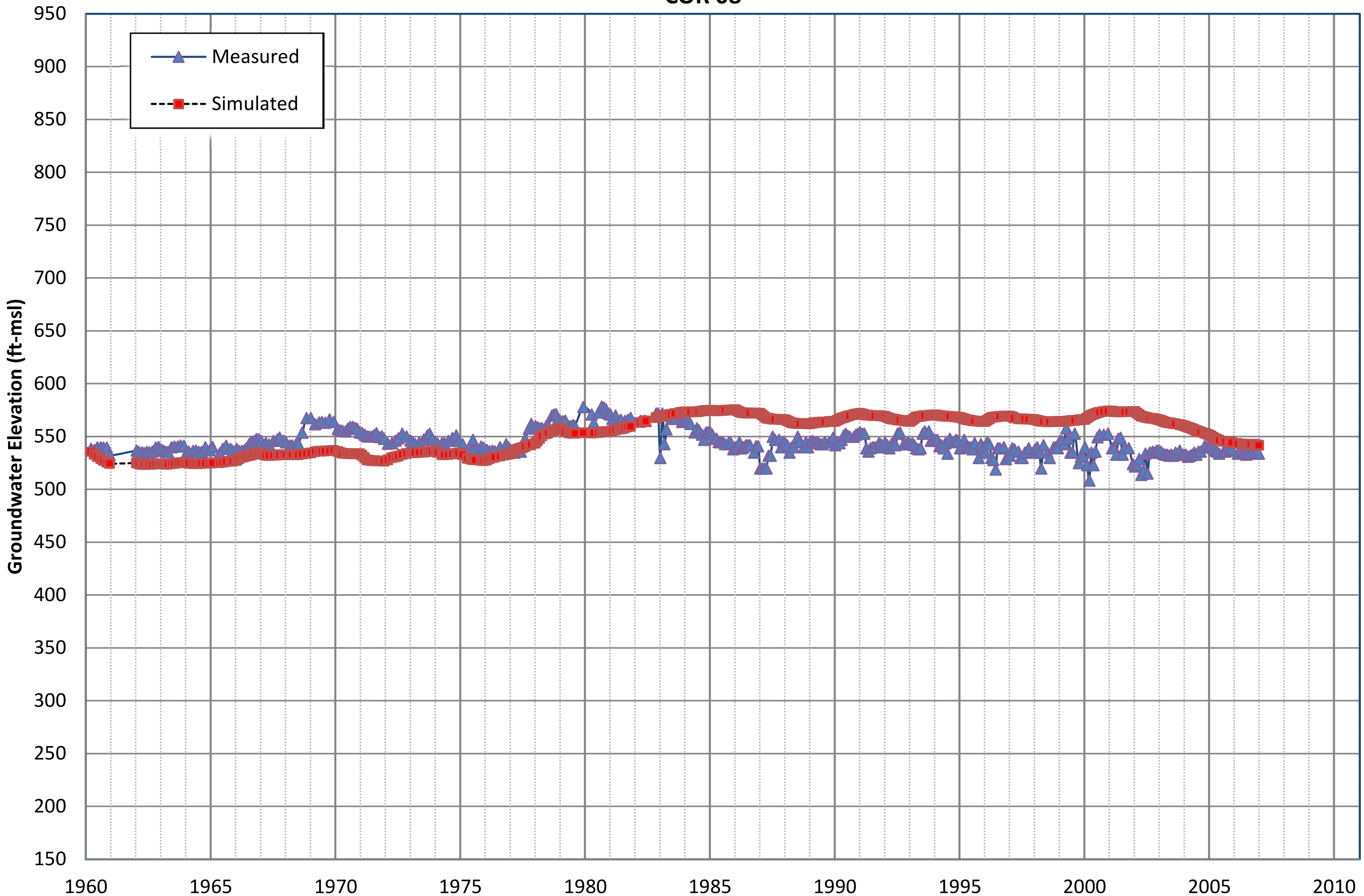

Appendix_C1_20150915_WW_WellHydrograph_calibrationwell_format.xlsm

Figure C1-19
Simulated and Measured Groundwater Elevations in the Wells Used in Model Calibration 1961 - 2011
COR 11

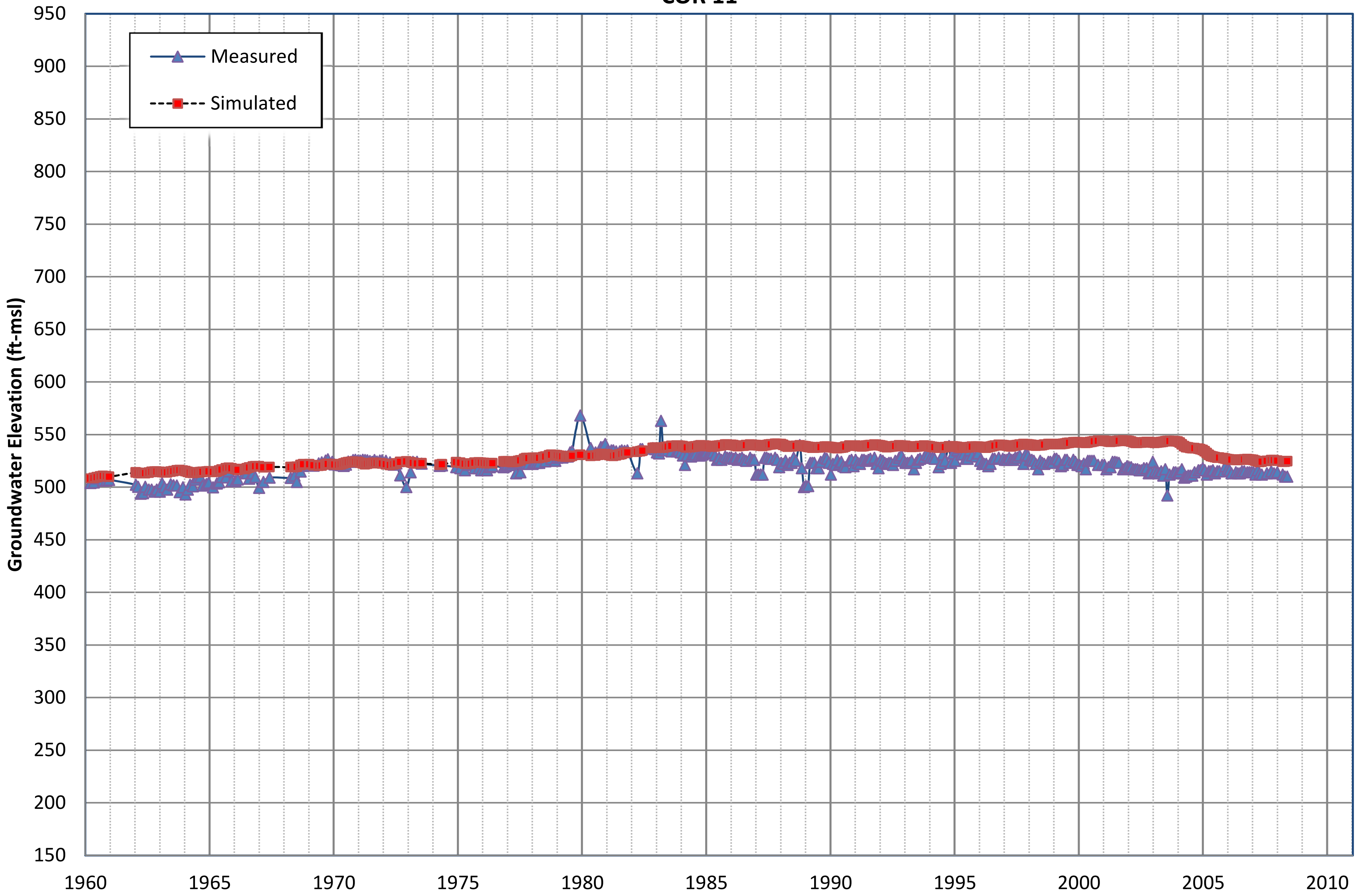

Appendix_C1_20150915_WW_WellHydrograph_calibrationwell_format.xlsm

Figure C1-20
Simulated and Measured Groundwater Elevations in the Wells Used in Model Calibration 1961 - 2011
COR 14

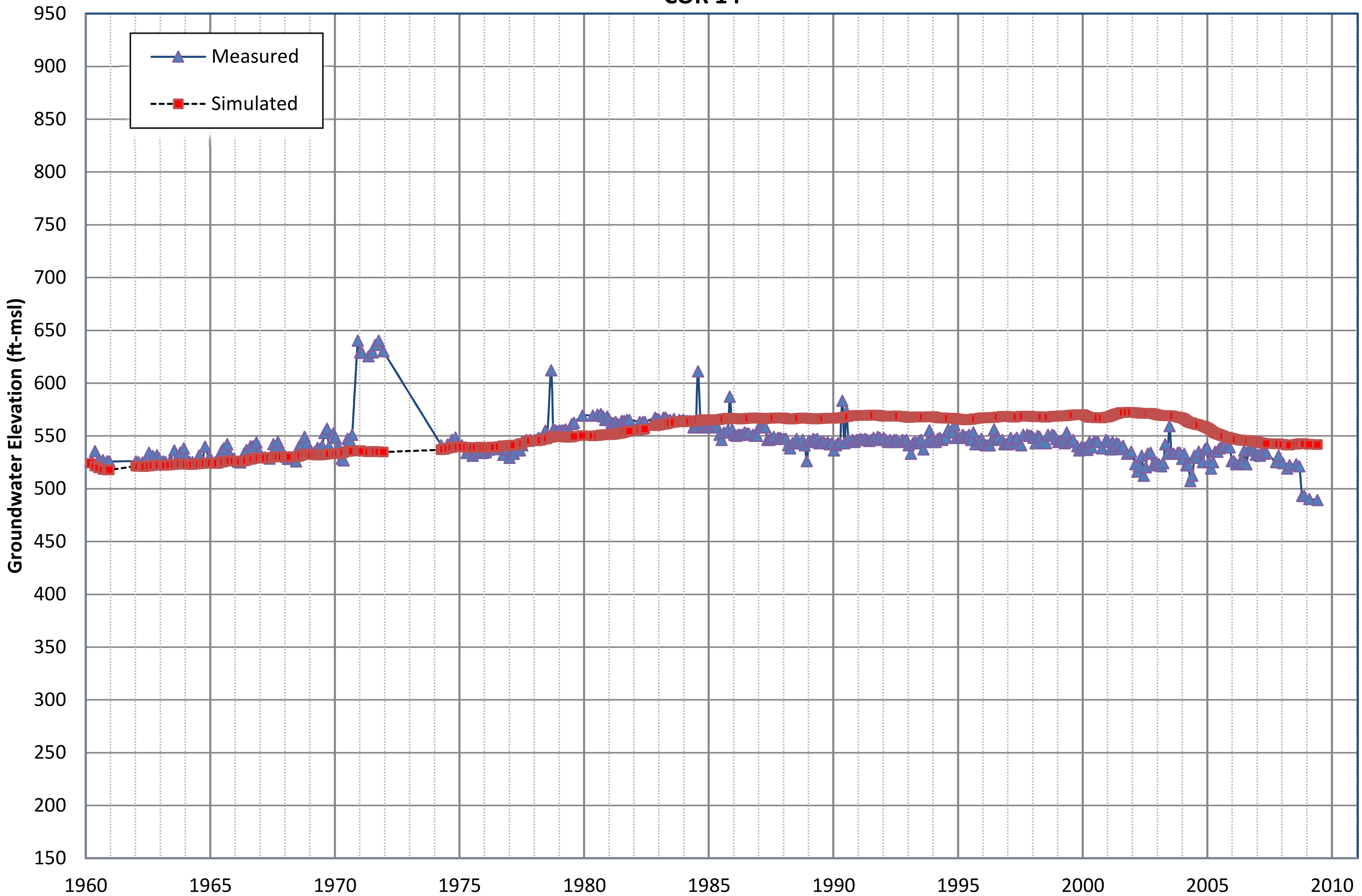

Appendix_C1_20150915_WW_WellHydrograph_calibrationwell_format.xlsm

Figure C1-21

Simulated and Measured Groundwater Elevations in the Wells Used in Model Calibration 1961 - 2011

COR 15

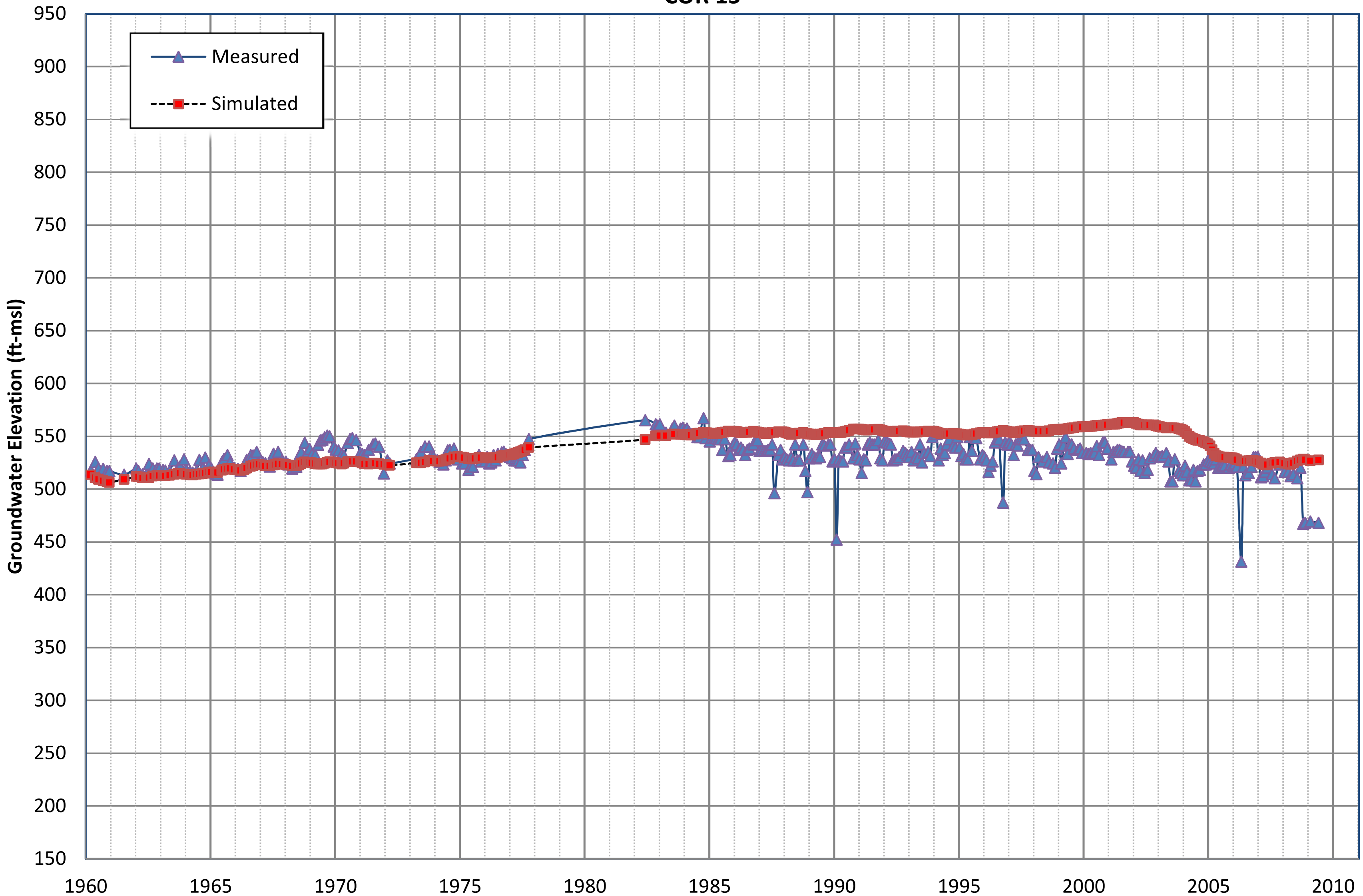

Appendix_C1_20150915_WW_WellHydrograph_calibrationwell_format.xlsm

Figure C1-22
Simulated and Measured Groundwater Elevations in the Wells Used in Model Calibration 1961 - 2011
NOR 11

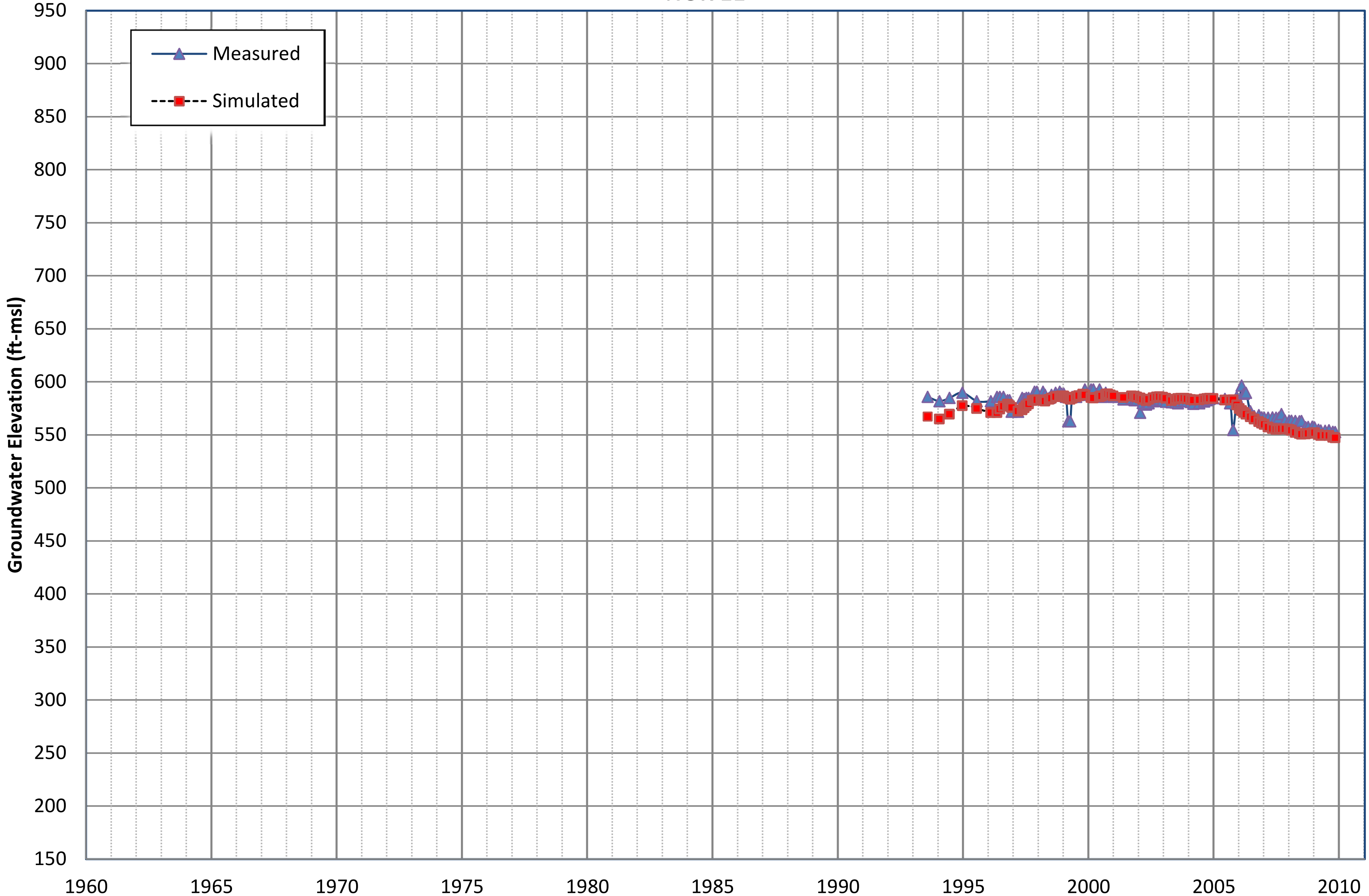

Appendix_C1_20150915_WW_WellHydrograph_calibrationwell_format.xlsm

Figure C1-23
Simulated and Measured Groundwater Elevations in the Wells Used in Model Calibration 1961 - 2011
ONT 04

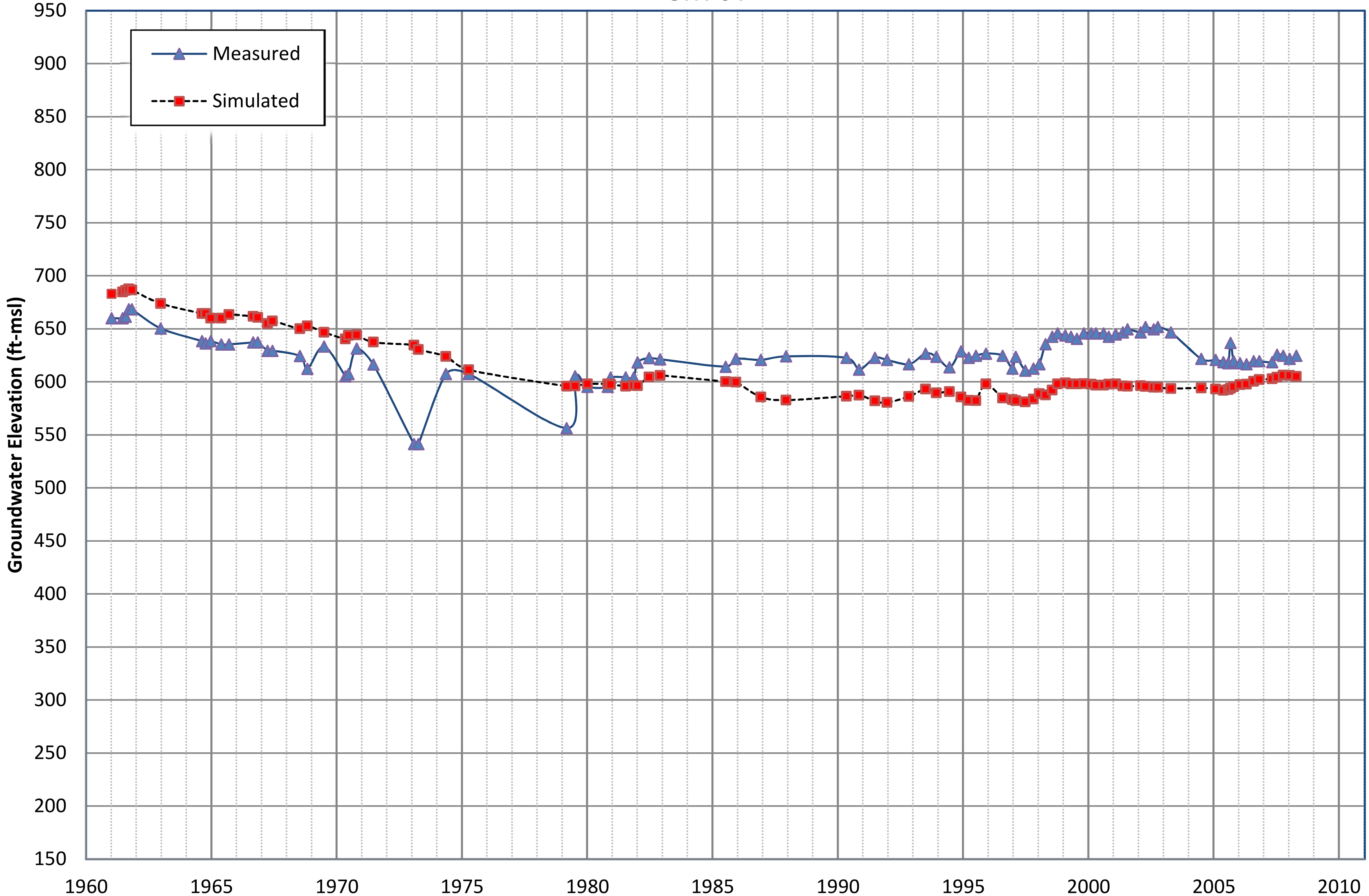

Figure C1-24

Simulated and Measured Groundwater Elevations in the Wells Used in Model Calibration 1961 - 2011

ONT 07

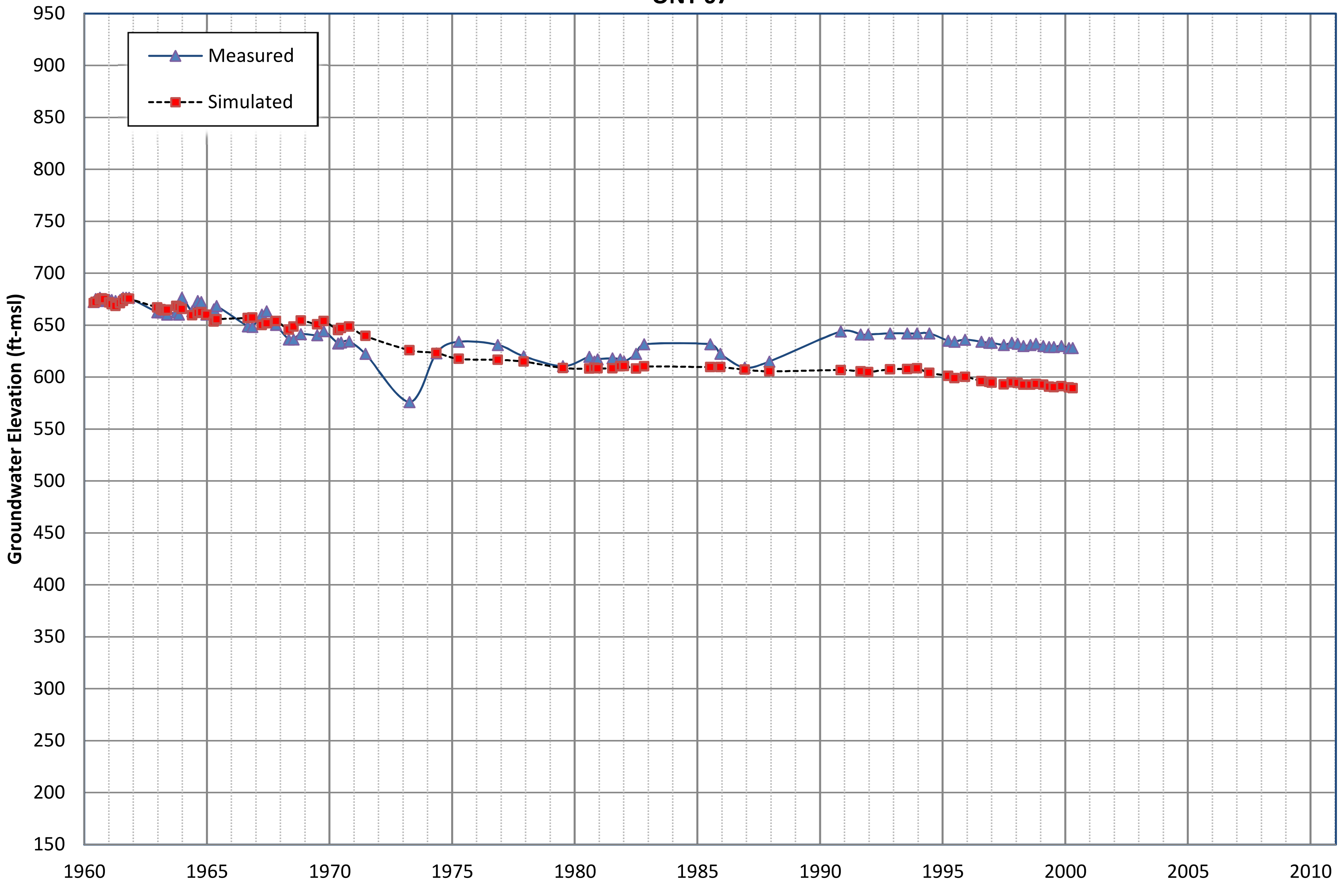

Figure C1-25
Simulated and Measured Groundwater Elevations in the Wells Used in Model Calibration 1961 - 2011
ONT 08

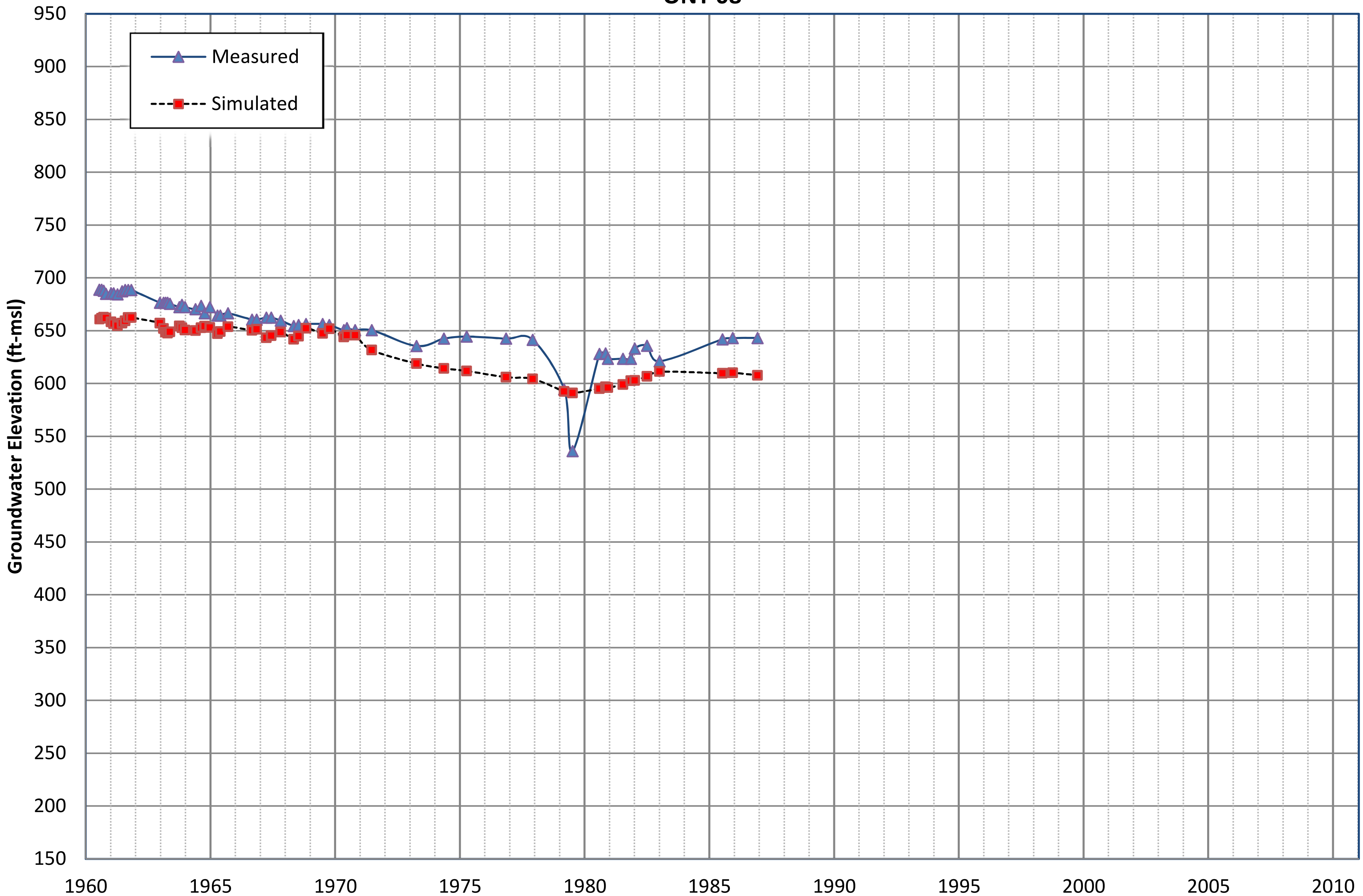

Appendix_C1_20150915_WW_WellHydrograph_calibrationwell_format.xlsm

Figure C1-26
Simulated and Measured Groundwater Elevations in the Wells Used in Model Calibration 1961 - 2011
ONT 09

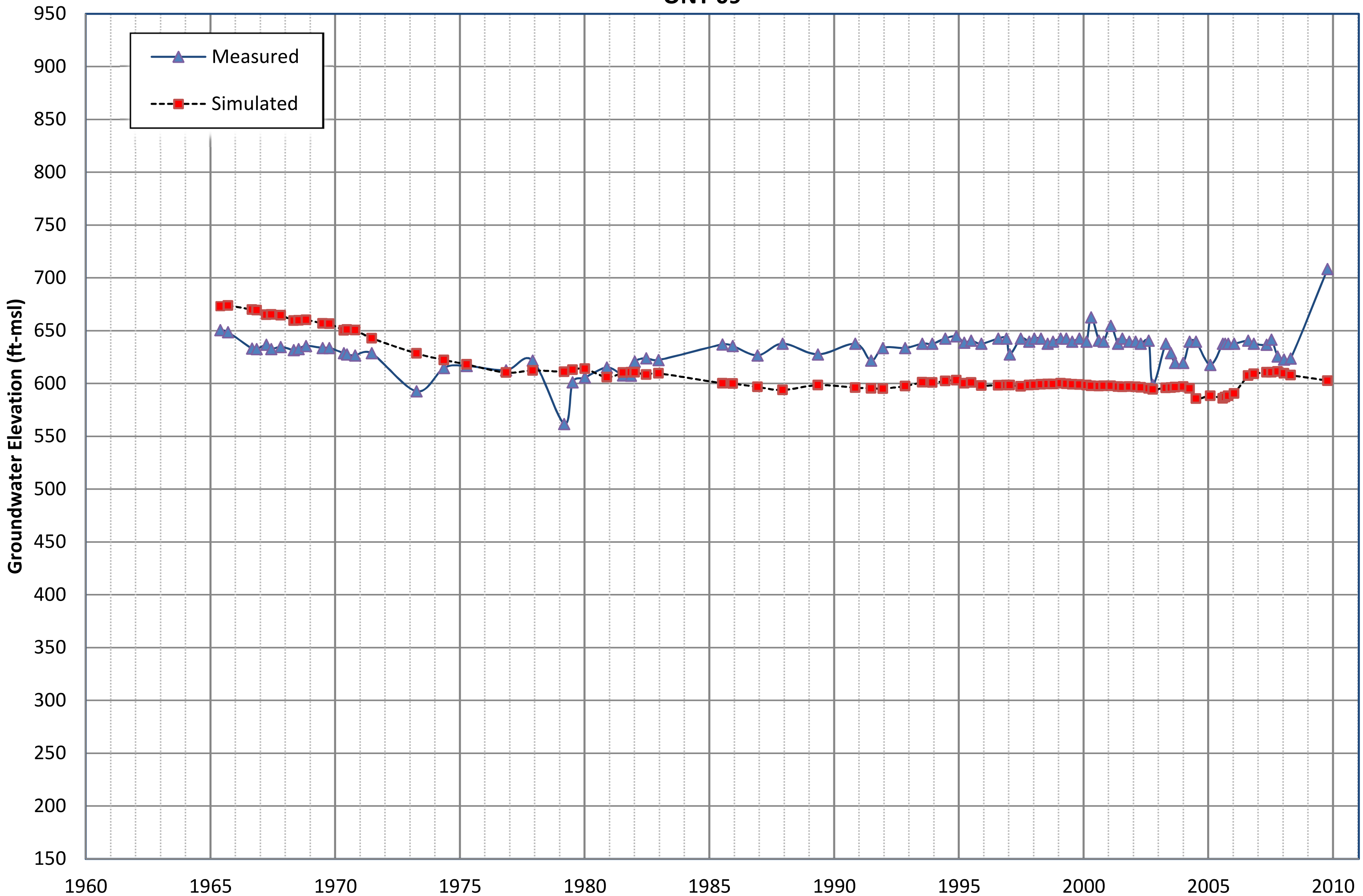

Figure C1-27
Simulated and Measured Groundwater Elevations in the Wells Used in Model Calibration 1961 - 2011
ONT 11

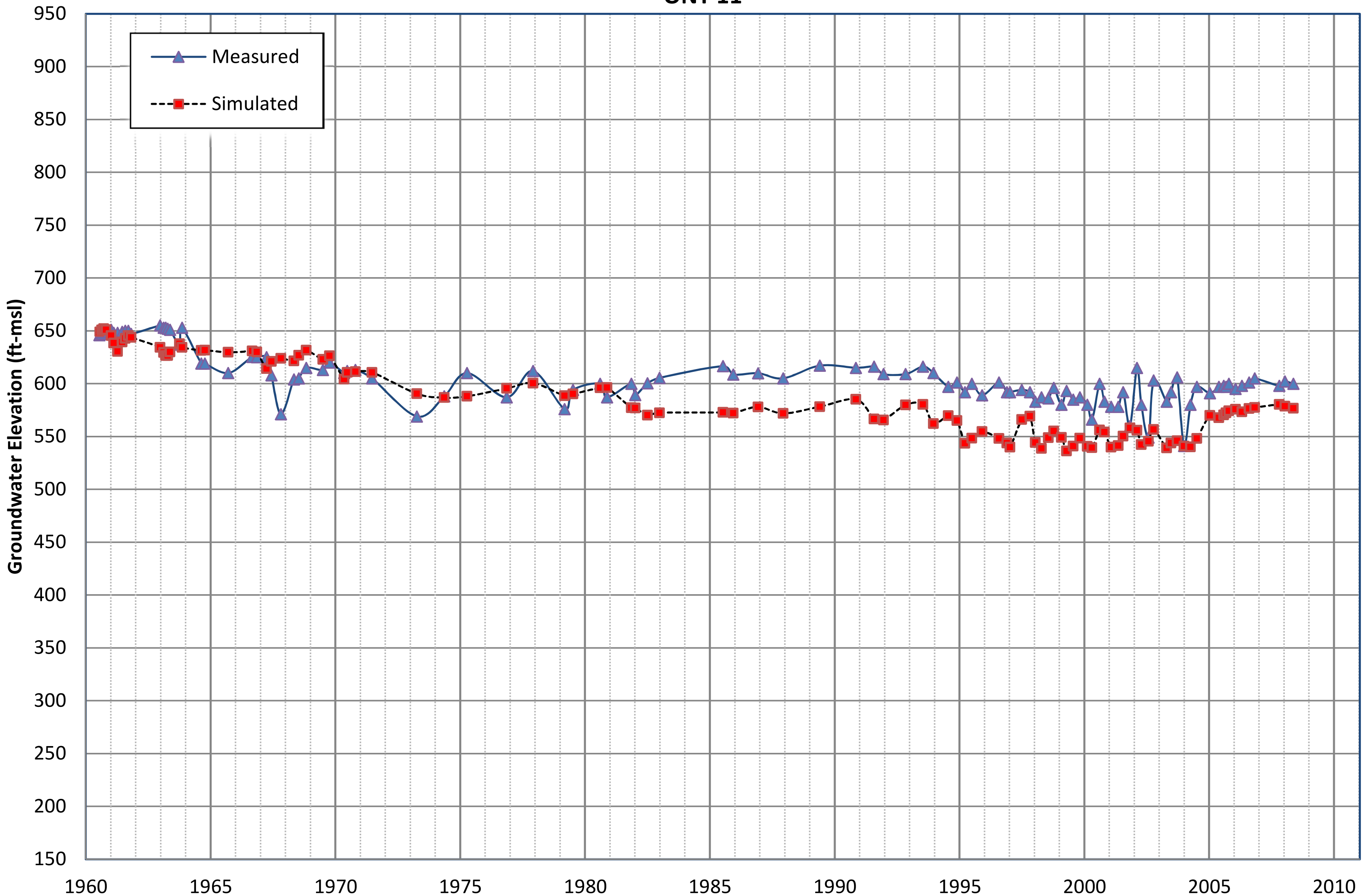

Appendix_C1_20150915_WW_WellHydrograph_calibrationwell_format.xlsm

Figure C1-28
Simulated and Measured Groundwater Elevations in the Wells Used in Model Calibration 1961 - 2011
ONT 20

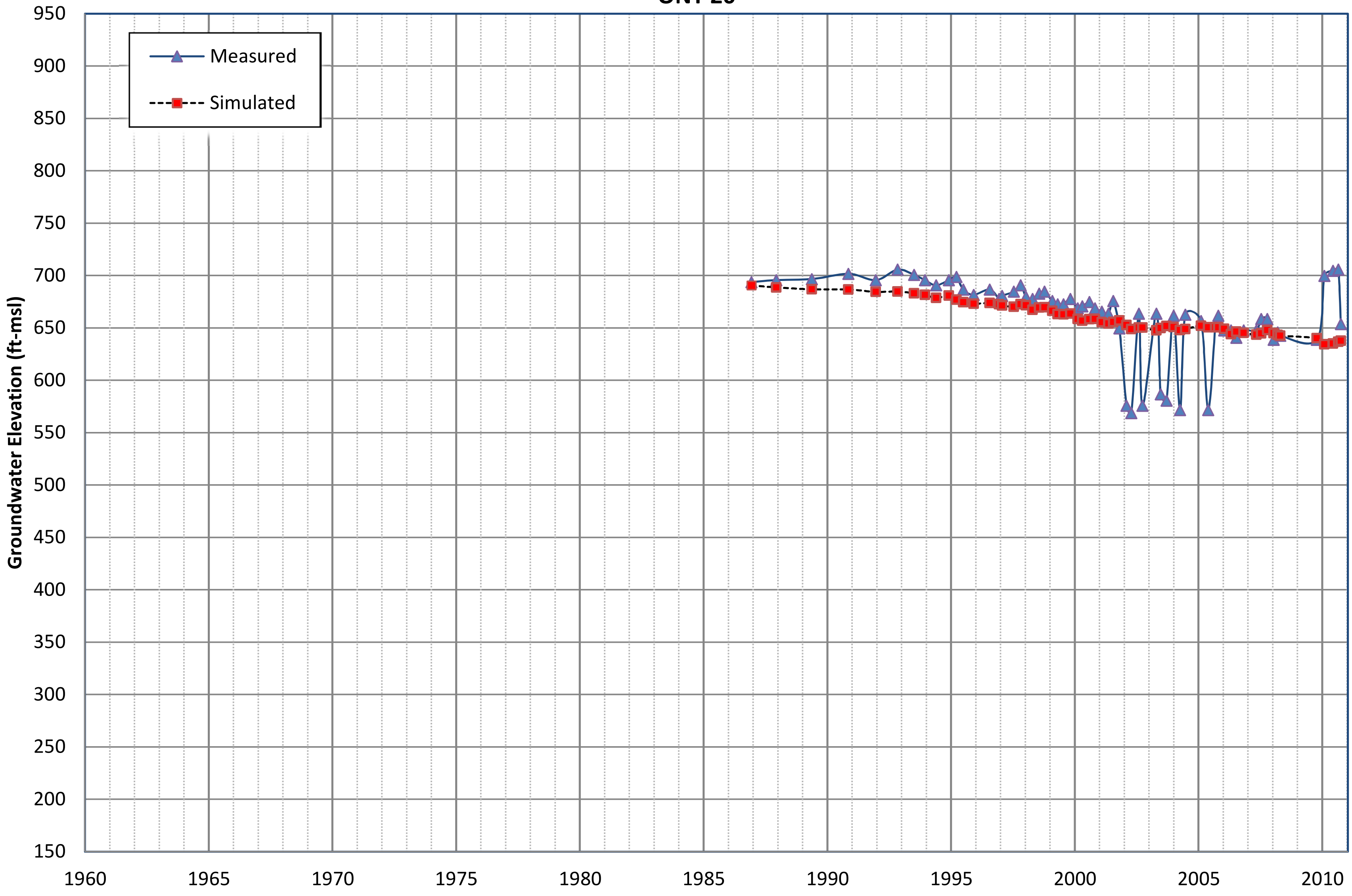

Figure C1-29
Simulated and Measured Groundwater Elevations in the Wells Used in Model Calibration 1961 - 2011
ONT 31

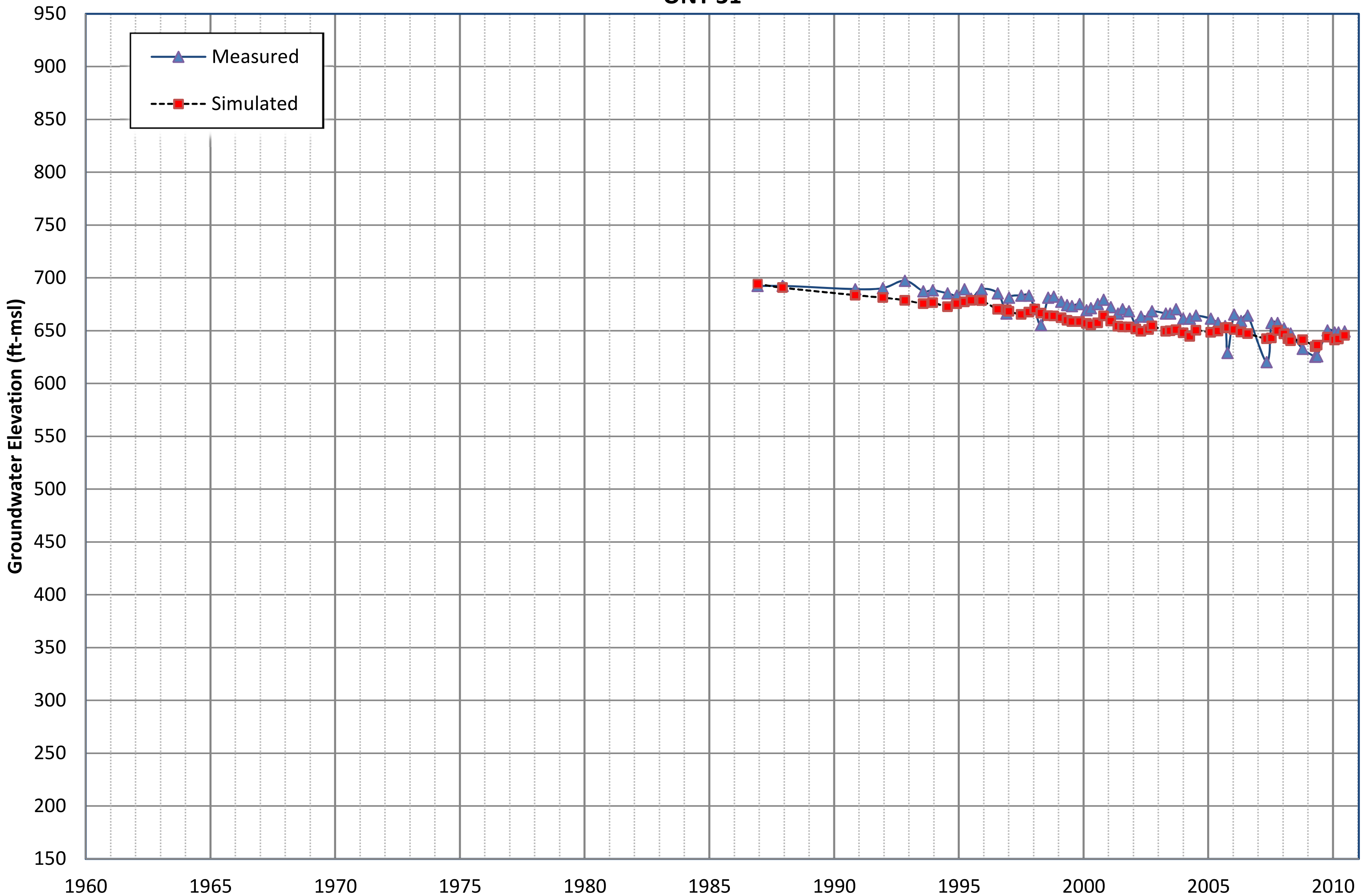

Figure C1-30
Simulated and Measured Groundwater Elevations in the Wells Used in Model Calibration 1961 - 2011
ONT 36

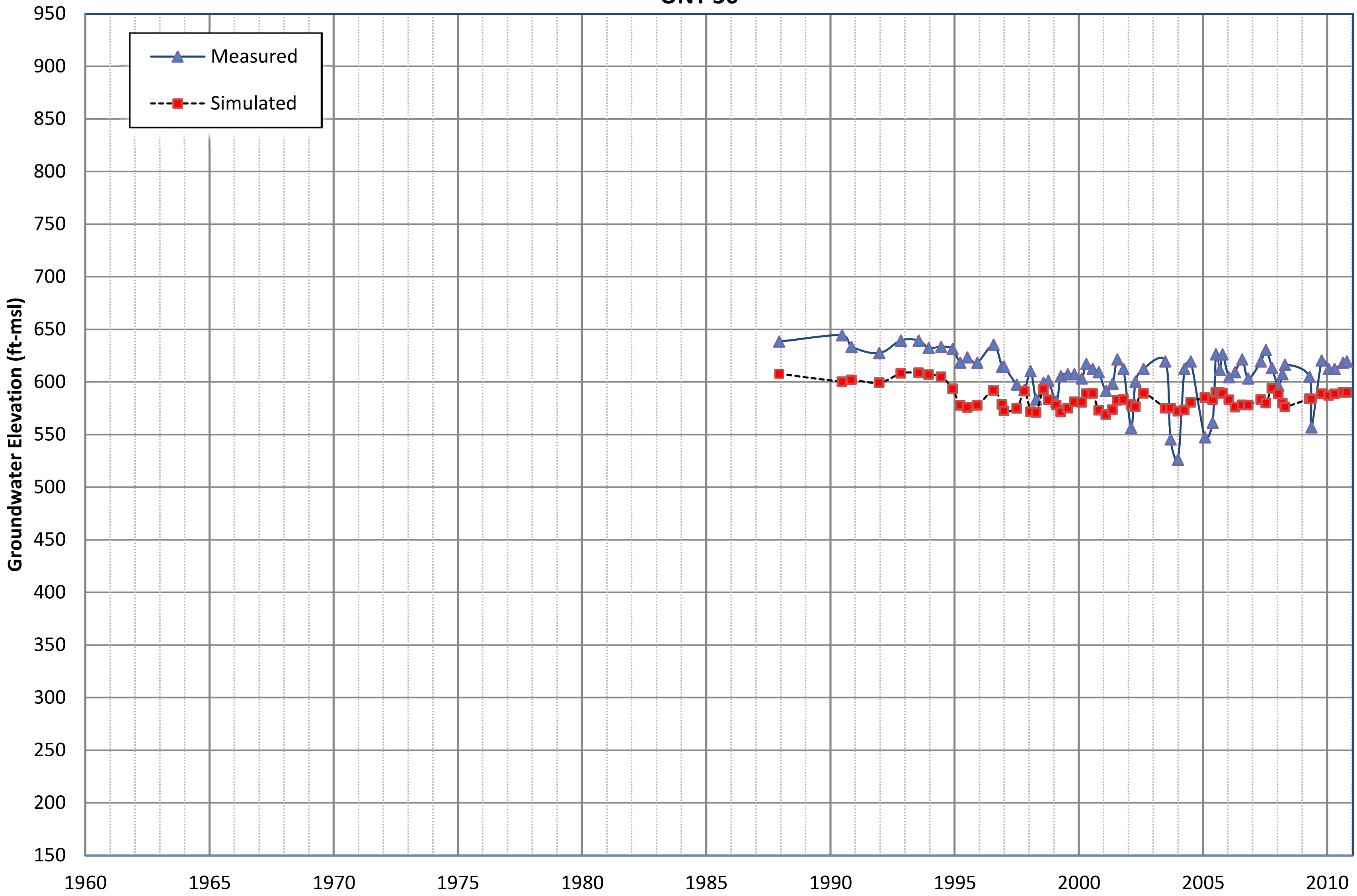

Figure C1-31
Simulated and Measured Groundwater Elevations in the Wells Used in Model Calibration 1961 - 2011
P 16

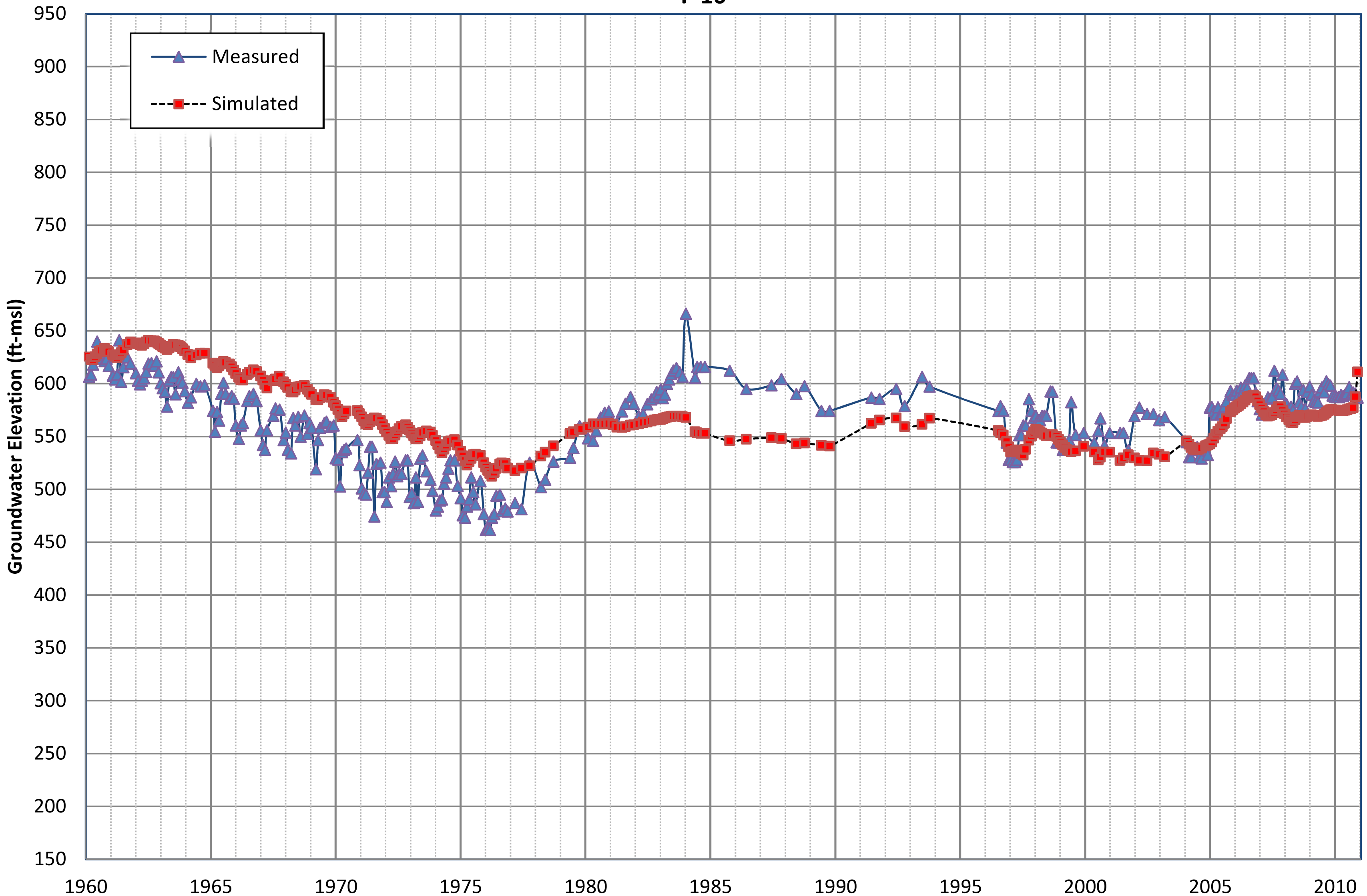

Figure C1-32
Simulated and Measured Groundwater Elevations in the Wells Used in Model Calibration 1961 - 2011
P 24 (OLD)

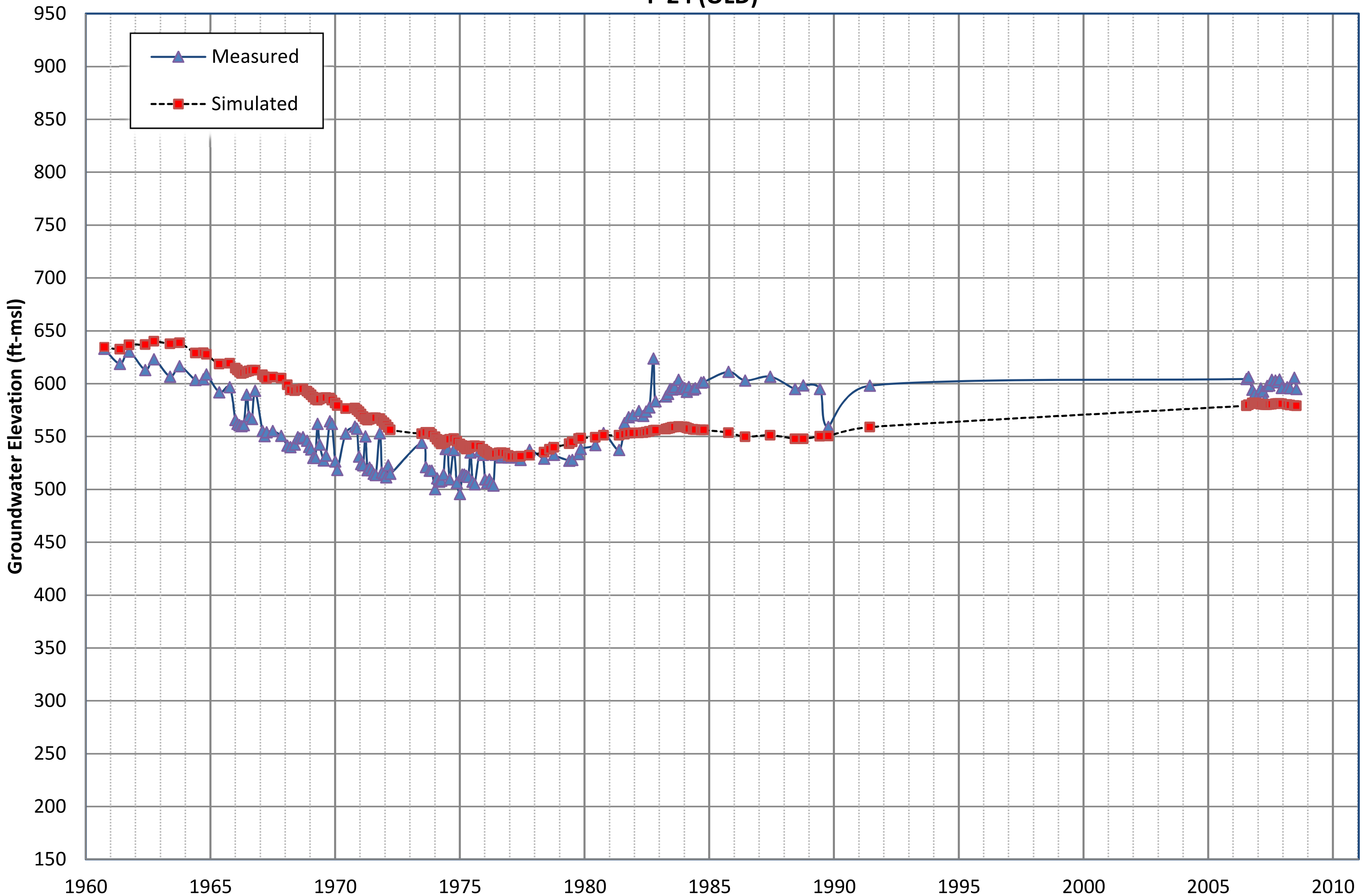

Appendix_C1_20150915_WW_WellHydrograph_calibrationwell_format.xlsm

Figure C1-33
Simulated and Measured Groundwater Elevations in the Wells Used in Model Calibration 1961 - 2011
P 29

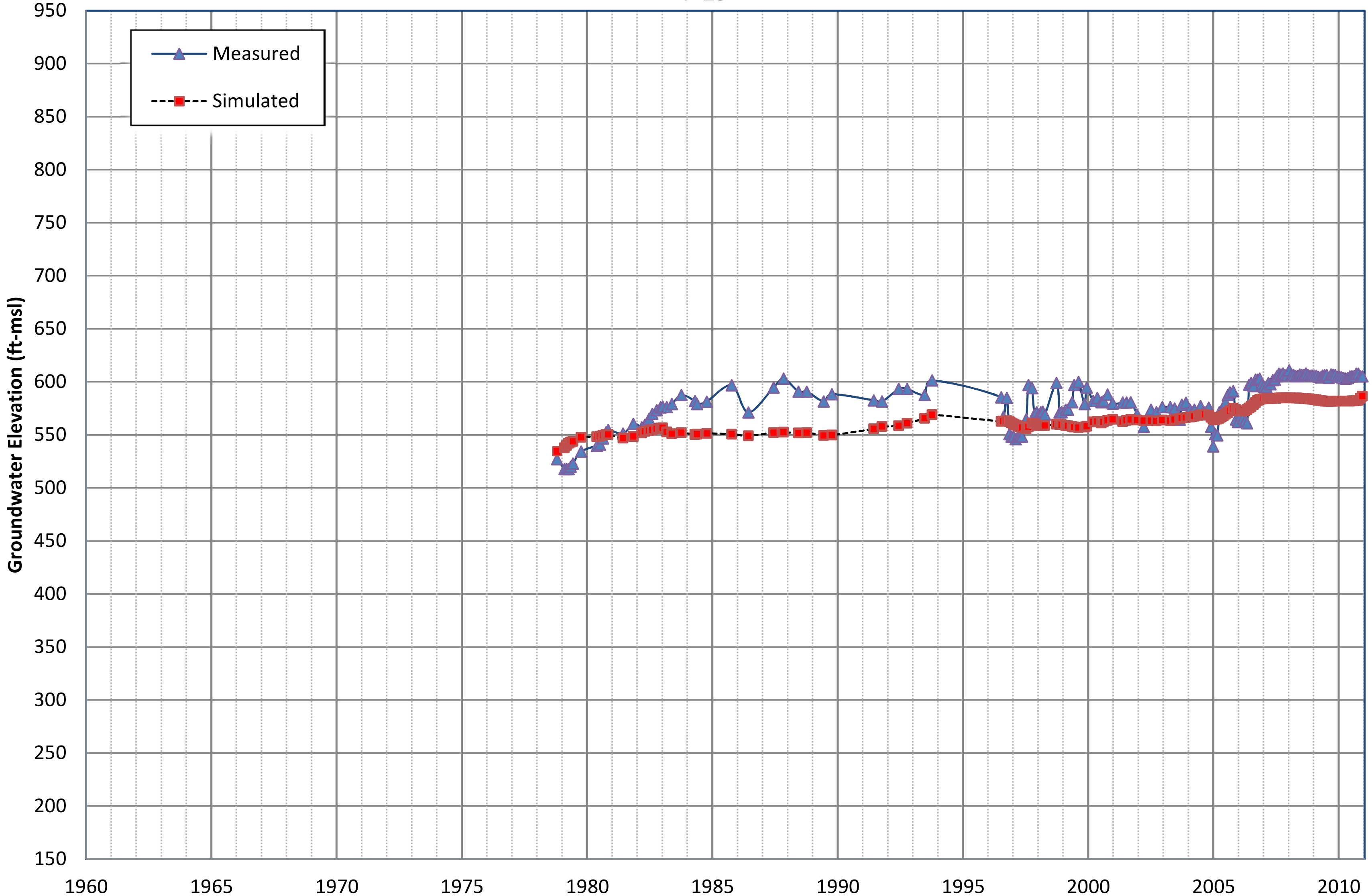

Figure C1-34
Simulated and Measured Groundwater Elevations in the Wells Used in Model Calibration 1961 - 2011
MIL M-03

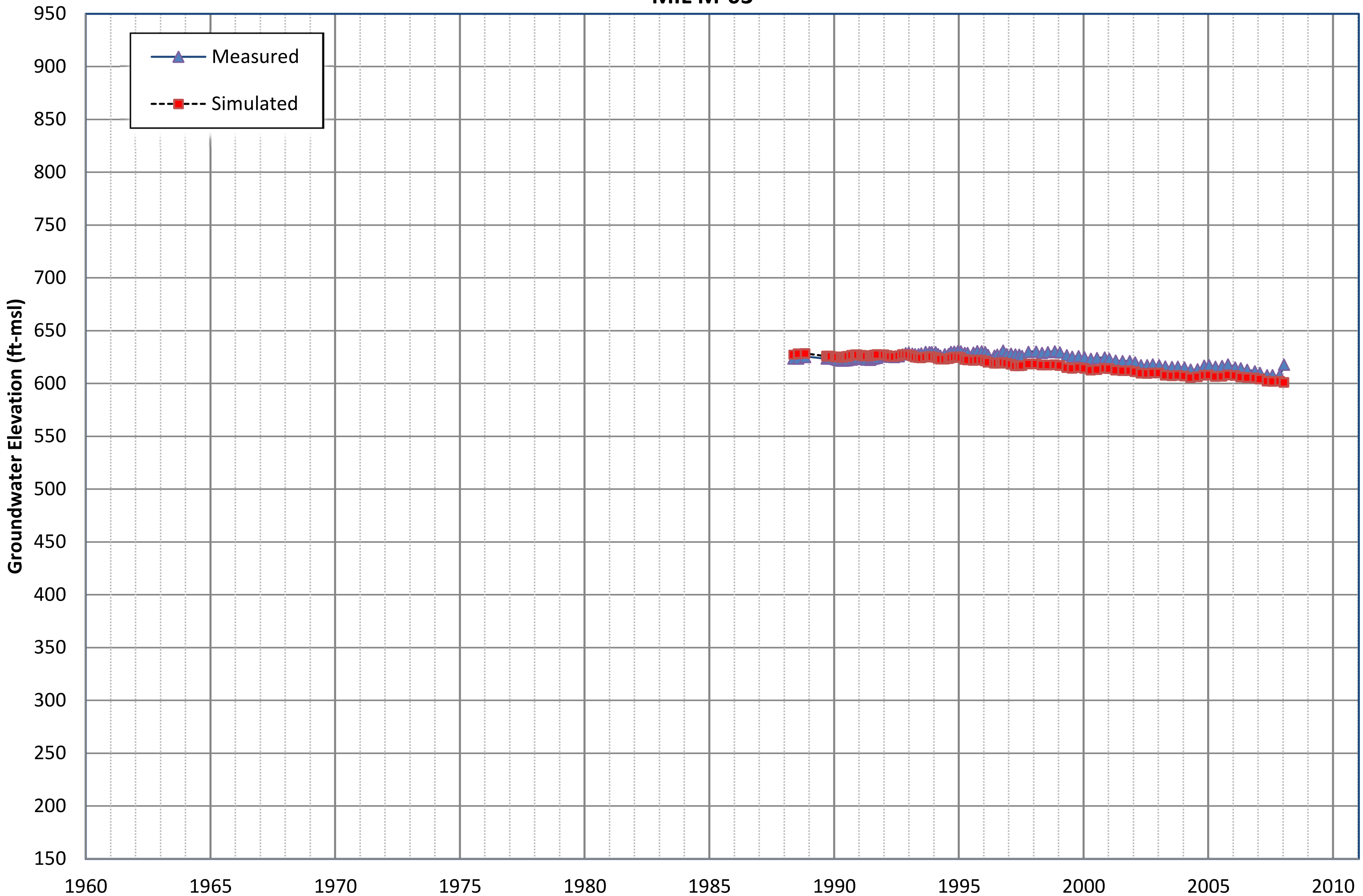

Figure C1-35
Simulated and Measured Groundwater Elevations in the Wells Used in Model Calibration 1961 - 2011
CVWD 3

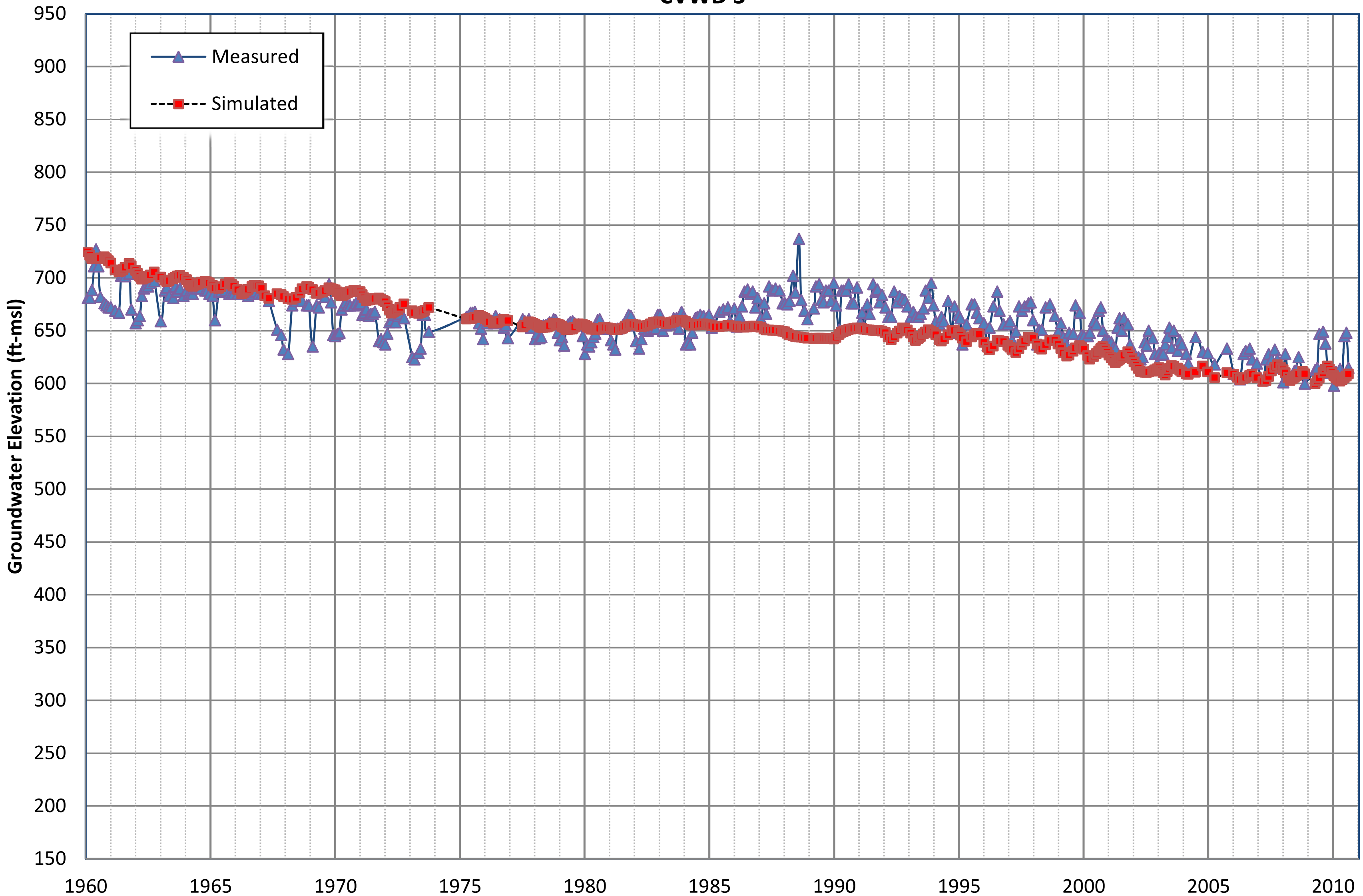

Figure C1-36
Simulated and Measured Groundwater Elevations in the Wells Used in Model Calibration 1961 - 2011
CVWD 35

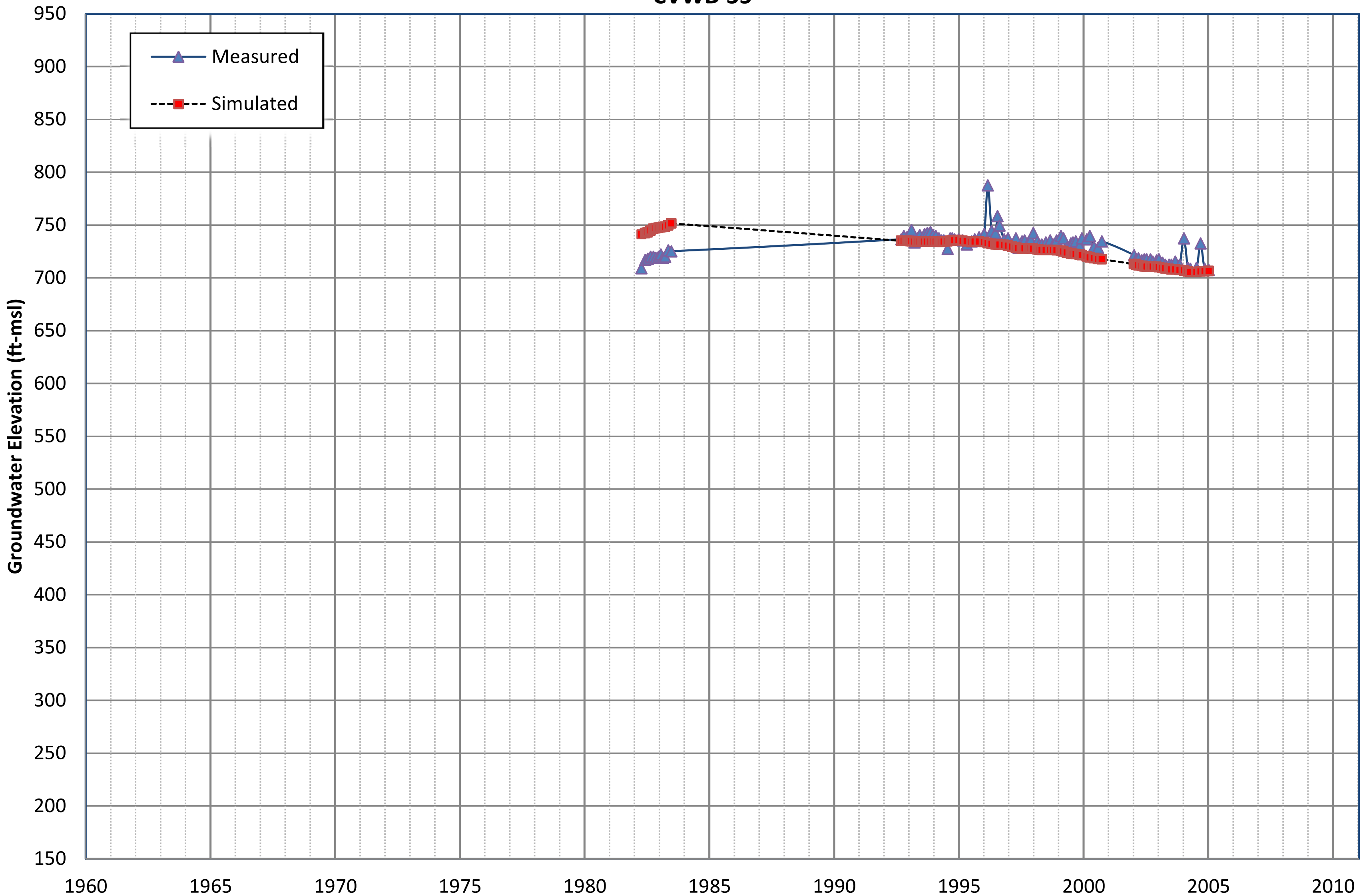

Figure C1-37
Simulated and Measured Groundwater Elevations in the Wells Used in Model Calibration 1961 - 2011
F21A

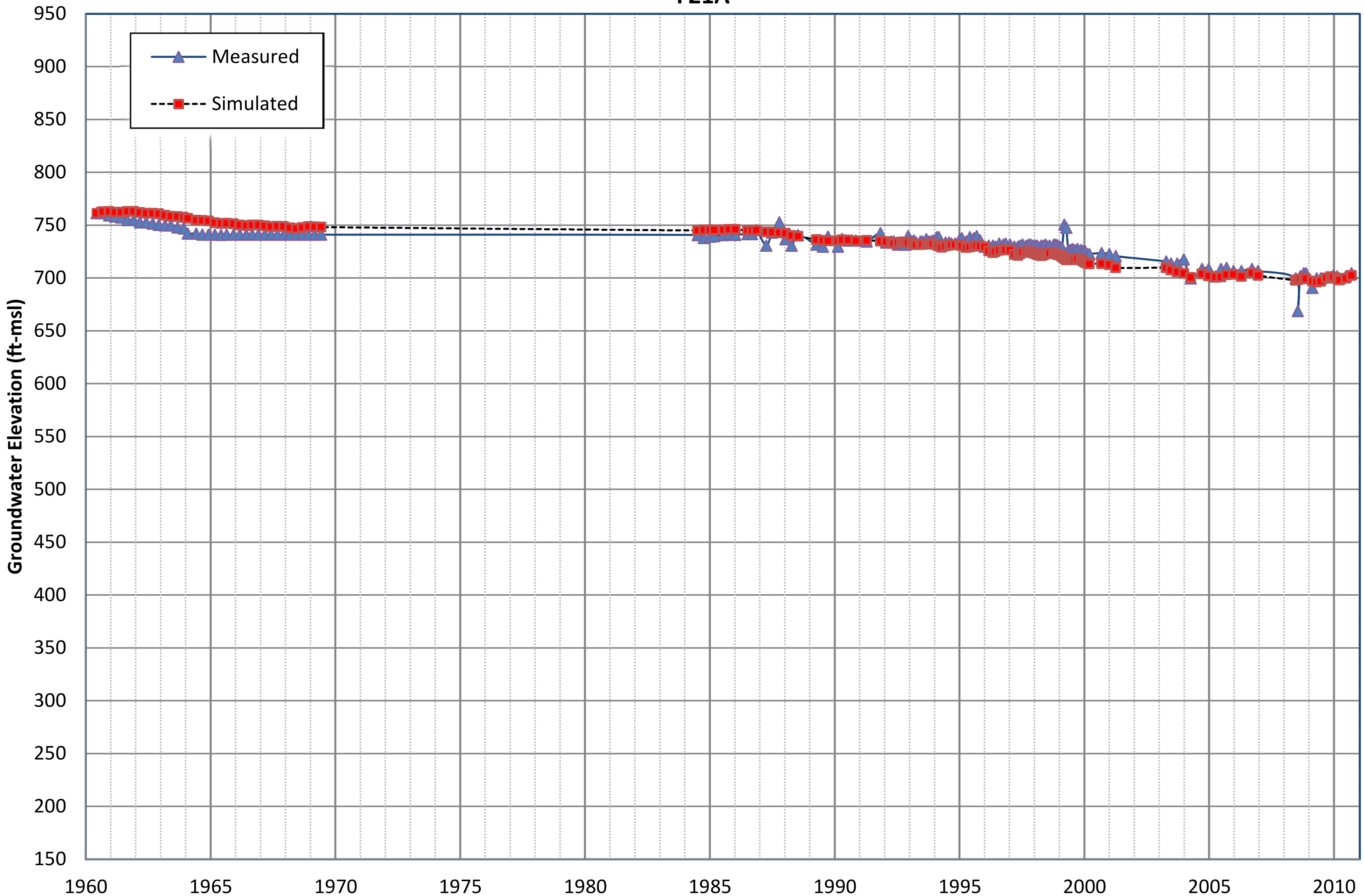

Appendix_C1_20150915_WW_WellHydrograph_calibrationwell_format.xlsm

Figure C1-38
Simulated and Measured Groundwater Elevations in the Wells Used in Model Calibration 1961 - 2011
F30A

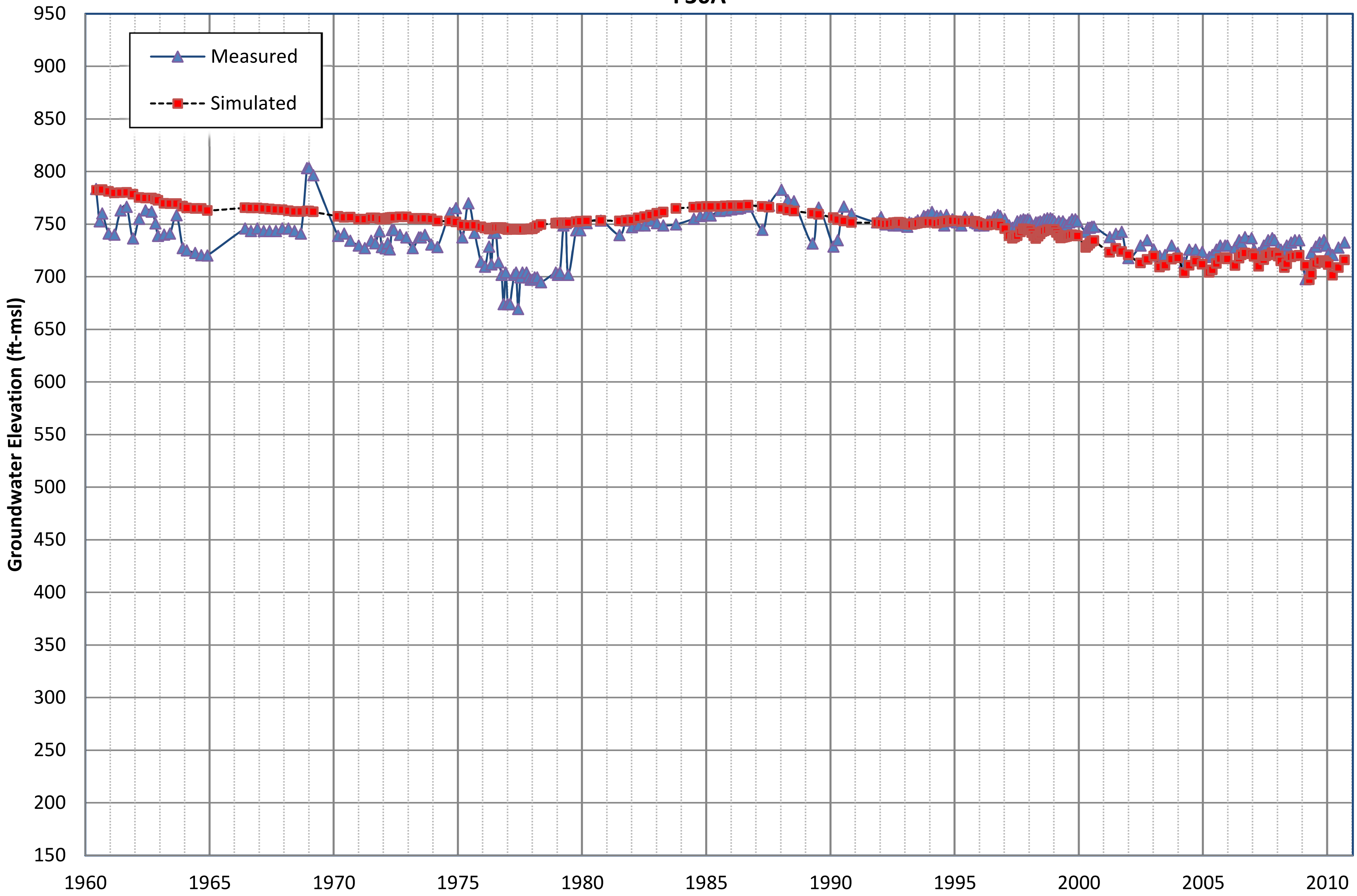

Appendix_C1_20150915_WW_WellHydrograph_calibrationwell_format.xlsm

Figure C1-39
Simulated and Measured Groundwater Elevations in the Wells Used in Model Calibration 1961 - 2011
F31A

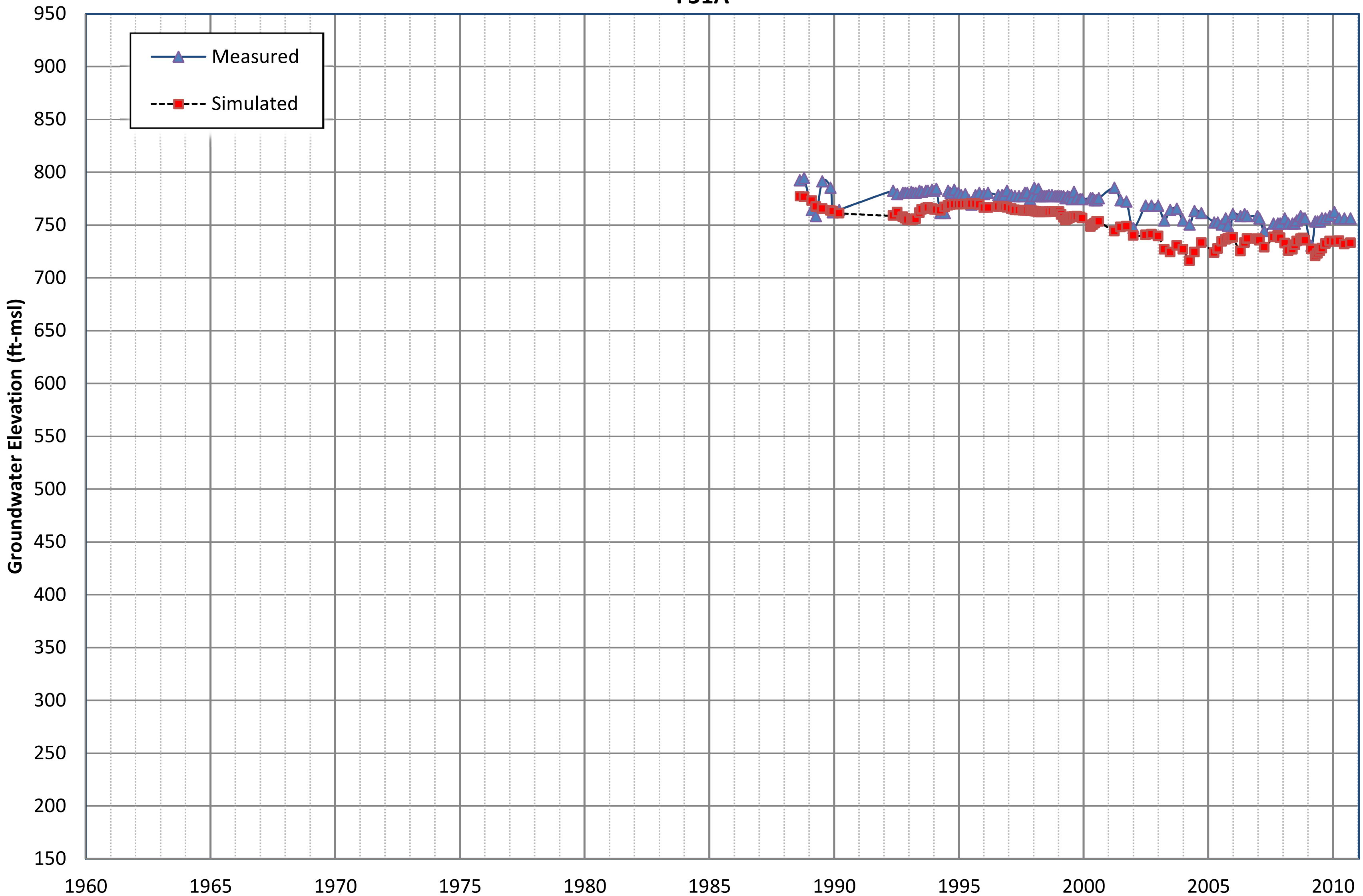

Figure C1-40
Simulated and Measured Groundwater Elevations in the Wells Used in Model Calibration 1961 - 2011
F35A

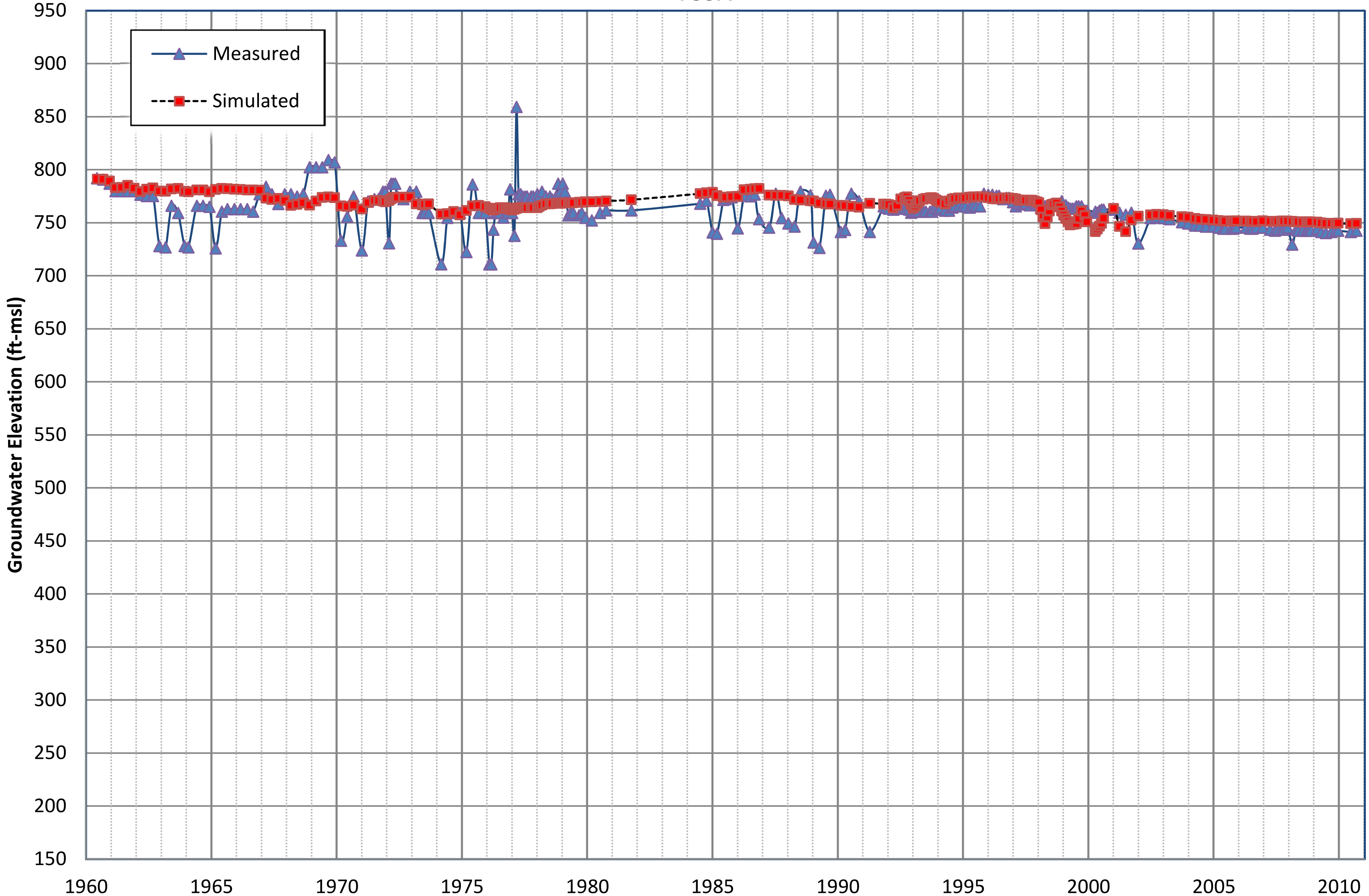

Figure C1-41
Simulated and Measured Groundwater Elevations in the Wells Used in Model Calibration 1961 - 2011
FU28

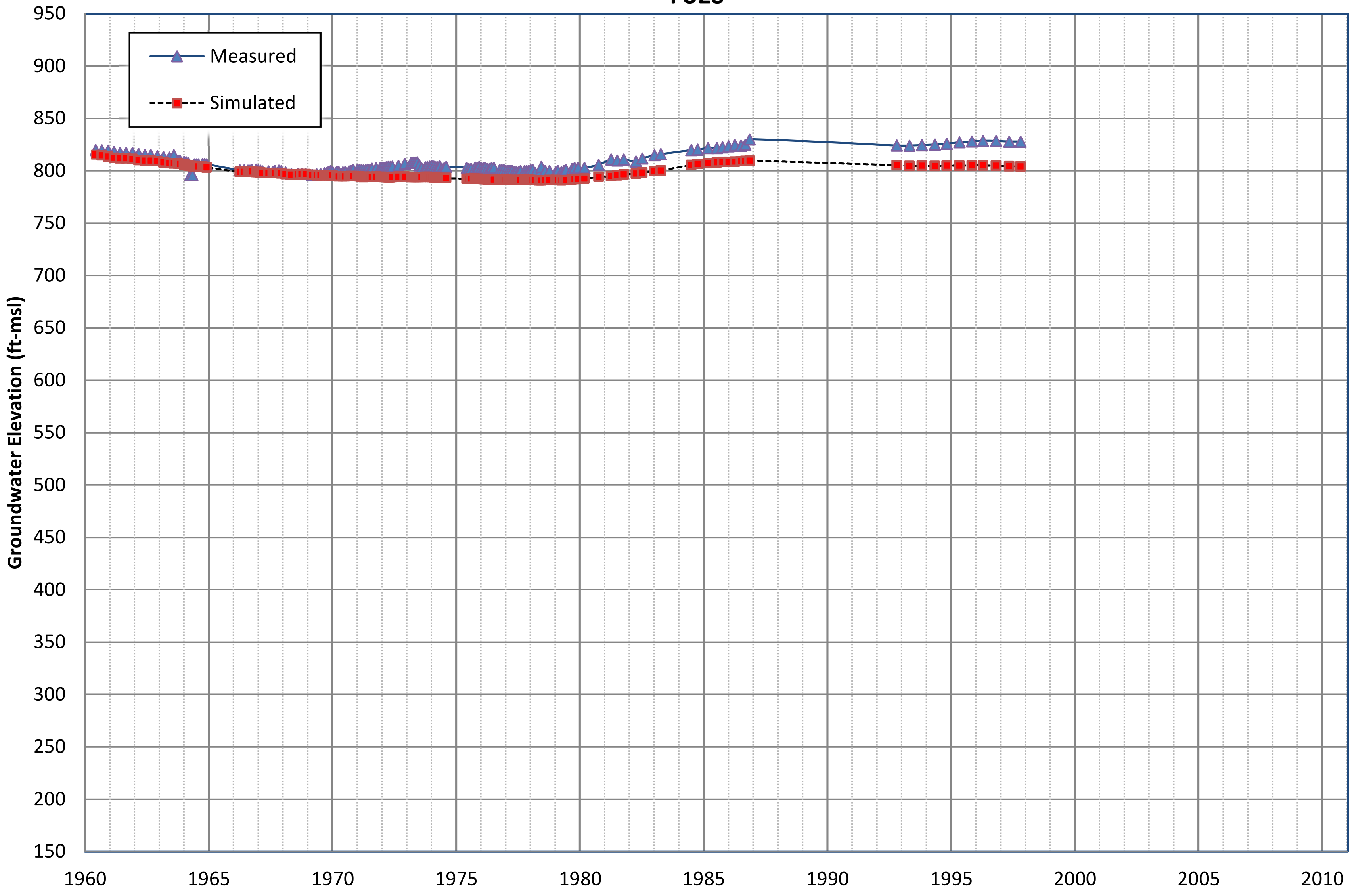

Figure C1-42
Simulated and Measured Groundwater Elevations in the Wells Used in Model Calibration 1961 - 2011
FU6

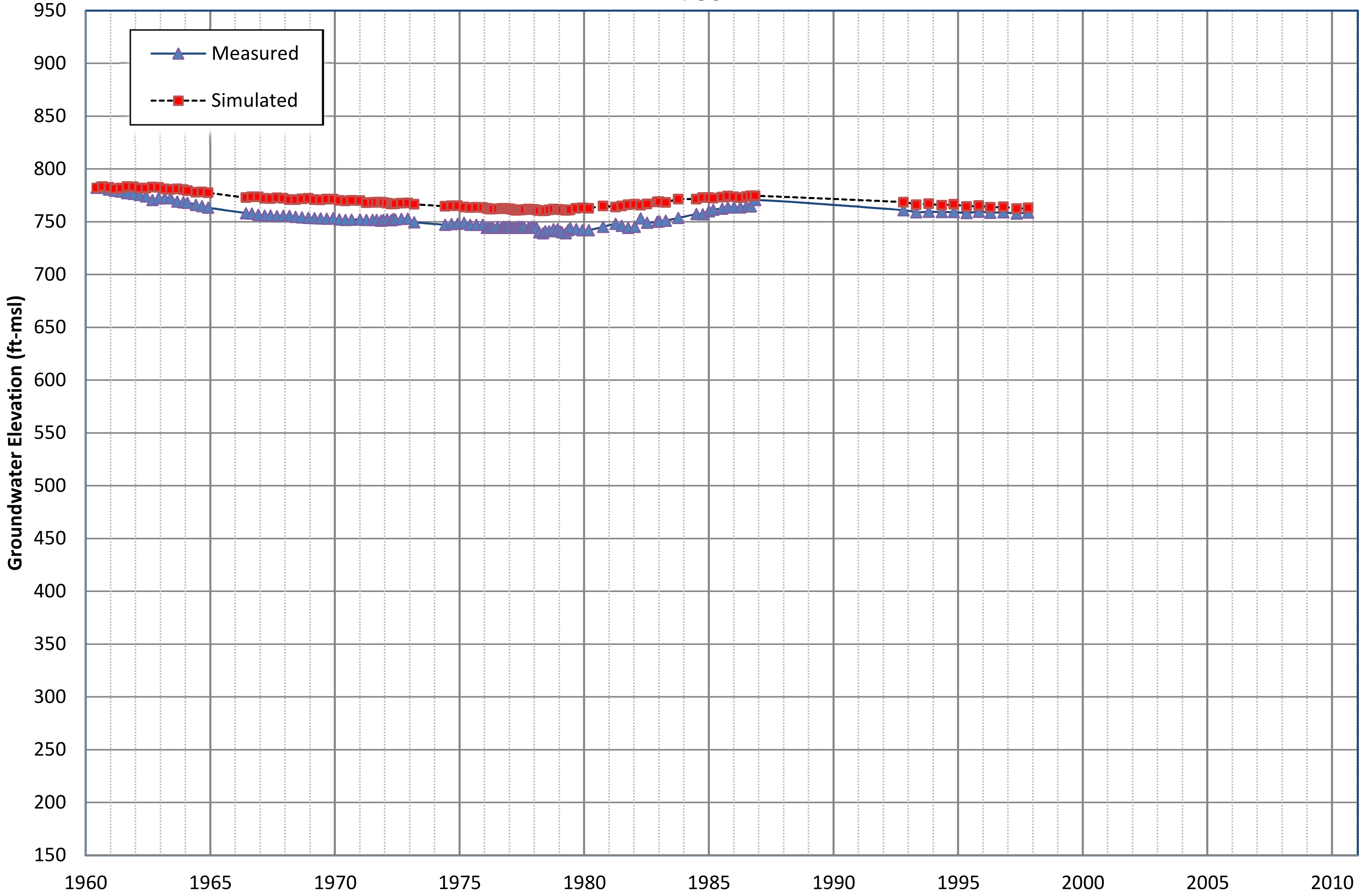

Appendix_C1_20150915_WW_WellHydrograph_calibrationwell_format.xlsm

Figure C1-43
Simulated and Measured Groundwater Elevations in the Wells Used in Model Calibration 1961 - 2011
GE MW-11

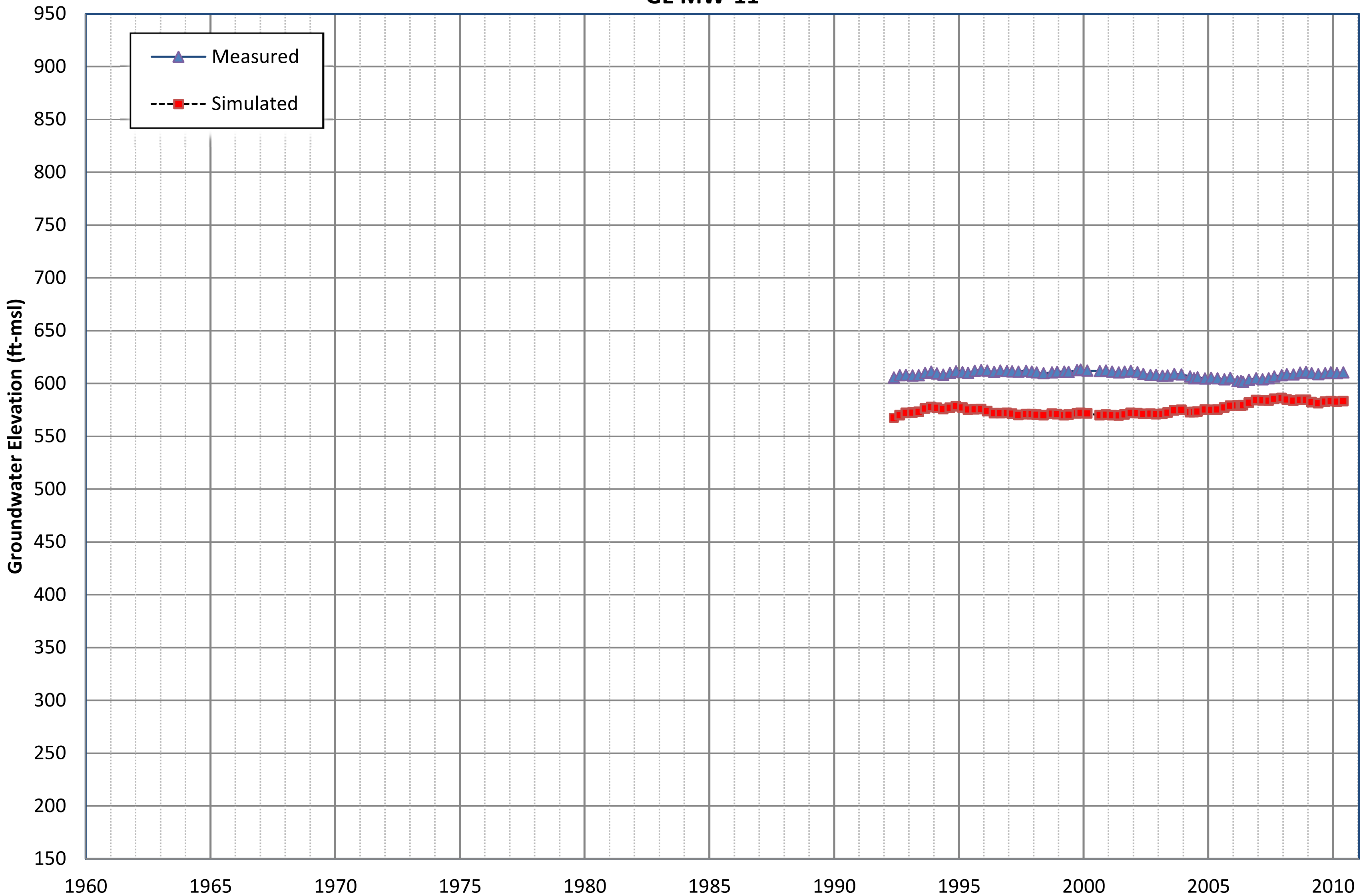

Figure C1-44
Simulated and Measured Groundwater Elevations in the Wells Used in Model Calibration 1961 - 2011
GSWC Margarita 1

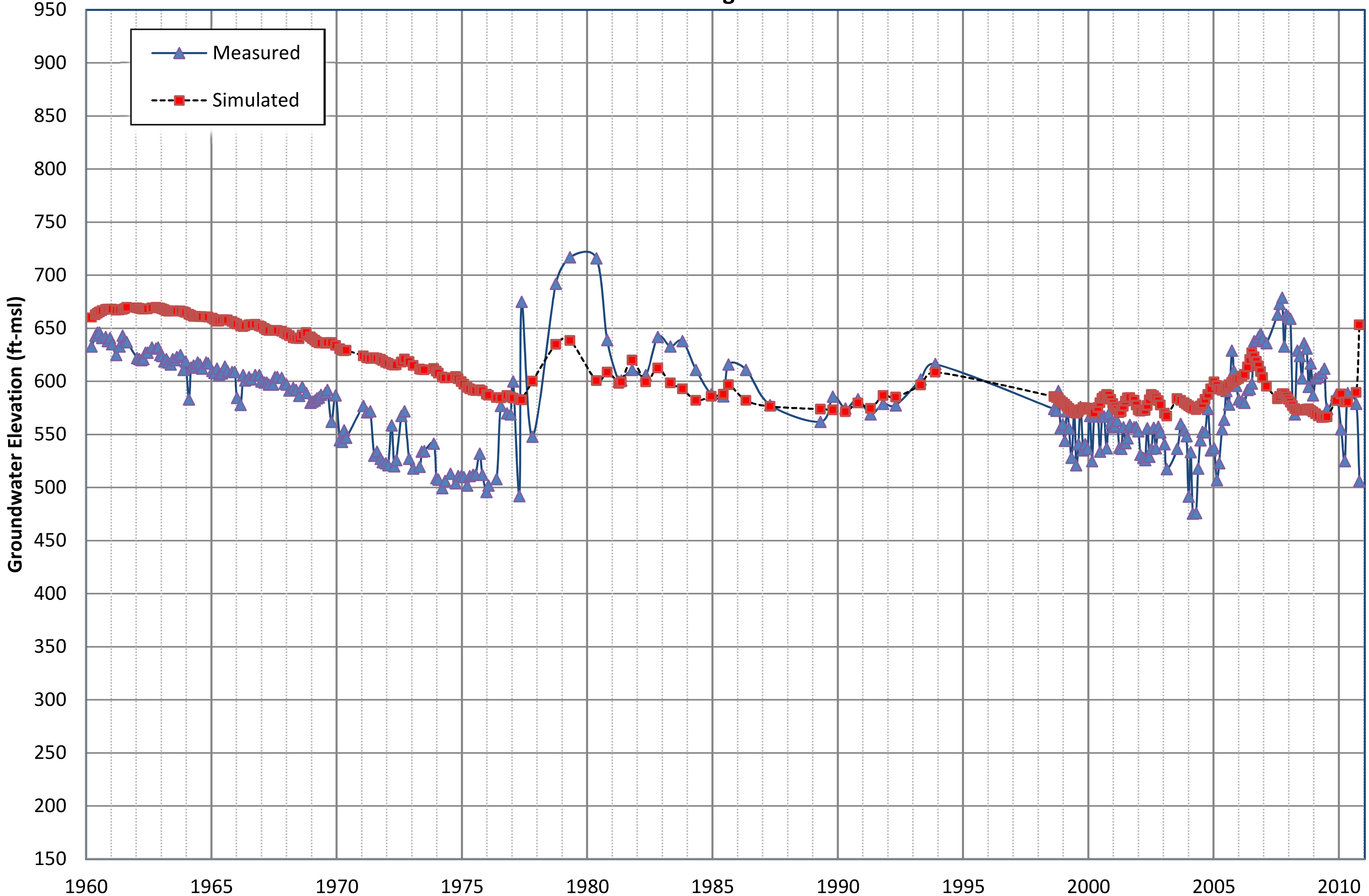

Appendix_C1_20150915_WW_WellHydrograph_calibrationwell_format.xlsm

Figure C1-45
Simulated and Measured Groundwater Elevations in the Wells Used in Model Calibration 1961 - 2011
PW 3

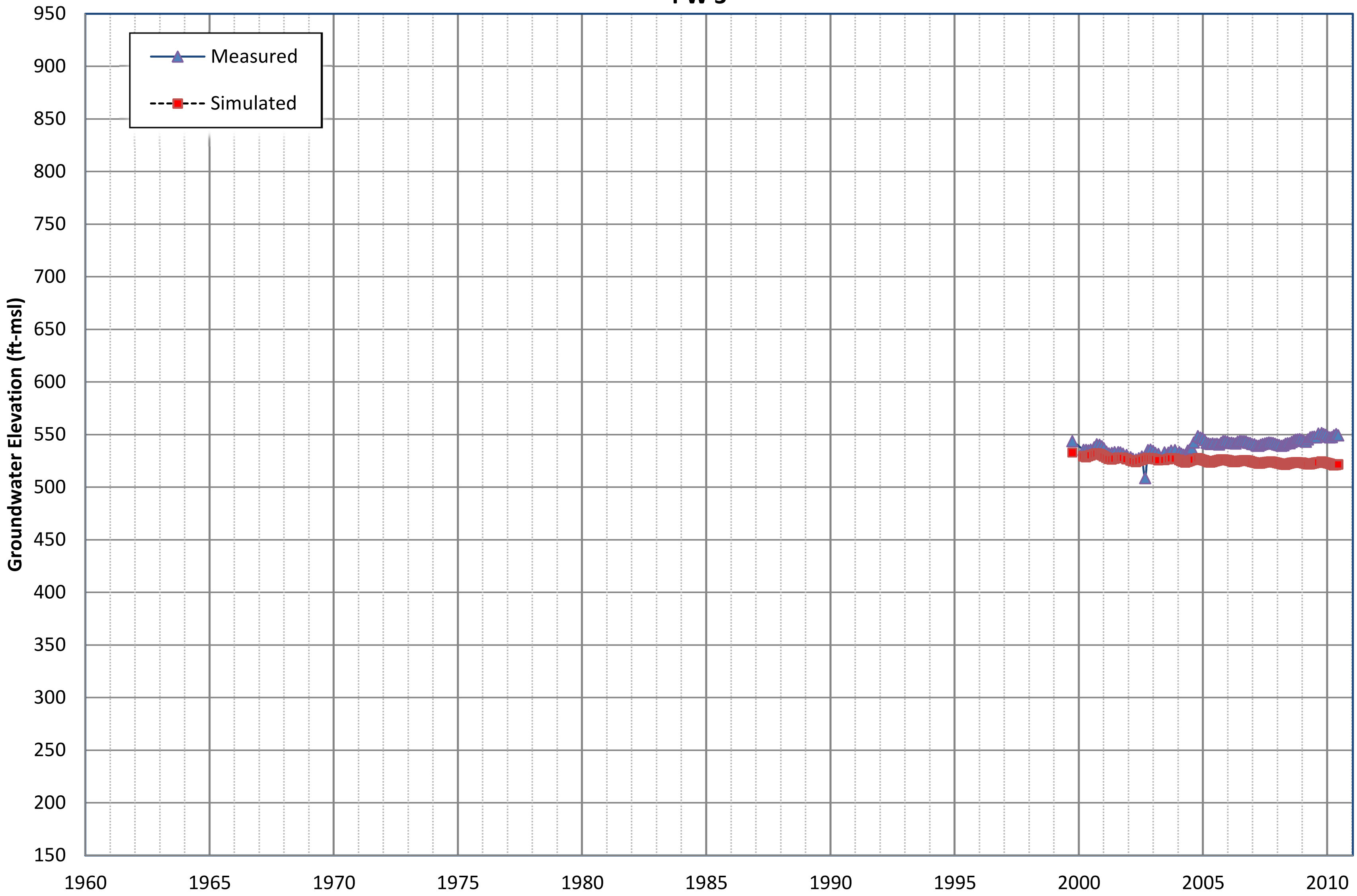

Appendix_C1_20150915_WW_WellHydrograph_calibrationwell_format.xlsm

Figure C1-46
Simulated and Measured Groundwater Elevations in the Wells Used in Model Calibration 1961 - 2011
IEUA MW-2

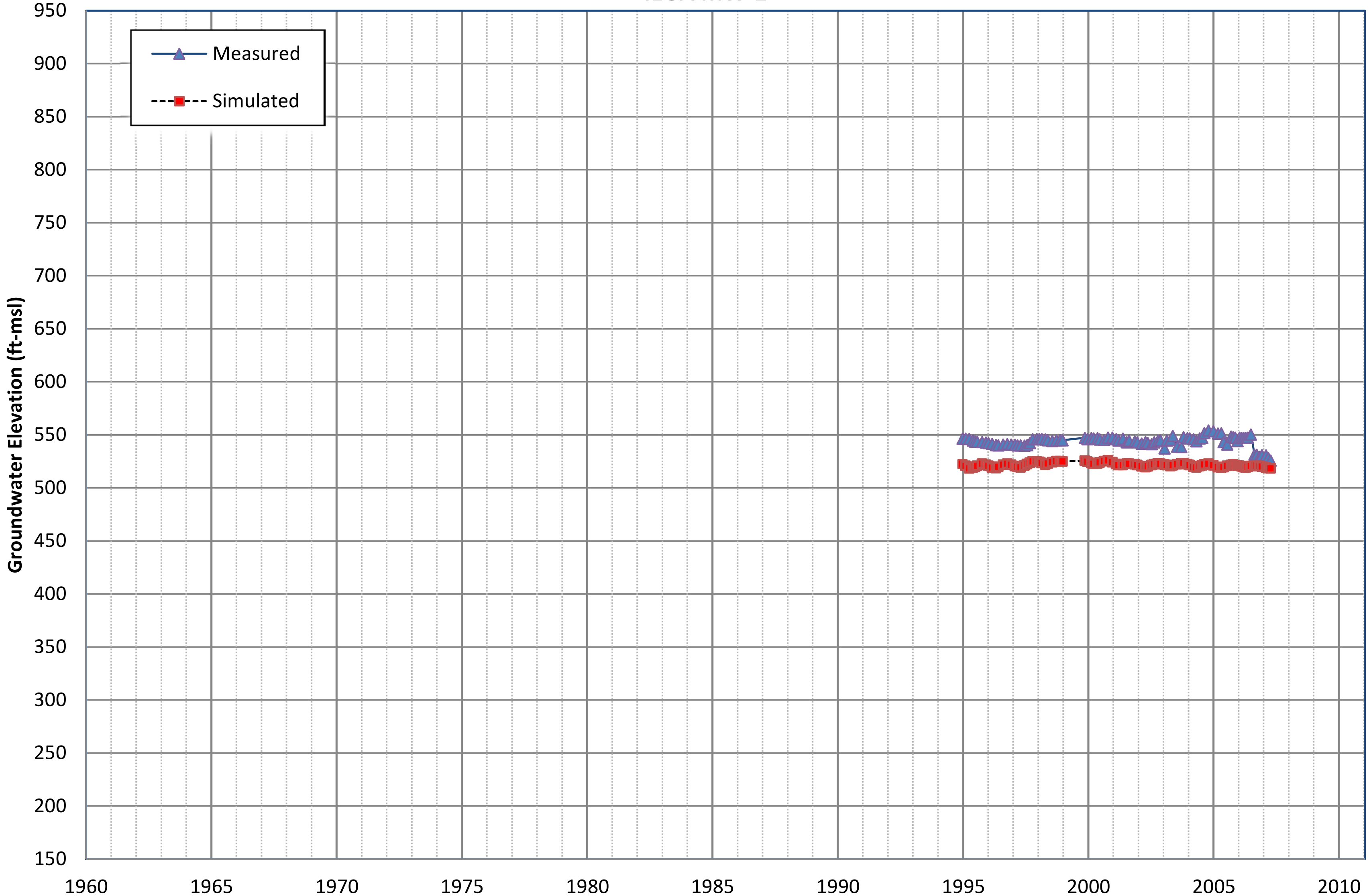

Appendix_C1_20150915_WW_WellHydrograph_calibrationwell_format.xlsm

Figure C1-47
Simulated and Measured Groundwater Elevations in the Wells Used in Model Calibration 1961 - 2011
JCSD 16

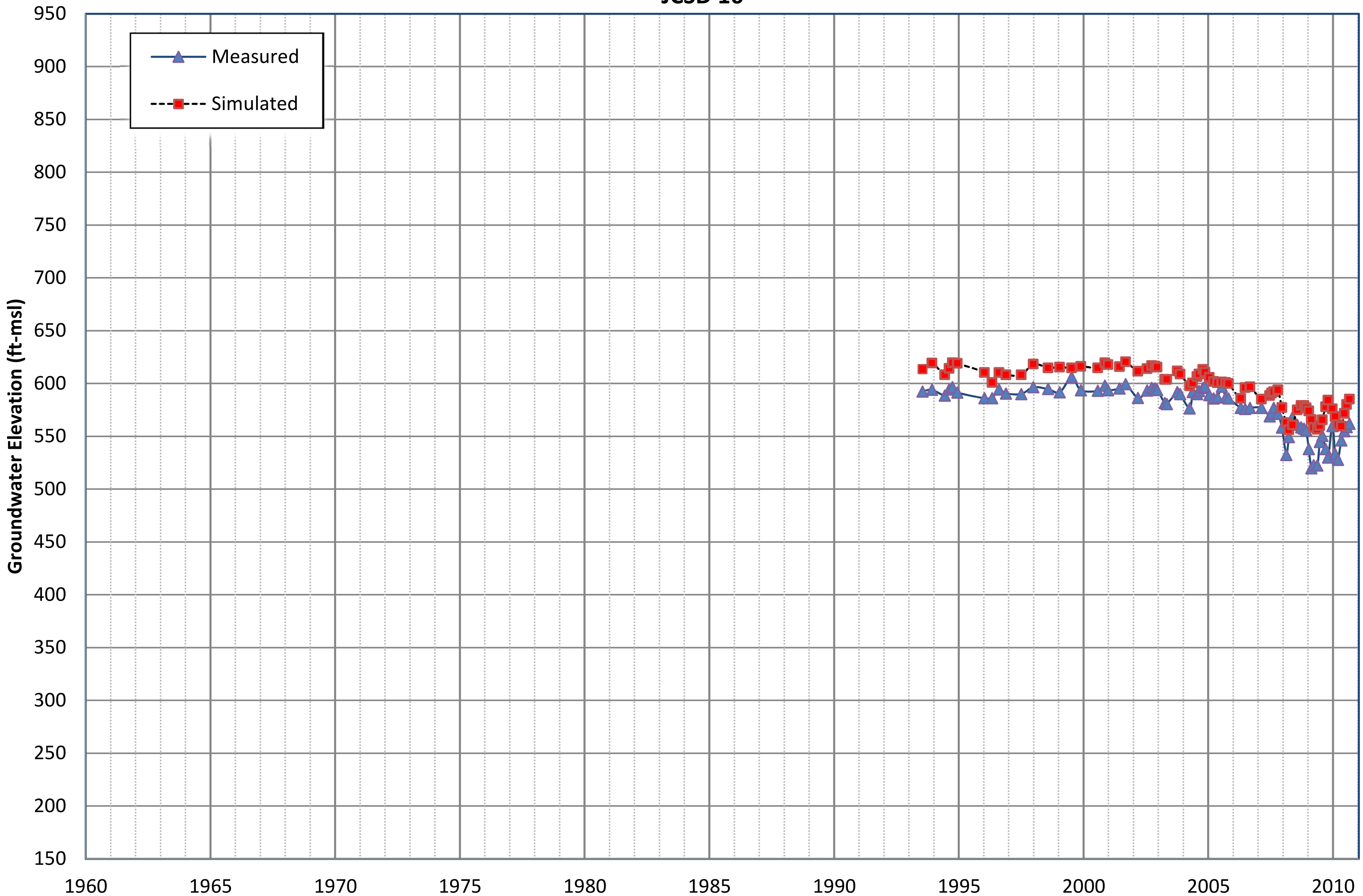

Figure C1-48
Simulated and Measured Groundwater Elevations in the Wells Used in Model Calibration 1961 - 2011
PW 7

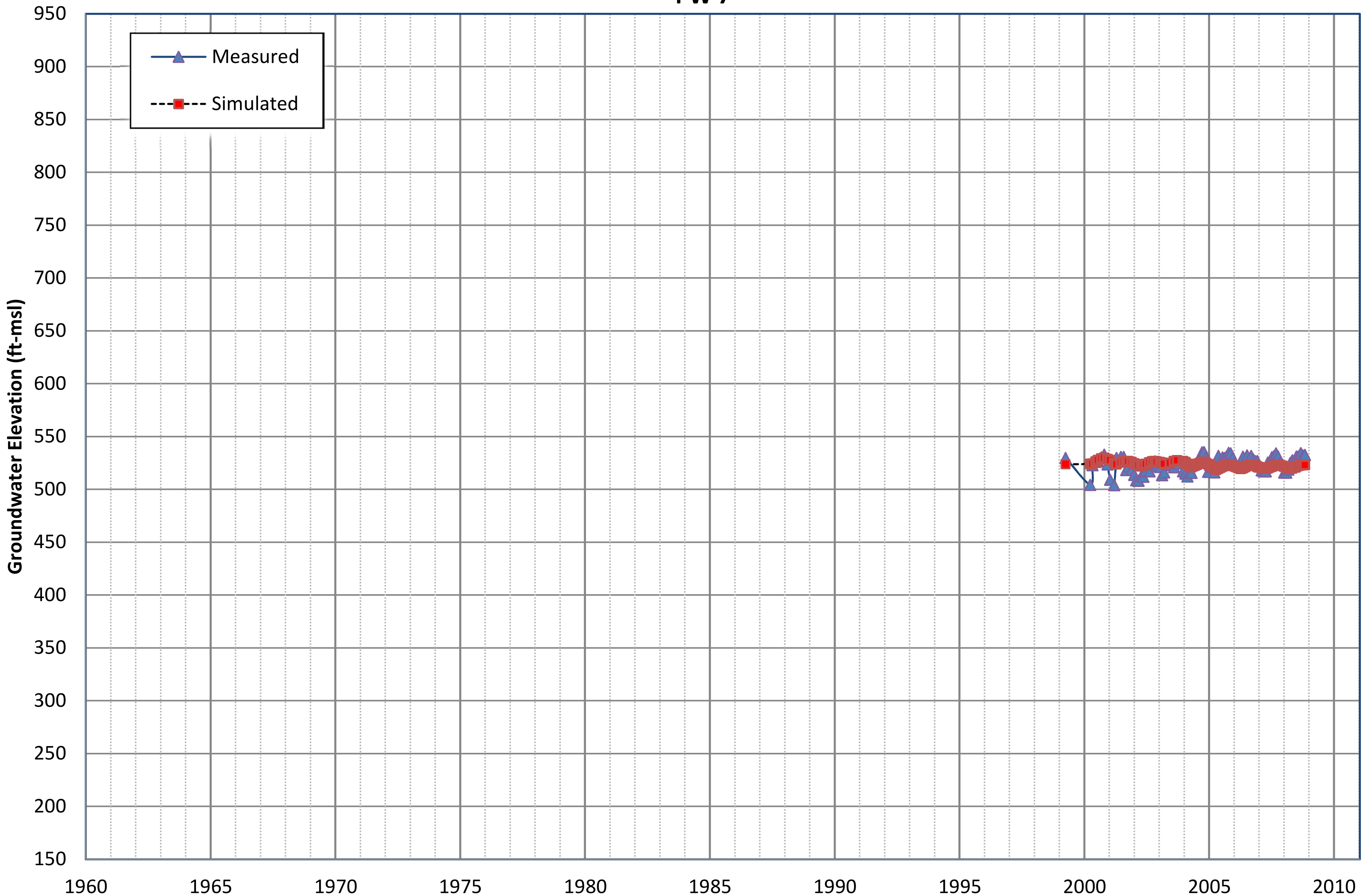

Appendix_C1_20150915_WW_WellHydrograph_calibrationwell_format.xlsm

Figure C1-49

Simulated and Measured Groundwater Elevations in the Wells Used in Model Calibration 1961 - 2011

PW 5

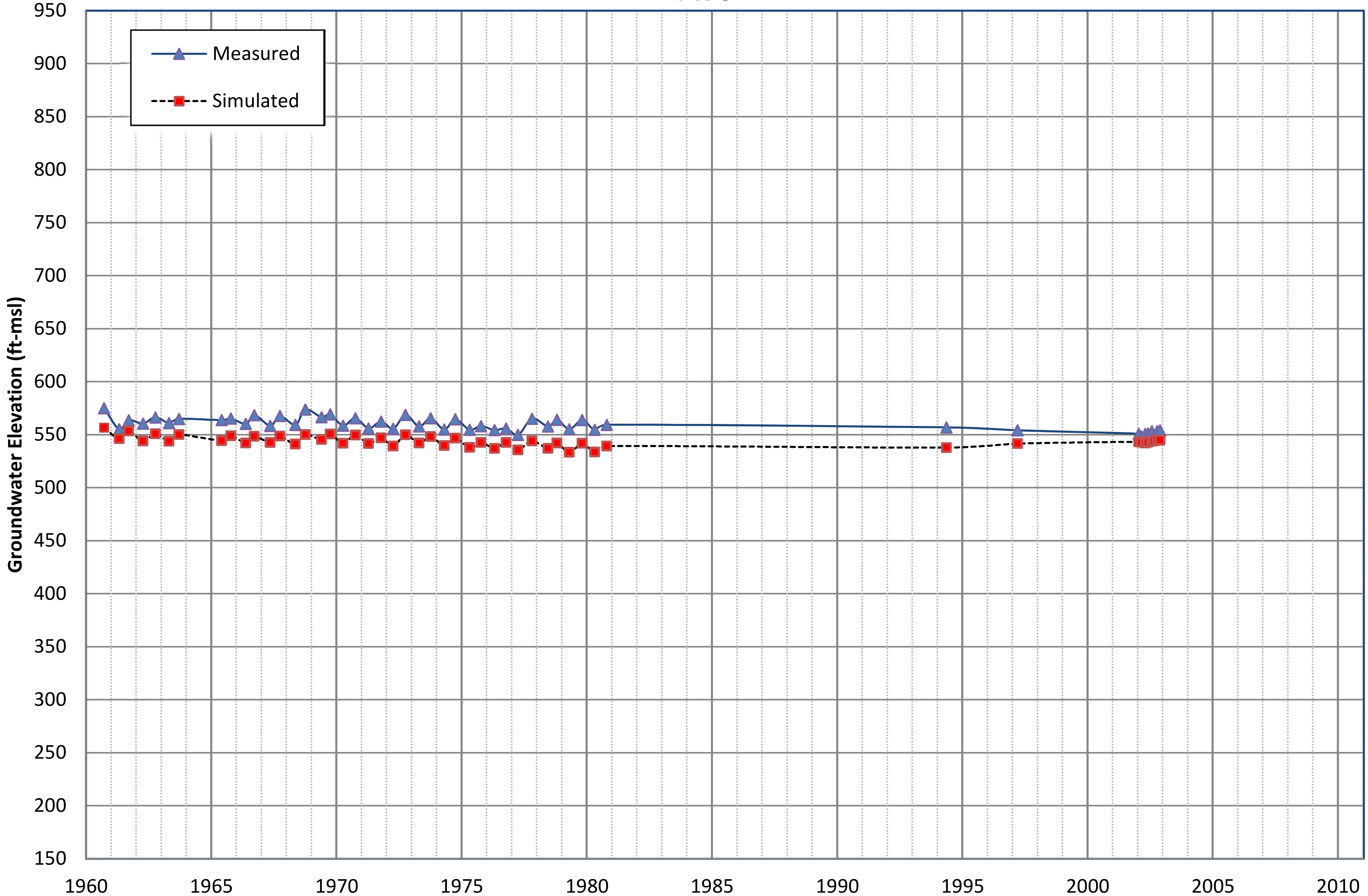

Appendix_C1_20150915_WW_WellHydrograph_calibrationwell_format.xlsm

Figure C1-50
Simulated and Measured Groundwater Elevations in the Wells Used in Model Calibration 1961 - 2011
Corona CG-1

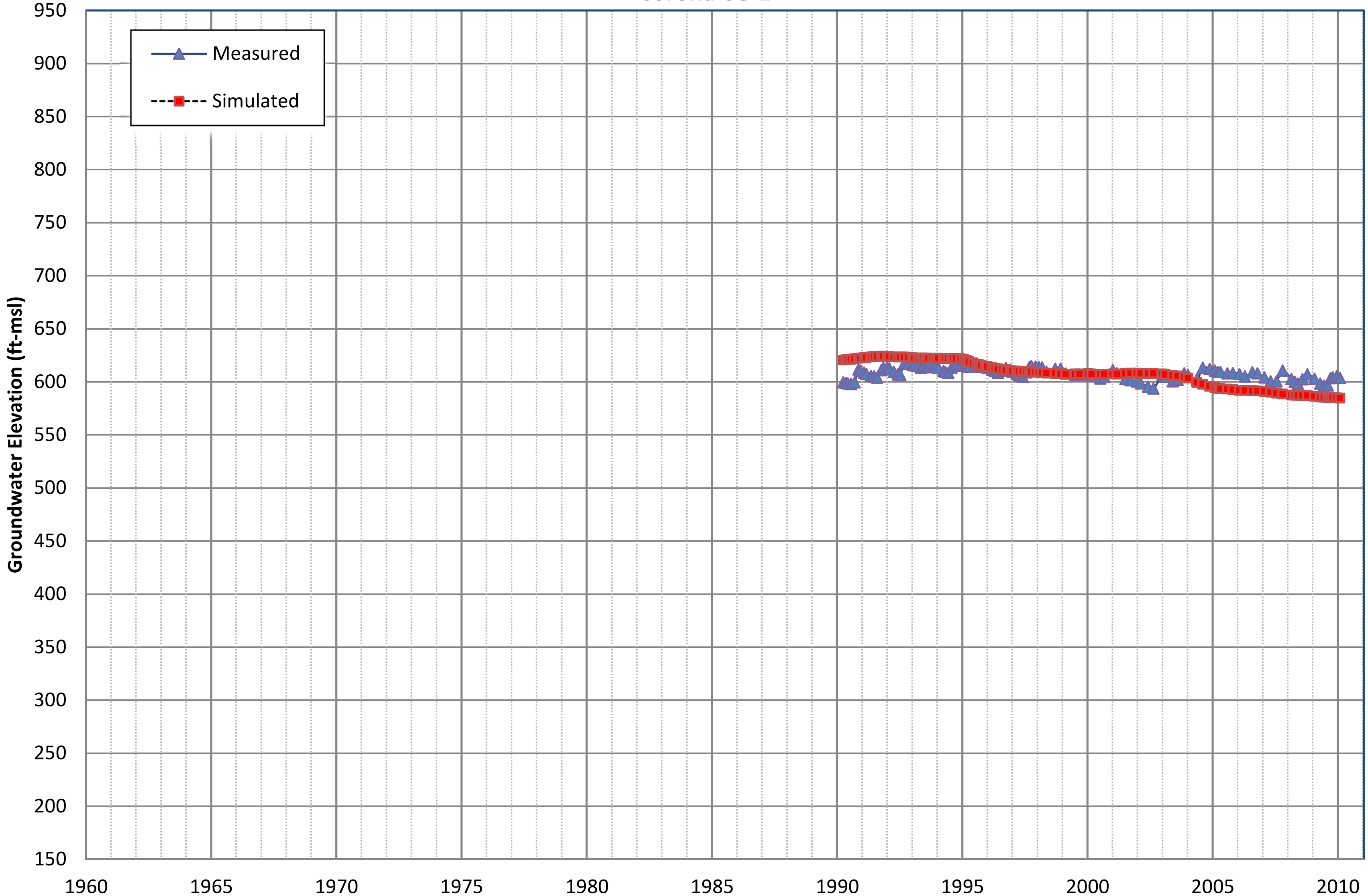

Figure C1-51

Simulated and Measured Groundwater Elevations in the Wells Used in Model Calibration 1961 - 2011

SAWC 18

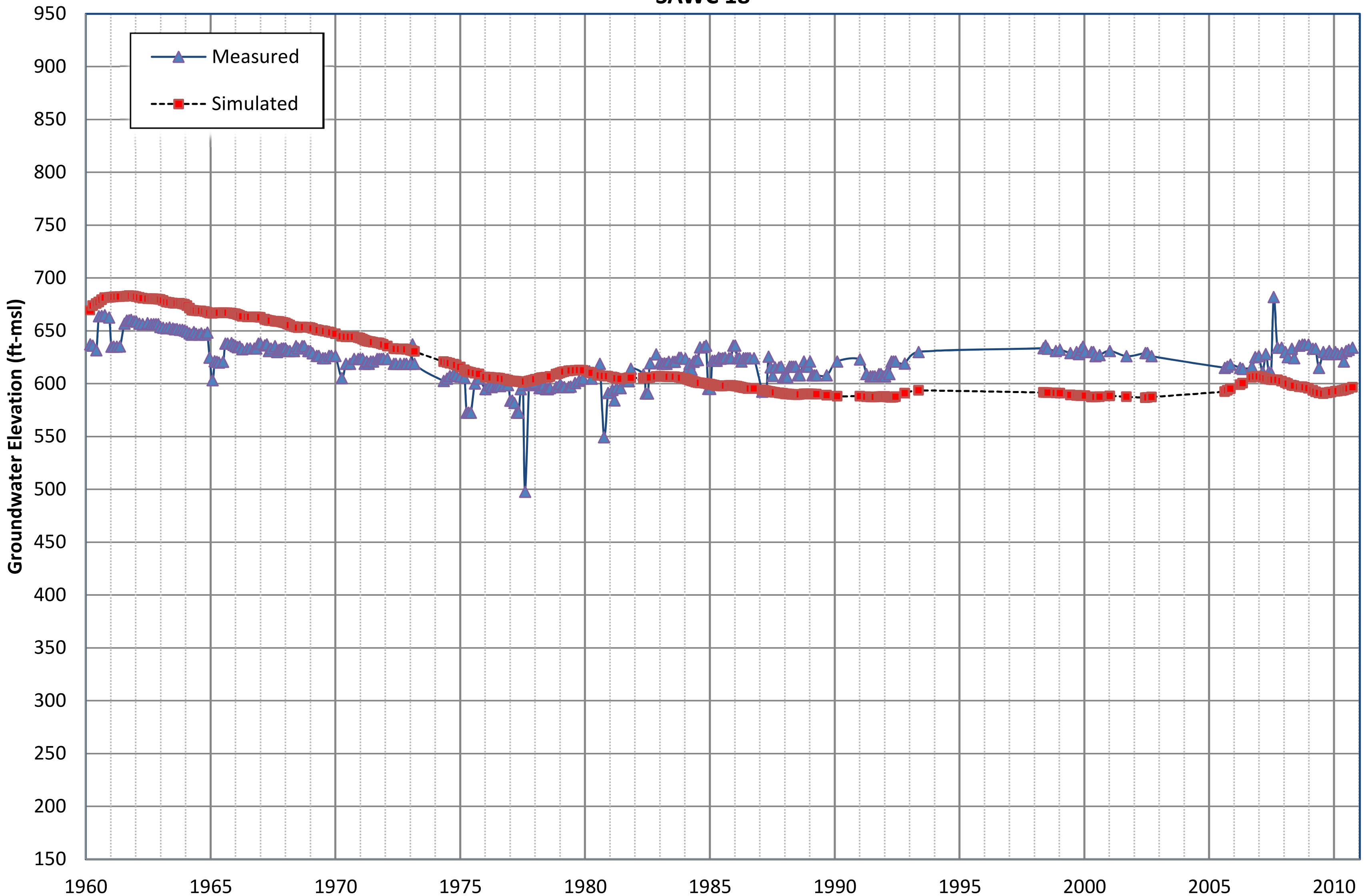

Figure C1-52

Simulated and Measured Groundwater Elevations in the Wells Used in Model Calibration 1961 - 2011

PW 8

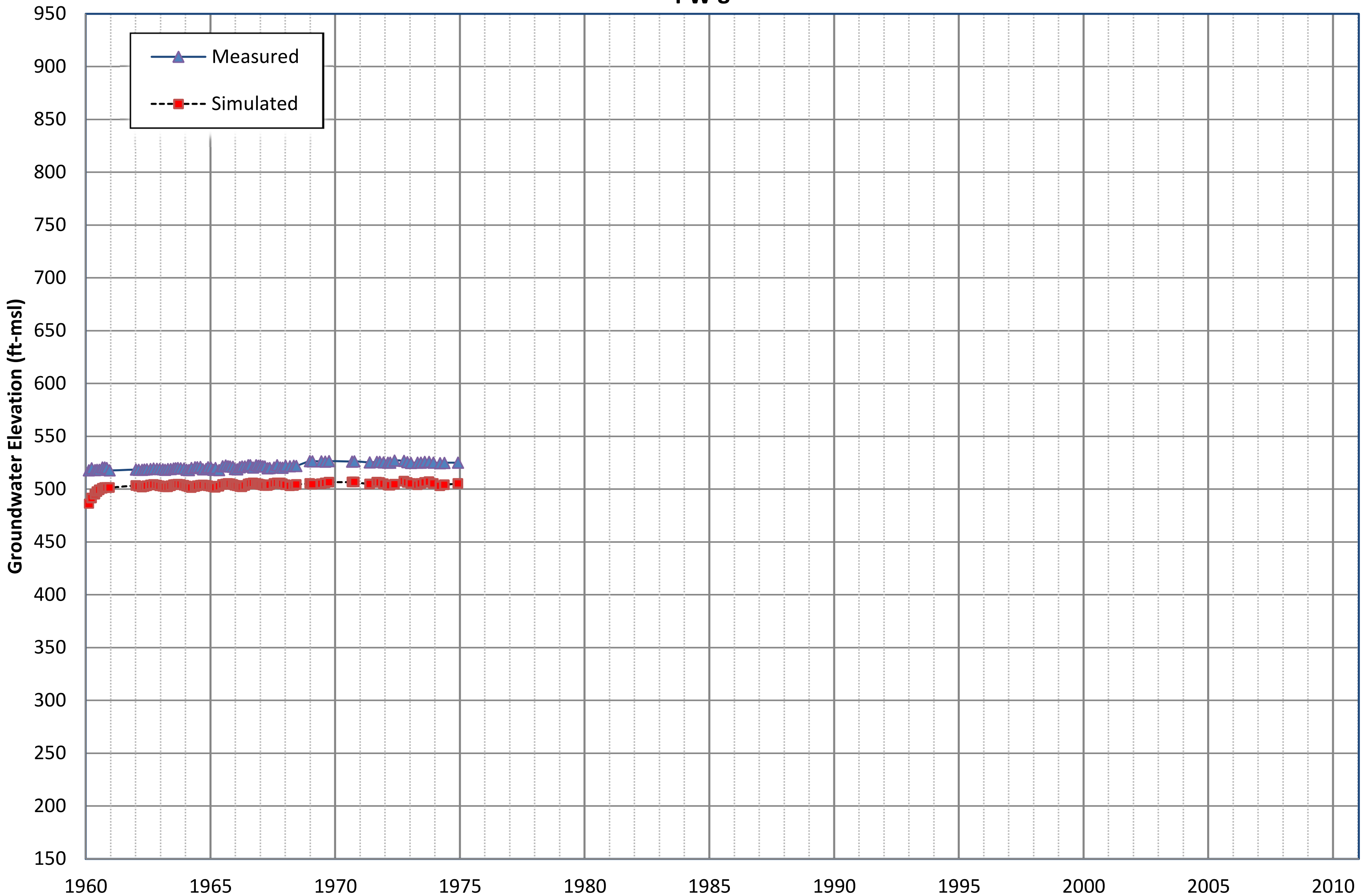

Figure C1-53
Simulated and Measured Groundwater Elevations in the Wells Used in Model Calibration 1961 - 2011
SARWC 07

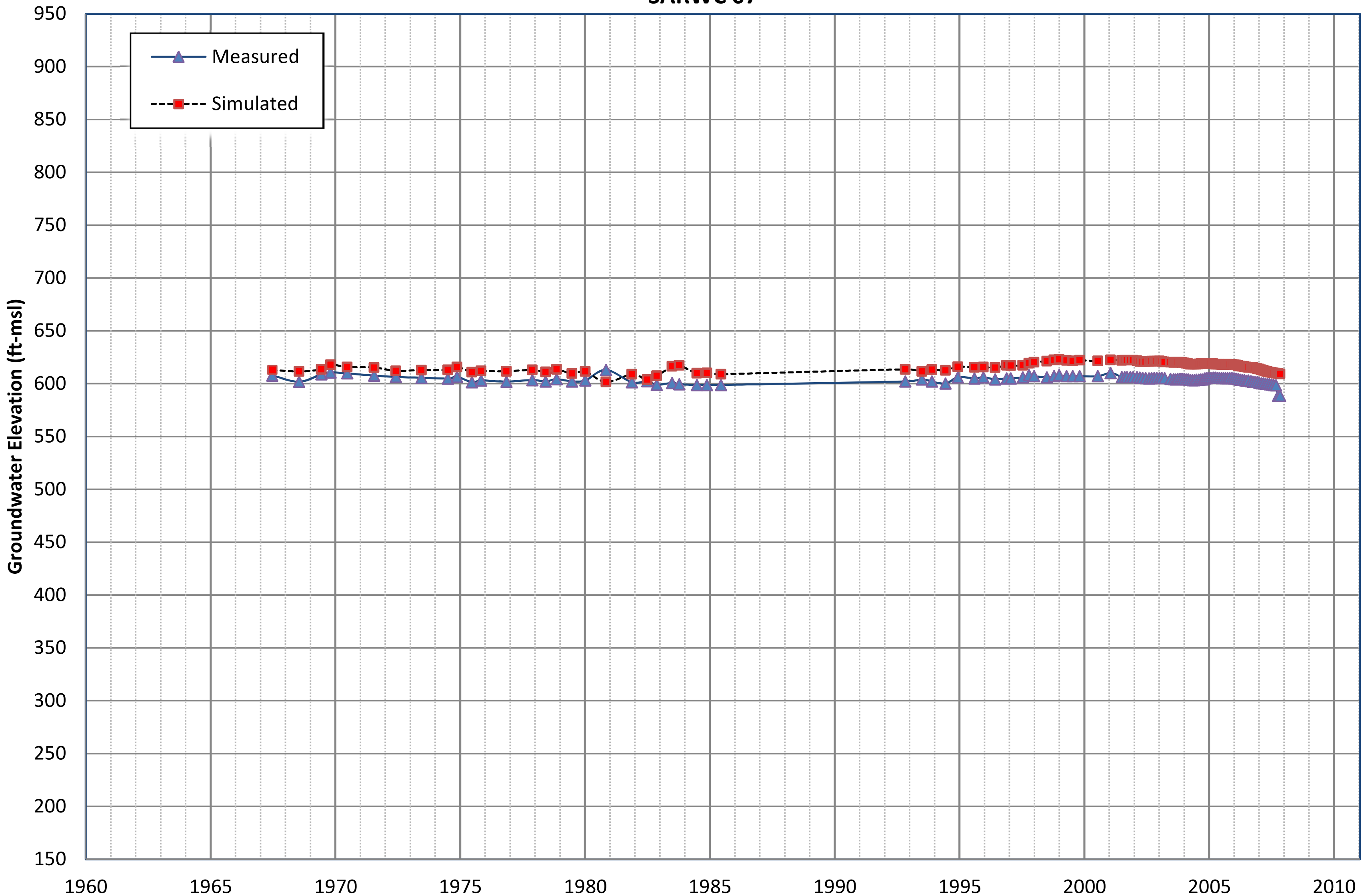

Appendix_C1_20150915_WW_WellHydrograph_calibrationwell_format.xlsm

Figure C1-54
Simulated and Measured Groundwater Elevations in the Wells Used in Model Calibration 1961 - 2011
PW 4

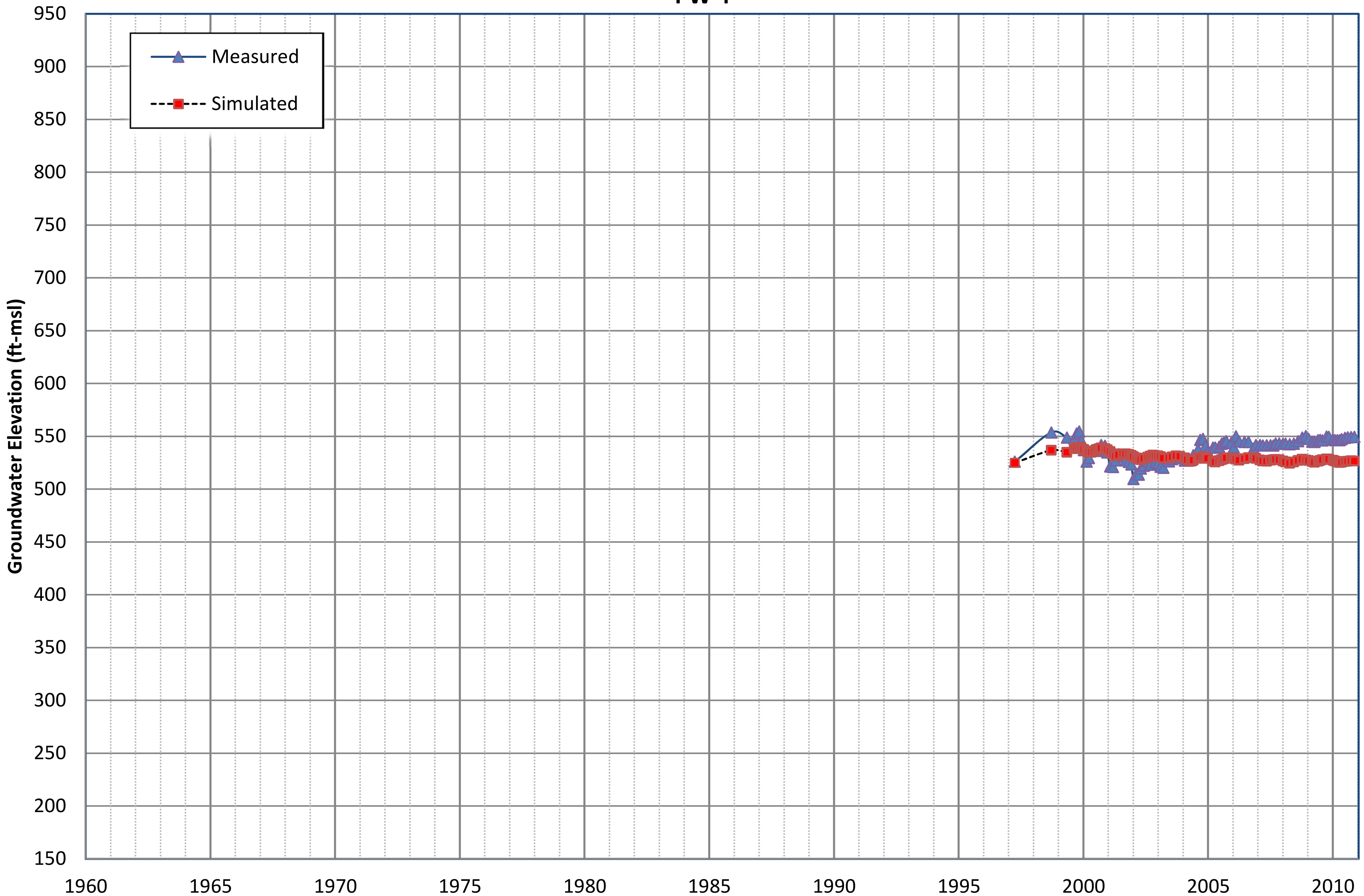

Figure C1-55
Simulated and Measured Groundwater Elevations in the Wells Used in Model Calibration 1961 - 2011
CIM 09

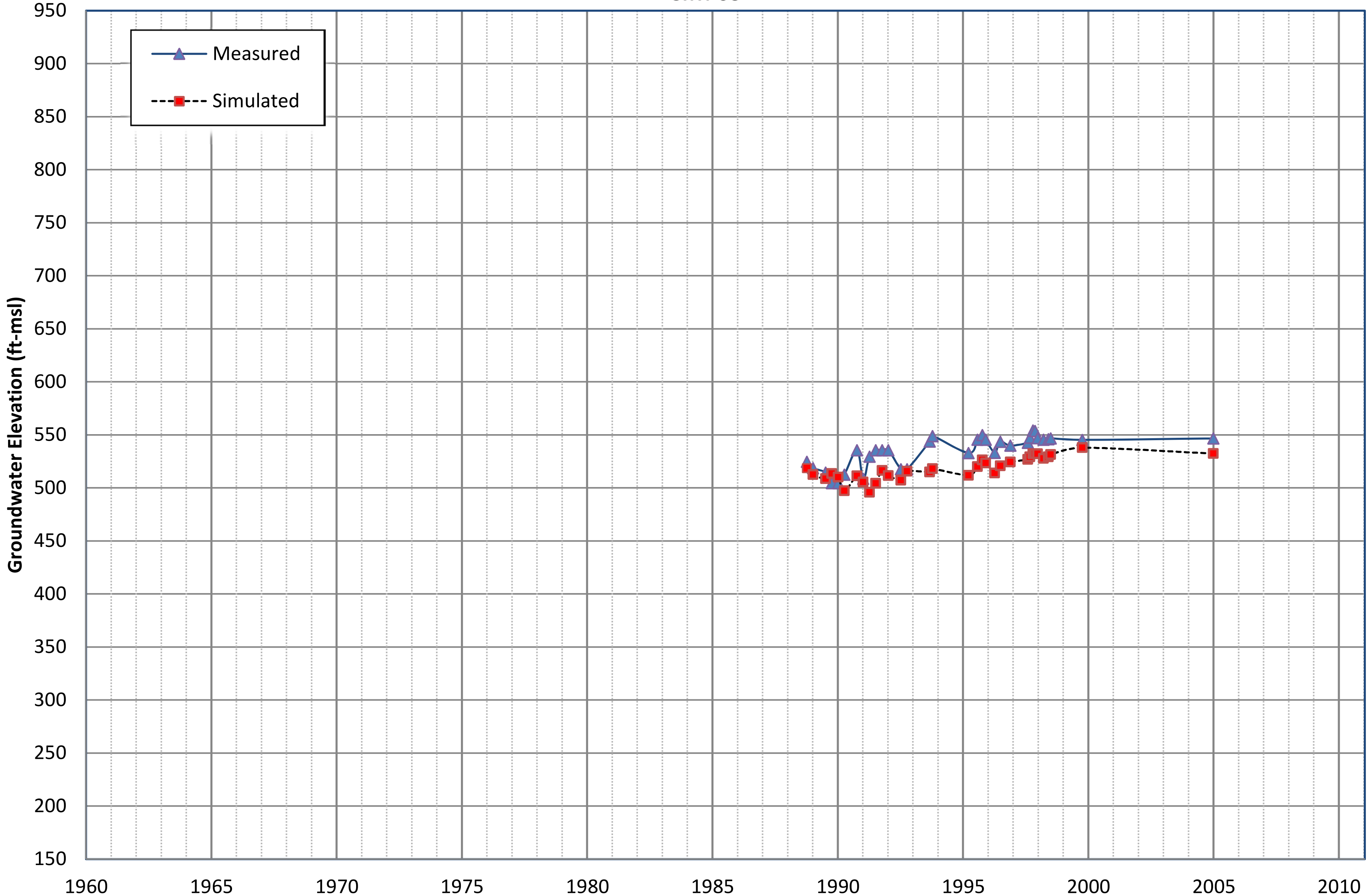

Figure C1-56

Simulated and Measured Groundwater Elevations in the Wells Used in Model Calibration 1961 - 2011

CIM MW 24I

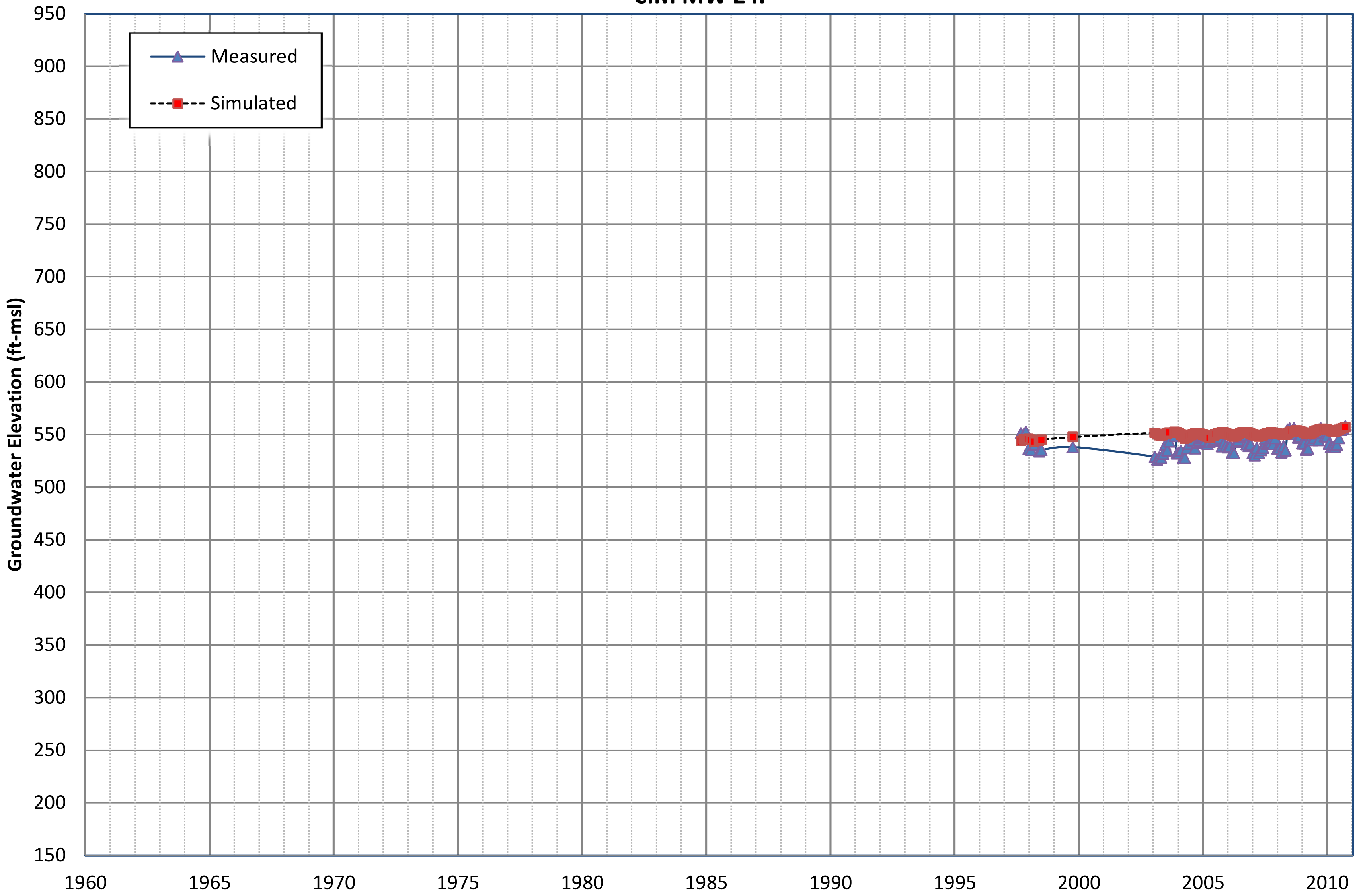

Figure C1-57
Simulated and Measured Groundwater Elevations in the Wells Used in Model Calibration 1961 - 2011
CIM MW 24S

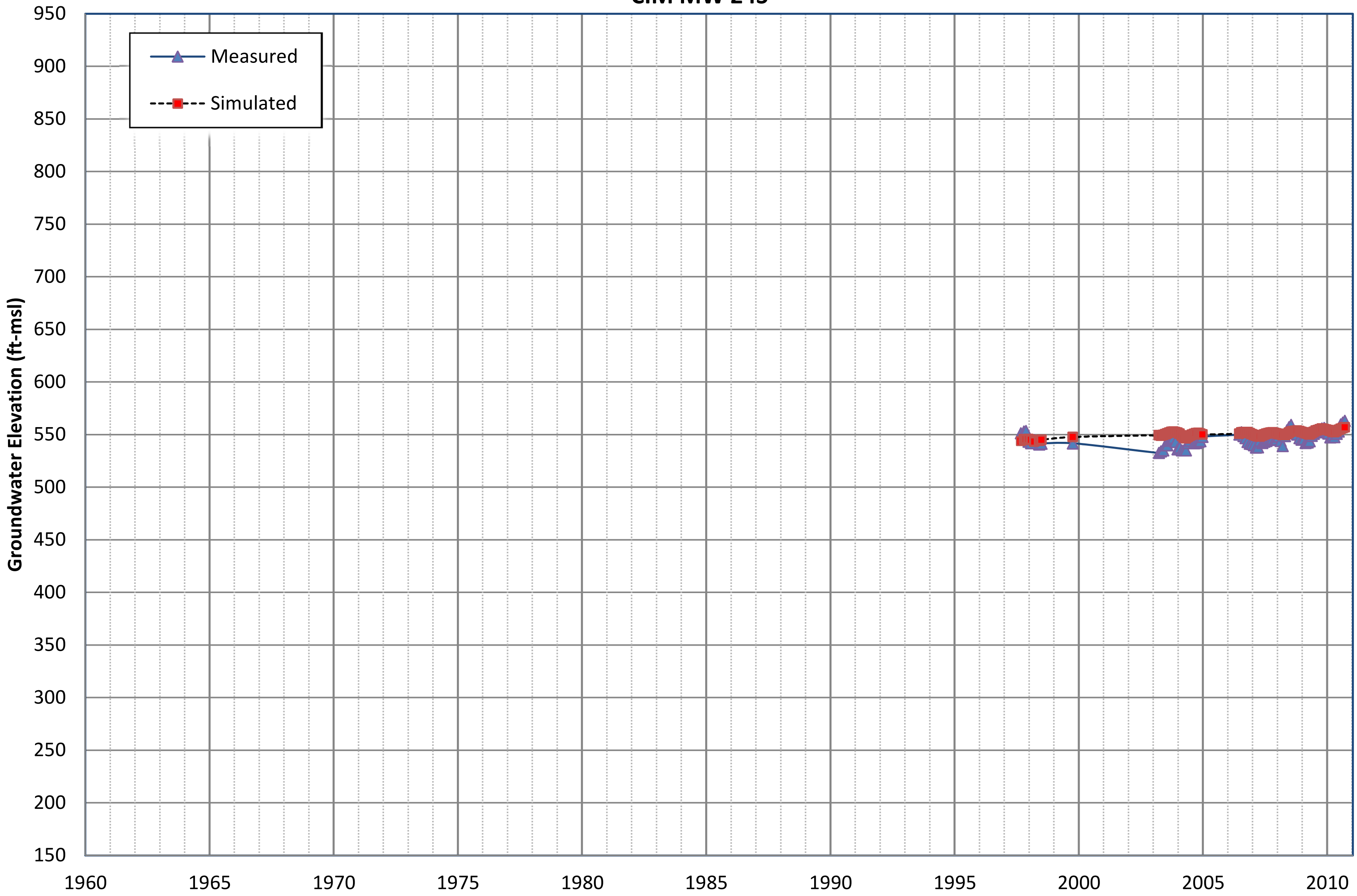

Figure C1-58
Simulated and Measured Groundwater Elevations in the Wells Used in Model Calibration 1961 - 2011
FC-936A2

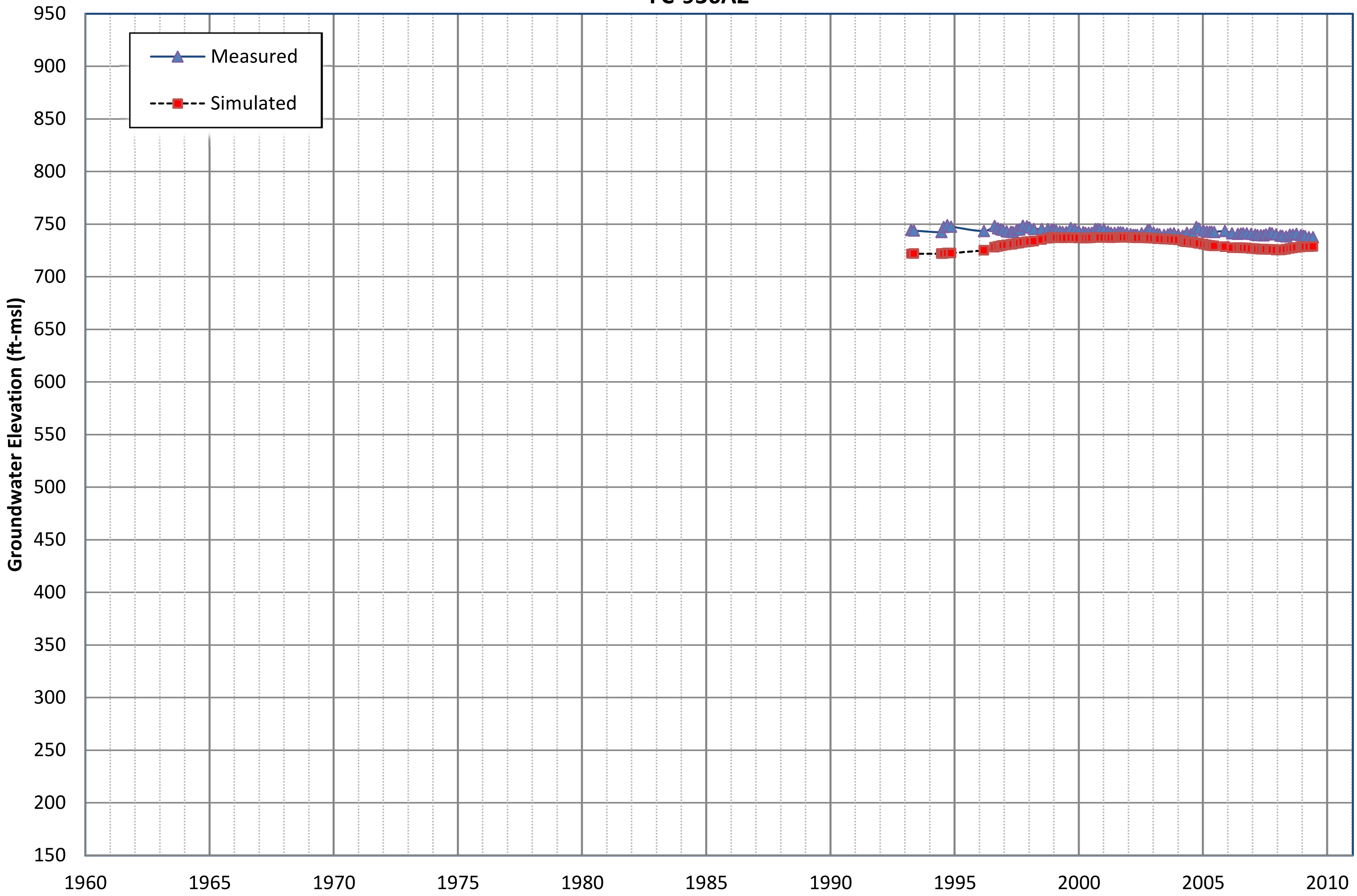

Figure C1-59
Simulated and Measured Groundwater Elevations in the Wells Used in Model Calibration 1961 - 2011
USGS Archibald 1

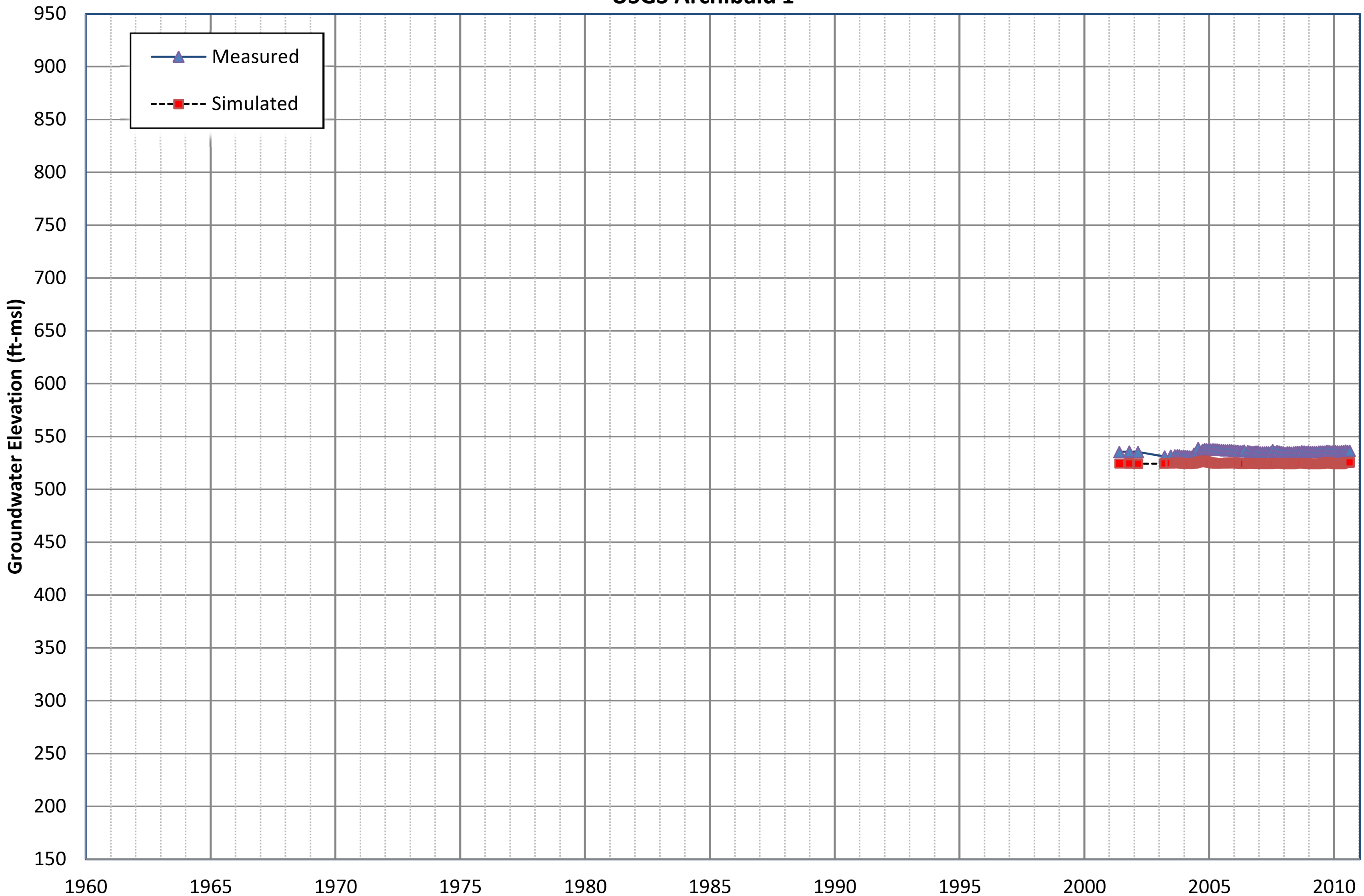

Appendix_C1_20150915_WW_WellHydrograph_calibrationwell_format.xlsm

Figure C1-60
Simulated and Measured Groundwater Elevations in the Wells Used in Model Calibration 1961 - 2011
COR 10

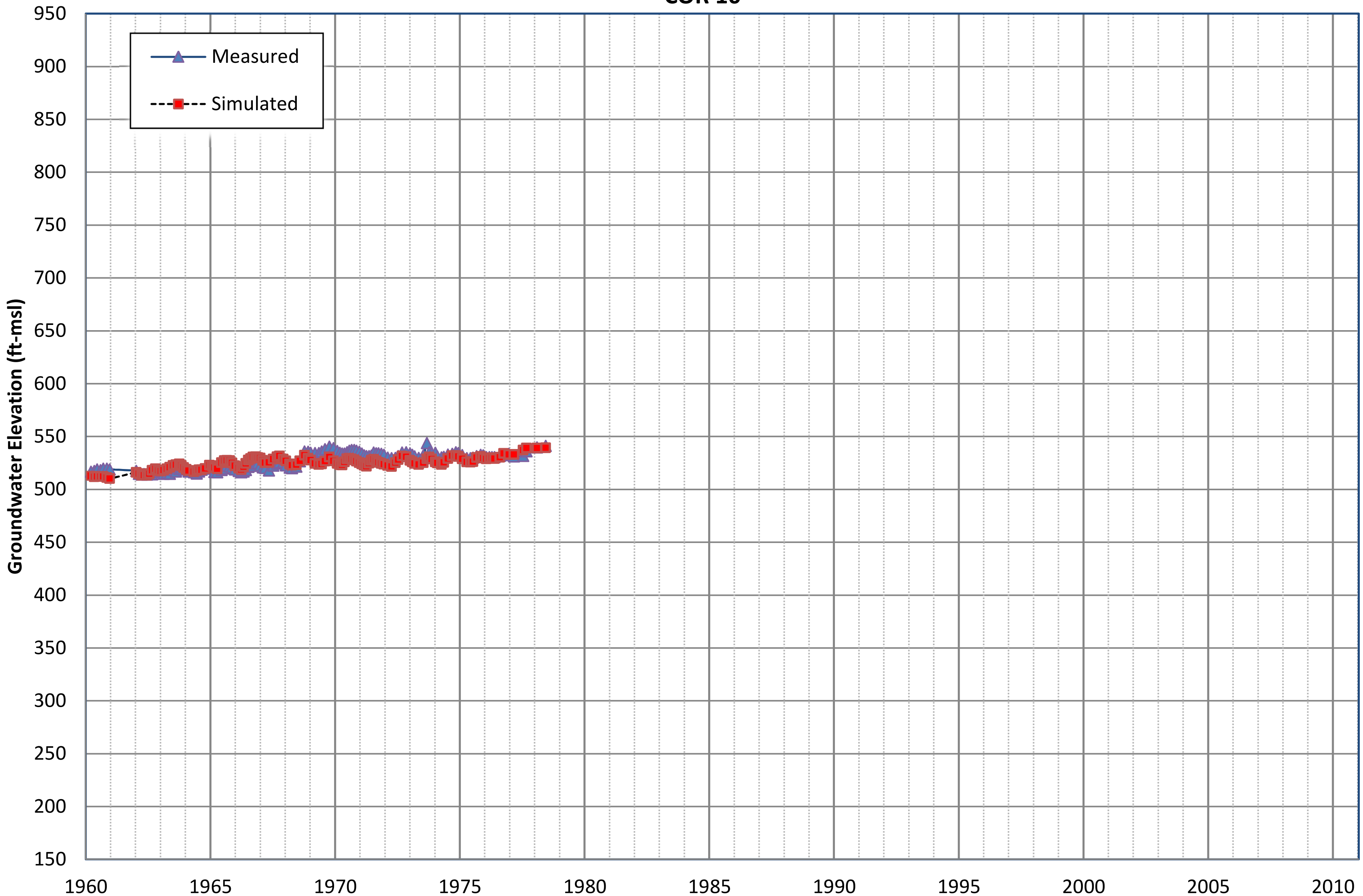

Figure C1-61
Simulated and Measured Groundwater Elevations in the Wells Used in Model Calibration 1961 - 2011
PW 10

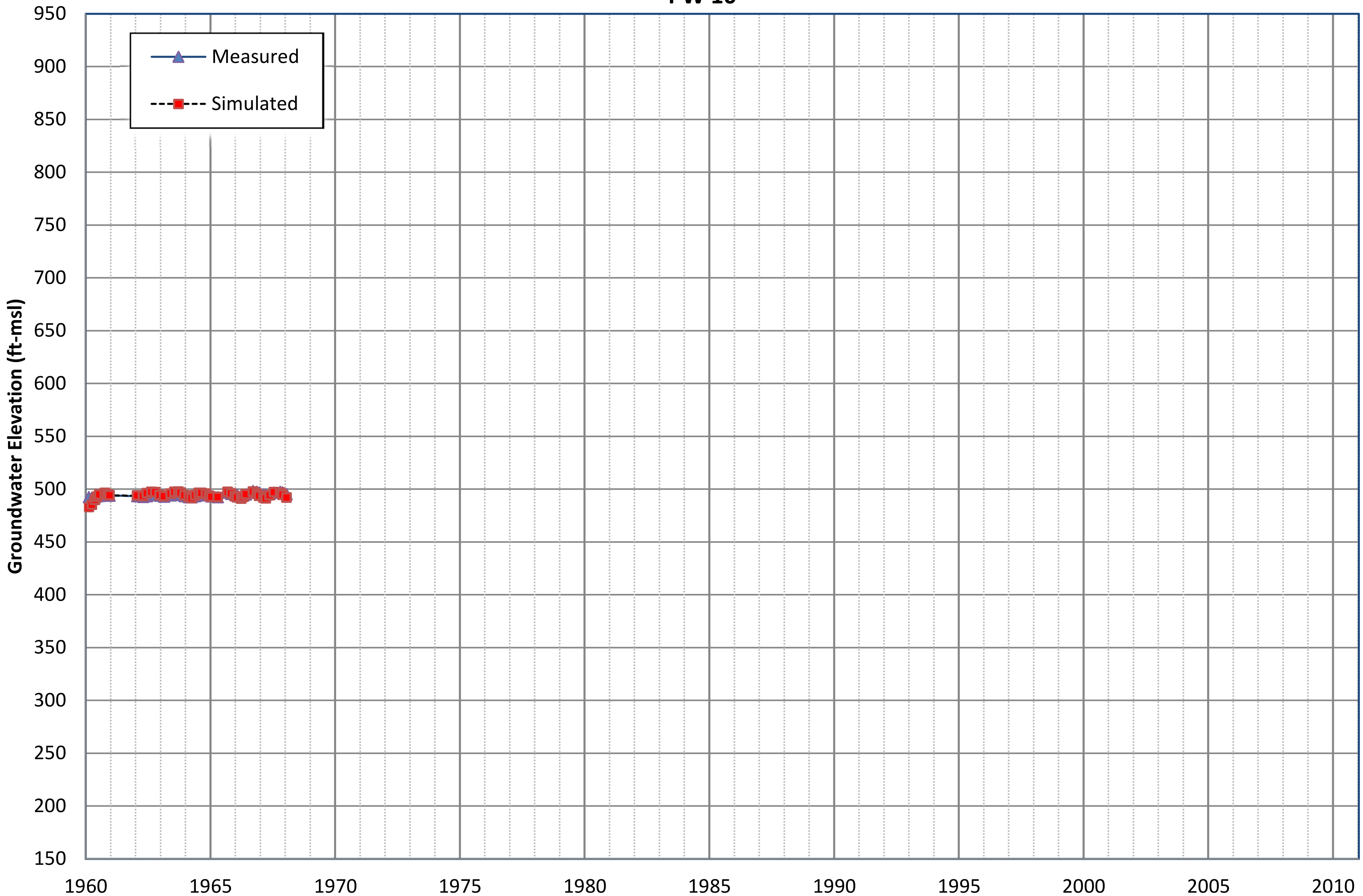

Figure C1-62

Simulated and Measured Groundwater Elevations in the Wells Used in Model Calibration 1961 - 2011

PW 6

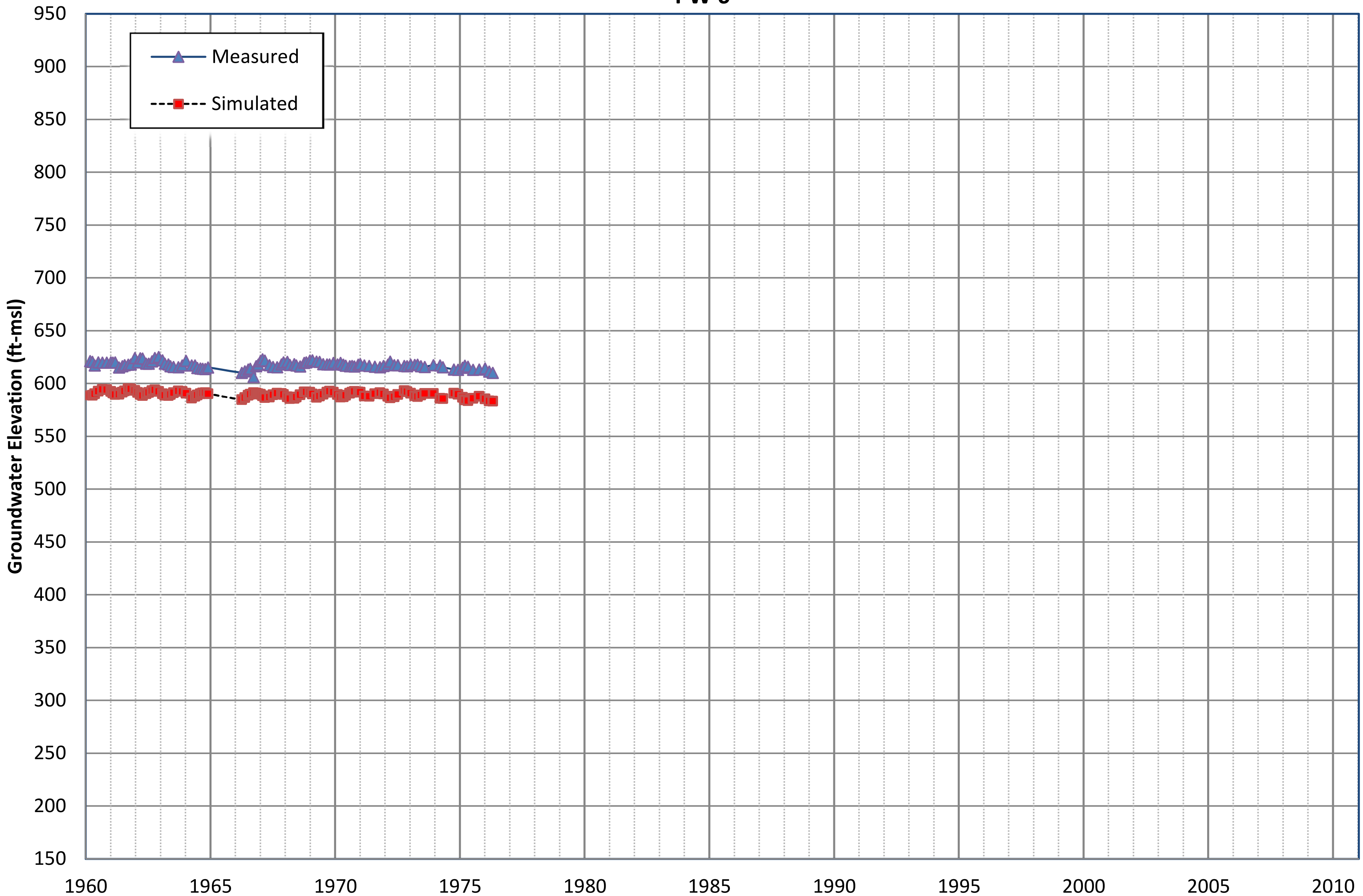

Figure C1-63

Simulated and Measured Groundwater Elevations in the Wells Used in Model Calibration 1961 - 2011

PW 9

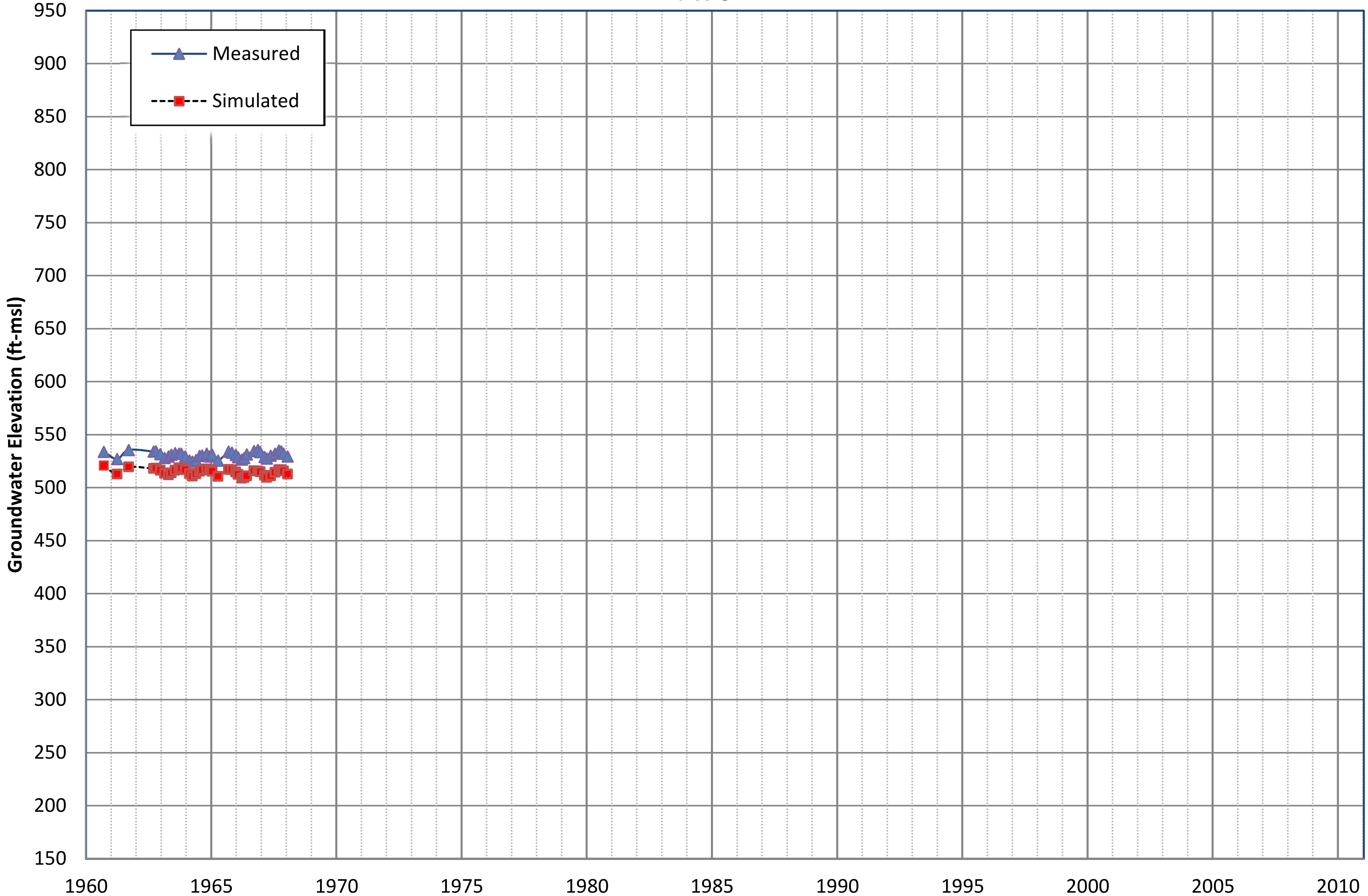

Figure C1-64
Simulated and Measured Groundwater Elevations in the Wells Used in Model Calibration 1961 - 2011
PW 11

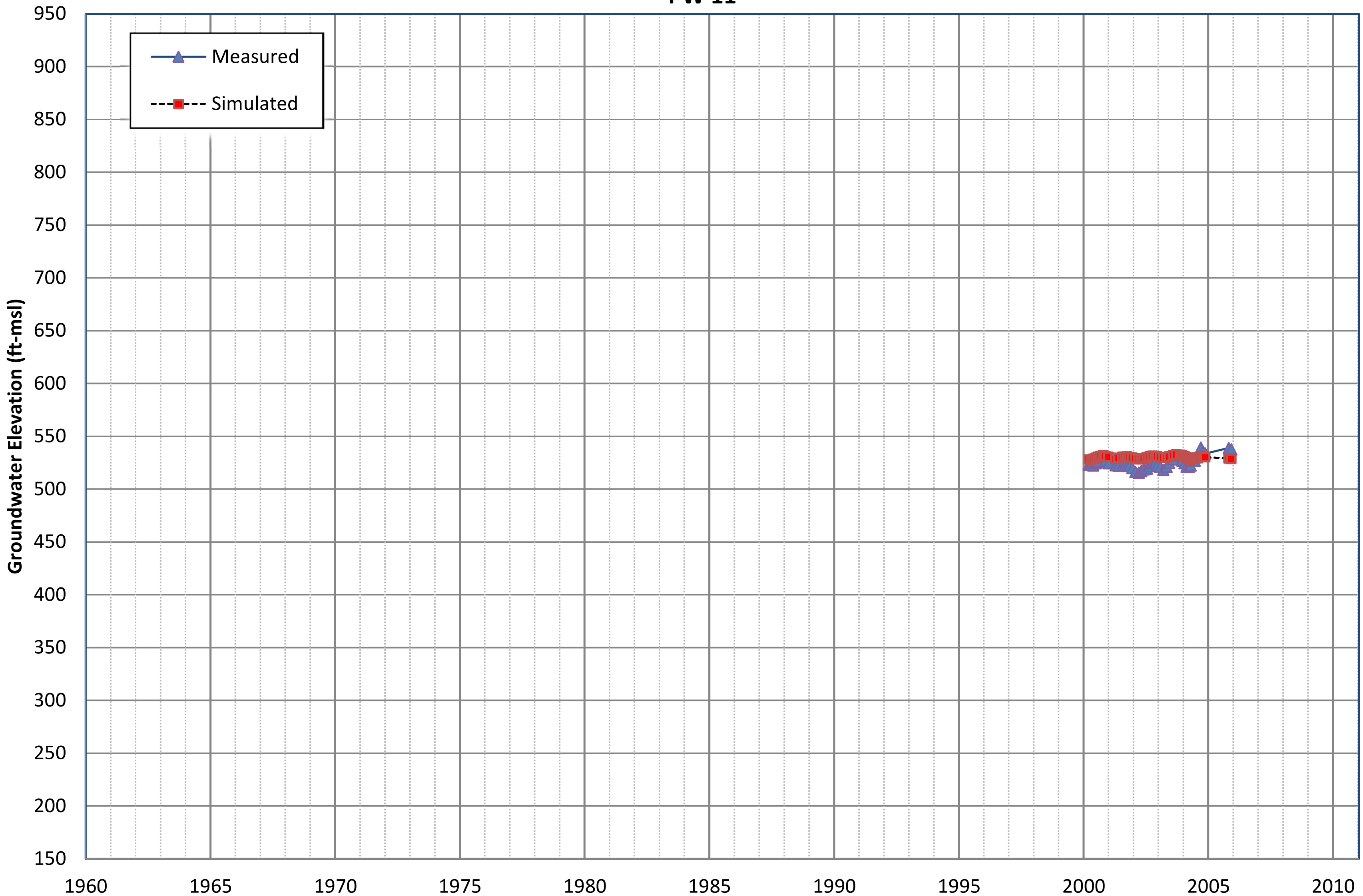

Figure C1-65
Simulated and Measured Groundwater Elevations in the Wells Used in Model Calibration 1961 - 2011
WECWC 1

Figure C1-66
Simulated and Measured Groundwater Elevations in the Wells Used in Model Calibration 1961 - 2011
WVWD 20

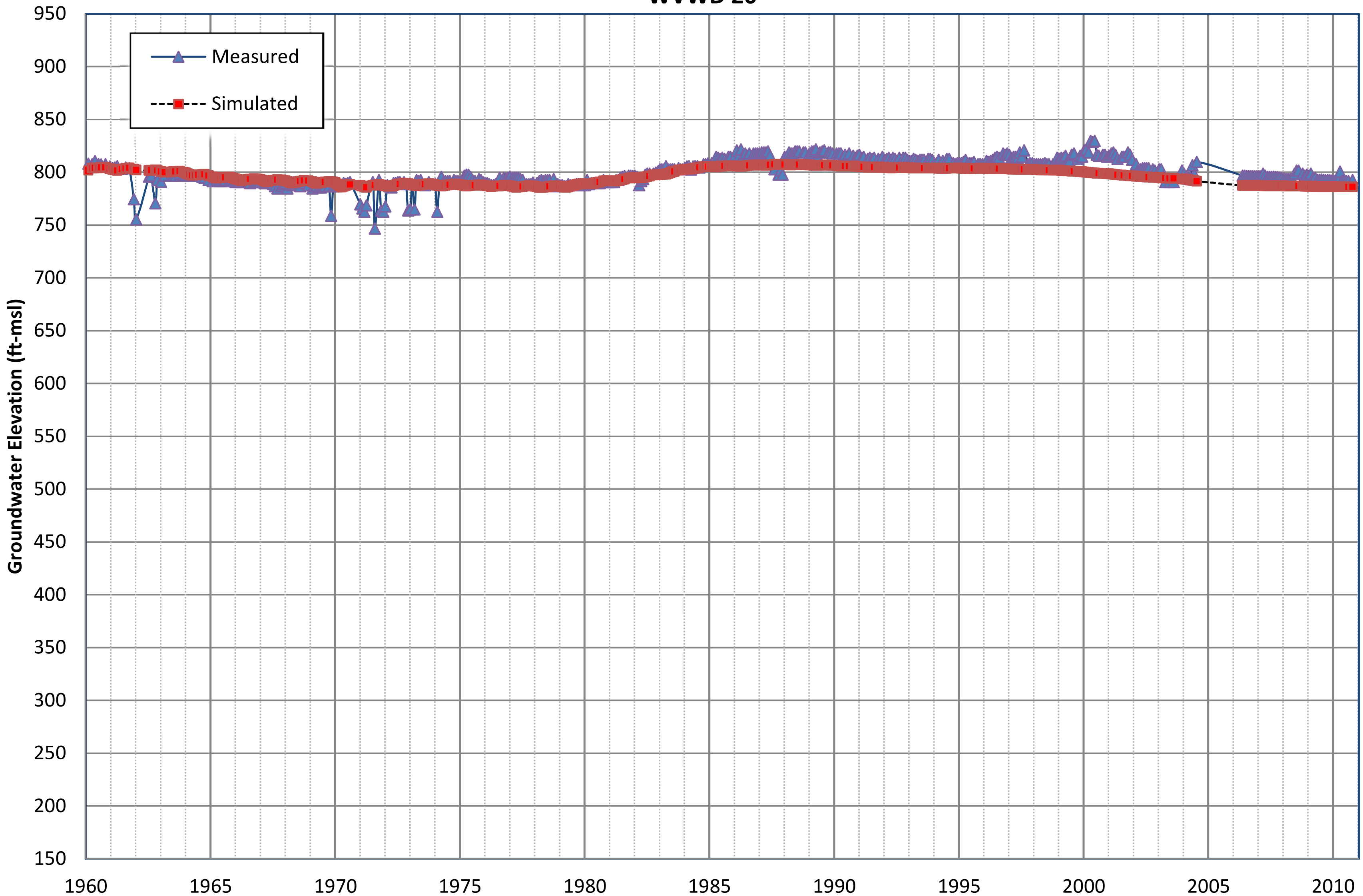

Appendix_C1_20150915_WW_WellHydrograph_calibrationwell_format.xlsm

Appendix C2

Time-History Plots of Simulated and Measured Groundwater Elevations in the Wells Used in Model Validation 1961 – 2011

Appendix C2
Time-History Plots of Simulated and Measured Groundwater Elevations in the Wells Used in Model Validation 1961 - 2011

Organization	Well Name	Chart Number
Chino Basin Desalter Authority	I-1	C2-1
Chino Basin Desalter Authority	I-2	C2-2
Chino Basin Desalter Authority	I-3	C2-3
Chino Basin Desalter Authority	I-4	C2-4
Chino Basin Desalter Authority	I-5	C2-5
Chino Basin Desalter Authority	I-6	C2-6
Chino Basin Desalter Authority	I-7	C2-7
Chino Basin Desalter Authority	I-8	C2-8
Chino Basin Desalter Authority	I-9	C2-9
Chino Basin Desalter Authority	I-10	C2-10
Chino Basin Desalter Authority	I-11	C2-11
Chino Basin Desalter Authority	I-13	C2-12
Chino Basin Desalter Authority	I-14	C2-13
Chino Basin Desalter Authority	I-15	C2-14
Chino Basin Desalter Authority	II-1	C2-15
Chino Basin Desalter Authority	II-2	C2-16
Chino Basin Desalter Authority	II-3	C2-17
Chino Basin Desalter Authority	II-4	C2-18
Chino Basin Desalter Authority	II-6	C2-19
Chino Basin Desalter Authority	II-7	C2-20
Chino Basin Desalter Authority	II-8	C2-21
Chino Basin Desalter Authority	II-9A	C2-22
Jurupa Community Services District	JCSD 05	C2-23
Jurupa Community Services District	JCSD 06 (Mira Loma #6)	C2-24
Jurupa Community Services District	JCSD 08 (Russell Well)	C2-25
Jurupa Community Services District	JCSD 11	C2-26
Jurupa Community Services District	JCSD 12	C2-27
Jurupa Community Services District	JCSD 13	C2-28
Jurupa Community Services District	JCSD 14	C2-29
Jurupa Community Services District	JCSD 15	C2-30
Jurupa Community Services District	JCSD 16	C2-31
Jurupa Community Services District	JCSD 17	C2-32
Jurupa Community Services District	JCSD 18	C2-33
Jurupa Community Services District	JCSD 19	C2-34
Jurupa Community Services District	JCSD 20	C2-35
Jurupa Community Services District	JCSD 22	C2-36
Jurupa Community Services District	JCSD 23	C2-37
Jurupa Community Services District	JCSD 24 (Glen Avon #6)	C2-38
Jurupa Community Services District	JCSD 25	C2-39
Jurupa Community Services District	JCSD 42	C2-40
Jurupa Community Services District	Mira Loma 4	C2-41

Figure C2-1
Comparison of Measured and Simulated Groundwater Levels in CDA Well I-1

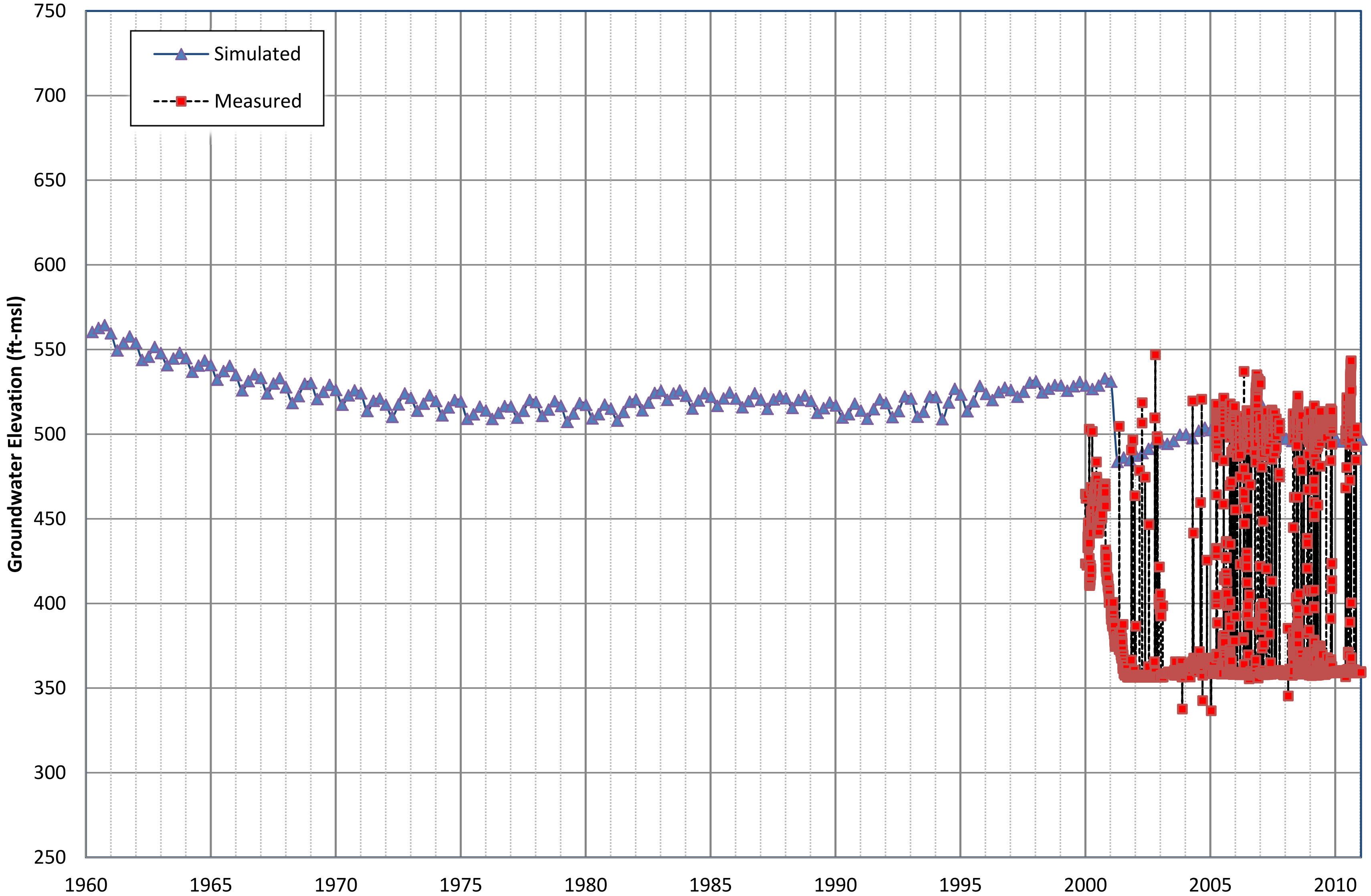

Figure C2-2
Comparison of Measured and Simulated Groundwater Levels in CDA Well I-2

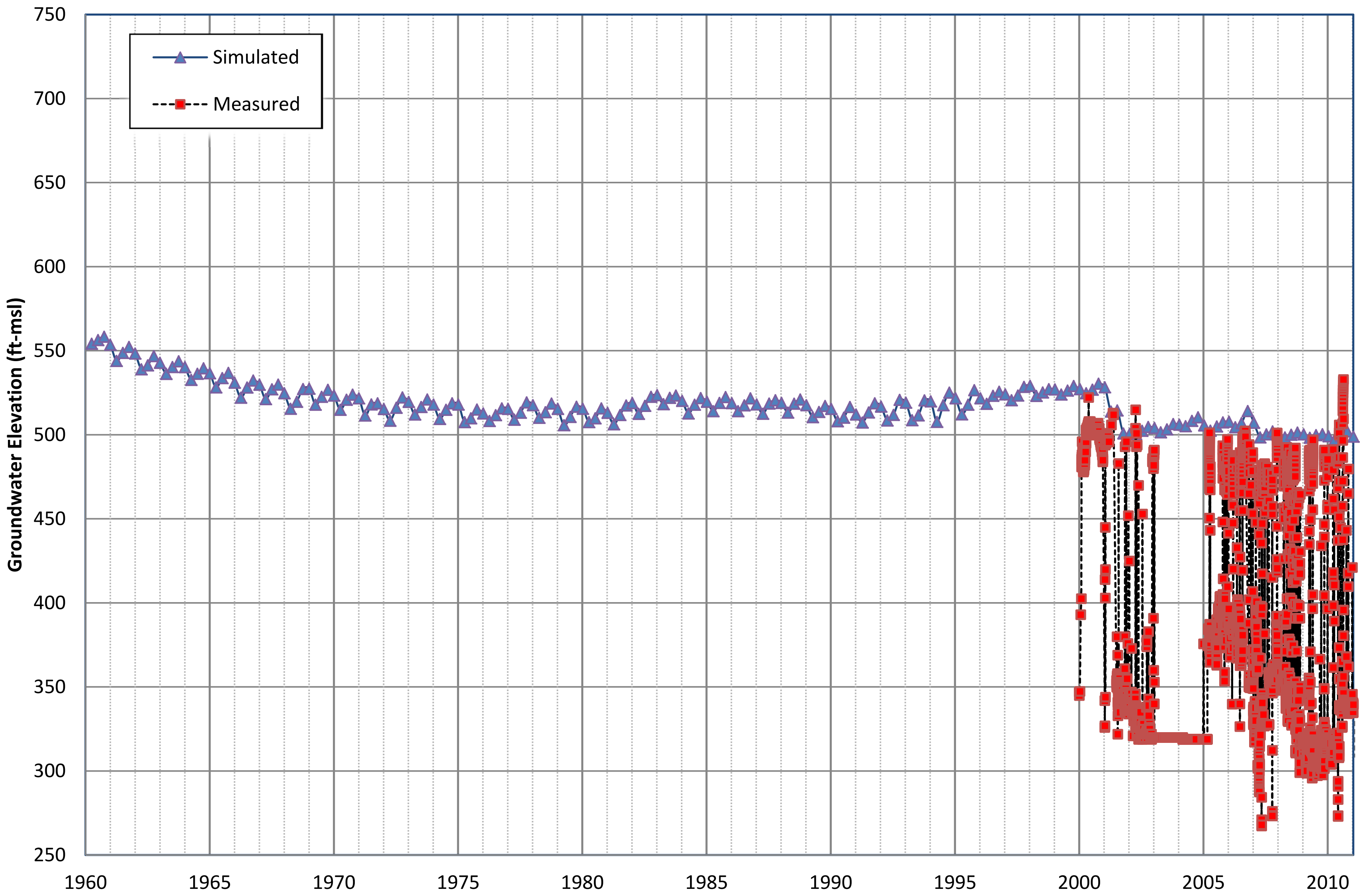

Figure C2-3
Comparison of Measured and Simulated Groundwater Levels in CDA Well I-3

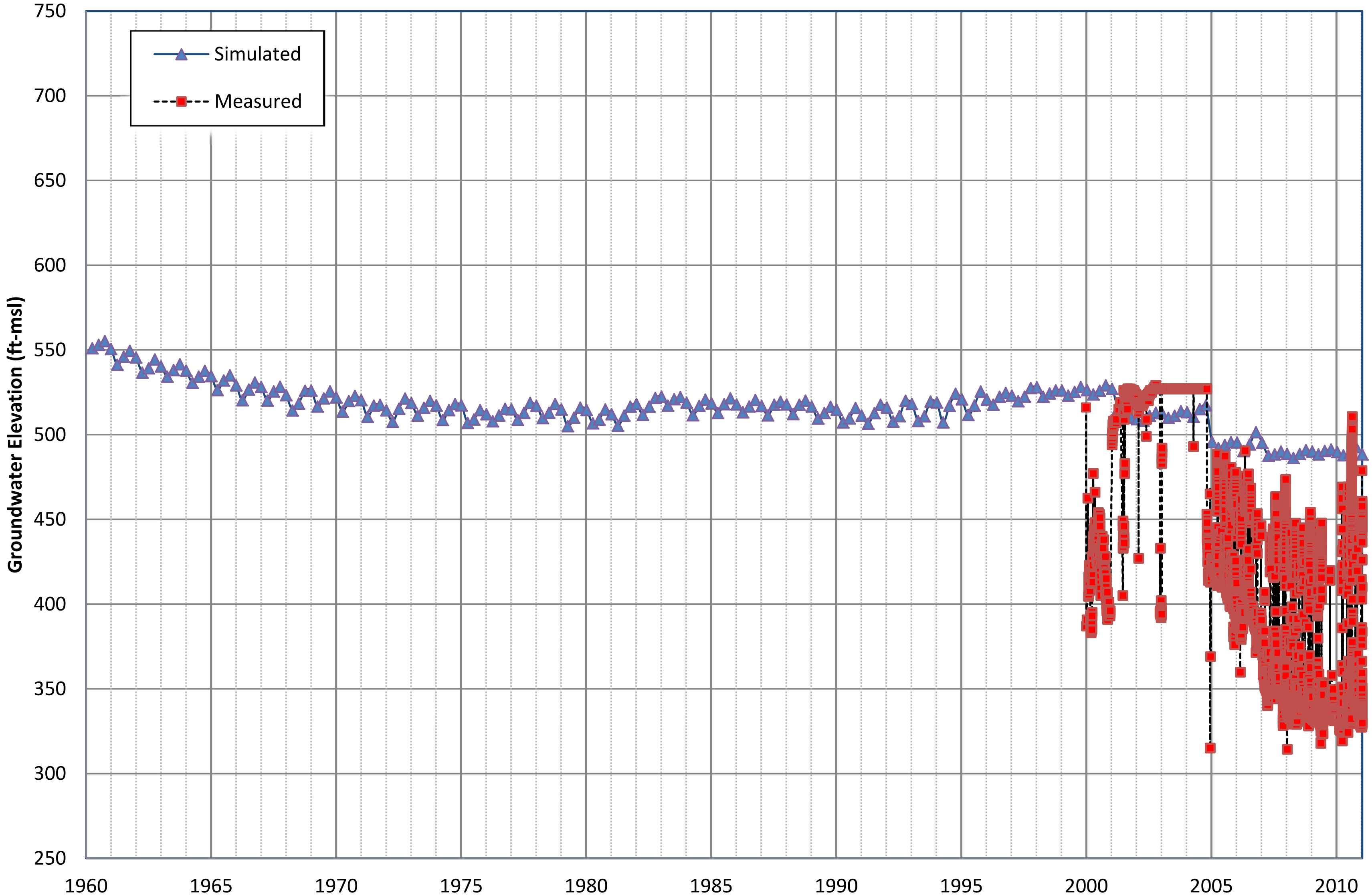

Figure C2-4
Comparison of Measured and Simulated Groundwater Levels in CDA Well I-4

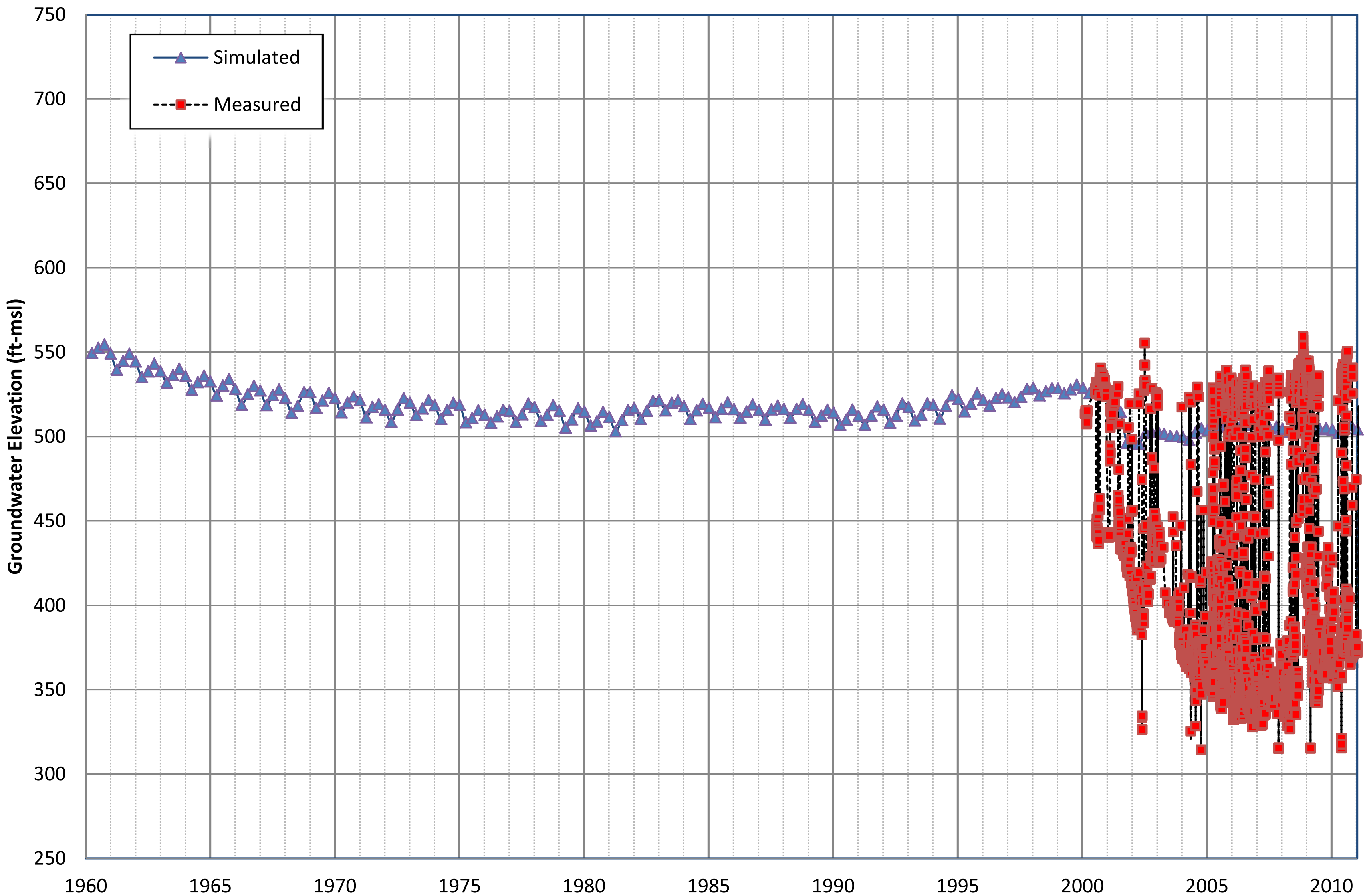

Figure C2-5
Comparison of Measured and Simulated Groundwater Levels in CDA Well I-5

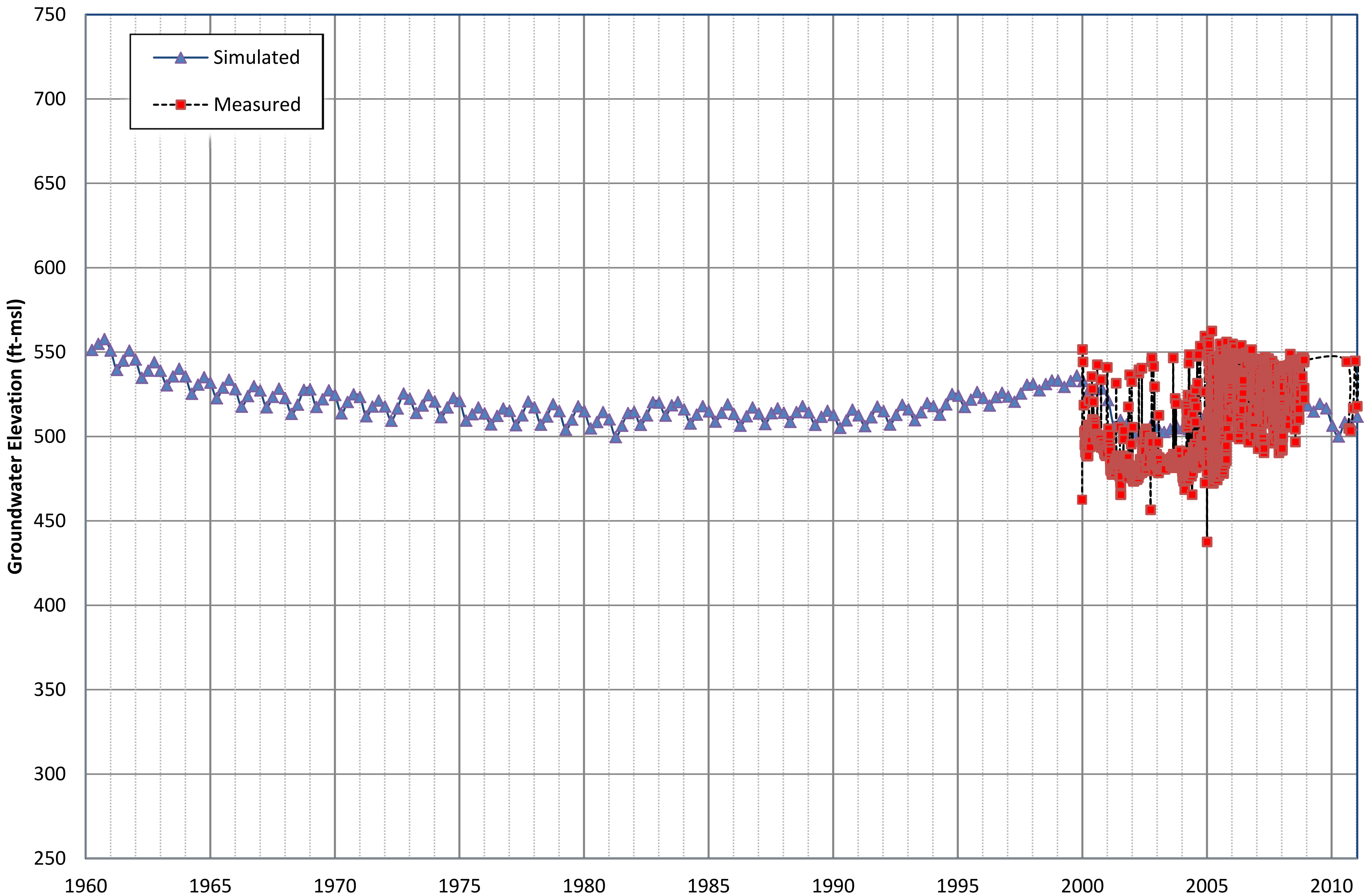

Appendix_C2_20151002_Validation_wells_Hydrographs.xlsm

Figure C2-6
Comparison of Measured and Simulated Groundwater Levels in CDA Well I-6

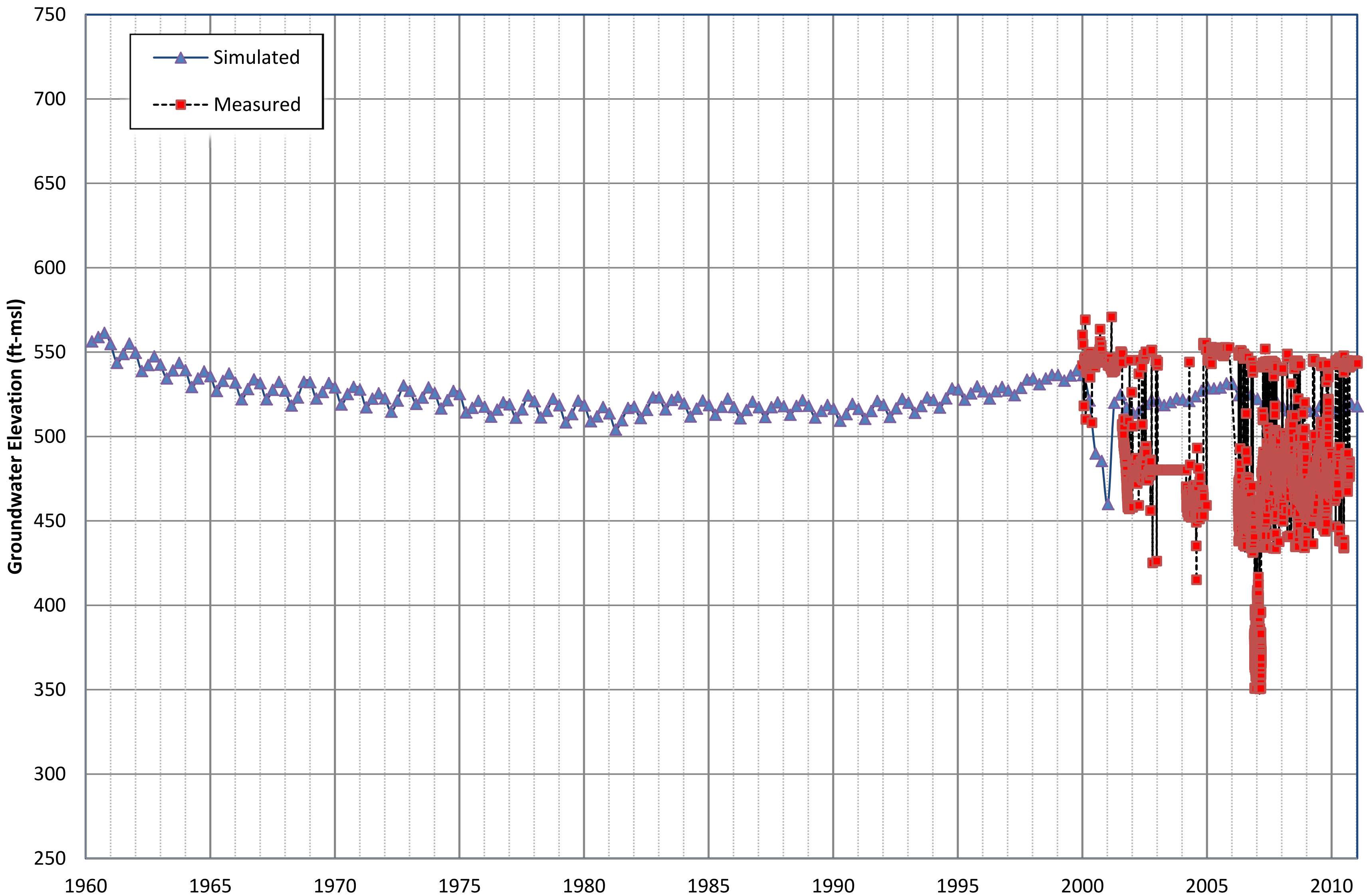

Appendix_C2_20151002_Validation_wells_Hydrographs.xlsm

Figure C2-7
Comparison of Measured and Simulated Groundwater Levels in CDA Well I-7

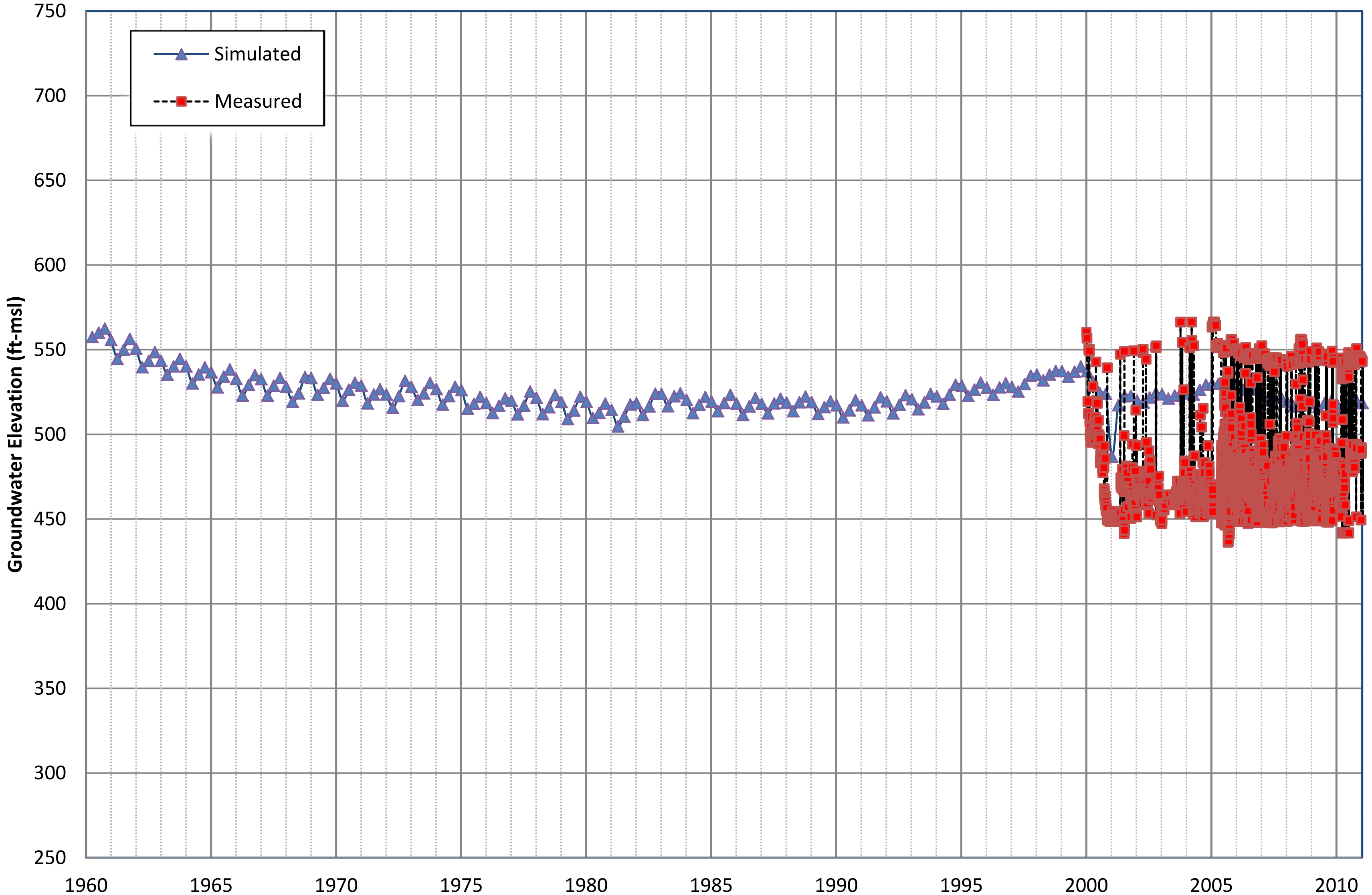

Appendix_C2_20151002_Validation_wells_Hydrographs.xlsm

Figure C2-8
Comparison of Measured and Simulated Groundwater Levels in CDA Well I-8

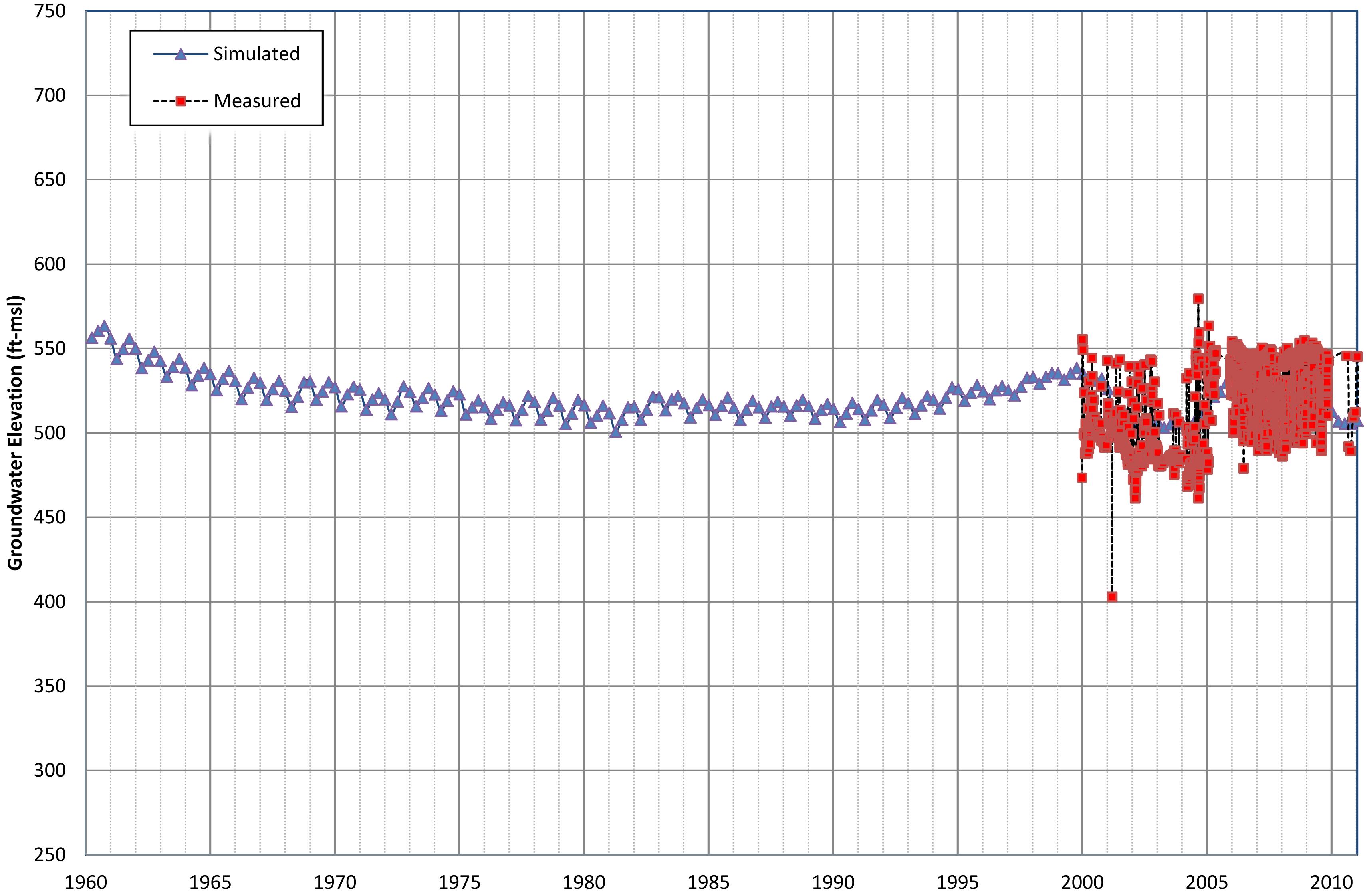

Figure C2-9
Comparison of Measured and Simulated Groundwater Levels in CDA Well I-9

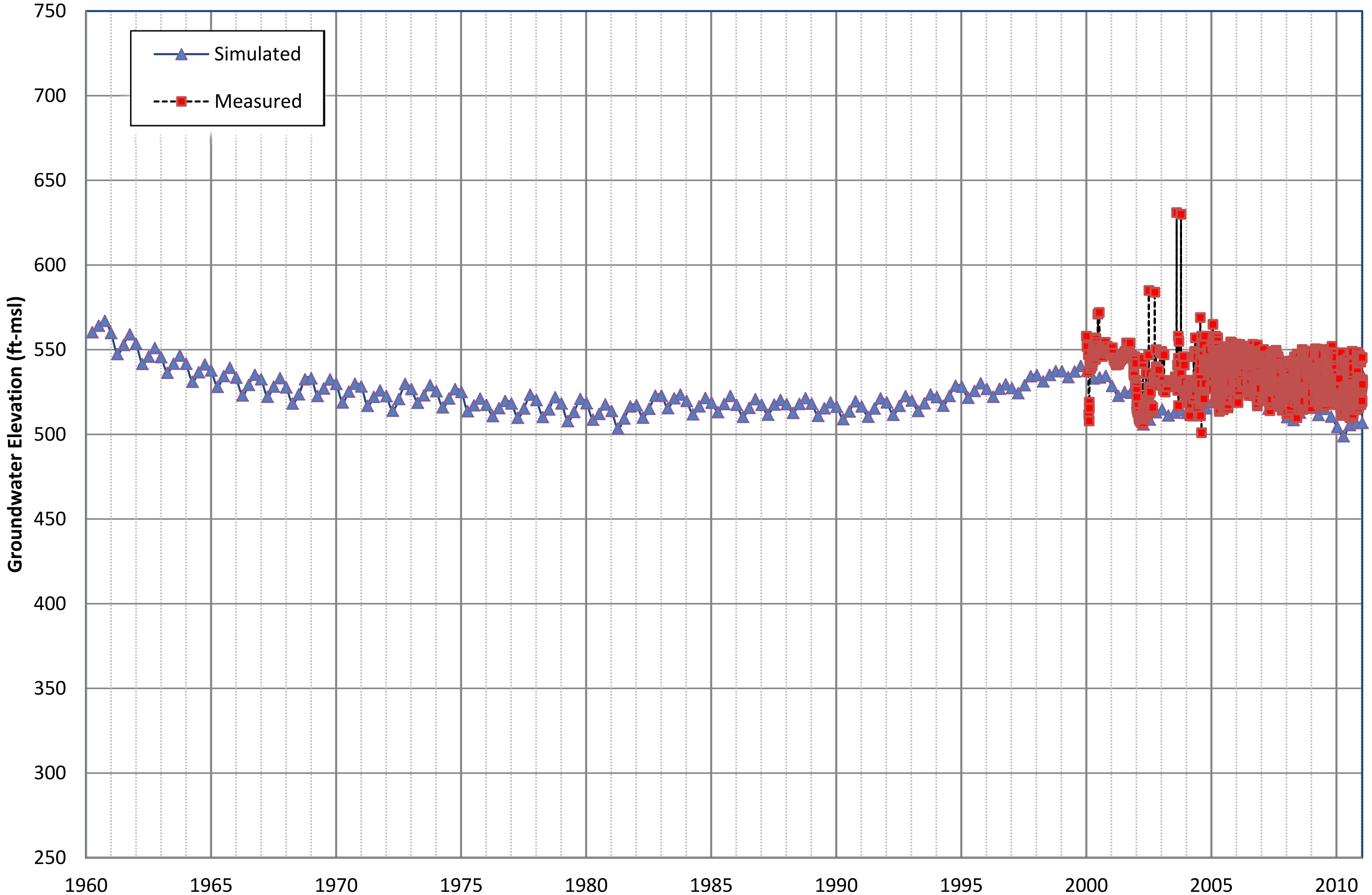

Figure C2-10
Comparison of Measured and Simulated Groundwater Levels in CDA Well I-10

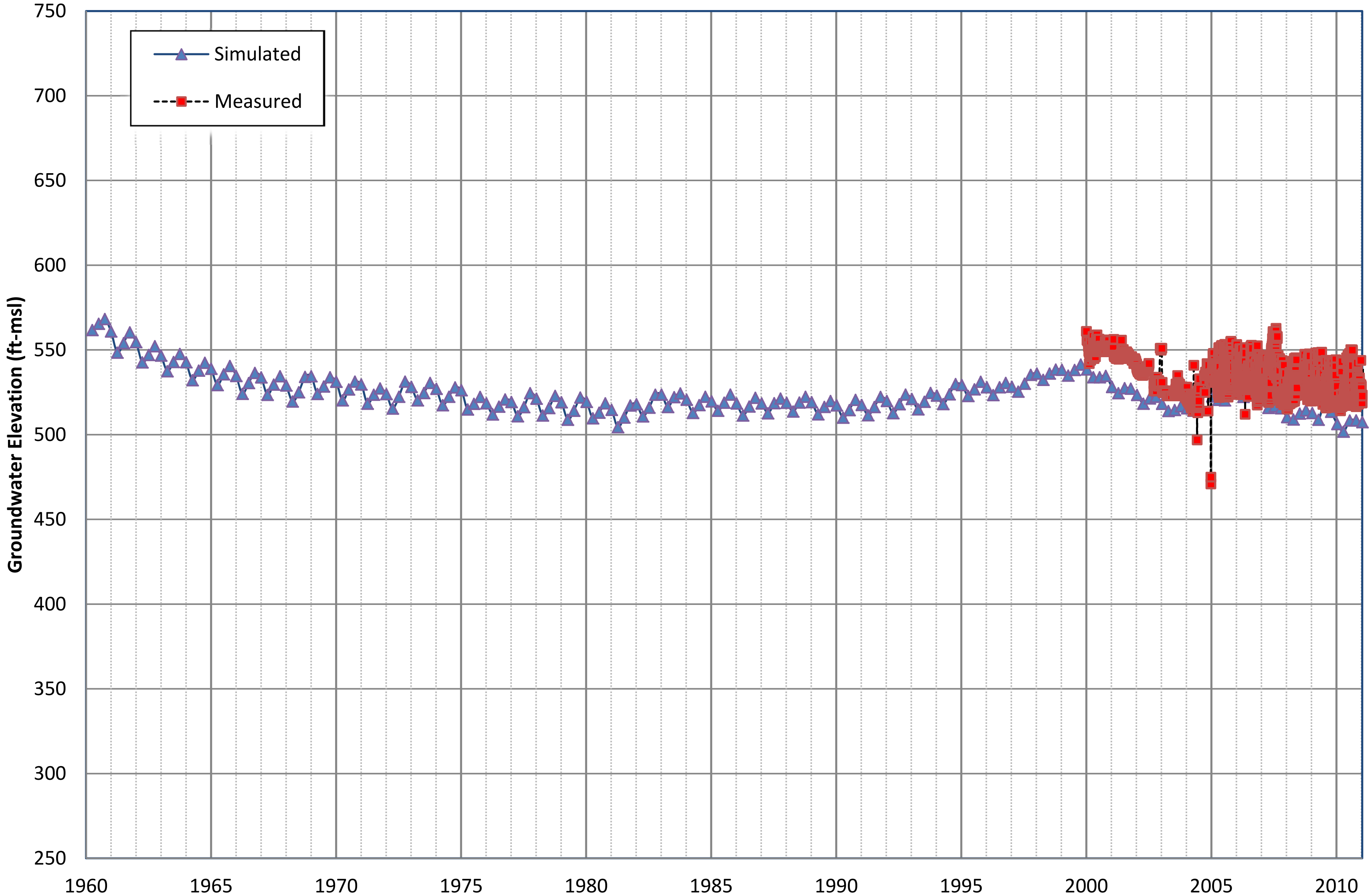

Appendix_C2_20151002_Validation_wells_Hydrographs.xlsm

Figure C2-11
Comparison of Measured and Simulated Groundwater Levels in CDA Well I-11

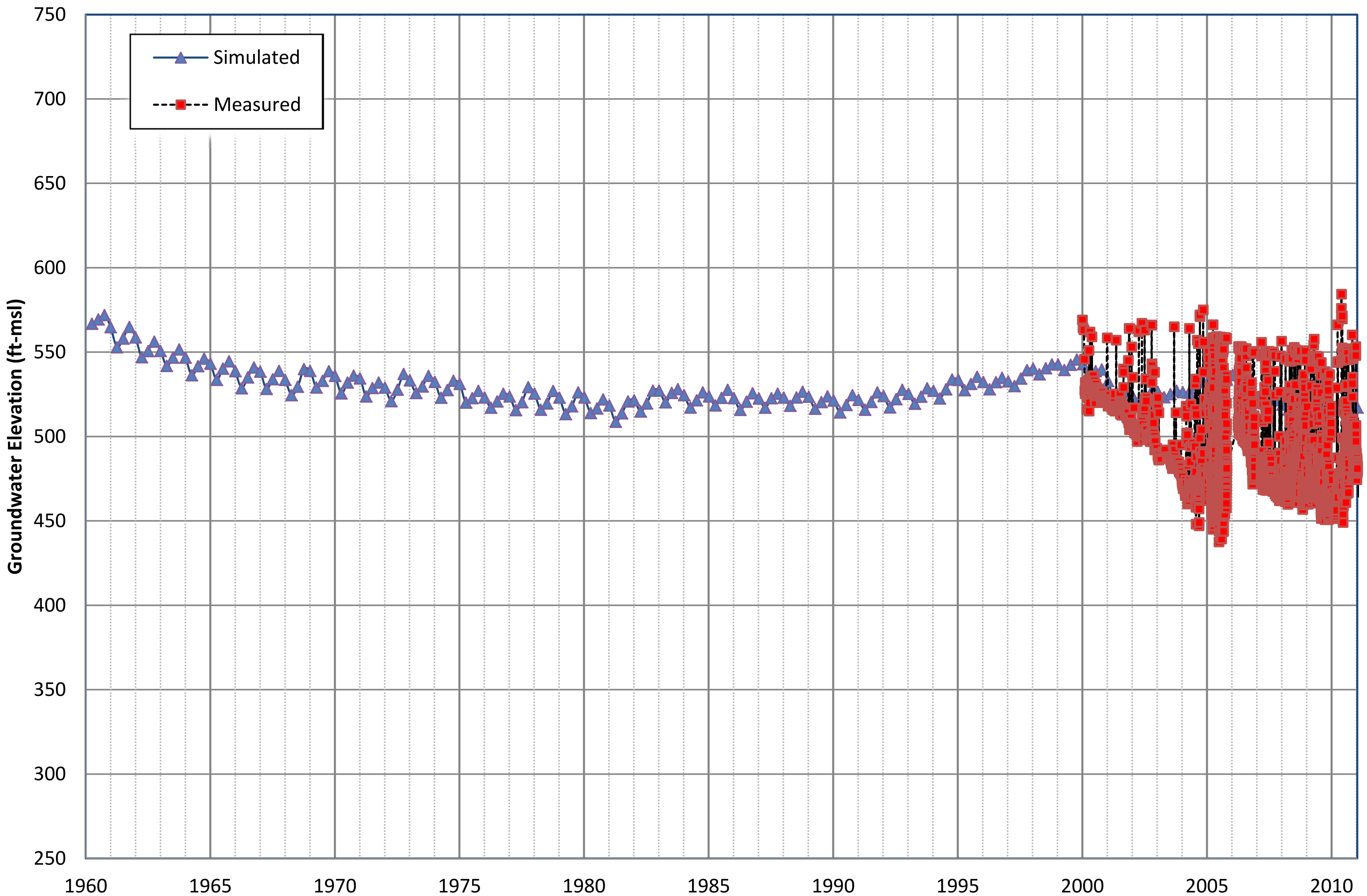

Appendix_C2_20151002_Validation_wells_Hydrographs.xlsm

Figure C2-12
Comparison of Measured and Simulated Groundwater Levels in CDA Well I-13

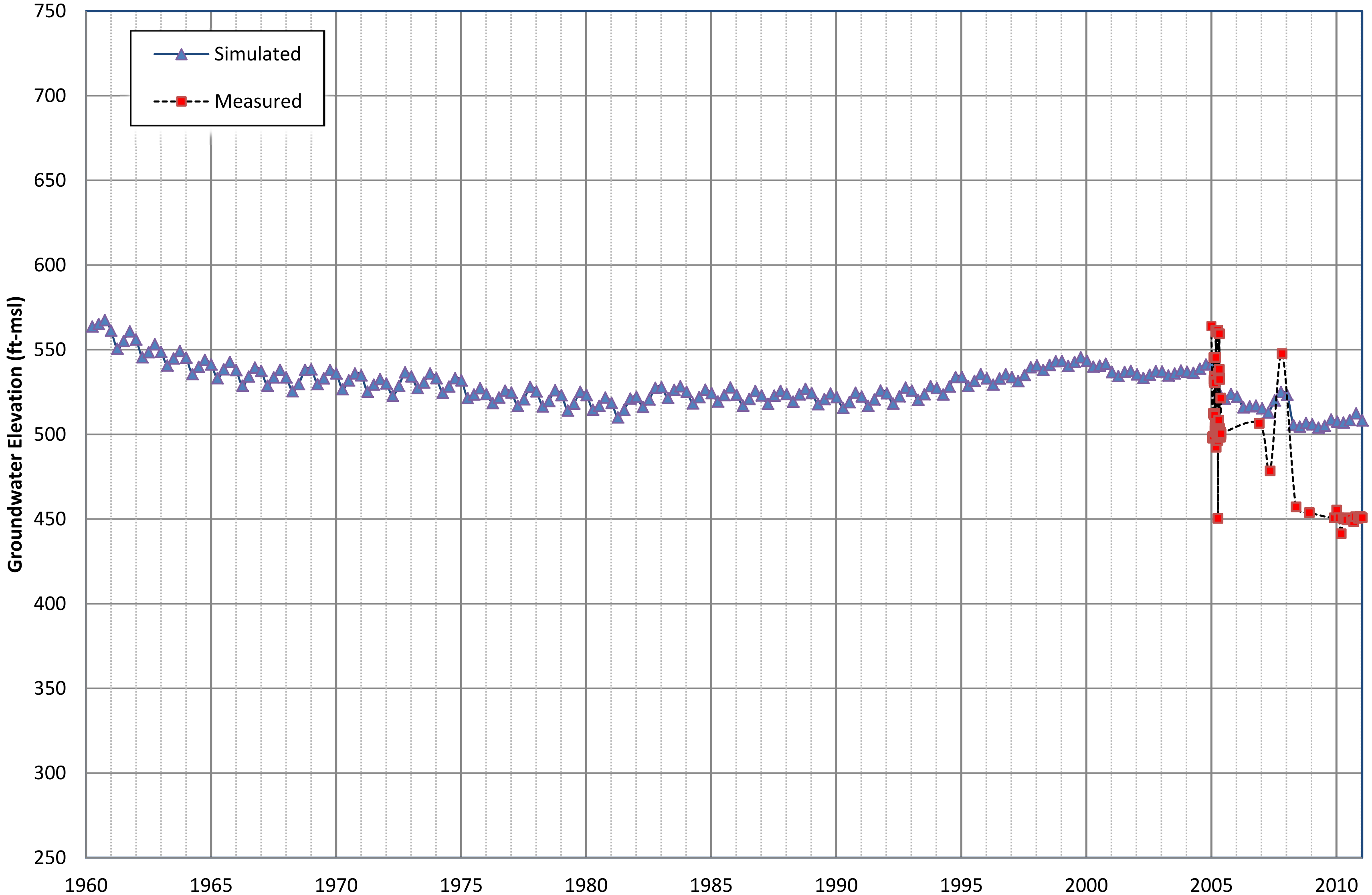

Figure C2-13
Comparison of Measured and Simulated Groundwater Levels in CDA Well I-14

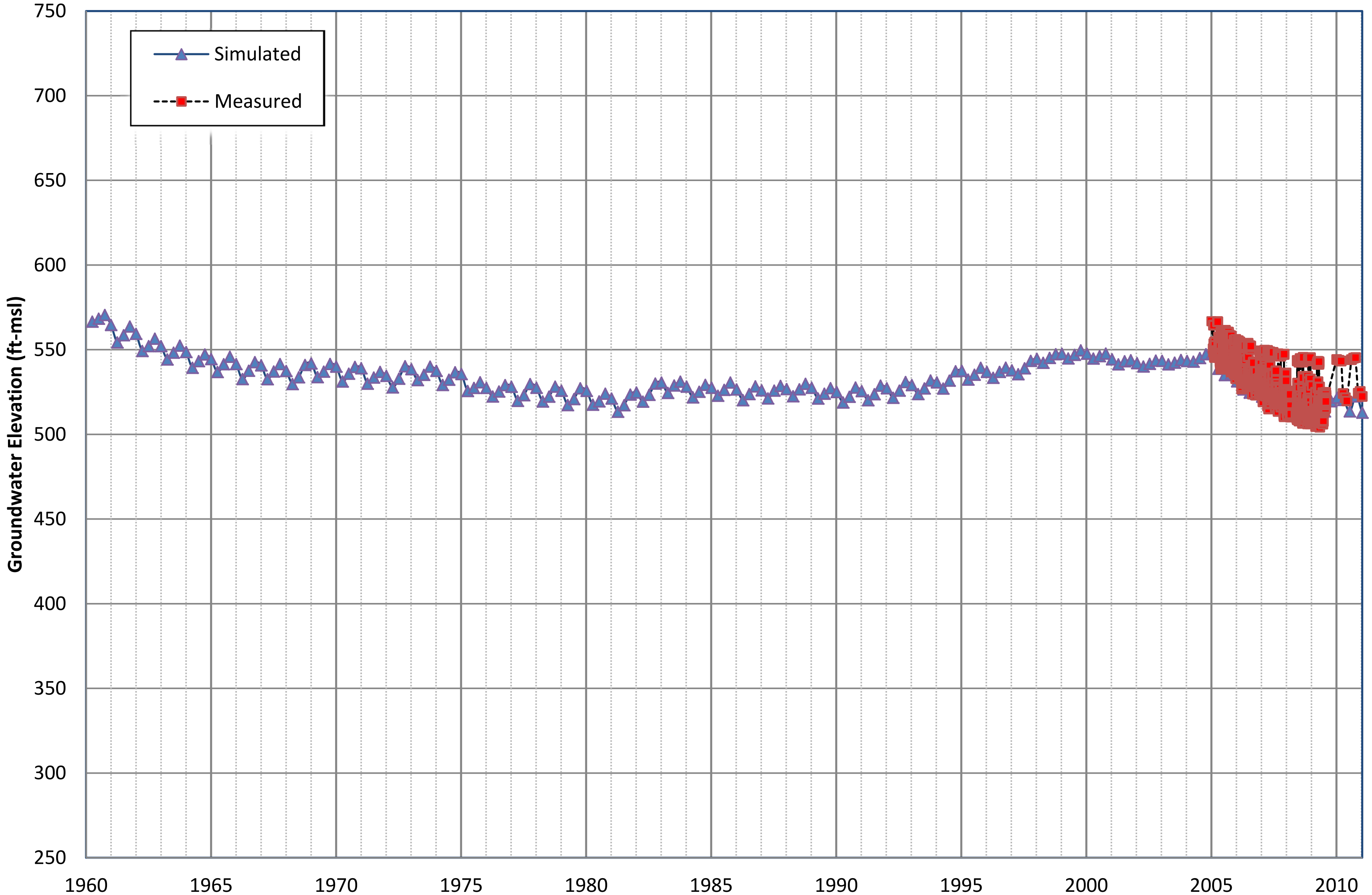

Figure C2-14
Comparison of Measured and Simulated Groundwater Levels in CDA Well I-15

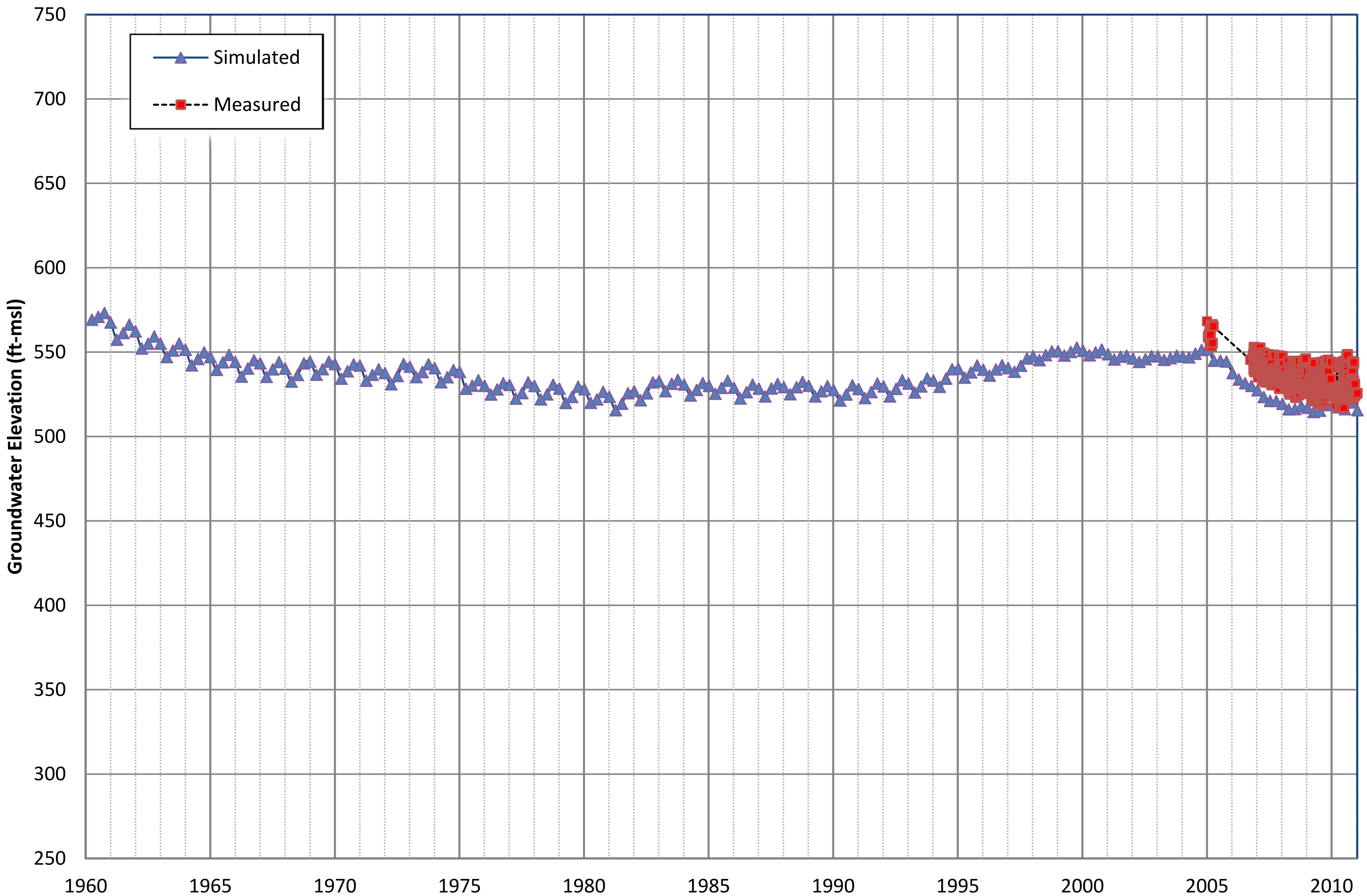

Figure C2-15
Comparison of Measured and Simulated Groundwater Levels in CDA Well II-1

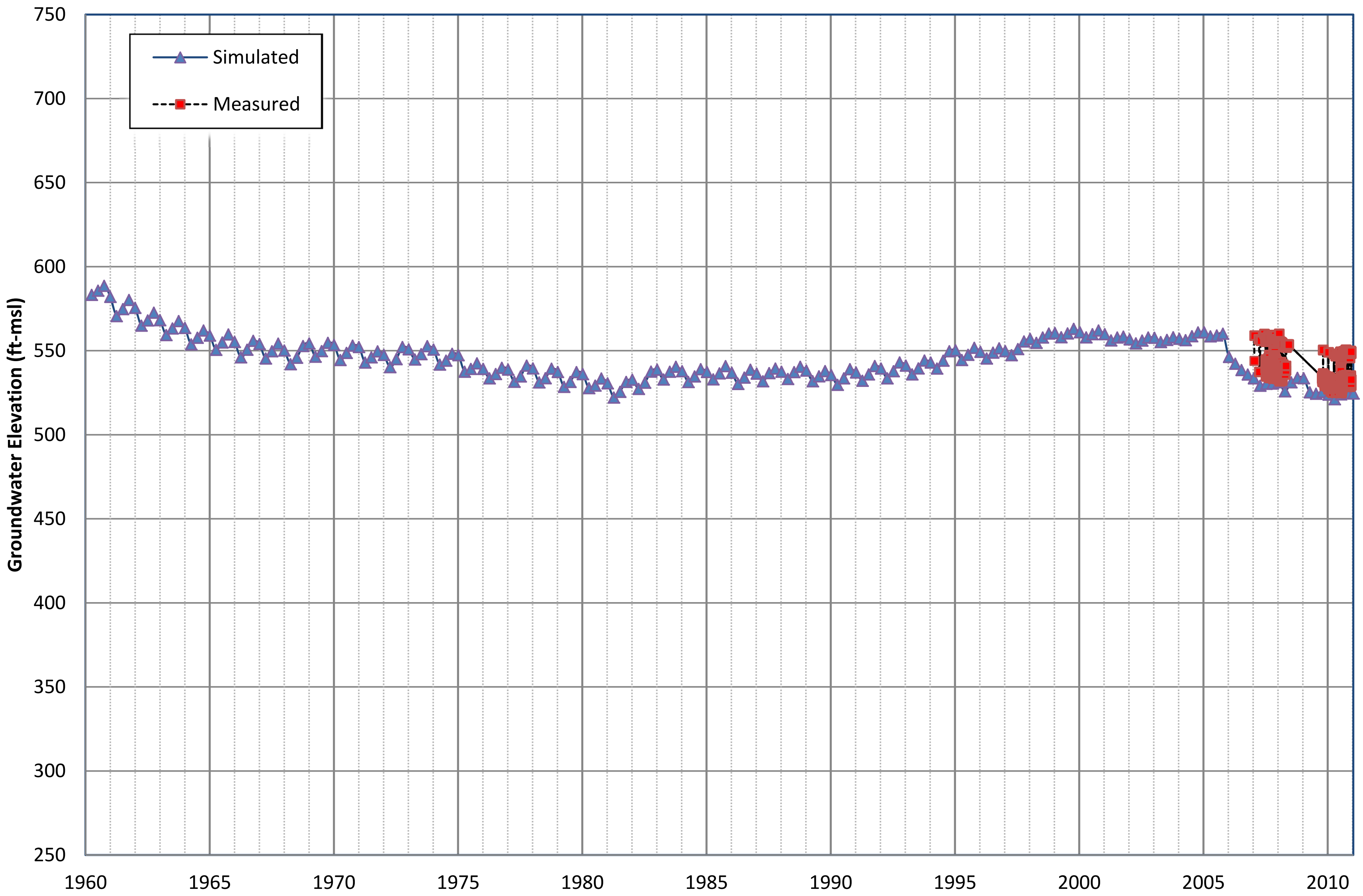

Figure C2-16
Comparison of Measured and Simulated Groundwater Levels in CDA Well II-2

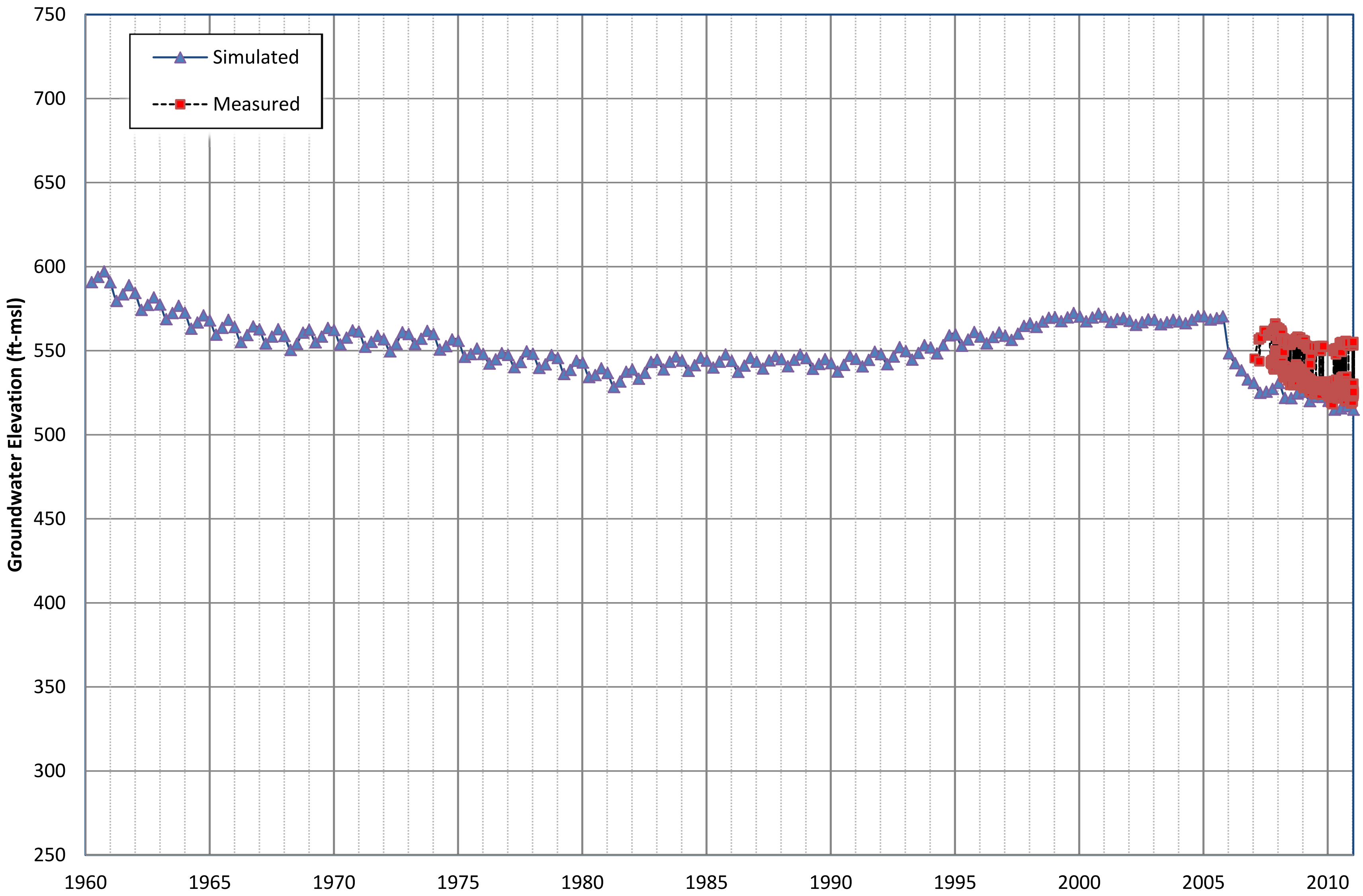

Figure C2-17
Comparison of Measured and Simulated Groundwater Levels in CDA Well II-3

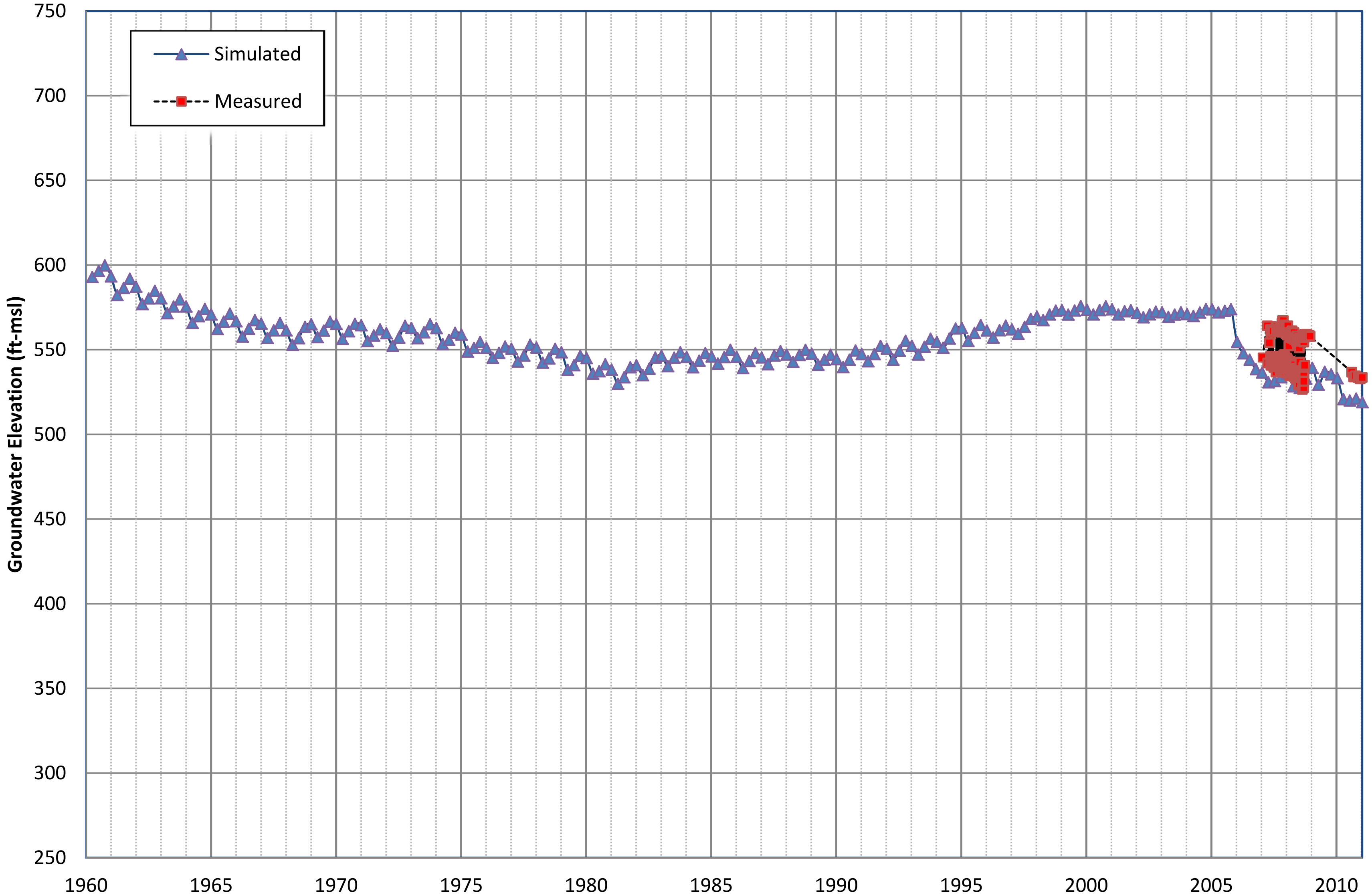

Appendix_C2_20151002_Validation_wells_Hydrographs.xlsm

Figure C2-18
Comparison of Measured and Simulated Groundwater Levels in CDA Well II-4

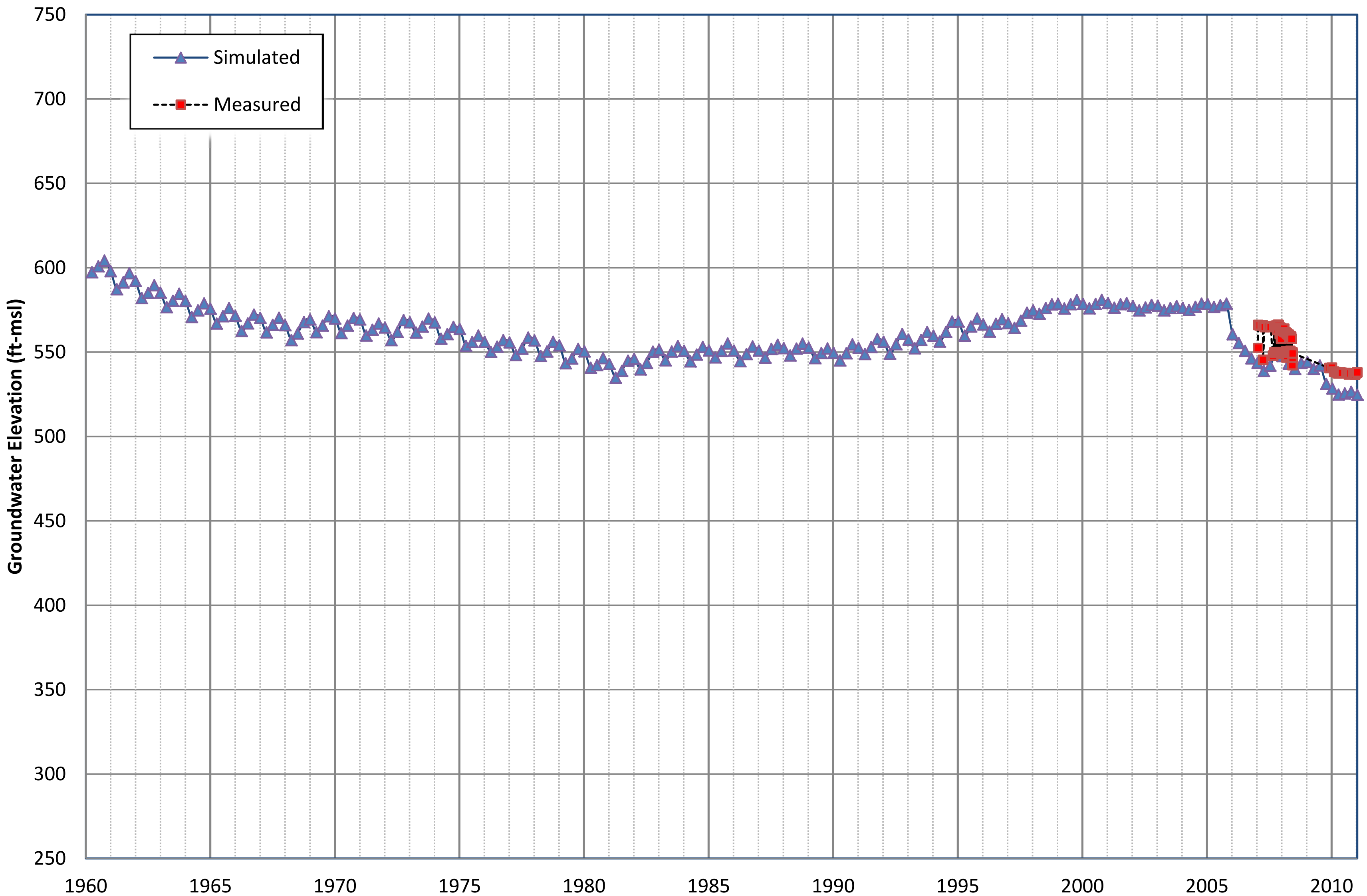

Figure C2-19

Comparison of Measured and Simulated Groundwater Levels in CDA Well II-6

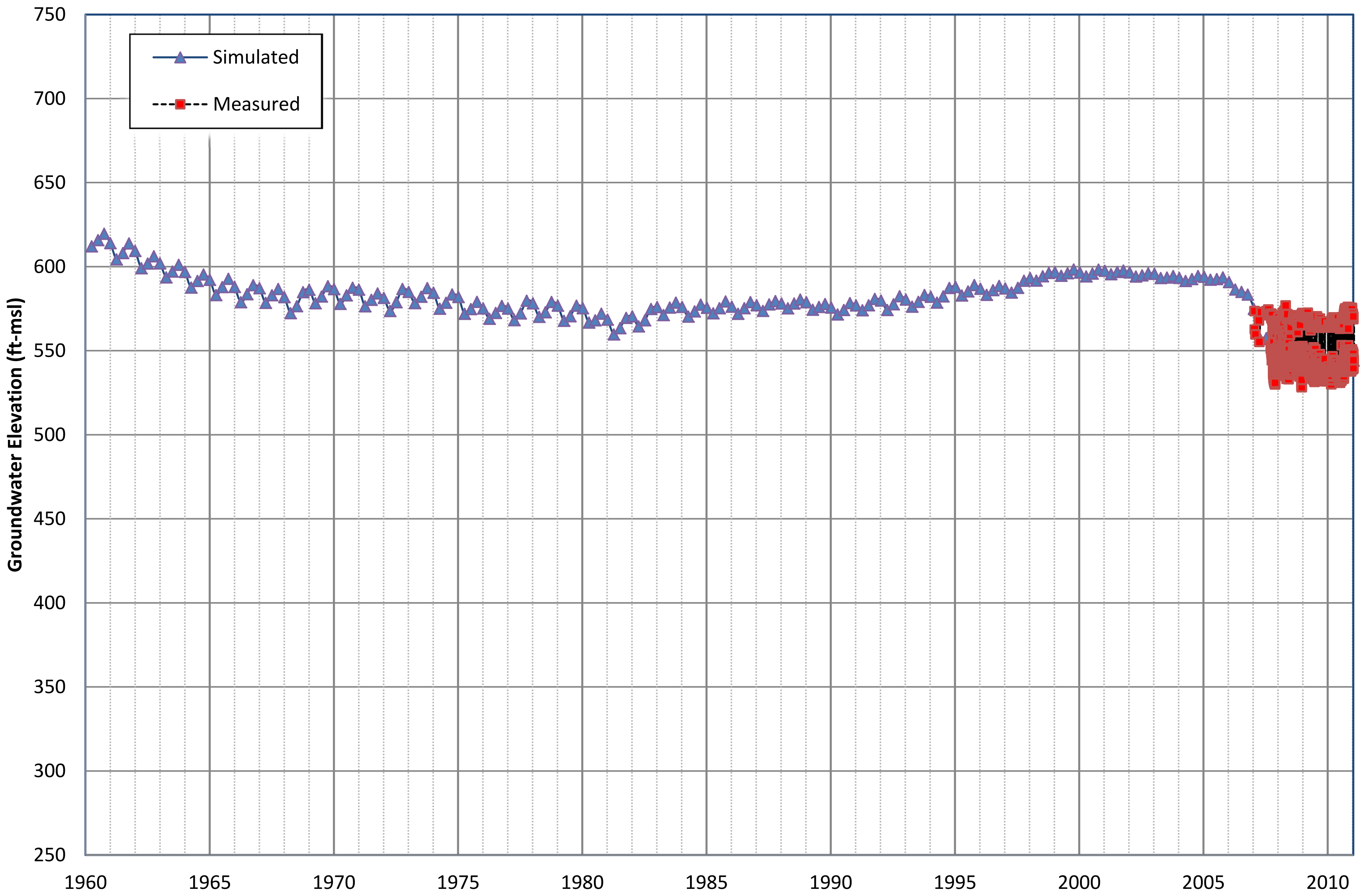

Figure C2-20
Comparison of Measured and Simulated Groundwater Levels in CDA Well II-7

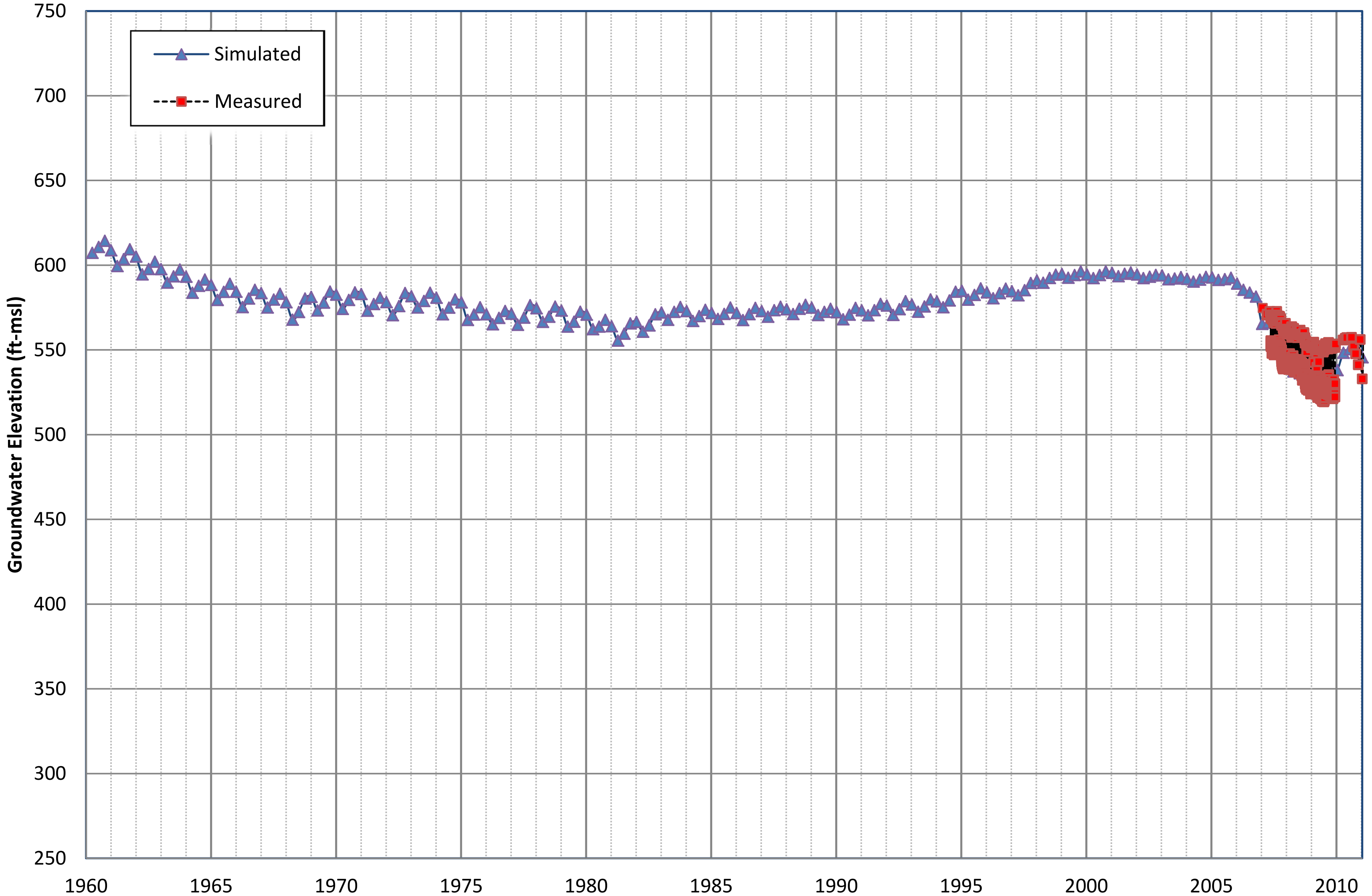

Figure C2-21
Comparison of Measured and Simulated Groundwater Levels in CDA Well II-8

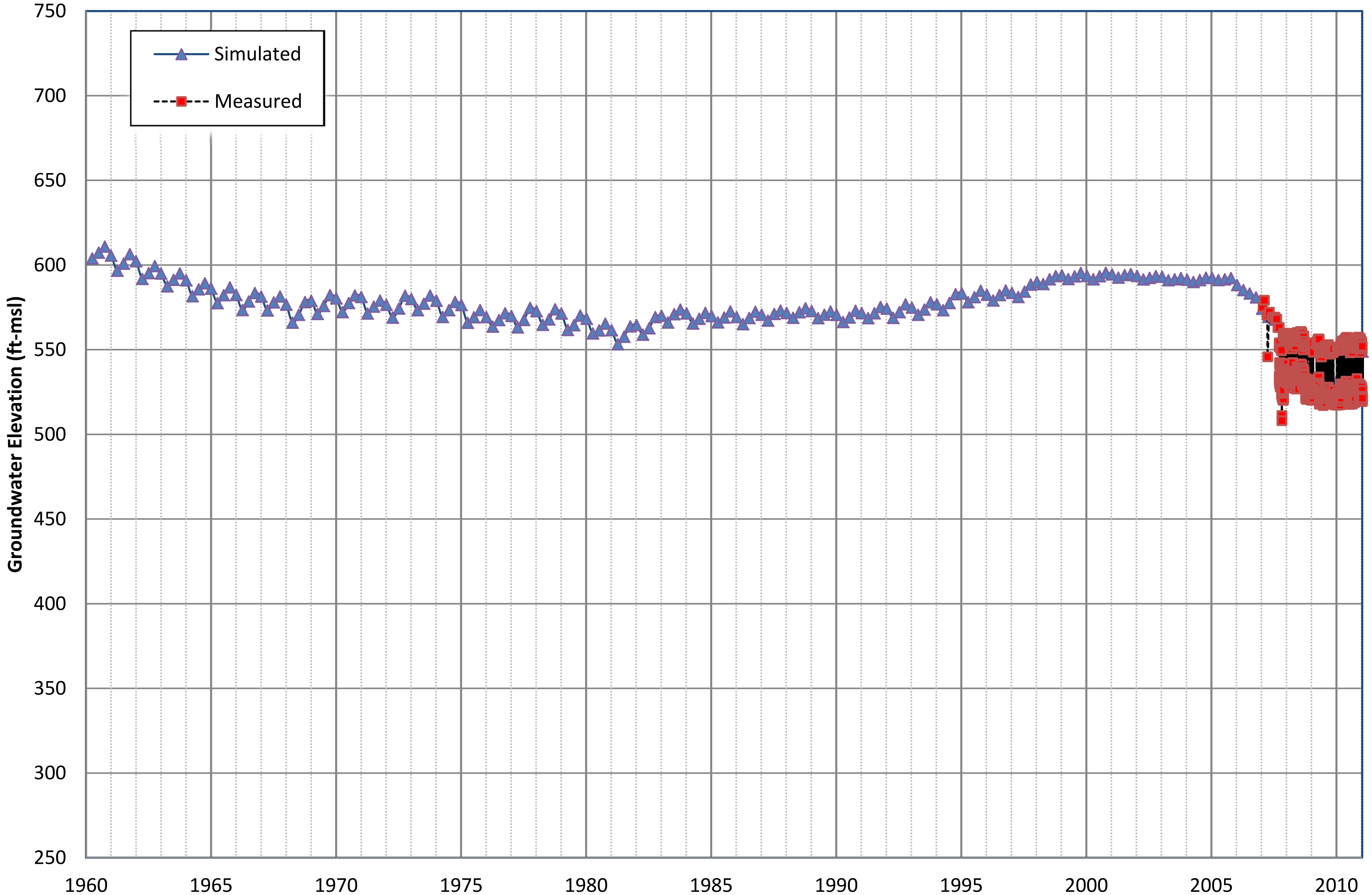

Appendix_C2_20151002_Validation_wells_Hydrographs.xlsm

Figure C2-22
Comparison of Measured and Simulated Groundwater Levels in CDA Well II-9A

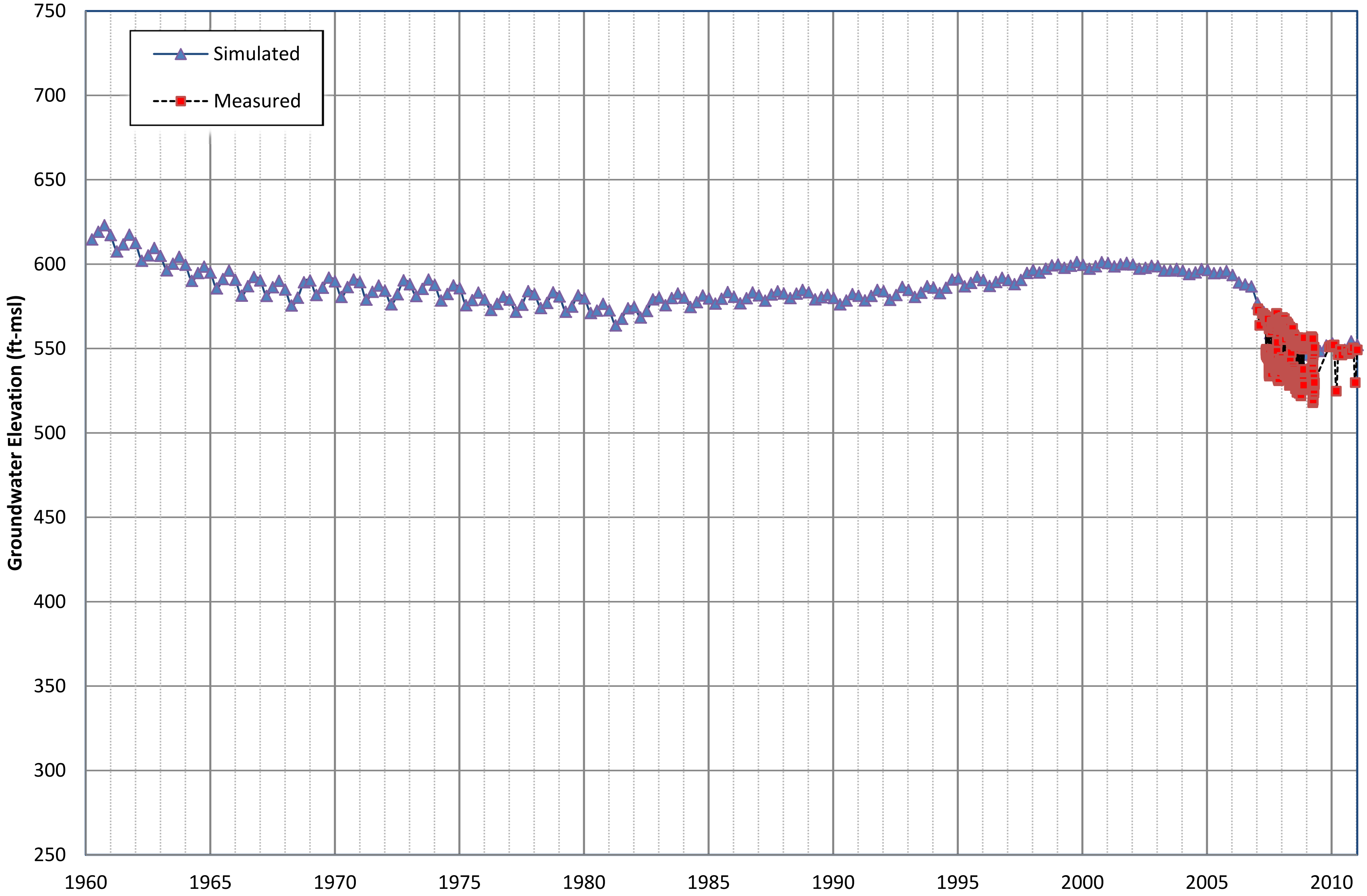

Figure C2-23
Comparison of Measured and Simulated Groundwater Levels in JCSD Well 5

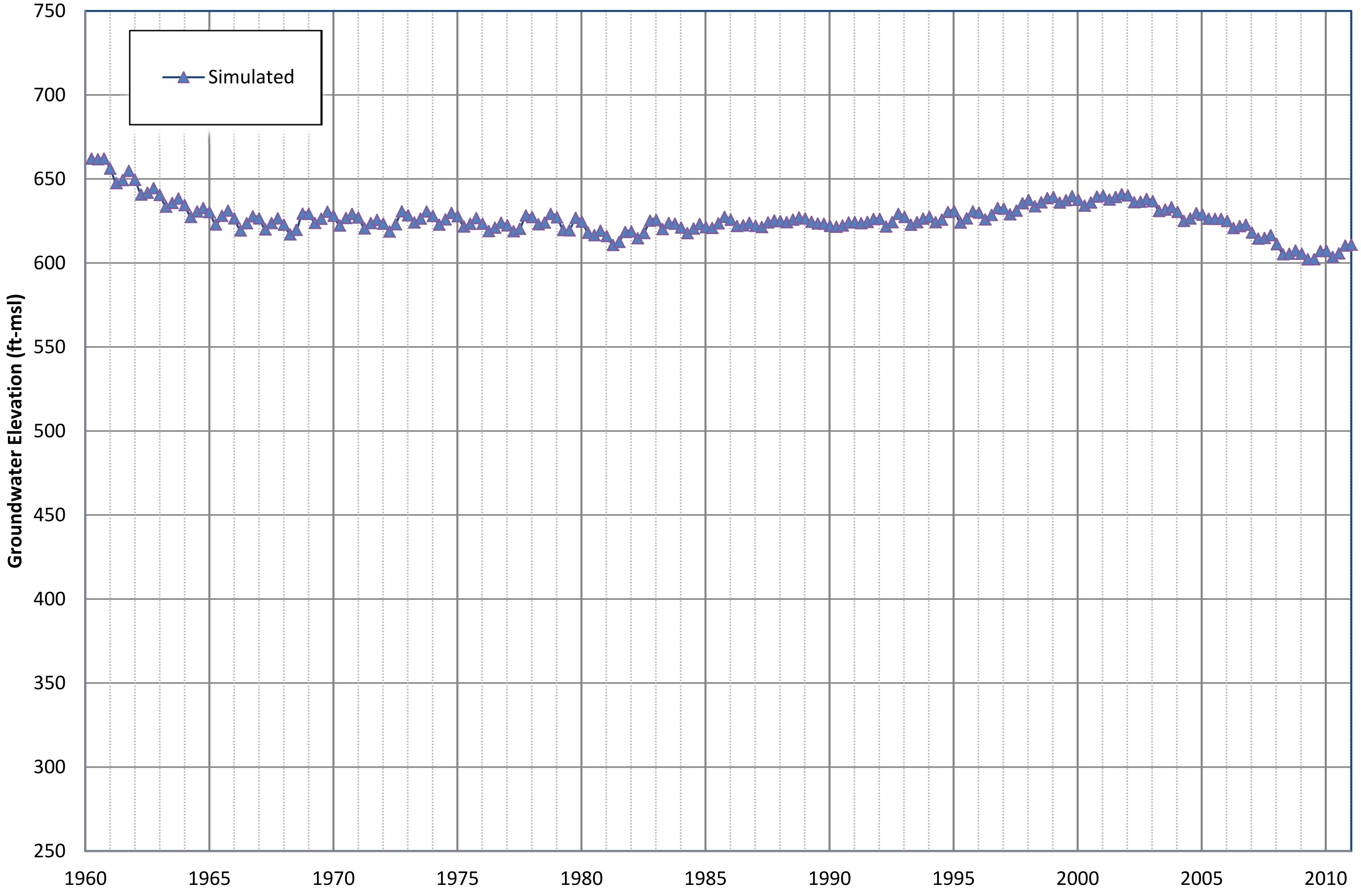

Figure C2-24
Comparison of Measured and Simulated Groundwater Levels in JCSD Well MIRA LOMA #6

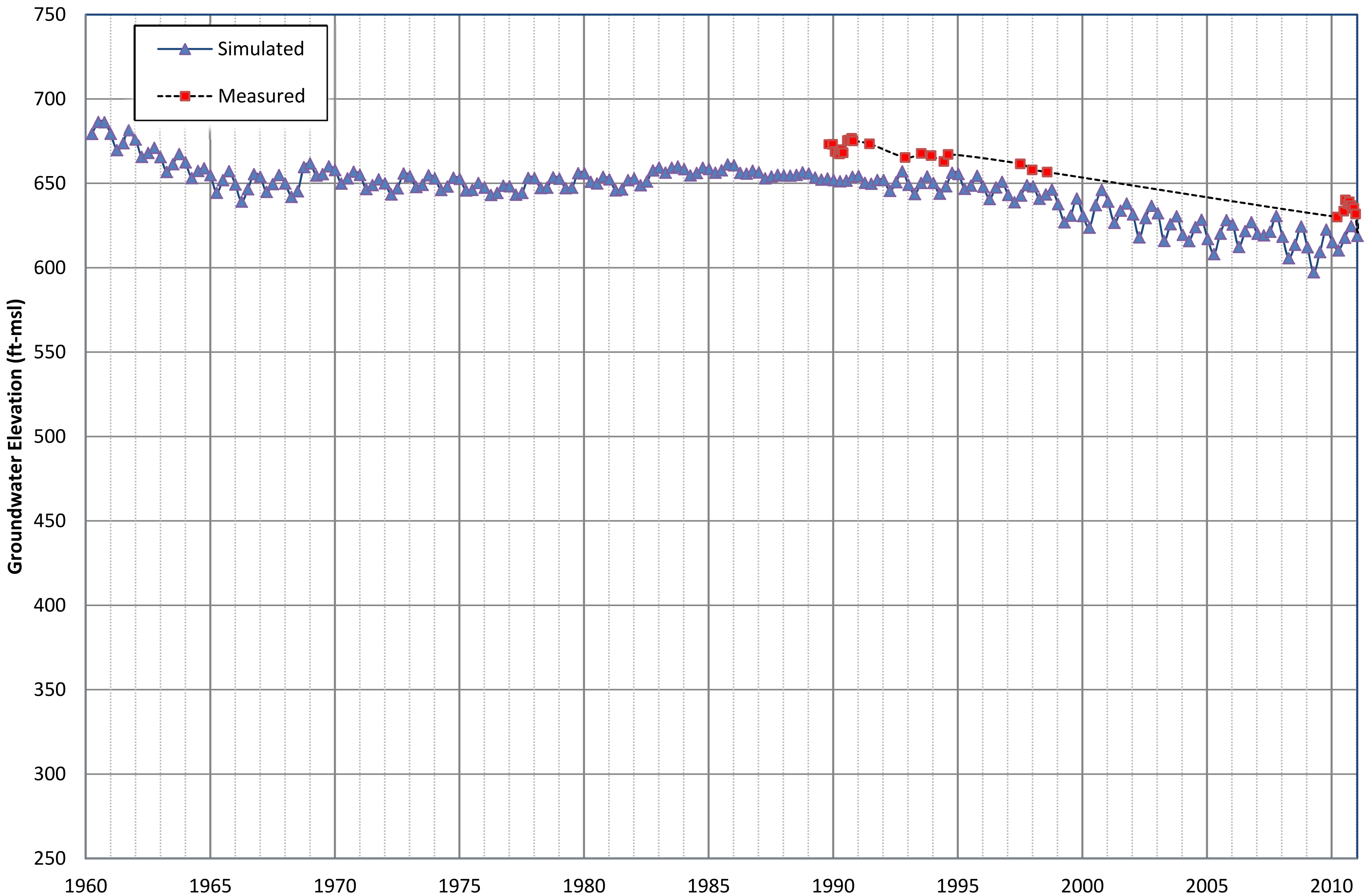

Figure C2-25
Comparison of Measured and Simulated Groundwater Levels in JCSD Well 8 (Russell Well)

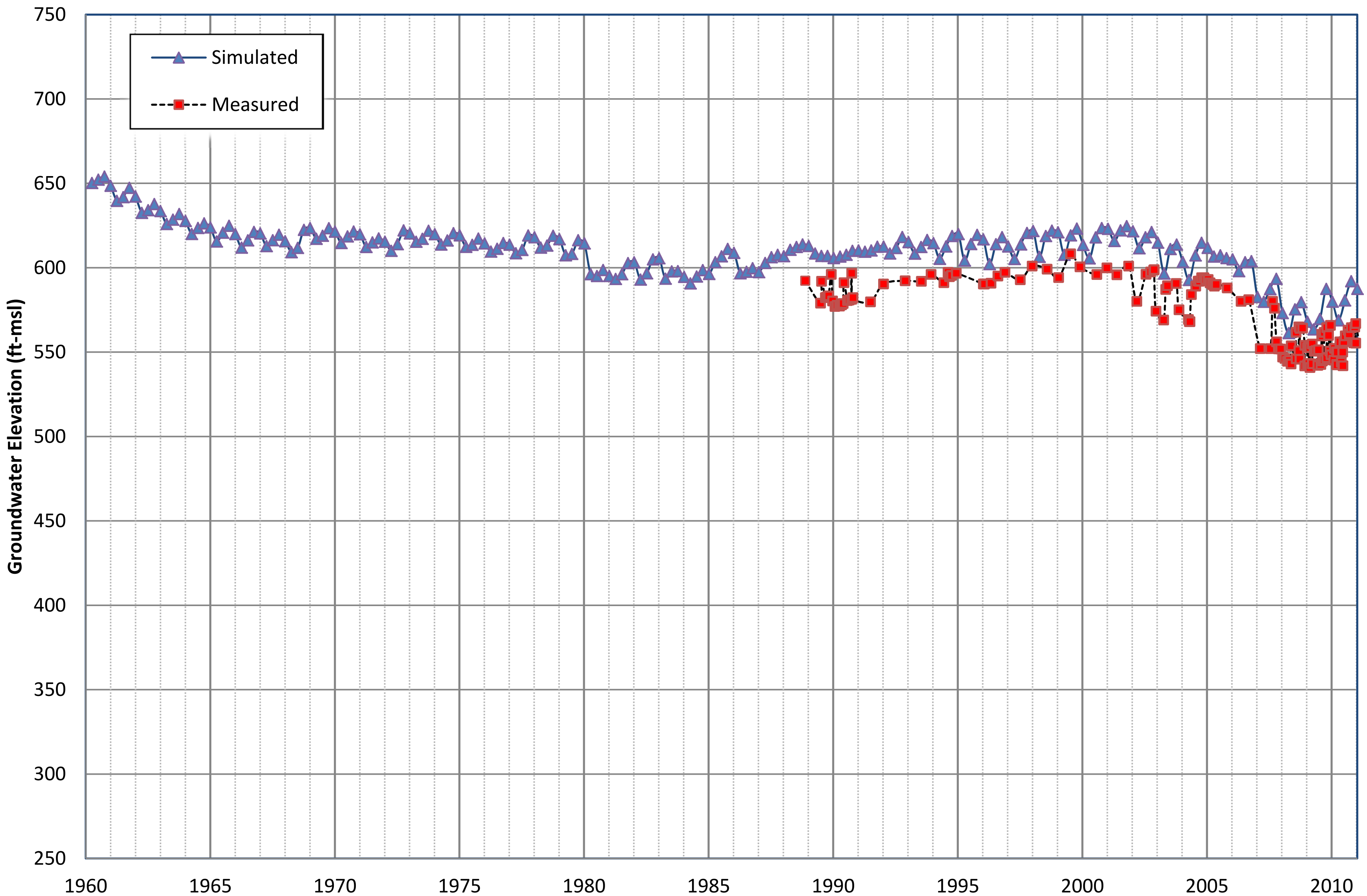

Figure C2-26
Comparison of Measured and Simulated Groundwater Levels in JCSD Well 11

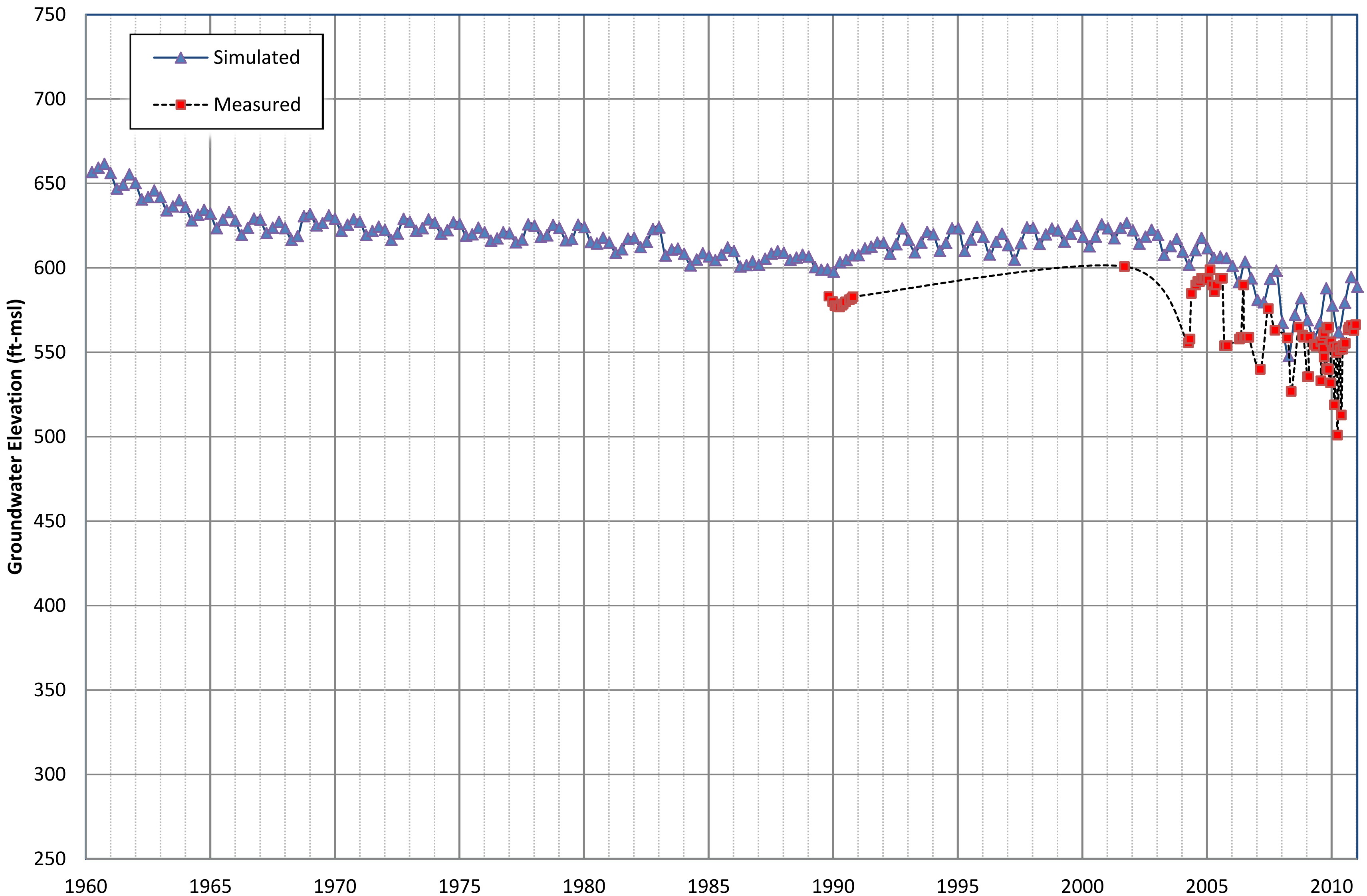

Figure C2-27
Comparison of Measured and Simulated Groundwater Levels in JCSD Well 12

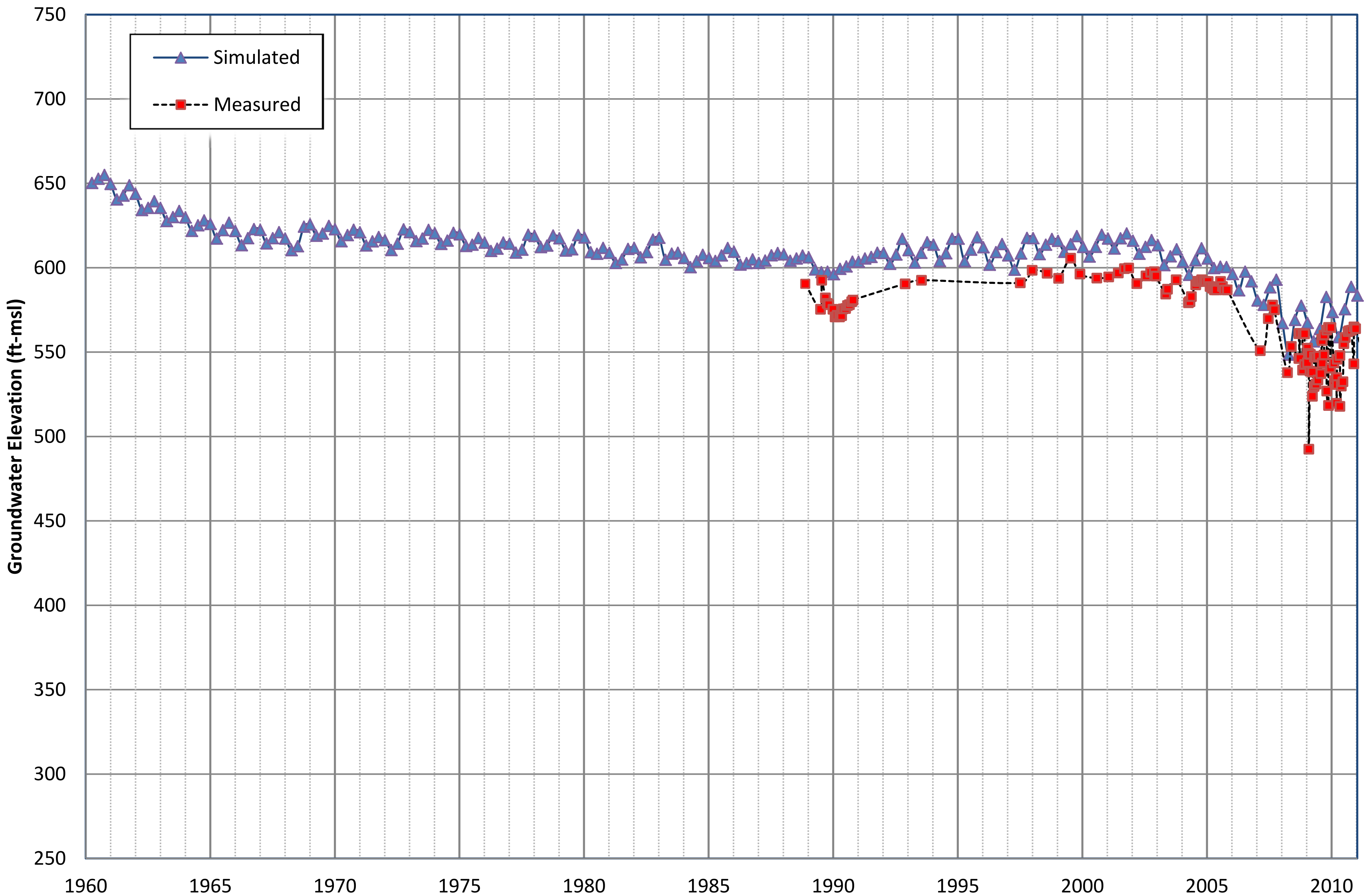

Appendix_C2_20151002_Validation_wells_Hydrographs.xlsm

Figure C2-28
Comparison of Measured and Simulated Groundwater Levels in JCSD Well 13

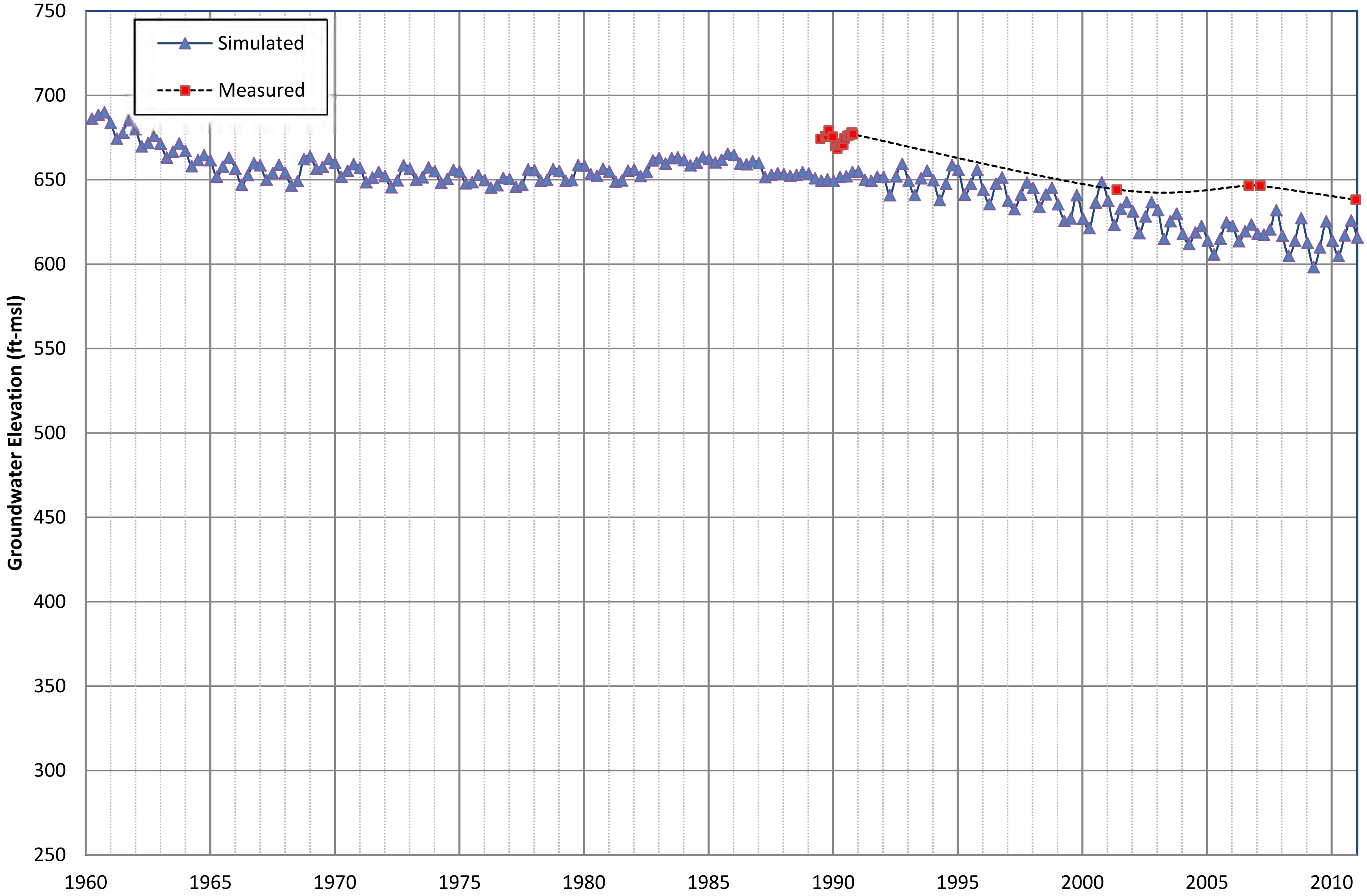

Figure C2-29
Comparison of Measured and Simulated Groundwater Levels in JCSD Well 14

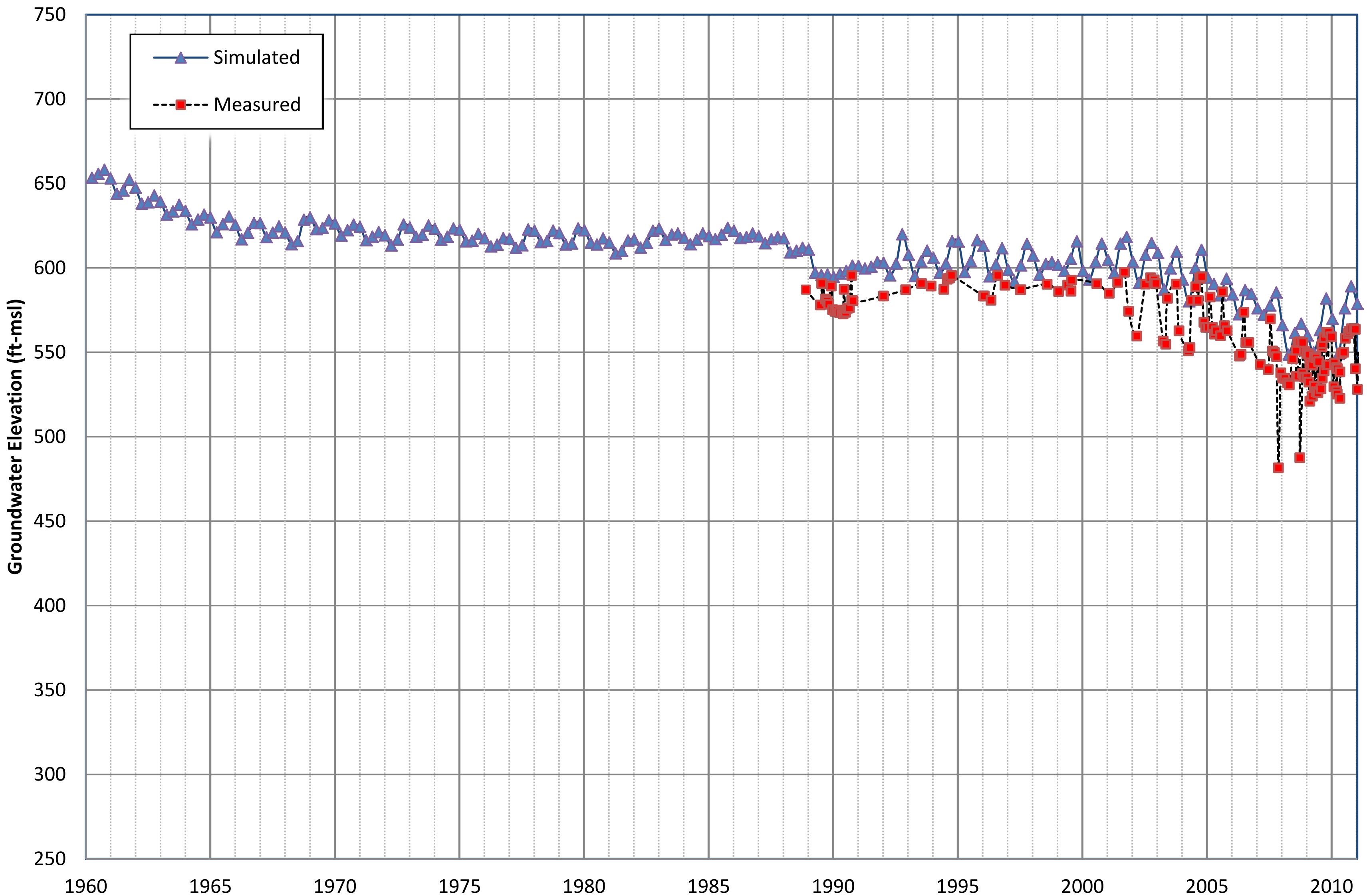

Figure C2-30
Comparison of Measured and Simulated Groundwater Levels in JCSD Well 15

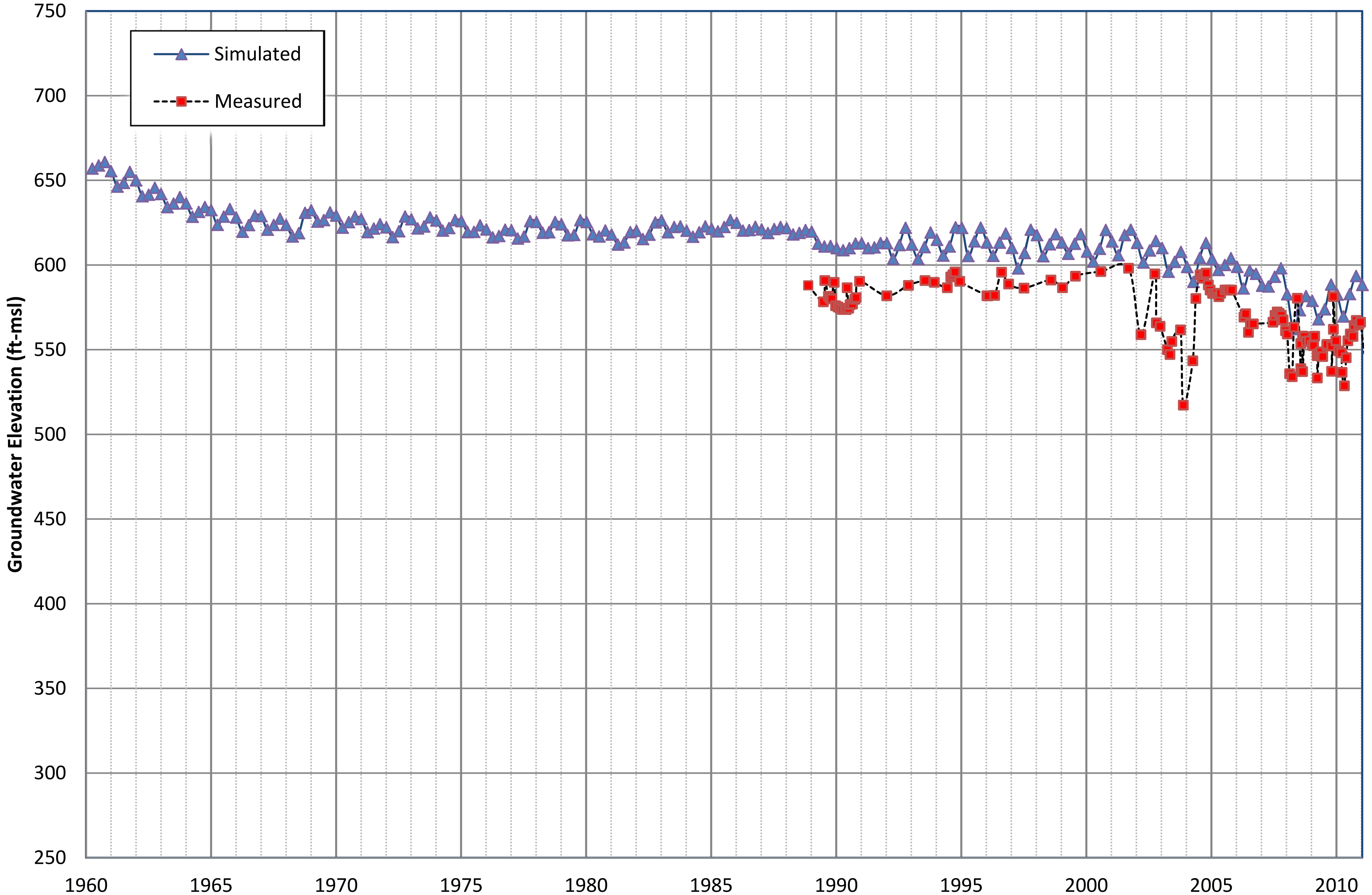

Figure C2-31
Comparison of Measured and Simulated Groundwater Levels in JCSD Well 16

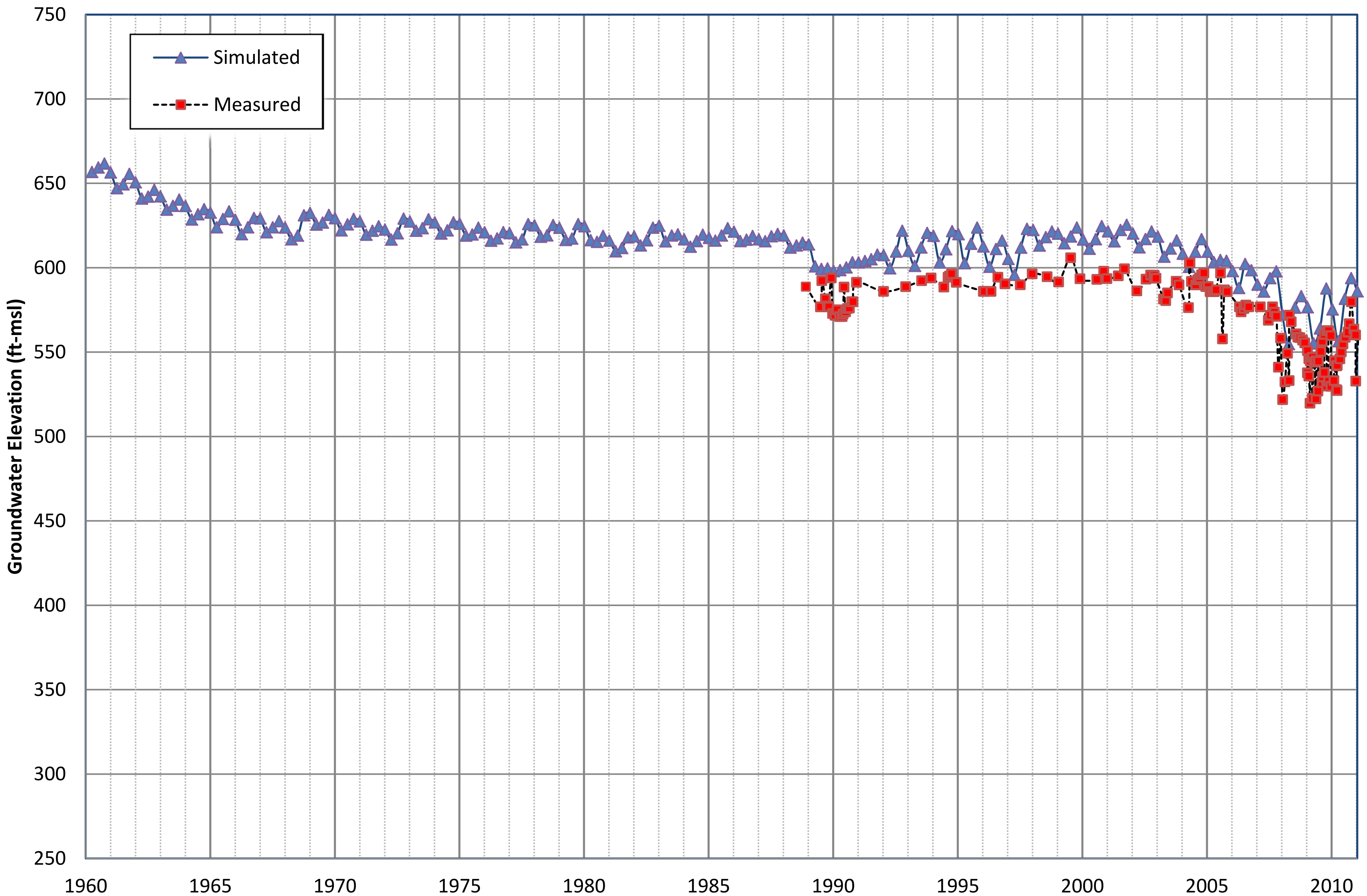

Appendix_C2_20151002_Validation_wells_Hydrographs.xlsm

Figure C2-32
Comparison of Measured and Simulated Groundwater Levels in JCSD Well 17

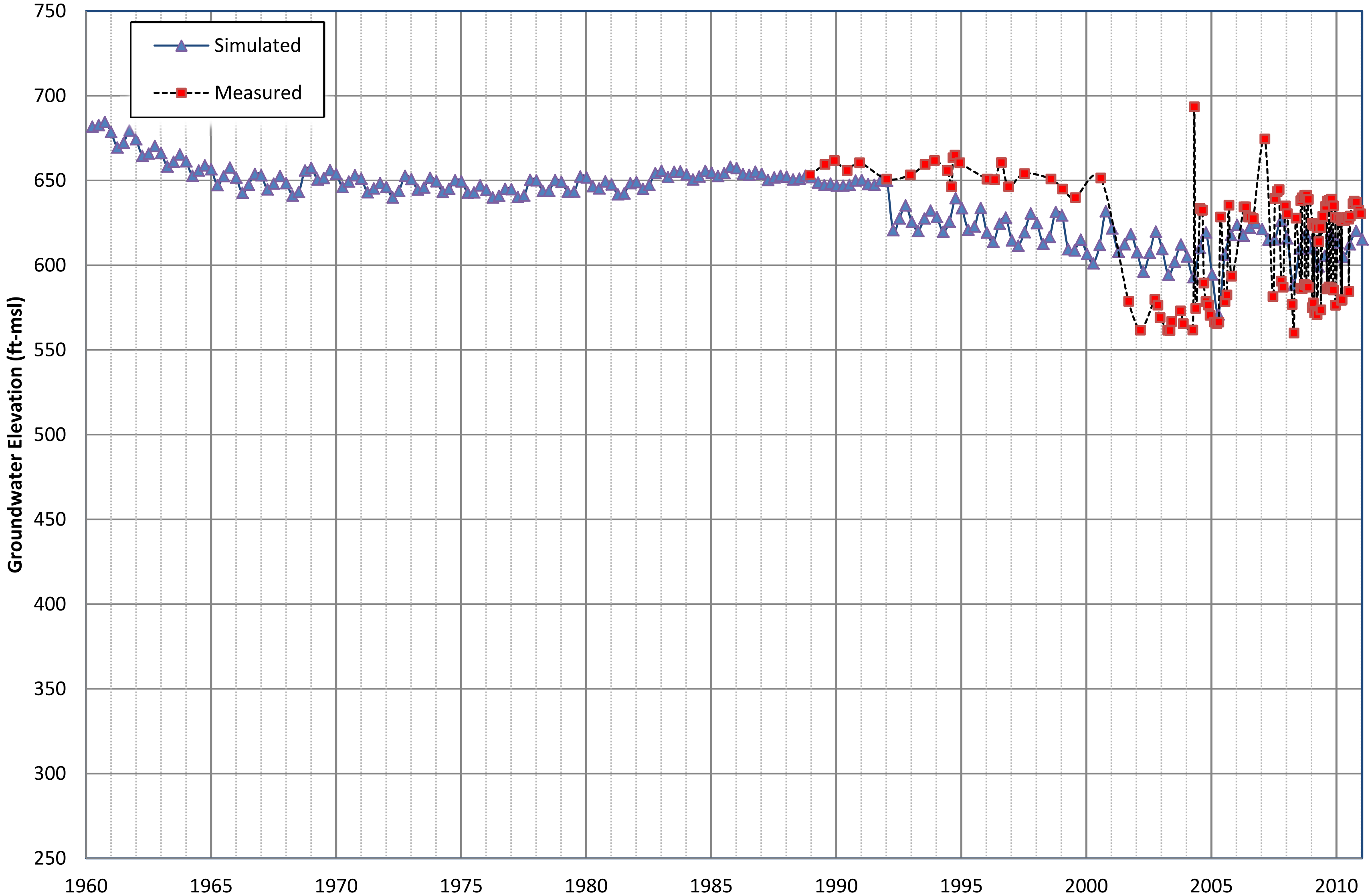

Figure C2-33
Comparison of Measured and Simulated Groundwater Levels in JCSD Well 18

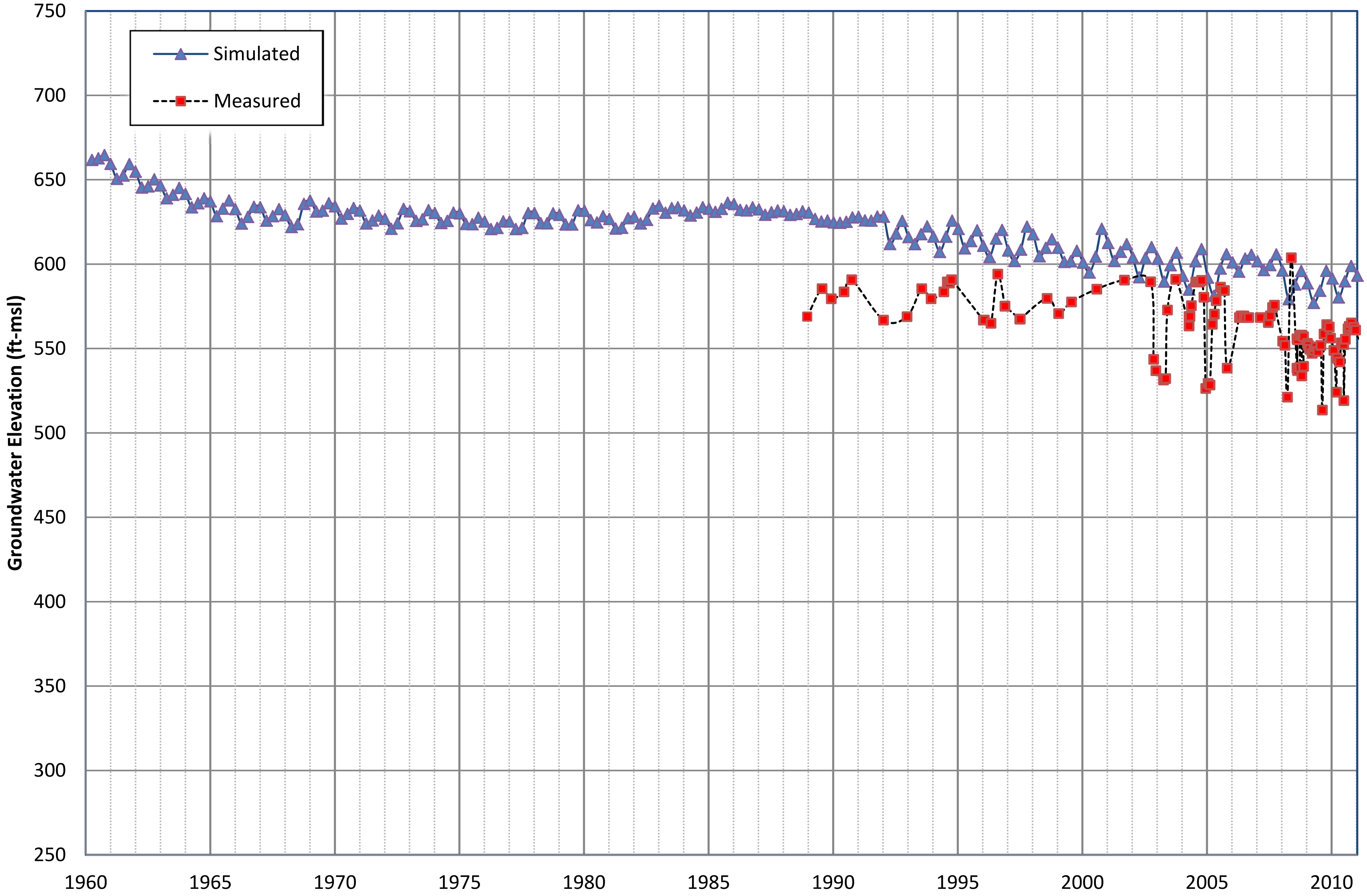

Figure C2-34
Comparison of Measured and Simulated Groundwater Levels in JCSD Well 19

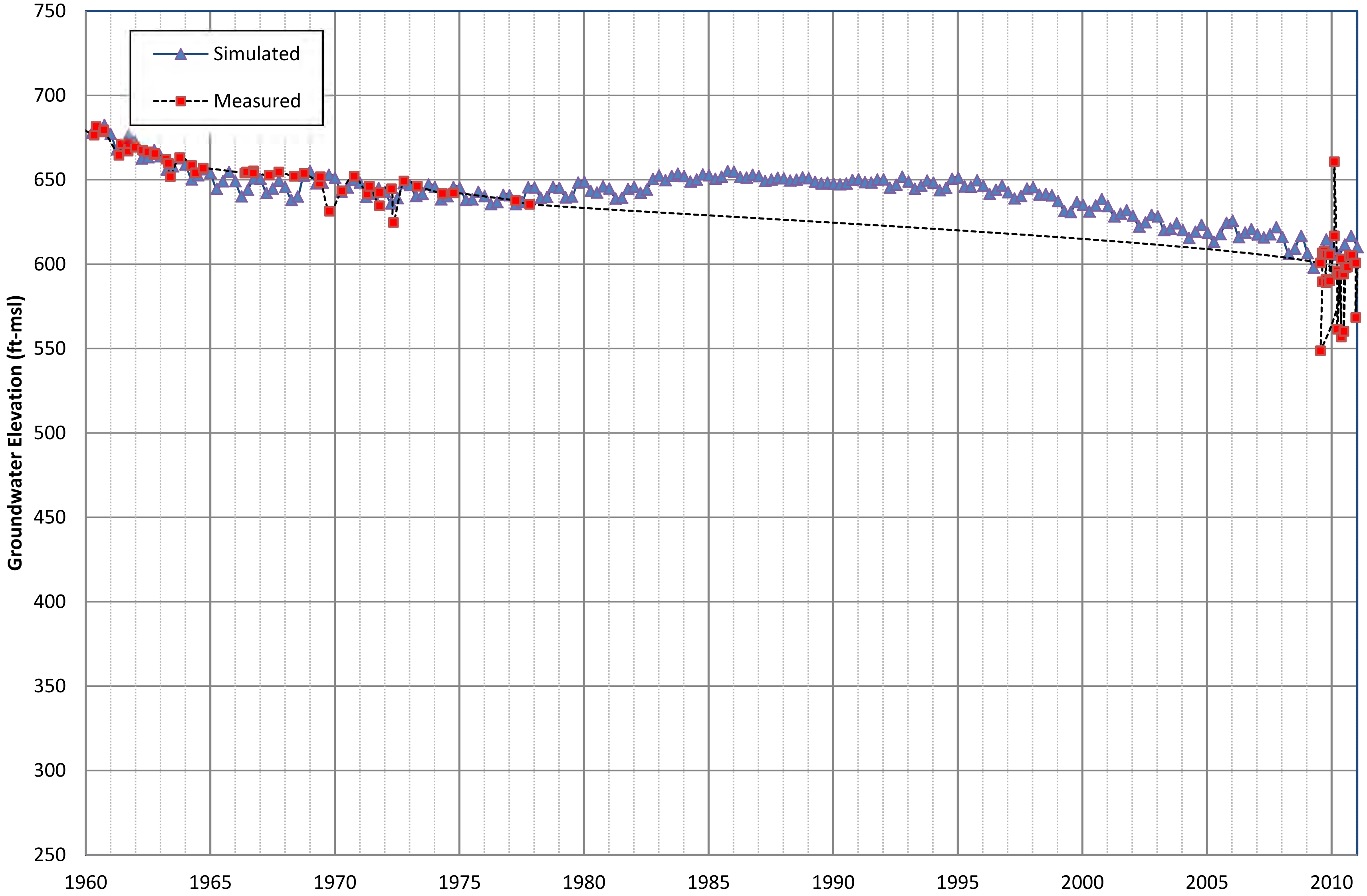

Figure C2-35
Comparison of Measured and Simulated Groundwater Levels in JCSD Well MLSC2

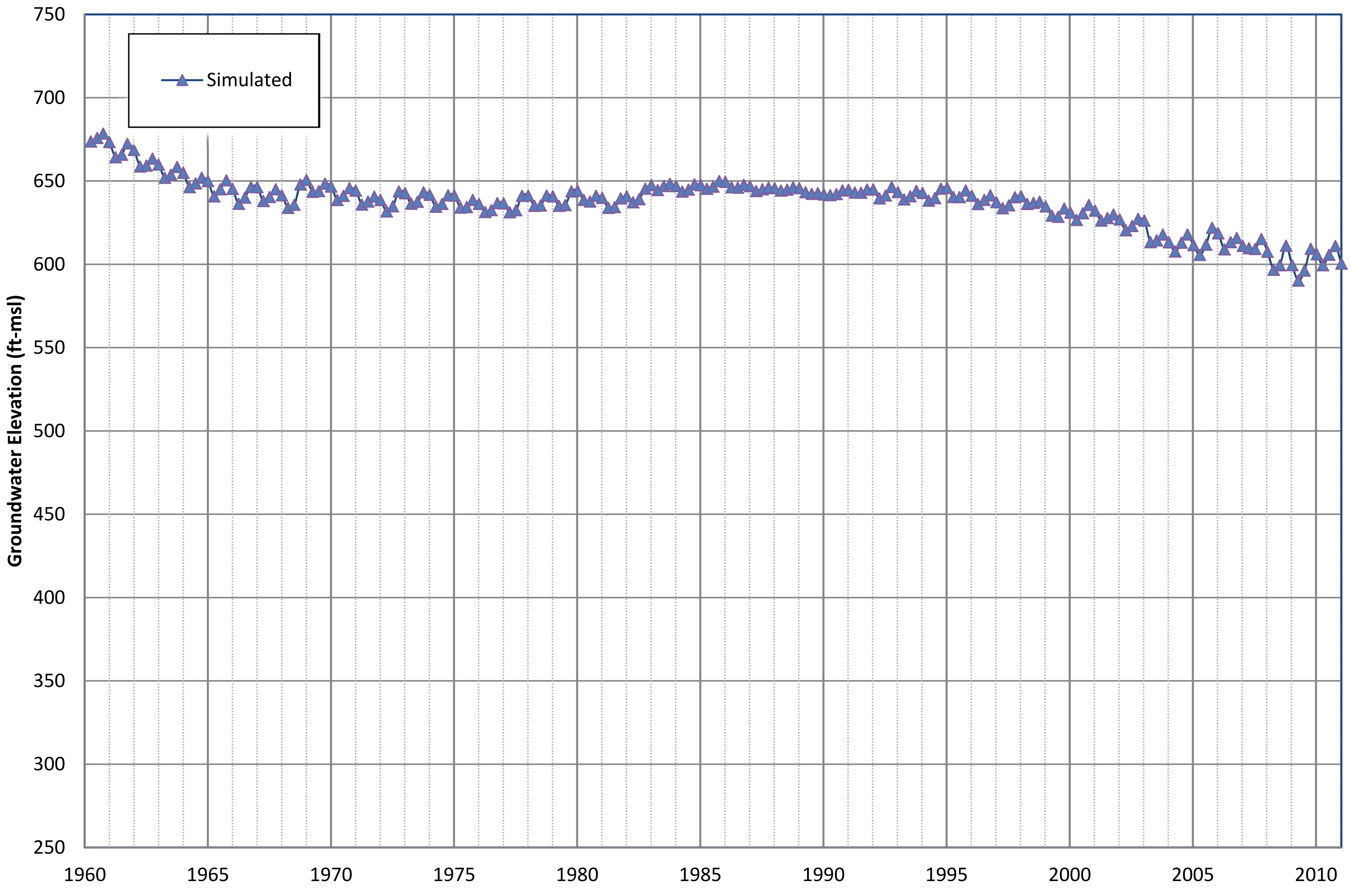

Figure C2-36
Comparison of Measured and Simulated Groundwater Levels in JCSD Well 22

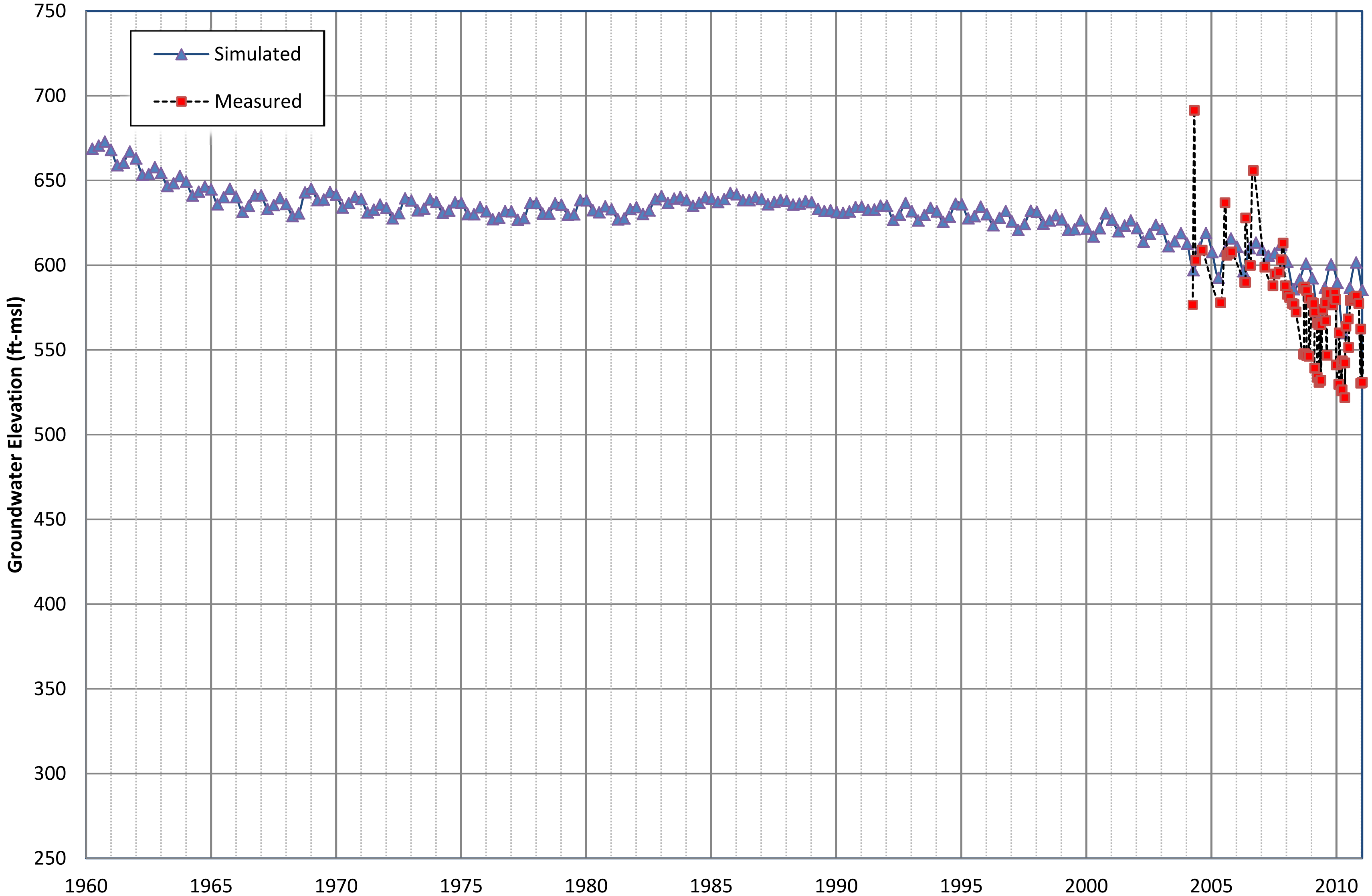

Appendix_C2_20151002_Validation_wells_Hydrographs.xlsm

Figure C2-37
Comparison of Measured and Simulated Groundwater Levels in JCSD Well 23

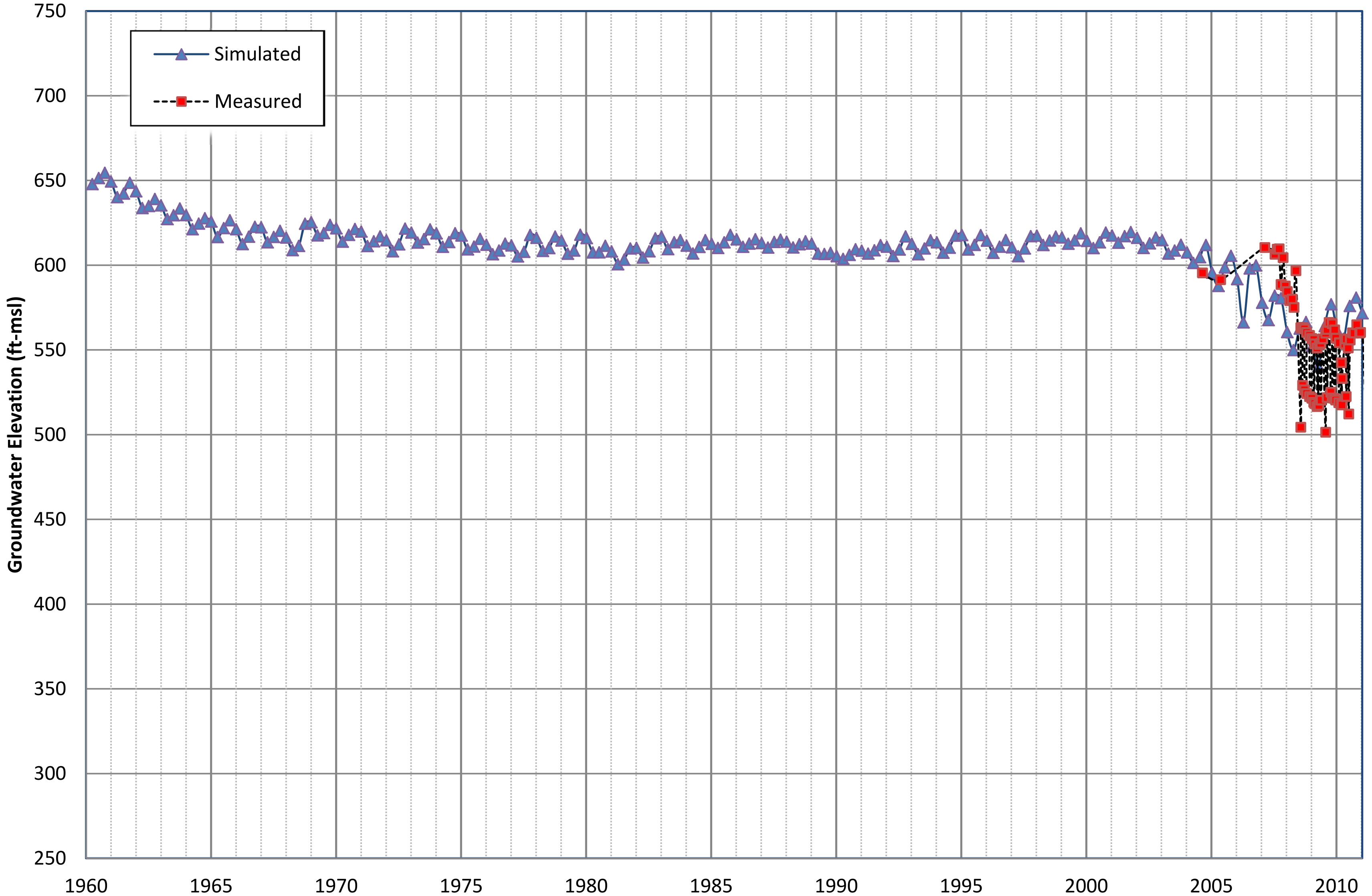

Figure C2-38
Comparison of Measured and Simulated Groundwater Levels in JCSD Well 6

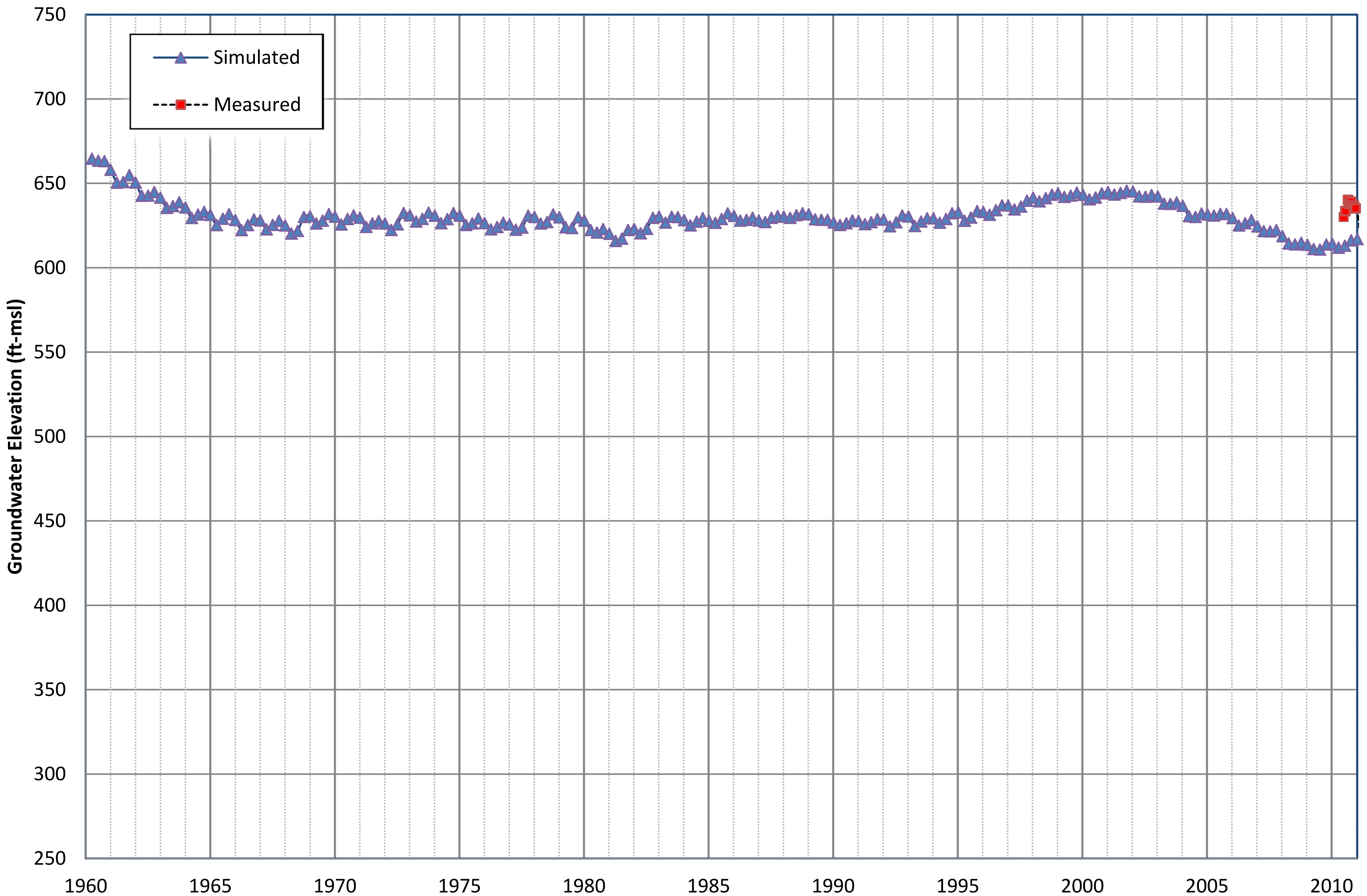

Figure C2-39
Comparison of Measured and Simulated Groundwater Levels in JCSD Well 25

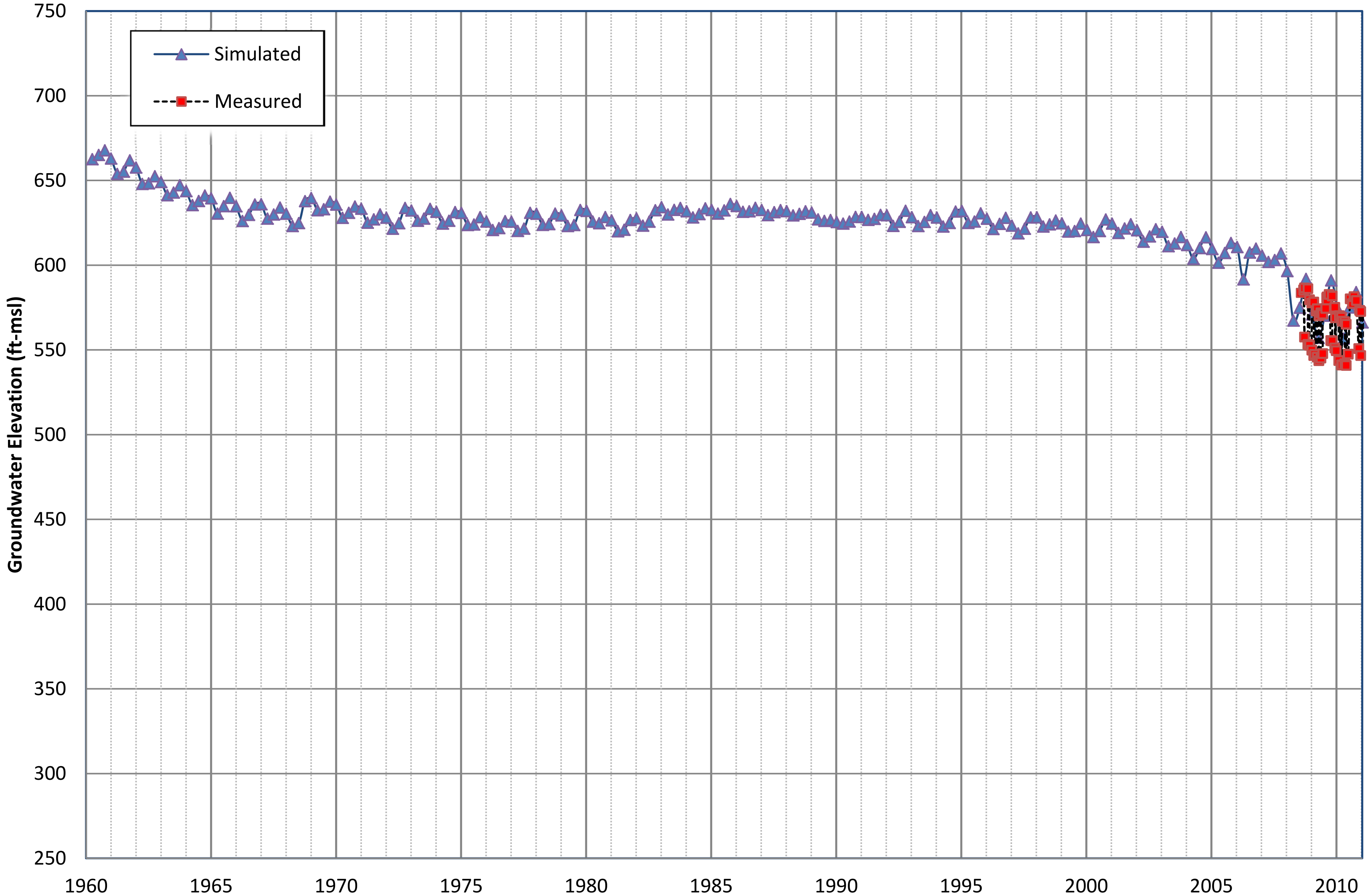

Appendix_C2_20151002_Validation_wells_Hydrographs.xlsm

Figure C2-40
Comparison of Measured and Simulated Groundwater Levels in JCSD Well 42

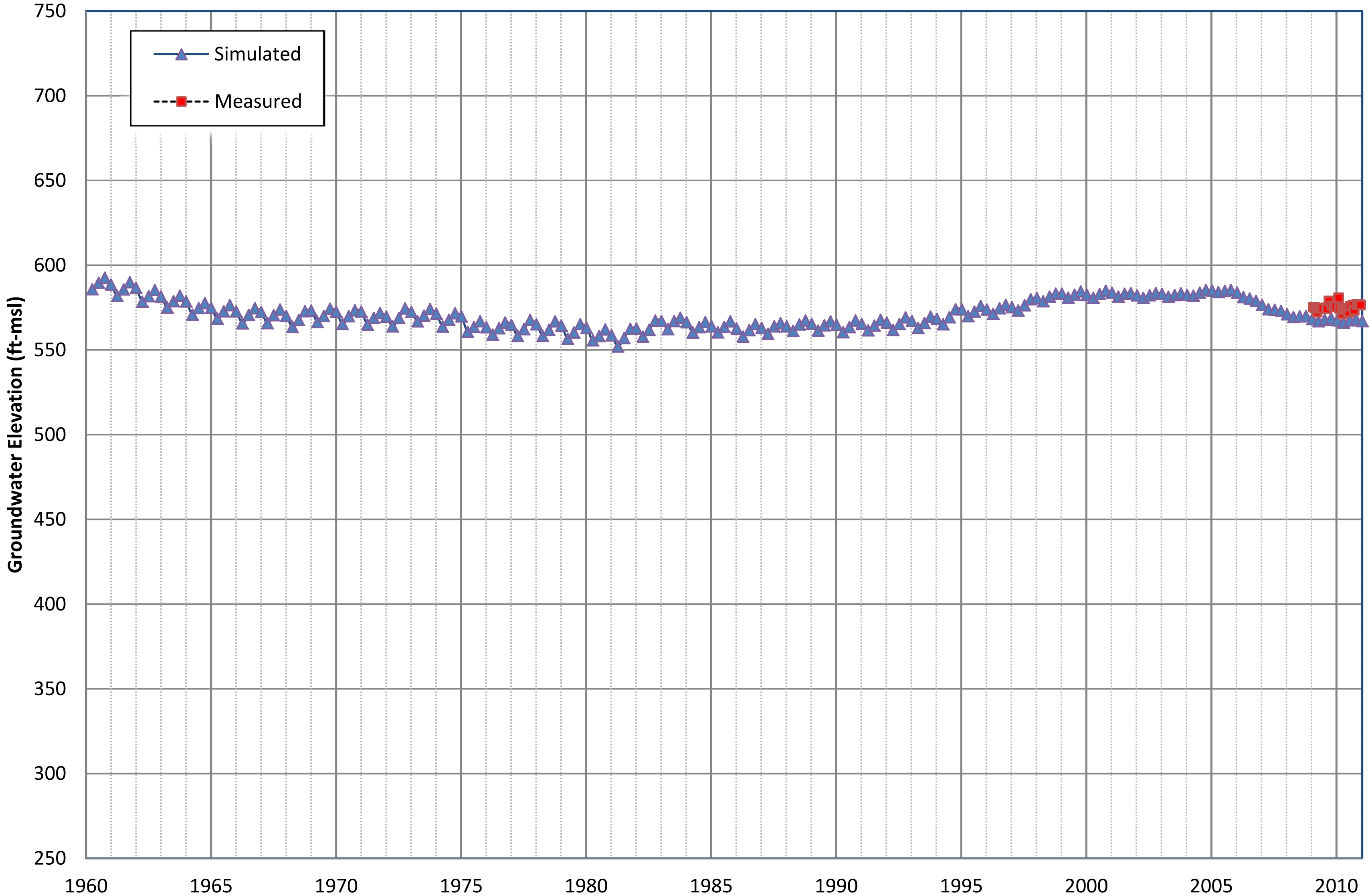

Figure C2-41
Comparison of Measured and Simulated Groundwater Levels in JCSD Well MIRA LOMA #4

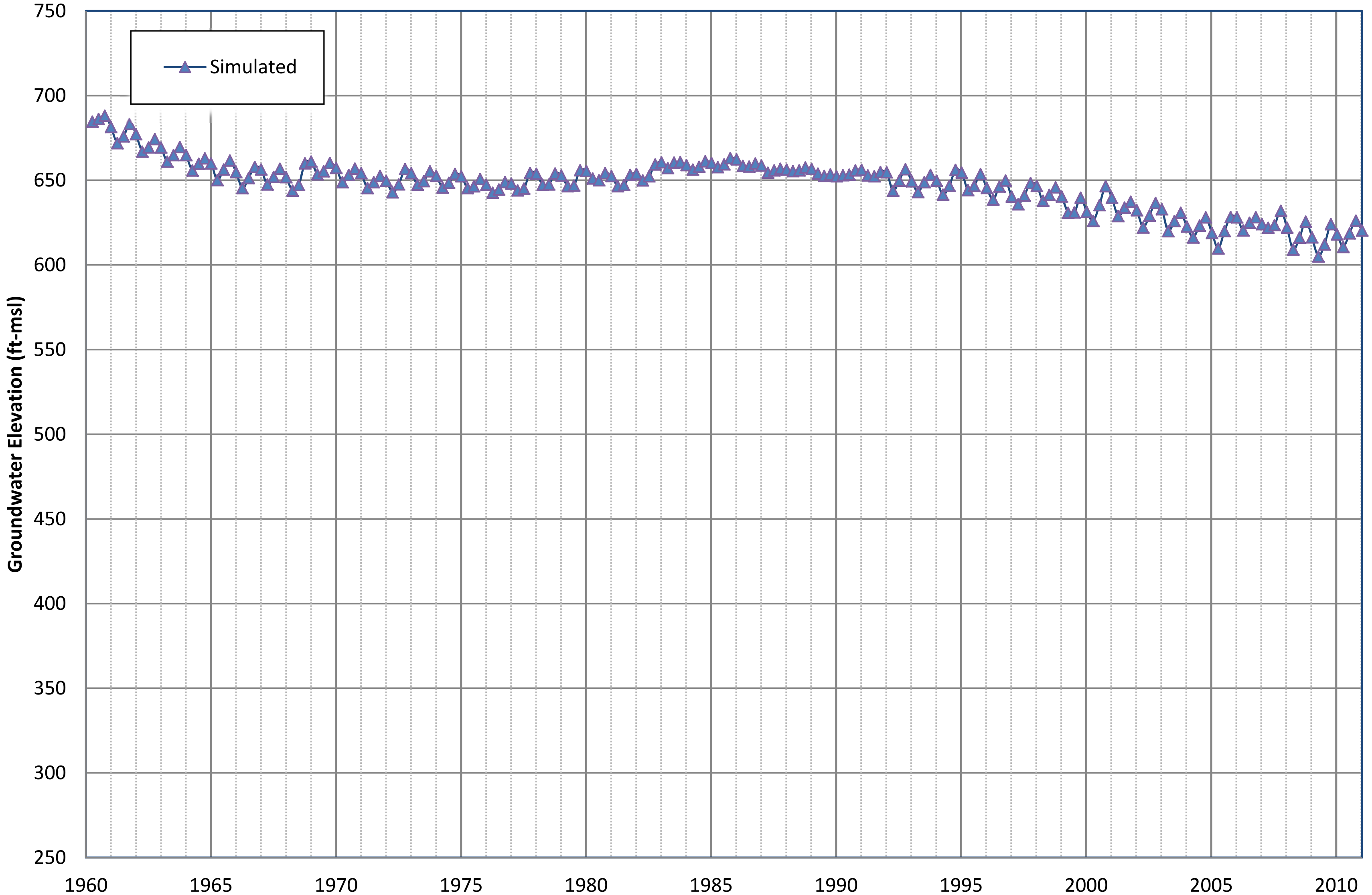

Appendix D

Time-History Plots of Projected Groundwater Elevations in Select Wells for Scenario 5A

Appendix D

Time-History Plots of Projected Groundwater Elevations in Select Wells for Scenario 5A

Owner	Well Name	Chart Number
Chino Basin Watermaster	AP-PA/7	D-1
Chino Desalter Authority	CDA I-1	D-2
	CDA I-10	D-3
	CDA I-11	D-4
	CDA I-13	D-5
	CDA I-14	D-6
	CDA I-15	D-7
	CDA I-16	D-8
	CDA I-17	D-9
	CDA I-18	D-10
	CDA I-19	D-11
	CDA I-2	D-12
	CDA I-20	D-13
	CDA I-21	D-14
	CDA I-3	D-15
	CDA I-4	D-16
	CDA I-5	D-17
	CDA I-6	D-18
	CDA I-7	D-19
	CDA I-8	D-20
	CDA I-9	D-21
	CDA II-1	D-22
	CDA II-2	D-23
	CDA II-3	D-24
	CDA II-4	D-25
	CDA II-7	D-26
	CDA-II-6	D-27
	CDA-II-8	D-28
	CDA-II-9a	D-29
Chino Hills, City of	5	D-30
	15	D-31
	16	D-32
	17	D-33
	1A	D-34
	7A	D-35
	7B	D-36
	4	D-37
	5	D-38
	6	D-39
	9	D-40
	10	D-41
	11	D-42
	12	D-43
	13	D-44
	14	D-45
	16	D-46
	17	D-47
	18	D-48
	Bon View	D-49
	Magnolia	D-50

Appendix D

Time-History Plots of Projected Groundwater Elevations in Select Wells for Scenario 5A

Owner	Well Name	Chart Number
Cucamonga Valley Water District	ASR1- CB-49	D-51
	ASR2-CB-50	D-52
	ASR3-CB-48	D-53
	CB-1	D-54
	CB-3	D-55
	CB-30	D-56
	CB-38	D-57
	CB-39	D-58
	CB-4	D-59
	CB-40	D-60
	CB-41	D-61
	CB-42	D-62
	CB-43	D-63
	CB-46	D-64
	CB-5	D-65
Fontana Water Company	F17B	D-66
	F17C	D-67
	F21A	D-68
	F21B	D-69
	F23A	D-70
	F2A	D-71
	F30A	D-72
	F31A	D-73
	F44A	D-74
	F44B	D-75
	F44C	D-76
	F7A	D-77
	F7B	D-78
Golden State Water Company	#1	D-79
Jurupa Community Services District	6	D-80
	8	D-81
	11	D-82
	12	D-83
	13	D-84
	14	D-85
	15	D-86
	16	D-87
	17	D-88
	18	D-89
	19	D-90
	20	D-91
	22	D-92
	23	D-93
	24	D-94
	25	D-95
	27	D-96
	28	D-97
	IDI-1	D-98
	IDI-2	D-99
Marygold Mutual Water Company	2	D-100
	3	D-101
	4	D-102

Appendix D

Time-History Plots of Projected Groundwater Elevations in Select Wells for Scenario 5A

Owner	Well Name	Chart Number
Monte Vista Water District	4	D-103
	5	D-104
	6	D-105
	10	D-106
	19	D-107
	26	D-108
	27	D-109
	28	D-110
	30	D-111
	31	D-112
	32	D-113
	34	D-114
	MVWD-33	D-115
	MVWD-33	D-116
Ontario, City of	9	D-117
	16	D-118
	17	D-119
	20	D-120
	24	D-121
	25	D-122
	26	D-123
	27	D-124
	29	D-125
	30	D-126
	31	D-127
	34	D-128
	35	D-129
	36	D-130
	37	D-131
	38	D-132
	39	D-133
	40	D-134
	41	D-135
	42	D-136
	43	D-137
	44	D-138
	45	D-139
	46	D-140
	47	D-141
	48	D-142
	49	D-143
	50	D-144
	51	D-145
	52	D-146
	100	D-147
	101	D-148
	103	D-149
	104	D-150
	105	D-151
	106	D-152
	109	D-153
	111	D-154
	115	D-155
	119	D-156
	120	D-157
	126	D-158
	134	D-159
	136	D-160
	138	D-161

Appendix D

Time-History Plots of Projected Groundwater Elevations in Select Wells for Scenario 5A

Owner	Well Name	Chart Number
Pomona, City of	2	D-162
	6	D-163
	10	D-164
	11	D-165
	12	D-166
	14	D-167
	15	D-168
	16	D-169
	17	D-170
	18	D-171
	21	D-172
	23	D-173
	25	D-174
	26	D-175
	27	D-176
	29	D-177
	30	D-178
	34	D-179
	35	D-180
	36	D-181
	5B	D-182
San Antonio Water Company	01A	D-183
	03A	D-184
Upland, City of	3	D-185
	8	D-186
	20	D-187
	21A	D-188
	7A	D-189

Figure D-1
Projected Groundwater Elevation for Scenario 5a
Chino Basin Watermaster Well AP-PA/7

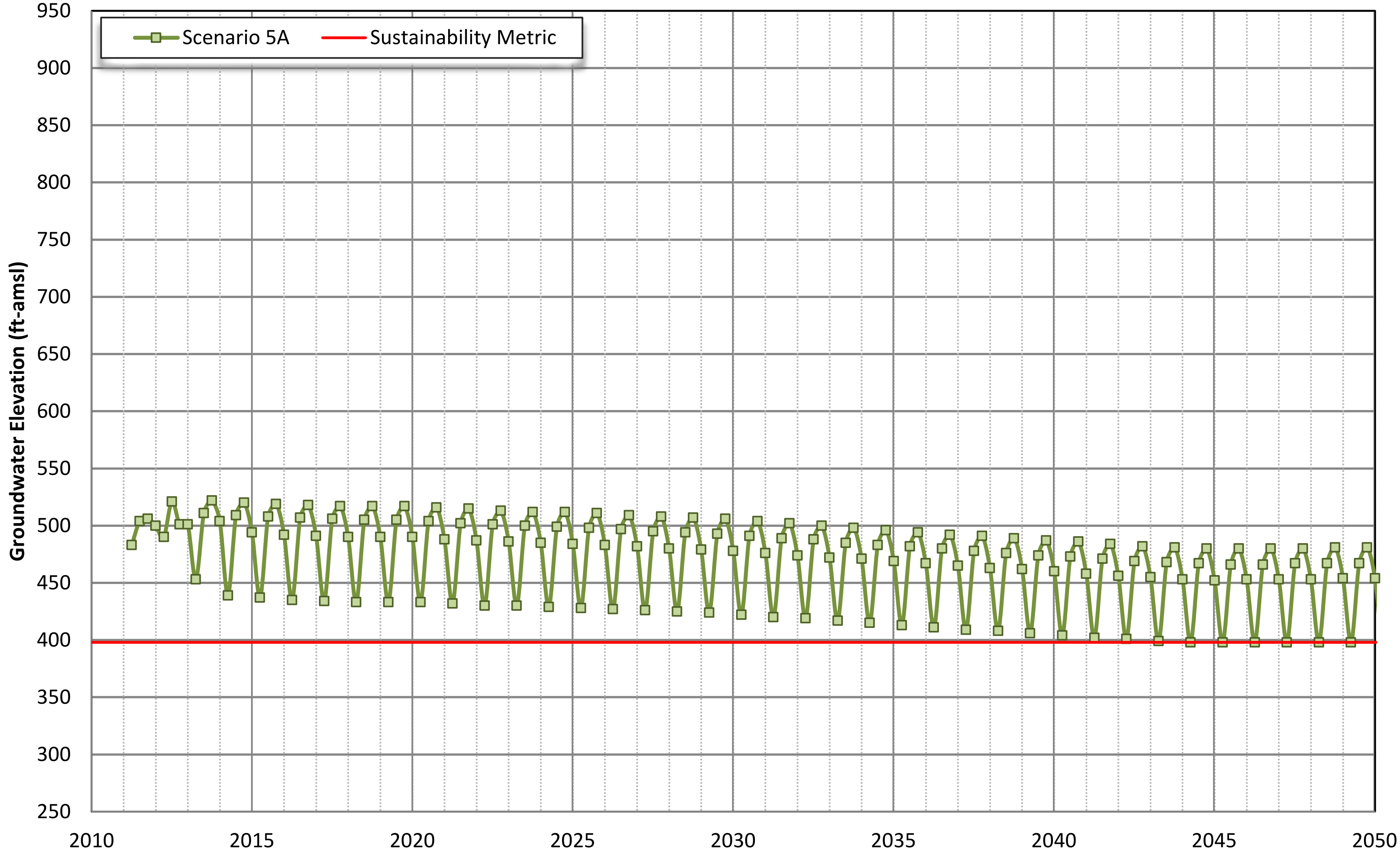

Appendix D_20150916_WellHydrographs_S5A4_Final_LBB2.xlsm
Created: 9/15/15
Printed: 9/16/2015

Figure D-2
Projected Groundwater Elevation for Scenario 5a
Chino Desalter Authority Well CDA I-1

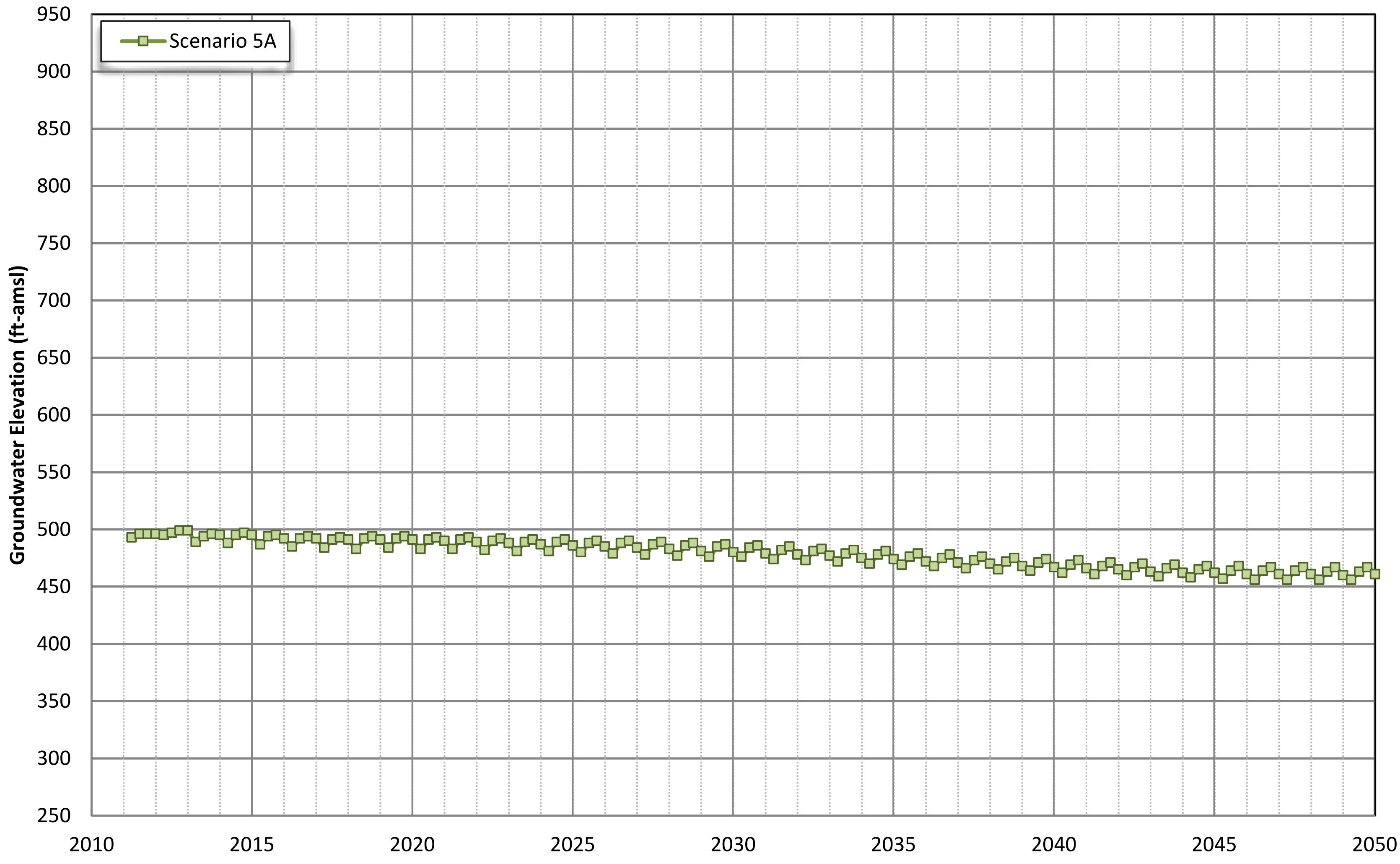

Appendix D_20150916_WellHydrographs_S5A4_Final_LBB2.xlsm
Created: 9/15/15
Printed: 9/16/2015

Figure D-3
Projected Groundwater Elevation for Scenario 5a
Chino Desalter Authority Well CDA I-10

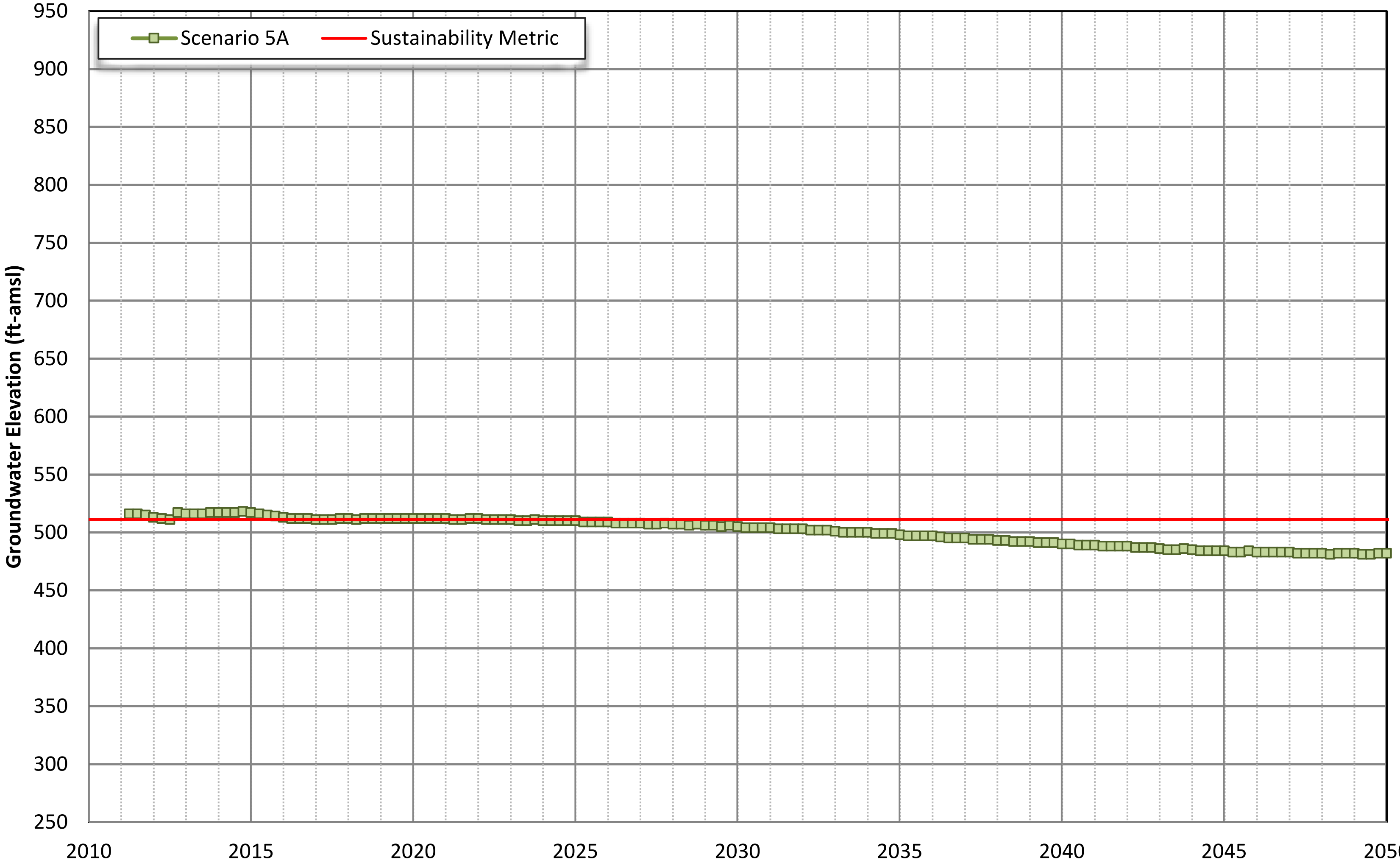

Appendix D_20150916_WellHydrographs_S5A4_Final_LBB2.xlsm
Created: 9/15/15
Printed: 9/16/2015

Figure D-4
Projected Groundwater Elevation for Scenario 5a
Chino Desalter Authority Well CDA I-11

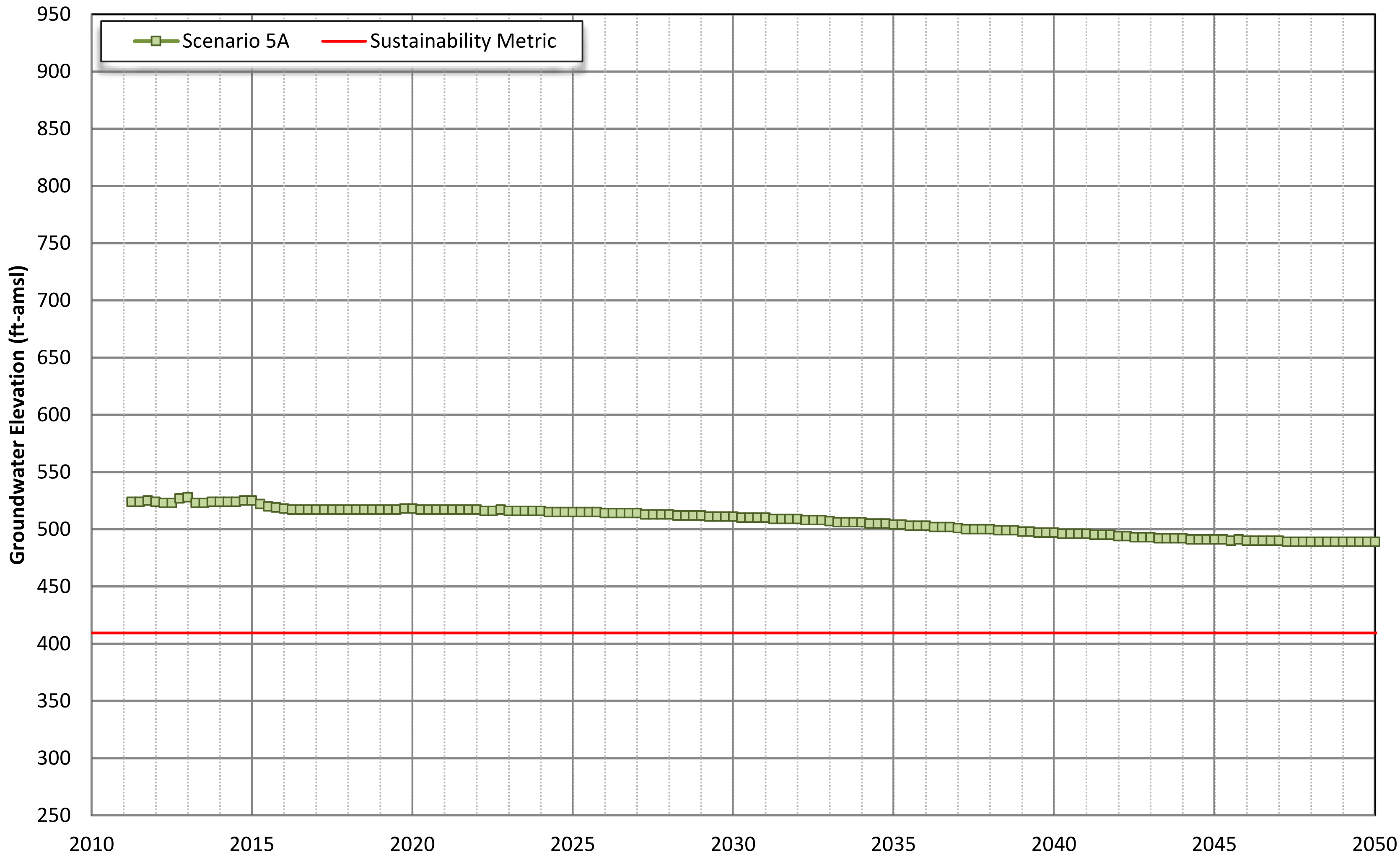

Appendix D_20150916_WellHydrographs_S5A4_Final_LBB2.xlsm
Created: 9/15/15
Printed: 9/16/2015

Figure D-5
Projected Groundwater Elevation for Scenario 5a
Chino Desalter Authority Well CDA I-13

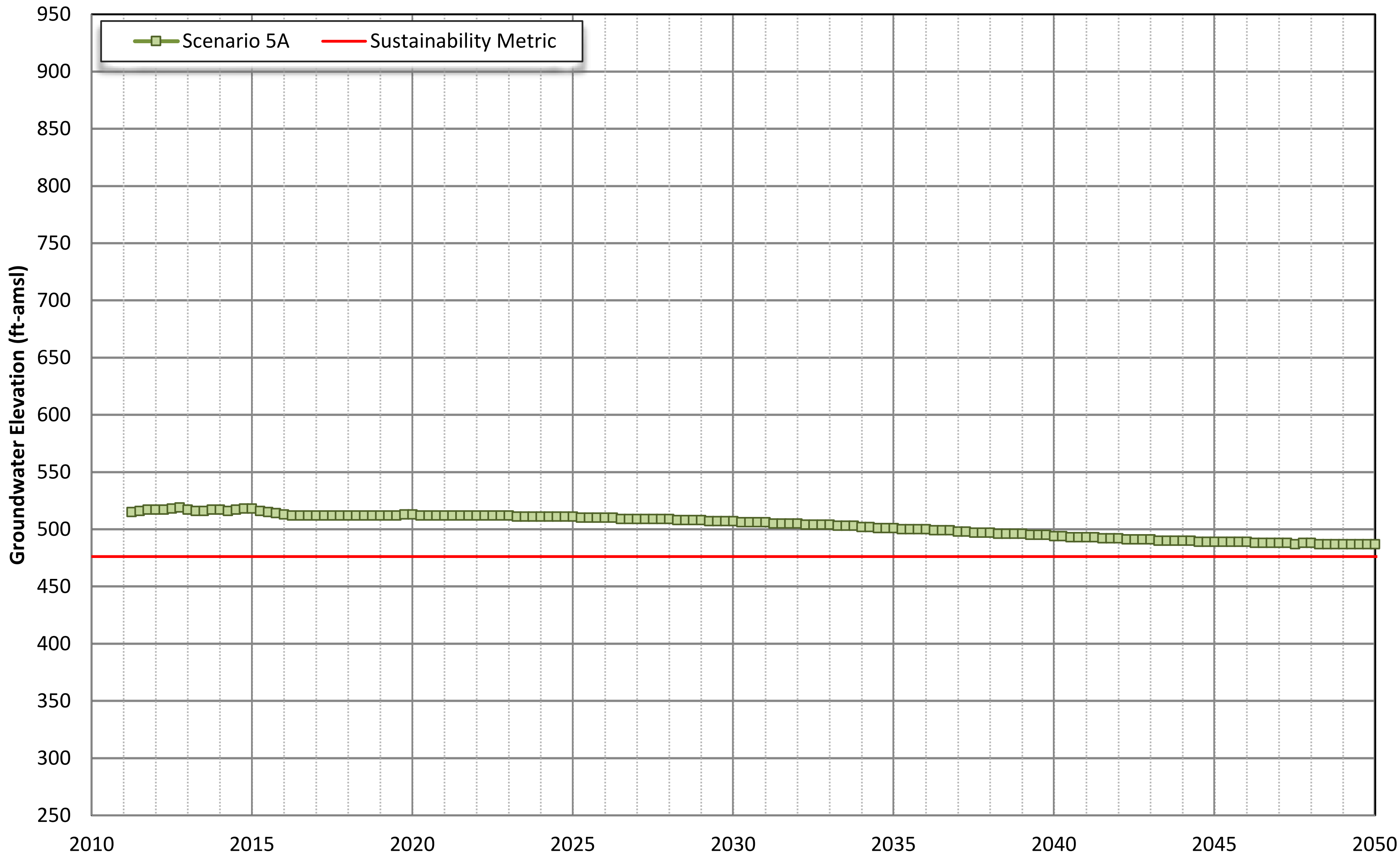

Appendix D_20150916_WellHydrographs_S5A4_Final_LBB2.xlsm
Created: 9/15/15
Printed: 9/16/2015

Figure D-6
Projected Groundwater Elevation for Scenario 5a
Chino Desalter Authority Well CDA I-14

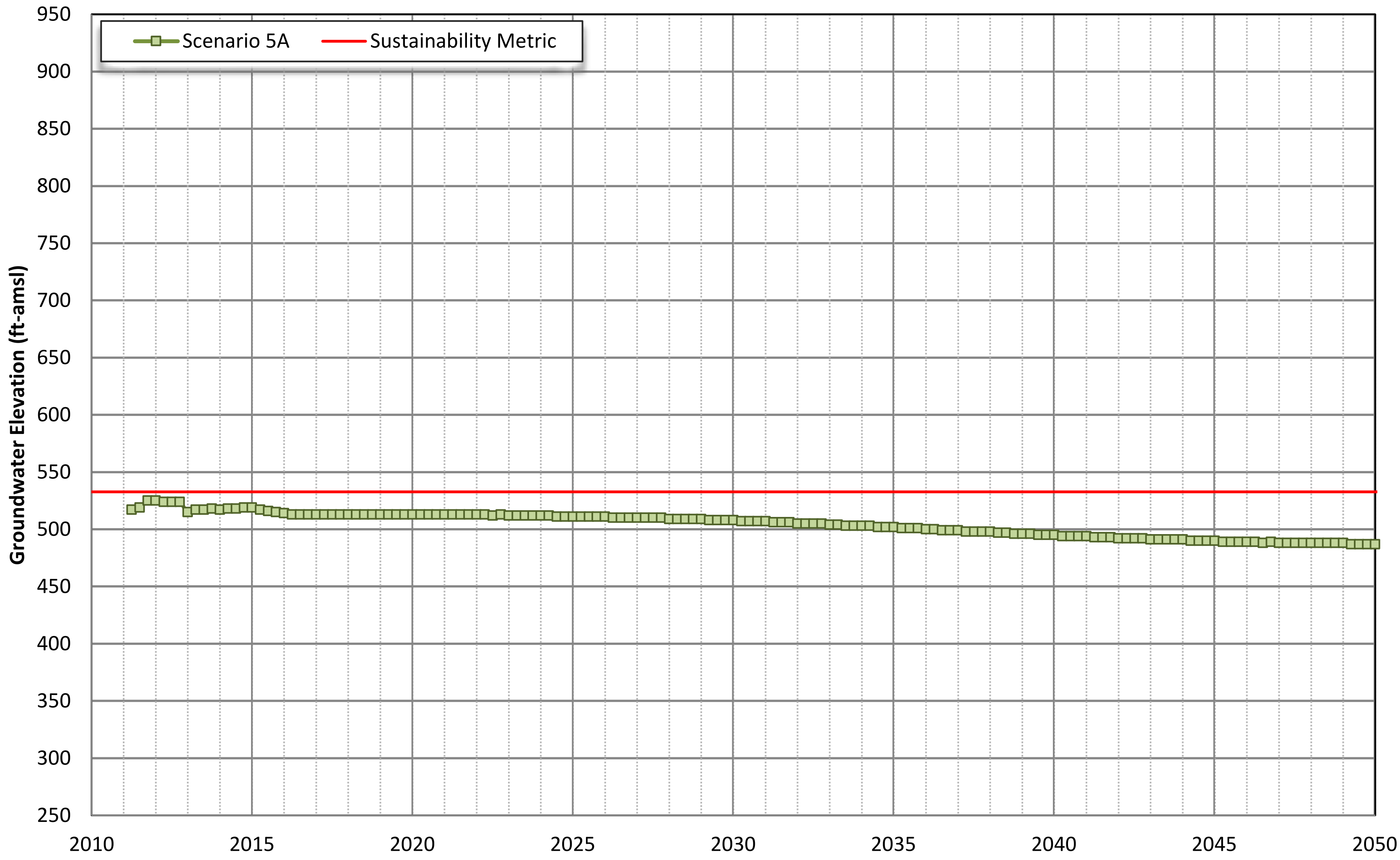

Appendix D_20150916_WellHydrographs_S5A4_Final_LBB2.xlsm
Created: 9/15/15
Printed: 9/16/2015

Figure D-7
Projected Groundwater Elevation for Scenario 5a
Chino Desalter Authority Well CDA I-15

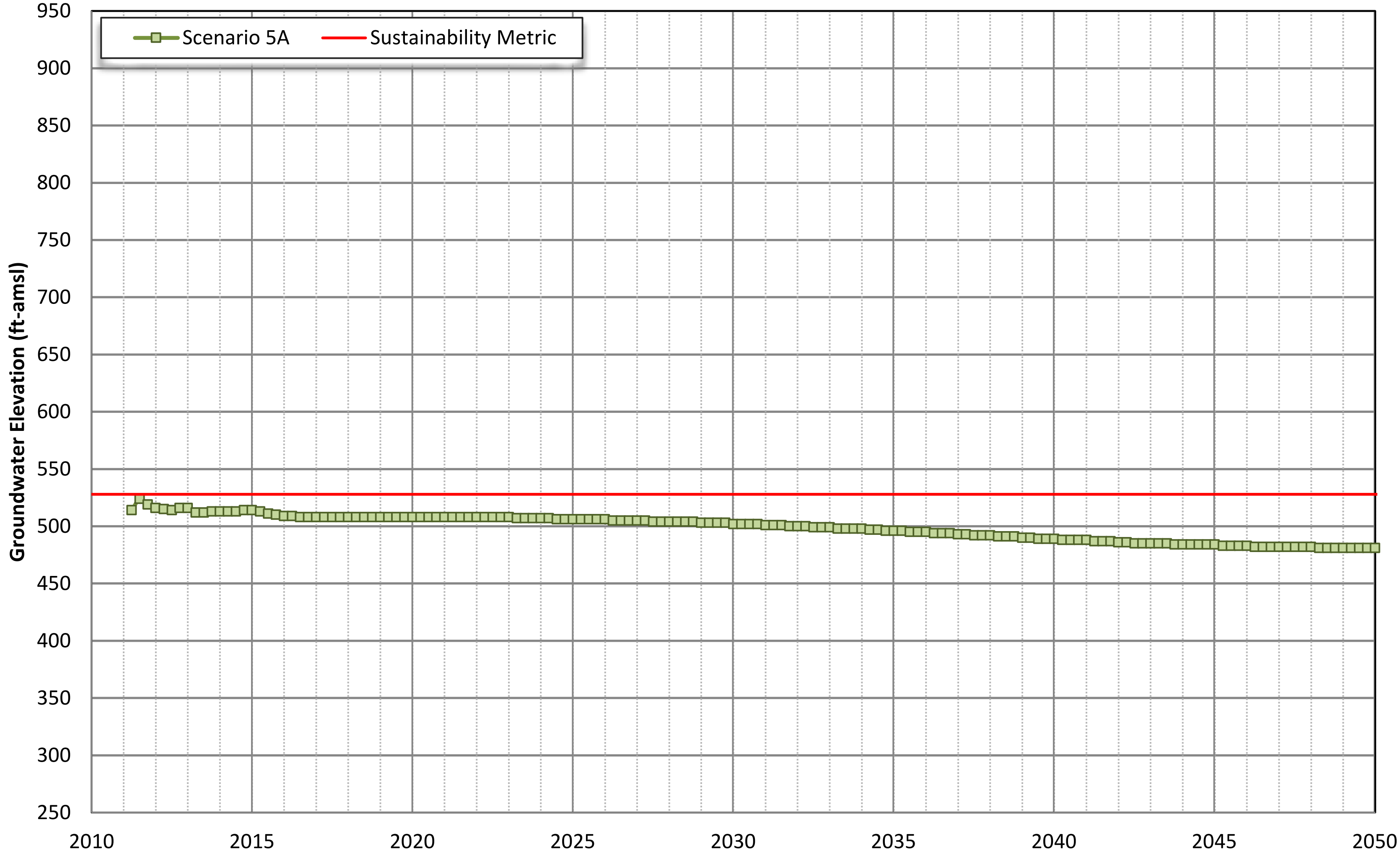

Appendix D_20150916_WellHydrographs_S5A4_Final_LBB2.xlsm
Created: 9/15/15
Printed: 9/16/2015

Figure D-8
Projected Groundwater Elevation for Scenario 5a
Chino Desalter Authority Well CDA I-16

Figure D-9
Projected Groundwater Elevation for Scenario 5a
Chino Desalter Authority Well CDA I-17

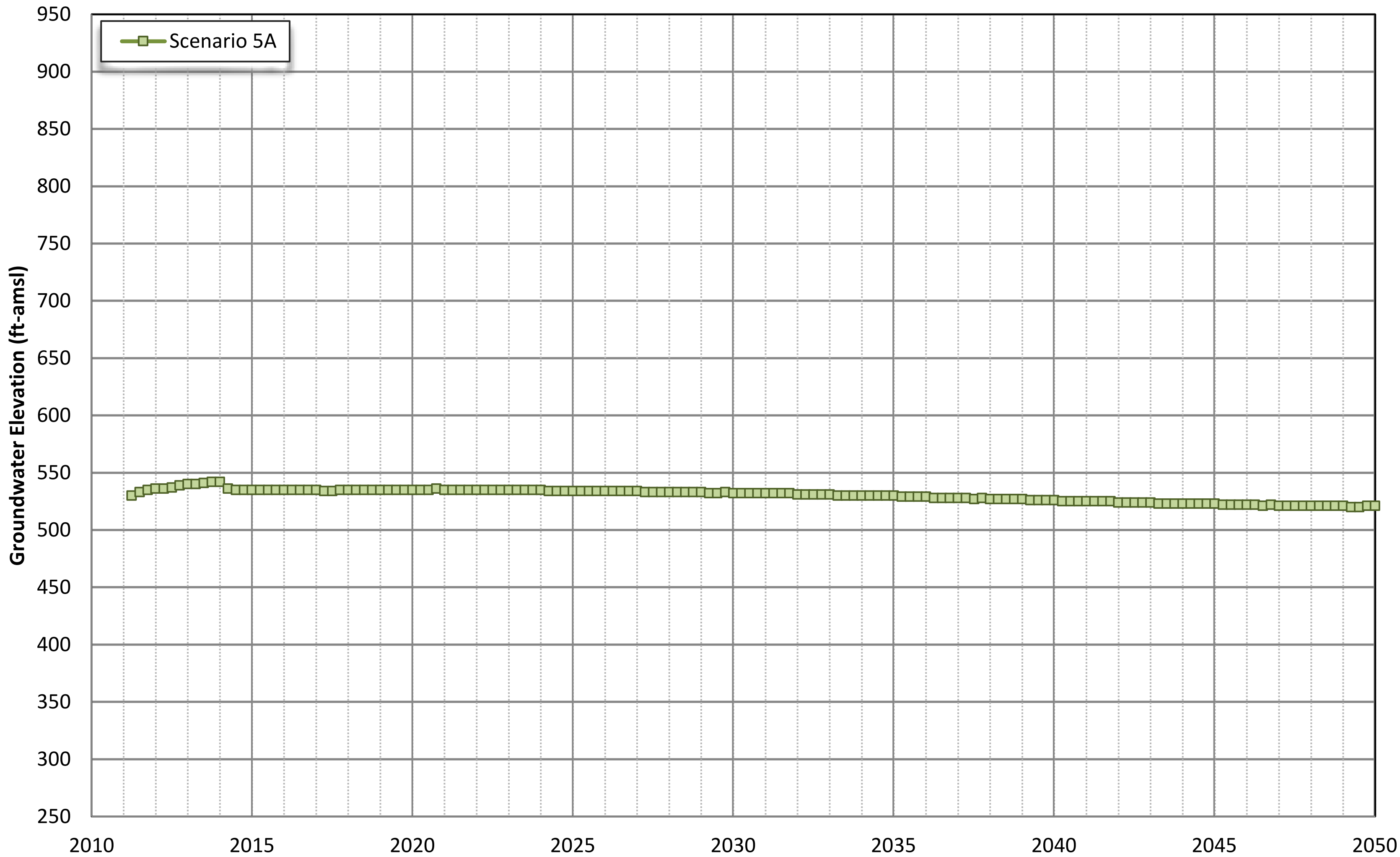

Appendix D_20150916_WellHydrographs_S5A4_Final_LBB2.xlsm
Created: 9/15/15
Printed: 9/16/2015

Figure D-10
Projected Groundwater Elevation for Scenario 5a
Chino Desalter Authority Well CDA I-18

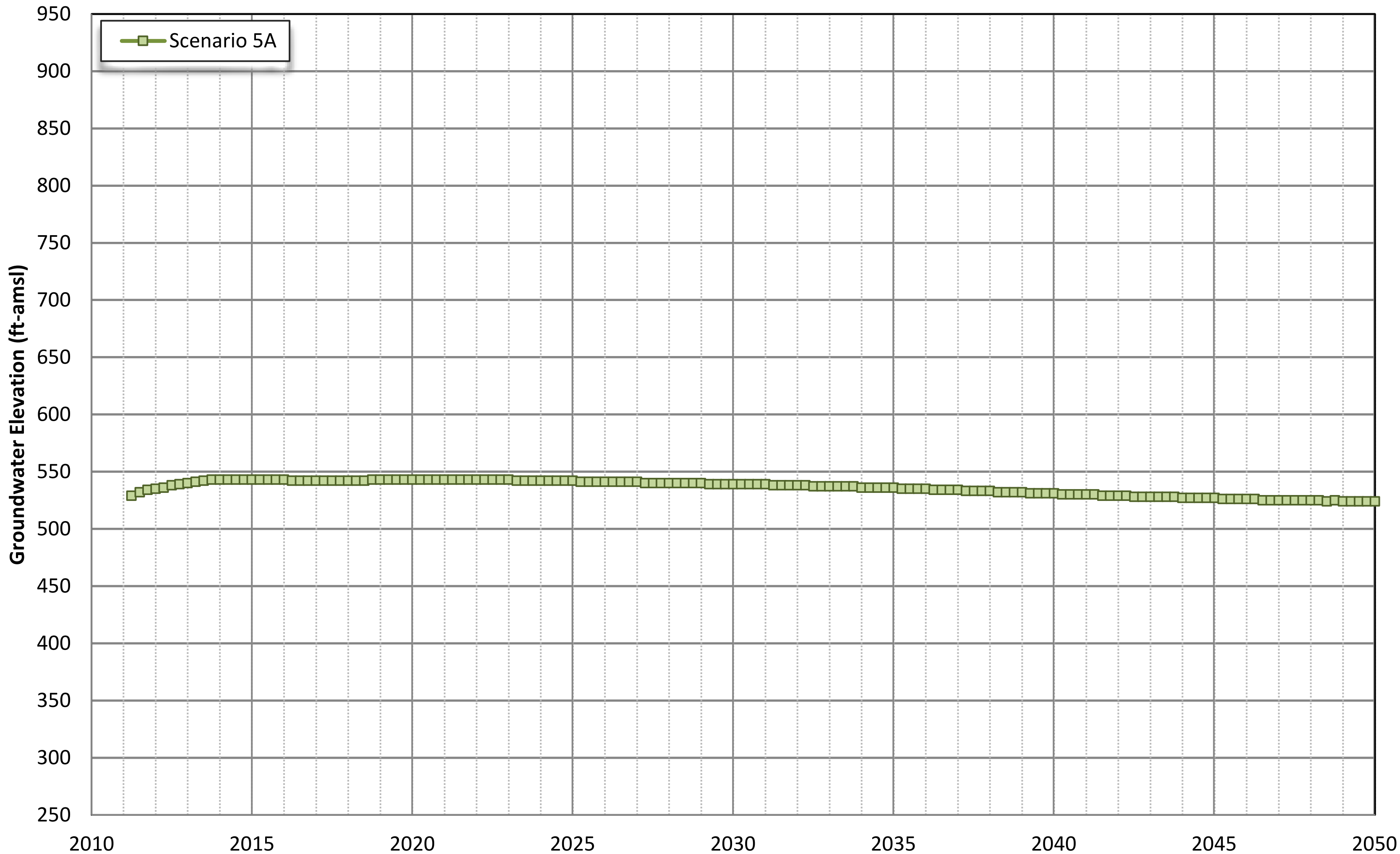

Appendix D_20150916_WellHydrographs_S5A4_Final_LBB2.xlsm
Created: 9/15/15
Printed: 9/16/2015

Figure D-11
Projected Groundwater Elevation for Scenario 5a
Chino Desalter Authority Well CDA I-19

Appendix D_20150916_WellHydrographs_S5A4_Final_LBB2.xlsm
Created: 9/15/15
Printed: 9/16/2015

Figure D-12
Projected Groundwater Elevation for Scenario 5a
Chino Desalter Authority Well CDA I-2

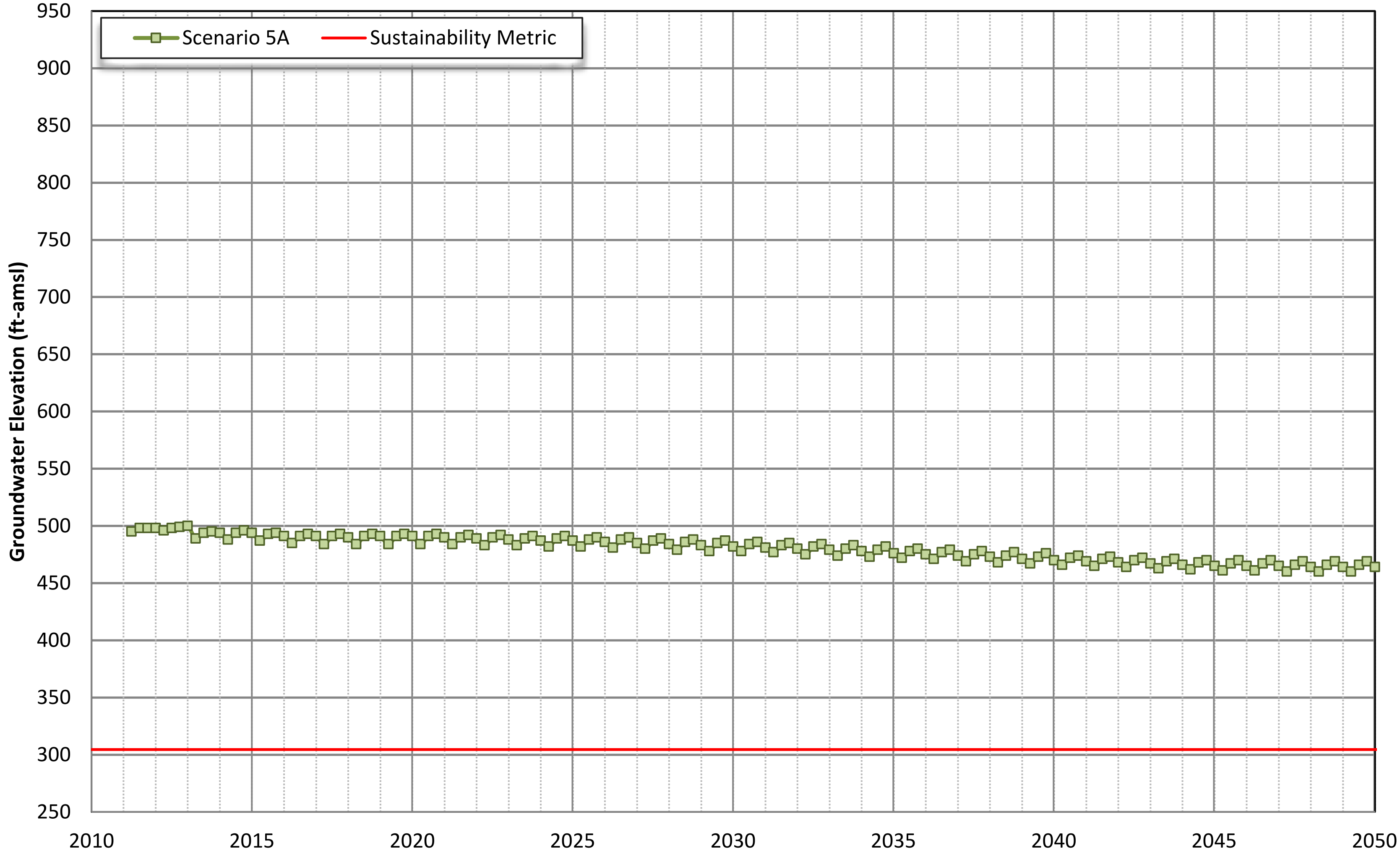

Appendix D_20150916_WellHydrographs_S5A4_Final_LBB2.xlsm
Created: 9/15/15
Printed: 9/16/2015

Figure D-13
Projected Groundwater Elevation for Scenario 5a
Chino Desalter Authority Well CDA I-20

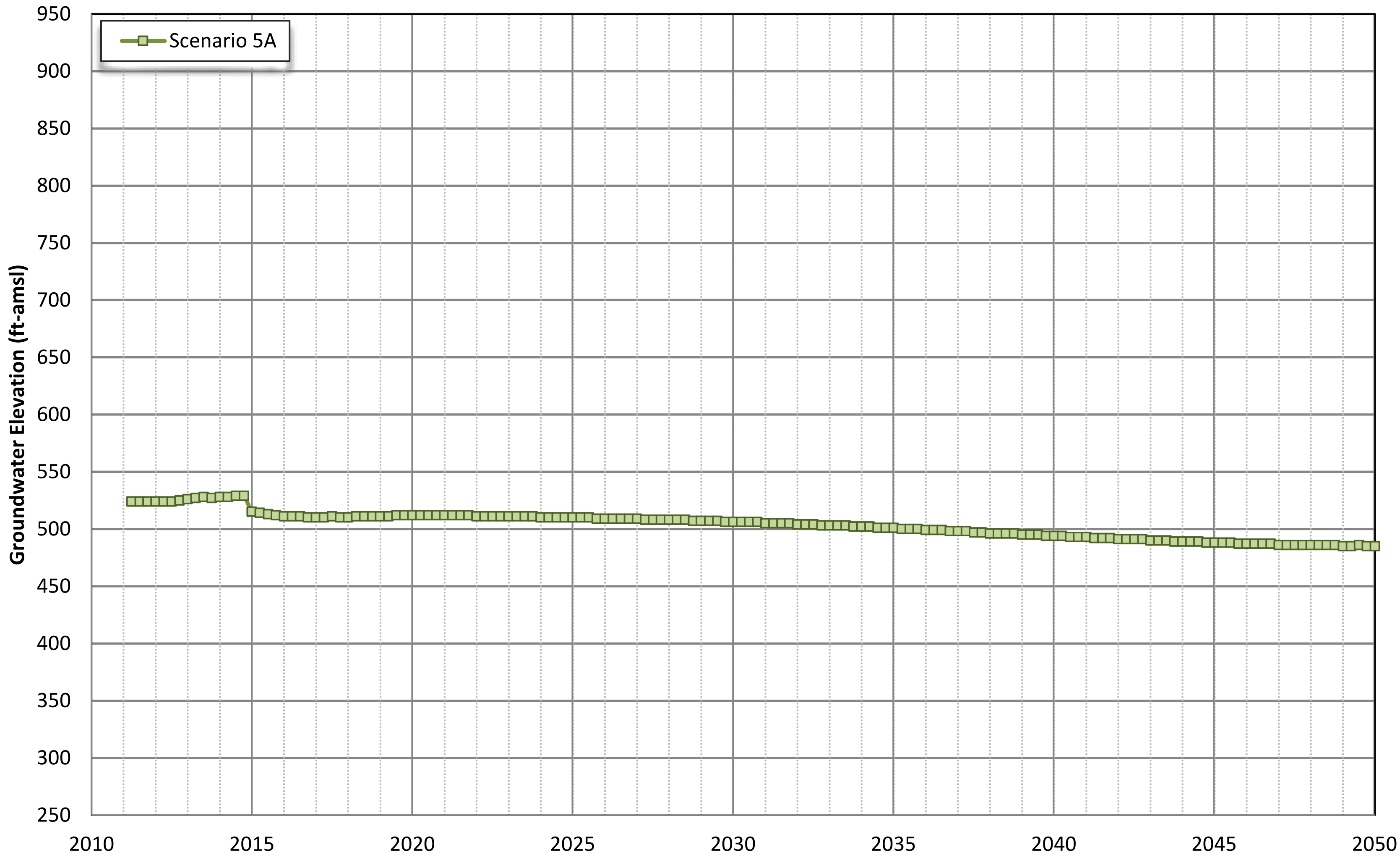

Appendix D_20150916_WellHydrographs_S5A4_Final_LBB2.xlsm
Created: 9/15/15
Printed: 9/16/2015

Figure D-14
Projected Groundwater Elevation for Scenario 5a
Chino Desalter Authority Well CDA I-21

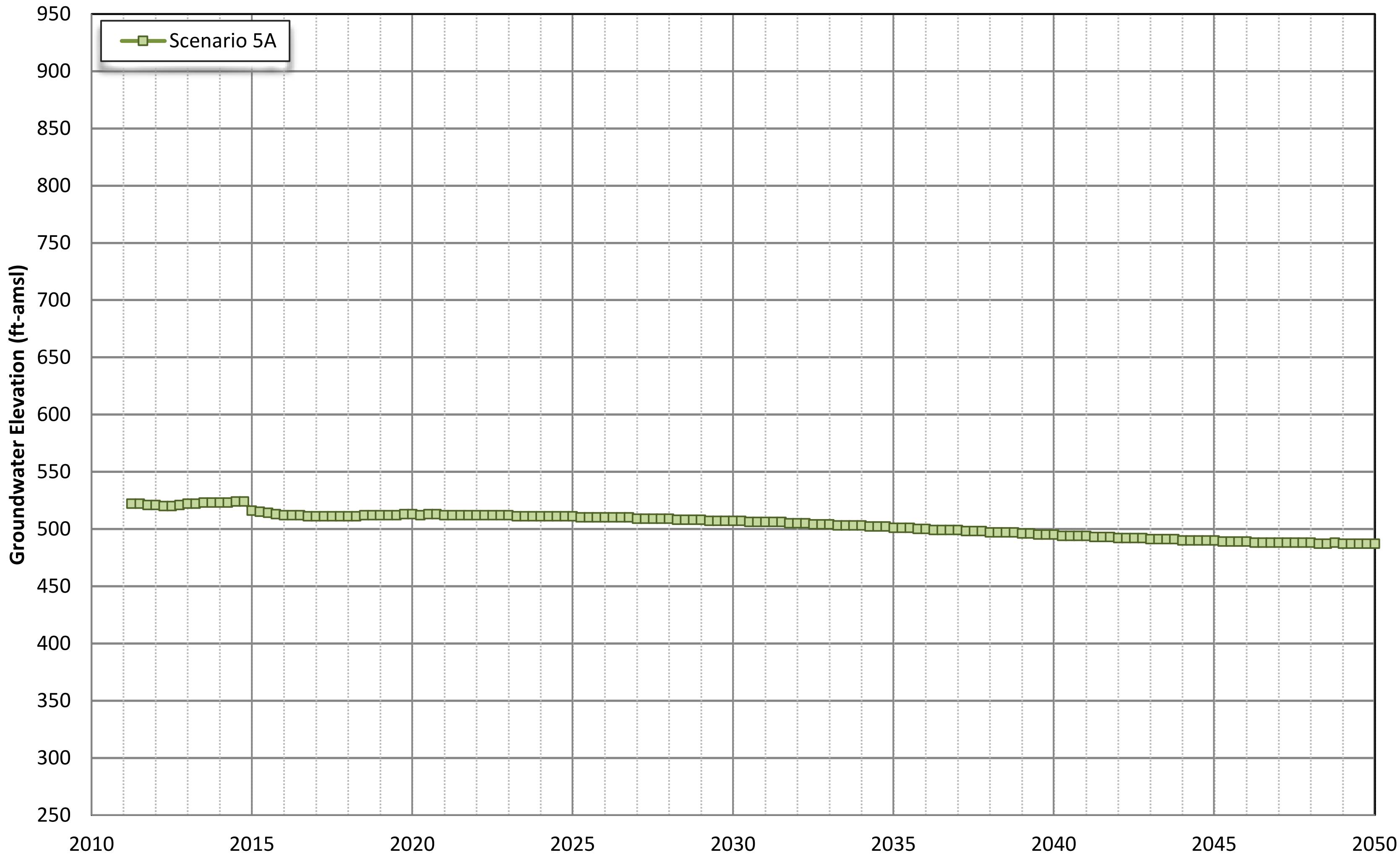

Appendix D_20150916_WellHydrographs_S5A4_Final_LBB2.xlsm
Created: 9/15/15
Printed: 9/16/2015

Figure D-15
Projected Groundwater Elevation for Scenario 5a
Chino Desalter Authority Well CDA I-3

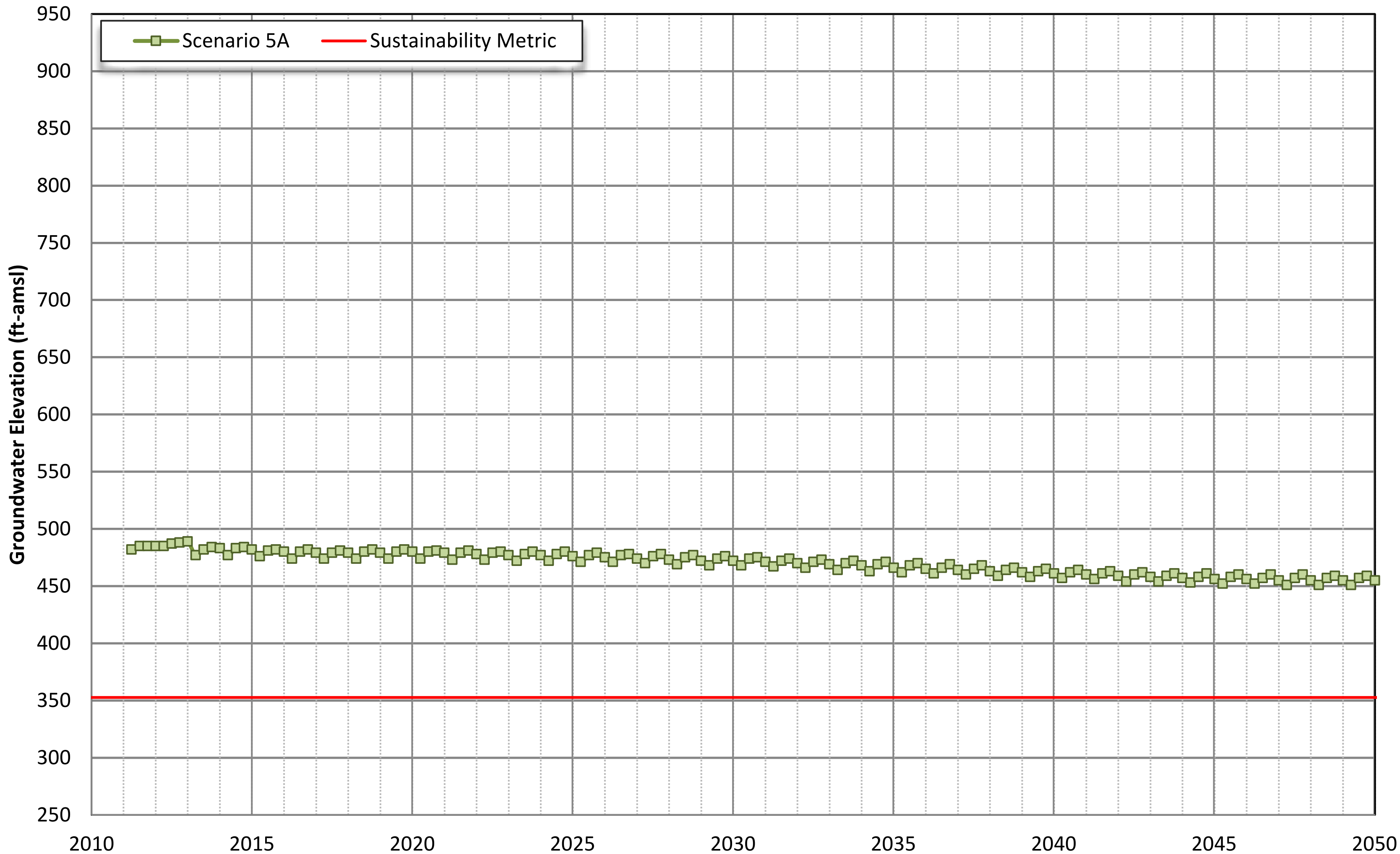

Appendix D_20150916_WellHydrographs_S5A4_Final_LBB2.xlsm
Created: 9/15/15
Printed: 9/16/2015

Figure D-16
Projected Groundwater Elevation for Scenario 5a
Chino Desalter Authority Well CDA I-4

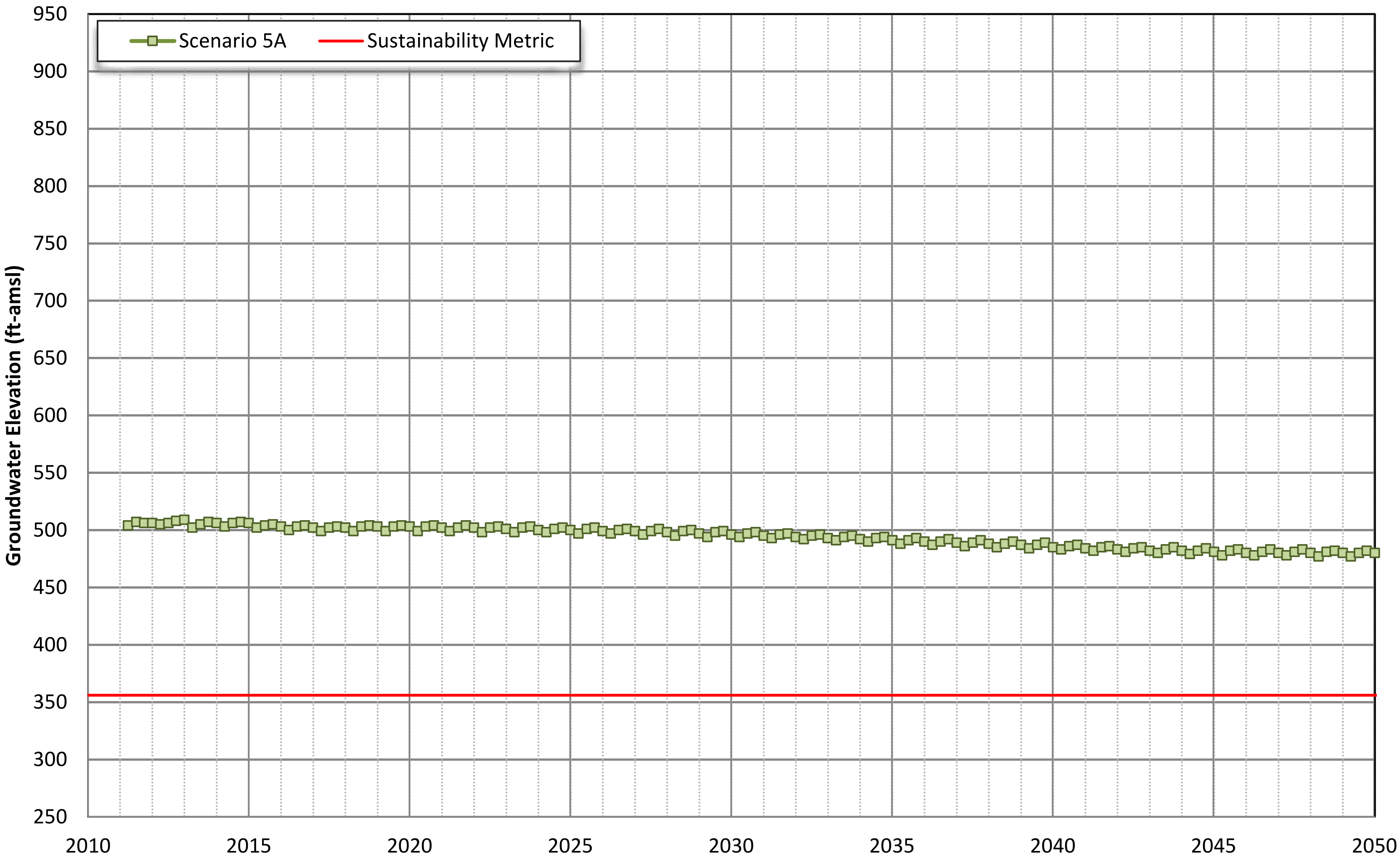

Appendix D_20150916_WellHydrographs_S5A4_Final_LBB2.xlsm
Created: 9/15/15
Printed: 9/16/2015

Figure D-17
Projected Groundwater Elevation for Scenario 5a
Chino Desalter Authority Well CDA I-5

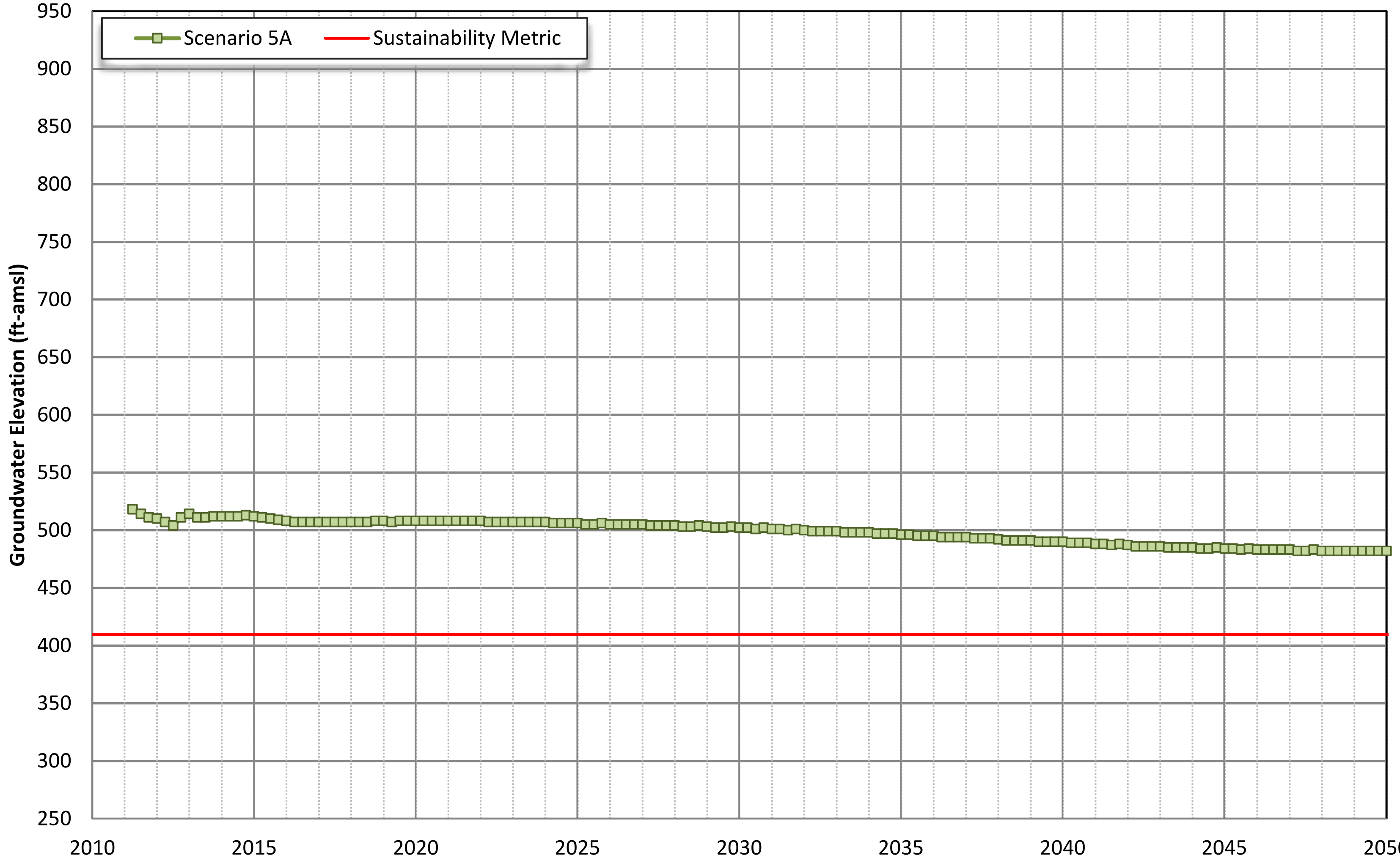

Appendix D_20150916_WellHydrographs_S5A4_Final_LBB2.xlsm
Created: 9/15/15
Printed: 9/16/2015

Figure D-18
Projected Groundwater Elevation for Scenario 5a
Chino Desalter Authority Well CDA I-6

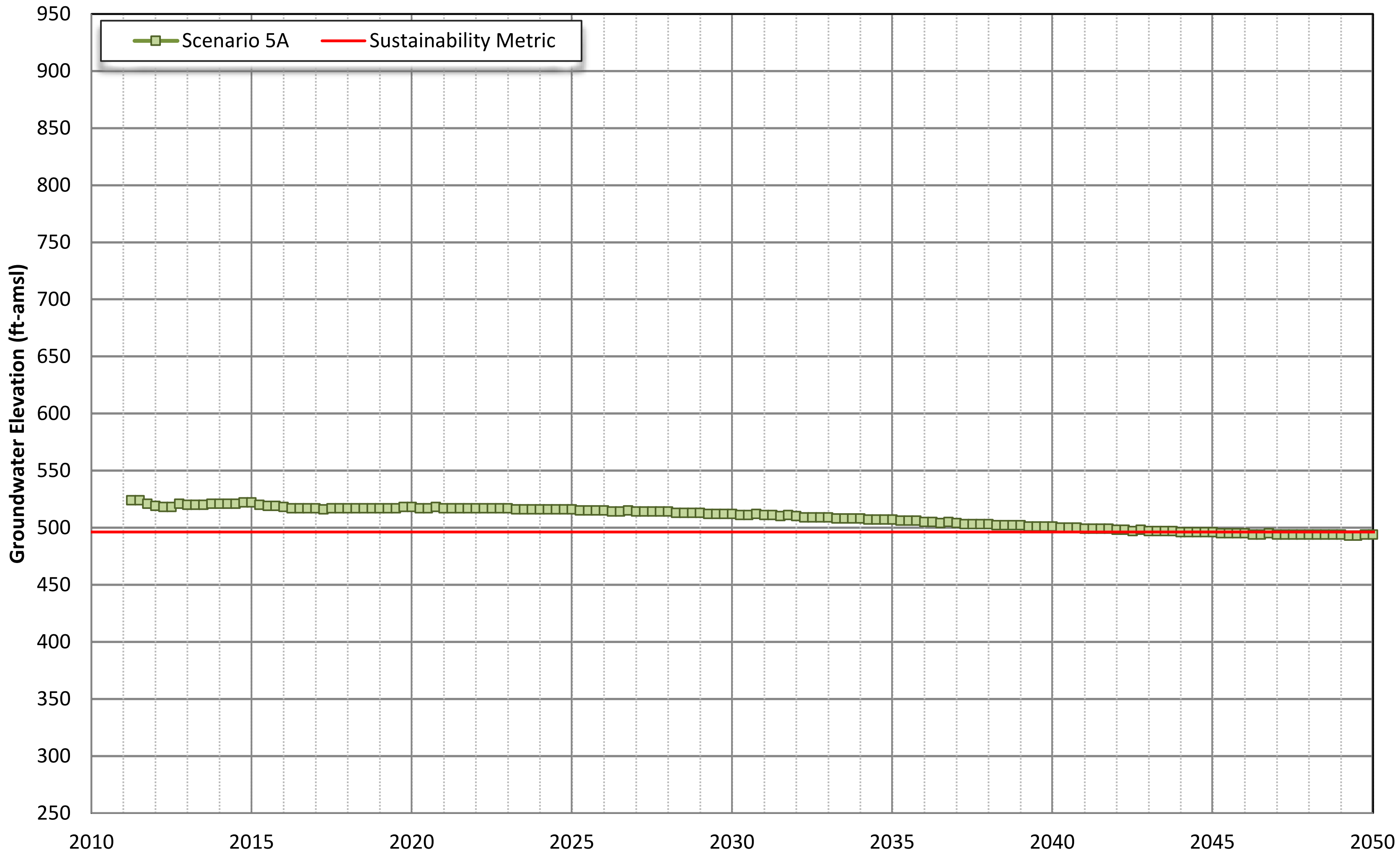

Appendix D_20150916_WellHydrographs_S5A4_Final_LBB2.xlsm
Created: 9/15/15
Printed: 9/16/2015

Figure D-19
Projected Groundwater Elevation for Scenario 5a
Chino Desalter Authority Well CDA I-7

Appendix D_20150916_WellHydrographs_S5A4_Final_LBB2.xlsm
Created: 9/15/15
Printed: 9/16/2015

Figure D-20
Projected Groundwater Elevation for Scenario 5a
Chino Desalter Authority Well CDA I-8

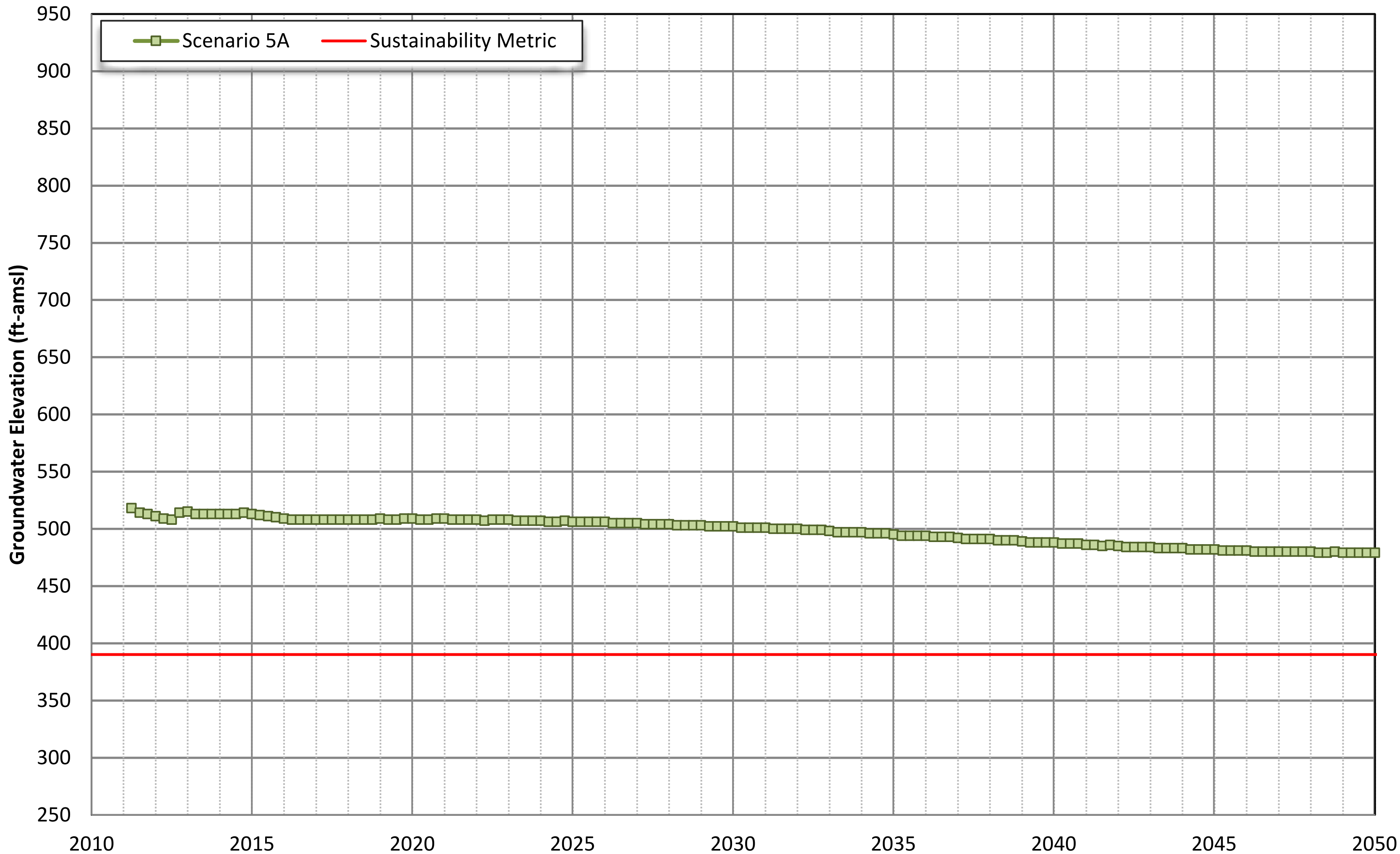

Appendix D_20150916_WellHydrographs_S5A4_Final_LBB2.xlsm
Created: 9/15/15
Printed: 9/16/2015

Figure D-21
Projected Groundwater Elevation for Scenario 5a
Chino Desalter Authority Well CDA I-9

Appendix D_20150916_WellHydrographs_S5A4_Final_LBB2.xlsm
Created: 9/15/15
Printed: 9/16/2015

Figure D-22
Projected Groundwater Elevation for Scenario 5a
Chino Desalter Authority Well CDA II-1

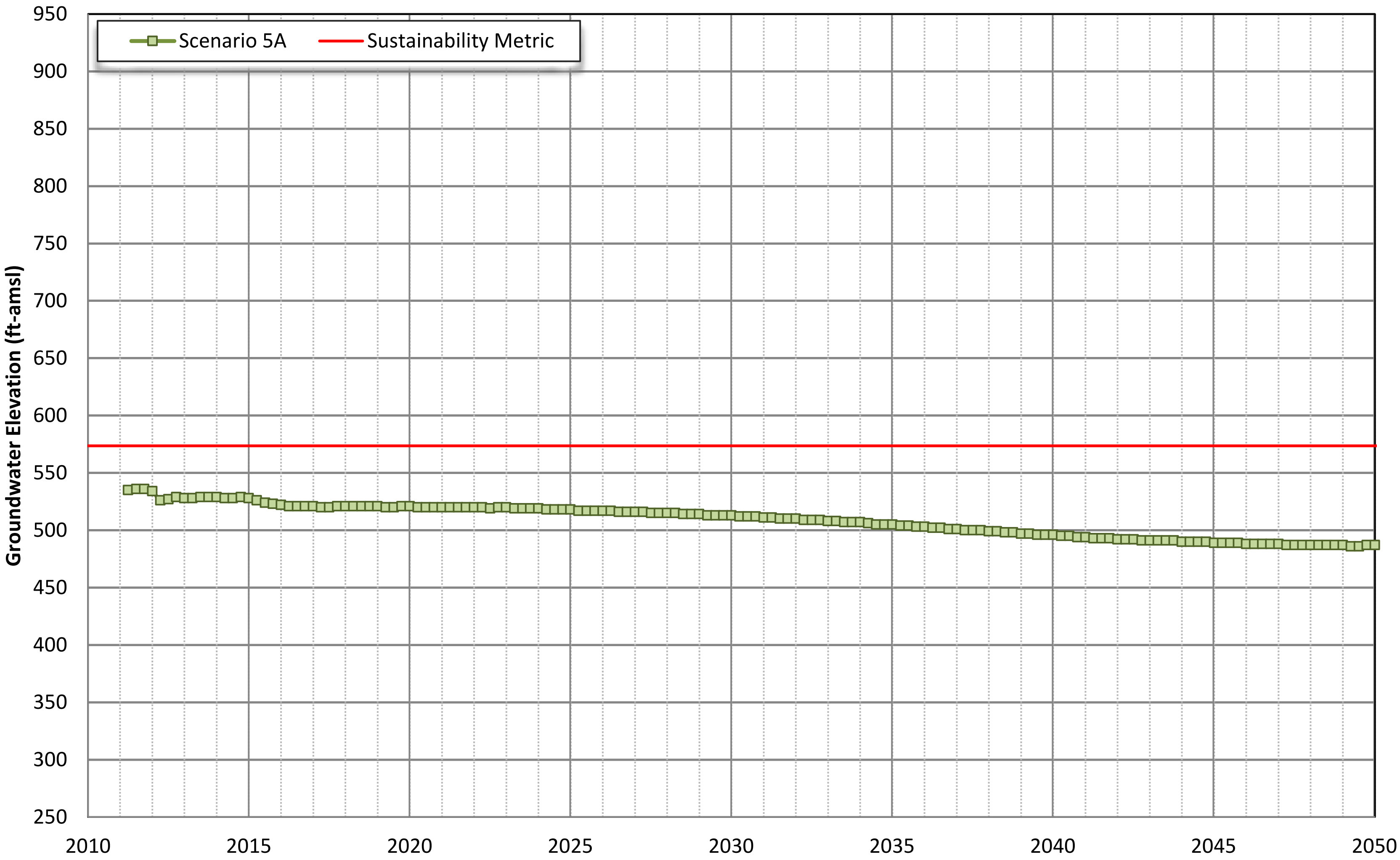

Appendix D_20150916_WellHydrographs_S5A4_Final_LBB2.xlsm
Created: 9/15/15
Printed: 9/16/2015

Figure D-23
Projected Groundwater Elevation for Scenario 5a
Chino Desalter Authority Well CDA II-2

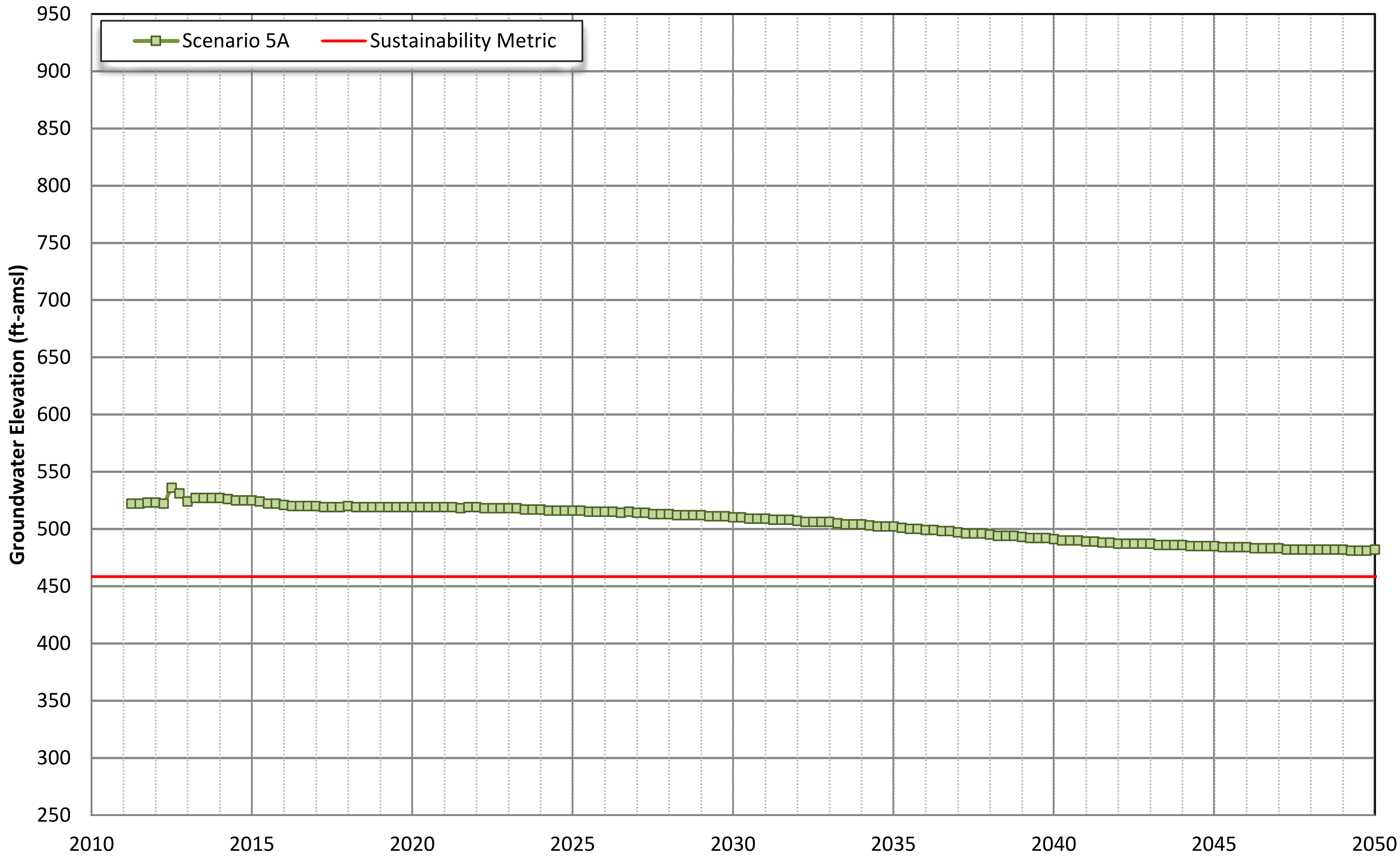

Appendix D_20150916_WellHydrographs_S5A4_Final_LBB2.xlsm
Created: 9/15/15
Printed: 9/16/2015

Figure D-24
Projected Groundwater Elevation for Scenario 5a
Chino Desalter Authority Well CDA II-3

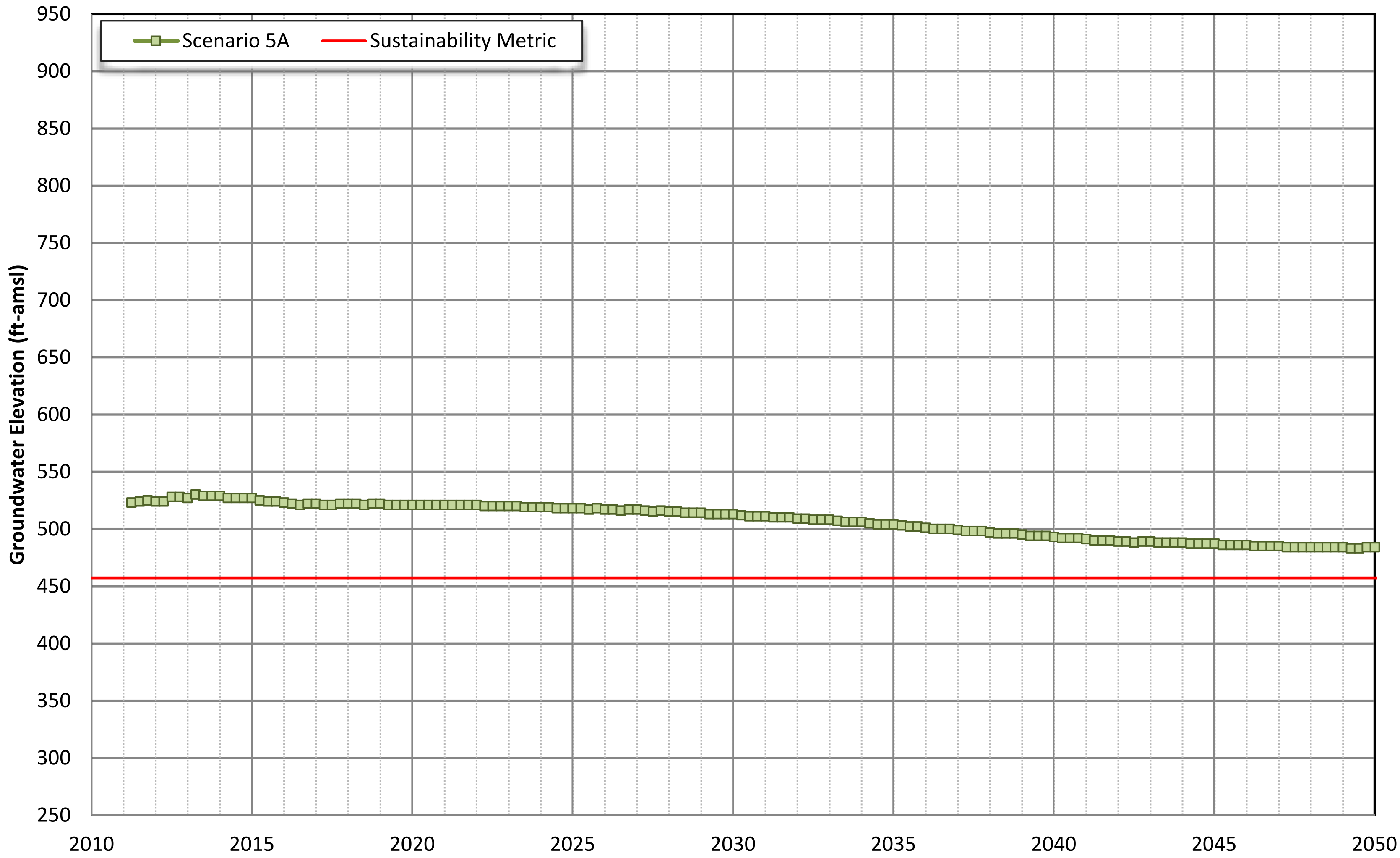

Appendix D_20150916_WellHydrographs_S5A4_Final_LBB2.xlsm
Created: 9/15/15
Printed: 9/16/2015

Figure D-25
Projected Groundwater Elevation for Scenario 5a
Chino Desalter Authority Well CDA II-4

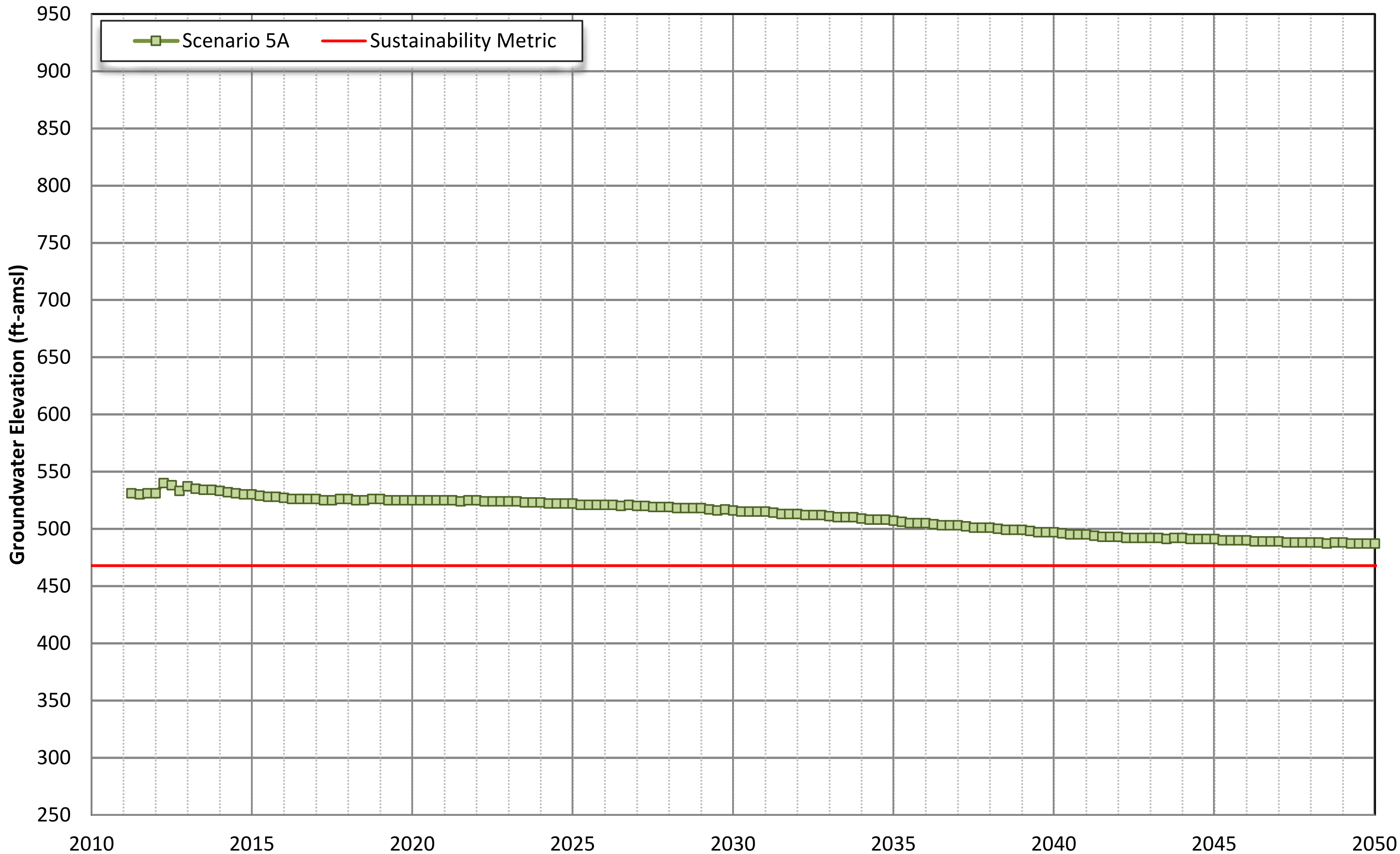

Appendix D_20150916_WellHydrographs_S5A4_Final_LBB2.xlsm
Created: 9/15/15
Printed: 9/16/2015

Figure D-26
Projected Groundwater Elevation for Scenario 5a
Chino Desalter Authority Well CDA II-7

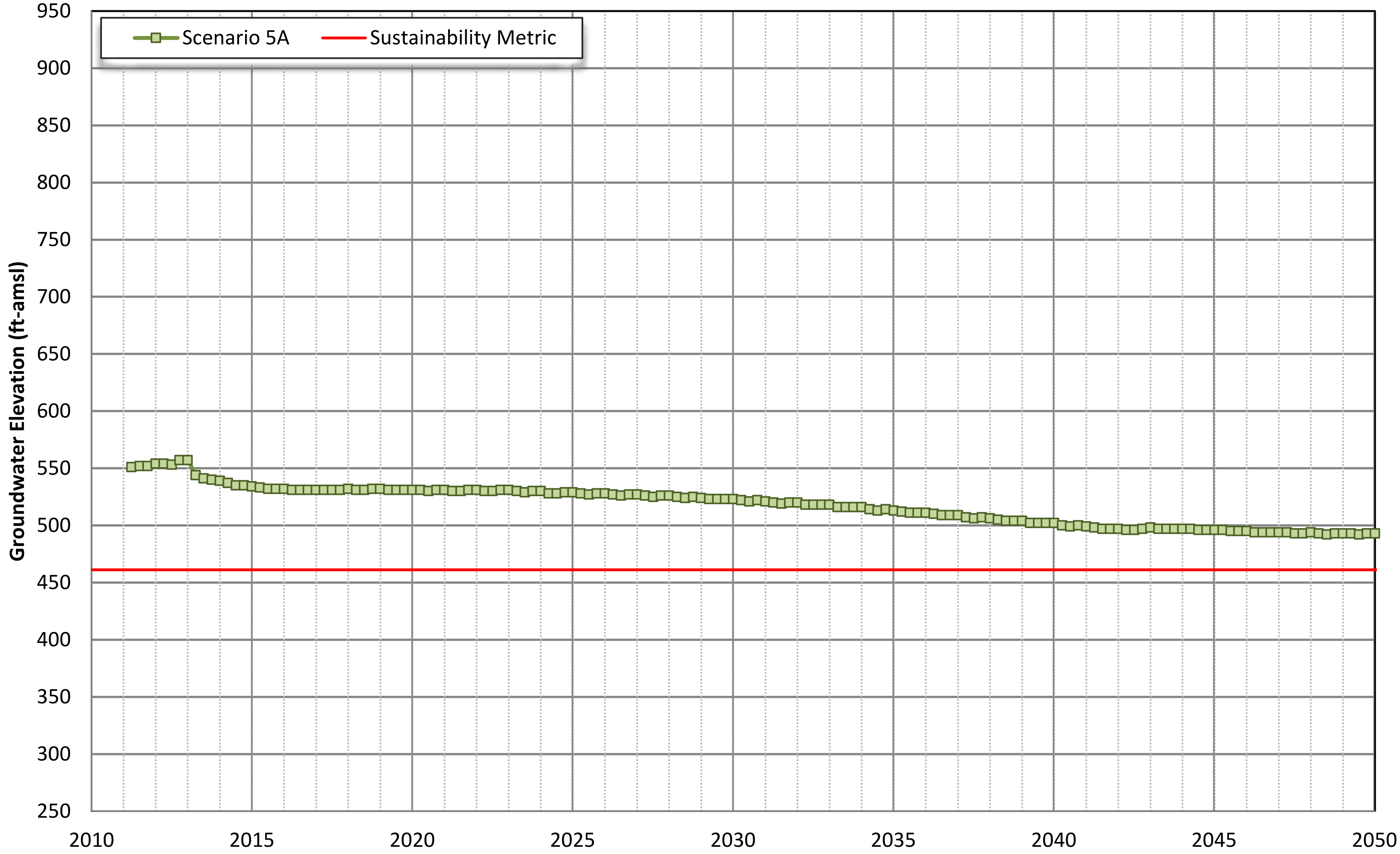

Appendix D_20150916_WellHydrographs_S5A4_Final_LBB2.xlsm
Created: 9/15/15
Printed: 9/16/2015

Figure D-27
Projected Groundwater Elevation for Scenario 5a
Chino Desalter Authority Well CDA-II-6

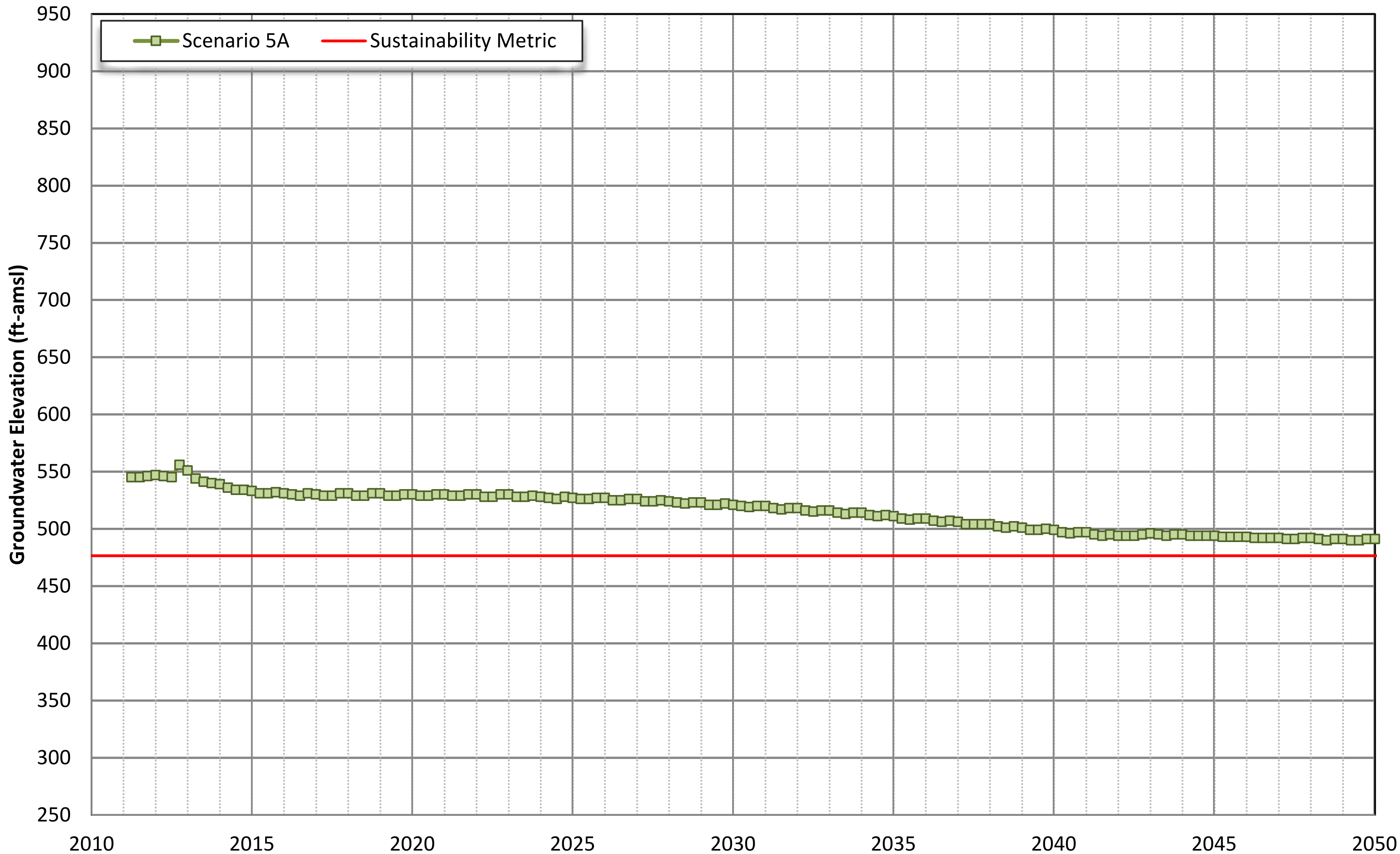

Appendix D_20150916_WellHydrographs_S5A4_Final_LBB2.xlsm
Created: 9/15/15
Printed: 9/16/2015

Figure D-28
Projected Groundwater Elevation for Scenario 5a
Chino Desalter Authority Well CDA-II-8

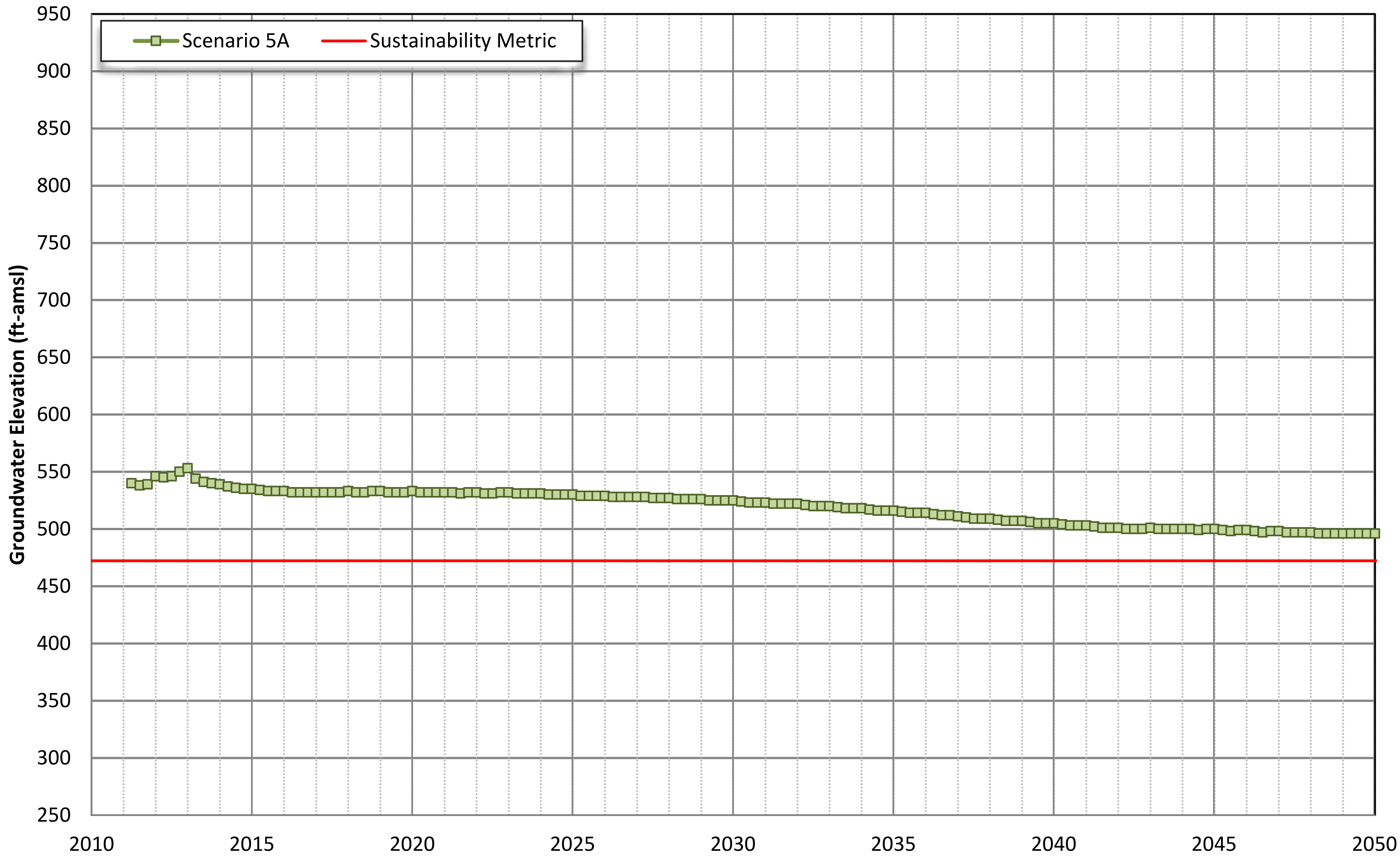

Appendix D_20150916_WellHydrographs_S5A4_Final_LBB2.xlsm
Created: 9/15/15
Printed: 9/16/2015

Figure D-29
Projected Groundwater Elevation for Scenario 5a
Chino Desalter Authority Well CDA-II-9a

Figure D-30
Projected Groundwater Elevation for Scenario 5a
City of Chino Hills Well 5

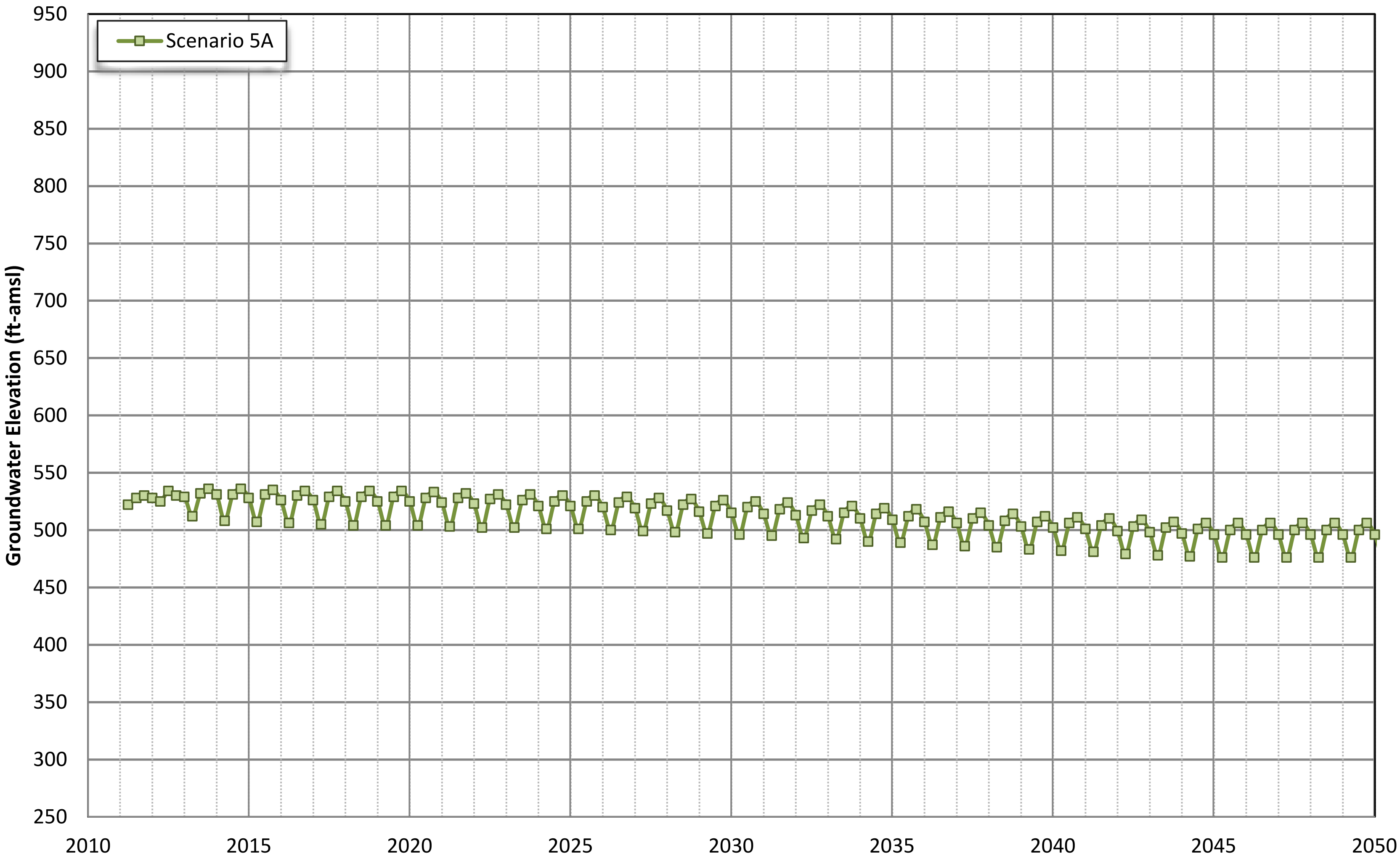

Appendix D_20150916_WellHydrographs_S5A4_Final_LBB2.xlsm
Created: 9/15/15
Printed: 9/16/2015

Figure D-31
Projected Groundwater Elevation for Scenario 5a
City of Chino Hills Well 15

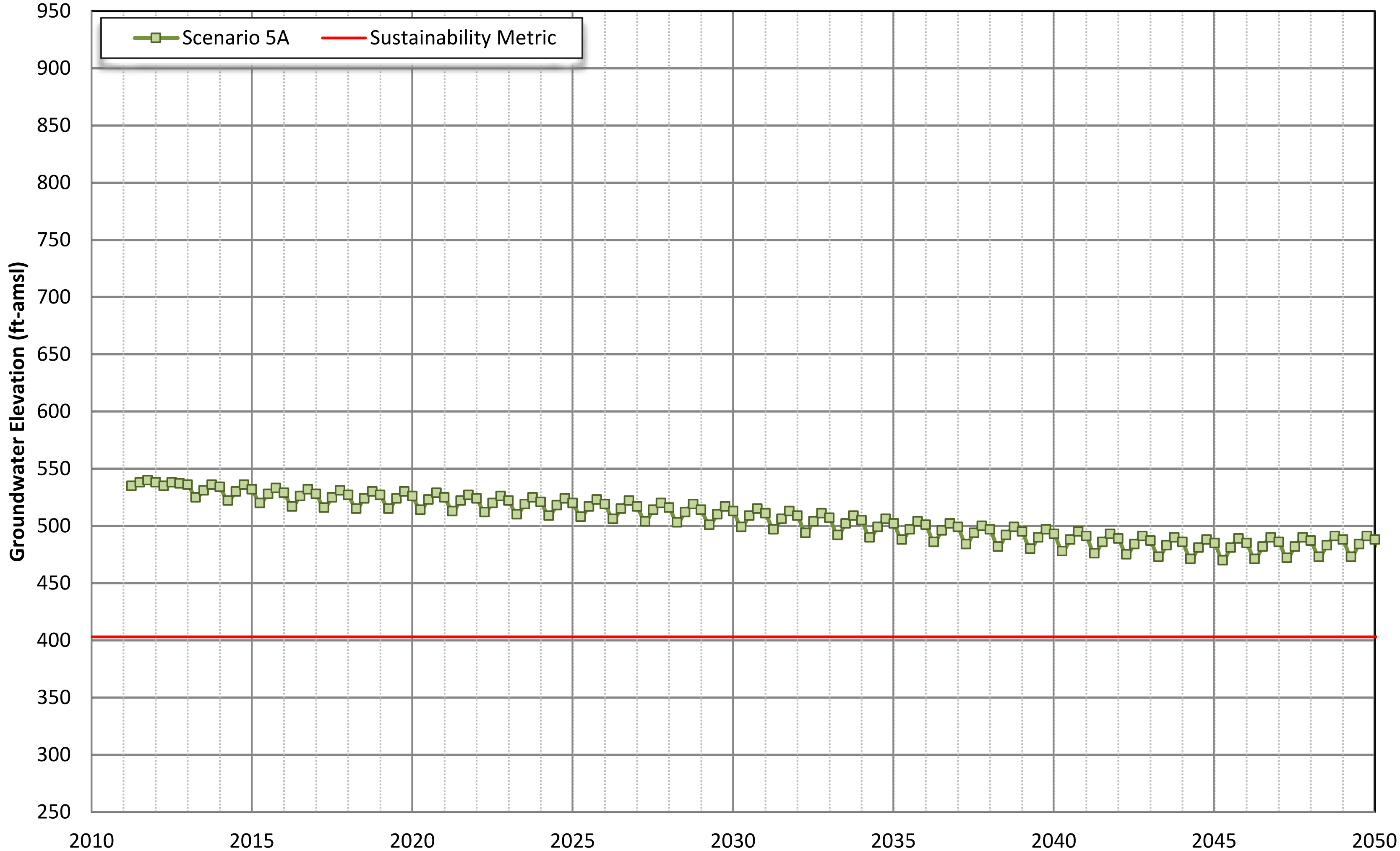

Appendix D_20150916_WellHydrographs_S5A4_Final_LBB2.xlsm
Created: 9/15/15
Printed: 9/16/2015

Figure D-32
Projected Groundwater Elevation for Scenario 5a
City of Chino Hills Well 16

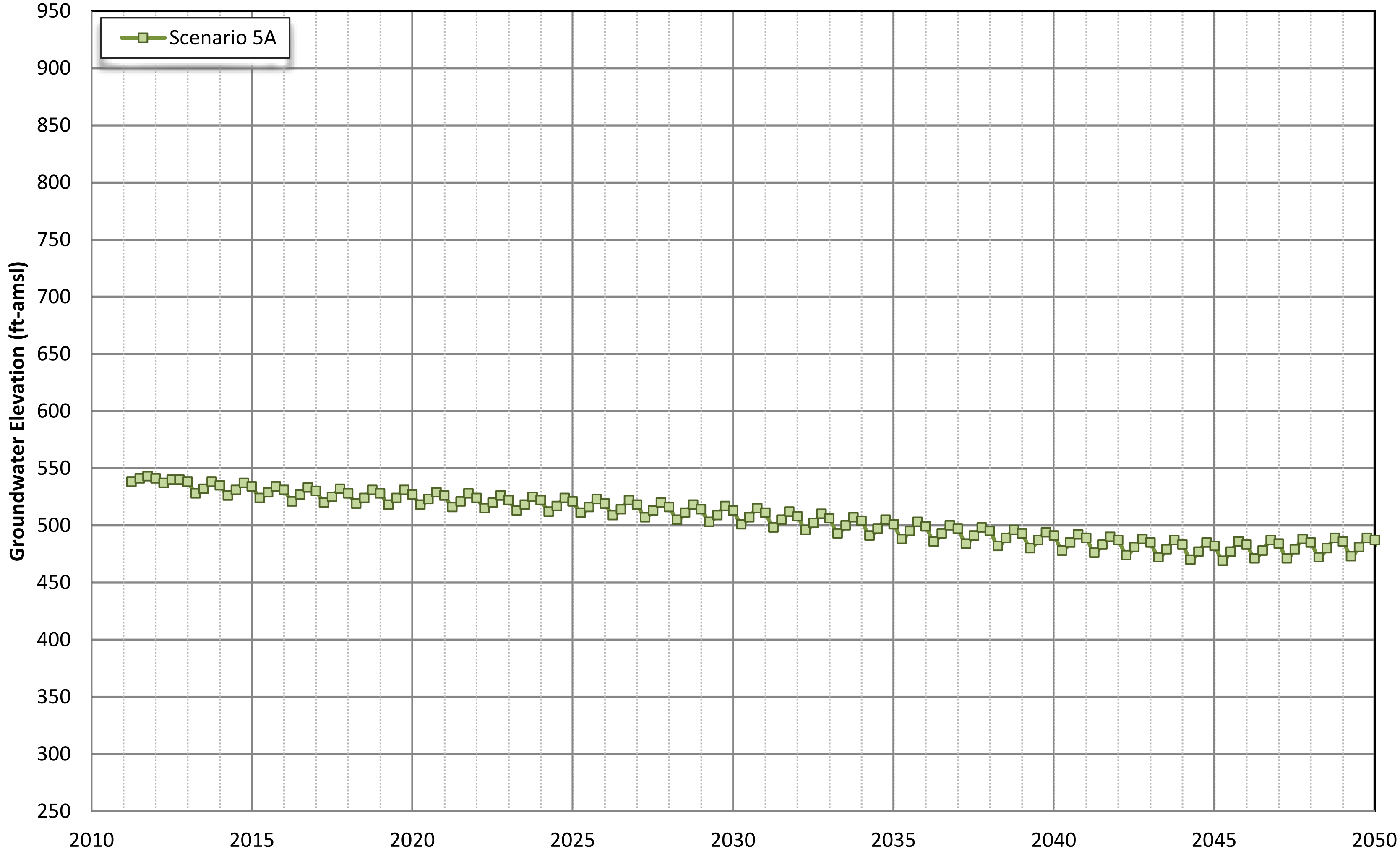

Appendix D_20150916_WellHydrographs_S5A4_Final_LBB2.xlsm
Created: 9/15/15
Printed: 9/16/2015

Figure D-33
Projected Groundwater Elevation for Scenario 5a
City of Chino Hills Well 17

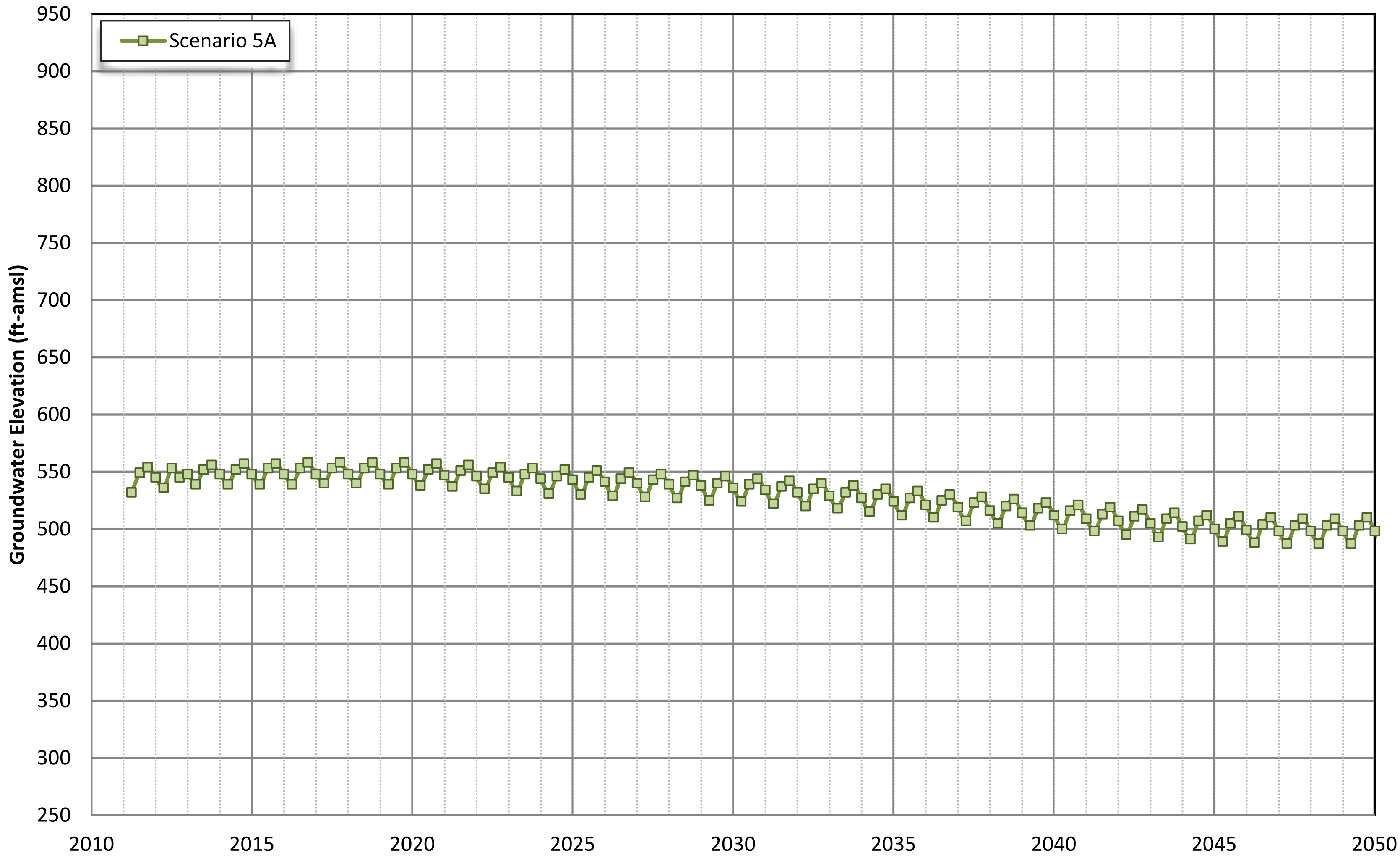

Appendix D_20150916_WellHydrographs_S5A4_Final_LBB2.xlsm
Created: 9/15/15
Printed: 9/16/2015

Figure D-34
Projected Groundwater Elevation for Scenario 5a
City of Chino Hills Well 1A

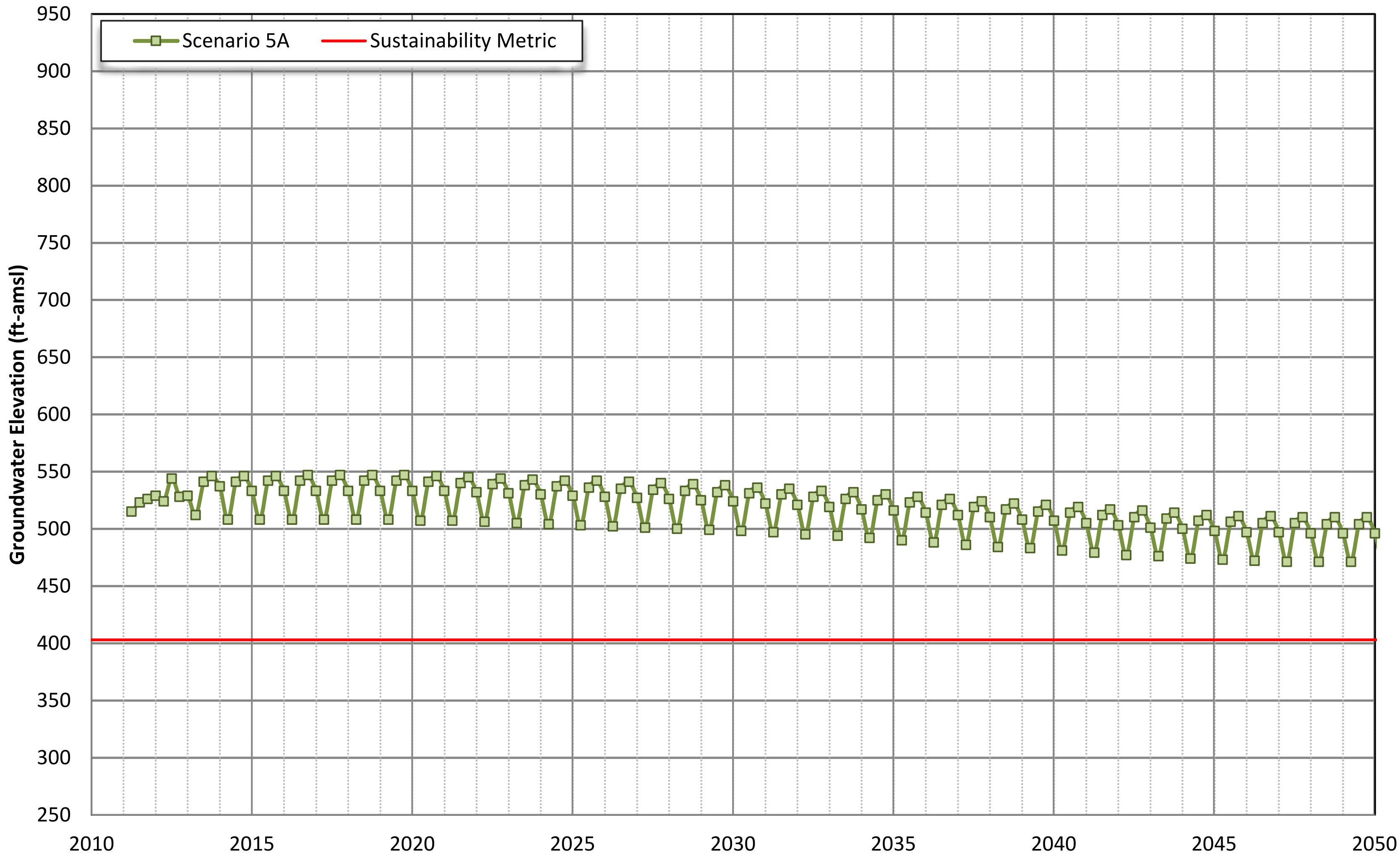

Appendix D_20150916_WellHydrographs_S5A4_Final_LBB2.xlsm
Created: 9/15/15
Printed: 9/16/2015

Figure D-35
Projected Groundwater Elevation for Scenario 5a
City of Chino Hills Well 7A

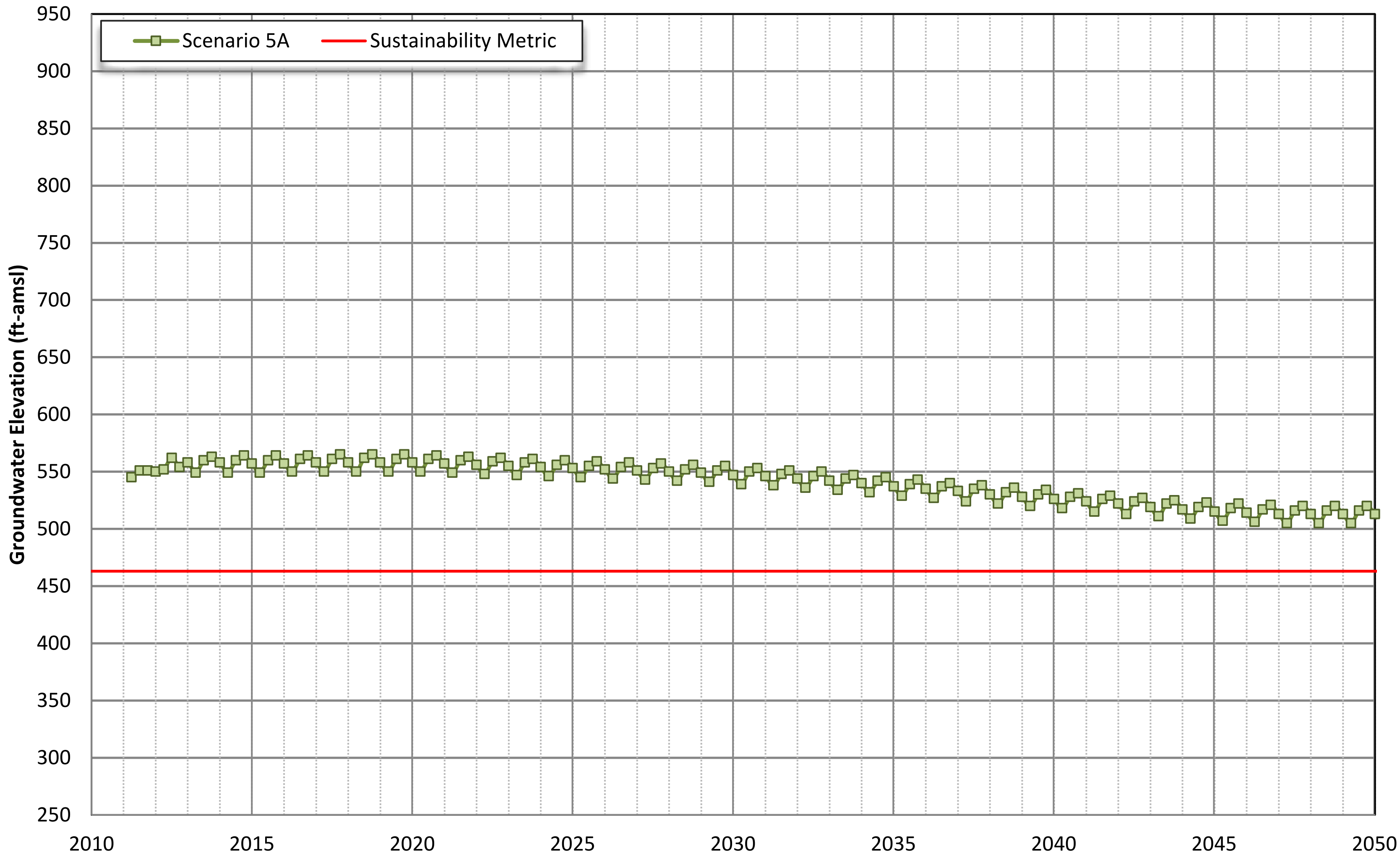

Appendix D_20150916_WellHydrographs_S5A4_Final_LBB2.xlsm
Created: 9/15/15
Printed: 9/16/2015

Figure D-36
Projected Groundwater Elevation for Scenario 5a
City of Chino Hills Well 7B

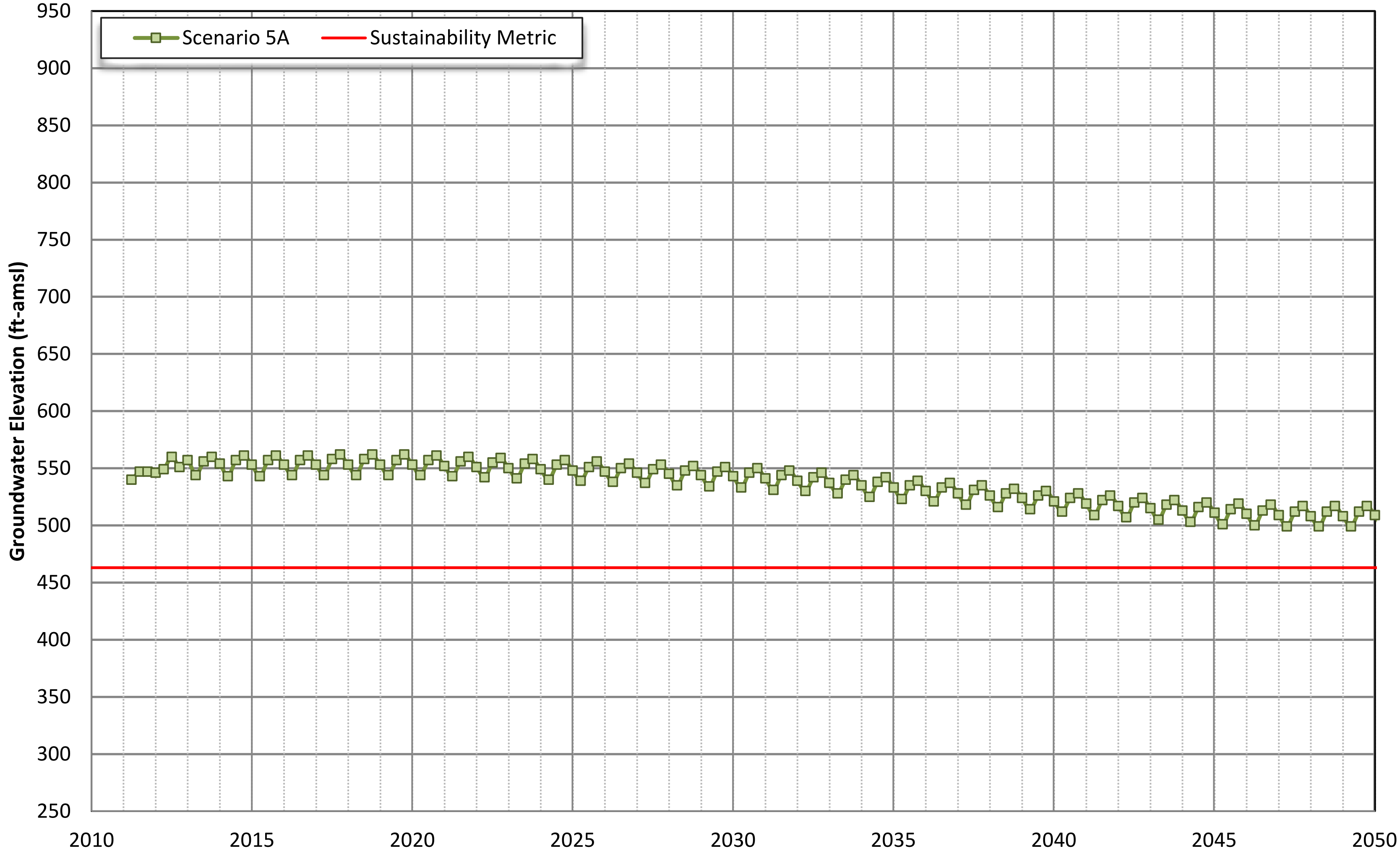

Appendix D_20150916_WellHydrographs_S5A4_Final_LBB2.xlsm
Created: 9/15/15
Printed: 9/16/2015

Figure D-37
Projected Groundwater Elevation for Scenario 5a
City of Chino Well 4

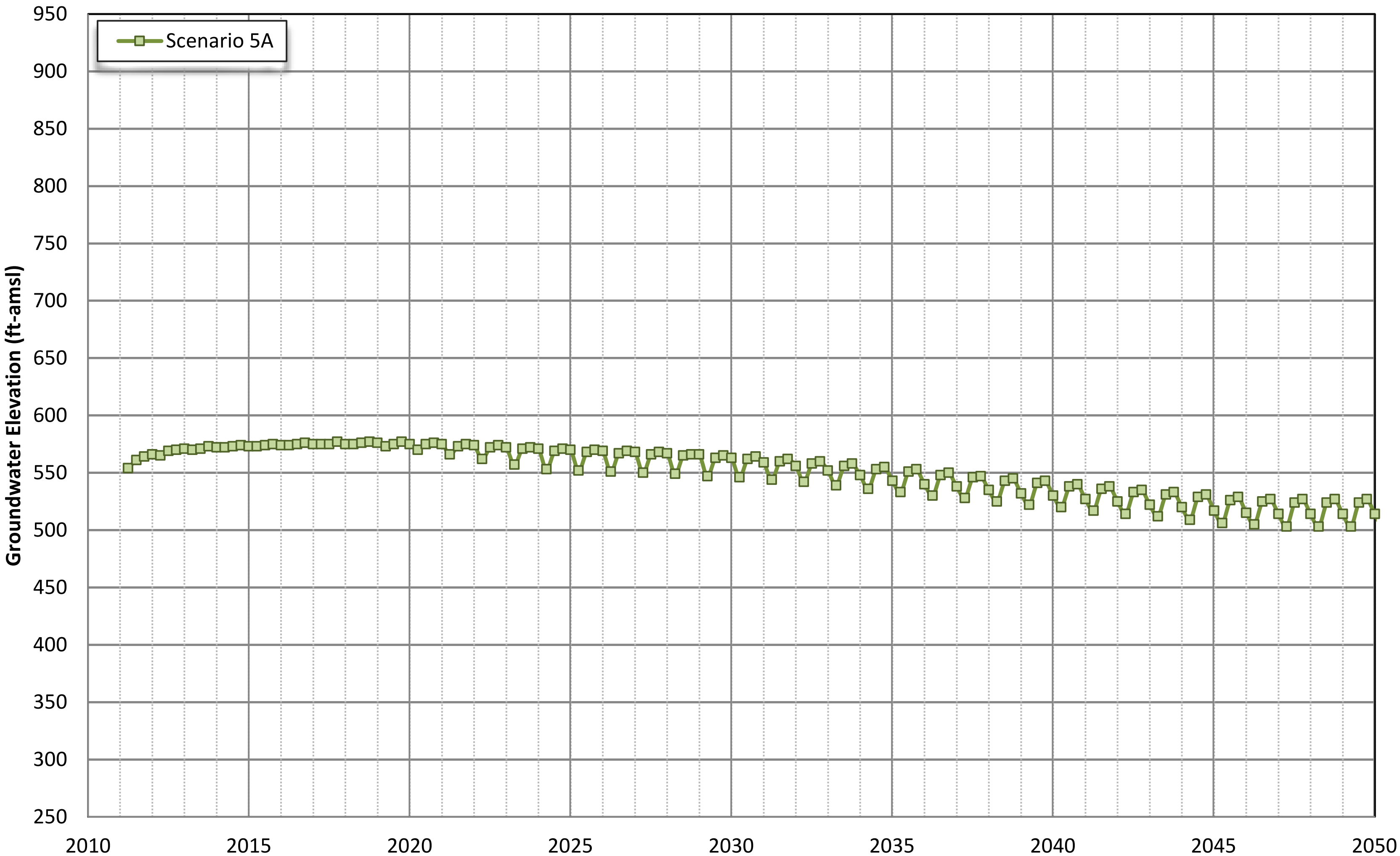

Appendix D_20150916_WellHydrographs_S5A4_Final_LBB2.xlsm
Created: 9/15/15
Printed: 9/16/2015

Figure D-38
Projected Groundwater Elevation for Scenario 5a
City of Chino Well 5

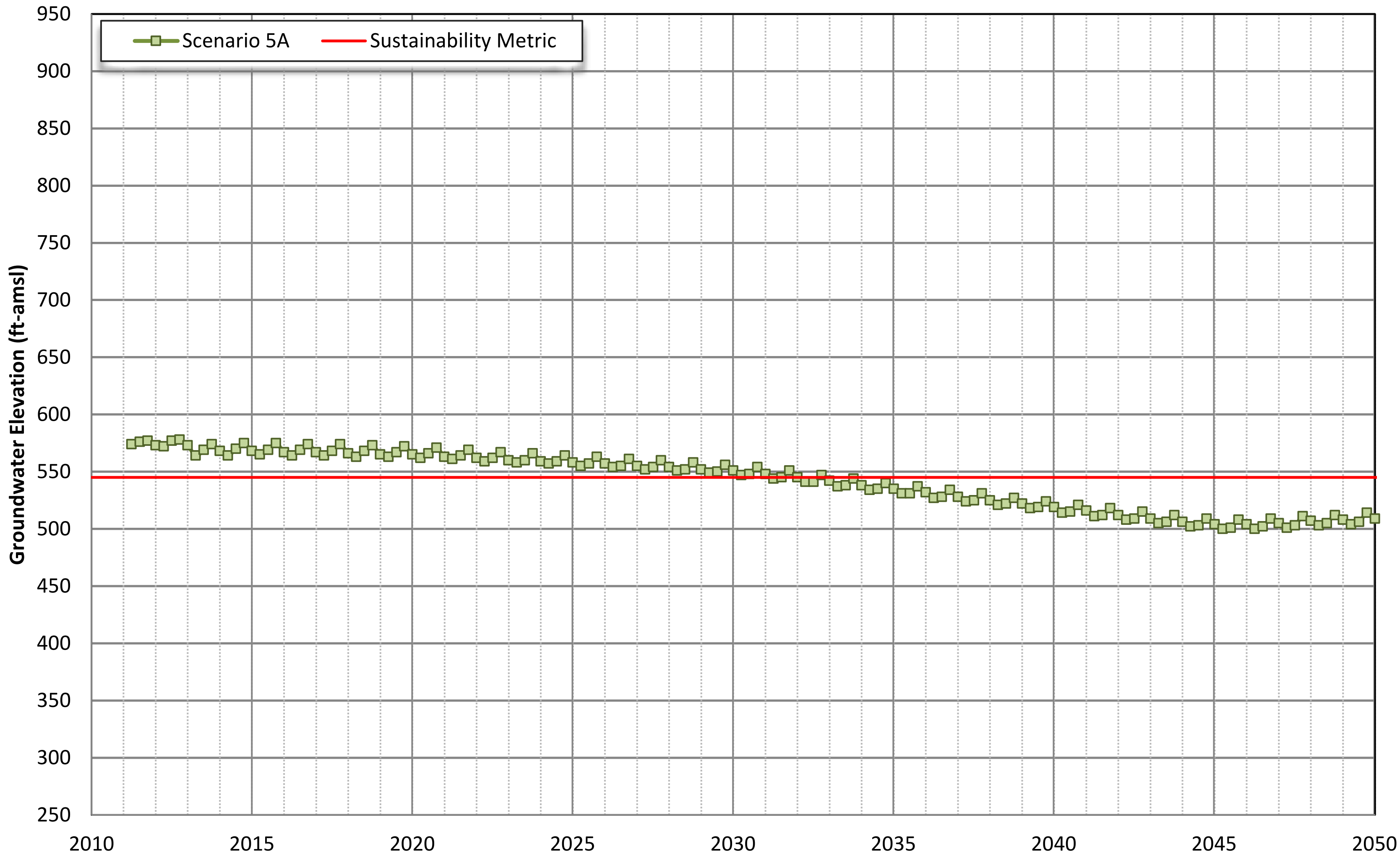

Appendix D_20150916_WellHydrographs_S5A4_Final_LBB2.xlsm
Created: 9/15/15
Printed: 9/16/2015

Figure D-39
Projected Groundwater Elevation for Scenario 5a
City of Chino Well 6

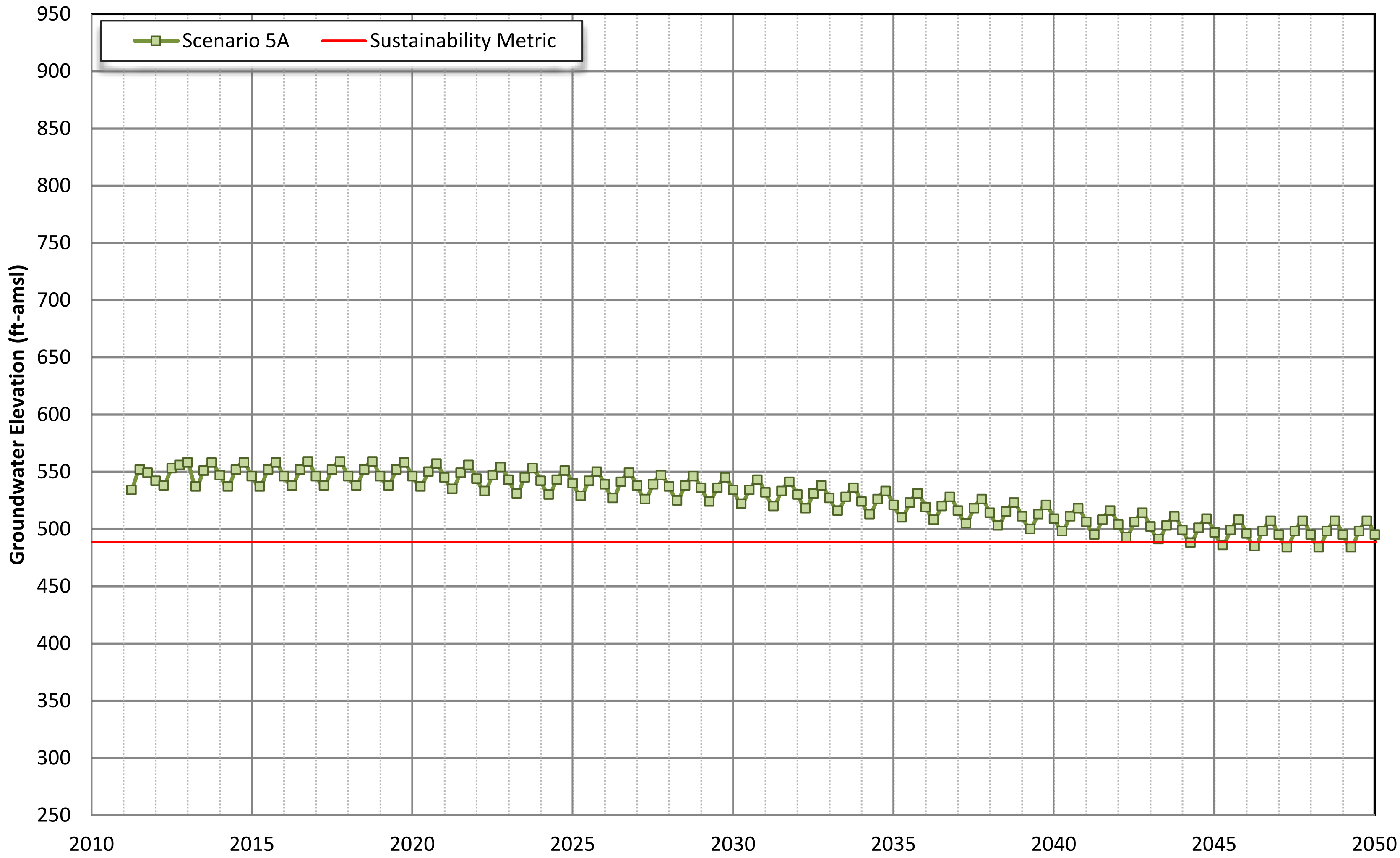

Appendix D_20150916_WellHydrographs_S5A4_Final_LBB2.xlsm
Created: 9/15/15
Printed: 9/16/2015

Figure D-40
Projected Groundwater Elevation for Scenario 5a
City of Chino Well 9

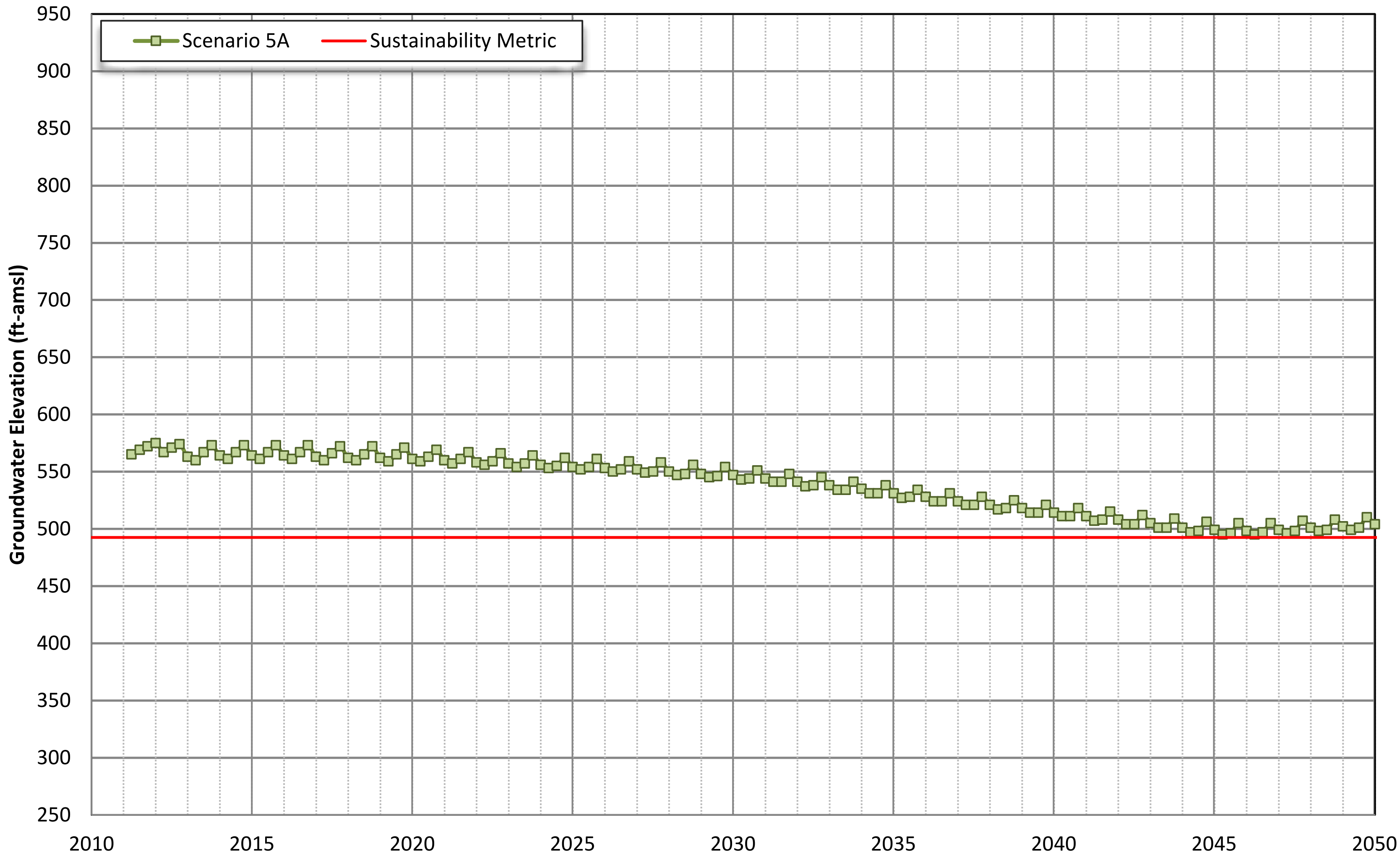

Appendix D_20150916_WellHydrographs_S5A4_Final_LBB2.xlsm
Created: 9/15/15
Printed: 9/16/2015

Figure D-41
Projected Groundwater Elevation for Scenario 5a
City of Chino Well 10

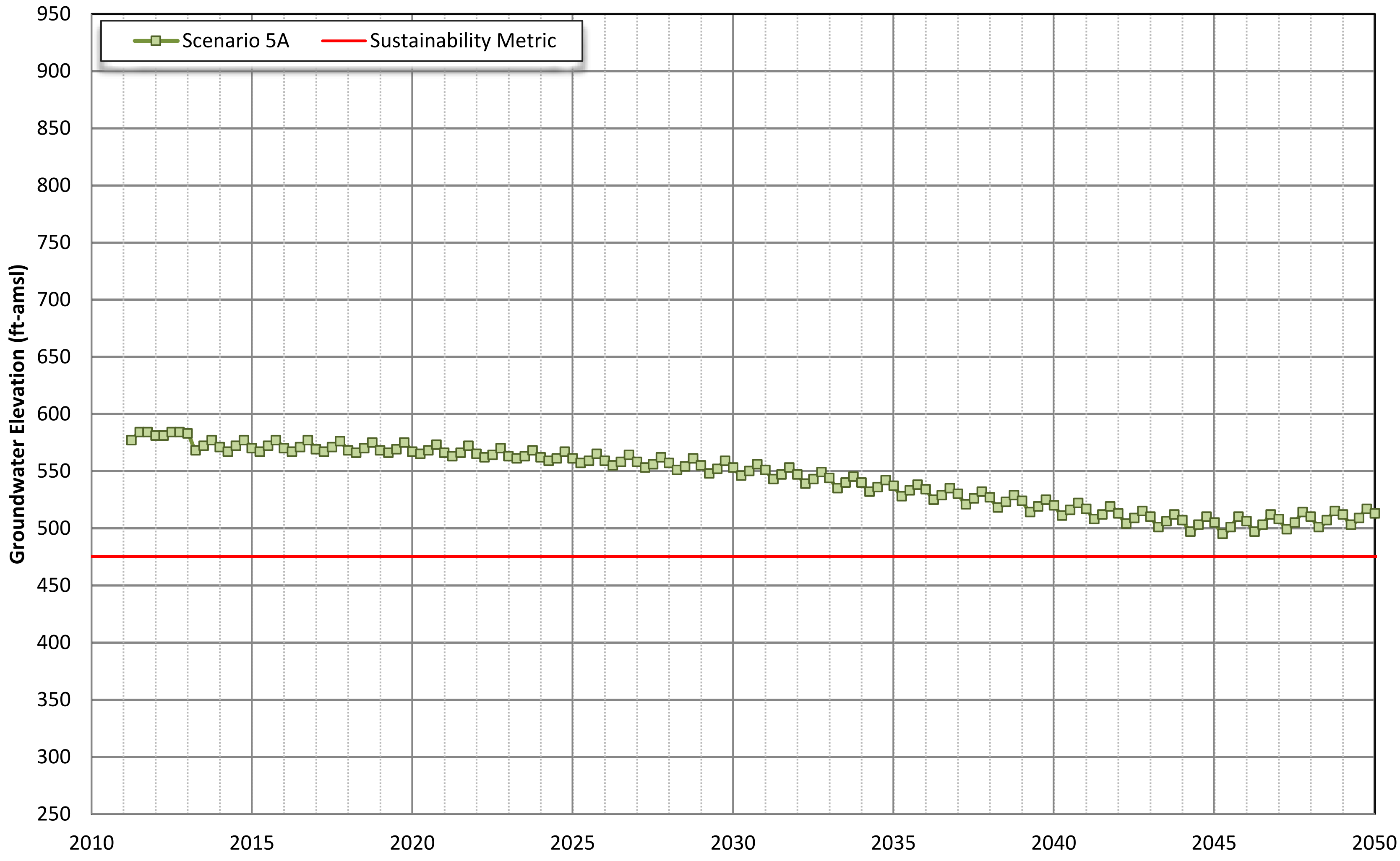

Appendix D_20150916_WellHydrographs_S5A4_Final_LBB2.xlsm
Created: 9/15/15
Printed: 9/16/2015

Figure D-42
Projected Groundwater Elevation for Scenario 5a
City of Chino Well 11

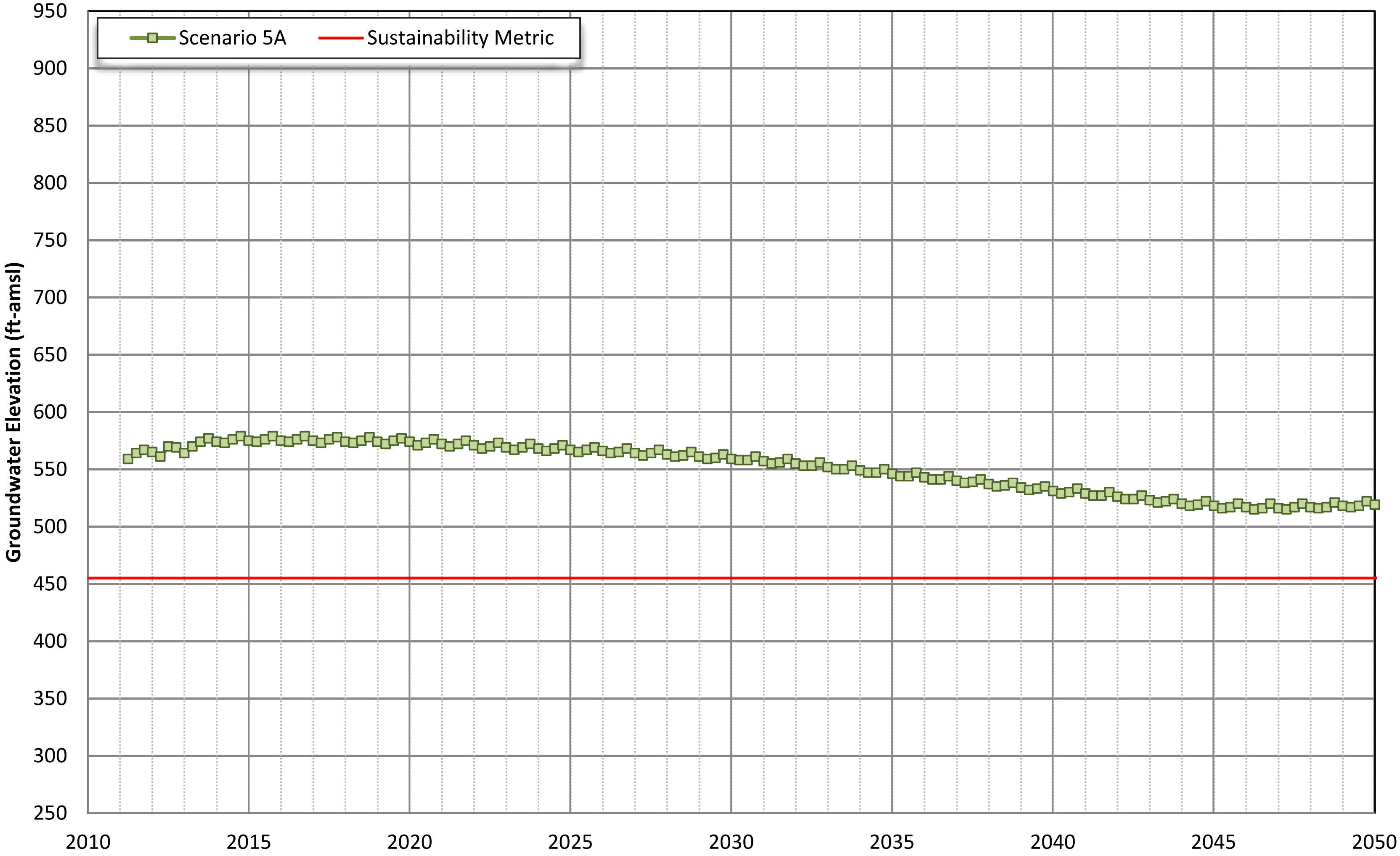

Appendix D_20150916_WellHydrographs_S5A4_Final_LBB2.xlsm
Created: 9/15/15
Printed: 9/16/2015

Figure D-43
Projected Groundwater Elevation for Scenario 5a
City of Chino Well 12

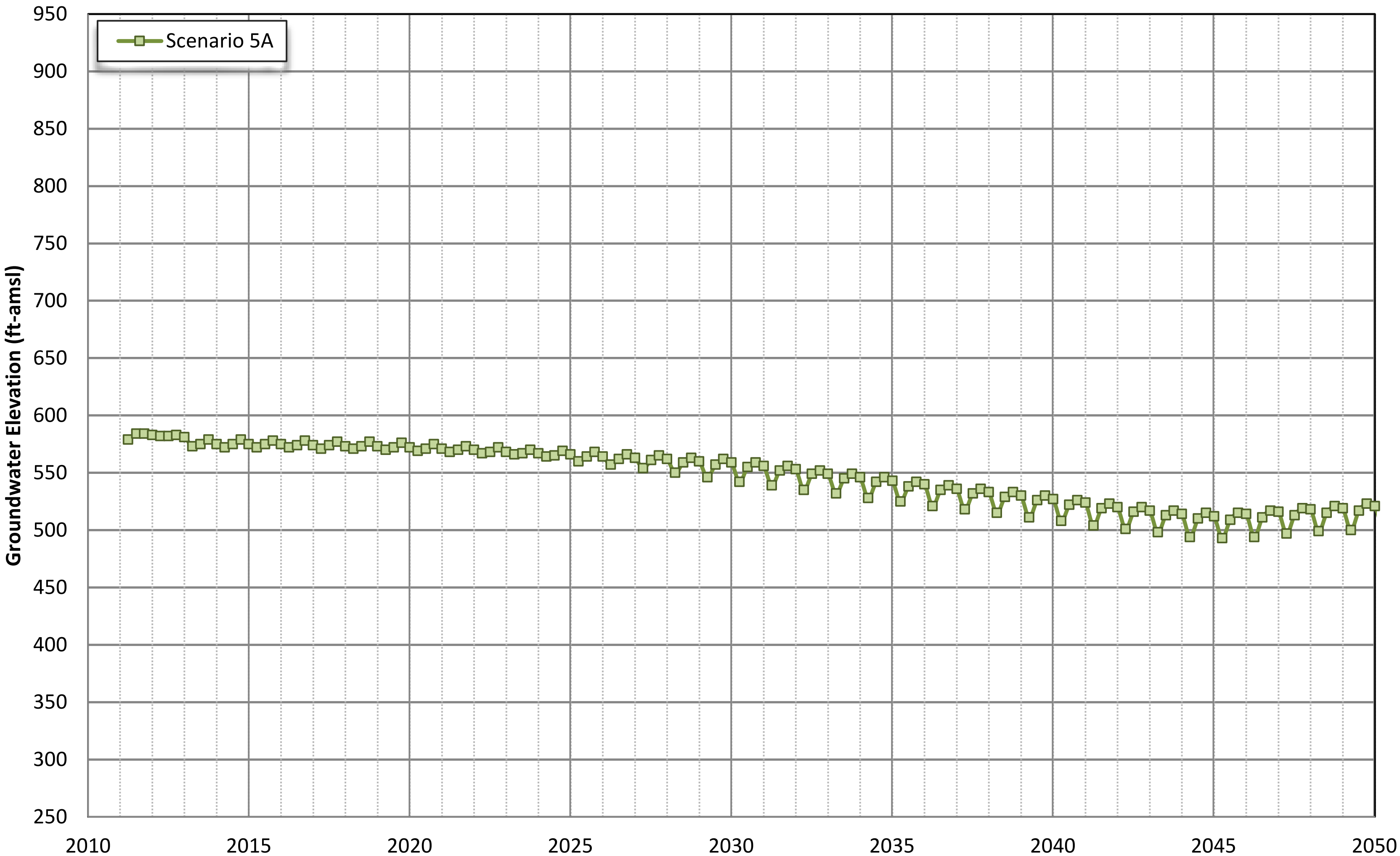

Appendix D_20150916_WellHydrographs_S5A4_Final_LBB2.xlsm
Created: 9/15/15
Printed: 9/16/2015

Figure D-44
Projected Groundwater Elevation for Scenario 5a
City of Chino Well 13

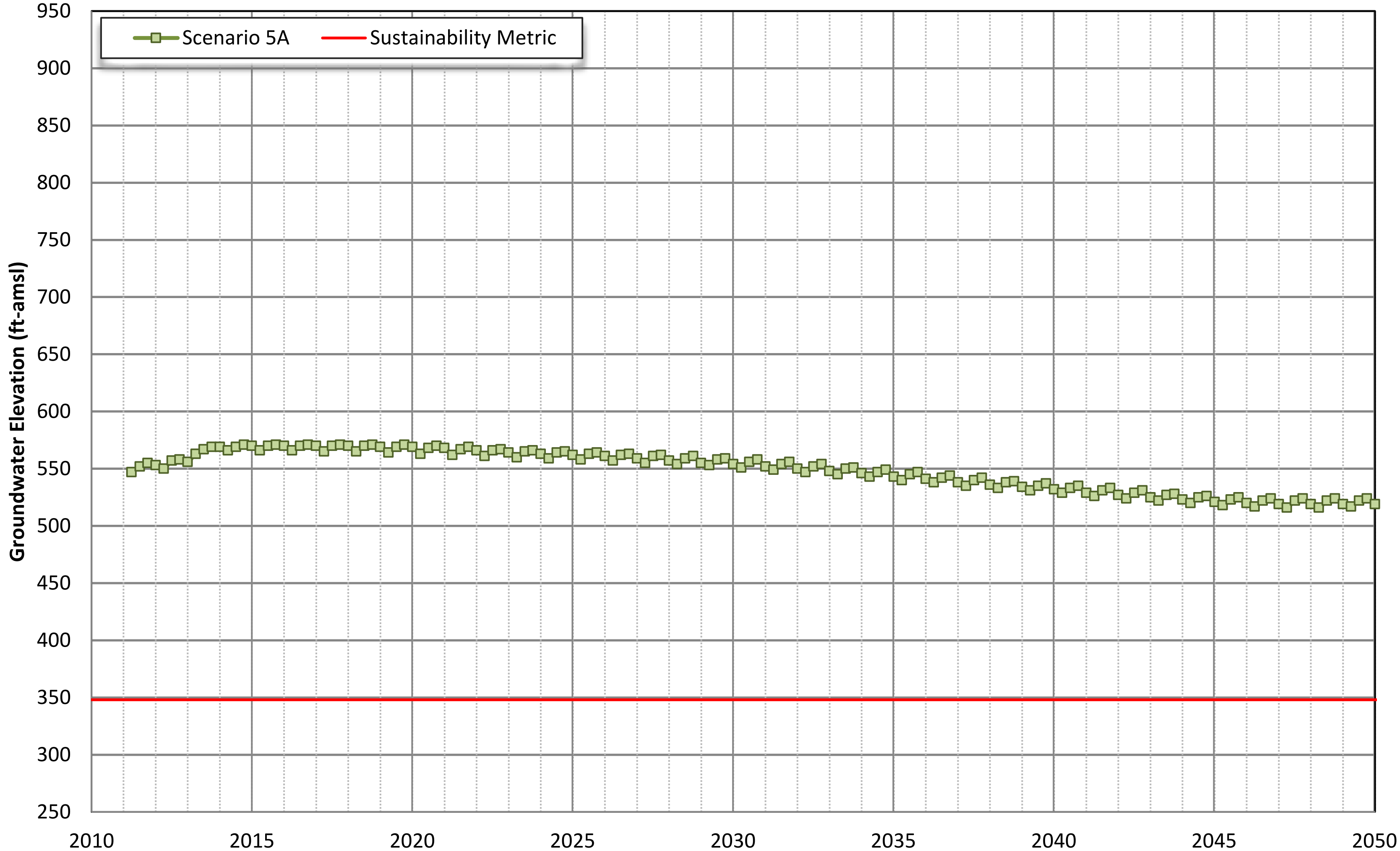

Appendix D_20150916_WellHydrographs_S5A4_Final_LBB2.xlsm
Created: 9/15/15
Printed: 9/16/2015

Figure D-45
Projected Groundwater Elevation for Scenario 5a
City of Chino Well 14

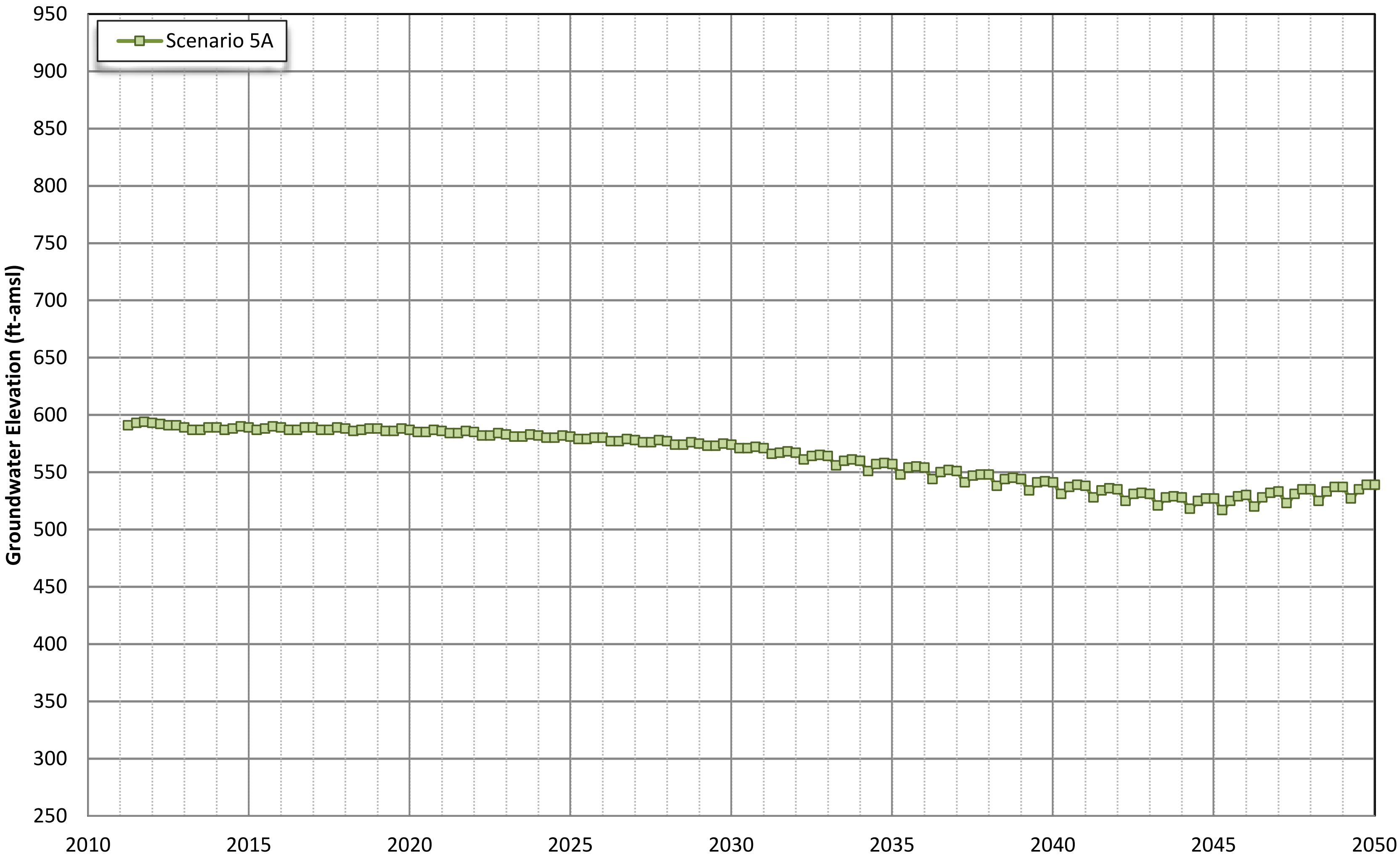

Appendix D_20150916_WellHydrographs_S5A4_Final_LBB2.xlsm
Created: 9/15/15
Printed: 9/16/2015

Figure D-46
Projected Groundwater Elevation for Scenario 5a
City of Chino Well 16

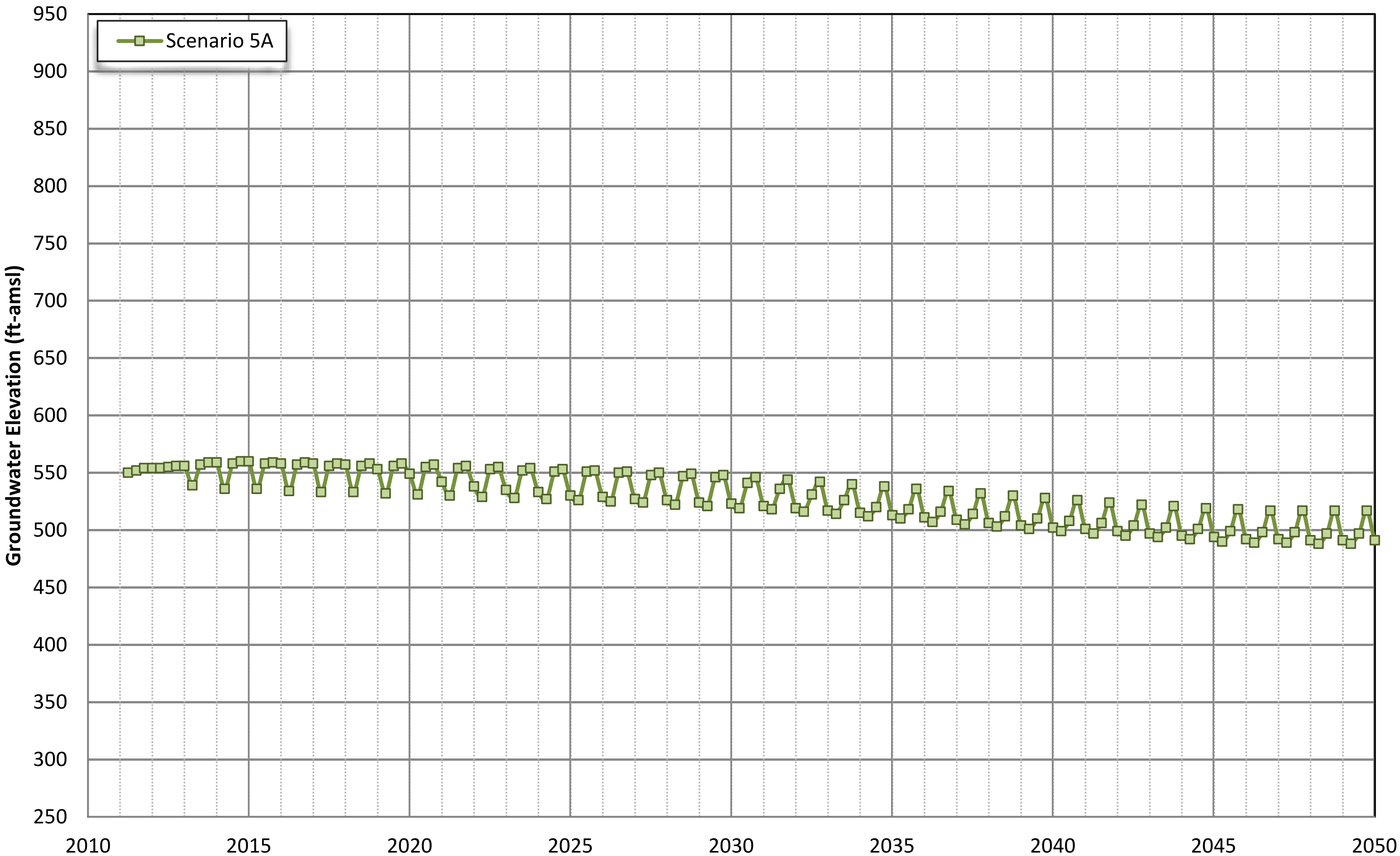

Appendix D_20150916_WellHydrographs_S5A4_Final_LBB2.xlsm
Created: 9/15/15
Printed: 9/16/2015

Figure D-47
Projected Groundwater Elevation for Scenario 5a
City of Chino Well 17

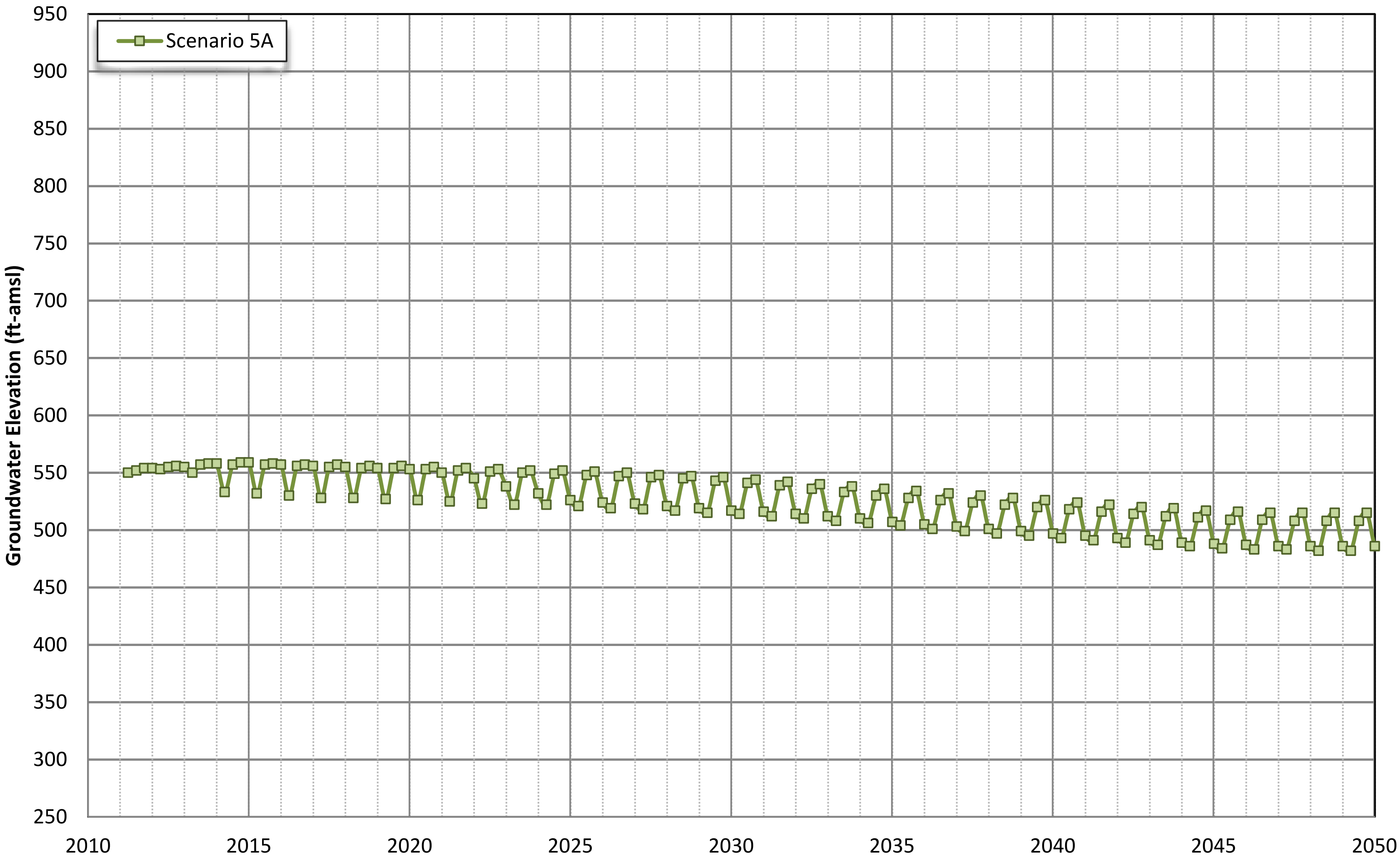

Appendix D_20150916_WellHydrographs_S5A4_Final_LBB2.xlsm
Created: 9/15/15
Printed: 9/16/2015

Figure D-48
Projected Groundwater Elevation for Scenario 5a
City of Chino Well 18

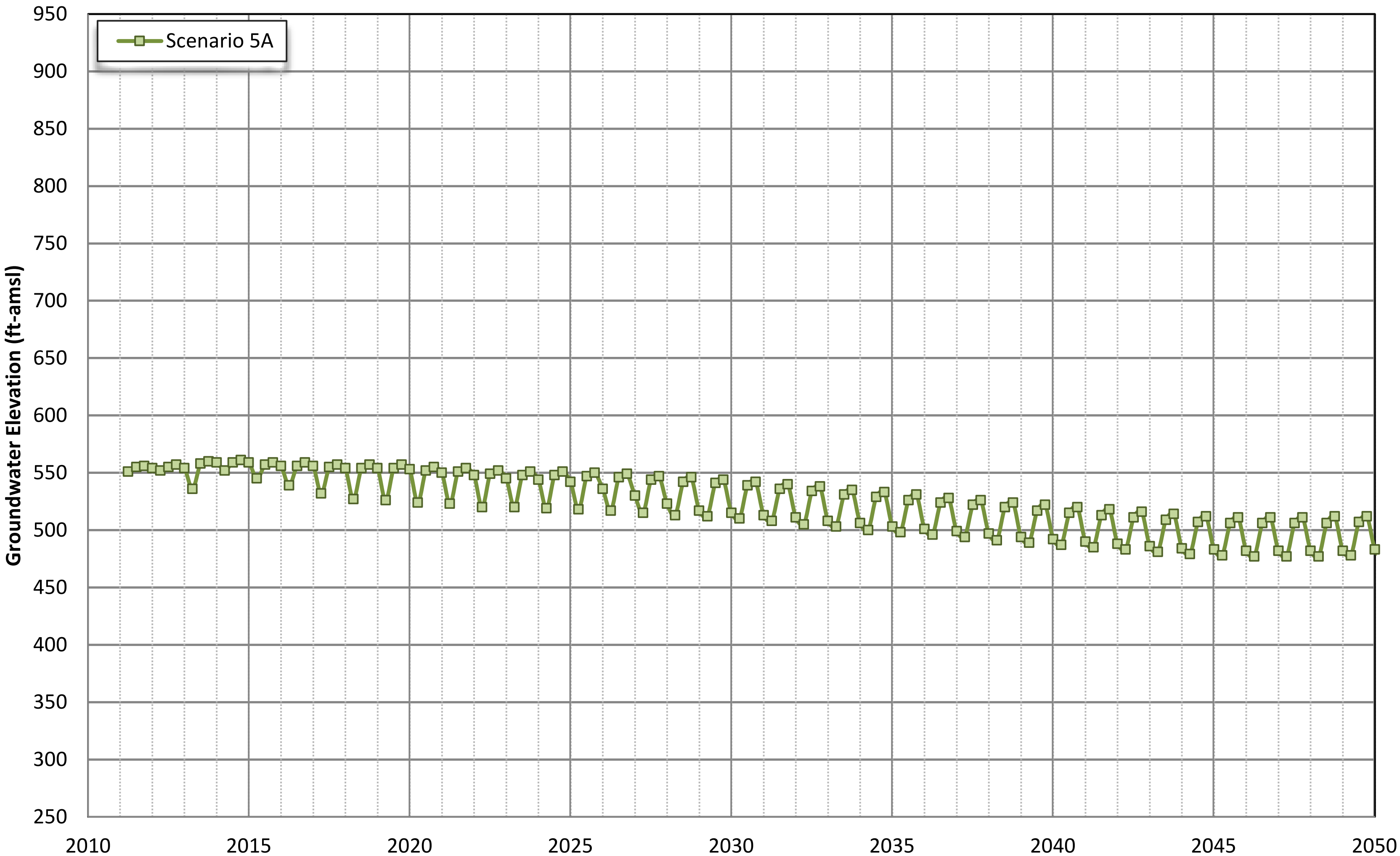

Appendix D_20150916_WellHydrographs_S5A4_Final_LBB2.xlsm
Created: 9/15/15
Printed: 9/16/2015

Figure D-49
Projected Groundwater Elevation for Scenario 5a
City of Chino Well Bon View

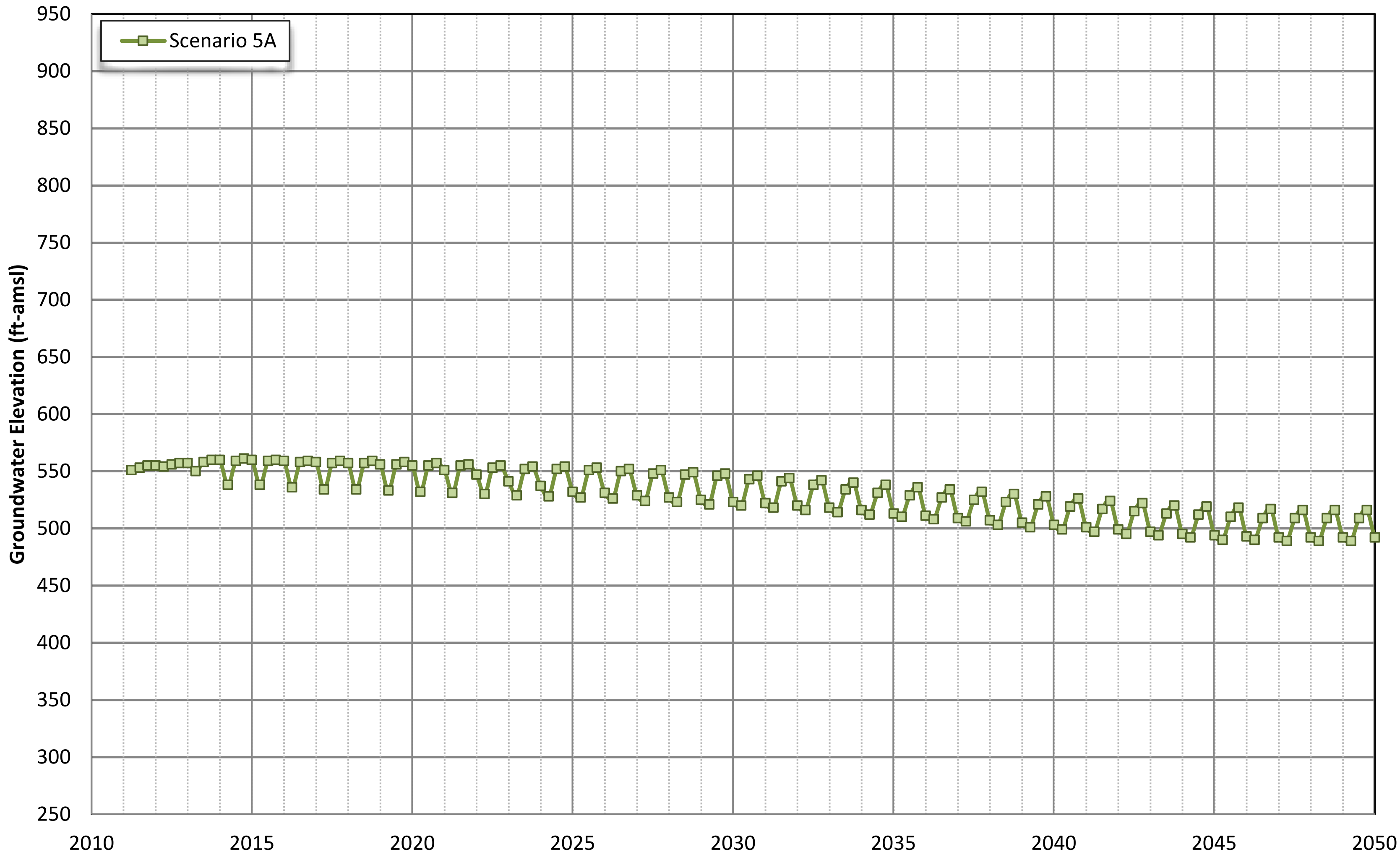

Appendix D_20150916_WellHydrographs_S5A4_Final_LBB2.xlsm
Created: 9/15/15
Printed: 9/16/2015

Figure D-50
Projected Groundwater Elevation for Scenario 5a
City of Chino Well Magnolia

Appendix D_20150916_WellHydrographs_S5A4_Final_LBB2.xlsm
Created: 9/15/15
Printed: 9/16/2015

Figure D-51
Projected Groundwater Elevation for Scenario 5a
Cucamonga Valley Water District Well ASR1- CB-49

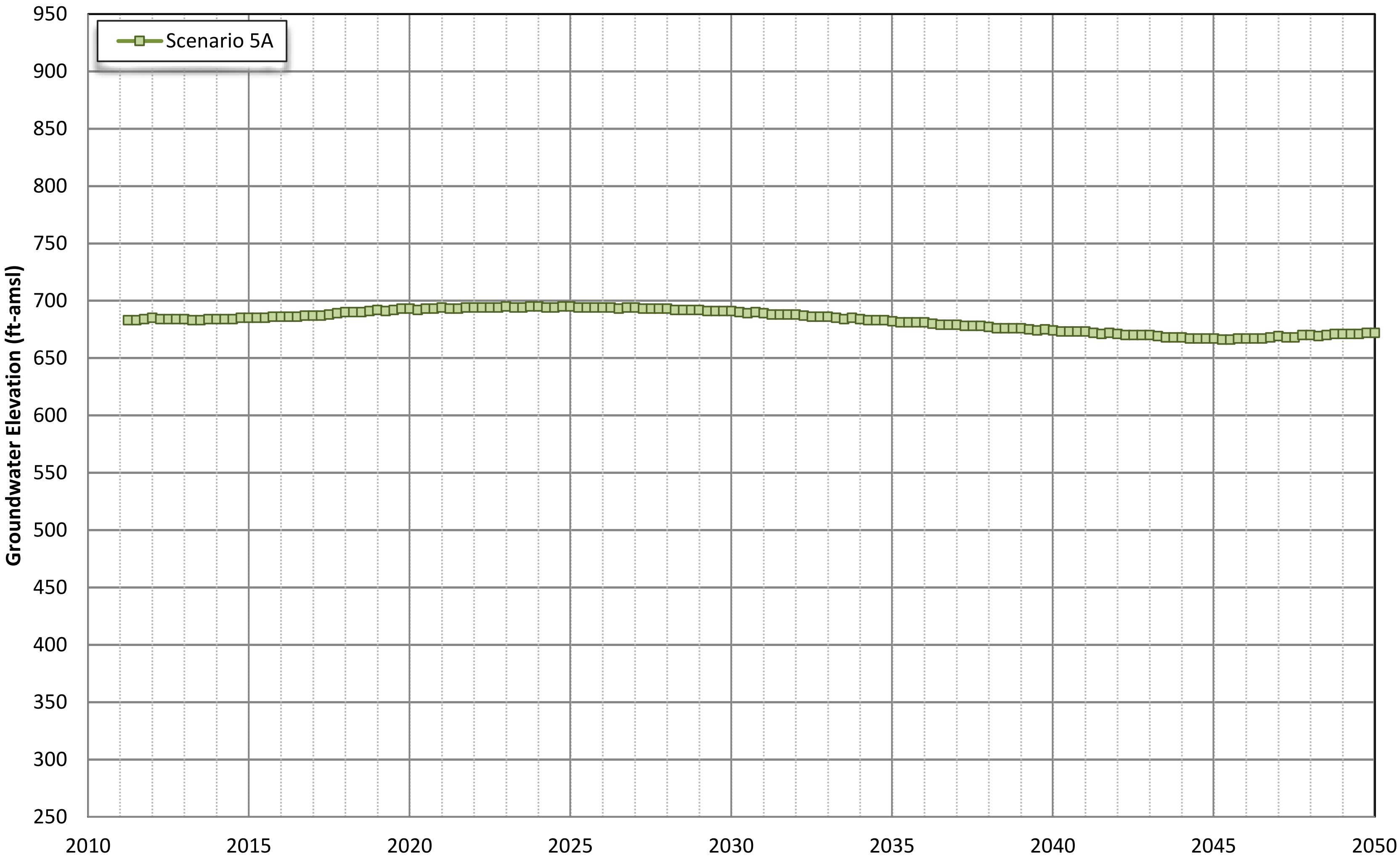

Appendix D_20150916_WellHydrographs_S5A4_Final_LBB2.xlsm
Created: 9/15/15
Printed: 9/16/2015

Figure D-52
Projected Groundwater Elevation for Scenario 5a
Cucamonga Valley Water District Well ASR2-CB-50

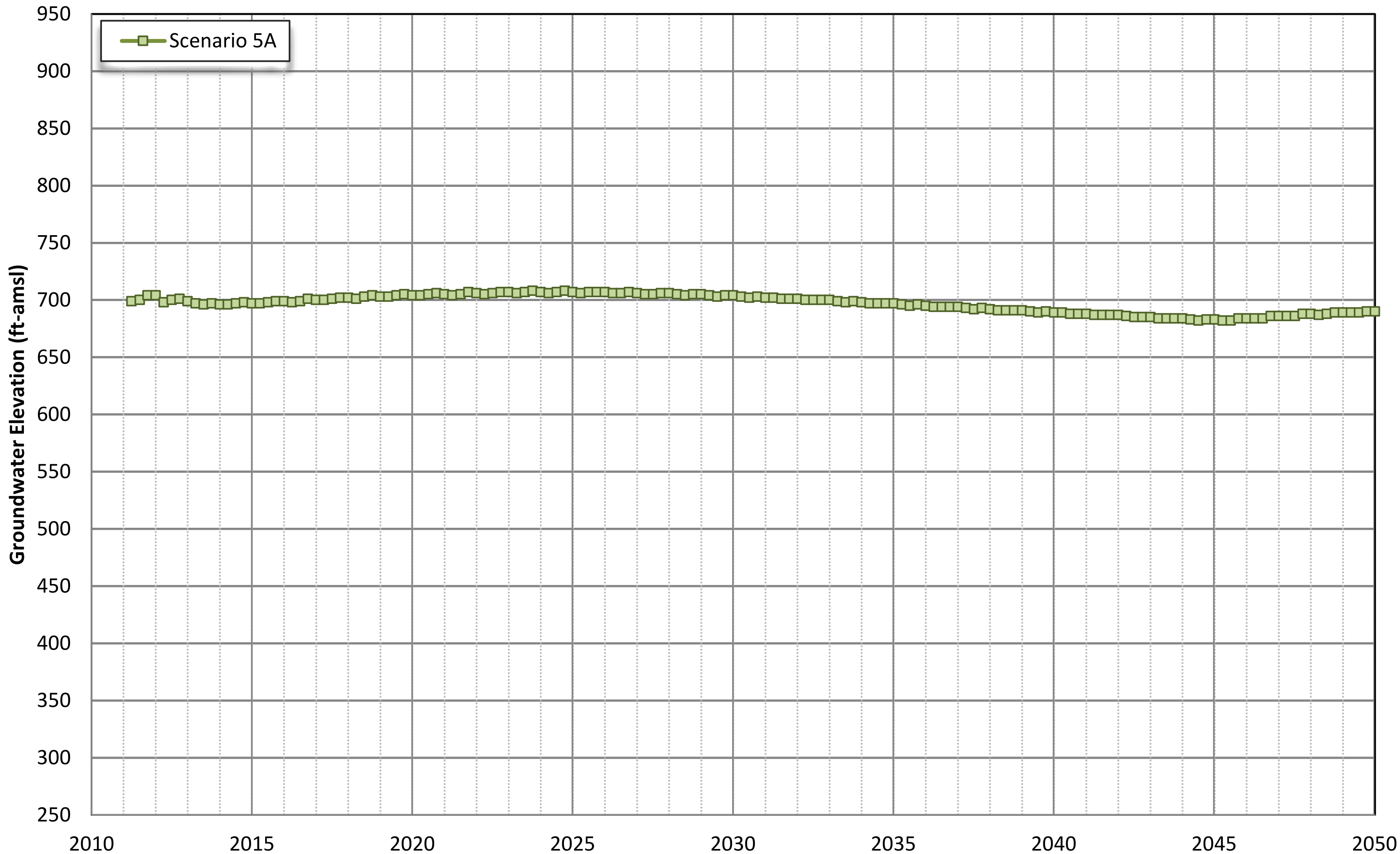

Appendix D_20150916_WellHydrographs_S5A4_Final_LBB2.xlsm
Created: 9/15/15
Printed: 9/16/2015

Figure D-53
Projected Groundwater Elevation for Scenario 5a
Cucamonga Valley Water District Well ASR3-CB-48

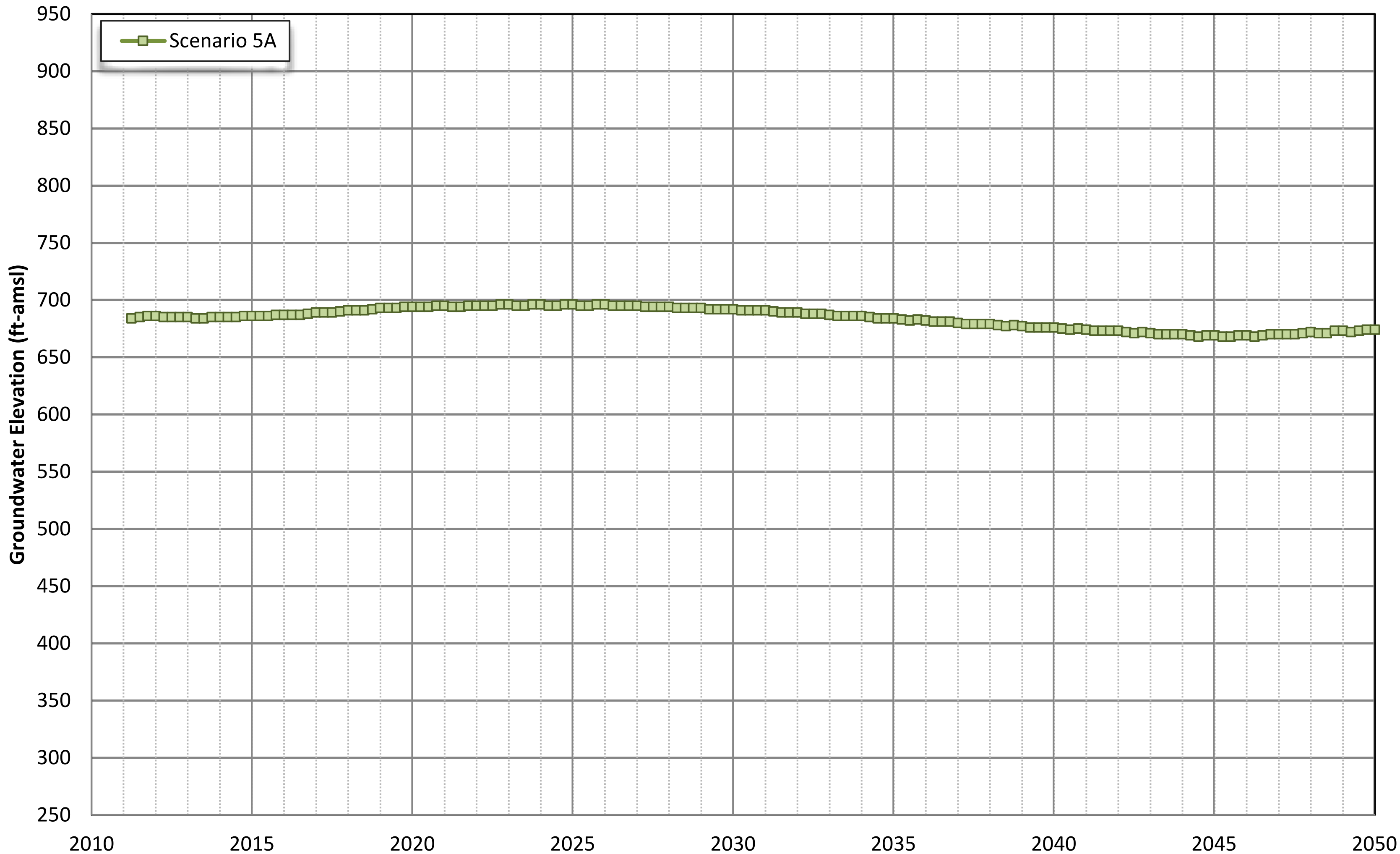

Appendix D_20150916_WellHydrographs_S5A4_Final_LBB2.xlsm
Created: 9/15/15
Printed: 9/16/2015

Figure D-54
Projected Groundwater Elevation for Scenario 5a
Cucamonga Valley Water District Well CB-1

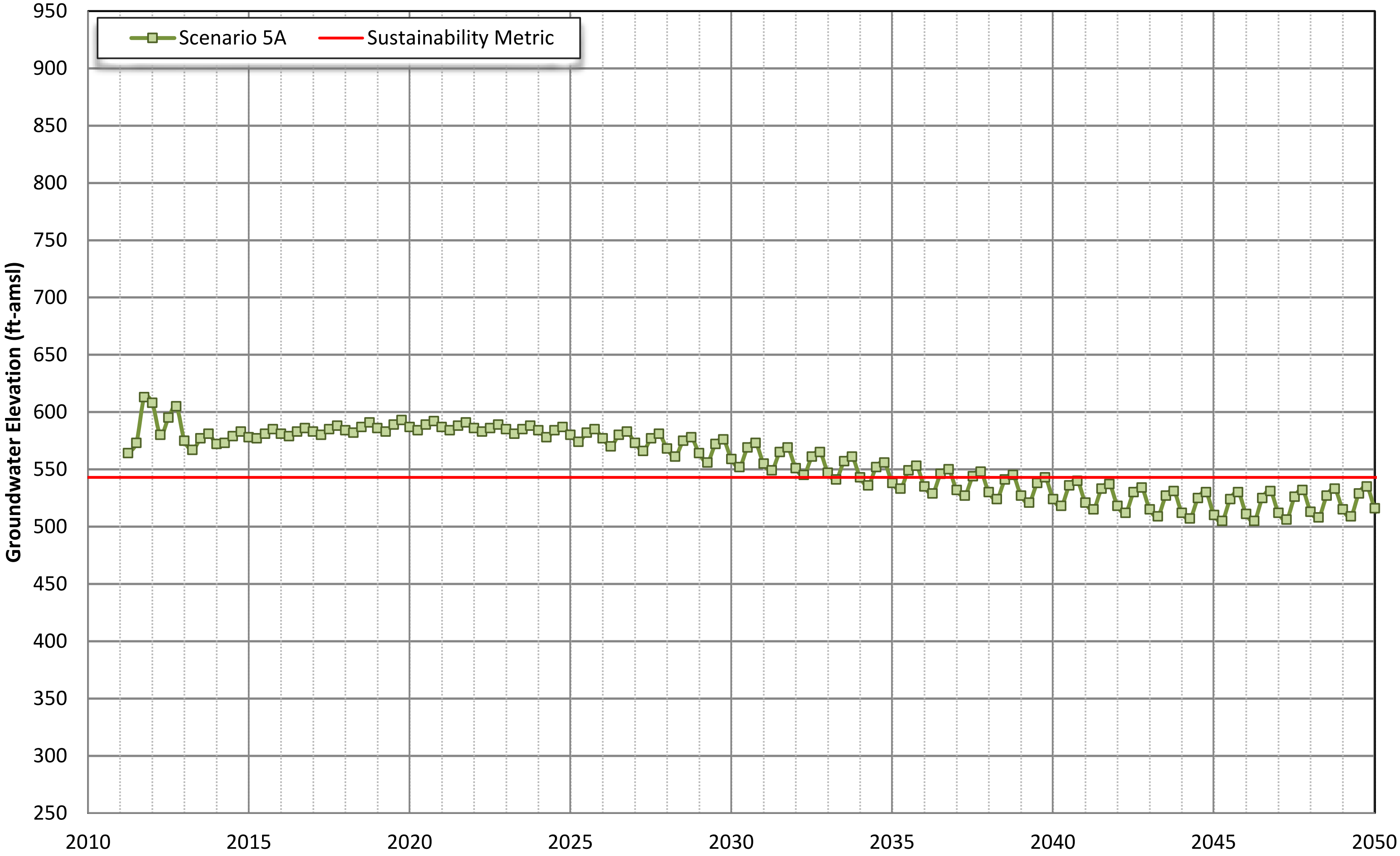

Appendix D_20150916_WellHydrographs_S5A4_Final_LBB2.xlsm
Created: 9/15/15
Printed: 9/16/2015

Figure D-55
Projected Groundwater Elevation for Scenario 5a
Cucamonga Valley Water District Well CB-3

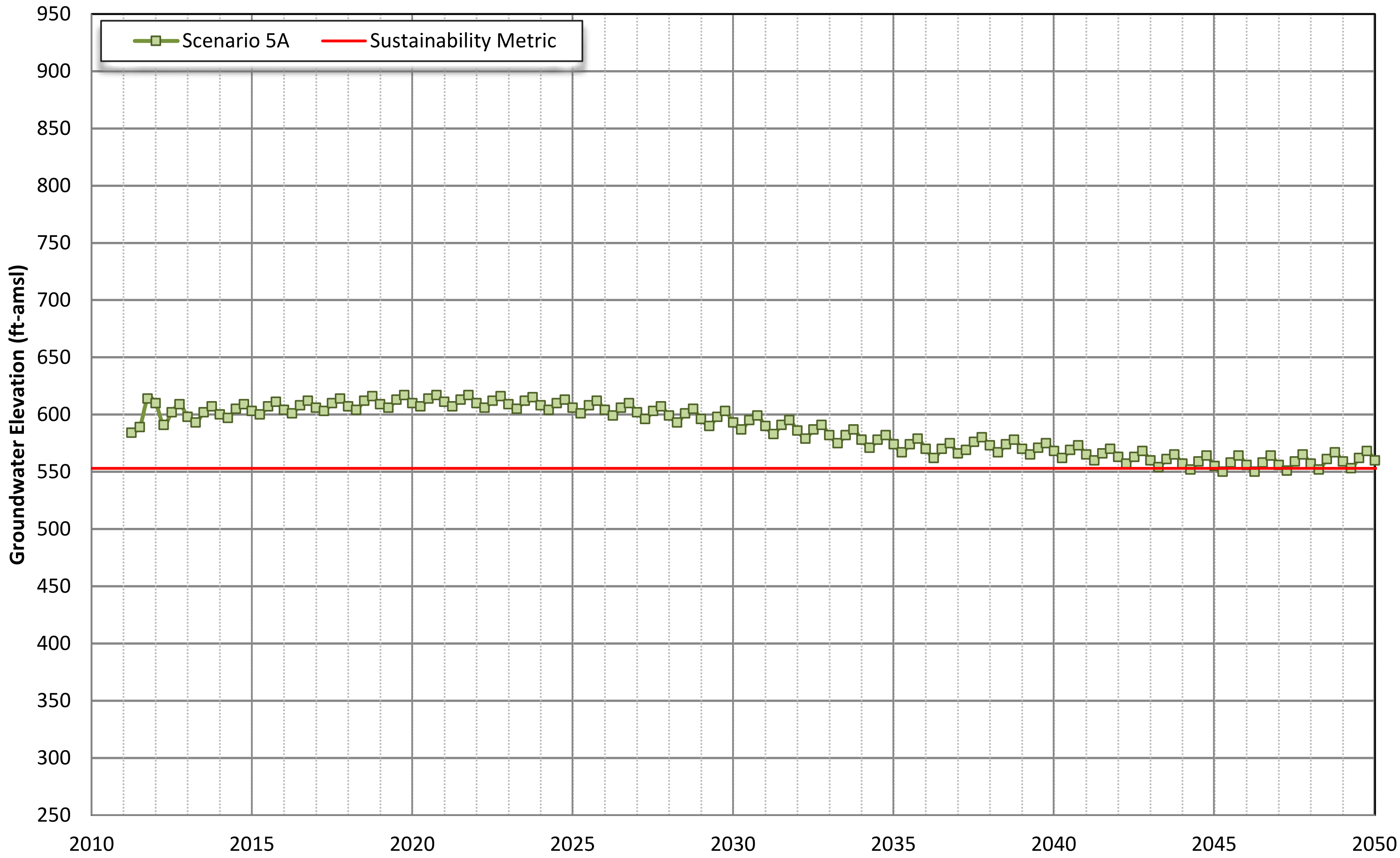

Appendix D_20150916_WellHydrographs_S5A4_Final_LBB2.xlsm
Created: 9/15/15
Printed: 9/16/2015

Figure D-56
Projected Groundwater Elevation for Scenario 5a
Cucamonga Valley Water District Well CB-30

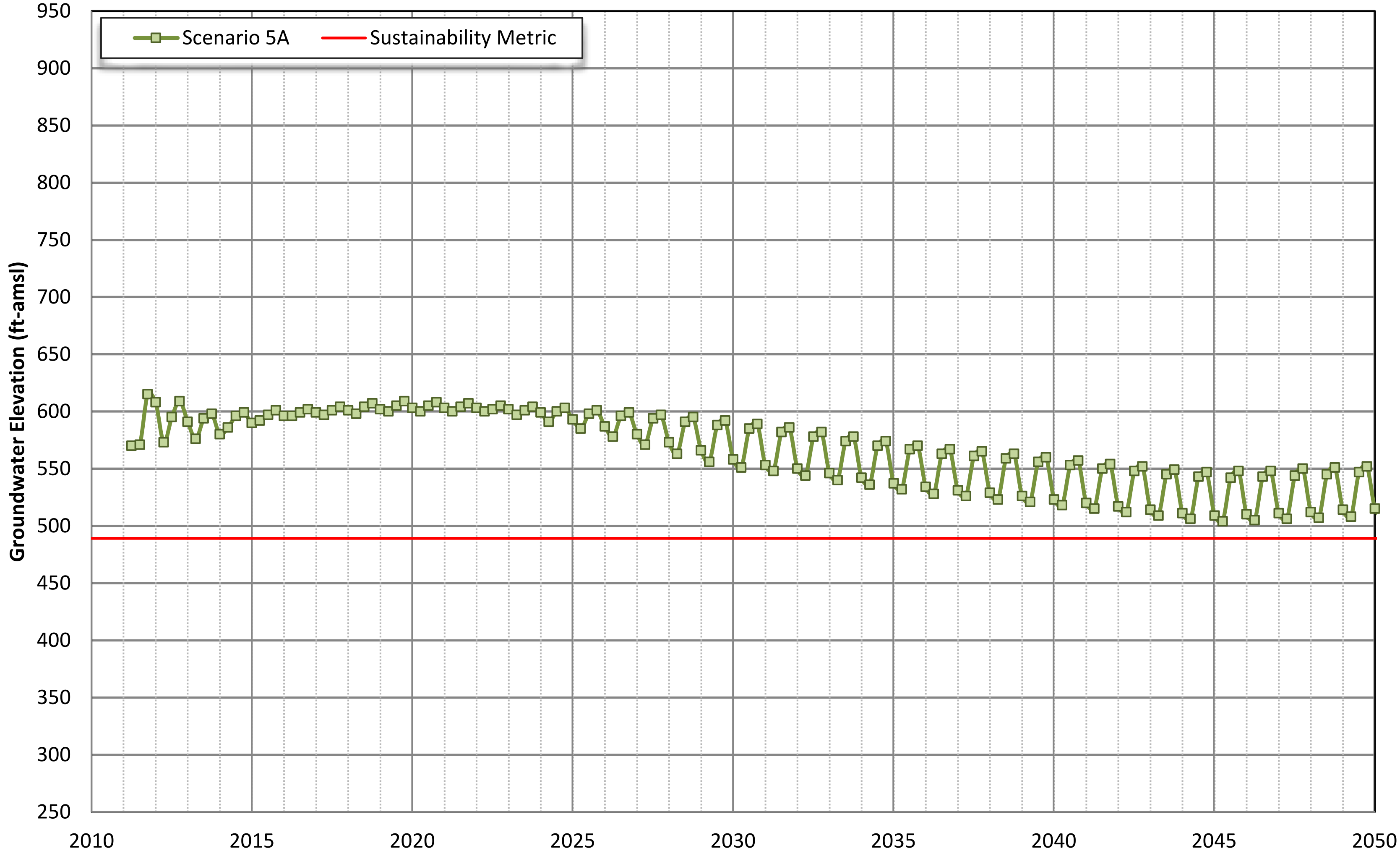

Appendix D_20150916_WellHydrographs_S5A4_Final_LBB2.xlsm
Created: 9/15/15
Printed: 9/16/2015

Figure D-57
Projected Groundwater Elevation for Scenario 5a
Cucamonga Valley Water District Well CB-38

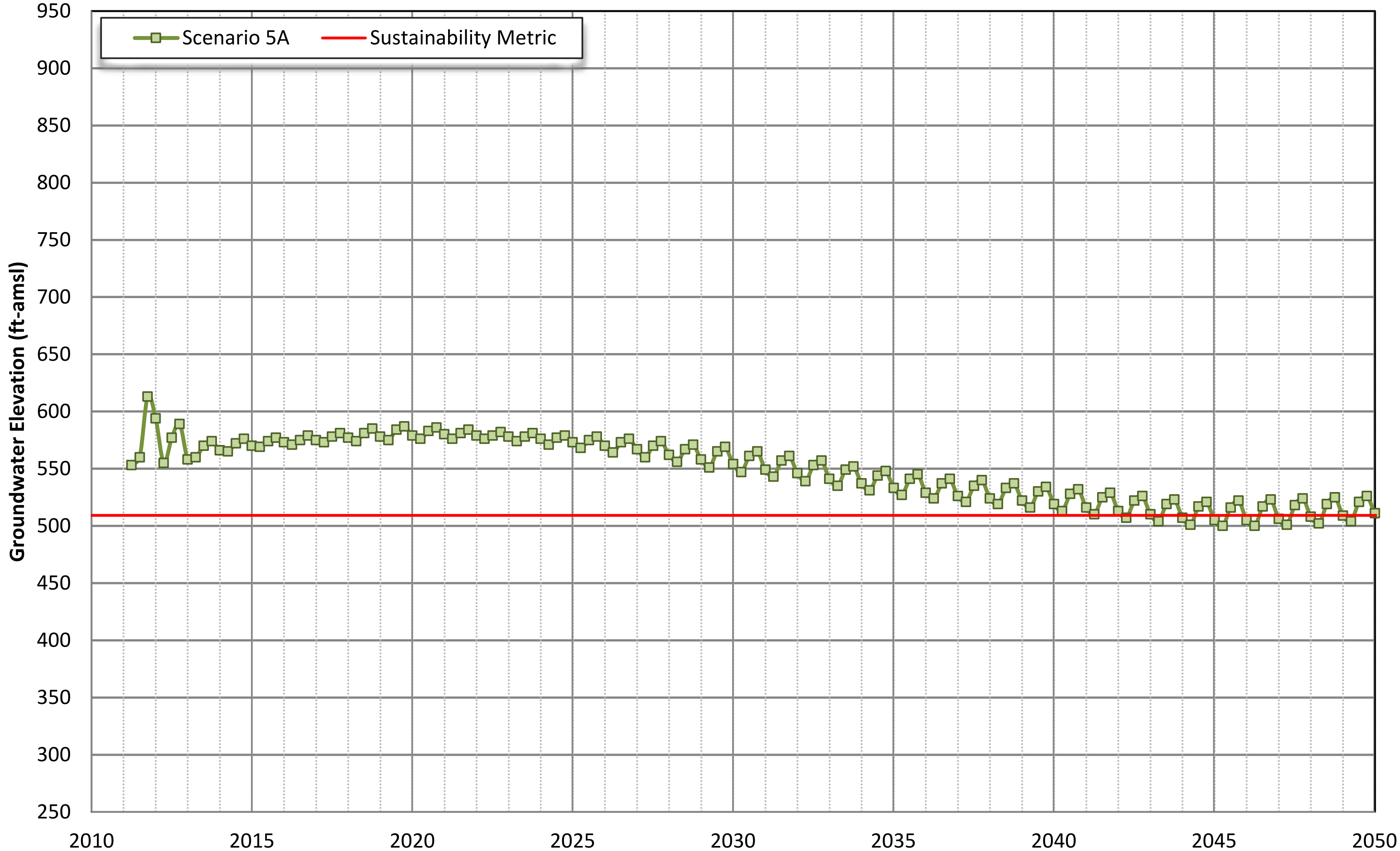

Figure D-58
Projected Groundwater Elevation for Scenario 5a
Cucamonga Valley Water District Well CB-39

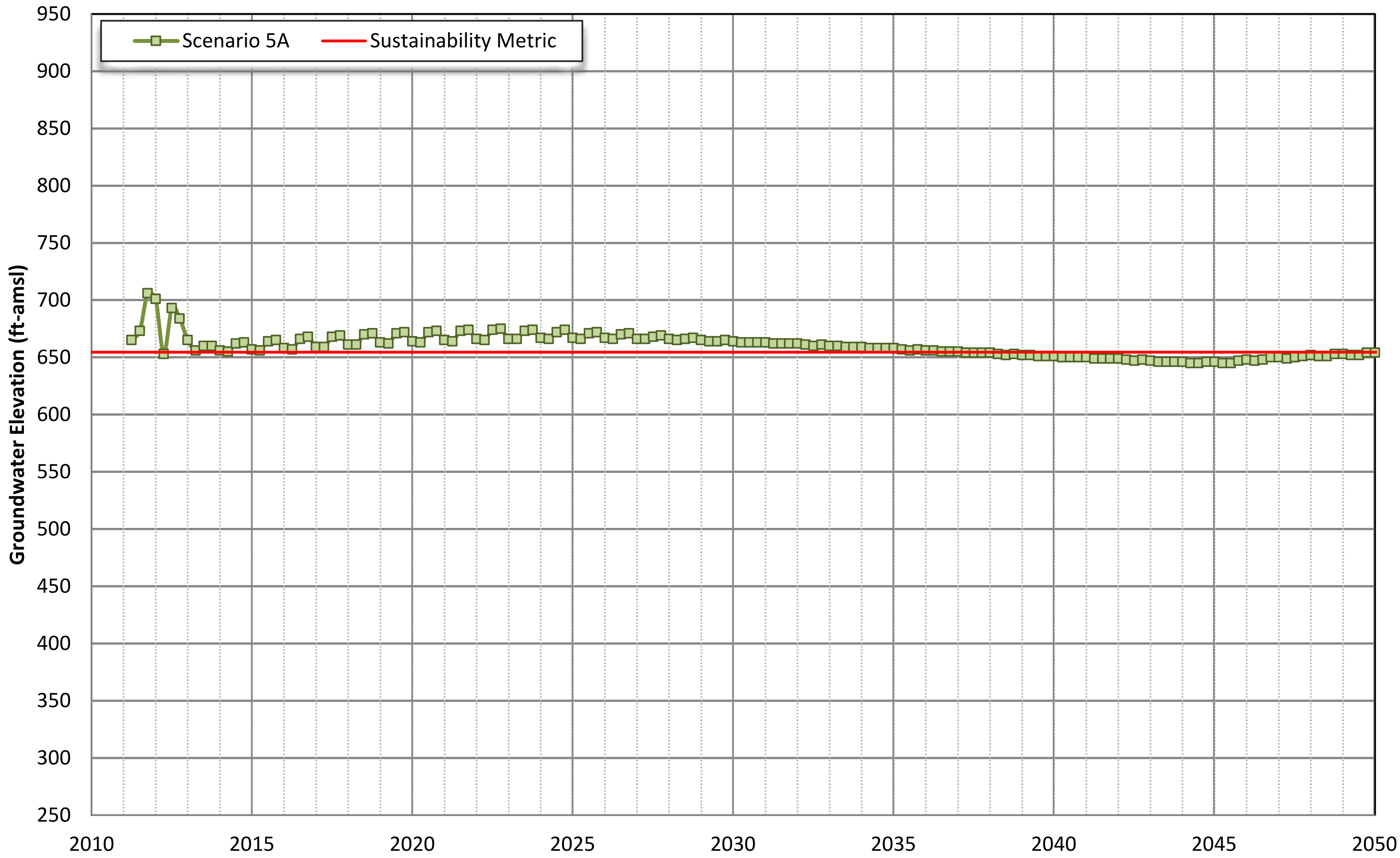

Appendix D_20150916_WellHydrographs_S5A4_Final_LBB2.xlsm
Created: 9/15/15
Printed: 9/16/2015

Figure D-59
Projected Groundwater Elevation for Scenario 5a
Cucamonga Valley Water District Well CB-4

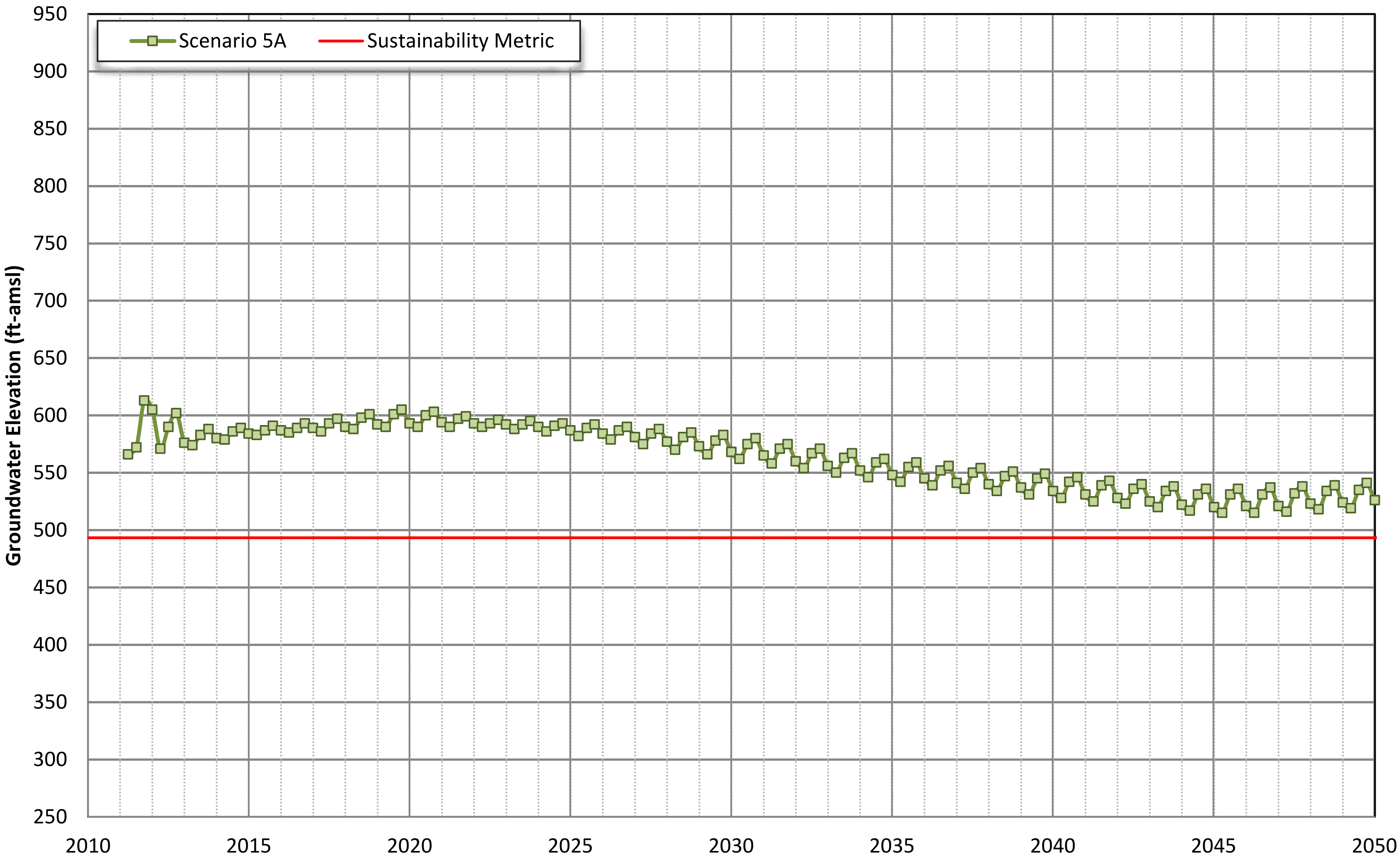

Appendix D_20150916_WellHydrographs_S5A4_Final_LBB2.xlsm
Created: 9/15/15
Printed: 9/16/2015

Figure D-60
Projected Groundwater Elevation for Scenario 5a
Cucamonga Valley Water District Well CB-40

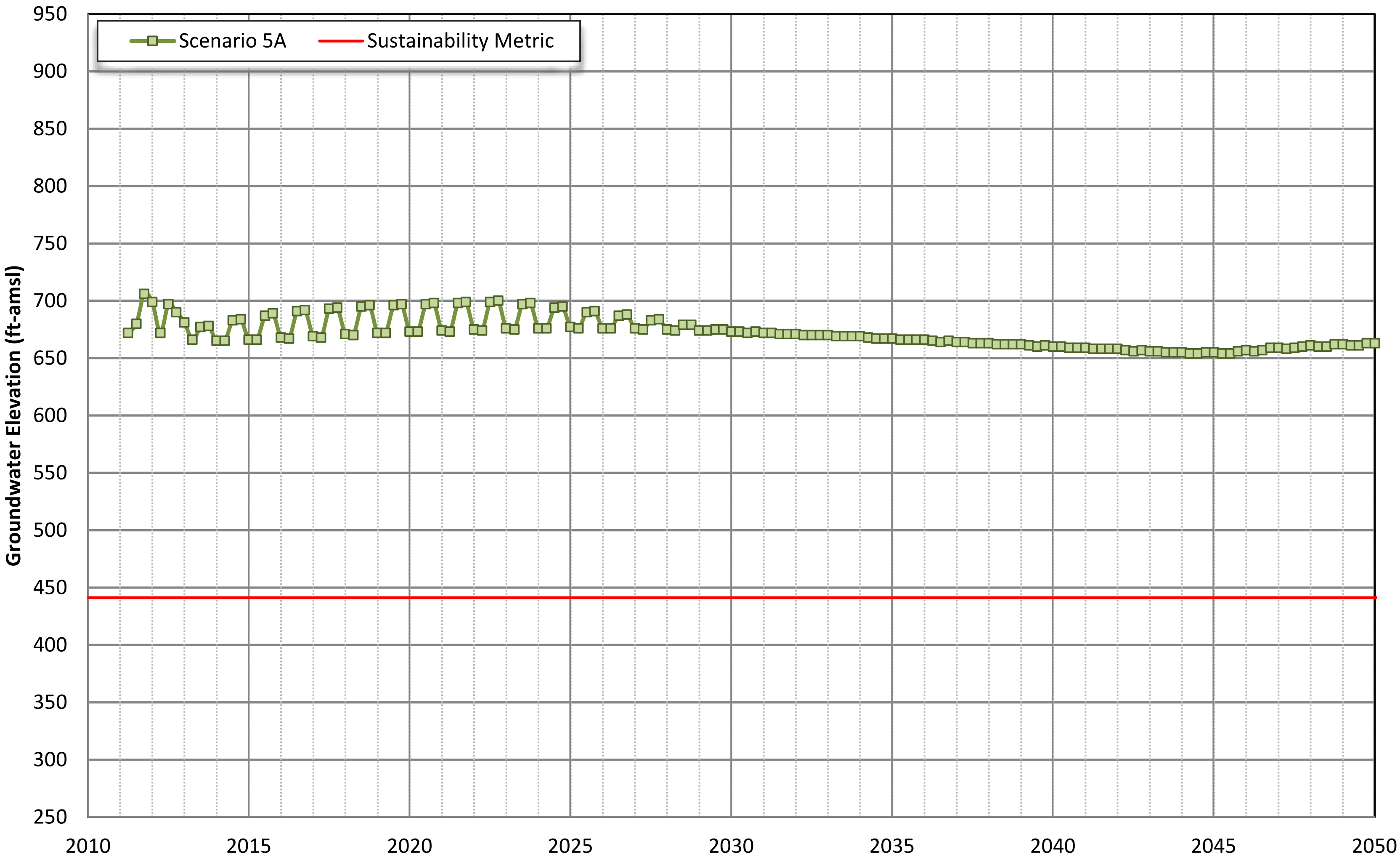

Appendix D_20150916_WellHydrographs_S5A4_Final_LBB2.xlsm
Created: 9/15/15
Printed: 9/16/2015

Figure D-61
Projected Groundwater Elevation for Scenario 5a
Cucamonga Valley Water District Well CB-41

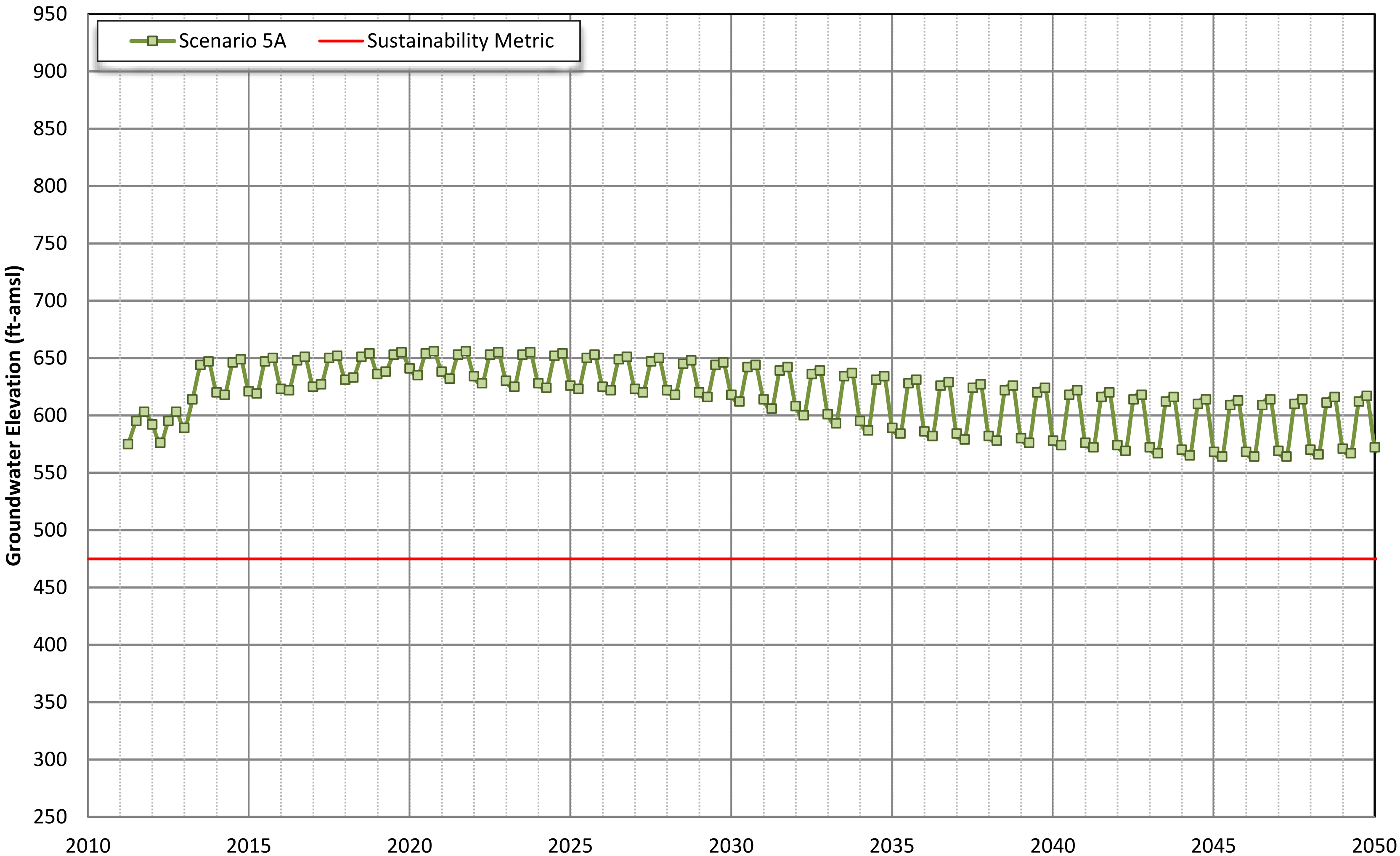

Appendix D_20150916_WellHydrographs_S5A4_Final_LBB2.xlsm
Created: 9/15/15
Printed: 9/16/2015

Figure D-62
Projected Groundwater Elevation for Scenario 5a
Cucamonga Valley Water District Well CB-42

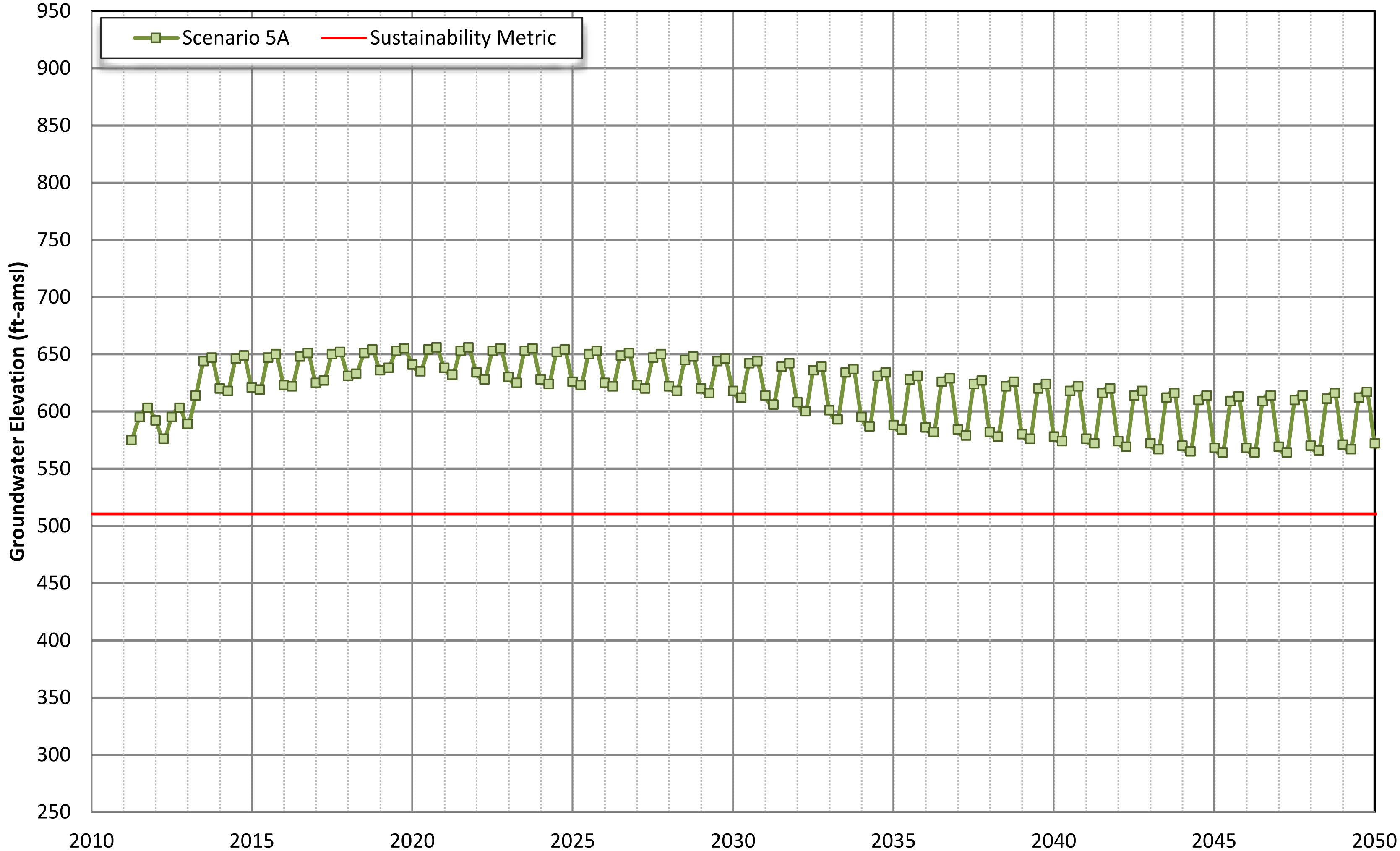

Appendix D_20150916_WellHydrographs_S5A4_Final_LBB2.xlsm
Created: 9/15/15
Printed: 9/16/2015

Figure D-63
Projected Groundwater Elevation for Scenario 5a
Cucamonga Valley Water District Well CB-43

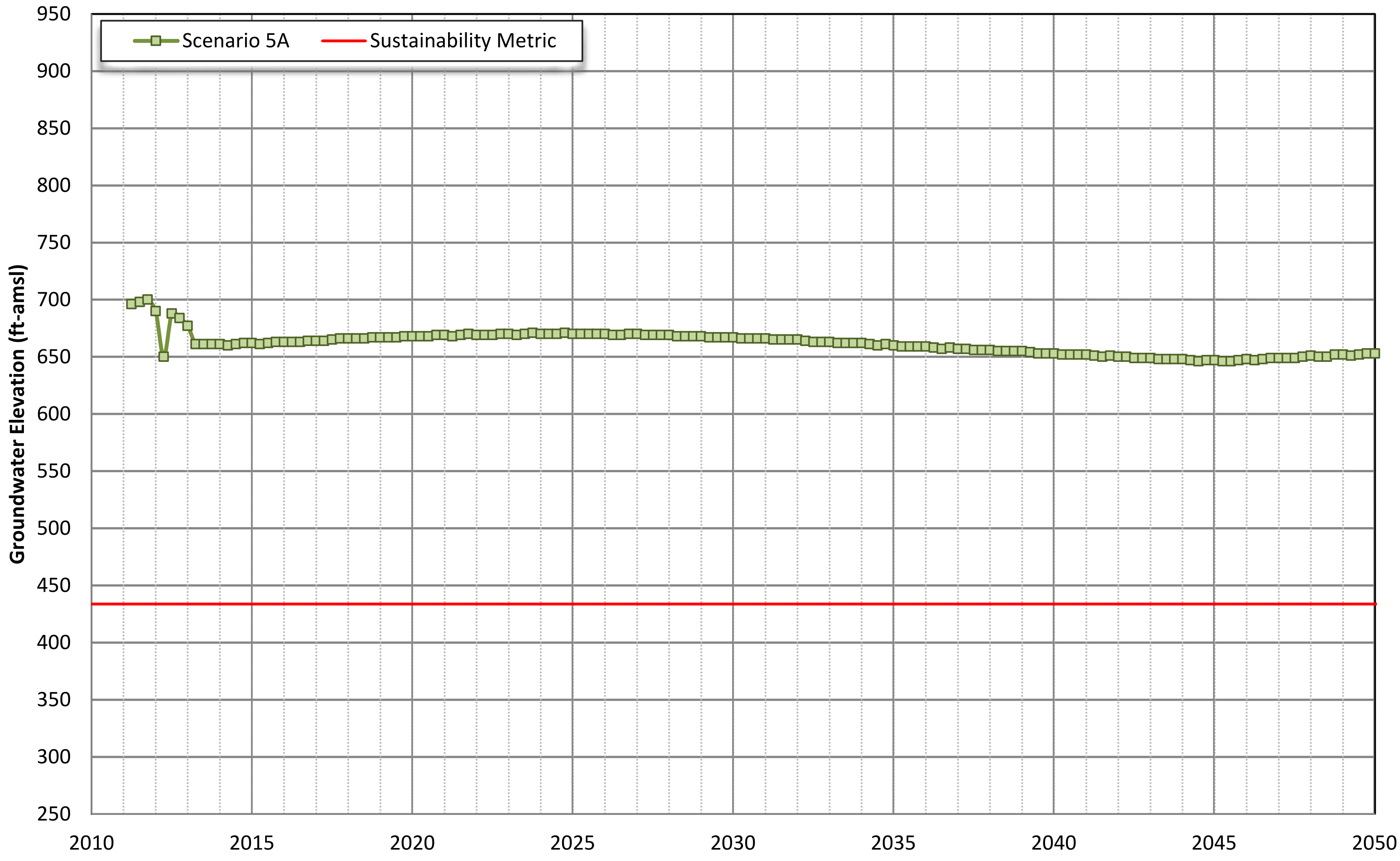

Appendix D_20150916_WellHydrographs_S5A4_Final_LBB2.xlsm
Created: 9/15/15
Printed: 9/16/2015

Figure D-64
Projected Groundwater Elevation for Scenario 5a
Cucamonga Valley Water District Well CB-46

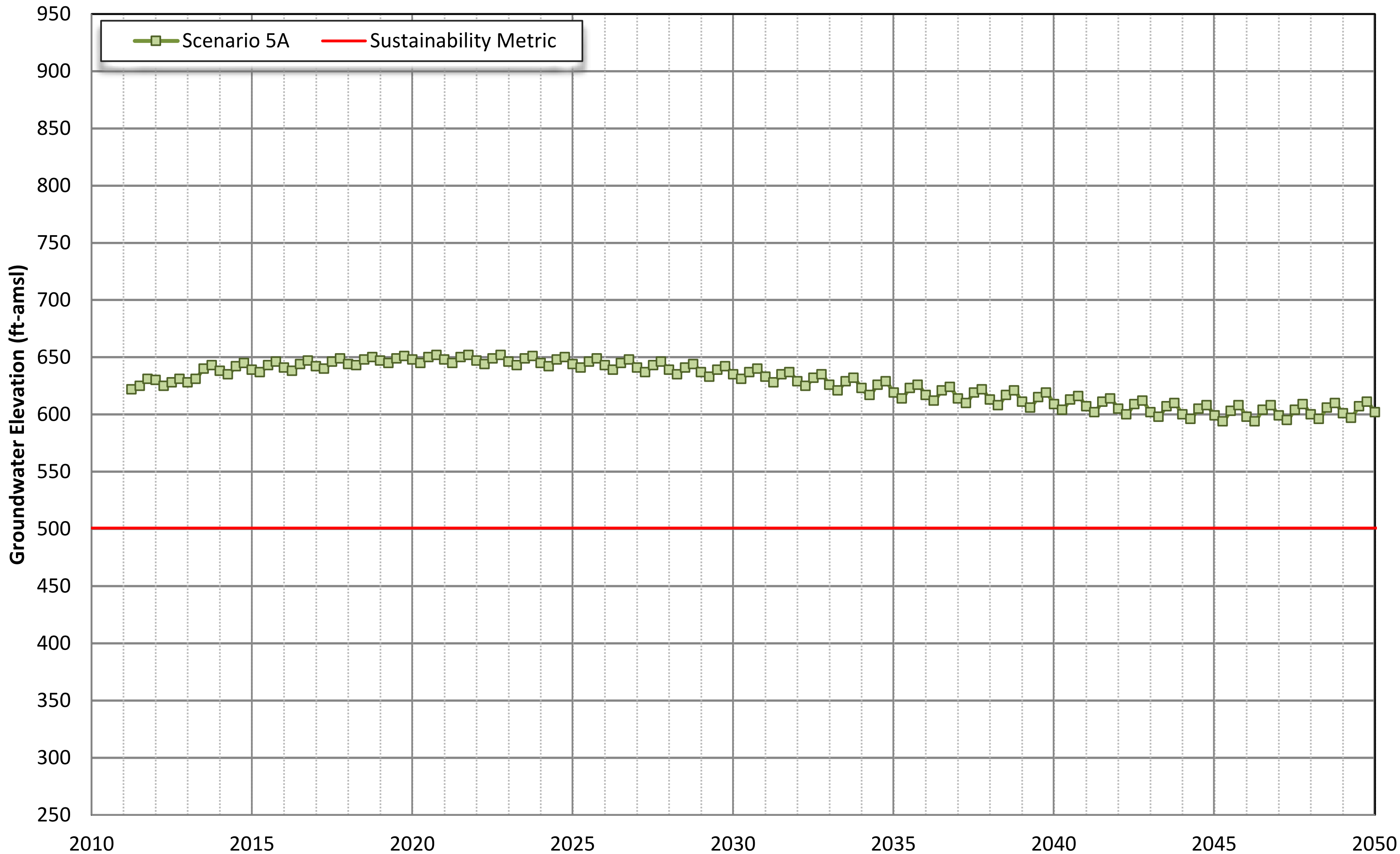

Appendix D_20150916_WellHydrographs_S5A4_Final_LBB2.xlsm
Created: 9/15/15
Printed: 9/16/2015

Figure D-65
Projected Groundwater Elevation for Scenario 5a
Cucamonga Valley Water District Well CB-5

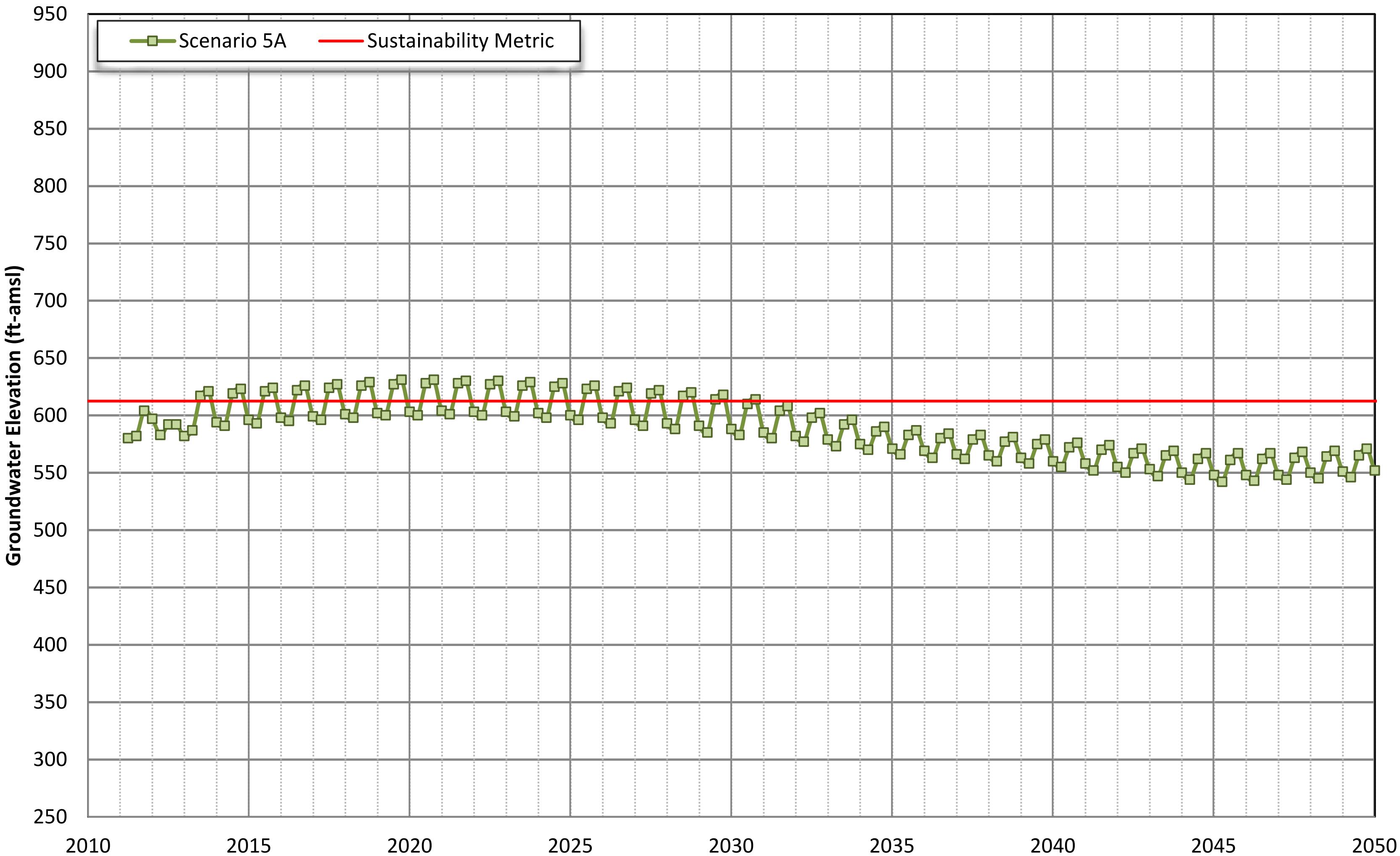

Appendix D_20150916_WellHydrographs_S5A4_Final_LBB2.xlsm
Created: 9/15/15
Printed: 9/16/2015

Figure D-66
Projected Groundwater Elevation for Scenario 5a
Fontana Water Company Well F17B

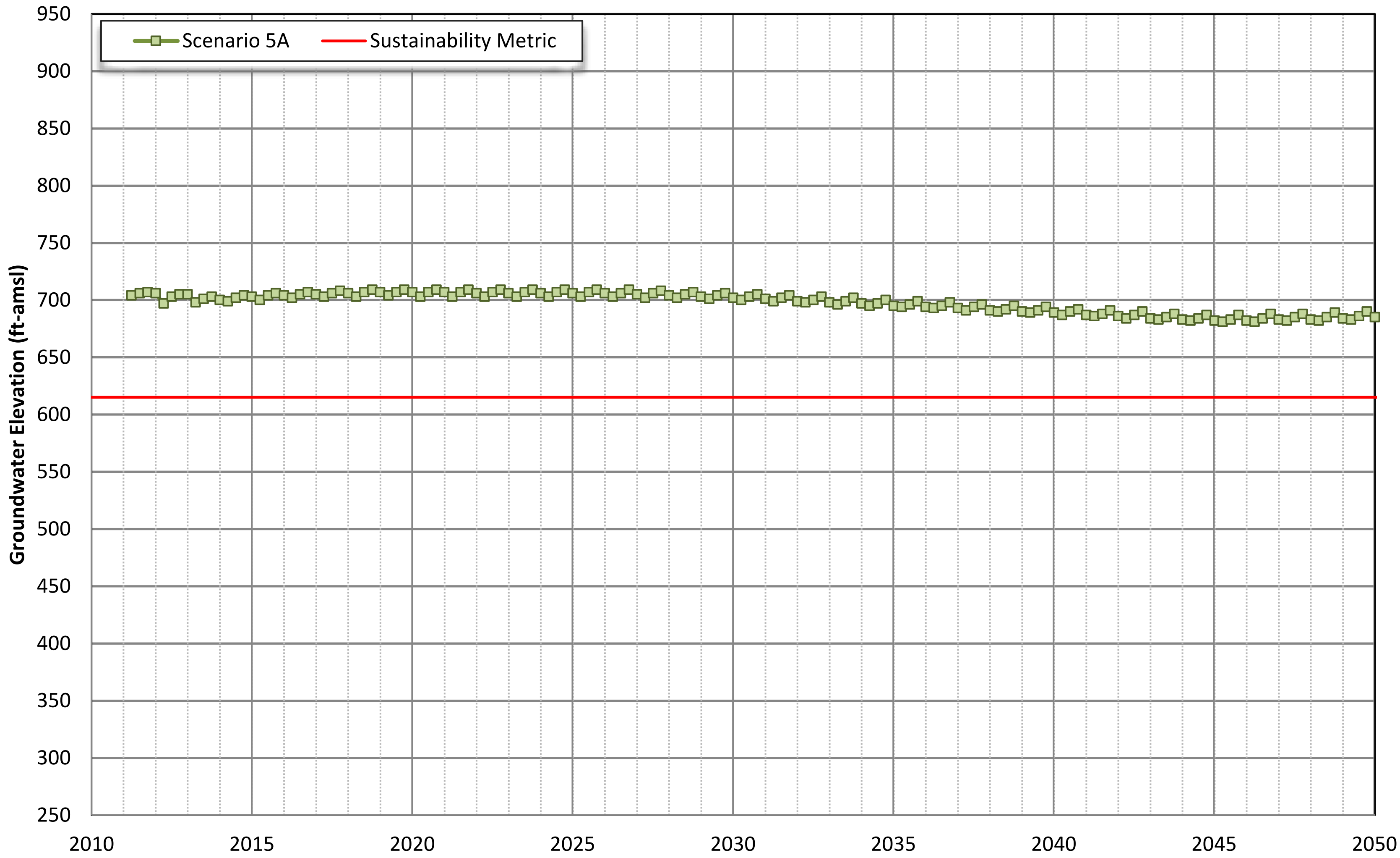

Appendix D_20150916_WellHydrographs_S5A4_Final_LBB2.xlsm
Created: 9/15/15
Printed: 9/16/2015

Figure D-67
Projected Groundwater Elevation for Scenario 5a
Fontana Water Company Well F17C

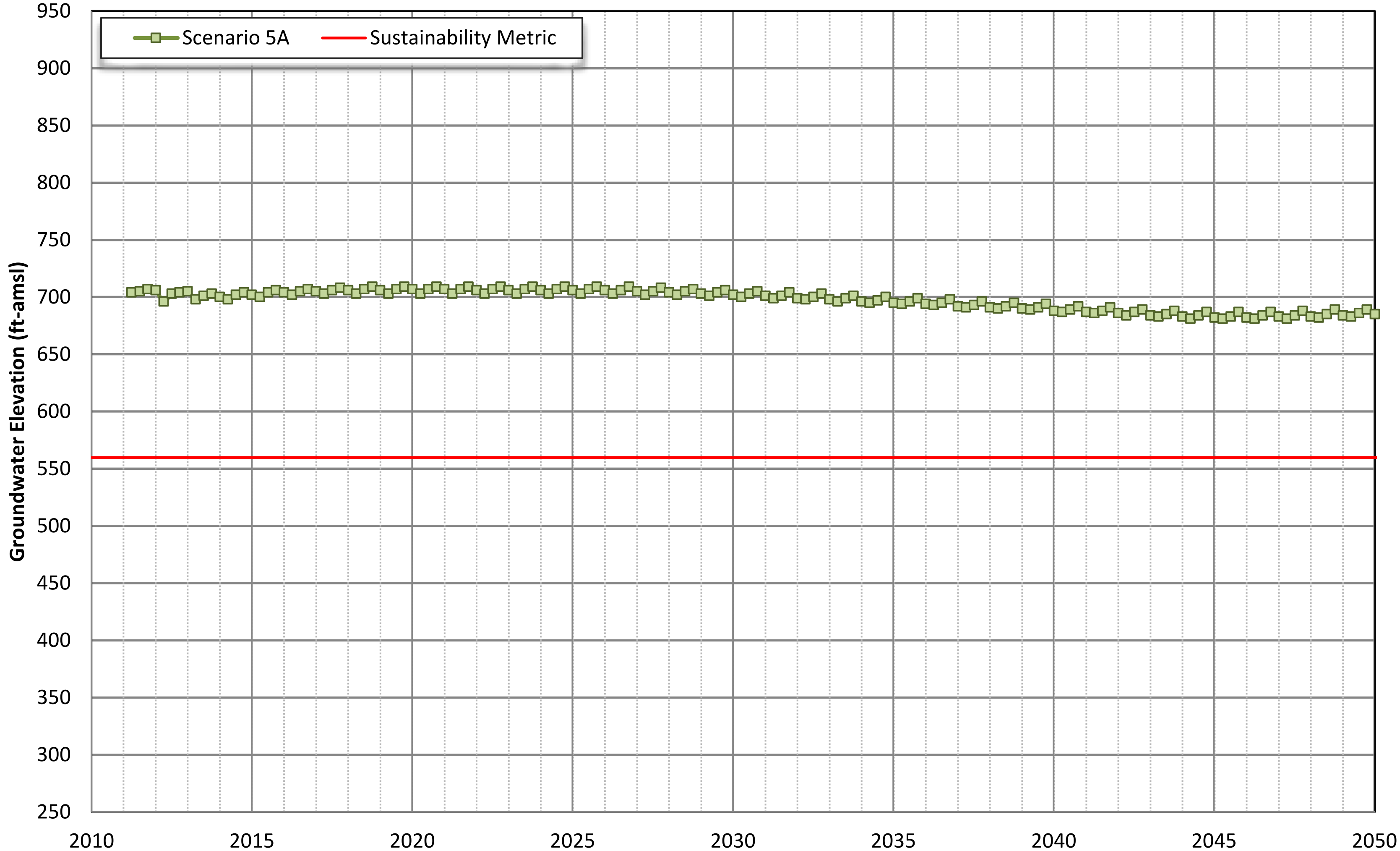

Appendix D_20150916_WellHydrographs_S5A4_Final_LBB2.xlsm
Created: 9/15/15
Printed: 9/16/2015

Figure D-68
Projected Groundwater Elevation for Scenario 5a
Fontana Water Company Well F21B

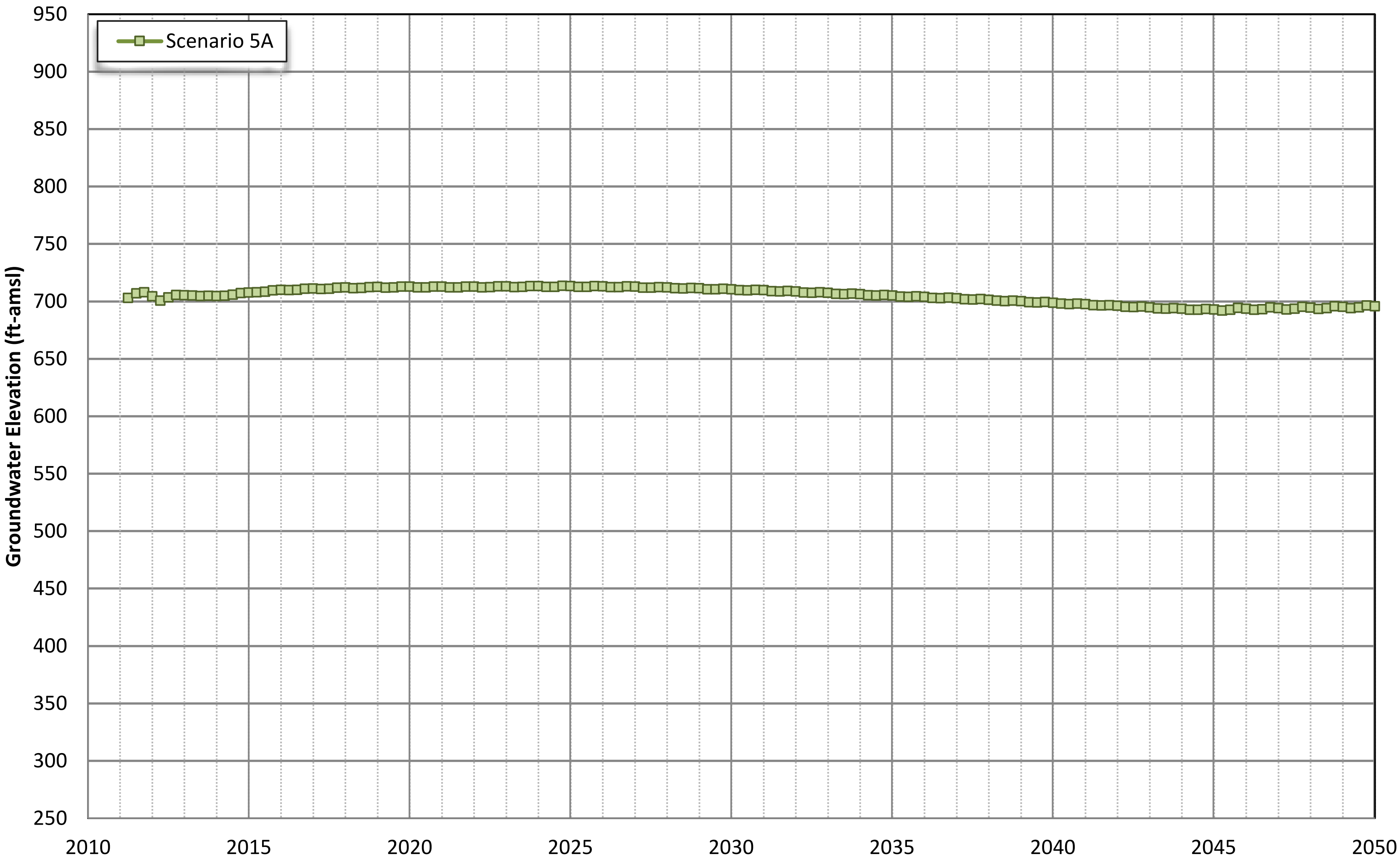

Appendix D_20150916_WellHydrographs_S5A4_Final_LBB2.xlsm
Created: 9/15/15
Printed: 9/16/2015

Figure D-69
Projected Groundwater Elevation for Scenario 5a
Fontana Water Company Well F21A

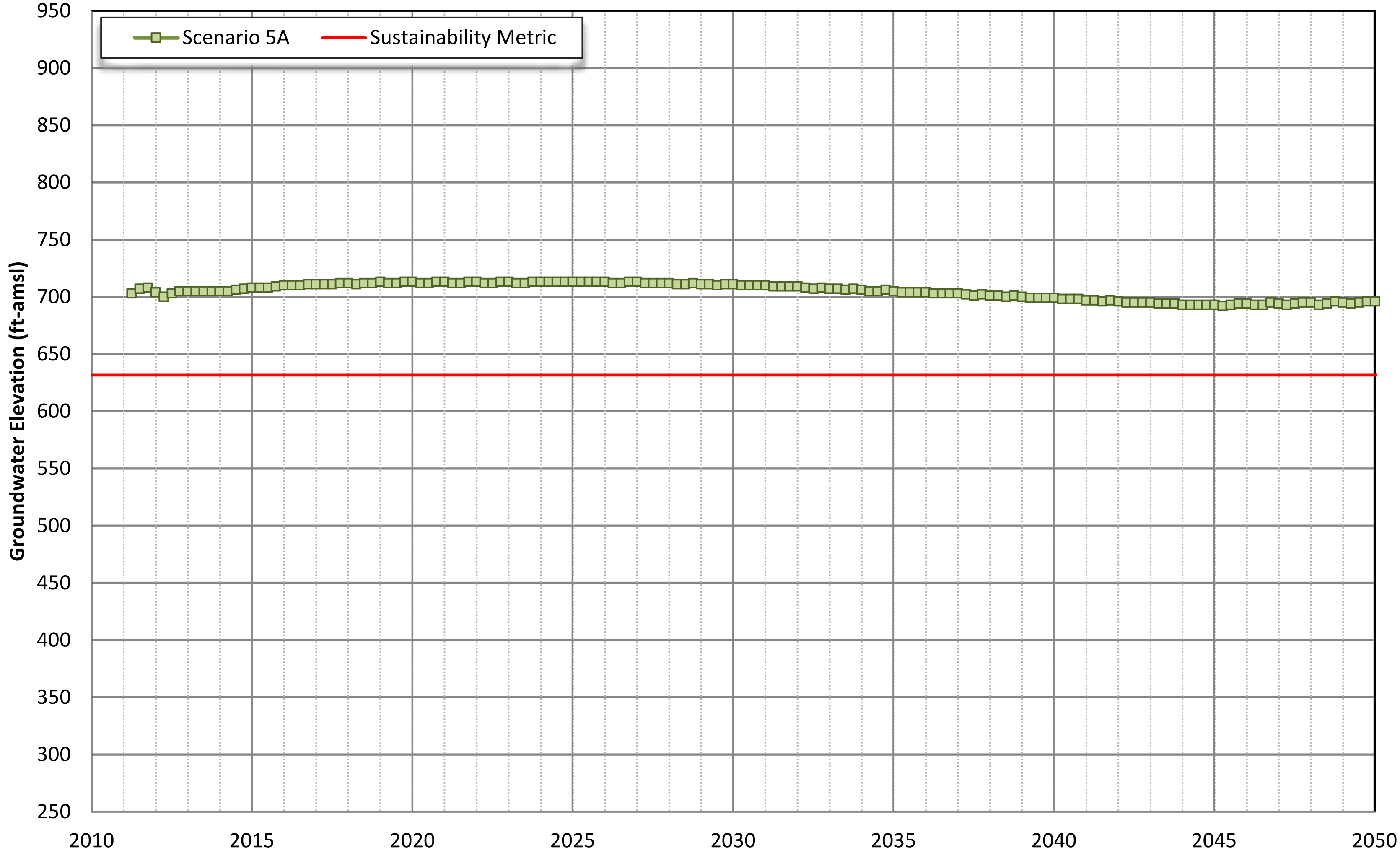

Appendix D_20150916_WellHydrographs_S5A4_Final_LBB2.xlsm
Created: 9/15/15
Printed: 9/16/2015

Figure D-70
Projected Groundwater Elevation for Scenario 5a
Fontana Water Company Well F23A

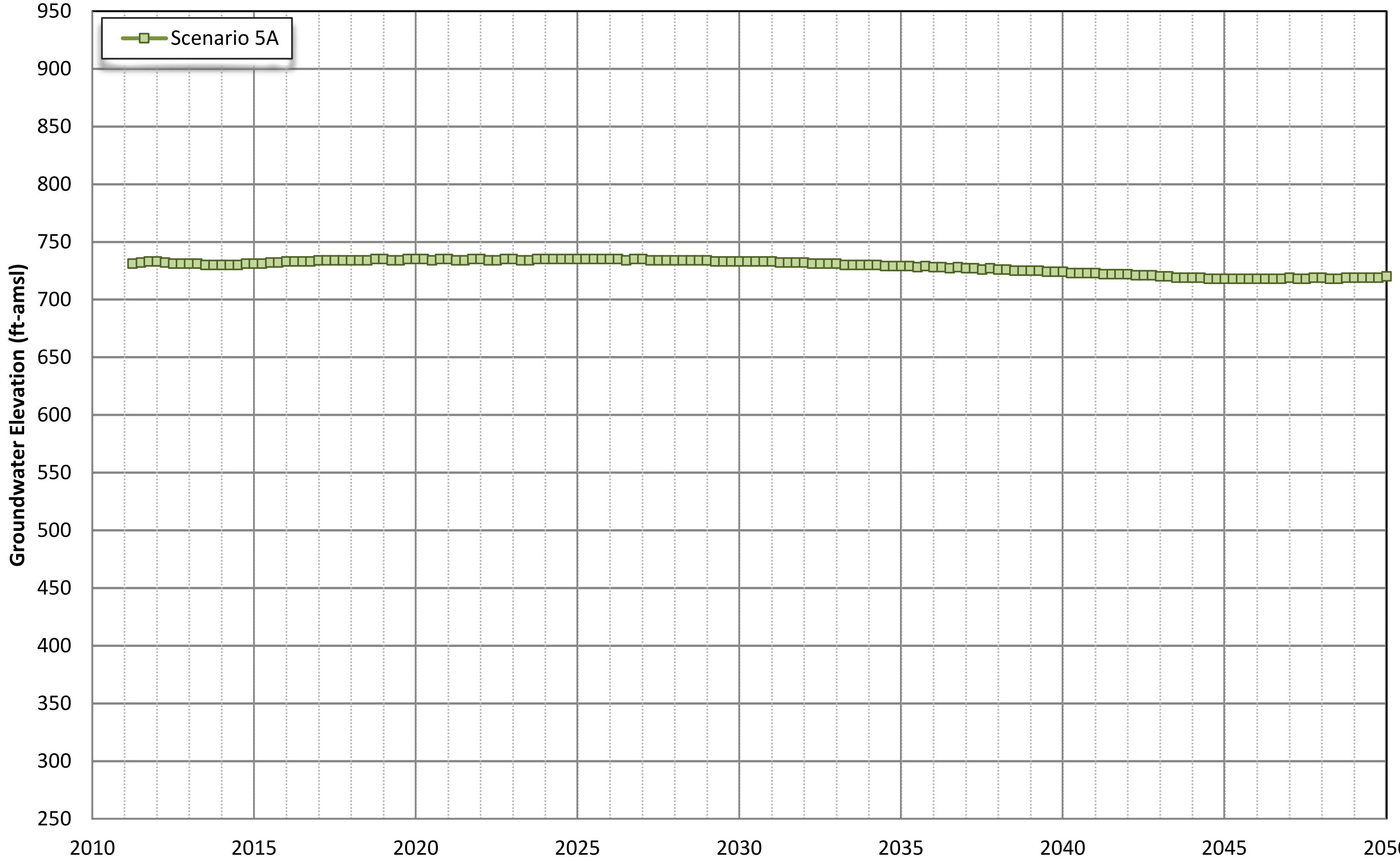

Appendix D_20150916_WellHydrographs_S5A4_Final_LBB2.xlsm
Created: 9/15/15
Printed: 9/16/2015

Figure D-71
Projected Groundwater Elevation for Scenario 5a
Fontana Water Company Well F2A

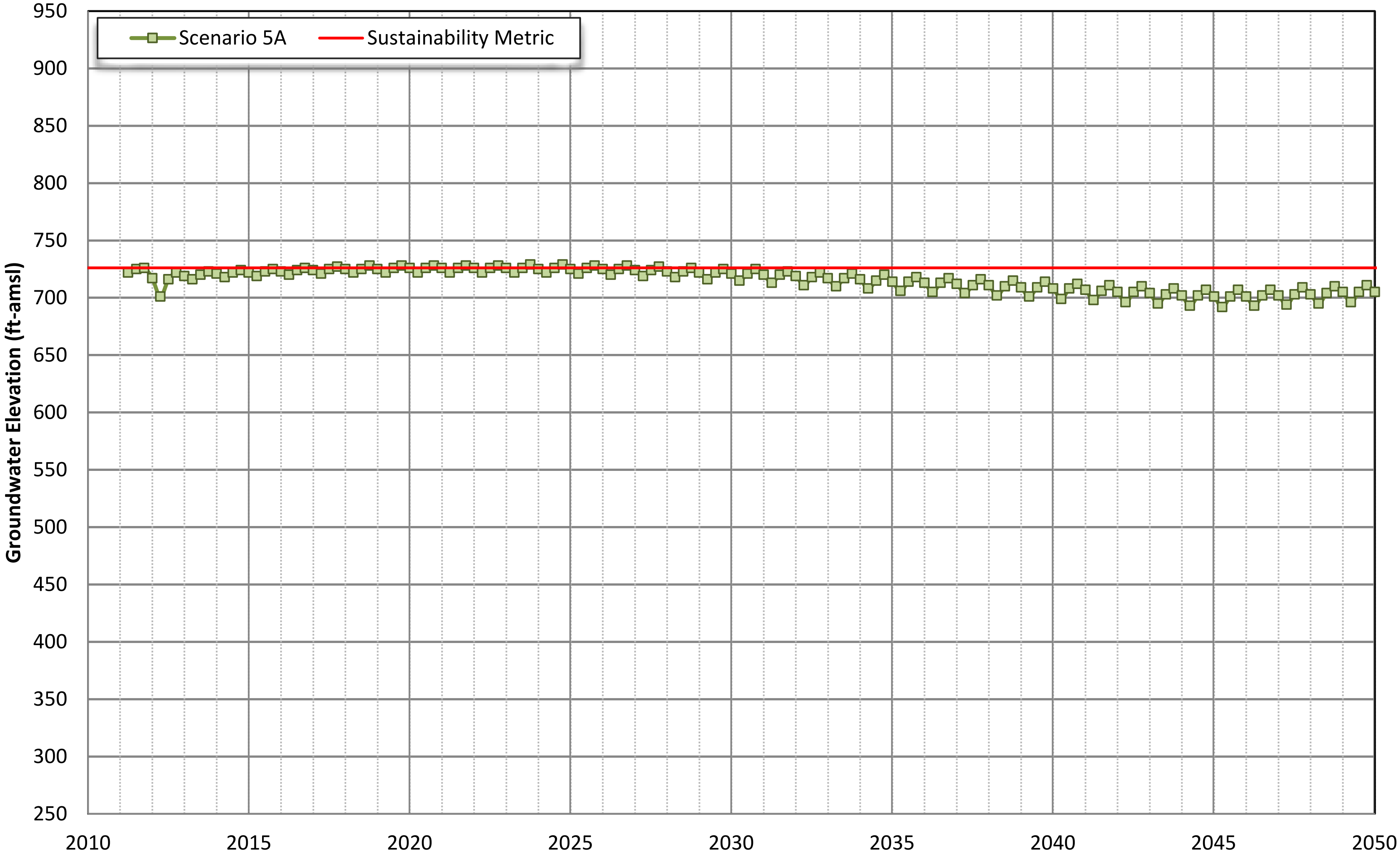

Appendix D_20150916_WellHydrographs_S5A4_Final_LBB2.xlsm
Created: 9/15/15
Printed: 9/16/2015

Figure D-72
Projected Groundwater Elevation for Scenario 5a
Fontana Water Company Well F30A

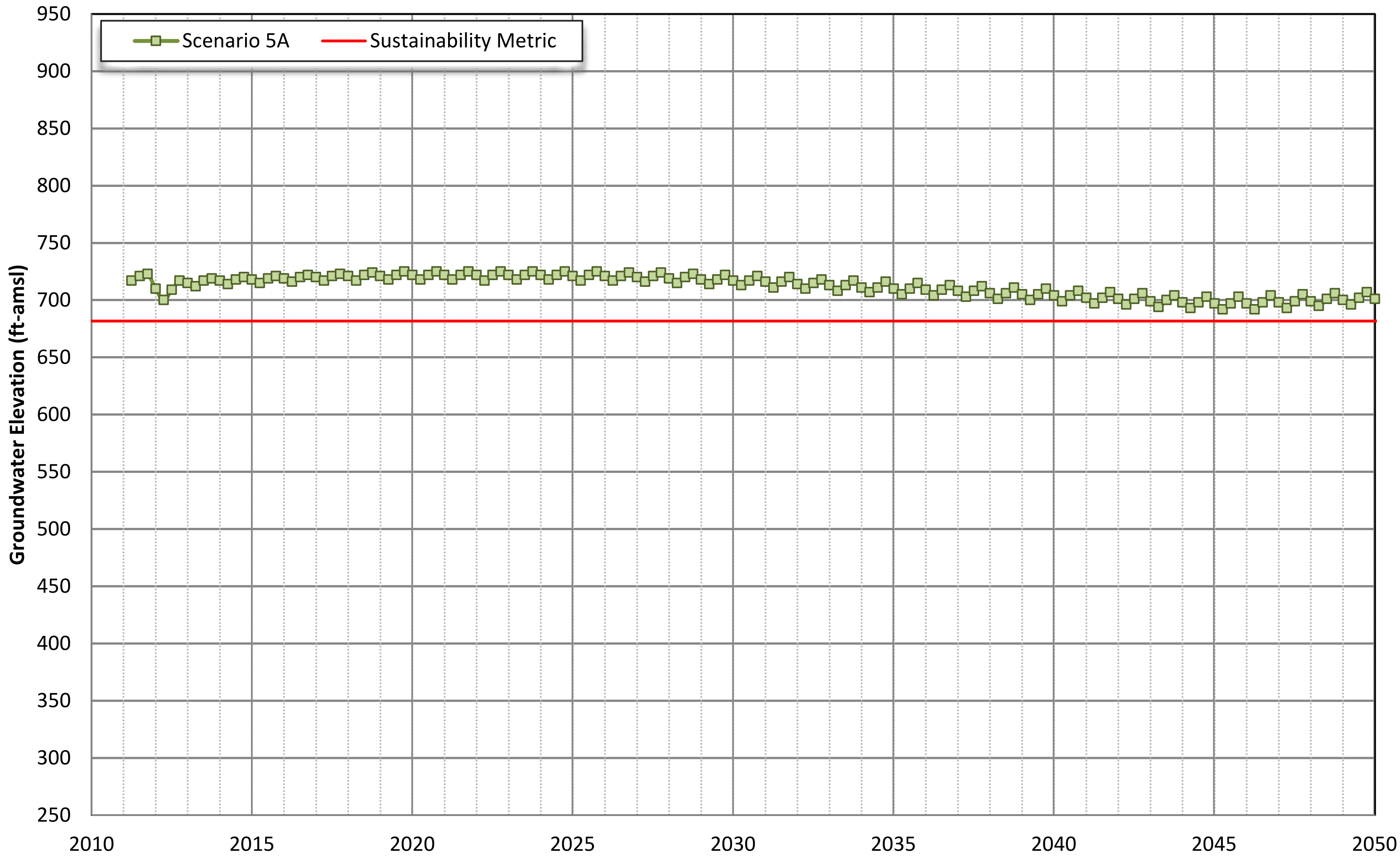

Appendix D_20150916_WellHydrographs_S5A4_Final_LBB2.xlsm
Created: 9/15/15
Printed: 9/16/2015

Figure D-73
Projected Groundwater Elevation for Scenario 5a
Fontana Water Company Well F31A

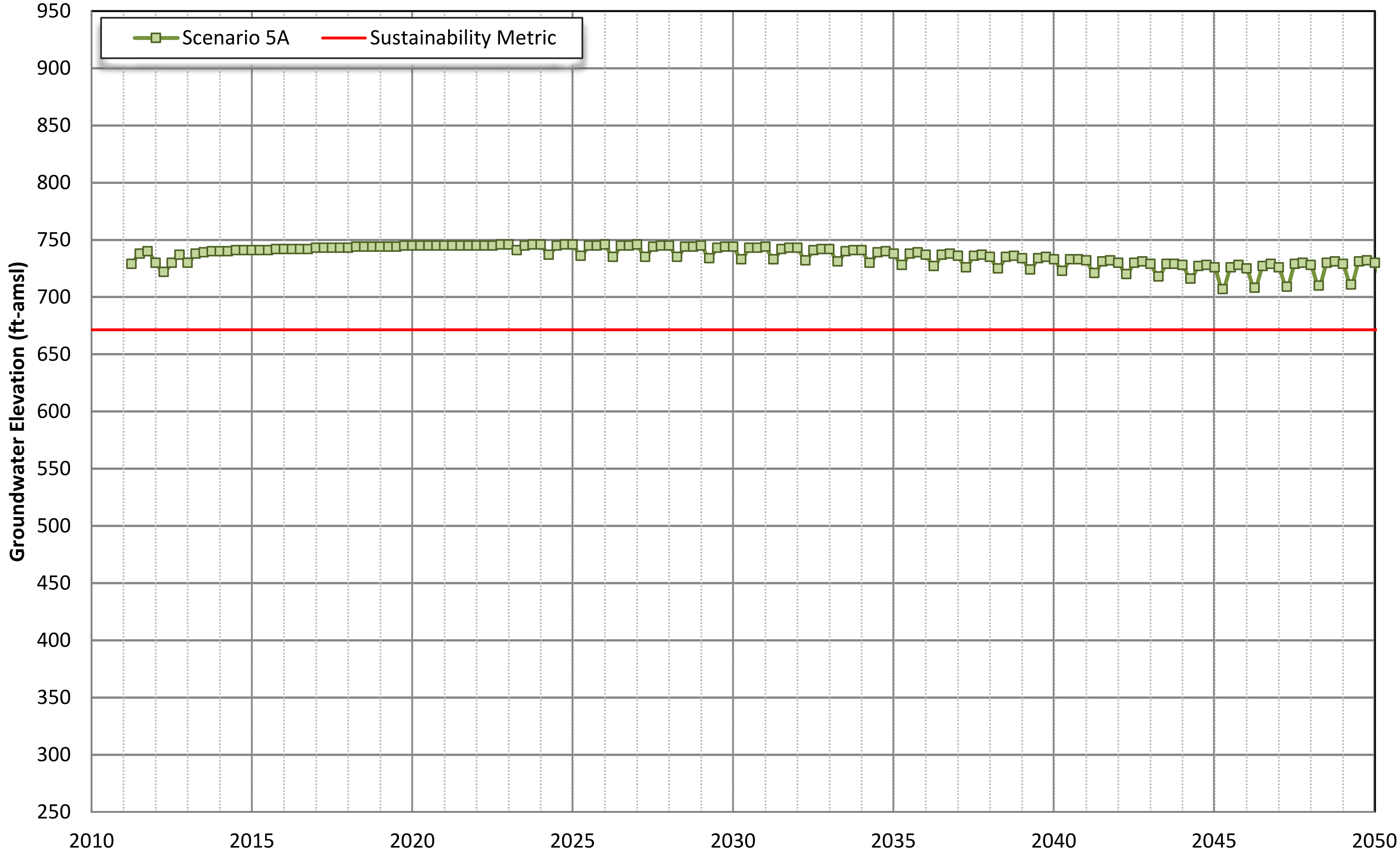

Appendix D_20150916_WellHydrographs_S5A4_Final_LBB2.xlsm
Created: 9/15/15
Printed: 9/16/2015

Figure D-74
Projected Groundwater Elevation for Scenario 5a
Fontana Water Company Well F44A

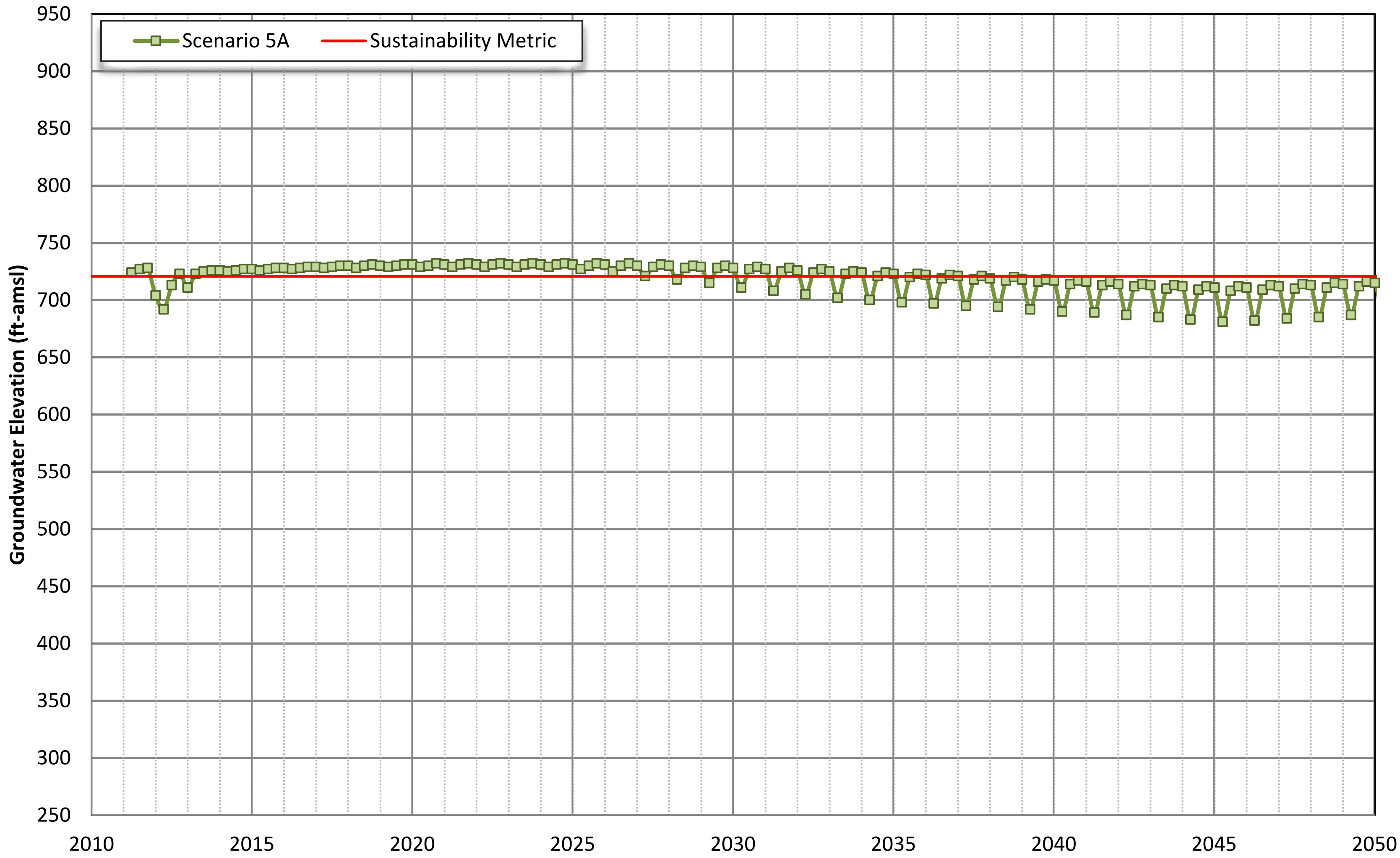

Appendix D_20150916_WellHydrographs_S5A4_Final_LBB2.xlsm
Created: 9/15/15
Printed: 9/16/2015

Figure D-75
Projected Groundwater Elevation for Scenario 5a
Fontana Water Company Well F44B

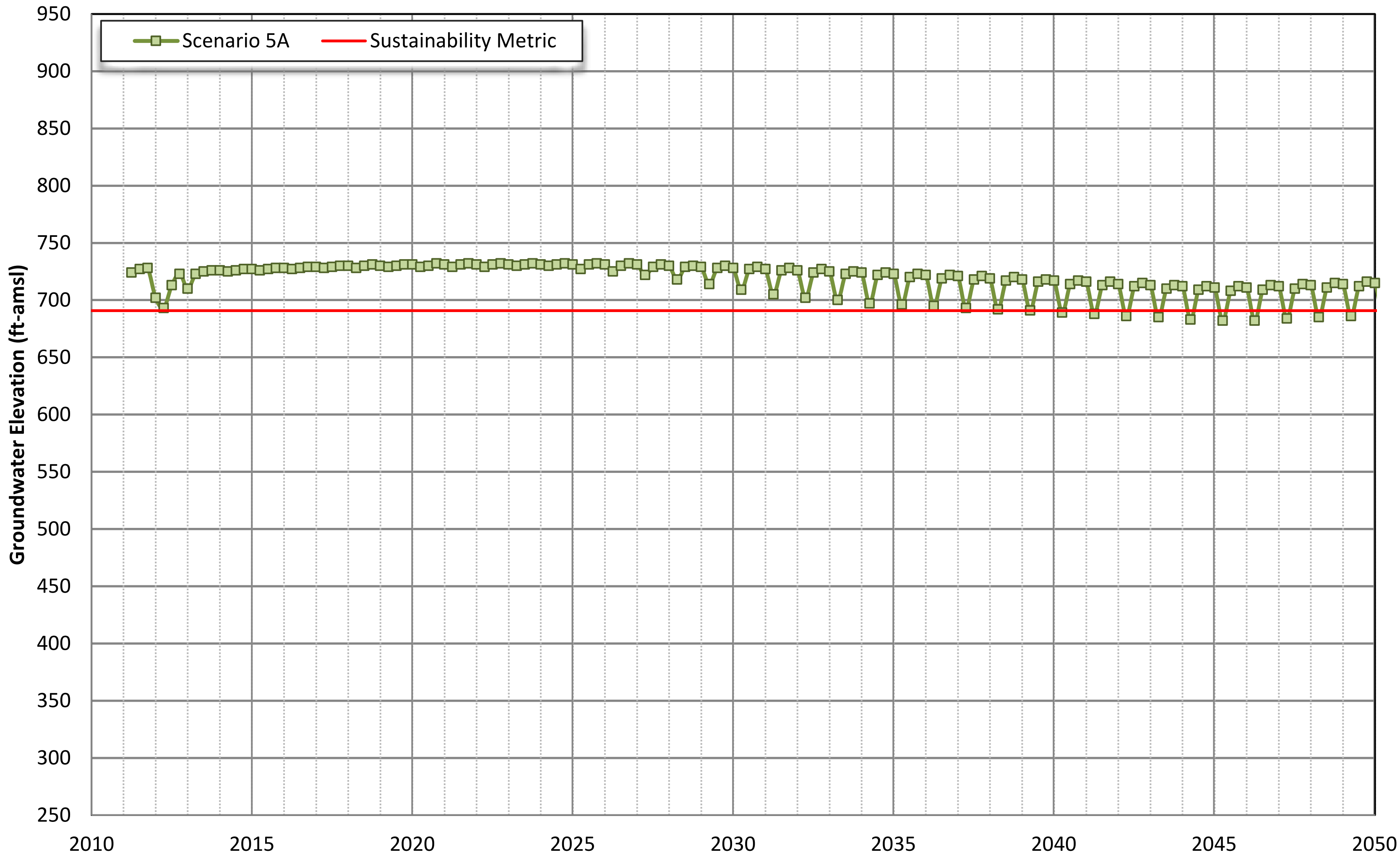

Appendix D_20150916_WellHydrographs_S5A4_Final_LBB2.xlsm
Created: 9/15/15
Printed: 9/16/2015

Figure D-76
Projected Groundwater Elevation for Scenario 5a
Fontana Water Company Well F44C

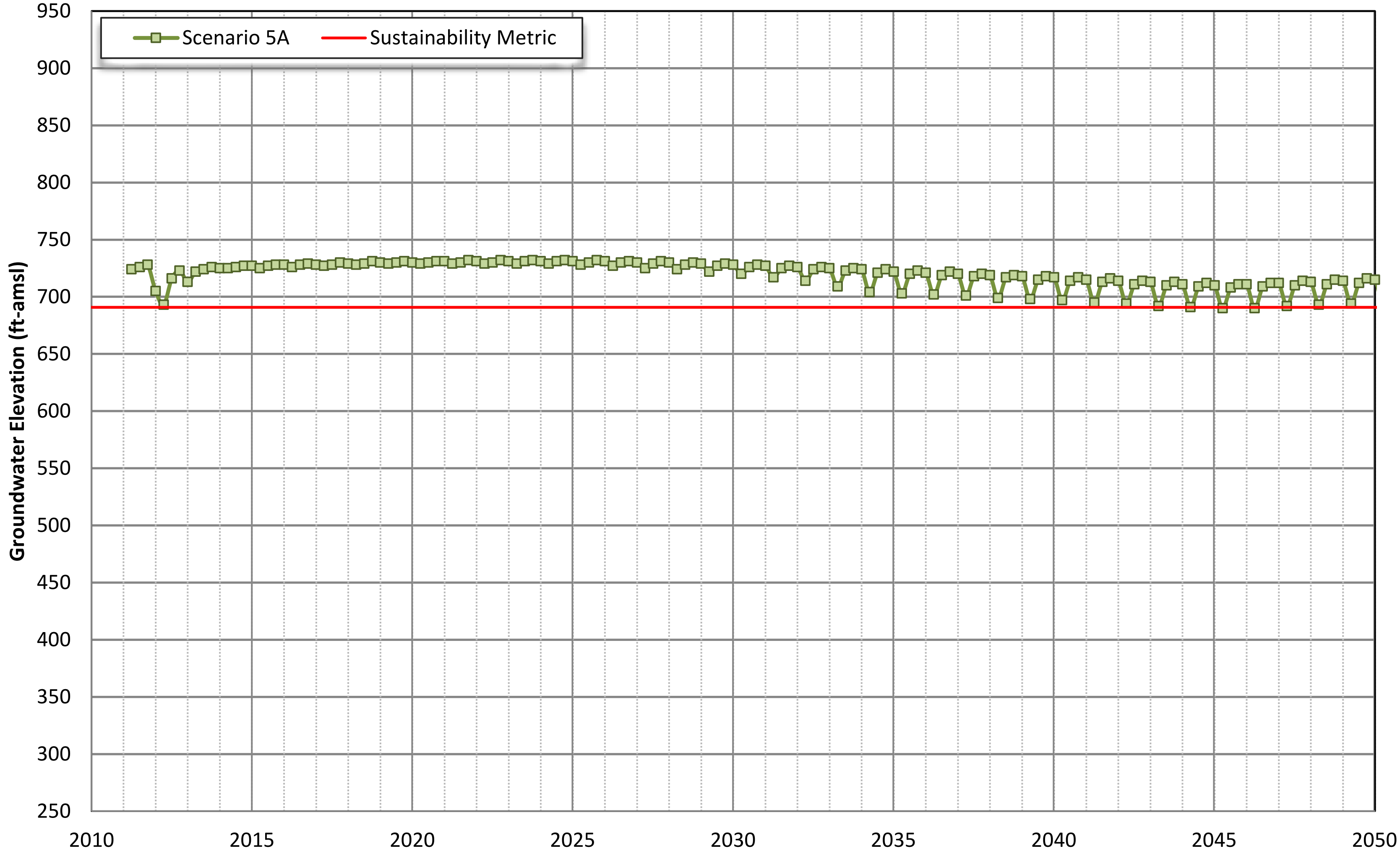

Appendix D_20150916_WellHydrographs_S5A4_Final_LBB2.xlsm
Created: 9/15/15
Printed: 9/16/2015

Figure D-77
Projected Groundwater Elevation for Scenario 5a
Fontana Water Company Well F7A

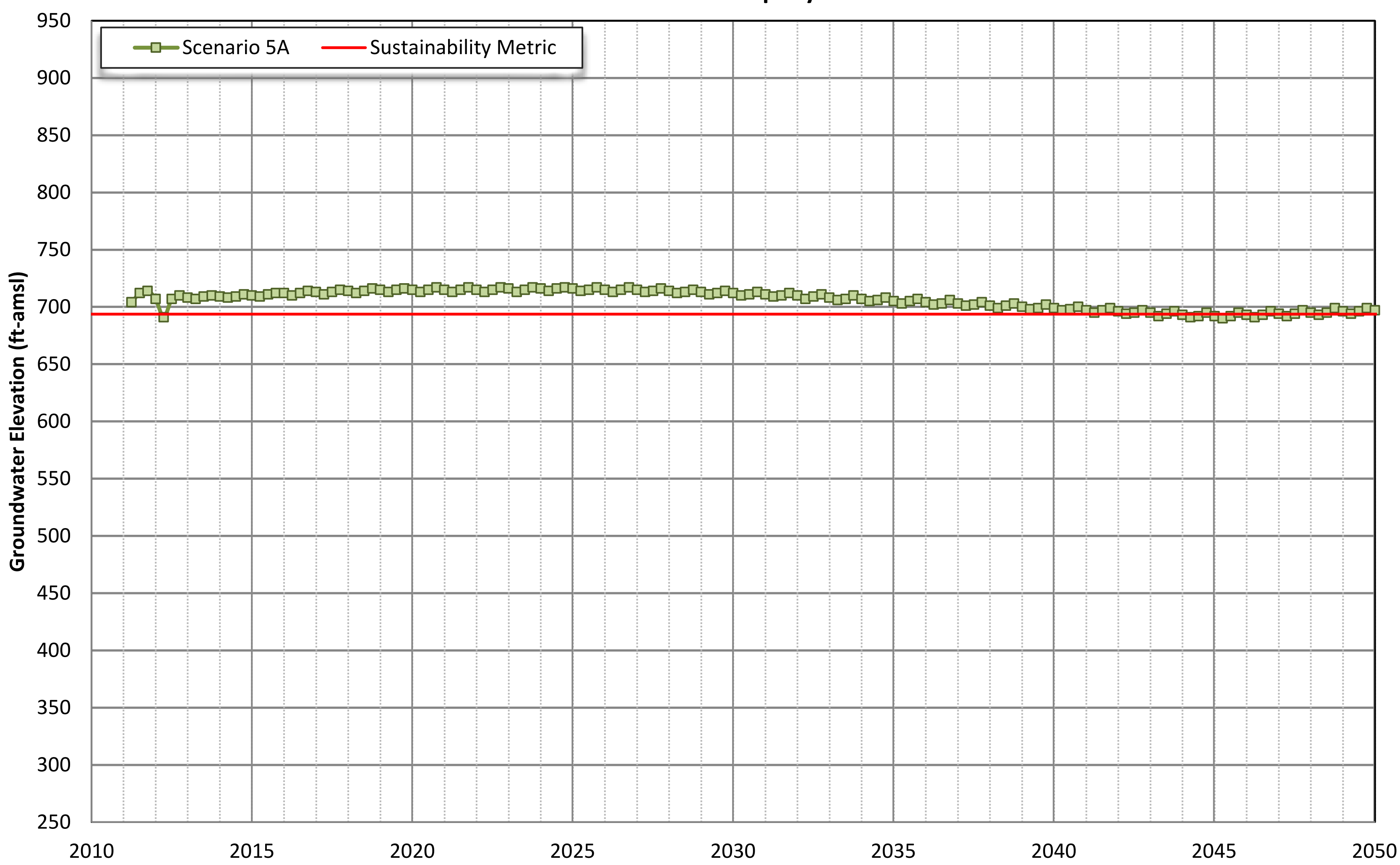

Appendix D_20150916_WellHydrographs_S5A4_Final_LBB2.xlsm
Created: 9/15/15
Printed: 9/16/2015

Figure D-78
Projected Groundwater Elevation for Scenario 5a
Fontana Water Company Well F7B

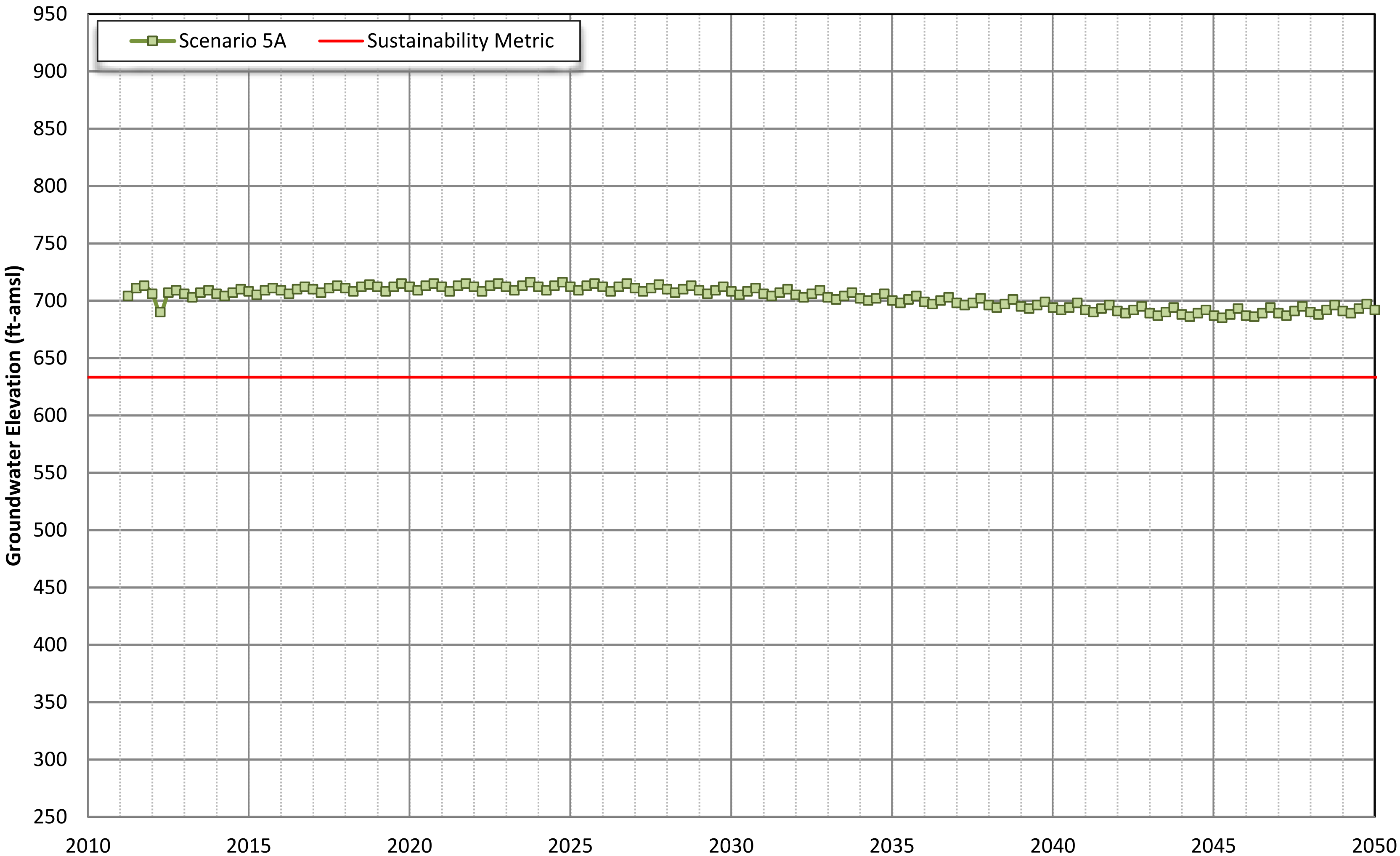

Appendix D_20150916_WellHydrographs_S5A4_Final_LBB2.xlsm
Created: 9/15/15
Printed: 9/16/2015

Figure D-79
Projected Groundwater Elevation for Scenario 5a
Golden State Water Company Well #1

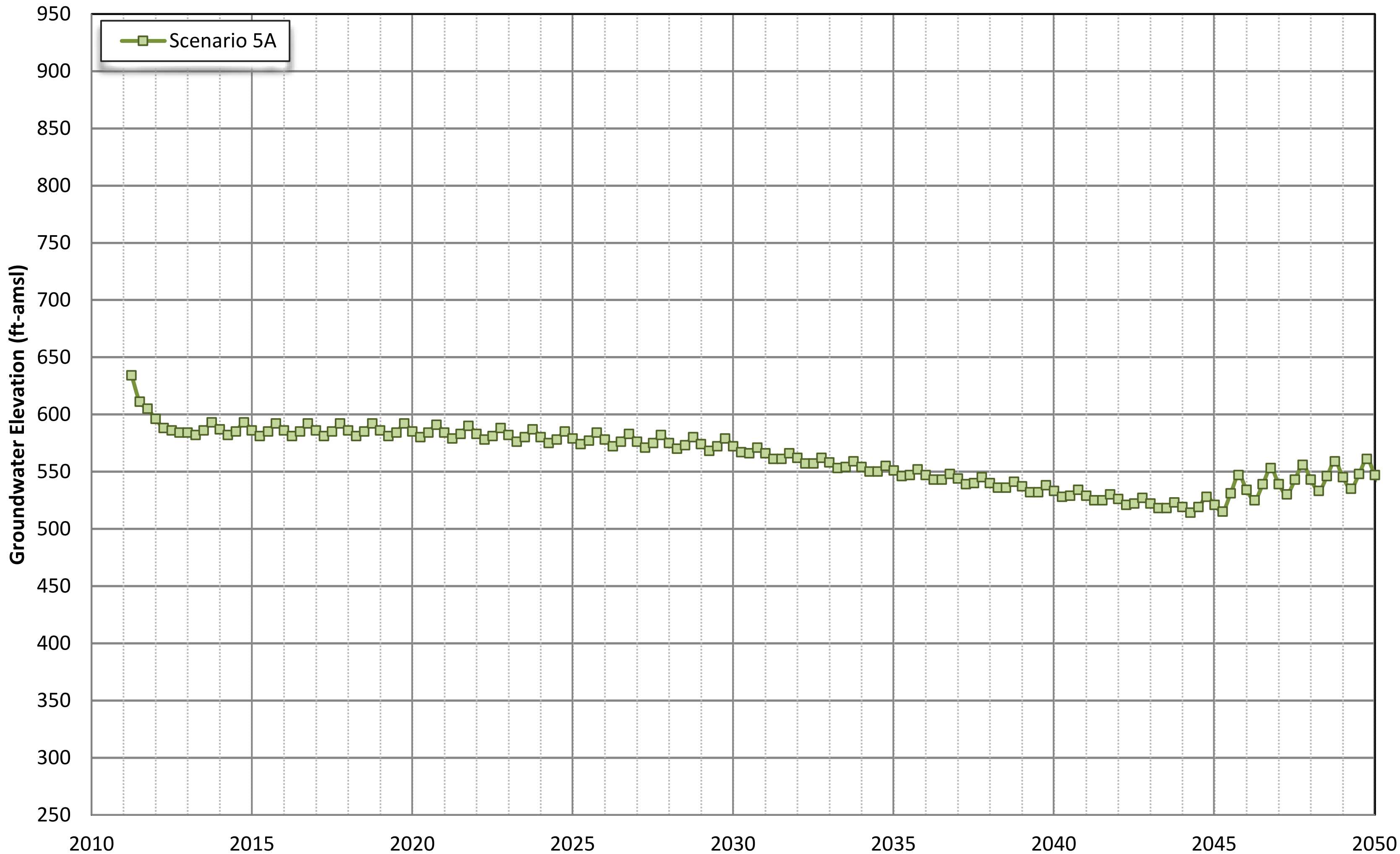

Appendix D_20150916_WellHydrographs_S5A4_Final_LBB2.xlsm
Created: 9/15/15
Printed: 9/16/2015

Figure D-80
Projected Groundwater Elevation for Scenario 5a
Jurupa Community Services District Well 6

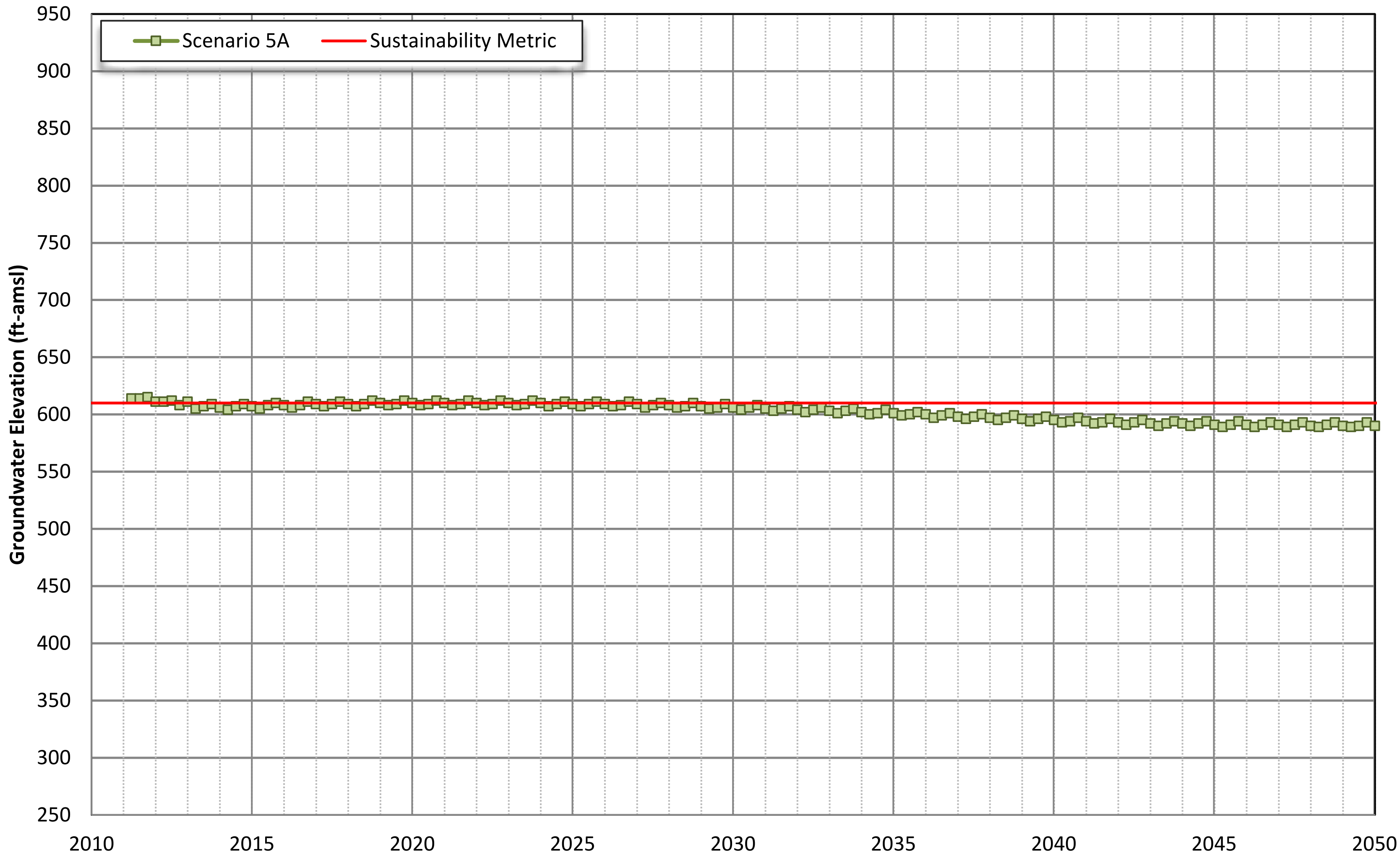

Appendix D_20150916_WellHydrographs_S5A4_Final_LBB2.xlsm
Created: 9/15/15
Printed: 9/16/2015

Figure D-81
Projected Groundwater Elevation for Scenario 5a
Jurupa Community Services District Well 8

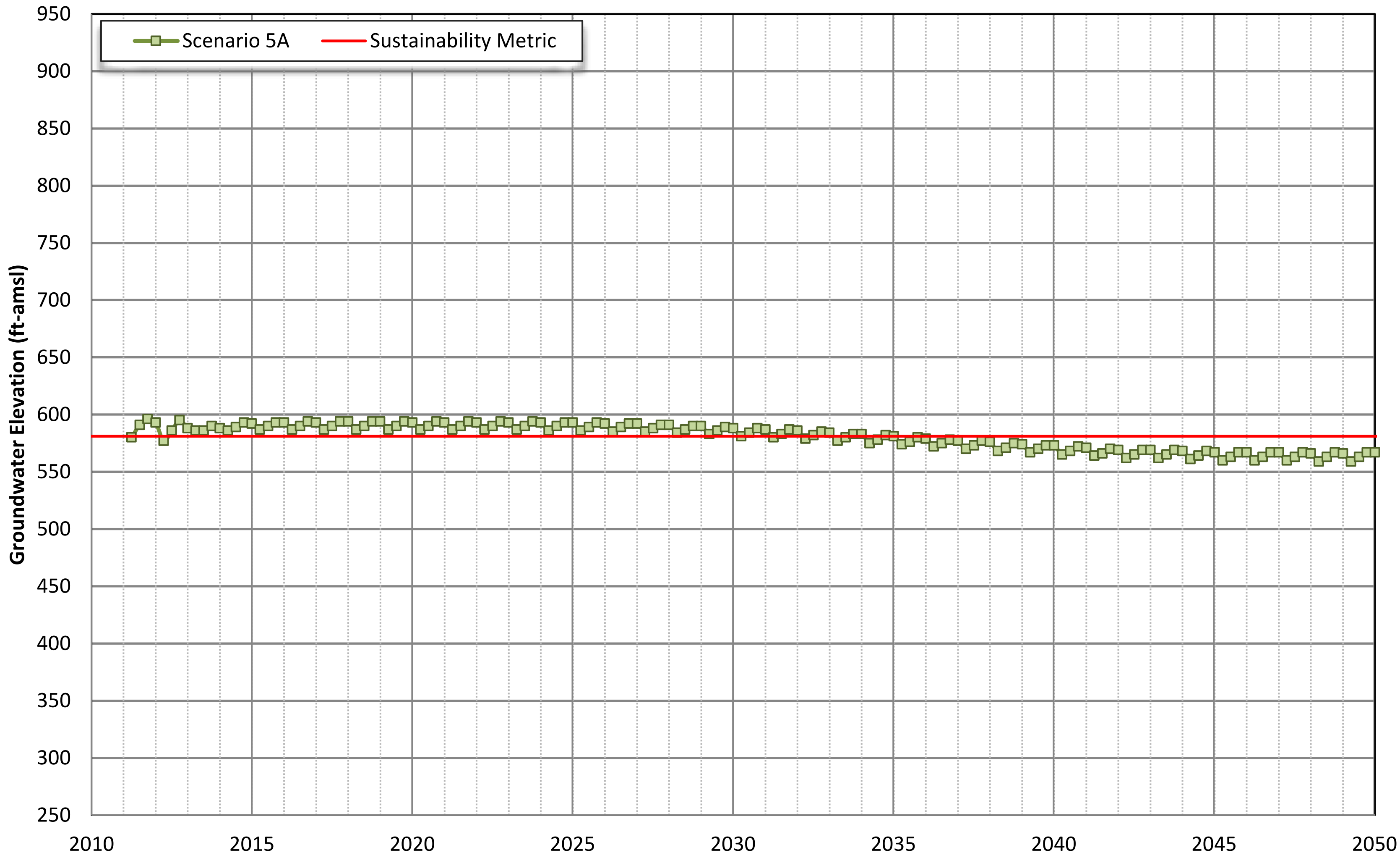

Appendix D_20150916_WellHydrographs_S5A4_Final_LBB2.xlsm
Created: 9/15/15
Printed: 9/16/2015

Figure D-82
Projected Groundwater Elevation for Scenario 5a
Jurupa Community Services District Well 11

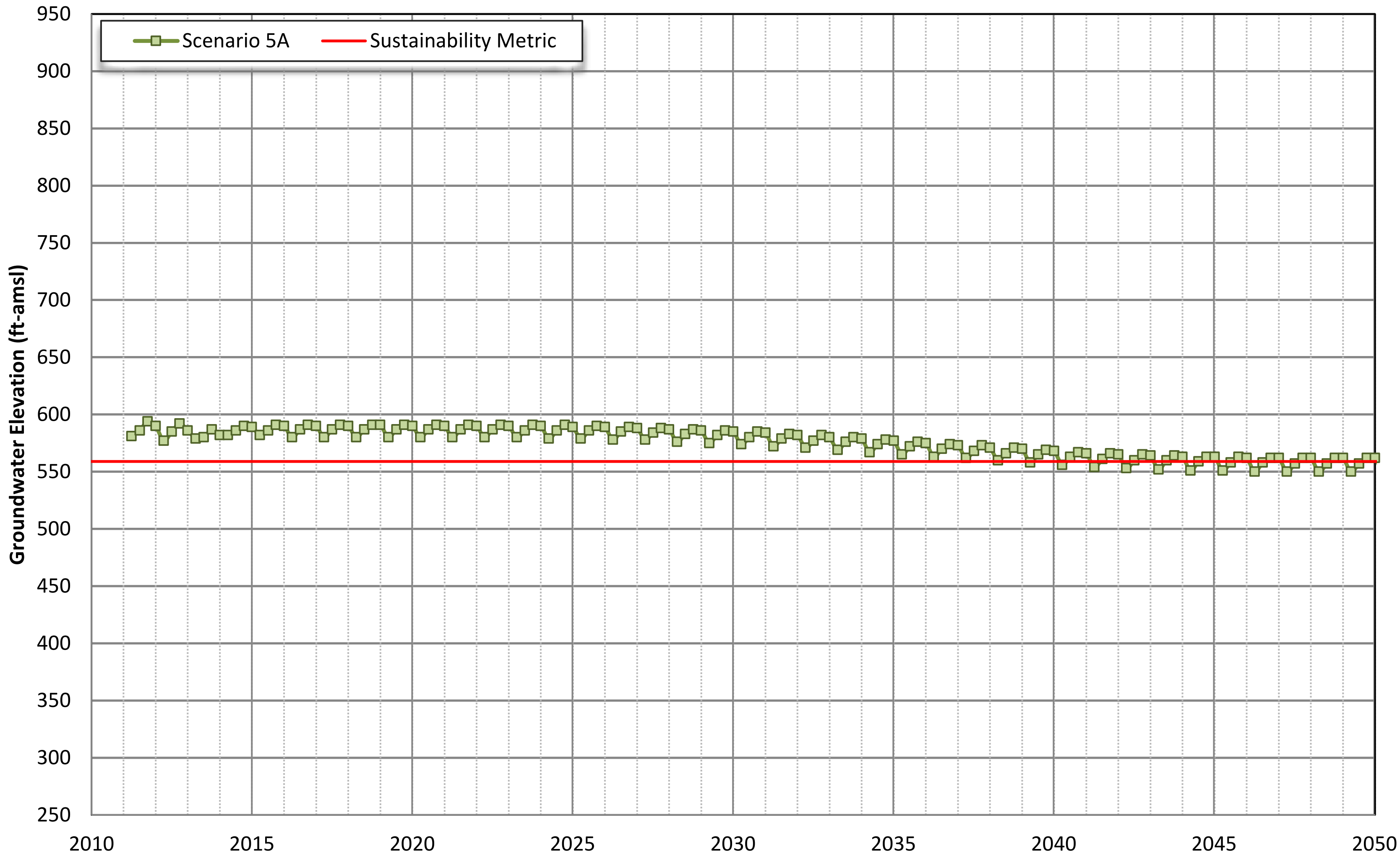

Appendix D_20150916_WellHydrographs_S5A4_Final_LBB2.xlsm
Created: 9/15/15
Printed: 9/16/2015

Figure D-83
Projected Groundwater Elevation for Scenario 5a
Jurupa Community Services District Well 12

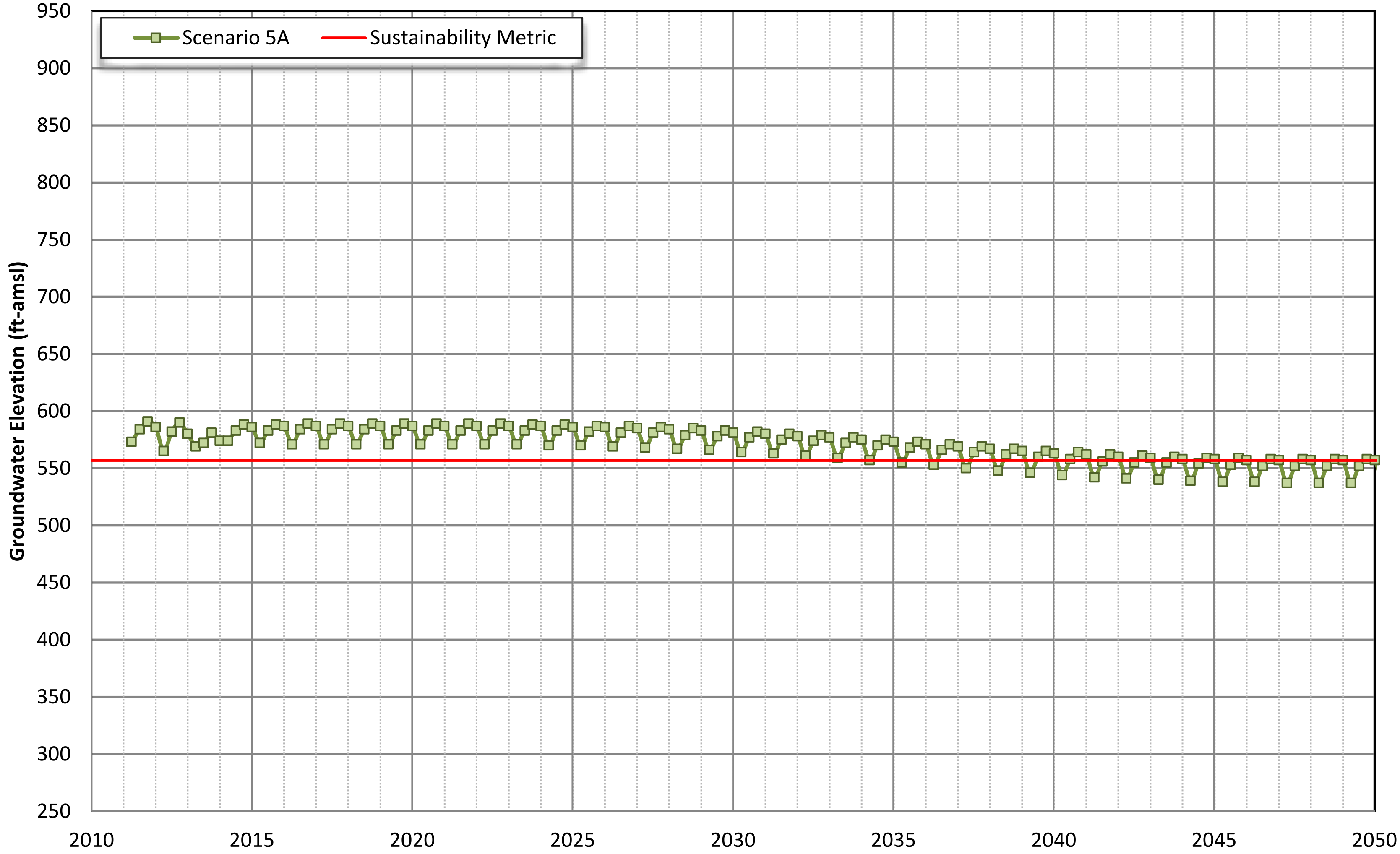

Appendix D_20150916_WellHydrographs_S5A4_Final_LBB2.xlsm
Created: 9/15/15
Printed: 9/16/2015

Figure D-84
Projected Groundwater Elevation for Scenario 5a
Jurupa Community Services District Well 13

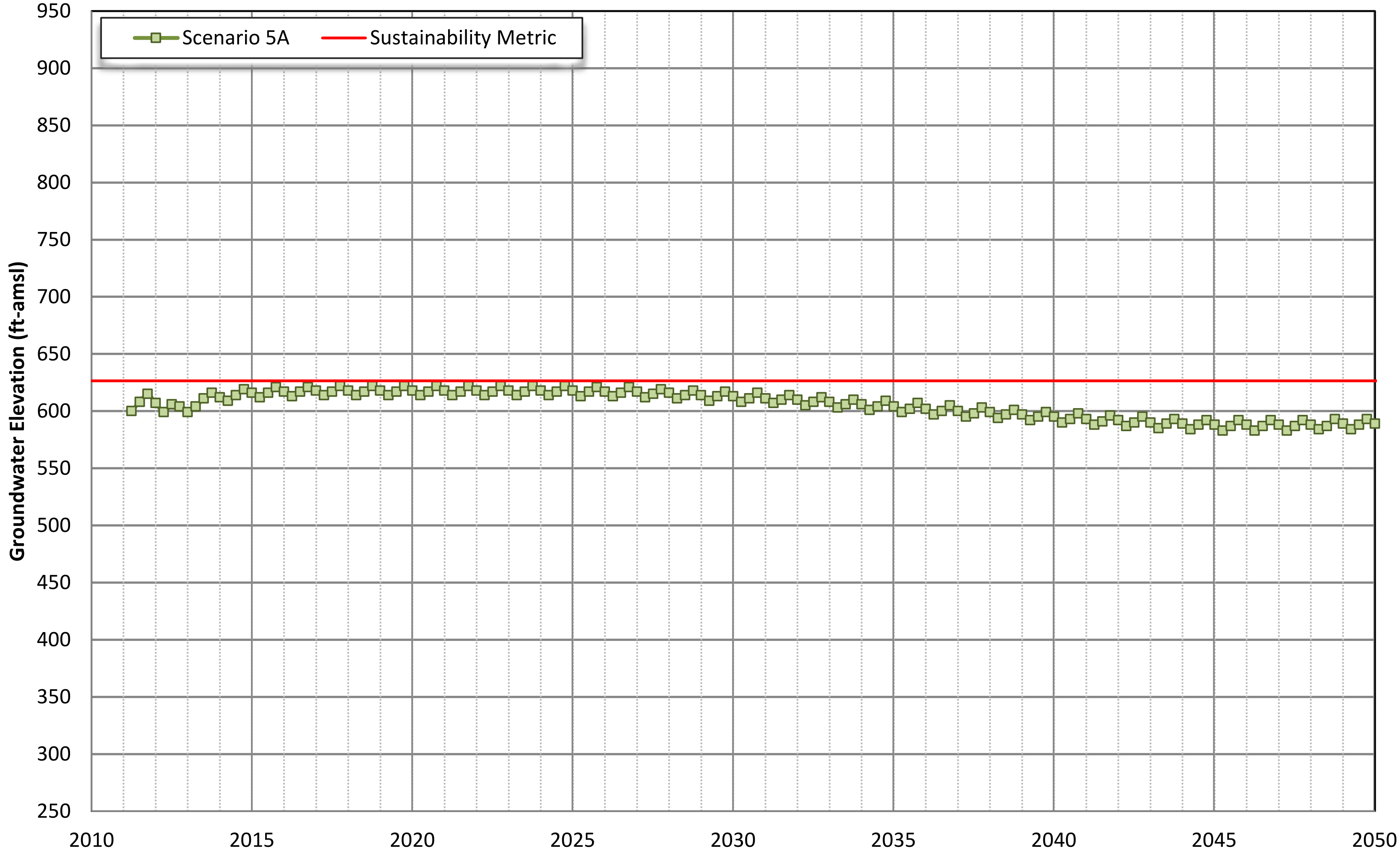

Figure D-85
Projected Groundwater Elevation for Scenario 5a
Jurupa Community Services District Well 14

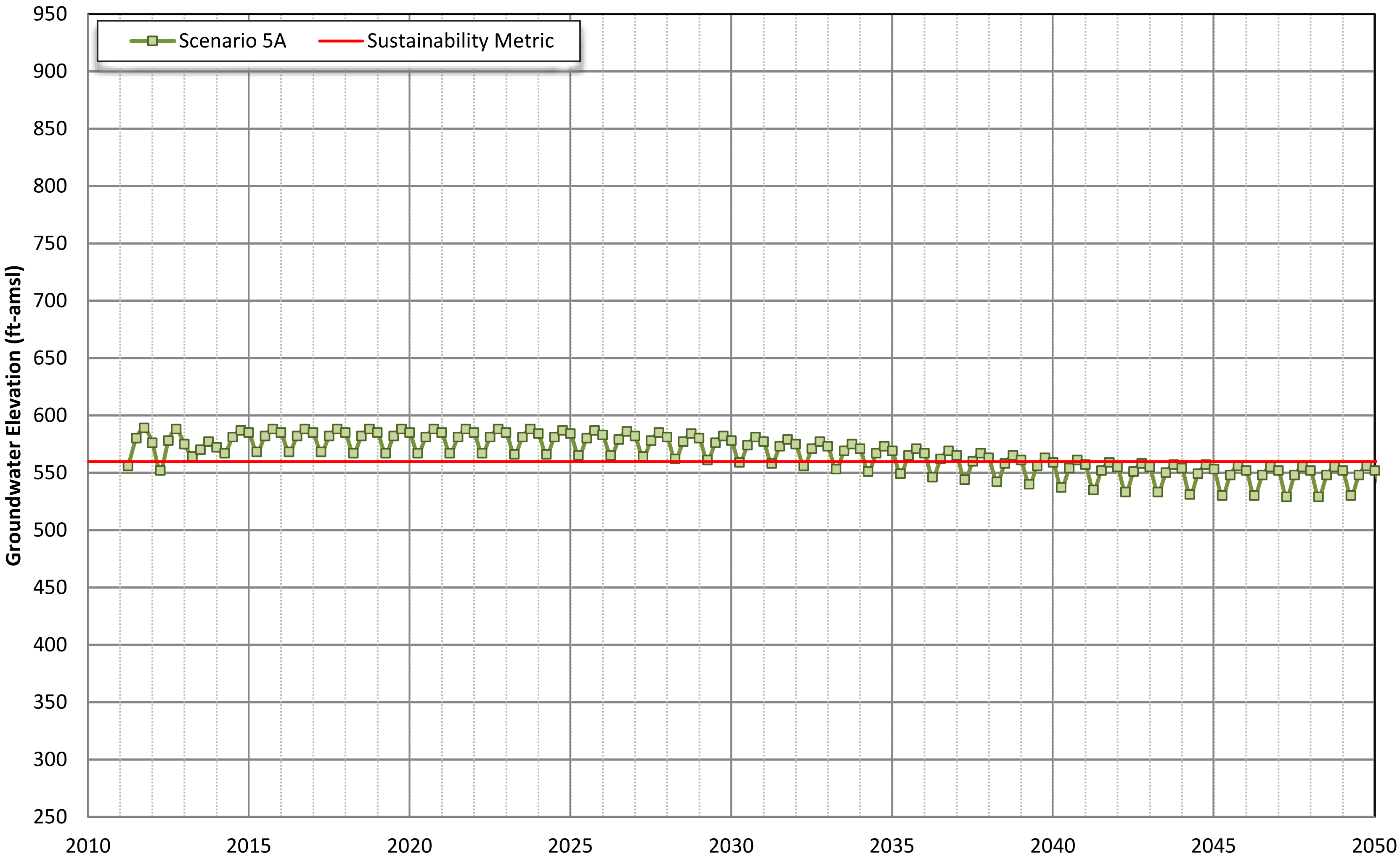

Appendix D_20150916_WellHydrographs_S5A4_Final_LBB2.xlsm
Created: 9/15/15
Printed: 9/16/2015

Figure D-86
Projected Groundwater Elevation for Scenario 5a
Jurupa Community Services District Well 15

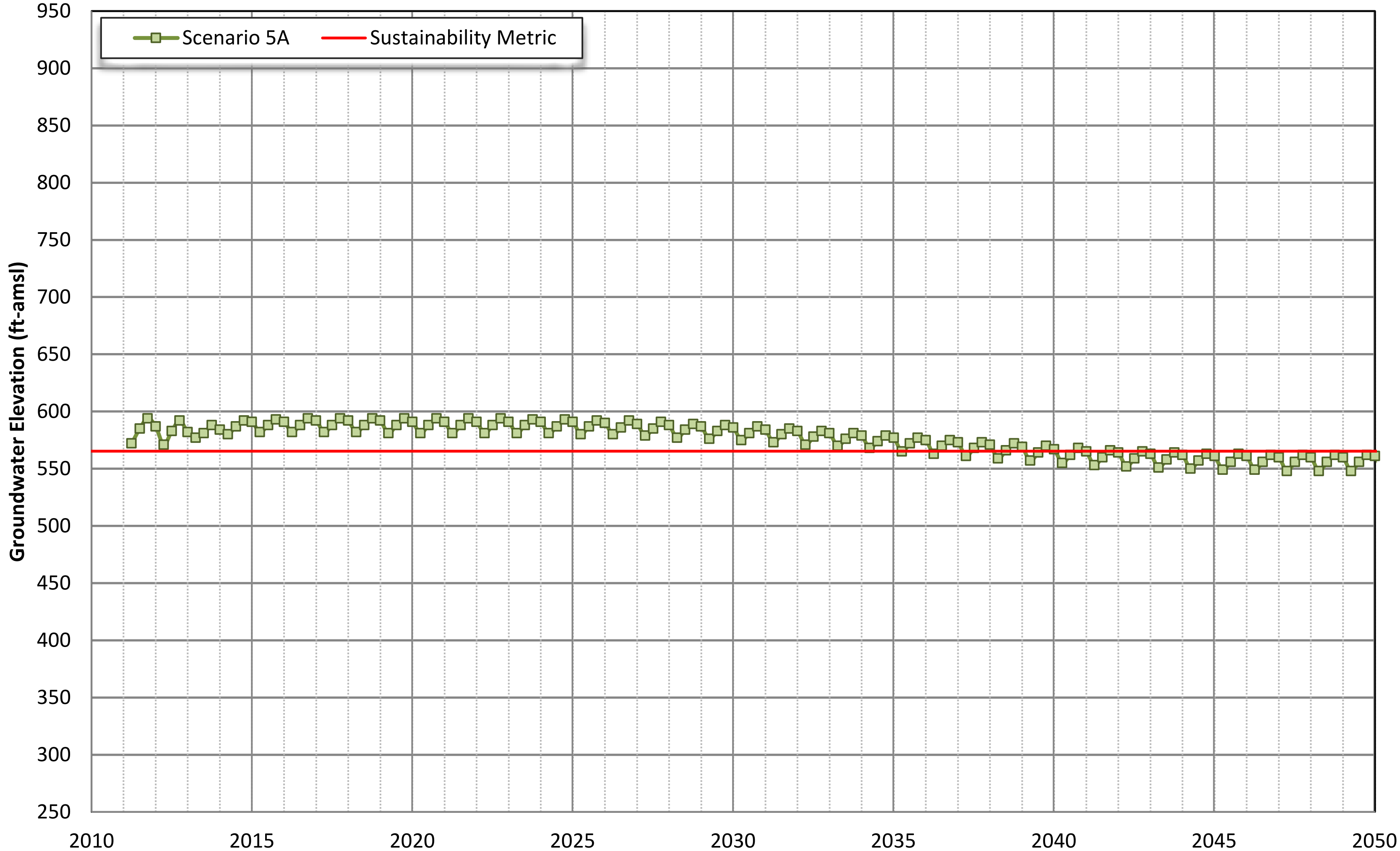

Appendix D_20150916_WellHydrographs_S5A4_Final_LBB2.xlsm
Created: 9/15/15
Printed: 9/16/2015

Figure D-87
Projected Groundwater Elevation for Scenario 5a
Jurupa Community Services District Well 16

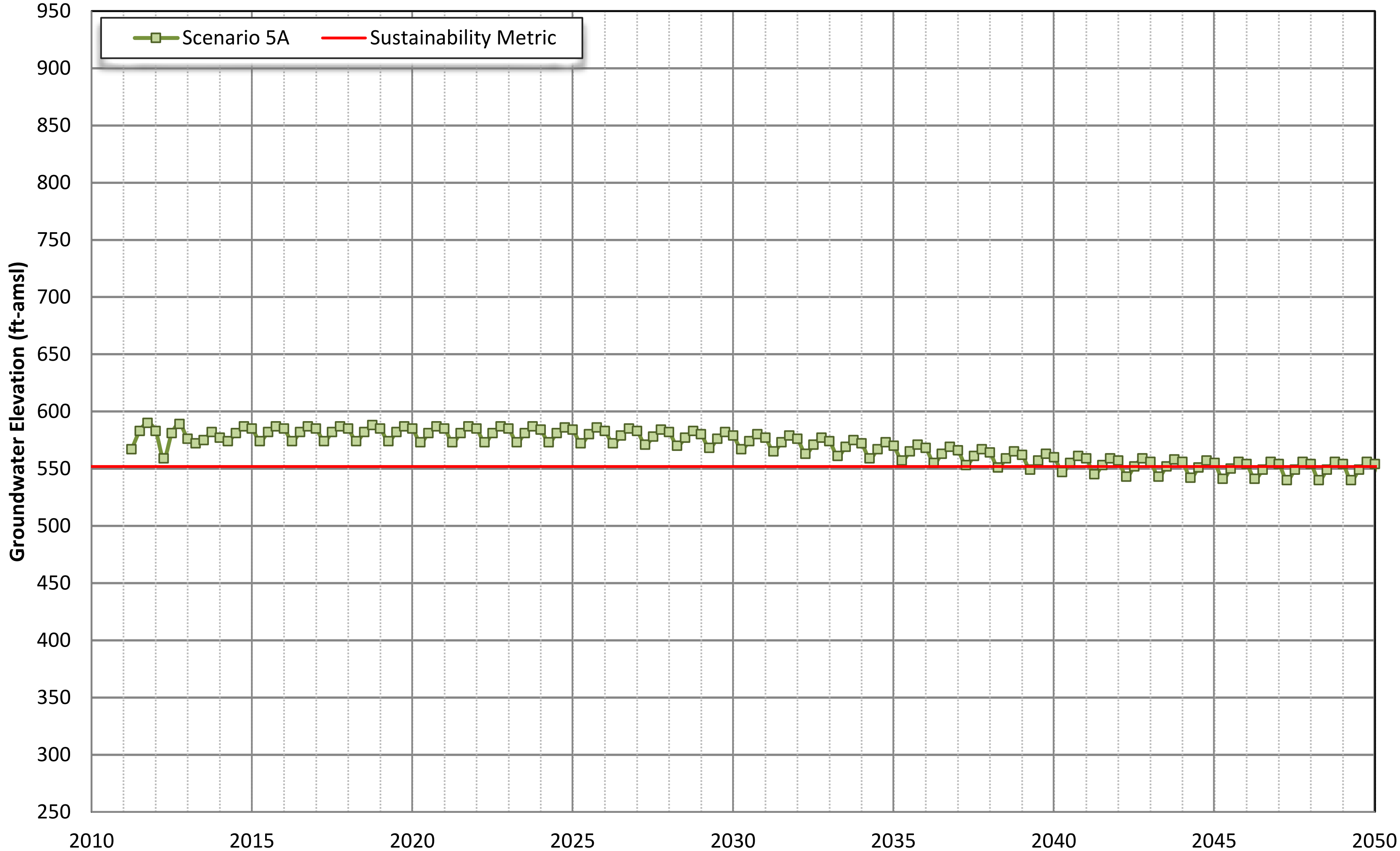

Appendix D_20150916_WellHydrographs_S5A4_Final_LBB2.xlsm
Created: 9/15/15
Printed: 9/16/2015

Figure D-88
Projected Groundwater Elevation for Scenario 5a
Jurupa Community Services District Well 17

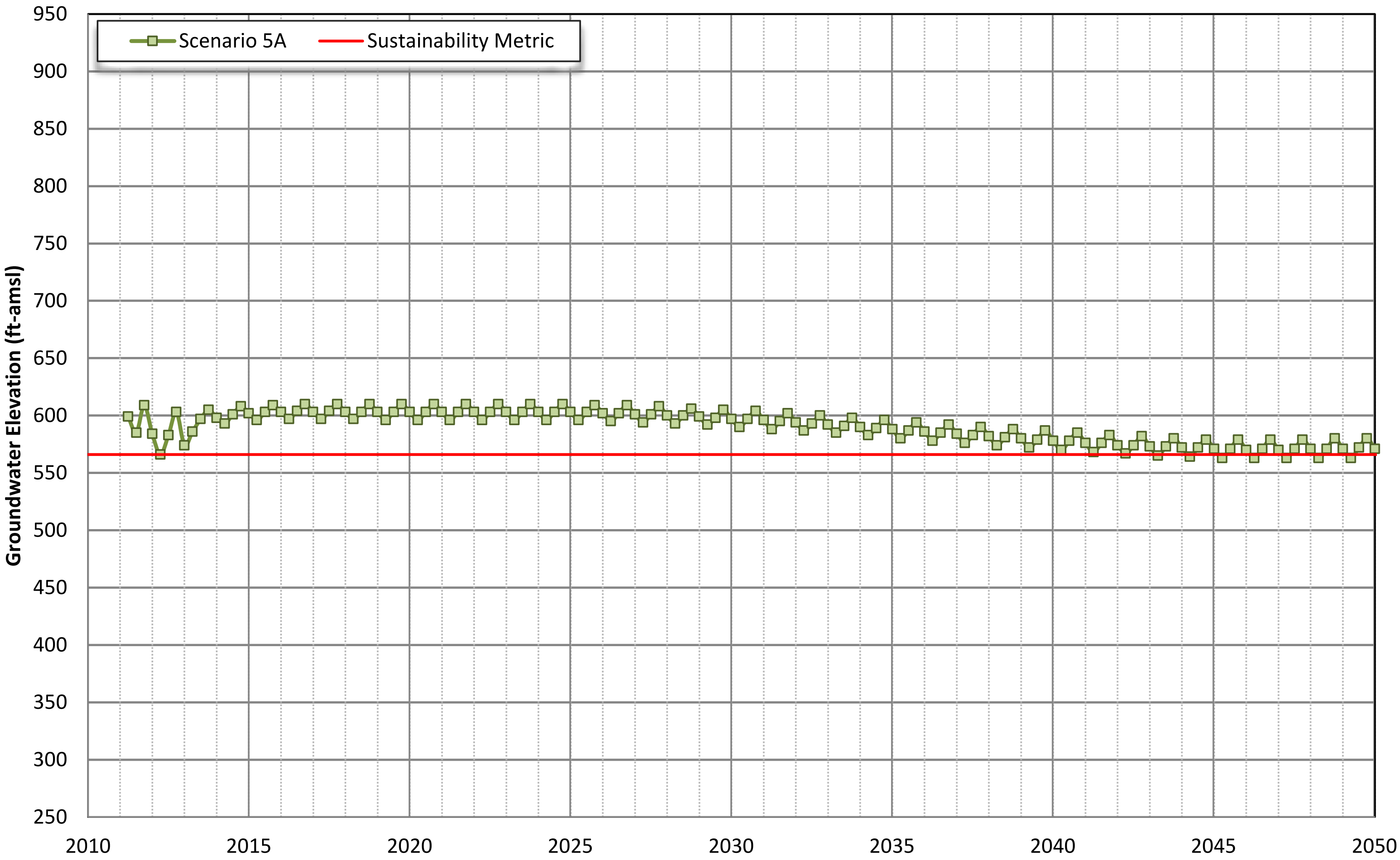

Appendix D_20150916_WellHydrographs_S5A4_Final_LBB2.xlsm
Created: 9/15/15
Printed: 9/16/2015

Figure D-89
Projected Groundwater Elevation for Scenario 5a
Jurupa Community Services District Well 18

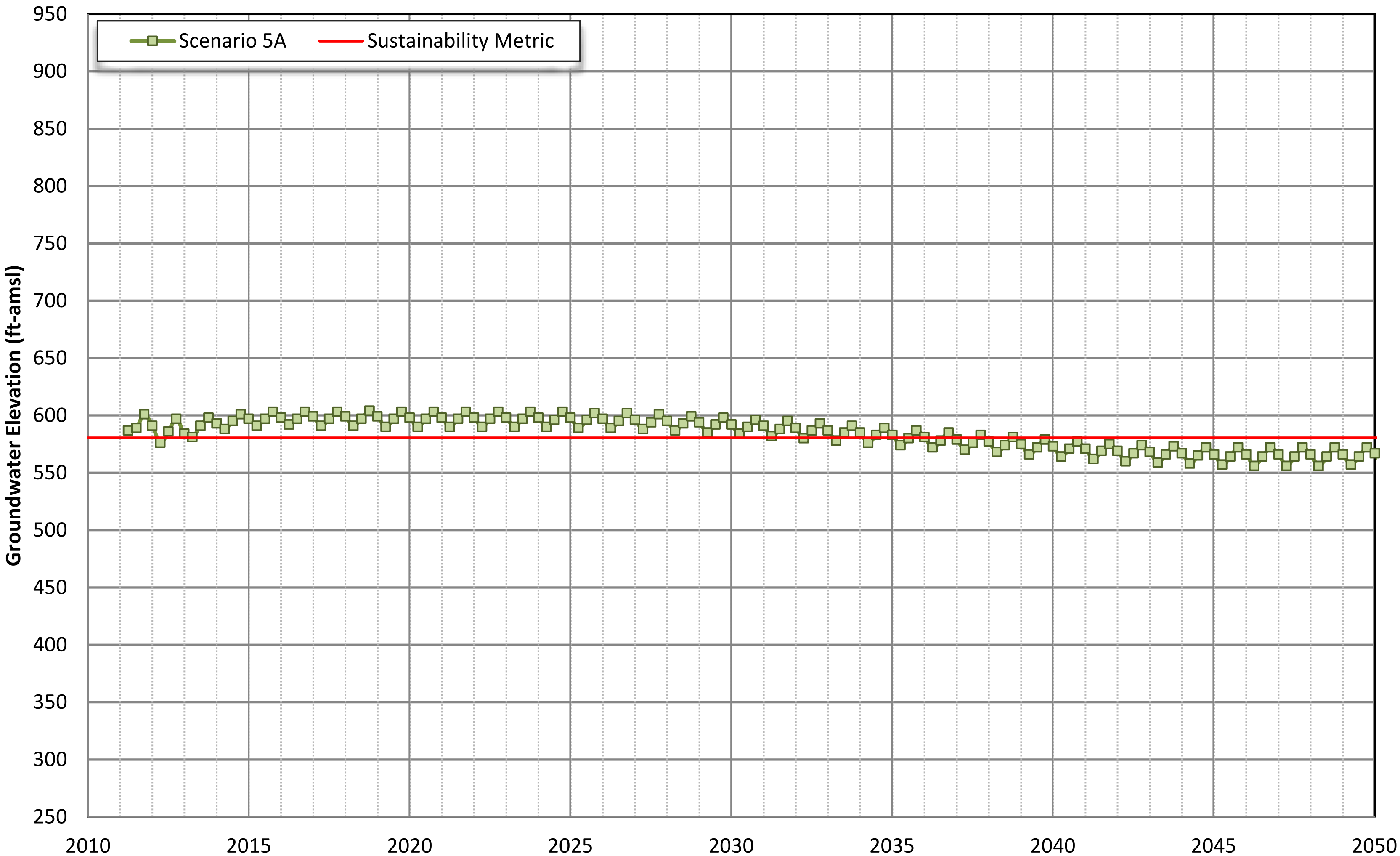

Appendix D_20150916_WellHydrographs_S5A4_Final_LBB2.xlsm
Created: 9/15/15
Printed: 9/16/2015

Figure D-90
Projected Groundwater Elevation for Scenario 5a
Jurupa Community Services District Well 19

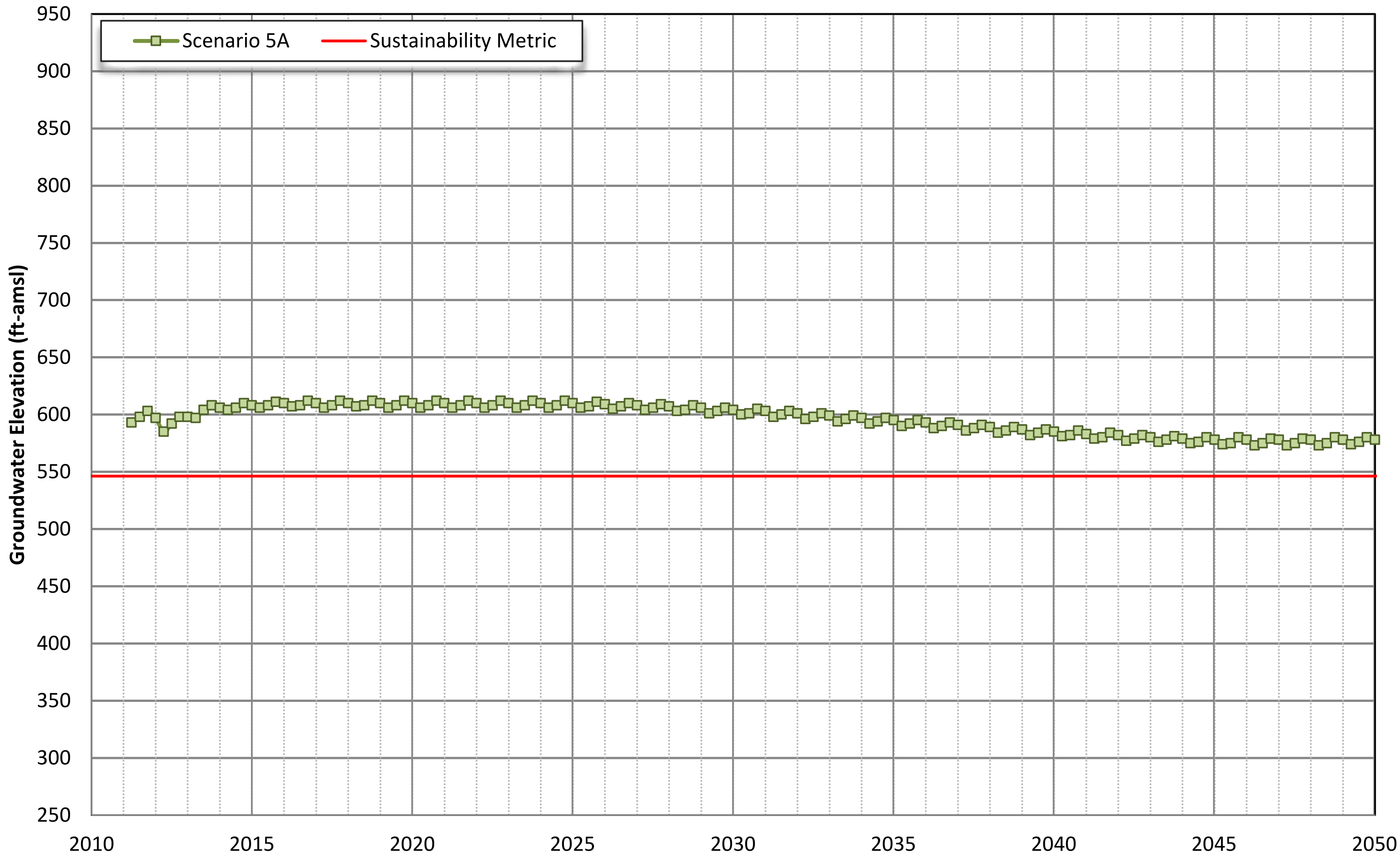

Appendix D_20150916_WellHydrographs_S5A4_Final_LBB2.xlsm
Created: 9/15/15
Printed: 9/16/2015

Figure D-91
Projected Groundwater Elevation for Scenario 5a
Jurupa Community Services District Well 20

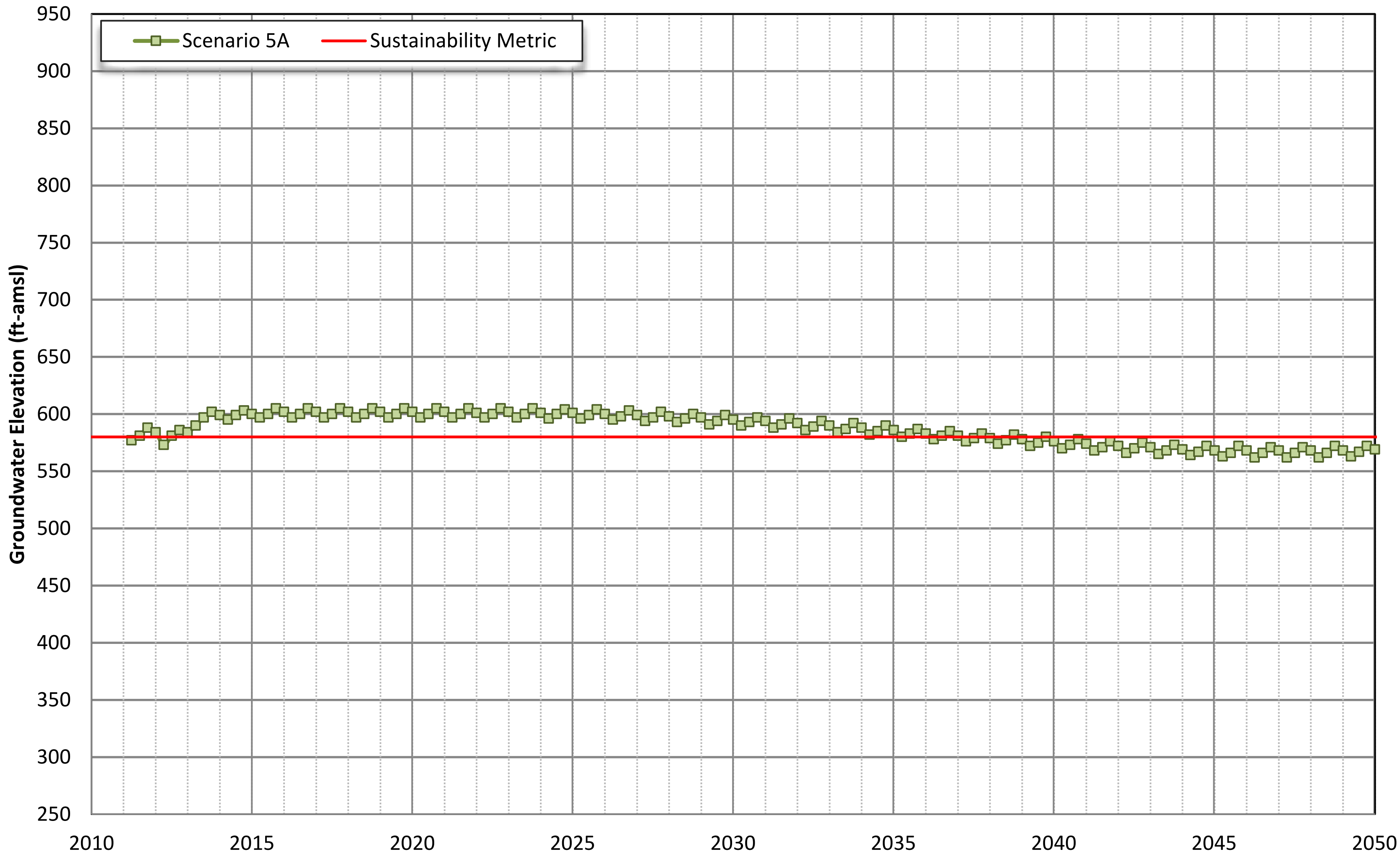

Appendix D_20150916_WellHydrographs_S5A4_Final_LBB2.xlsm
Created: 9/15/15
Printed: 9/16/2015

Figure D-92
Projected Groundwater Elevation for Scenario 5a
Jurupa Community Services District Well 22

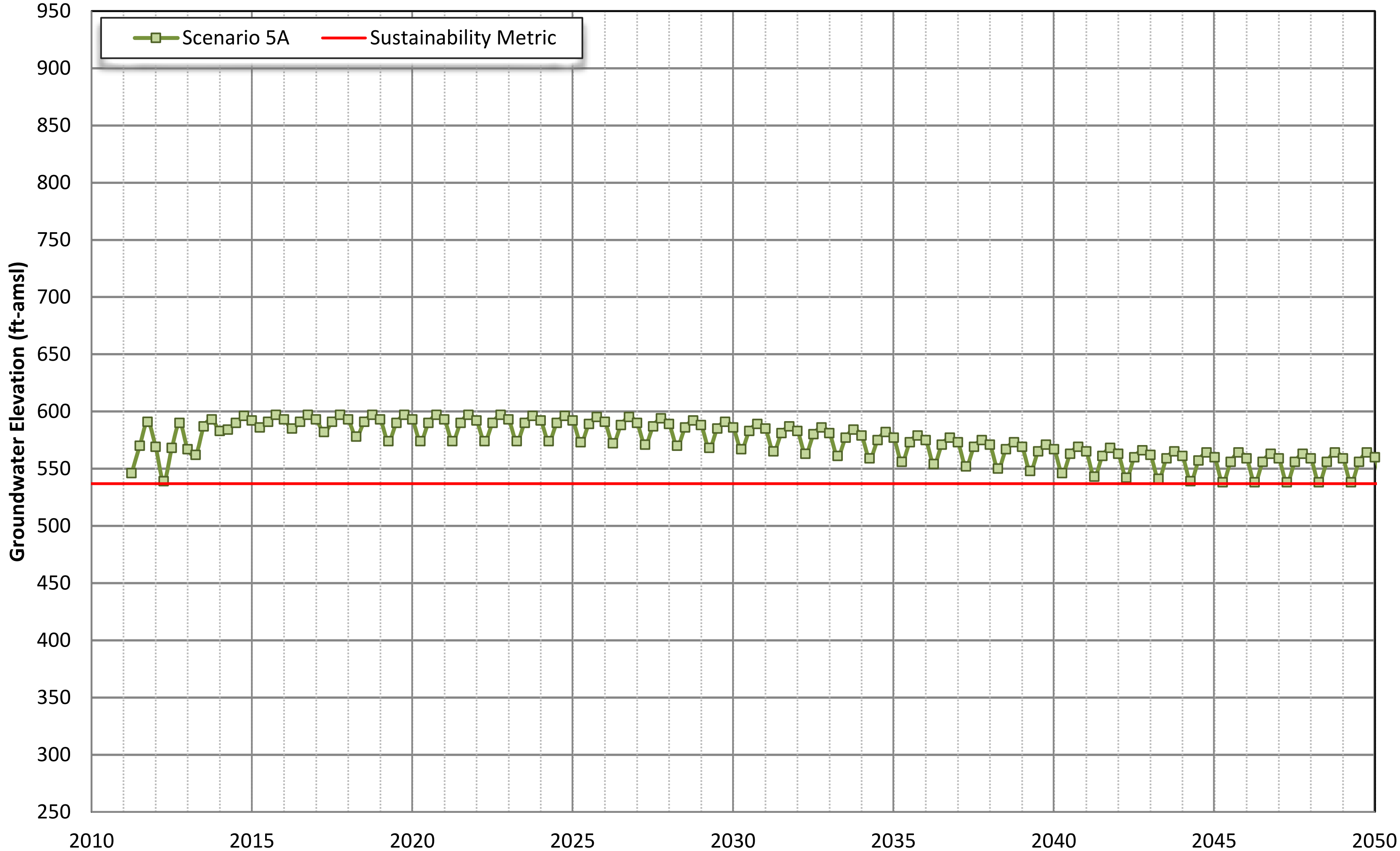

Appendix D_20150916_WellHydrographs_S5A4_Final_LBB2.xlsm
Created: 9/15/15
Printed: 9/16/2015

Figure D-93
Projected Groundwater Elevation for Scenario 5a
Jurupa Community Services District Well 23

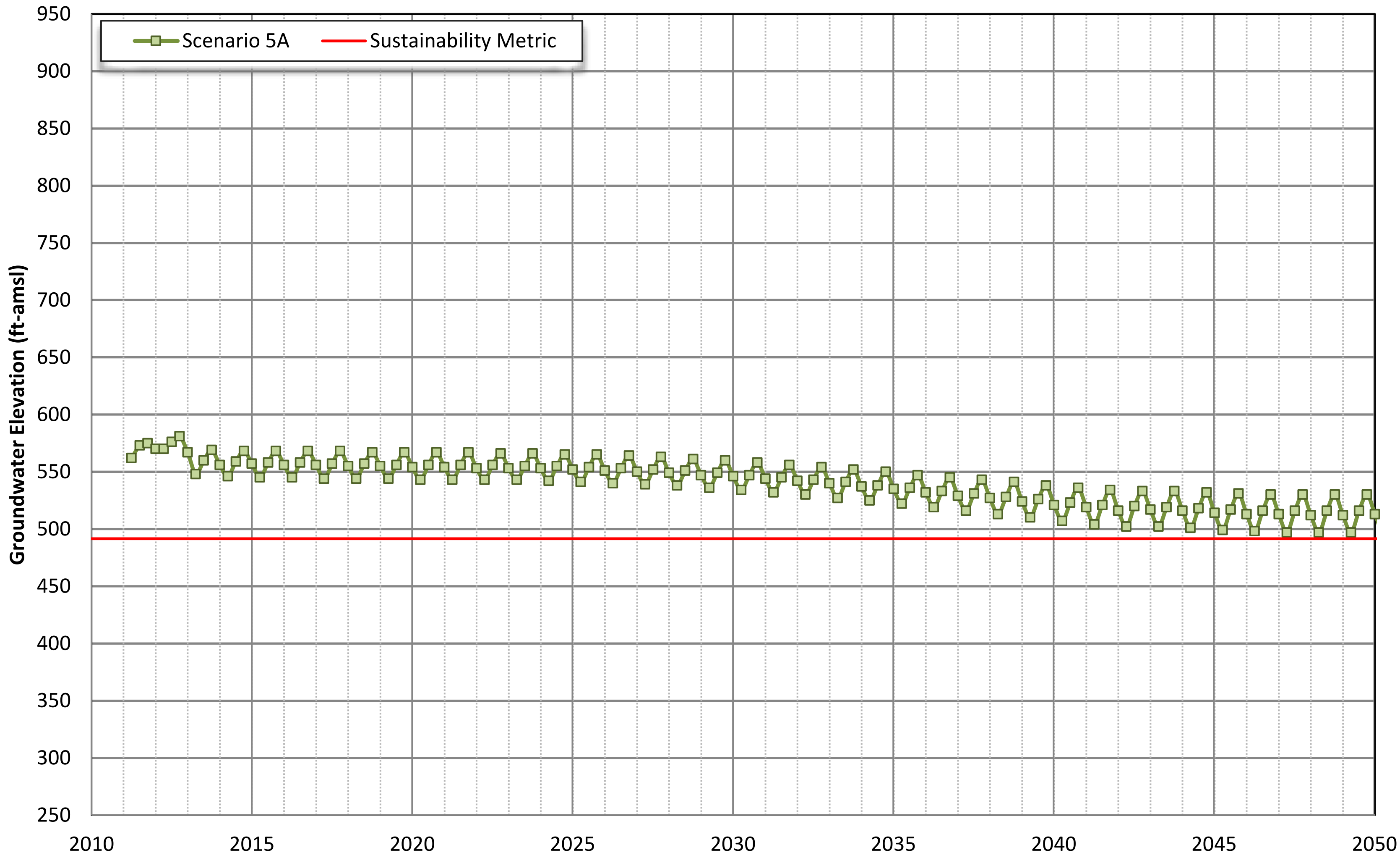

Appendix D_20150916_WellHydrographs_S5A4_Final_LBB2.xlsm
Created: 9/15/15
Printed: 9/16/2015

Figure D-94
Projected Groundwater Elevation for Scenario 5a
Jurupa Community Services District Well 24

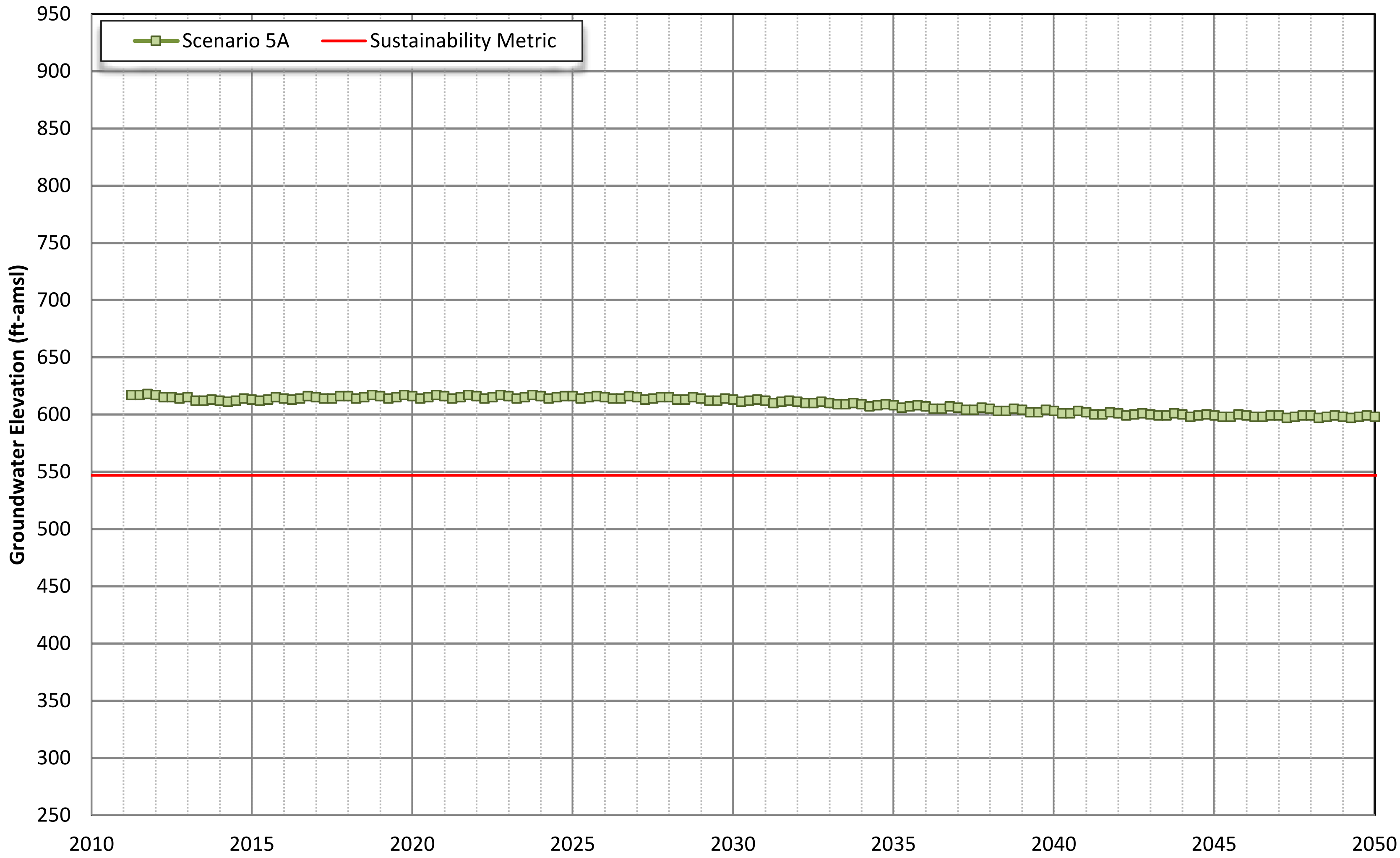

Appendix D_20150916_WellHydrographs_S5A4_Final_LBB2.xlsm
Created: 9/15/15
Printed: 9/16/2015

Figure D-95
Projected Groundwater Elevation for Scenario 5a
Jurupa Community Services District Well 25

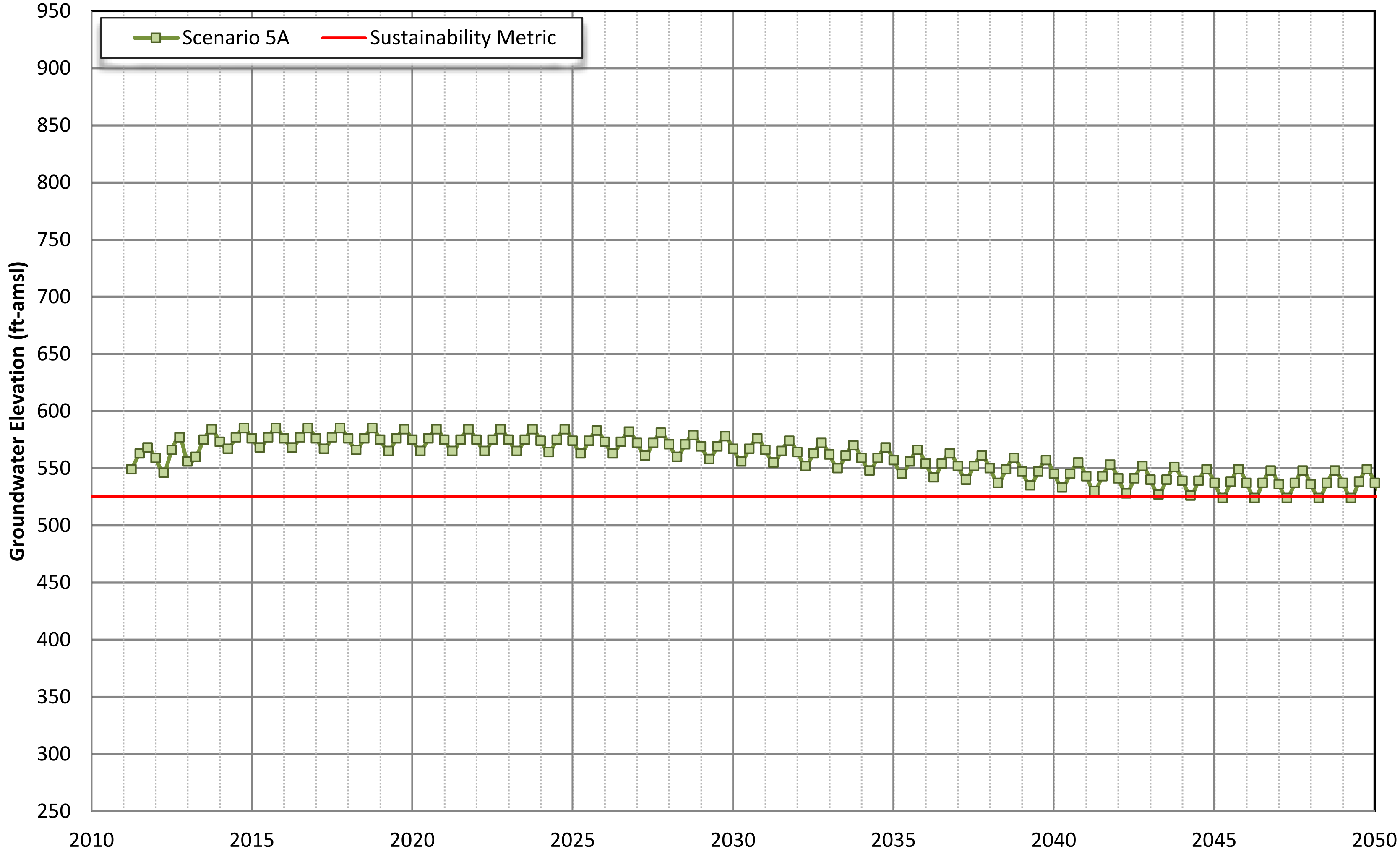

Appendix D_20150916_WellHydrographs_S5A4_Final_LBB2.xlsm
Created: 9/15/15
Printed: 9/16/2015

Figure D-96
Projected Groundwater Elevation for Scenario 5a
Jurupa Community Services District Well 27

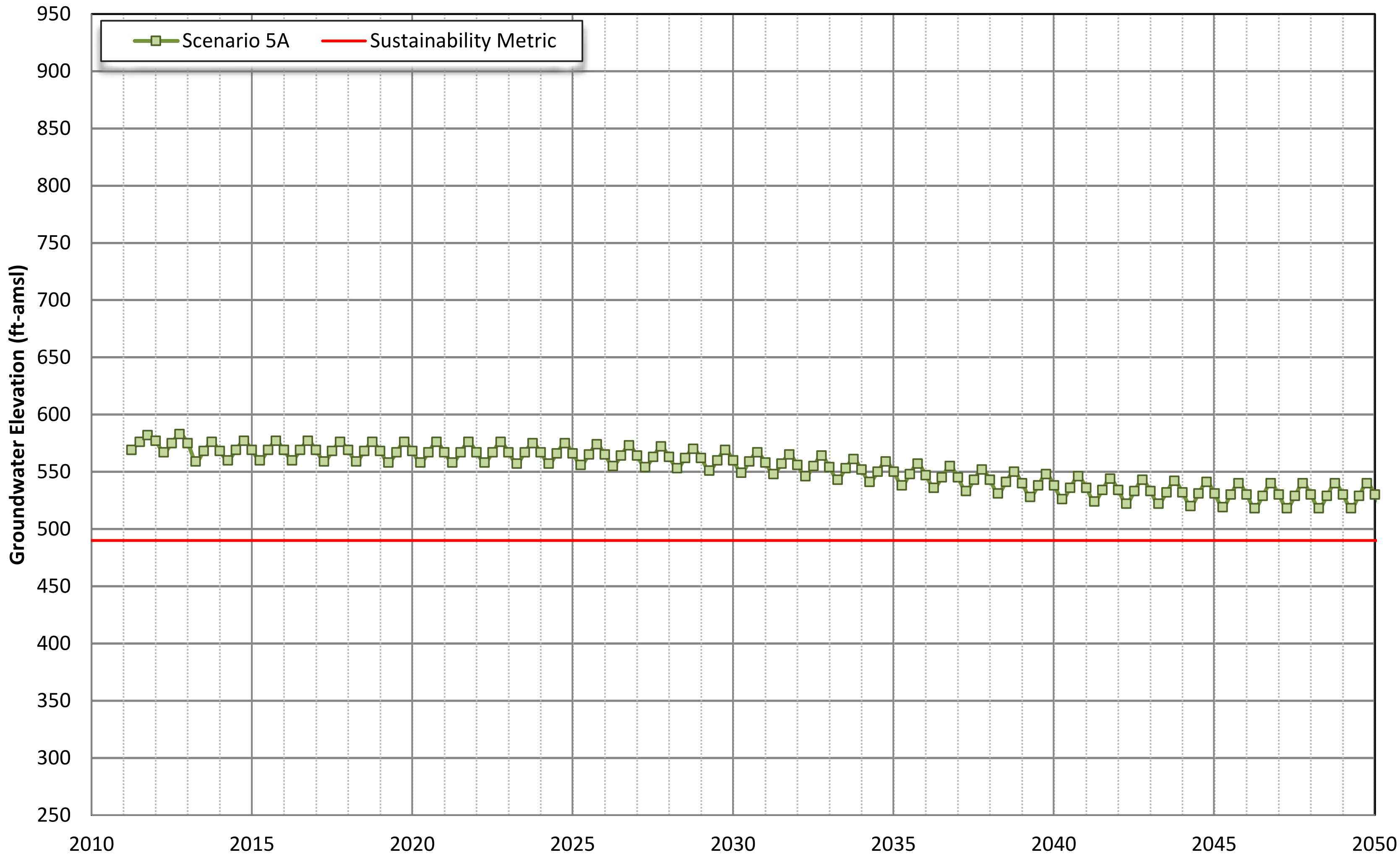

Appendix D_20150916_WellHydrographs_S5A4_Final_LBB2.xlsm
Created: 9/15/15
Printed: 9/16/2015

Figure D-97
Projected Groundwater Elevation for Scenario 5a
Jurupa Community Services District Well 28

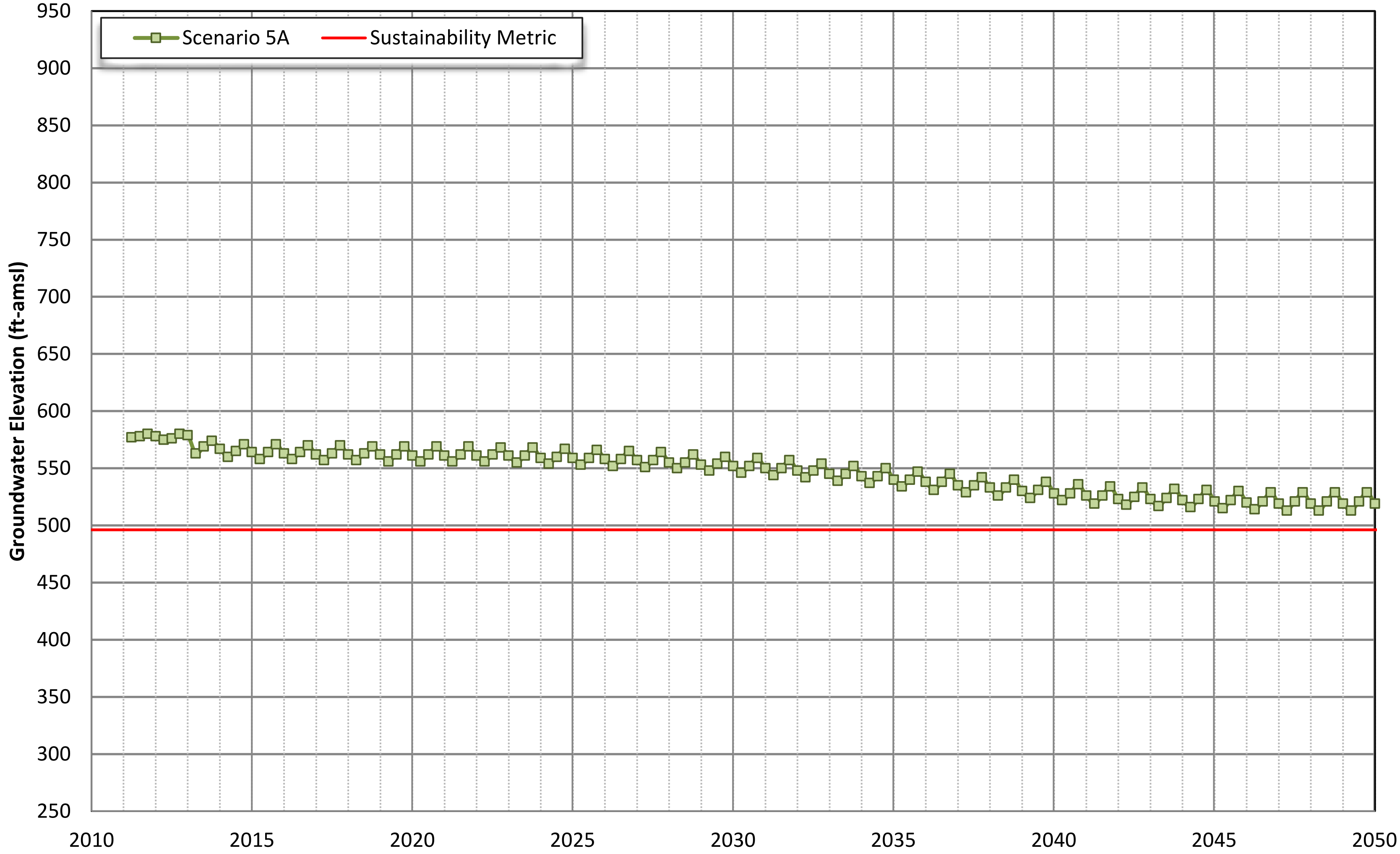

Appendix D_20150916_WellHydrographs_S5A4_Final_LBB2.xlsm
Created: 9/15/15
Printed: 9/16/2015

Figure D-98
Projected Groundwater Elevation for Scenario 5a
Jurupa Community Services District Well IDI-1

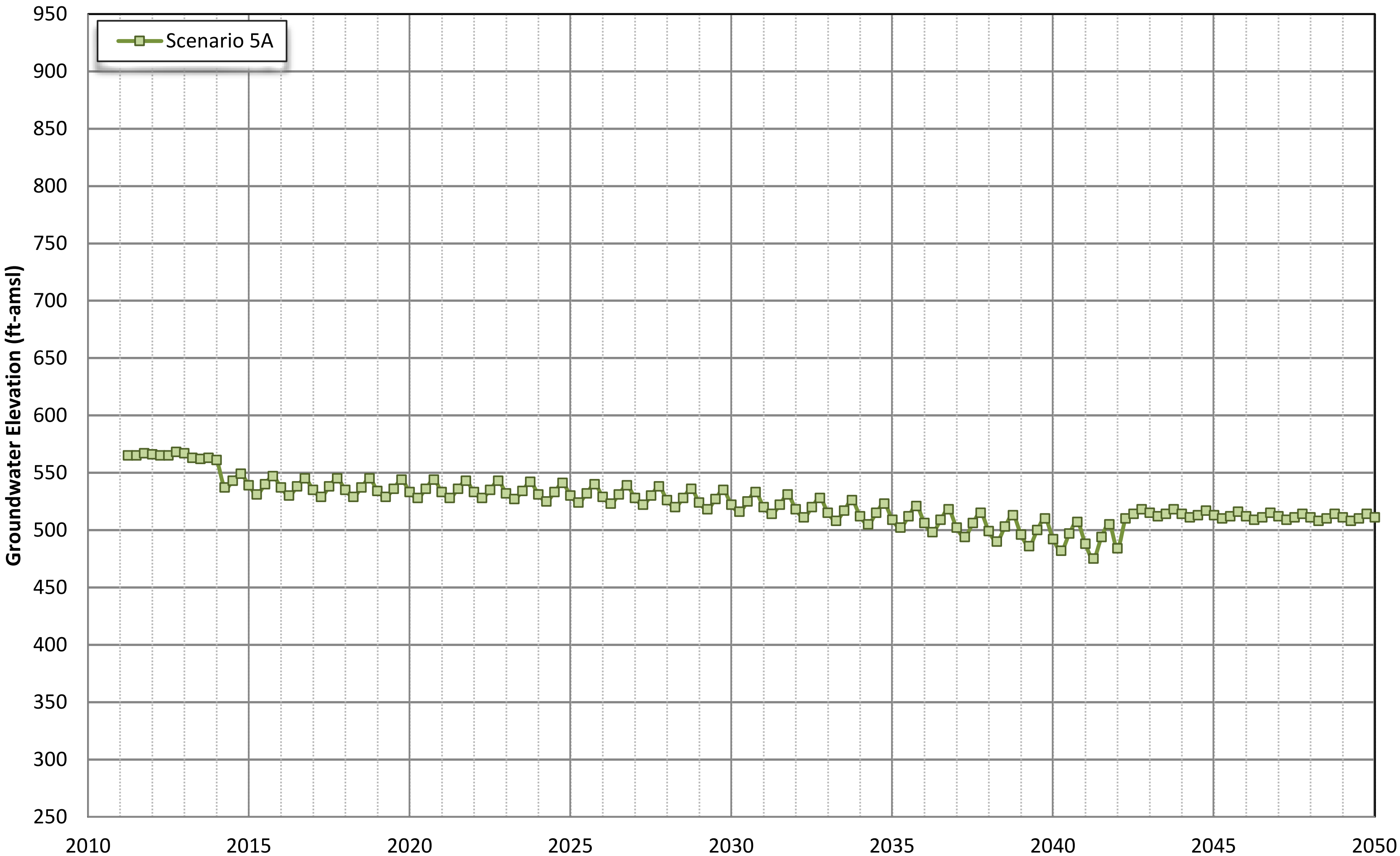

Appendix D_20150916_WellHydrographs_S5A4_Final_LBB2.xlsm
Created: 9/15/15
Printed: 9/16/2015

Figure D-99
Projected Groundwater Elevation for Scenario 5a
Jurupa Community Services District Well IDI-2

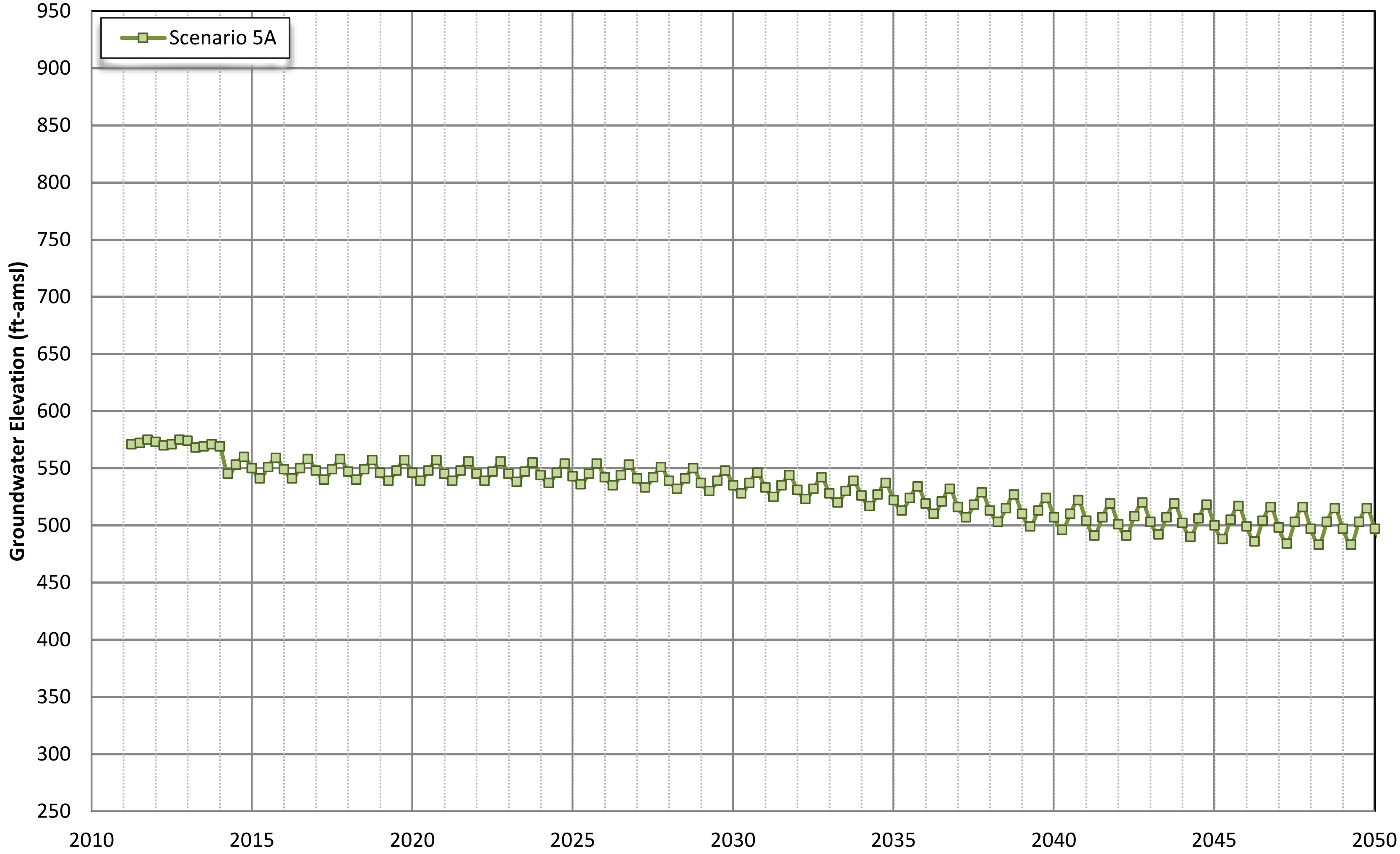

Appendix D_20150916_WellHydrographs_S5A4_Final_LBB2.xlsm
Created: 9/15/15
Printed: 9/16/2015

Figure D-100
Projected Groundwater Elevation for Scenario 5a
Marygold Mutual Water Company Well 2

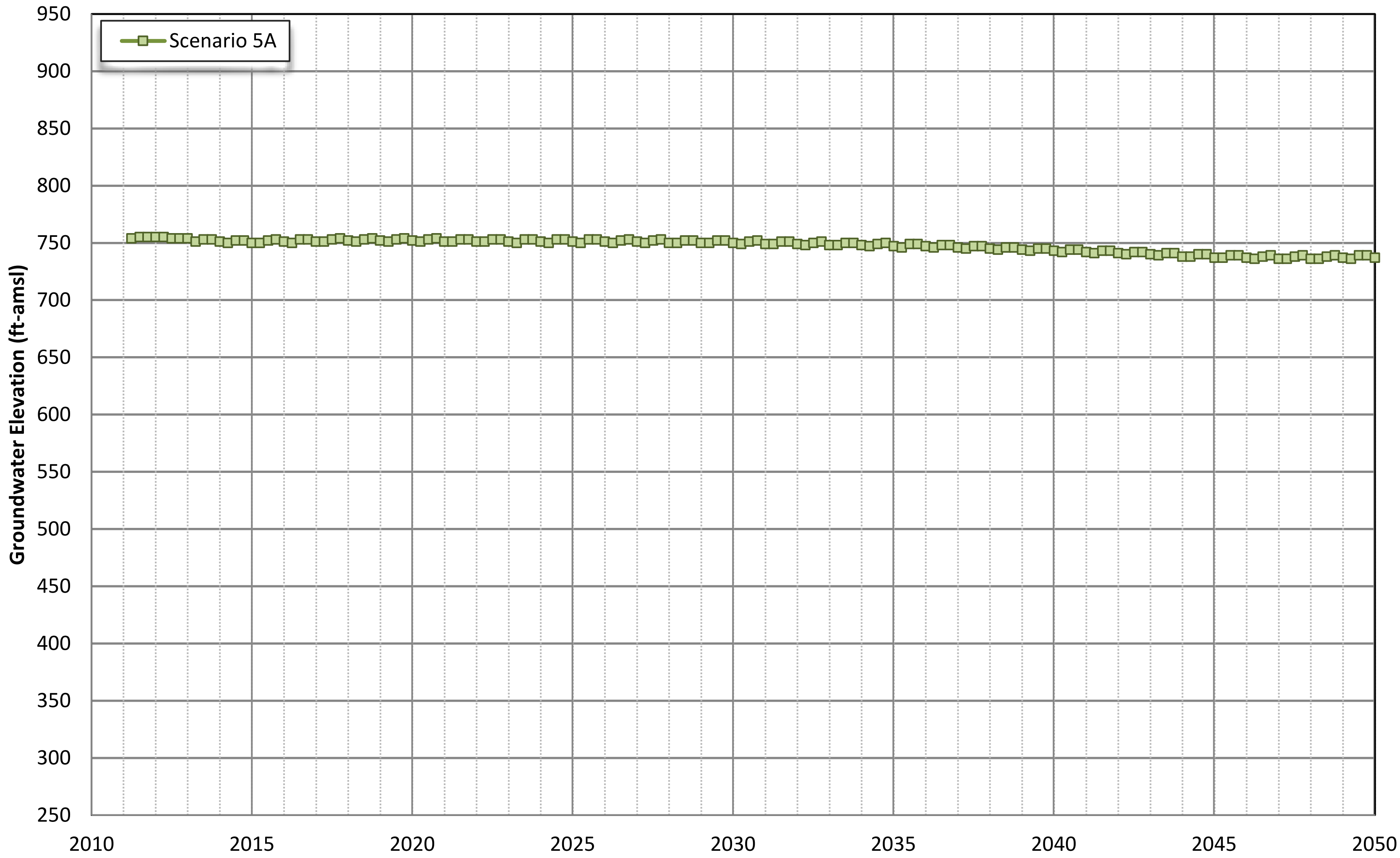

Appendix D_20150916_WellHydrographs_S5A4_Final_LBB2.xlsm
Created: 9/15/15
Printed: 9/16/2015

Figure D-101
Projected Groundwater Elevation for Scenario 5a
Marygold Mutual Water Company Well 3

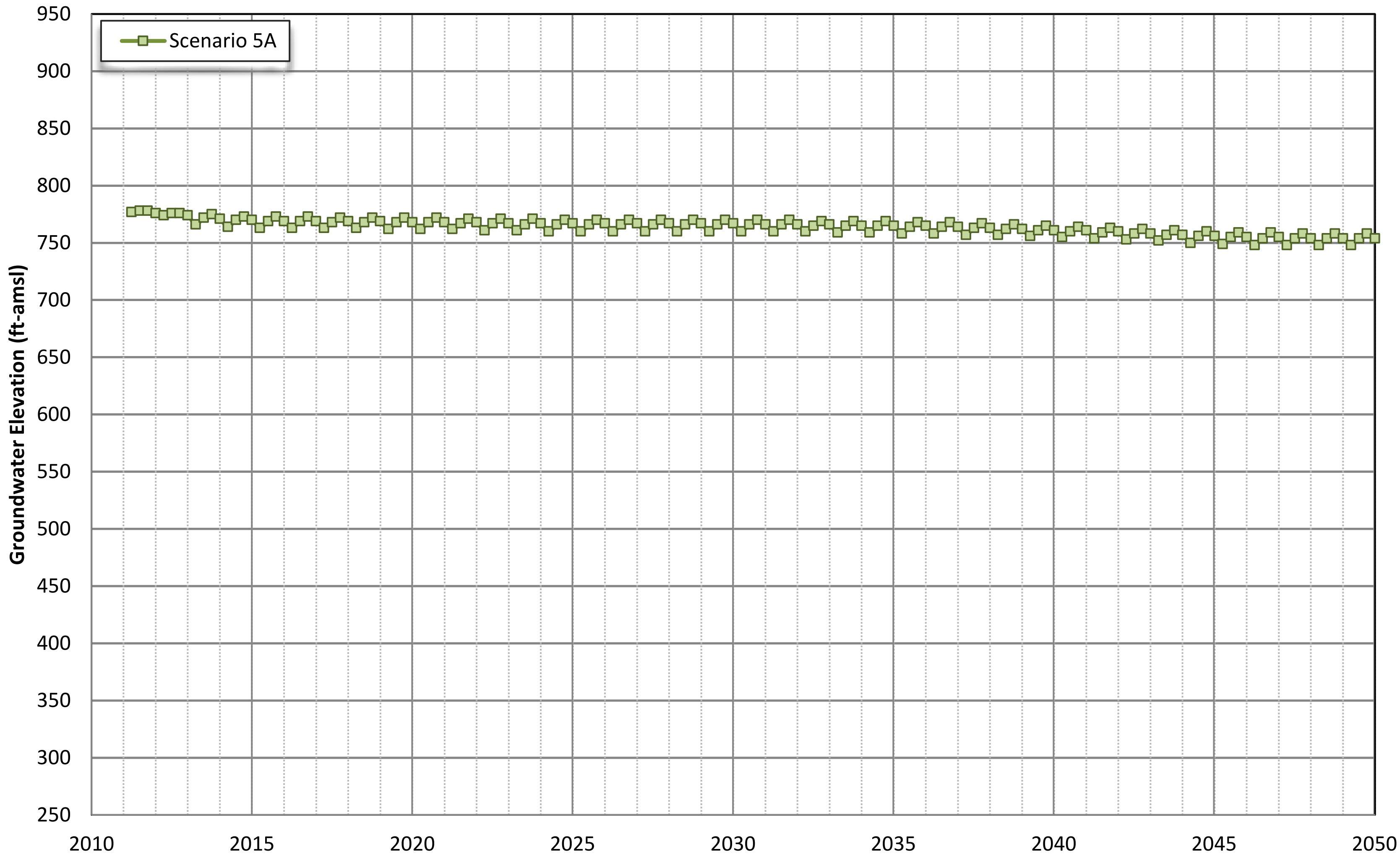

Appendix D_20150916_WellHydrographs_S5A4_Final_LBB2.xlsm
Created: 9/15/15
Printed: 9/16/2015

Figure D-102
Projected Groundwater Elevation for Scenario 5a
Marygold Mutual Water Company Well 4

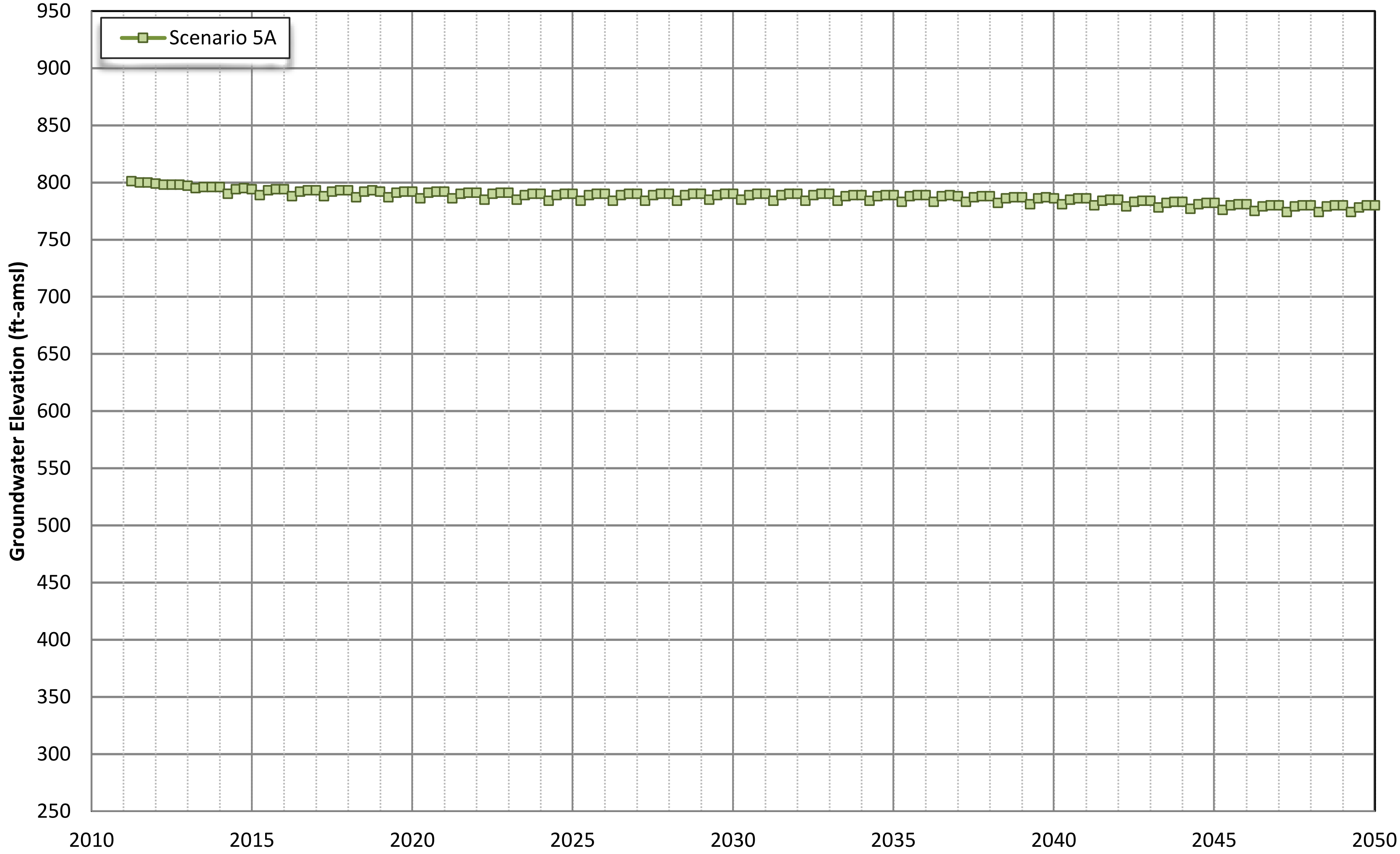

Appendix D_20150916_WellHydrographs_S5A4_Final_LBB2.xlsm
Created: 9/15/15
Printed: 9/16/2015

Figure D-103
Projected Groundwater Elevation for Scenario 5a
Monte Vista Water District Well 4

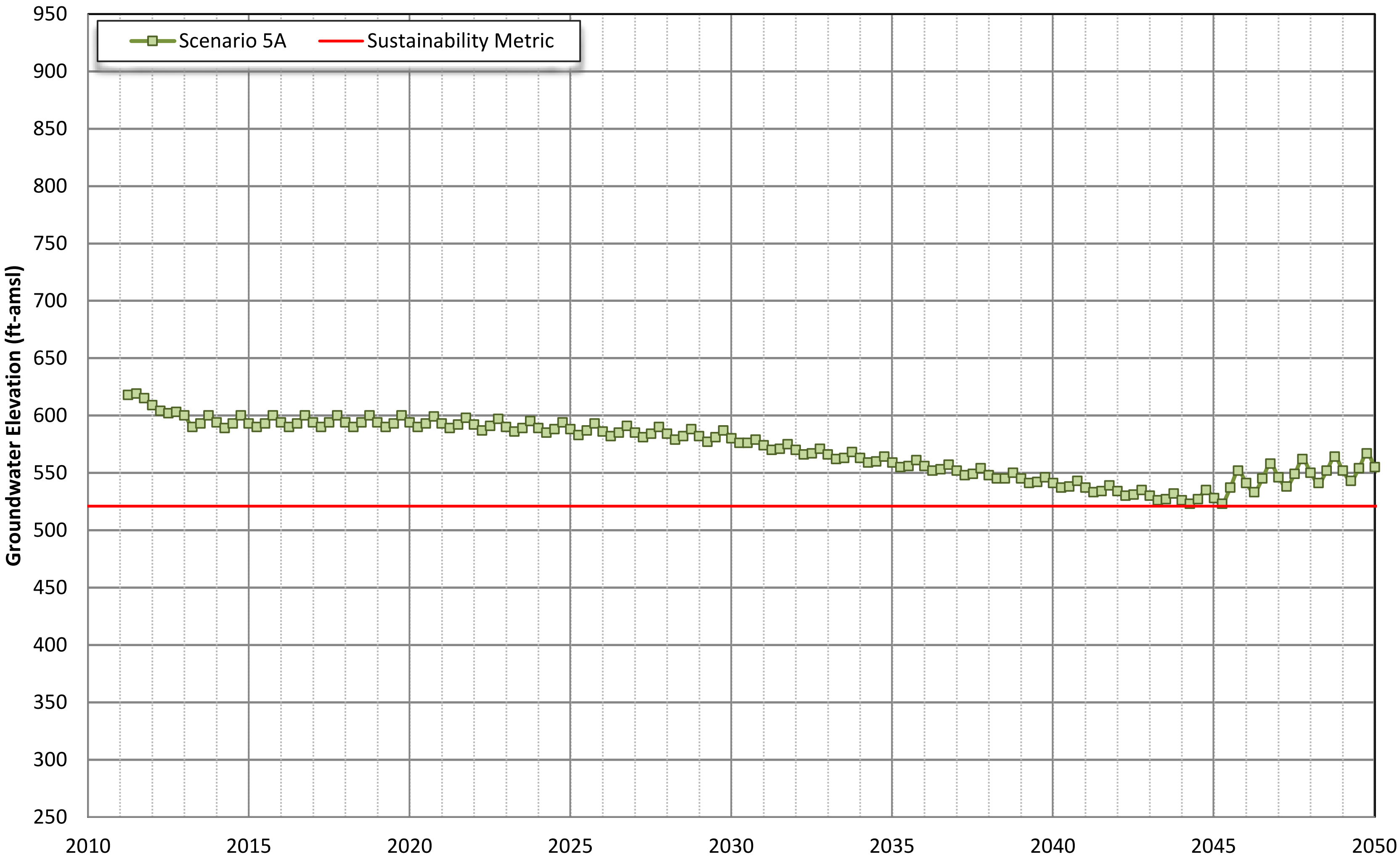

Appendix D_20150916_WellHydrographs_S5A4_Final_LBB2.xlsm
Created: 9/15/15
Printed: 9/16/2015

Figure D-104
Projected Groundwater Elevation for Scenario 5a
Monte Vista Water District Well 5

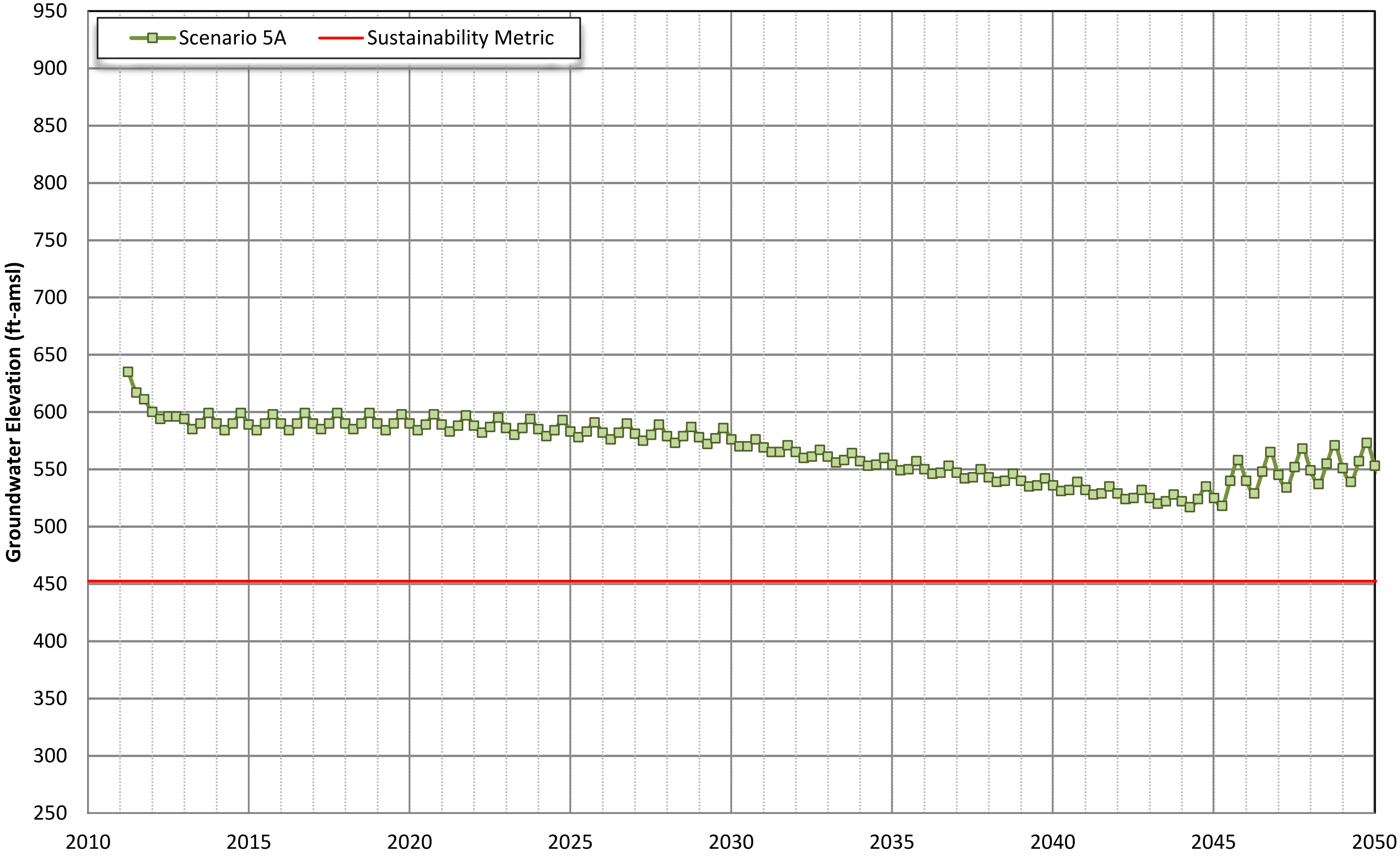

Appendix D_20150916_WellHydrographs_S5A4_Final_LBB2.xlsm
Created: 9/15/15
Printed: 9/16/2015

Figure D-105
Projected Groundwater Elevation for Scenario 5a
Monte Vista Water District Well 6

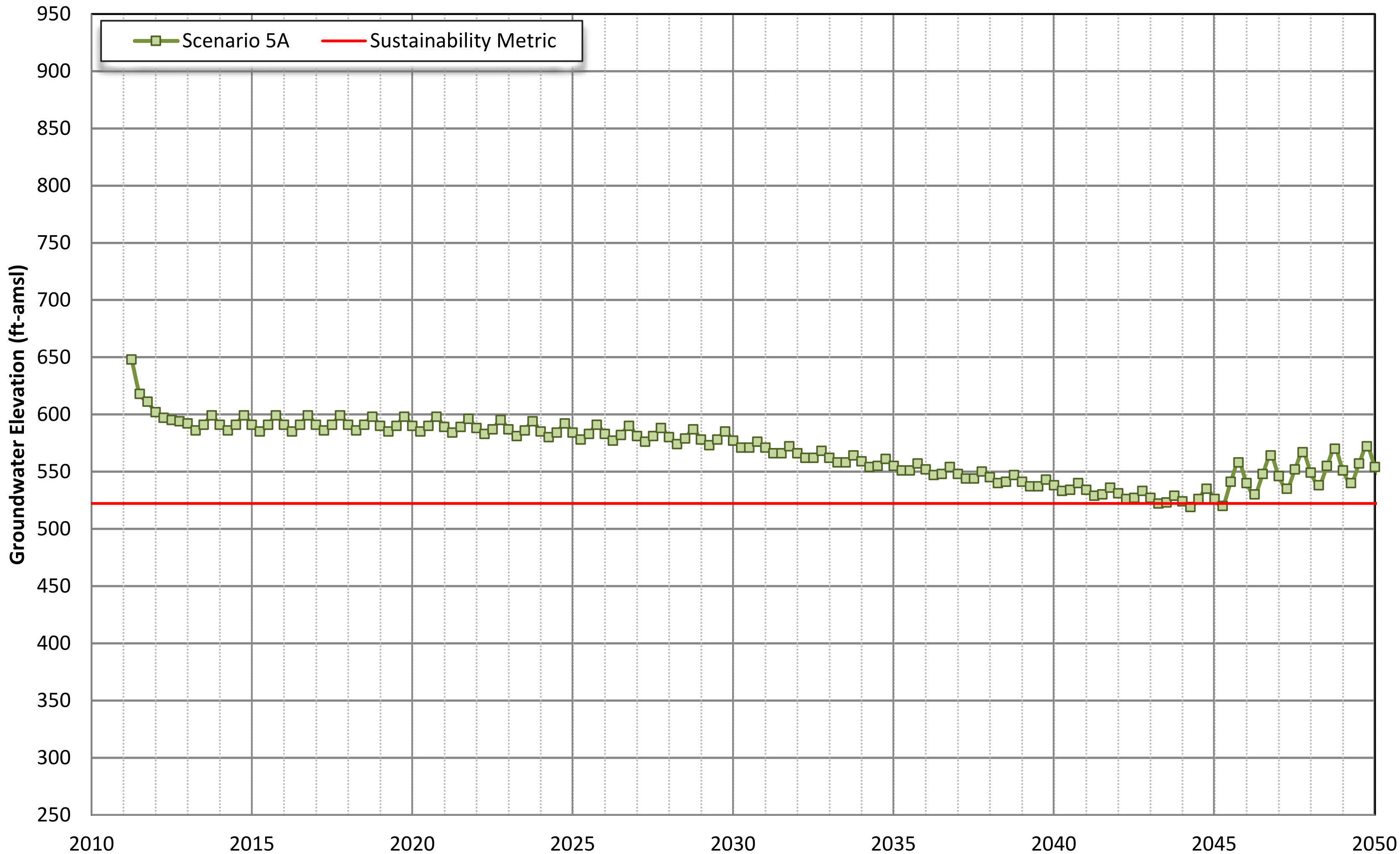

Appendix D_20150916_WellHydrographs_S5A4_Final_LBB2.xlsm
Created: 9/15/15
Printed: 9/16/2015

Figure D-106
Projected Groundwater Elevation for Scenario 5a
Monte Vista Water District Well 10

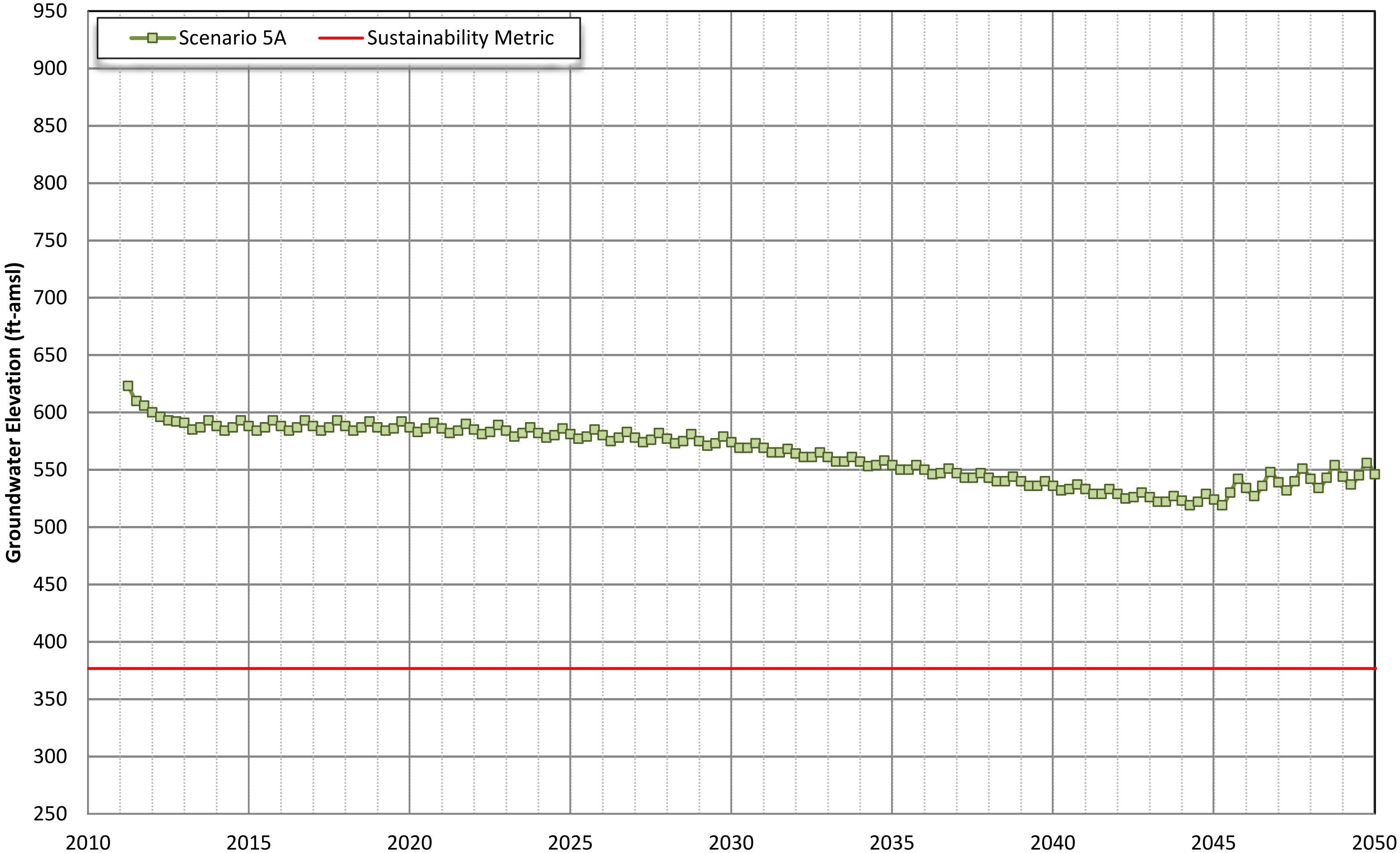

Appendix D_20150916_WellHydrographs_S5A4_Final_LBB2.xlsm
Created: 9/15/15
Printed: 9/16/2015

Figure D-107
Projected Groundwater Elevation for Scenario 5a
Monte Vista Water District Well 19

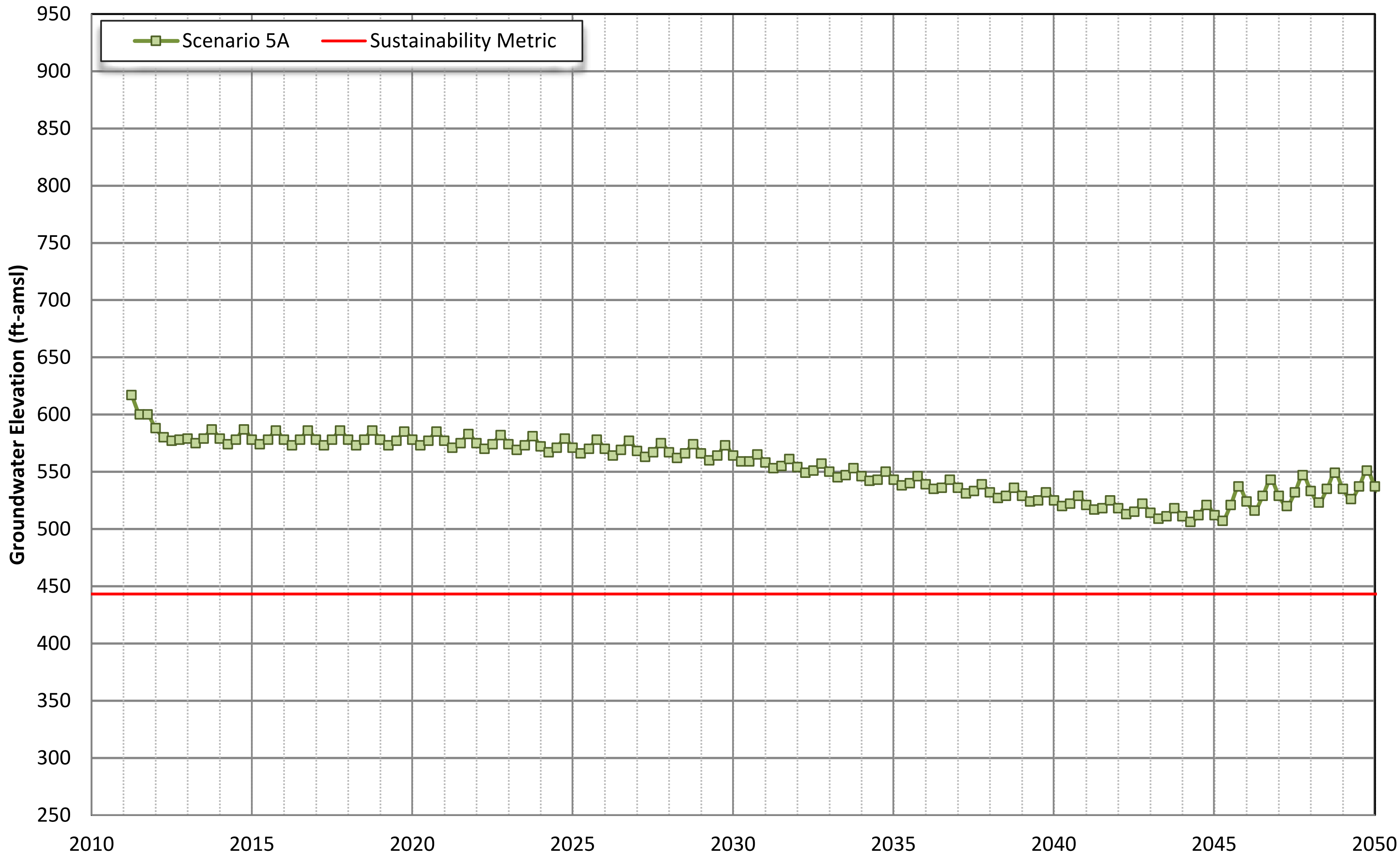

Appendix D_20150916_WellHydrographs_S5A4_Final_LBB2.xlsm
Created: 9/15/15
Printed: 9/16/2015

Figure D-108
Projected Groundwater Elevation for Scenario 5a
Monte Vista Water District Well 26

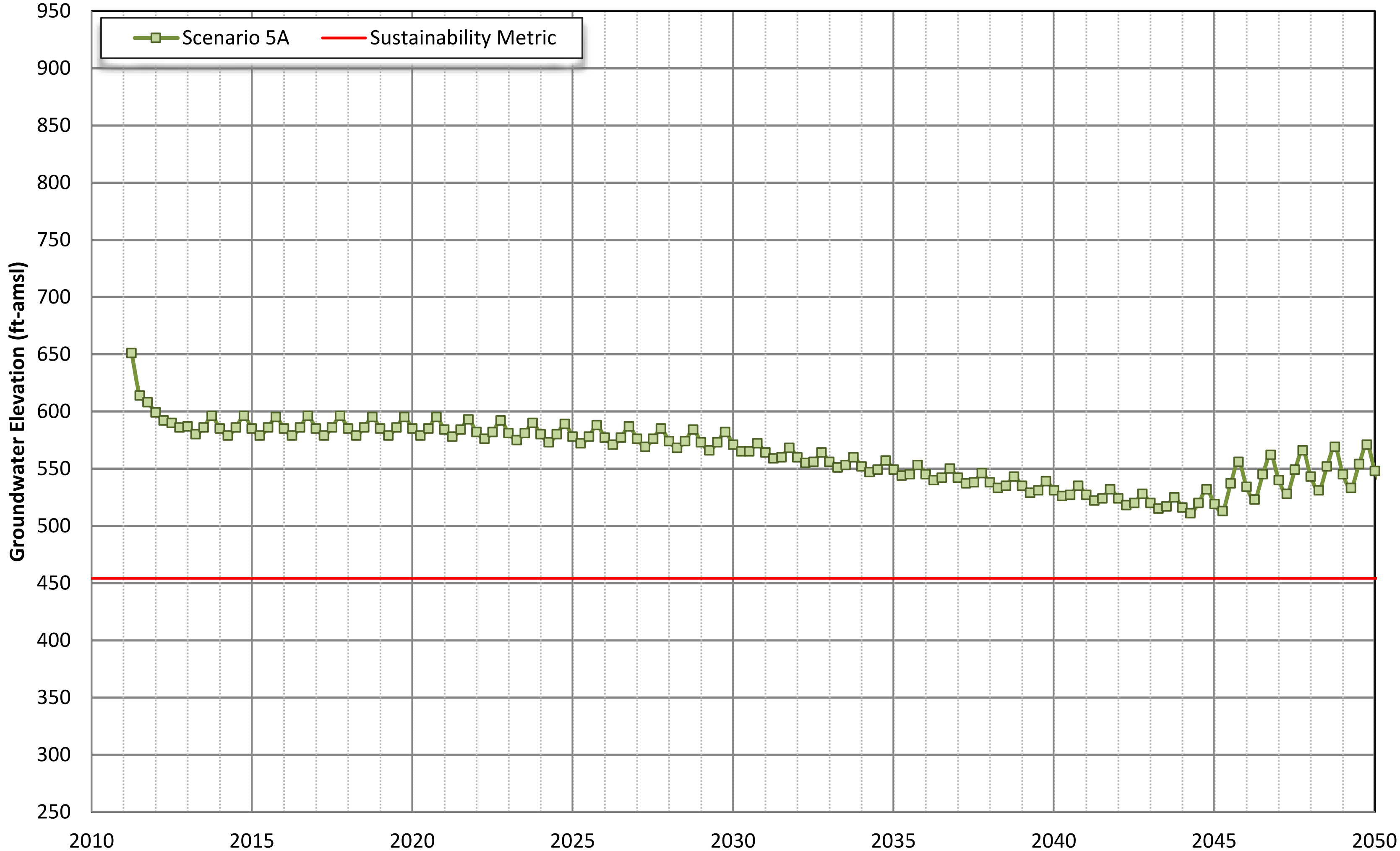

Appendix D_20150916_WellHydrographs_S5A4_Final_LBB2.xlsm
Created: 9/15/15
Printed: 9/16/2015

Figure D-109
Projected Groundwater Elevation for Scenario 5a
Monte Vista Water District Well 27

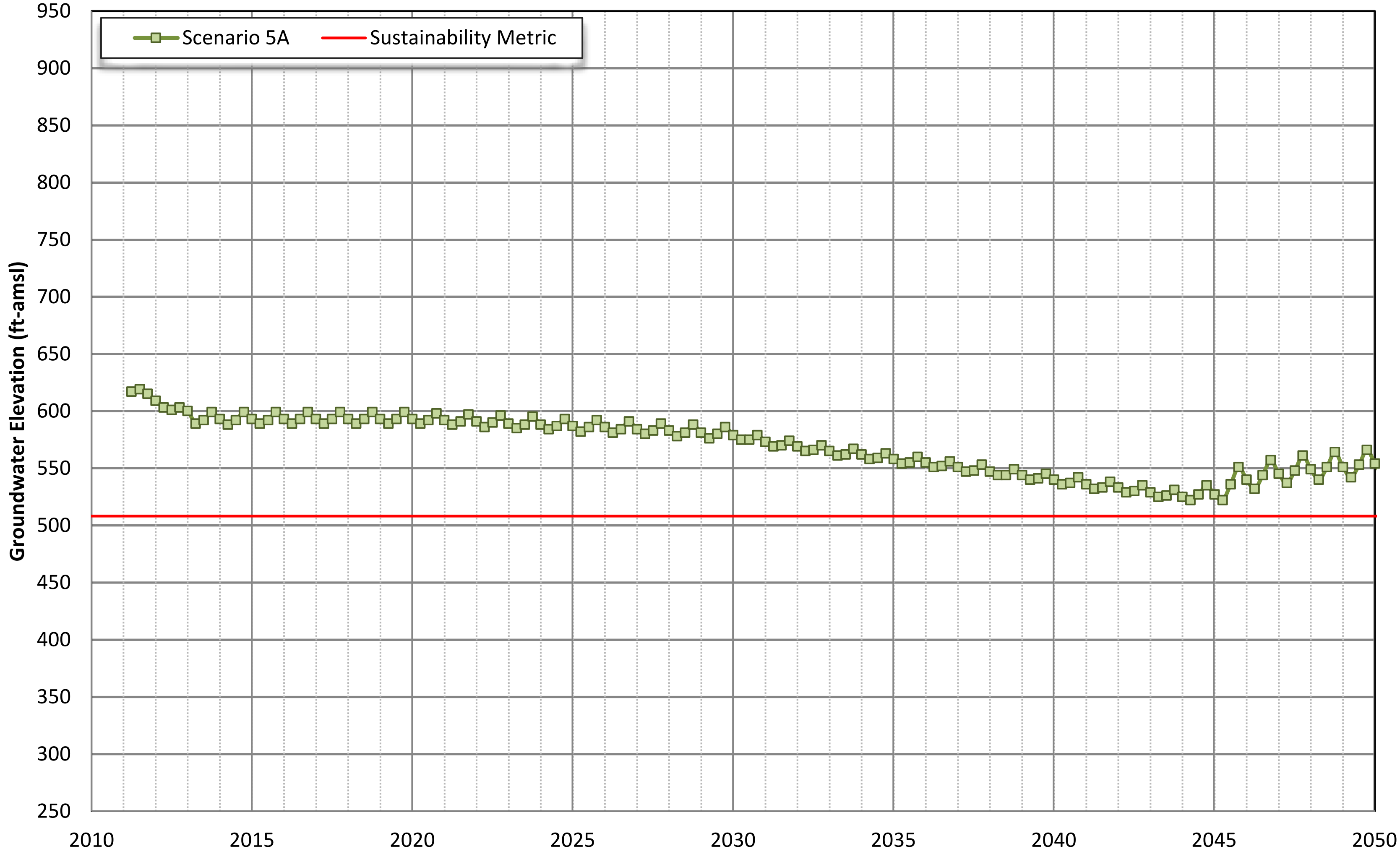

Appendix D_20150916_WellHydrographs_S5A4_Final_LBB2.xlsm
Created: 9/15/15
Printed: 9/16/2015

Figure D-110
Projected Groundwater Elevation for Scenario 5a
Monte Vista Water District Well 28

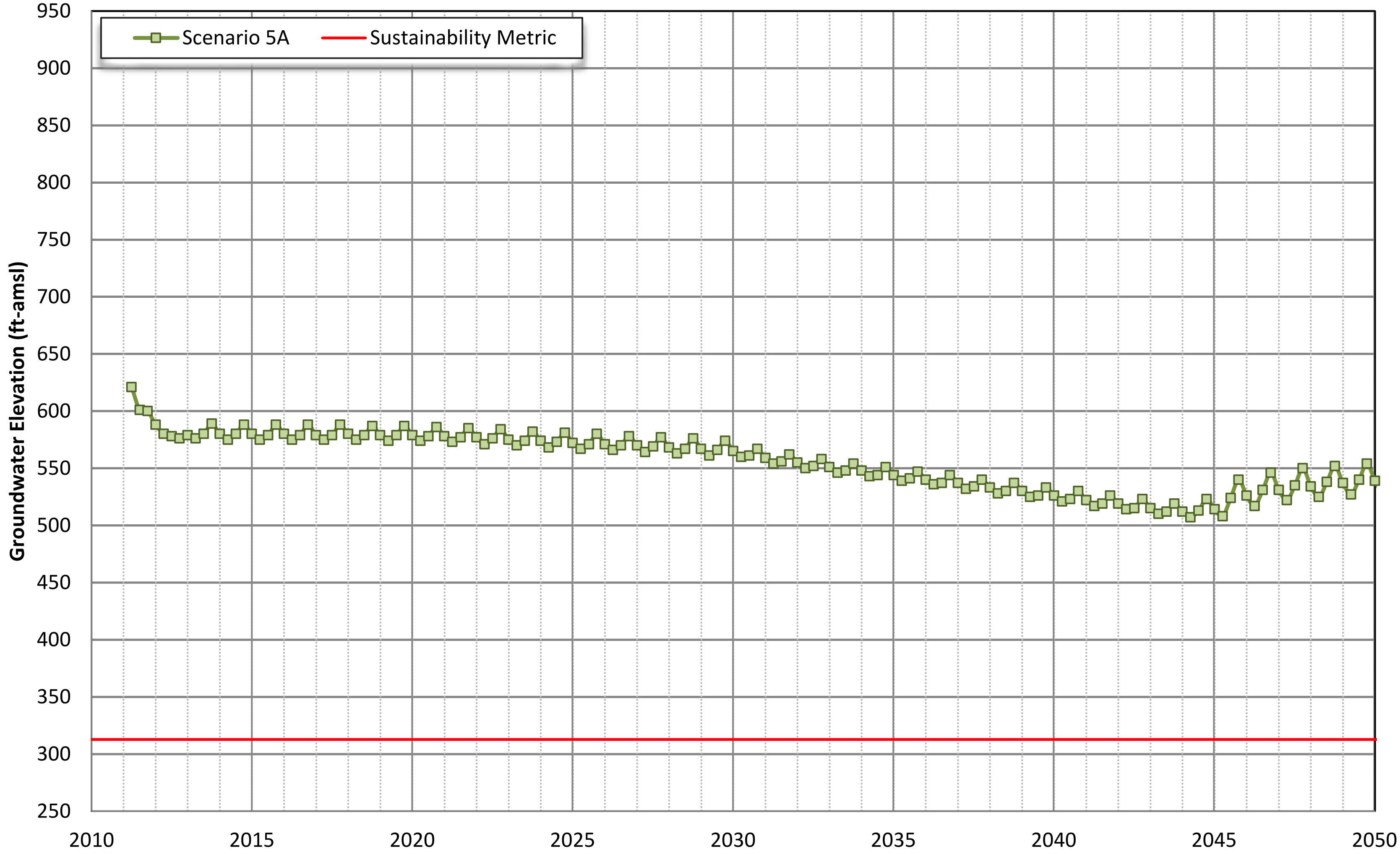

Appendix D_20150916_WellHydrographs_S5A4_Final_LBB2.xlsm
Created: 9/15/15
Printed: 9/16/2015

Figure D-111
Projected Groundwater Elevation for Scenario 5a
Monte Vista Water District Well 30

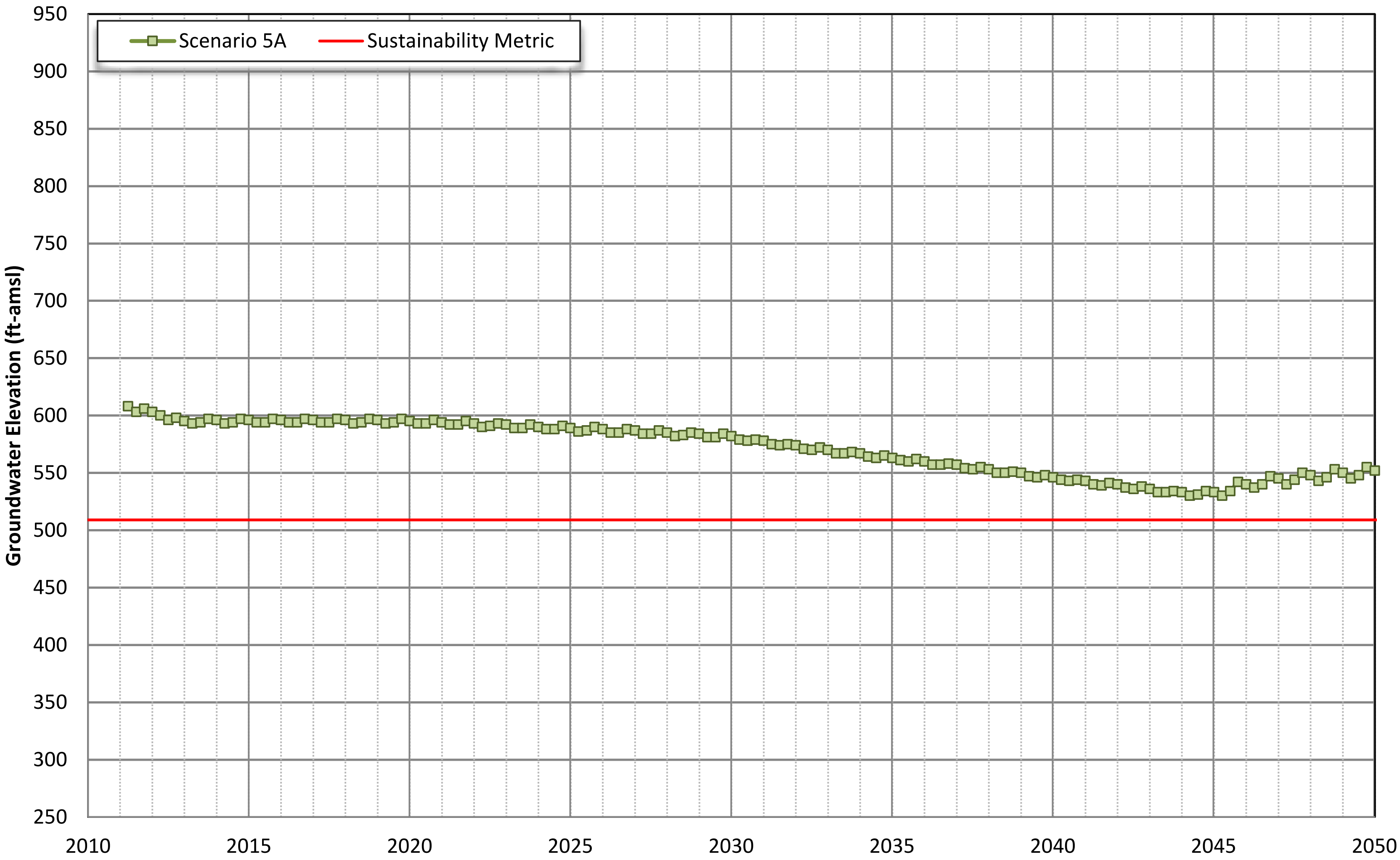

Appendix D_20150916_WellHydrographs_S5A4_Final_LBB2.xlsm
Created: 9/15/15
Printed: 9/16/2015

Figure D-112
Projected Groundwater Elevation for Scenario 5a
Monte Vista Water District Well 31

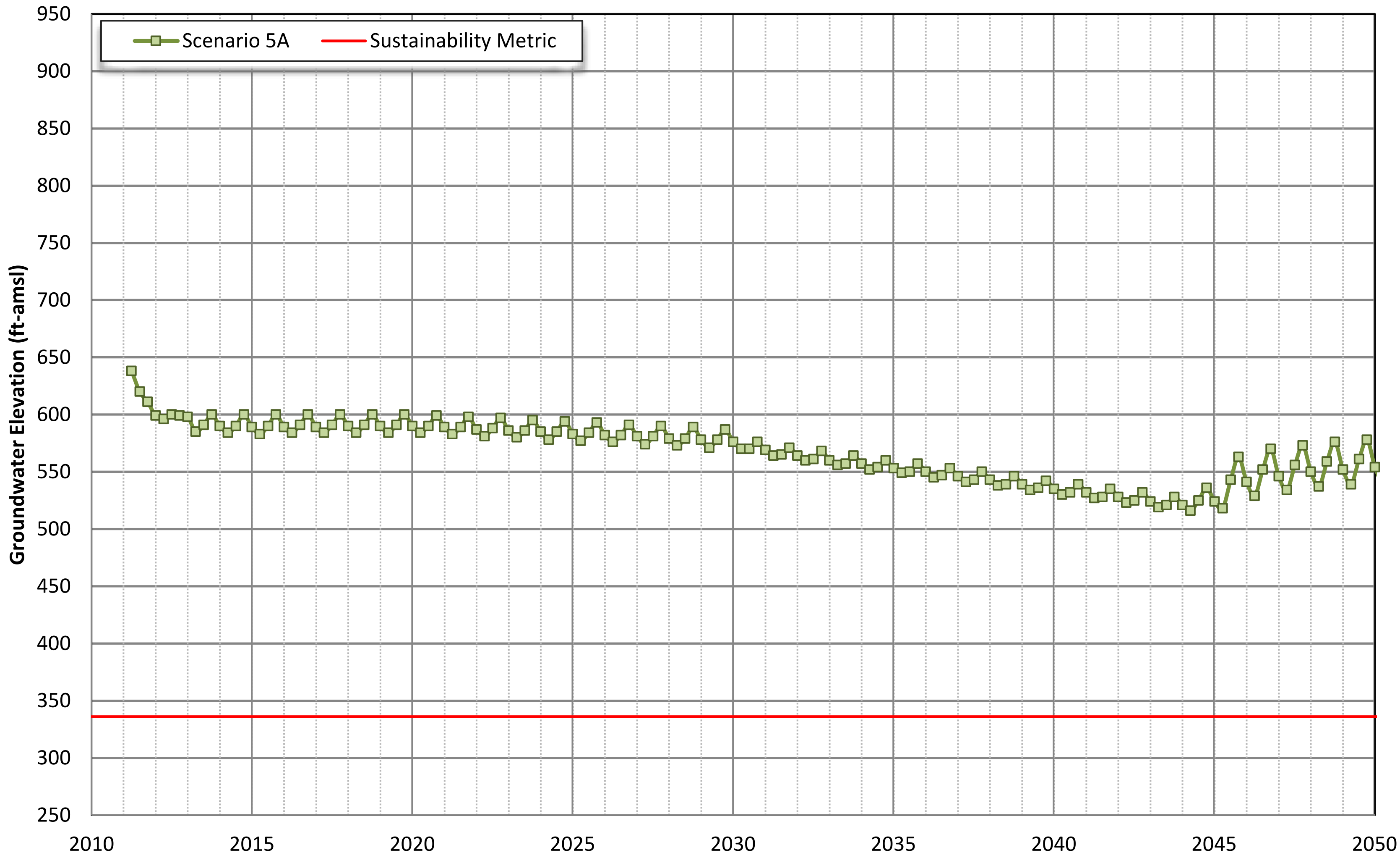

Appendix D_20150916_WellHydrographs_S5A4_Final_LBB2.xlsm
Created: 9/15/15
Printed: 9/16/2015

Figure D-113
Projected Groundwater Elevation for Scenario 5a
Monte Vista Water District Well 32

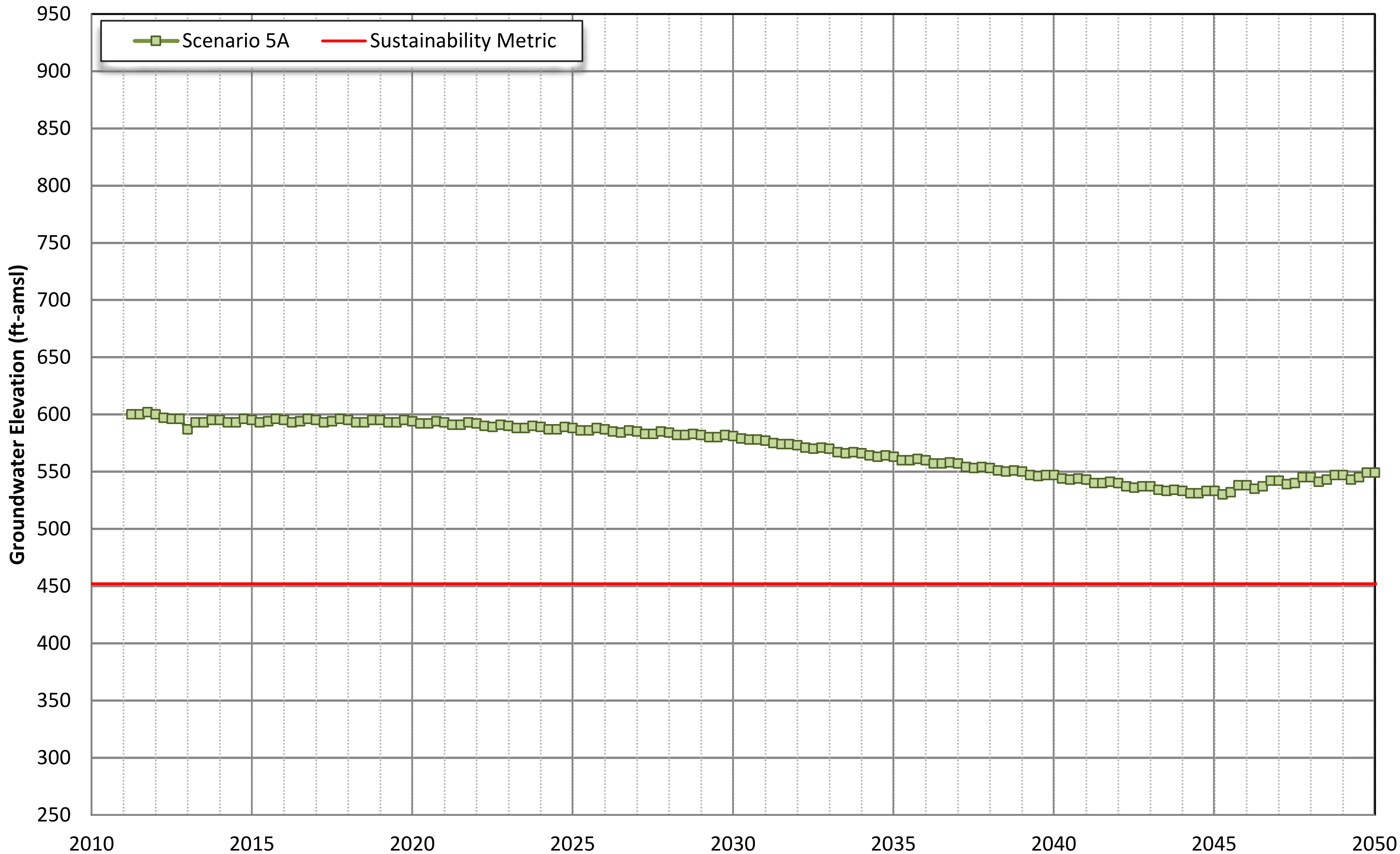

Appendix D_20150916_WellHydrographs_S5A4_Final_LBB2.xlsm
Created: 9/15/15
Printed: 9/16/2015

Figure D-114
Projected Groundwater Elevation for Scenario 5a
Monte Vista Water District Well 34

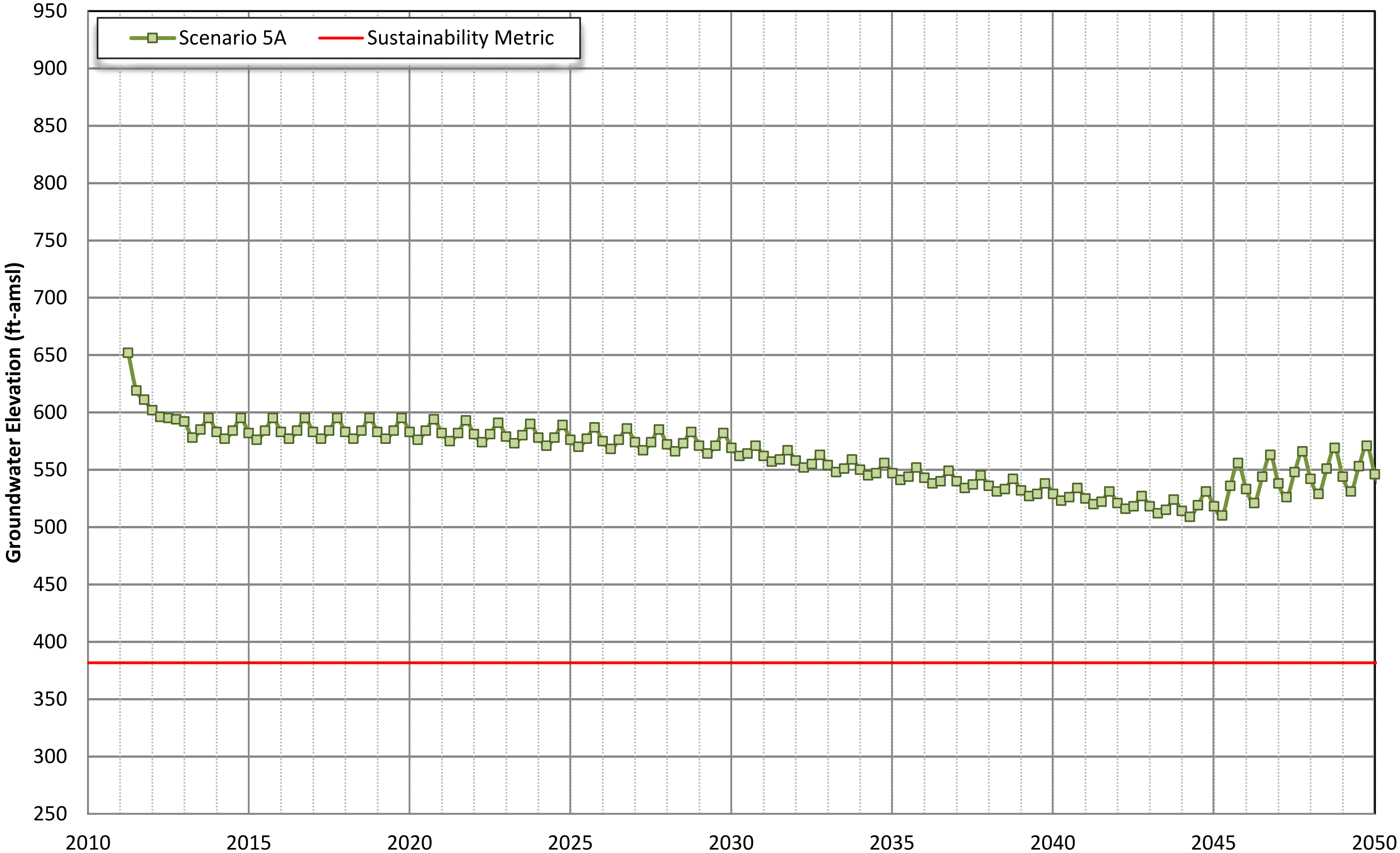

Appendix D_20150916_WellHydrographs_S5A4_Final_LBB2.xlsm
Created: 9/15/15
Printed: 9/16/2015

Figure D-115
Projected Groundwater Elevation for Scenario 5a
Monte Vista Water District Well MVWD-33

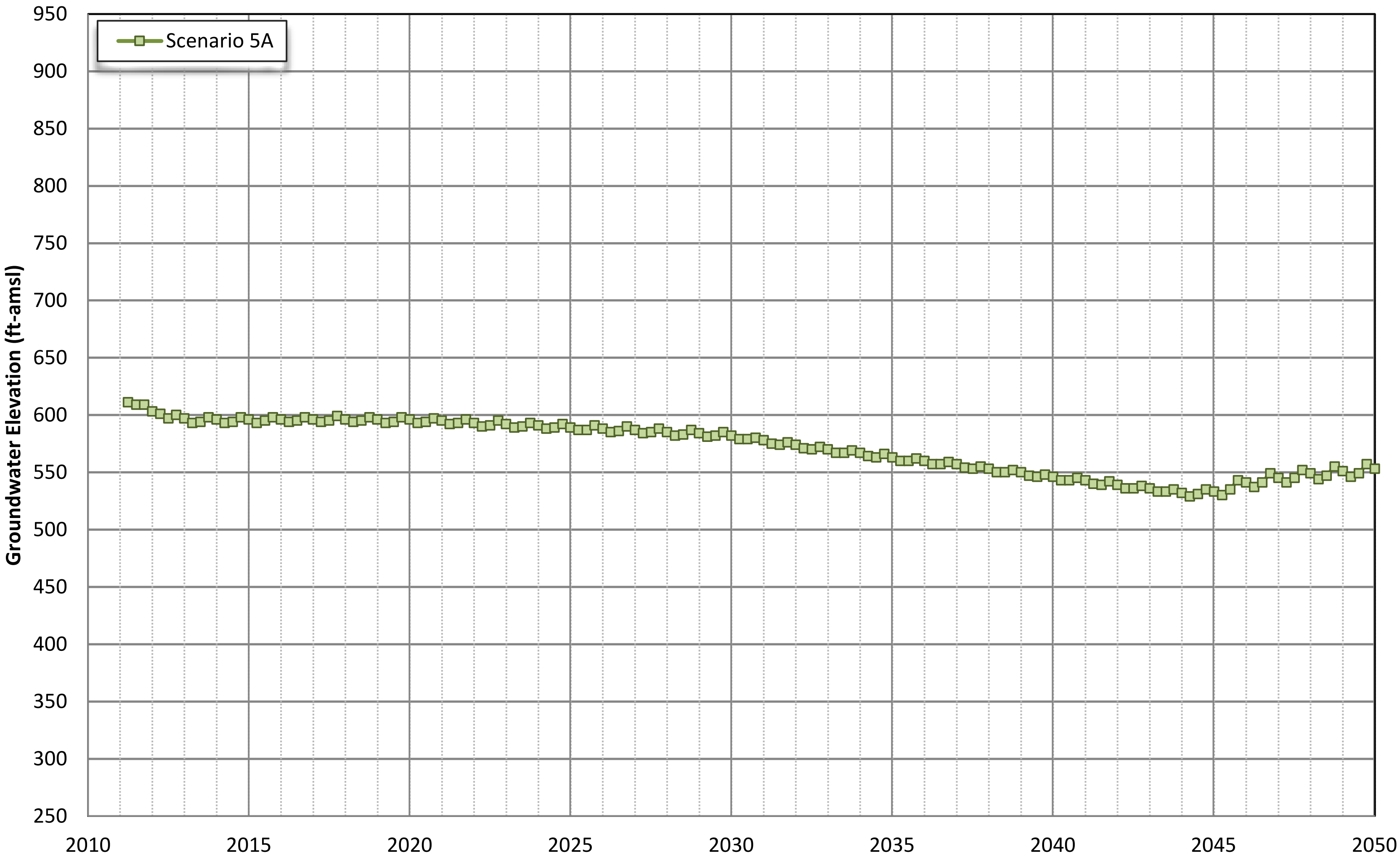

Appendix D_20150916_WellHydrographs_S5A4_Final_LBB2.xlsm
Created: 9/15/15
Printed: 9/16/2015

Figure D-116
Projected Groundwater Elevation for Scenario 5a
Monte Vista Water District Well MVWD-33

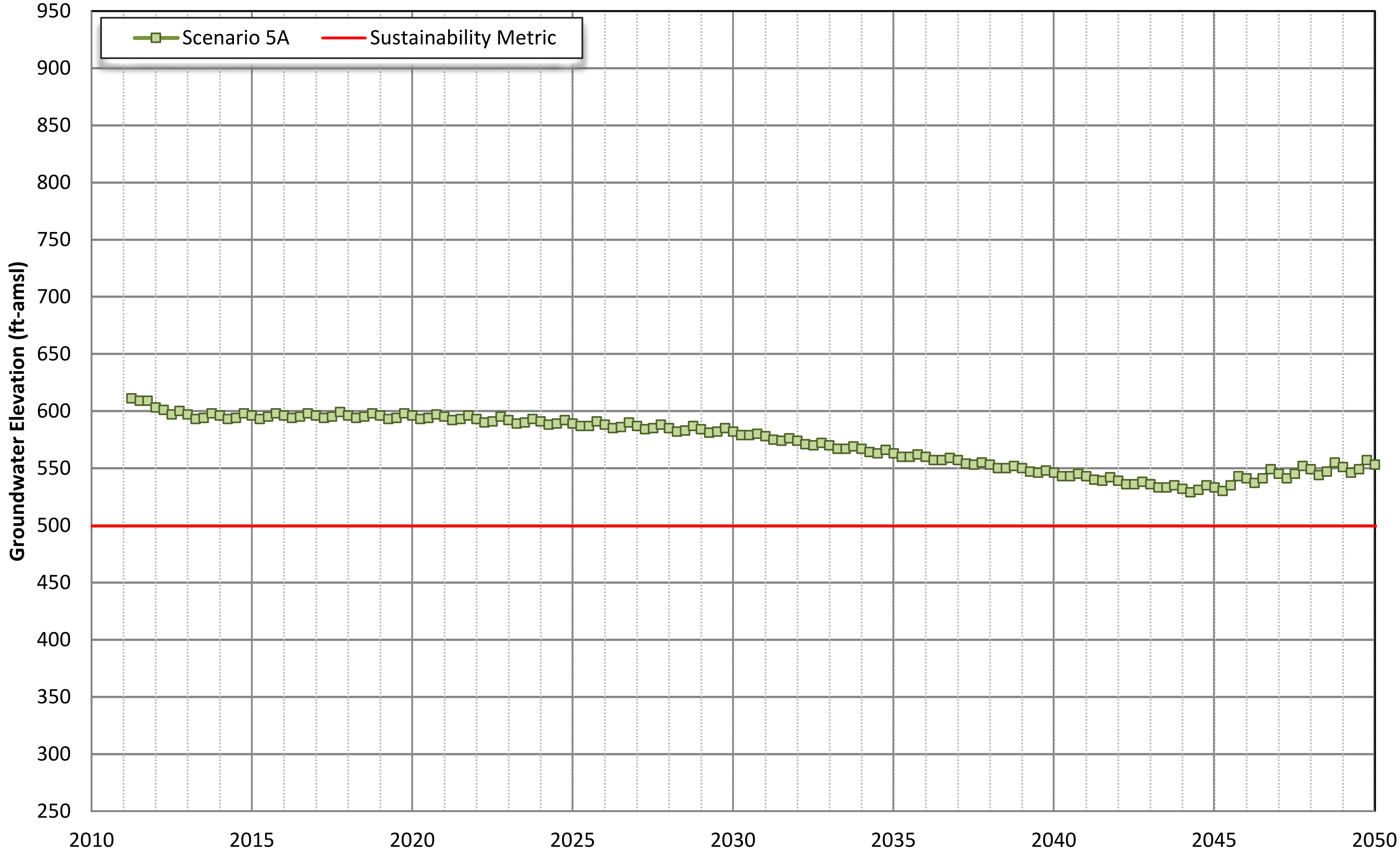

Appendix D_20150916_WellHydrographs_S5A4_Final_LBB2.xlsm
Created: 9/15/15
Printed: 9/16/2015

Figure D-117
Projected Groundwater Elevation for Scenario 5a
City of Ontario Well 9

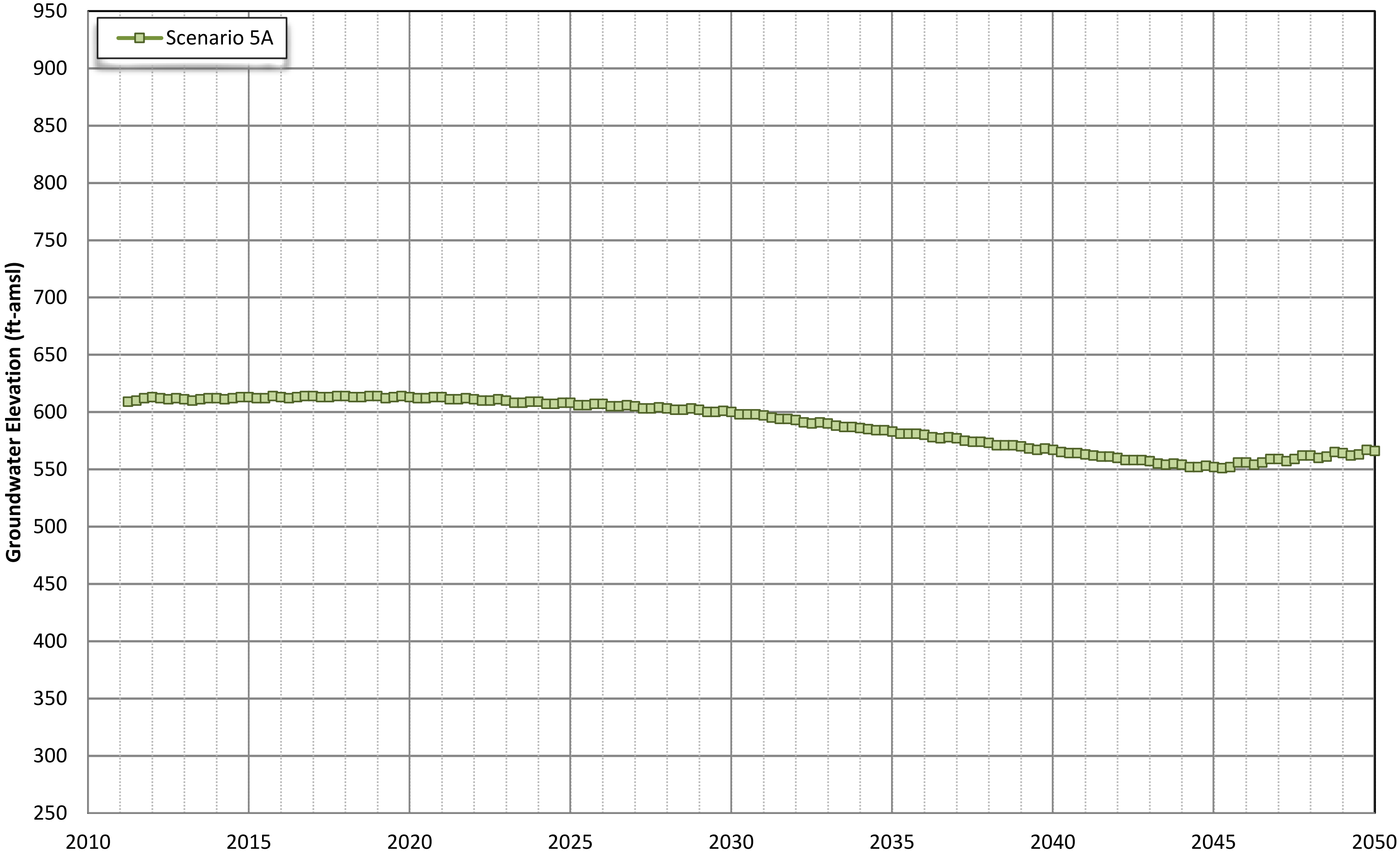

Appendix D_20150916_WellHydrographs_S5A4_Final_LBB2.xlsm
Created: 9/15/15
Printed: 9/16/2015

Figure D-118
Projected Groundwater Elevation for Scenario 5a
City of Ontario Well 16

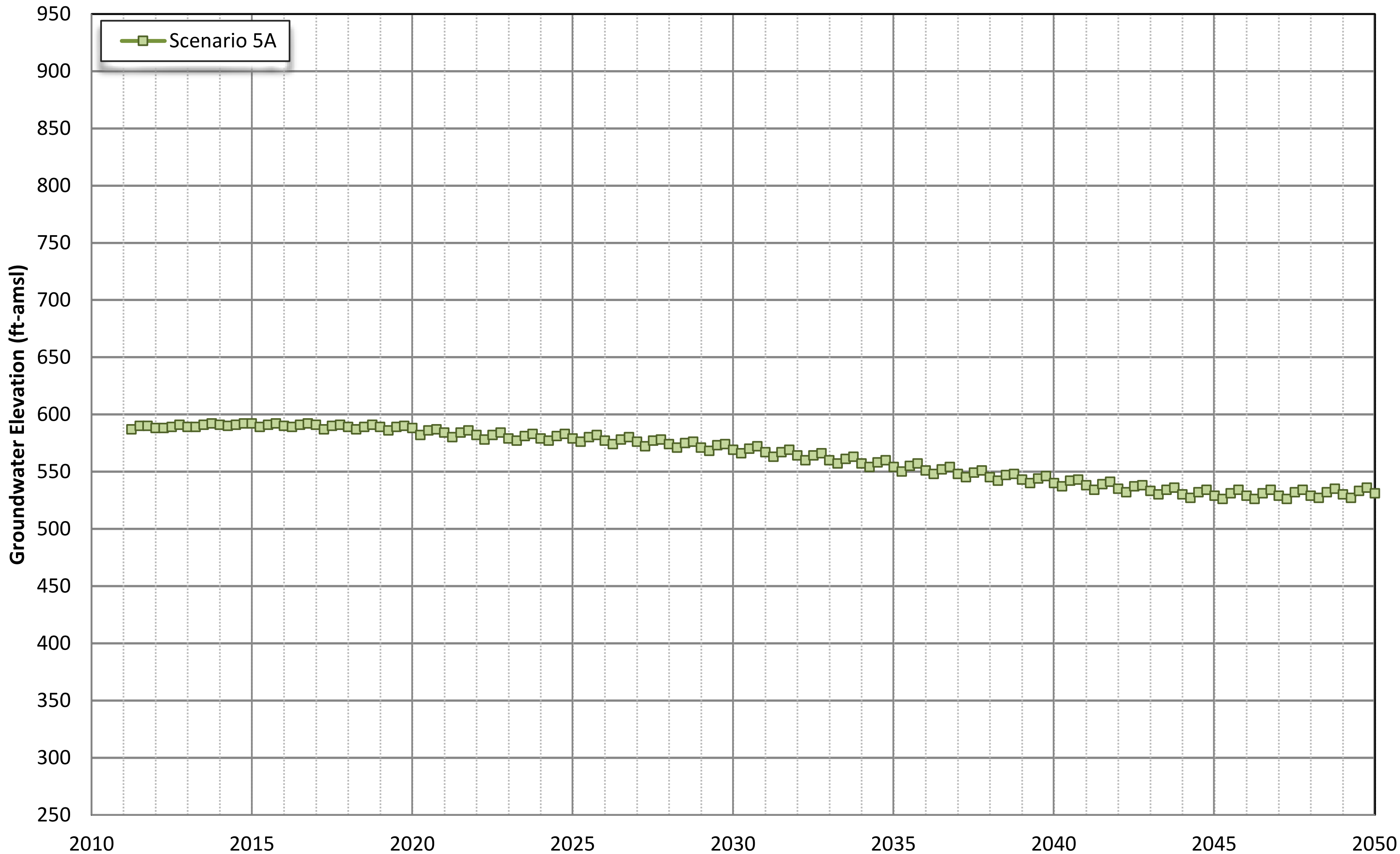

Appendix D_20150916_WellHydrographs_S5A4_Final_LBB2.xlsm
Created: 9/15/15
Printed: 9/16/2015

Figure D-119
Projected Groundwater Elevation for Scenario 5a
City of Ontario Well 17

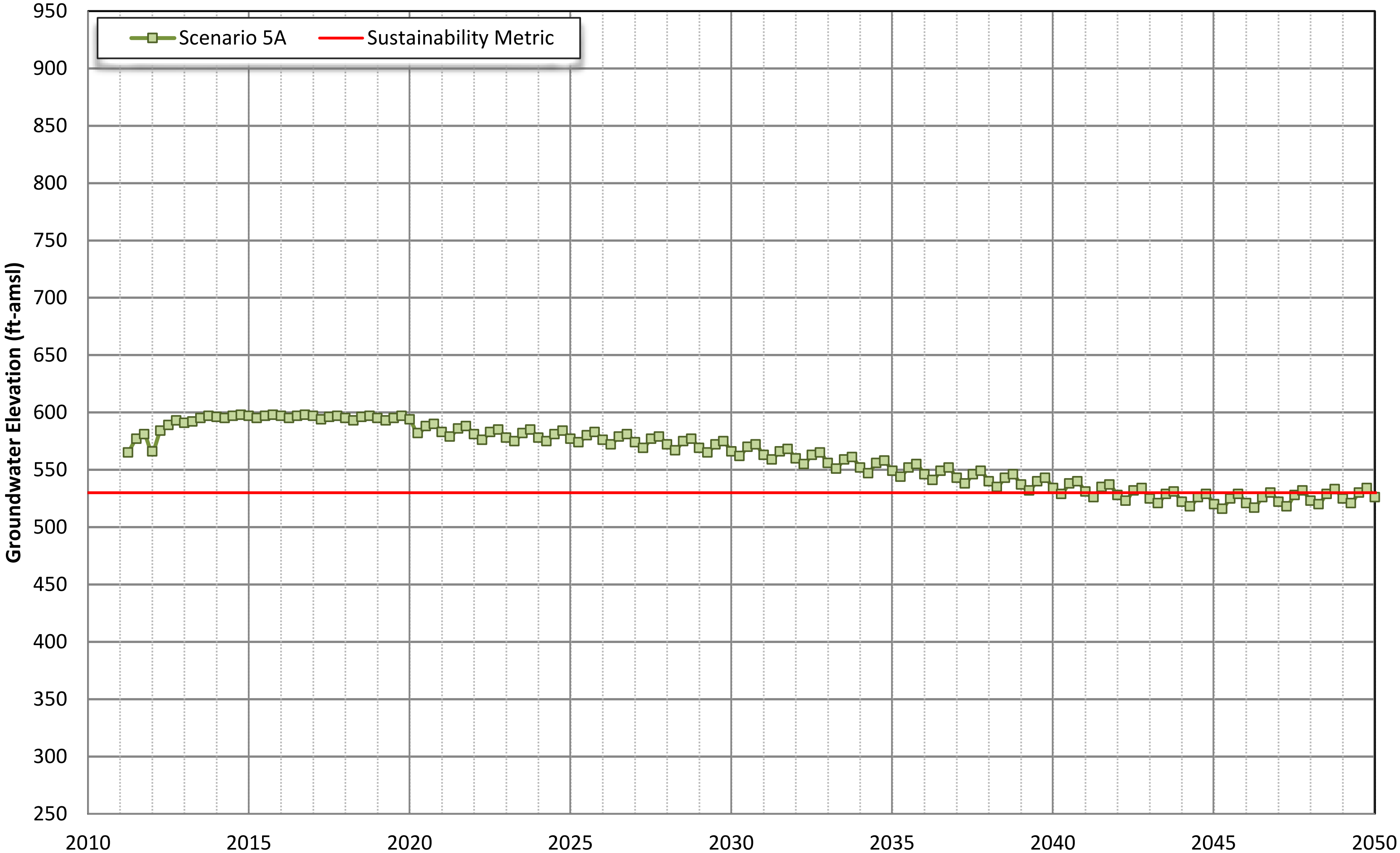

Appendix D_20150916_WellHydrographs_S5A4_Final_LBB2.xlsm
Created: 9/15/15
Printed: 9/16/2015

Figure D-120
Projected Groundwater Elevation for Scenario 5a
City of Ontario Well 20

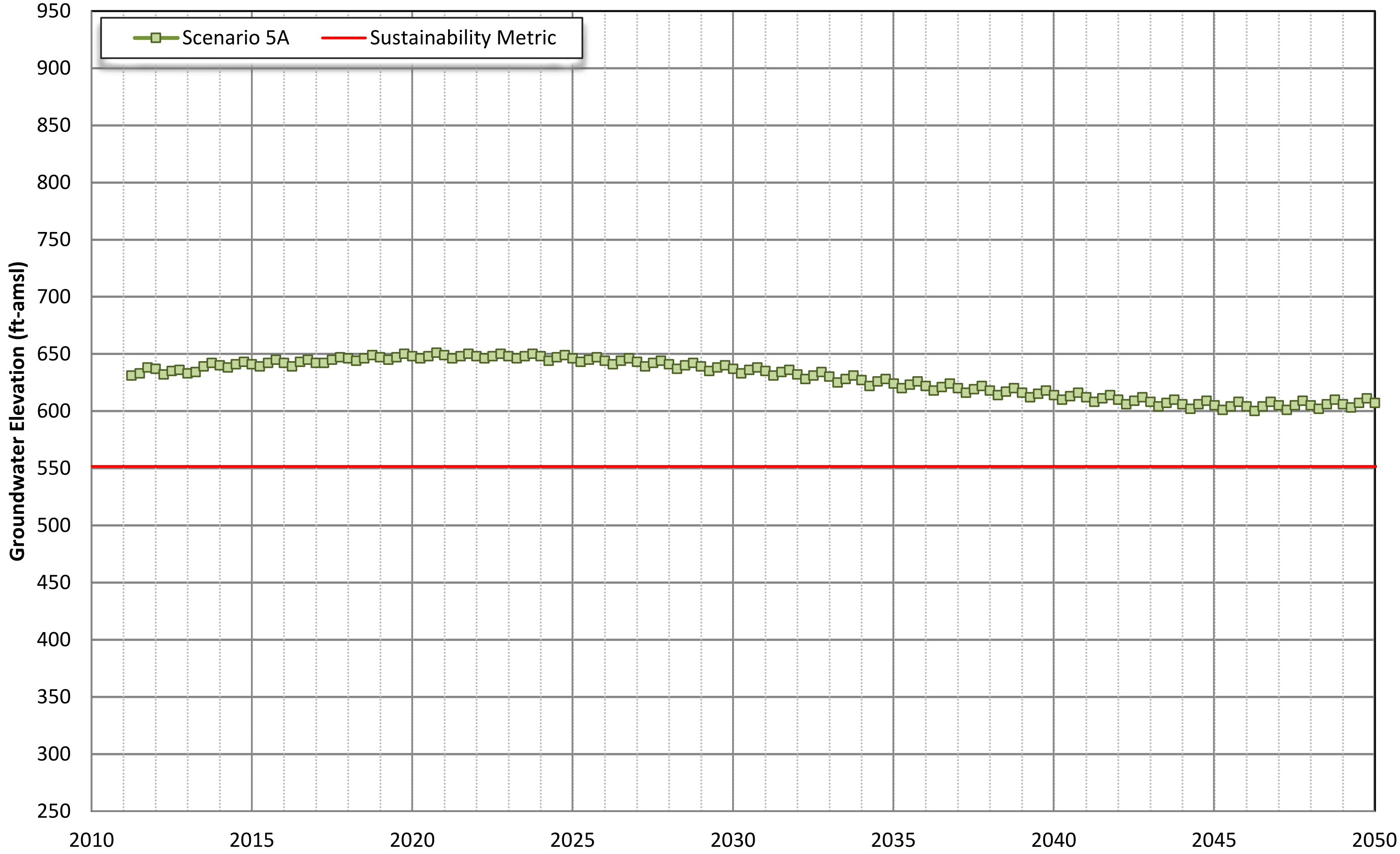

Appendix D_20150916_WellHydrographs_S5A4_Final_LBB2.xlsm
Created: 9/15/15
Printed: 9/16/2015

Figure D-121
Projected Groundwater Elevation for Scenario 5a
City of Ontario Well 24

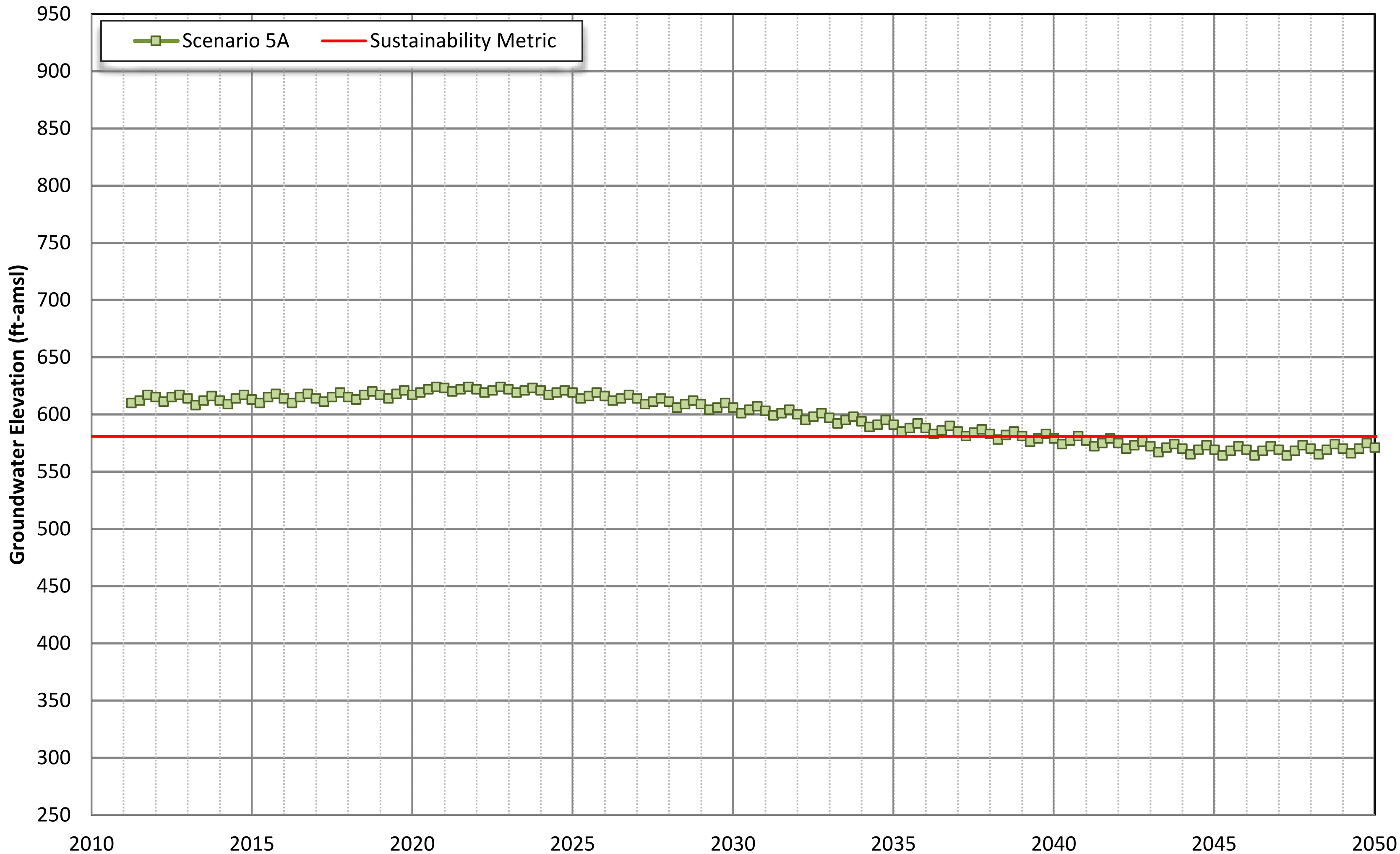

Appendix D_20150916_WellHydrographs_S5A4_Final_LBB2.xlsm
Created: 9/15/15
Printed: 9/16/2015

Figure D-122
Projected Groundwater Elevation for Scenario 5a
City of Ontario Well 25

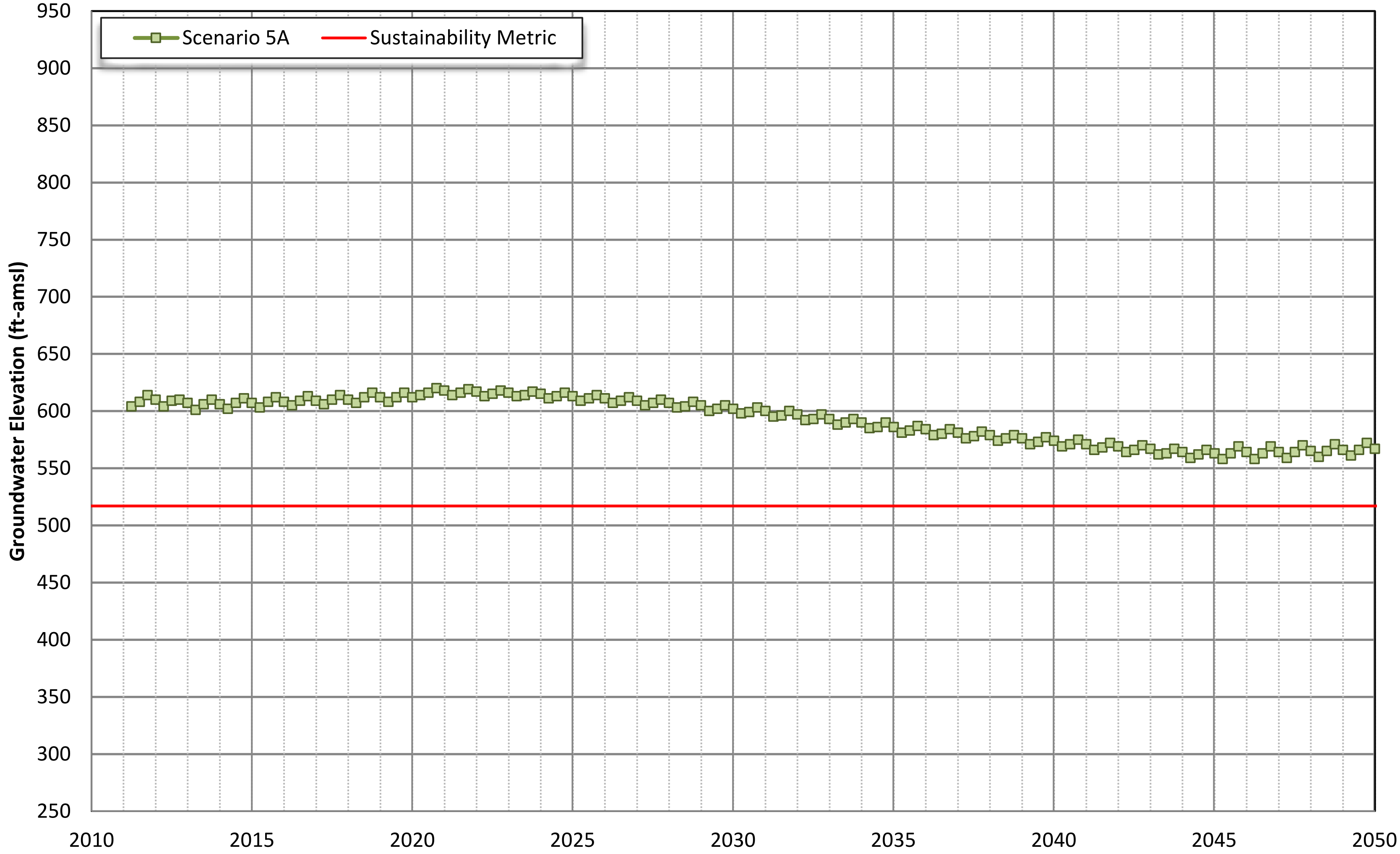

Appendix D_20150916_WellHydrographs_S5A4_Final_LBB2.xlsm
Created: 9/15/15
Printed: 9/16/2015

Figure D-123
Projected Groundwater Elevation for Scenario 5a
City of Ontario Well 26

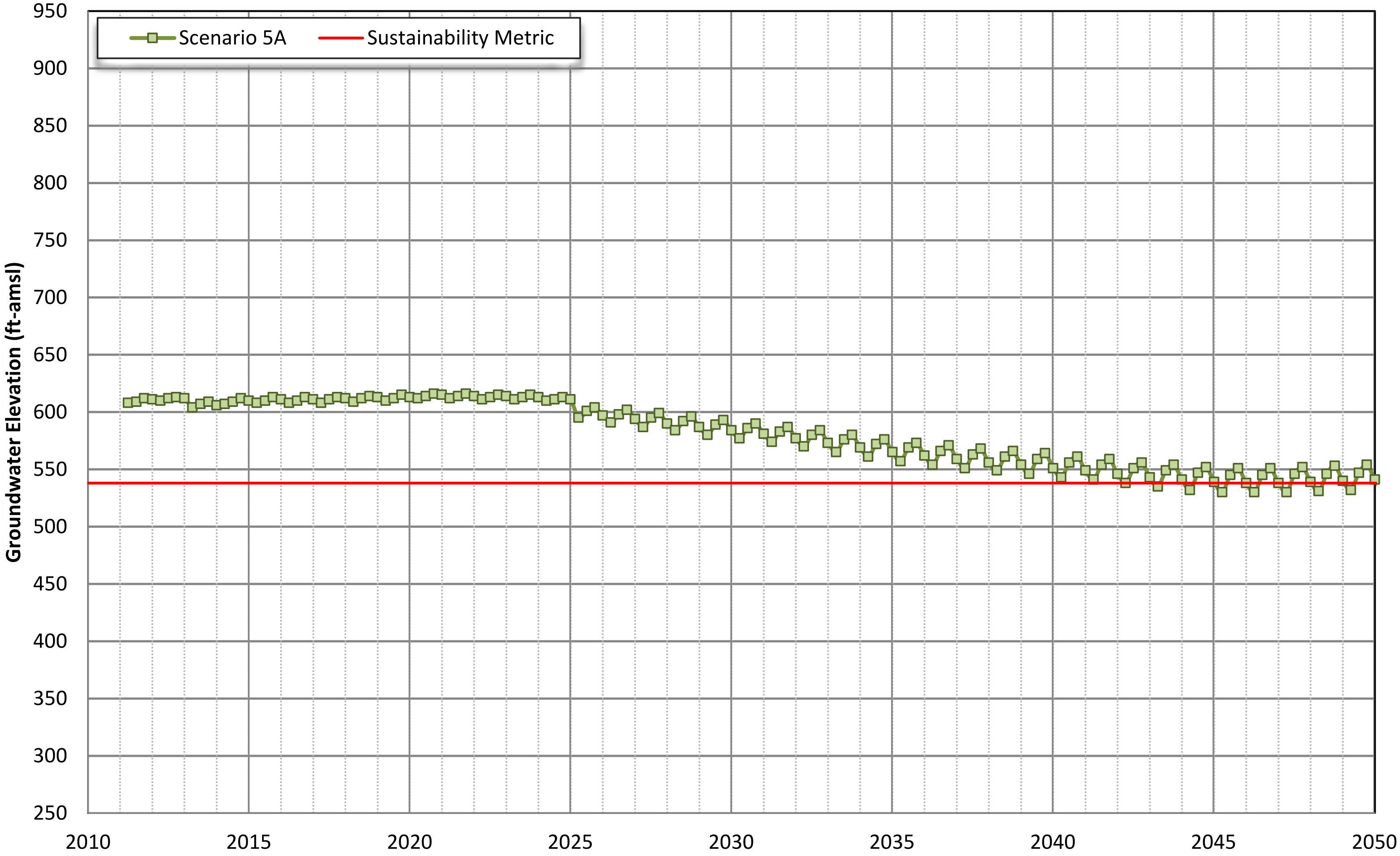

Appendix D_20150916_WellHydrographs_S5A4_Final_LBB2.xlsm
Created: 9/15/15
Printed: 9/16/2015

Figure D-124
Projected Groundwater Elevation for Scenario 5a
City of Ontario Well 27

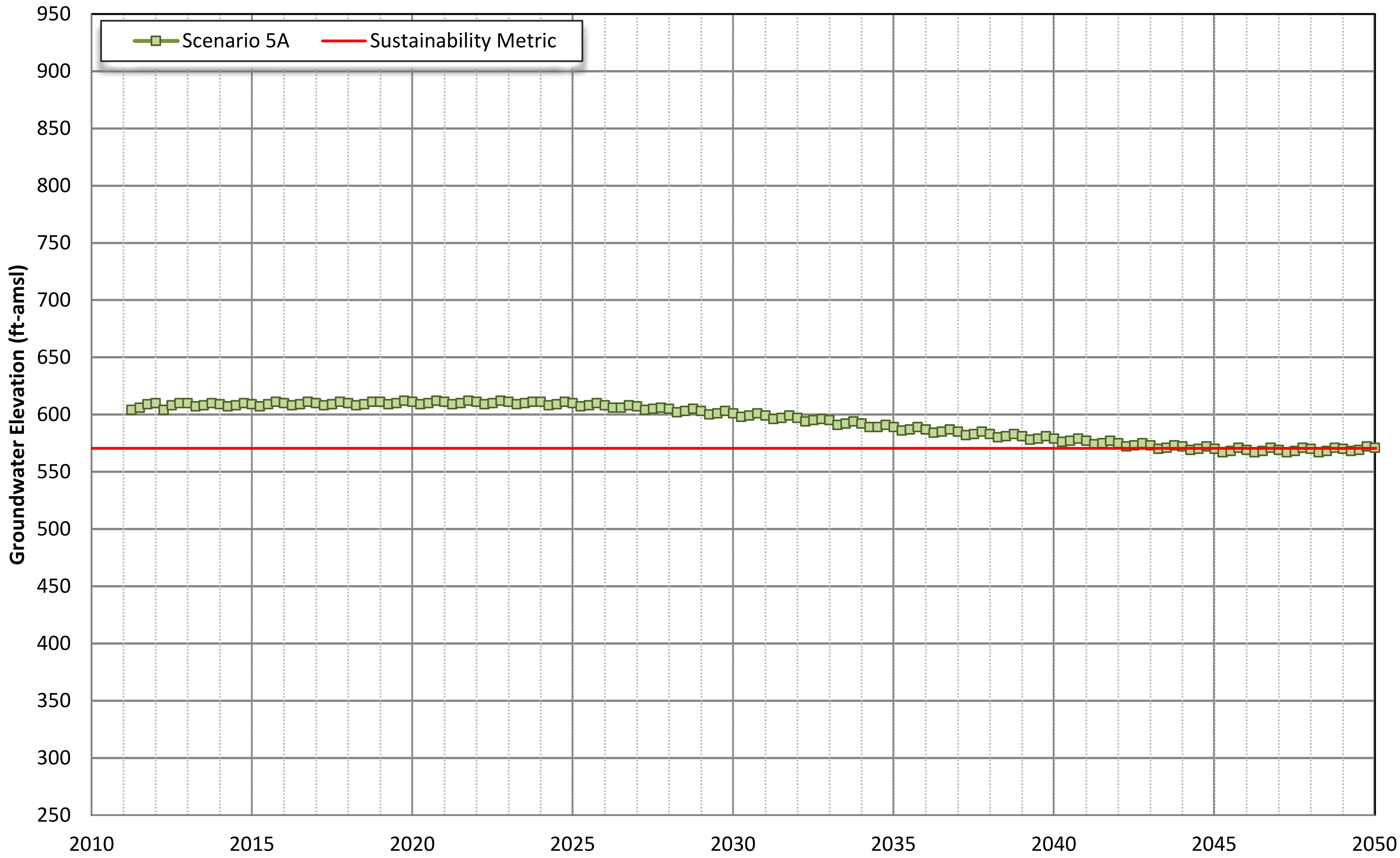

Appendix D_20150916_WellHydrographs_S5A4_Final_LBB2.xlsm
Created: 9/15/15
Printed: 9/16/2015

Figure D-125
Projected Groundwater Elevation for Scenario 5a
City of Ontario Well 29

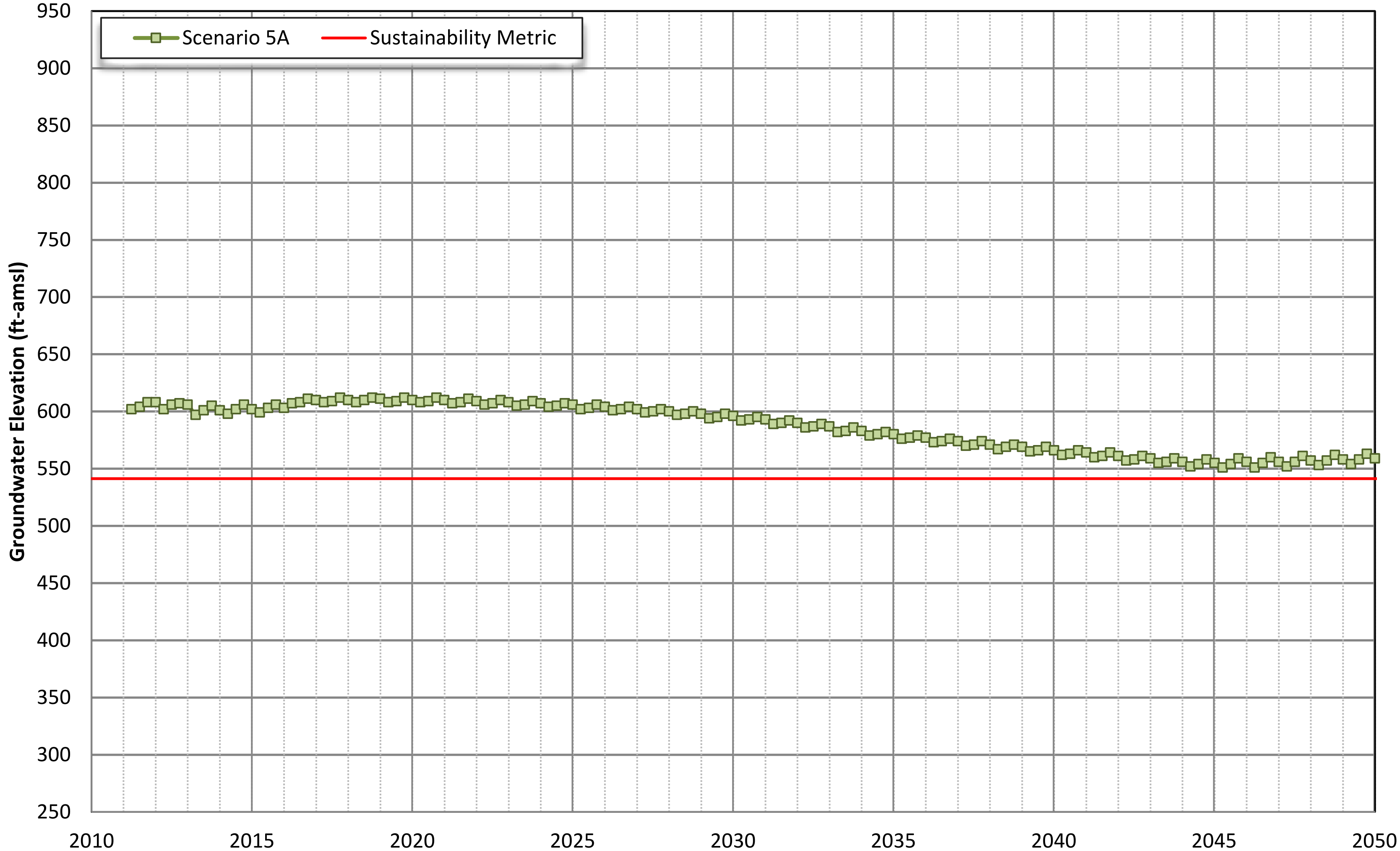

Appendix D_20150916_WellHydrographs_S5A4_Final_LBB2.xlsm
Created: 9/15/15
Printed: 9/16/2015

Figure D-126
Projected Groundwater Elevation for Scenario 5a
City of Ontario Well 30

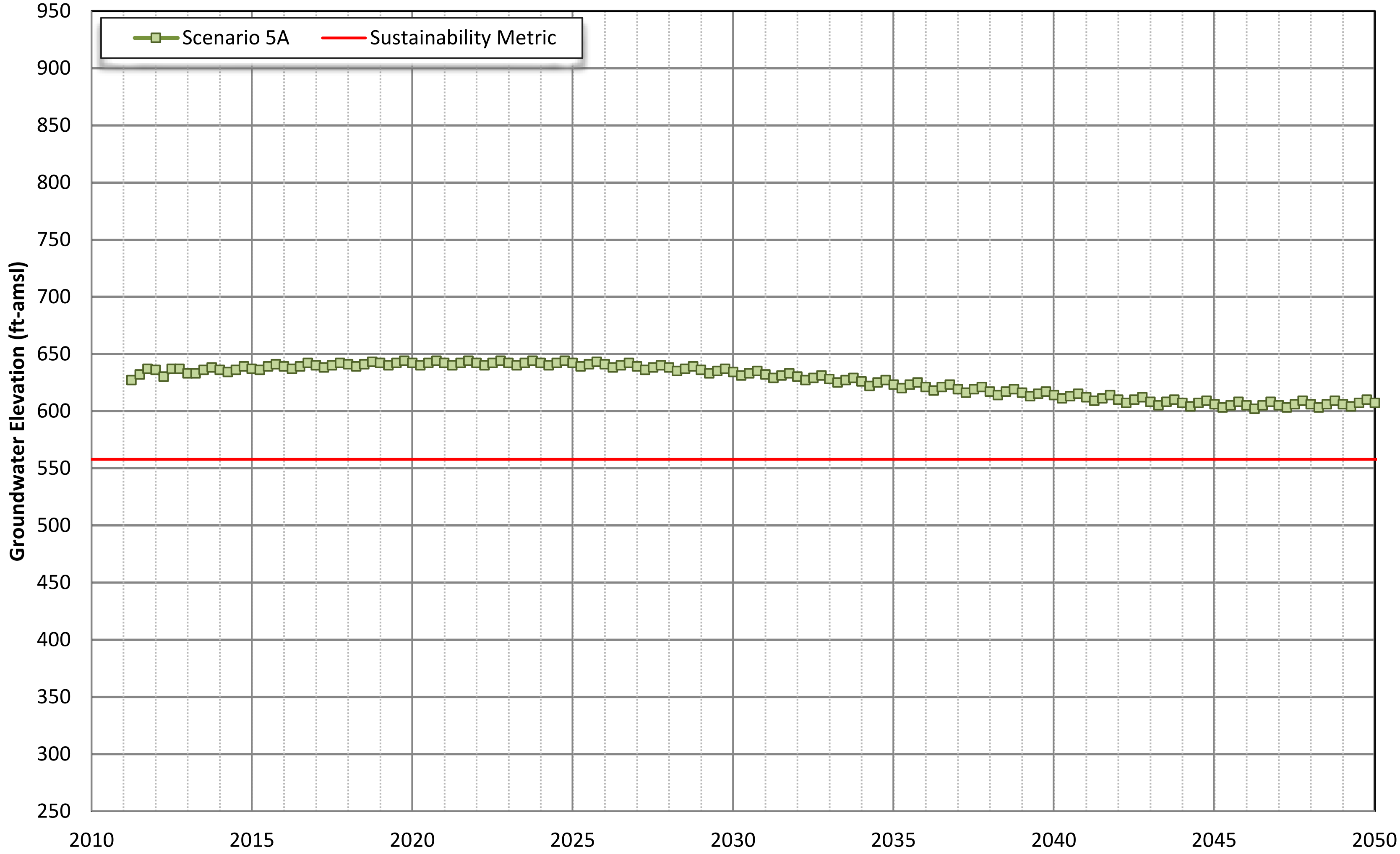

Appendix D_20150916_WellHydrographs_S5A4_Final_LBB2.xlsm
Created: 9/15/15
Printed: 9/16/2015

Figure D-127
Projected Groundwater Elevation for Scenario 5a
City of Ontario Well 31

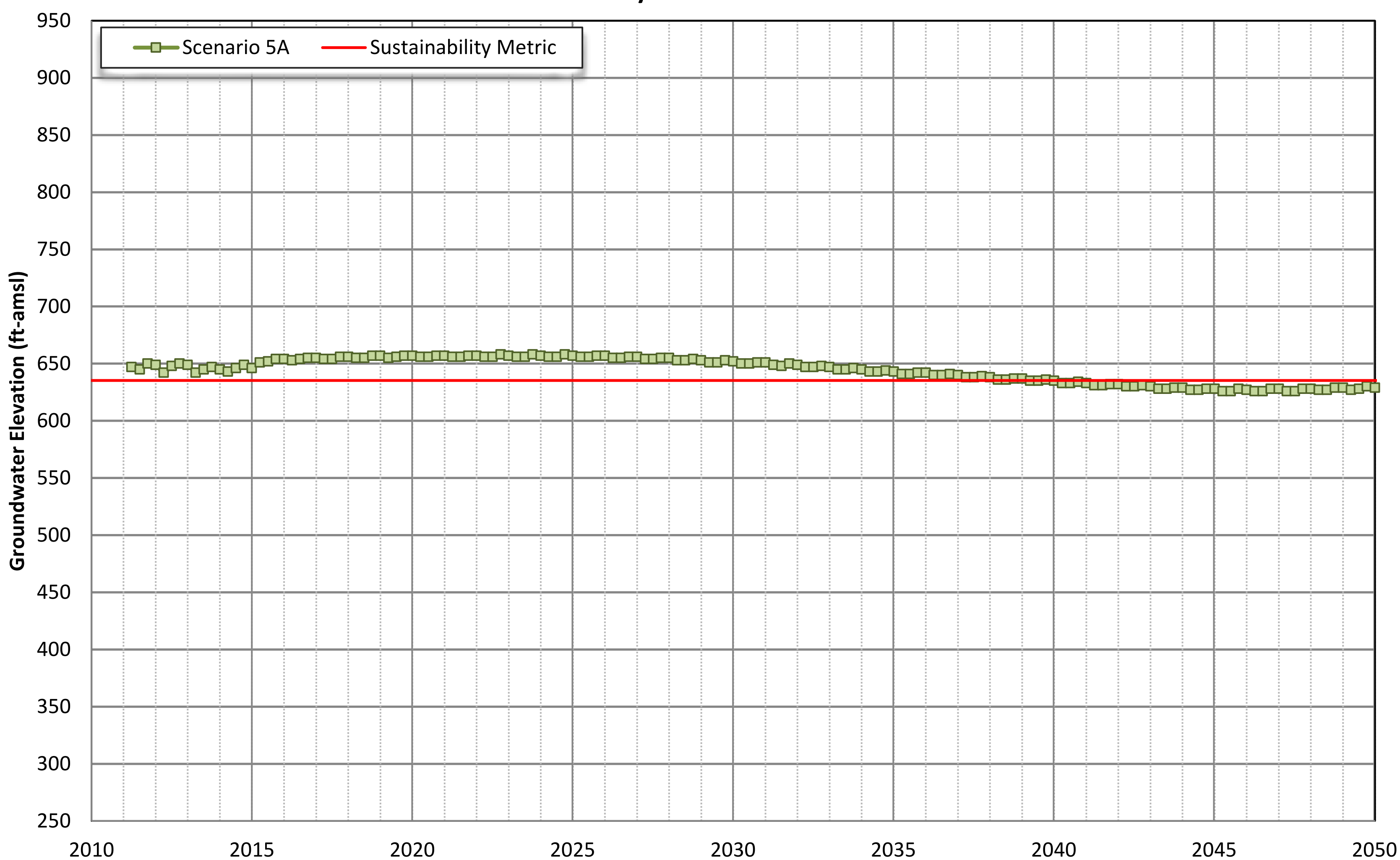

Appendix D_20150916_WellHydrographs_S5A4_Final_LBB2.xlsm
Created: 9/15/15
Printed: 9/16/2015

Figure D-128
Projected Groundwater Elevation for Scenario 5a
City of Ontario Well 34

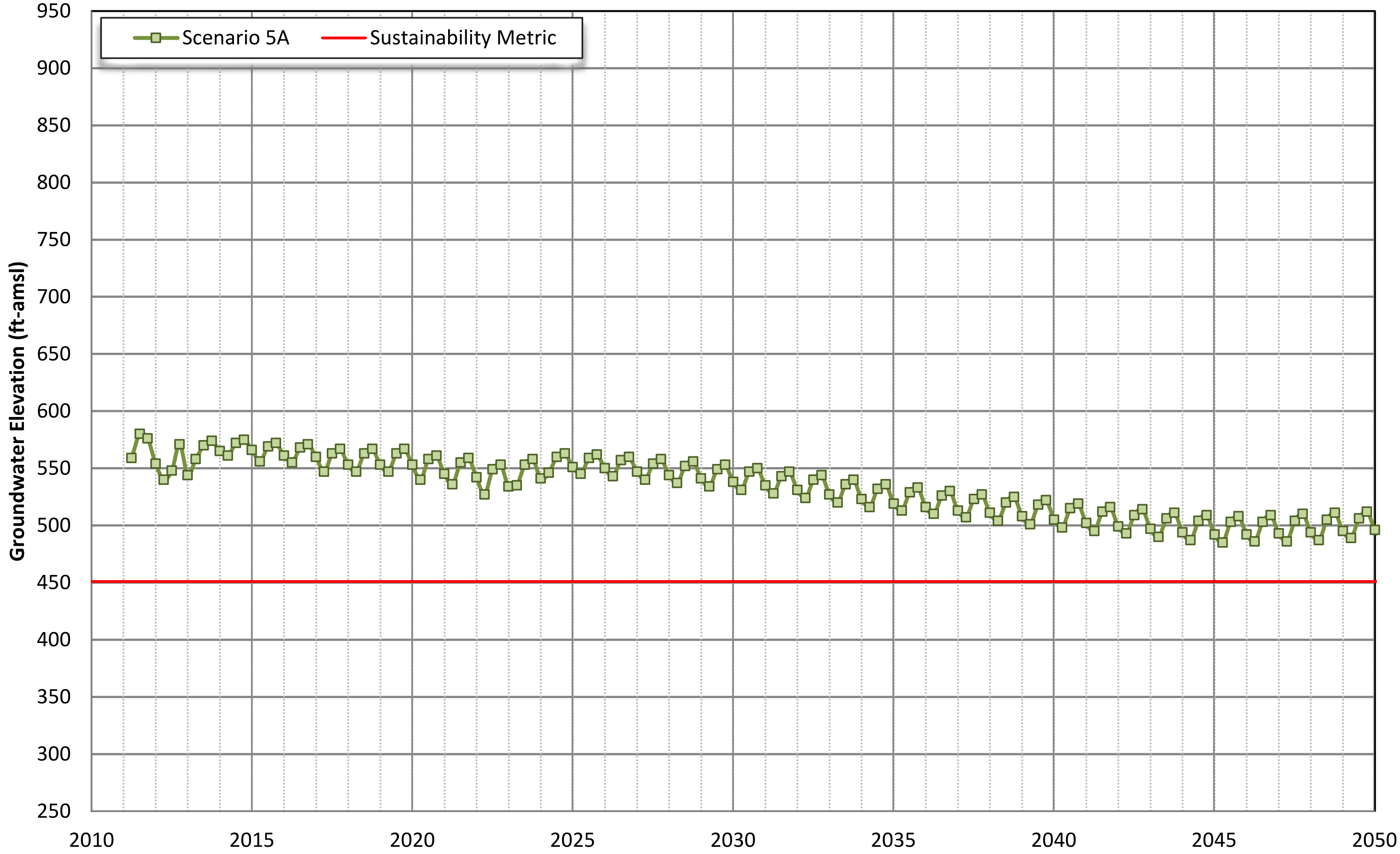

Appendix D_20150916_WellHydrographs_S5A4_Final_LBB2.xlsm
Created: 9/15/15
Printed: 9/16/2015

Figure D-129
Projected Groundwater Elevation for Scenario 5a
City of Ontario Well 35

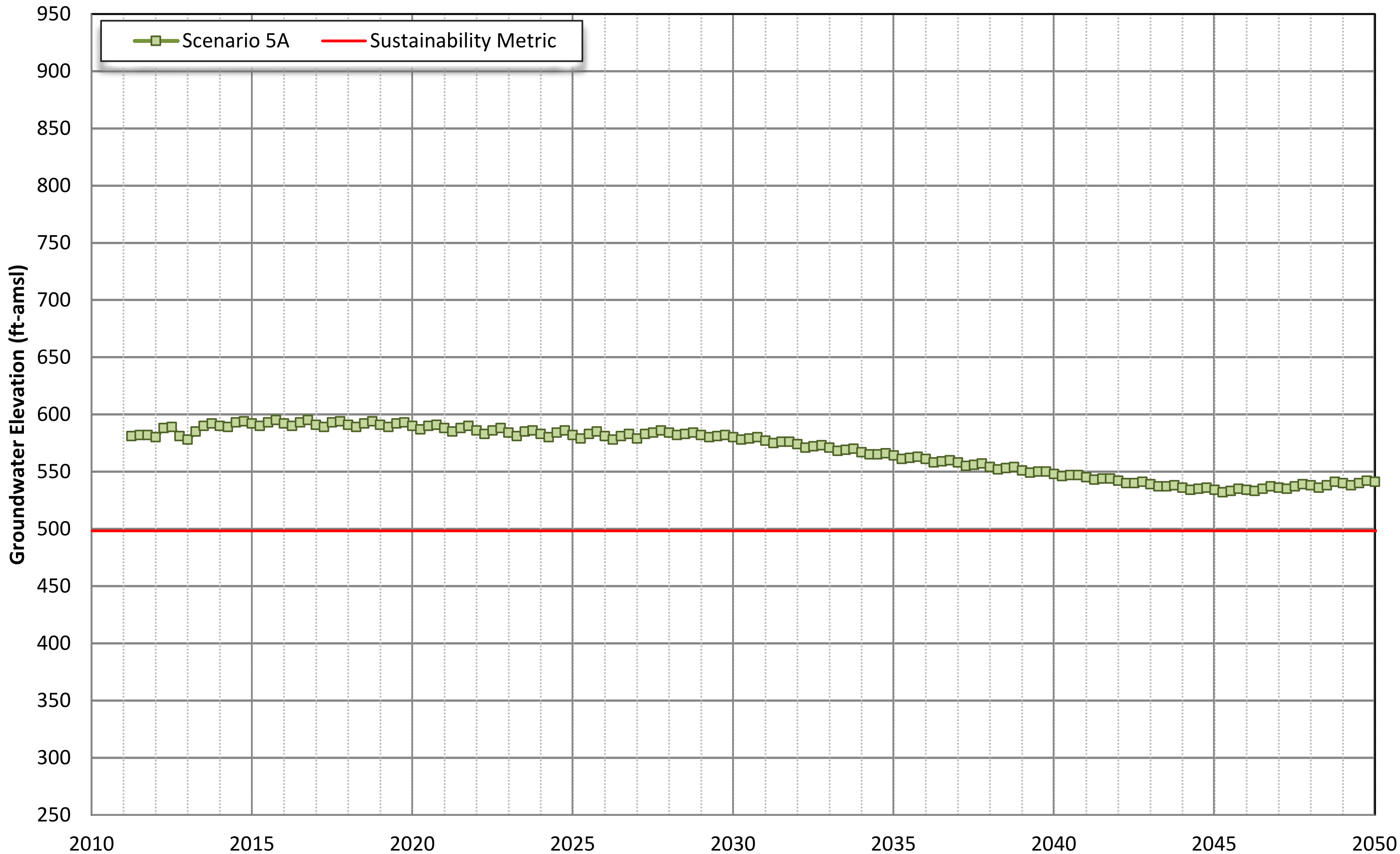

Appendix D_20150916_WellHydrographs_S5A4_Final_LBB2.xlsm
Created: 9/15/15
Printed: 9/16/2015

Figure D-130
Projected Groundwater Elevation for Scenario 5a
City of Ontario Well 36

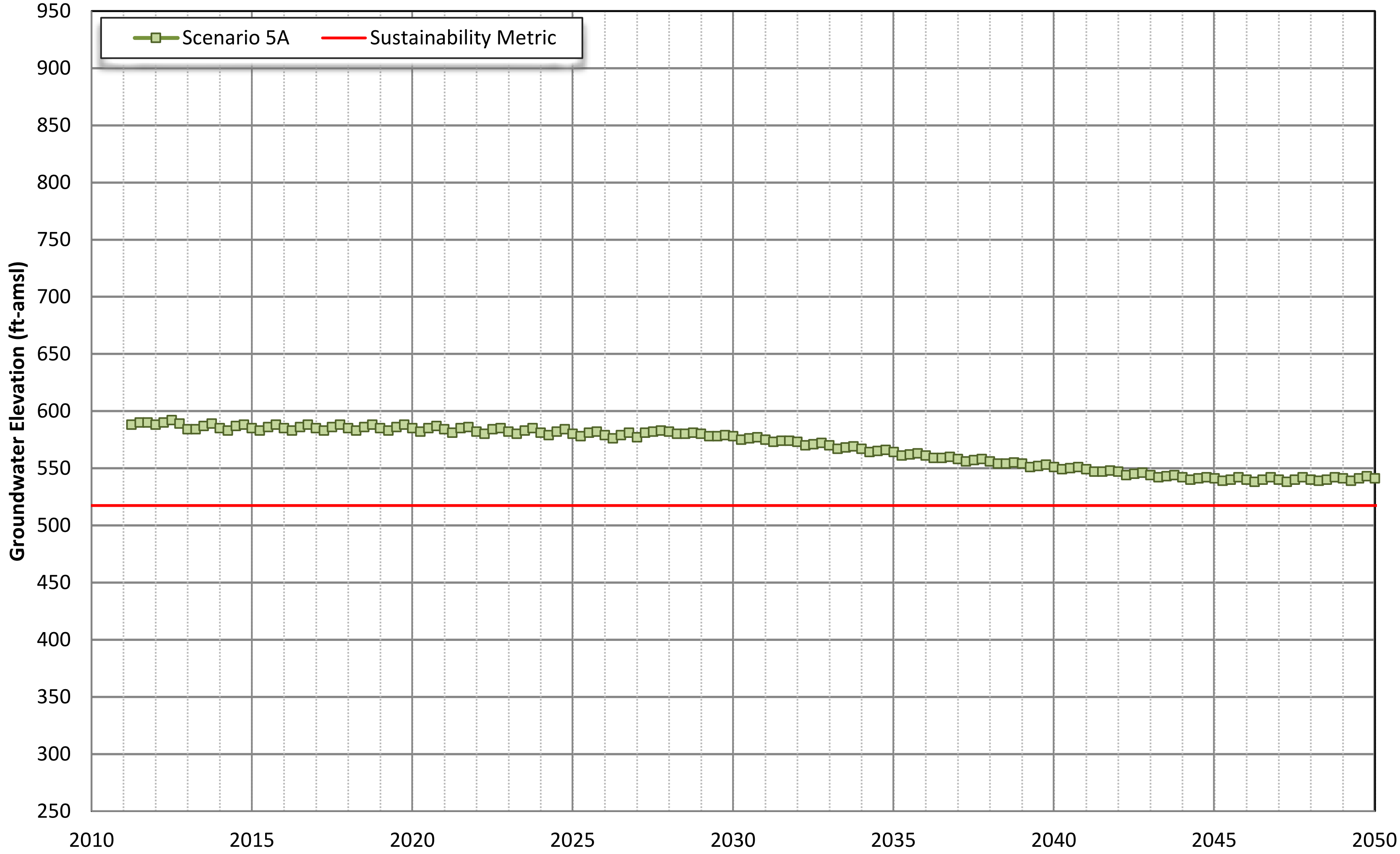

Appendix D_20150916_WellHydrographs_S5A4_Final_LBB2.xlsm
Created: 9/15/15
Printed: 9/16/2015

Figure D-131
Projected Groundwater Elevation for Scenario 5a
City of Ontario Well 37

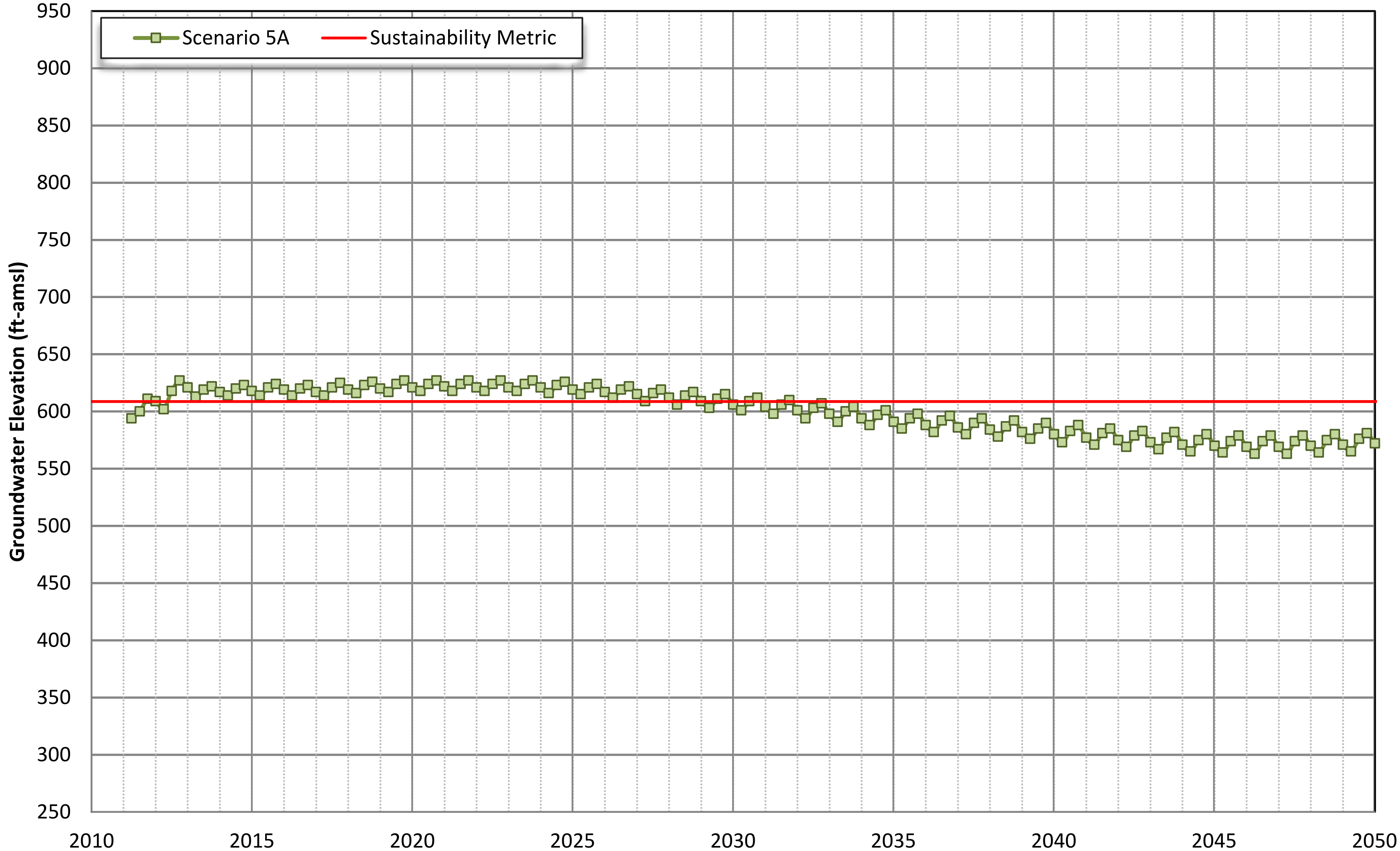

Appendix D_20150916_WellHydrographs_S5A4_Final_LBB2.xlsm
Created: 9/15/15
Printed: 9/16/2015

Figure D-132
Projected Groundwater Elevation for Scenario 5a
City of Ontario Well 38

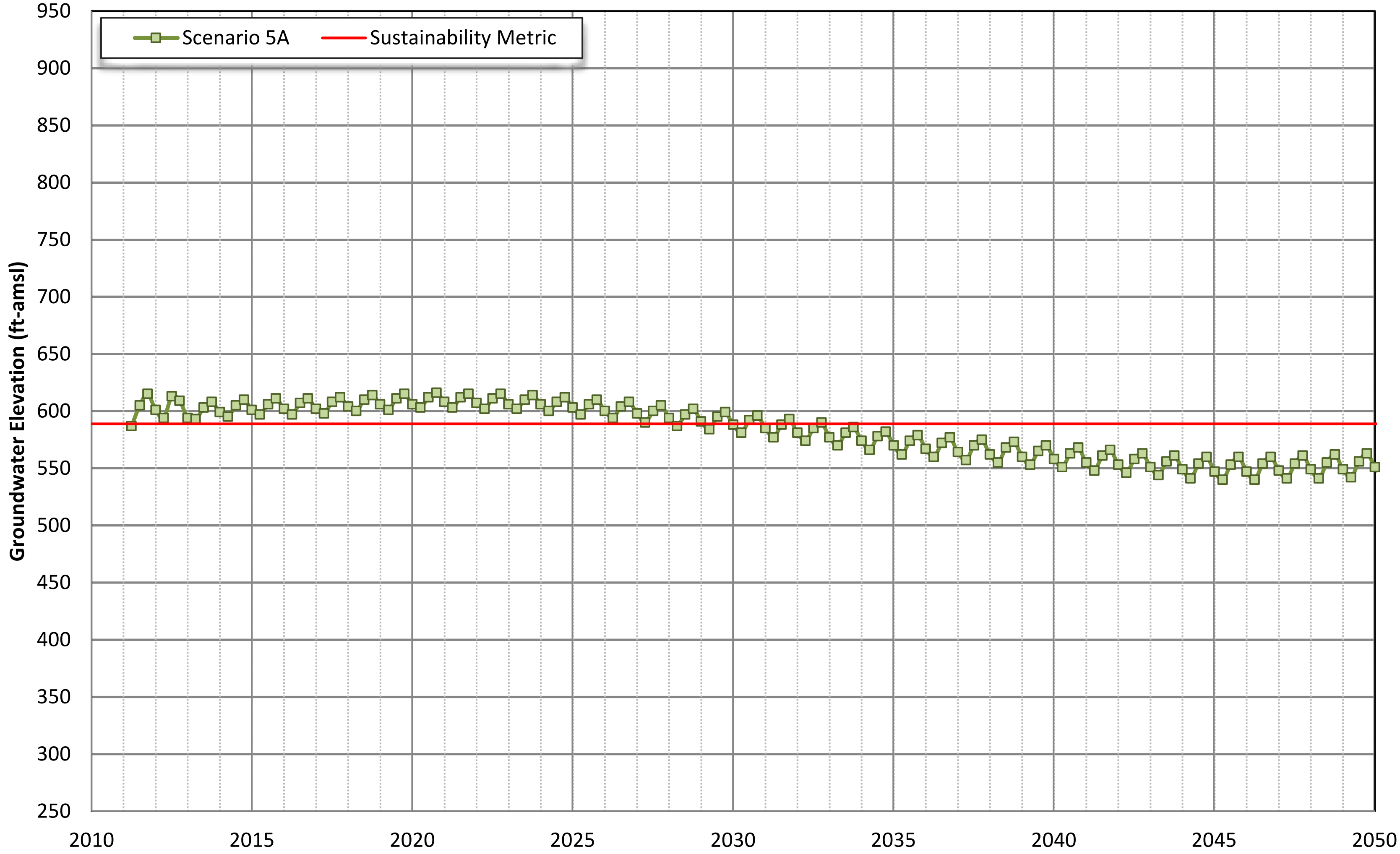

Appendix D_20150916_WellHydrographs_S5A4_Final_LBB2.xlsm
Created: 9/15/15
Printed: 9/16/2015

Figure D-133
Projected Groundwater Elevation for Scenario 5a
City of Ontario Well 39

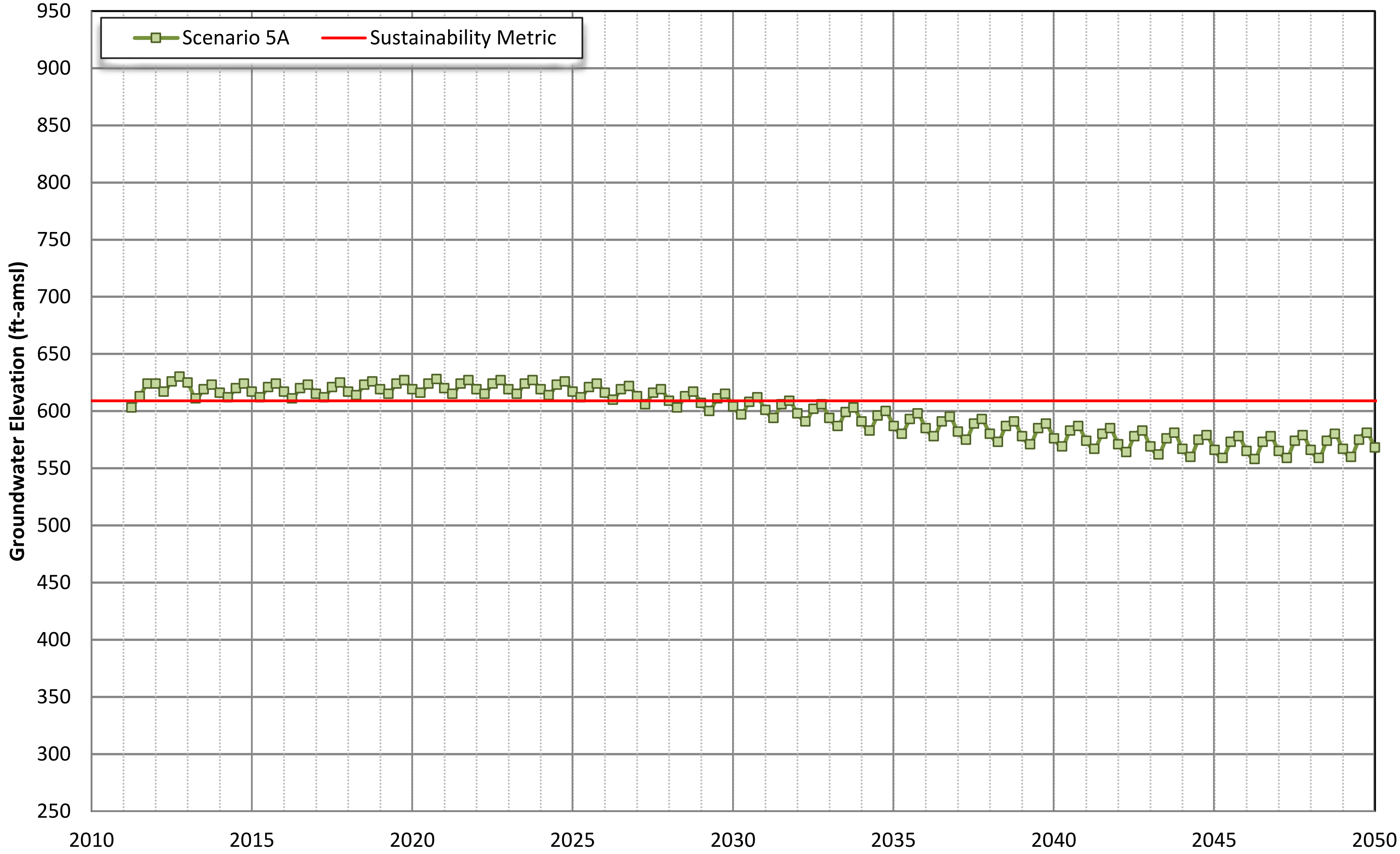

Appendix D_20150916_WellHydrographs_S5A4_Final_LBB2.xlsm
Created: 9/15/15
Printed: 9/16/2015

Figure D-134
Projected Groundwater Elevation for Scenario 5a
City of Ontario Well 40

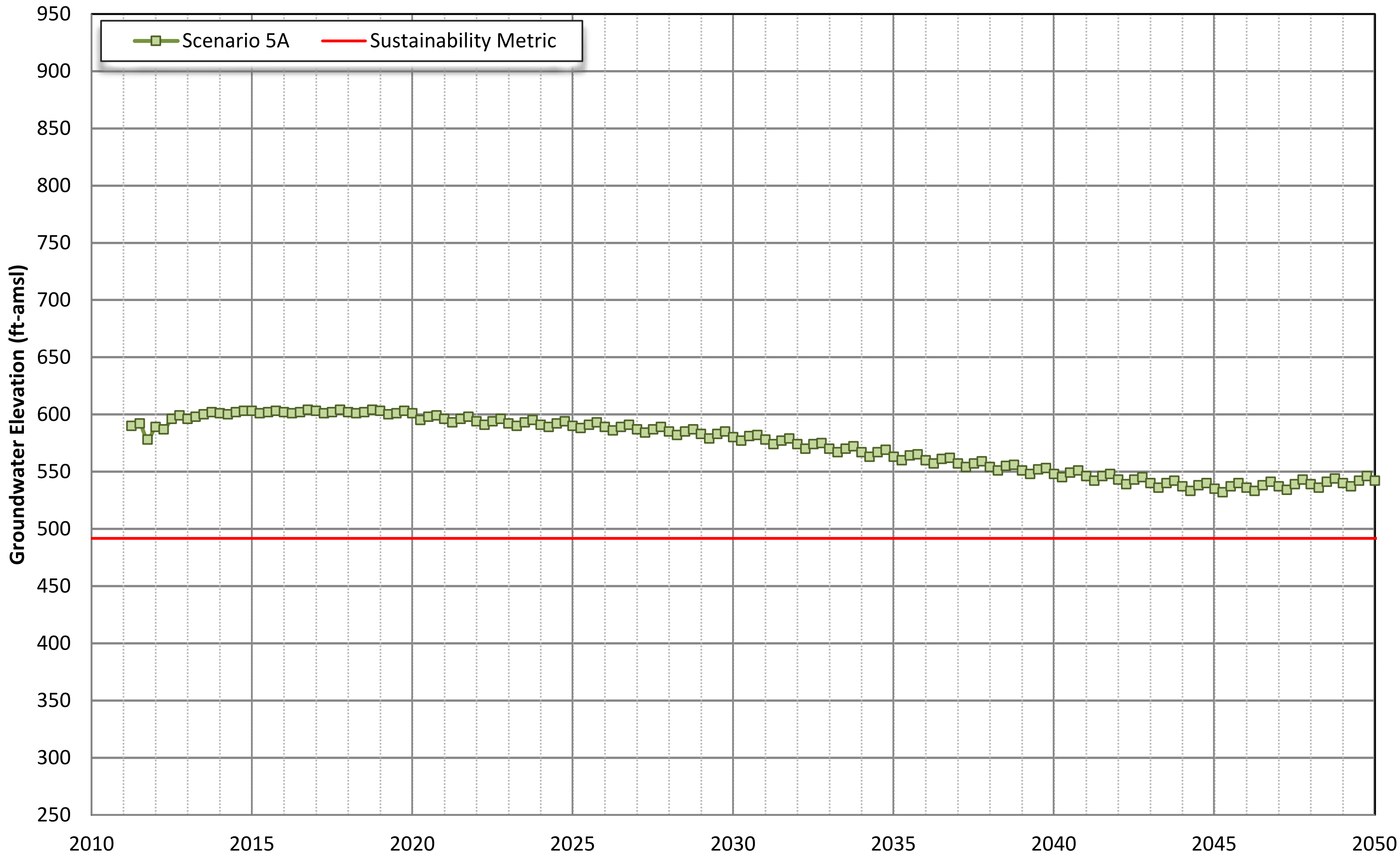

Appendix D_20150916_WellHydrographs_S5A4_Final_LBB2.xlsm
Created: 9/15/15
Printed: 9/16/2015

Figure D-135
Projected Groundwater Elevation for Scenario 5a
City of Ontario Well 41

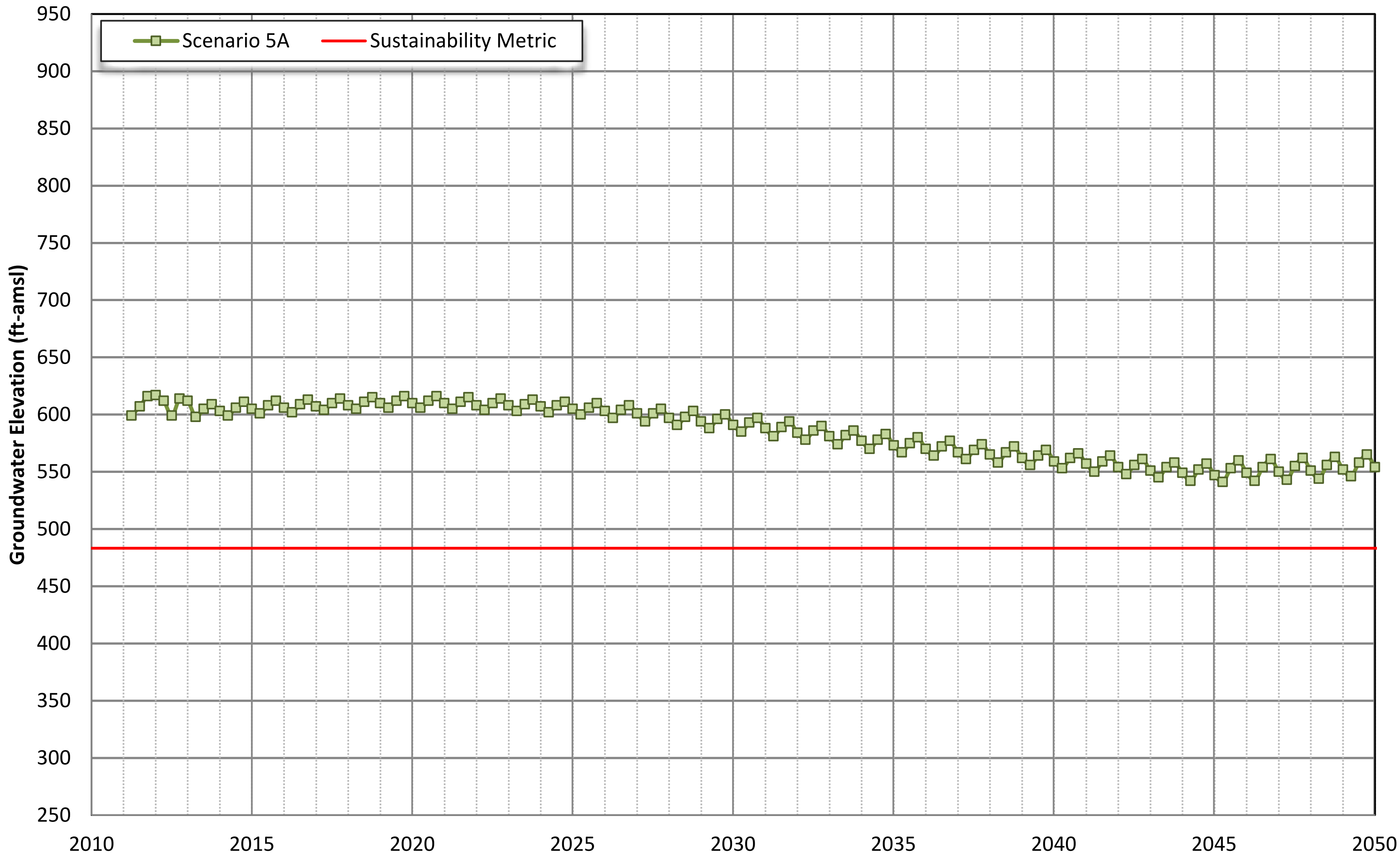

Appendix D_20150916_WellHydrographs_S5A4_Final_LBB2.xlsm
Created: 9/15/15
Printed: 9/16/2015

Figure D-136
Projected Groundwater Elevation for Scenario 5a
City of Ontario Well 42

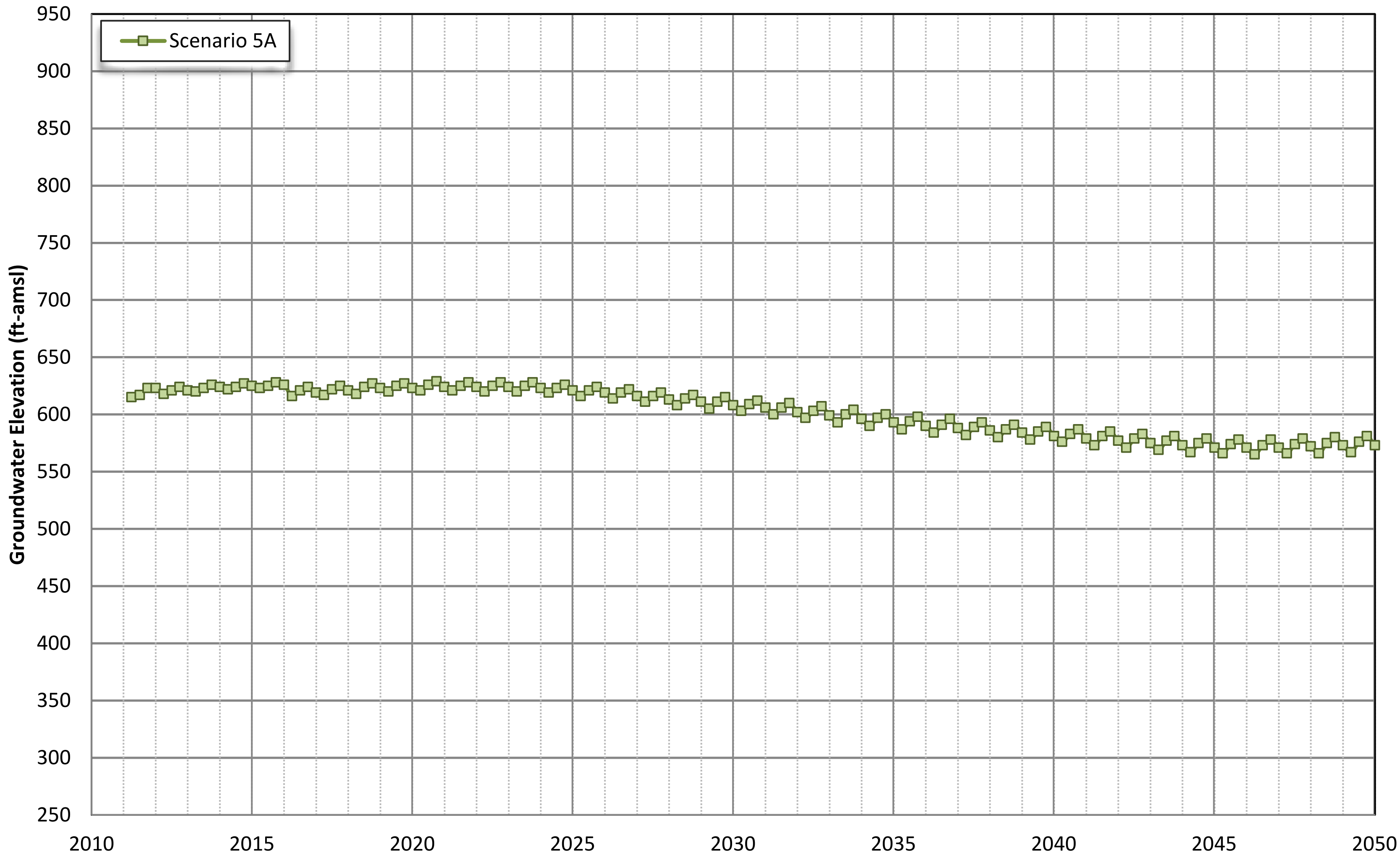

Figure D-137
Projected Groundwater Elevation for Scenario 5a
City of Ontario Well 43

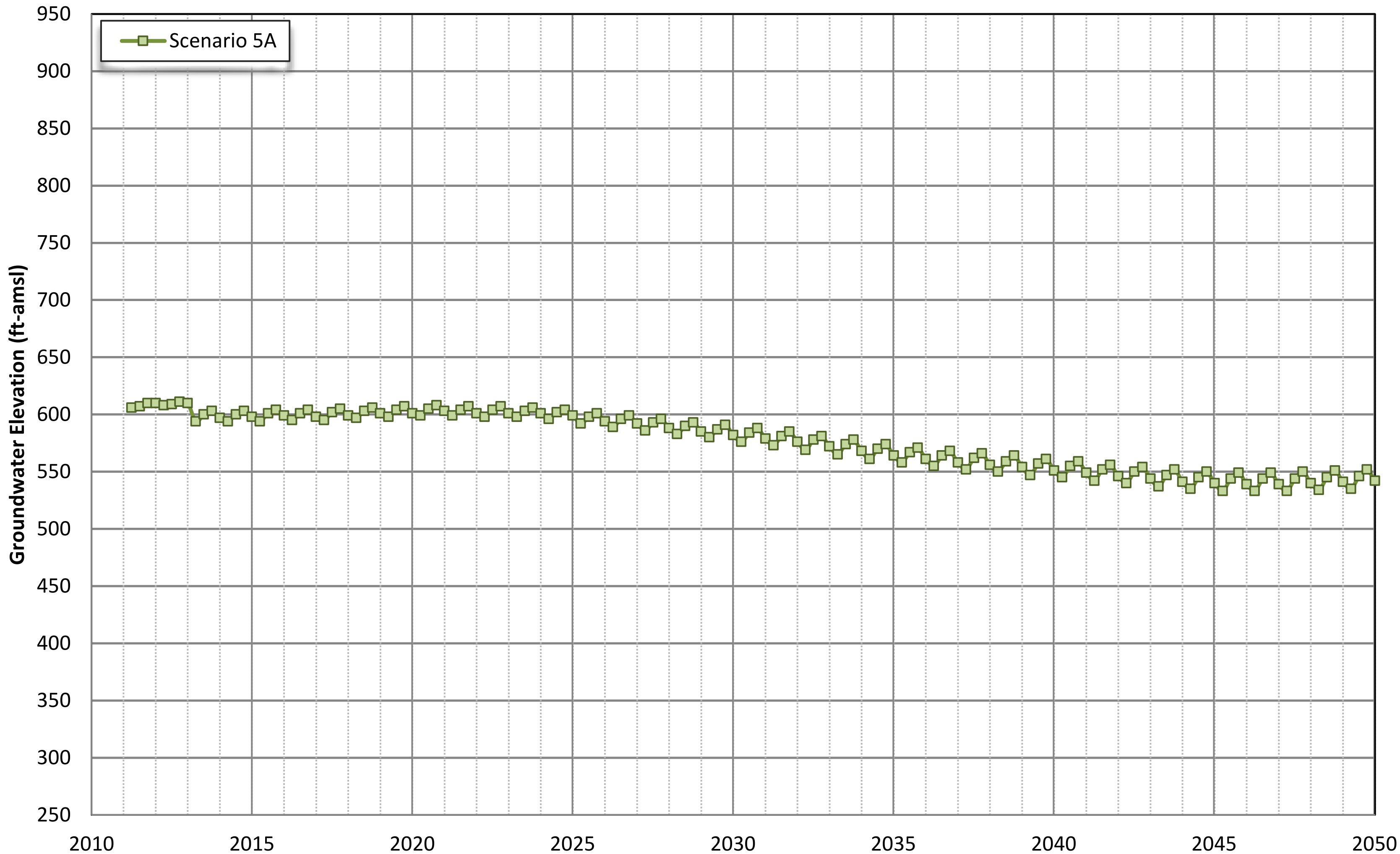

Appendix D_20150916_WellHydrographs_S5A4_Final_LBB2.xlsm
Created: 9/15/15
Printed: 9/16/2015

Figure D-138
Projected Groundwater Elevation for Scenario 5a
City of Ontario Well 44

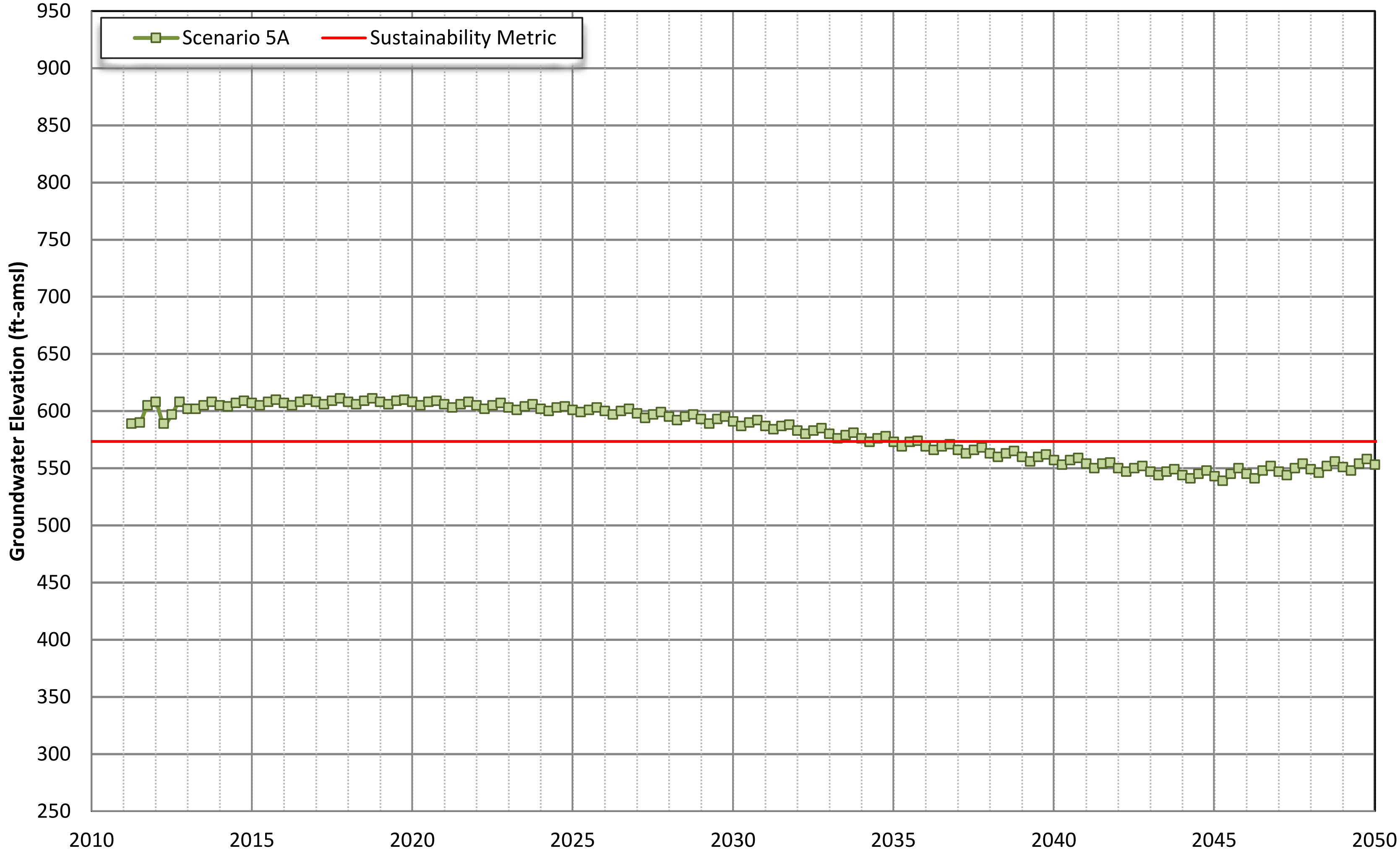

Appendix D_20150916_WellHydrographs_S5A4_Final_LBB2.xlsm
Created: 9/15/15
Printed: 9/16/2015

Figure D-139
Projected Groundwater Elevation for Scenario 5a
City of Ontario Well 45

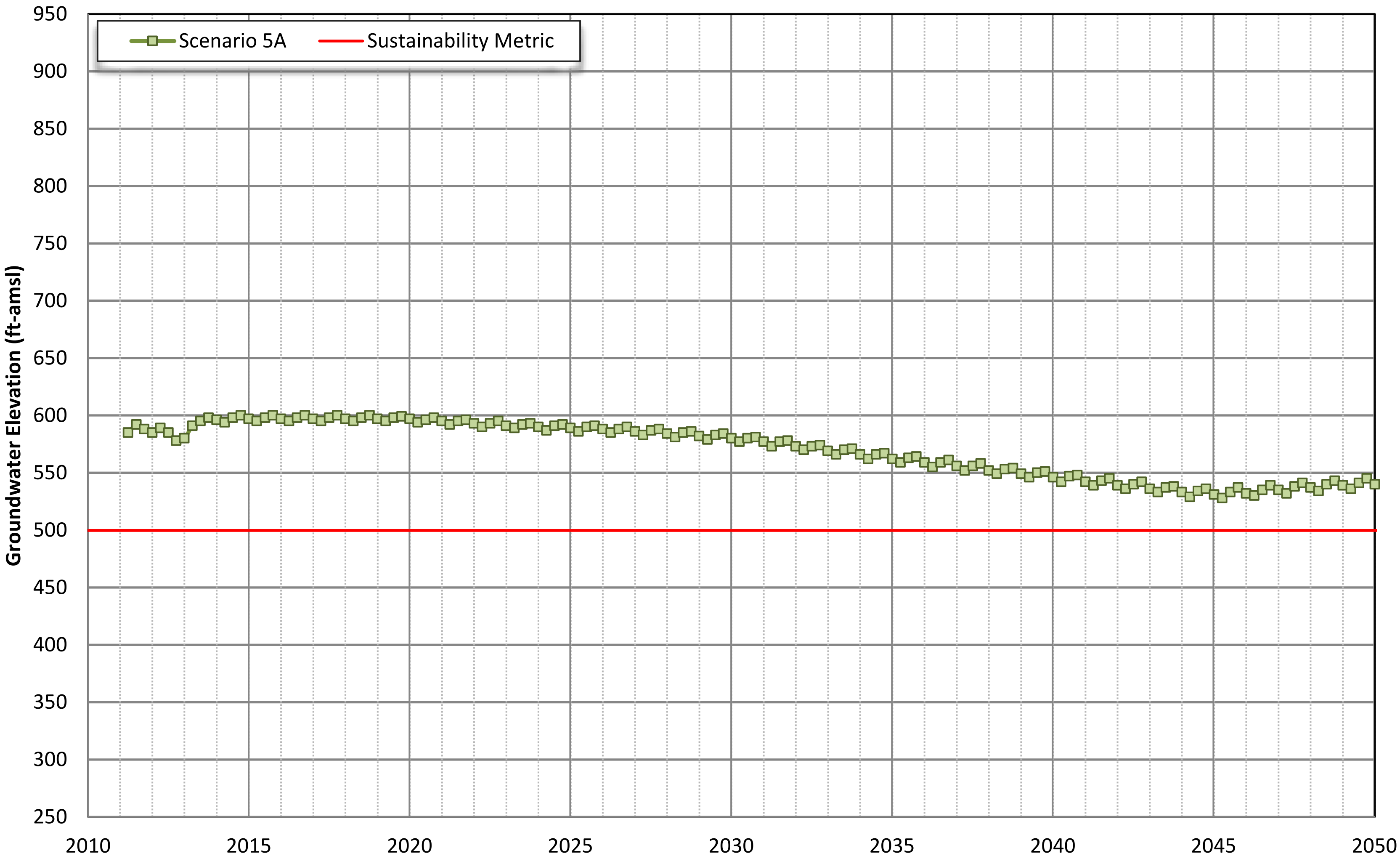

Appendix D_20150916_WellHydrographs_S5A4_Final_LBB2.xlsm
Created: 9/15/15
Printed: 9/16/2015

Figure D-140
Projected Groundwater Elevation for Scenario 5a
City of Ontario Well 46

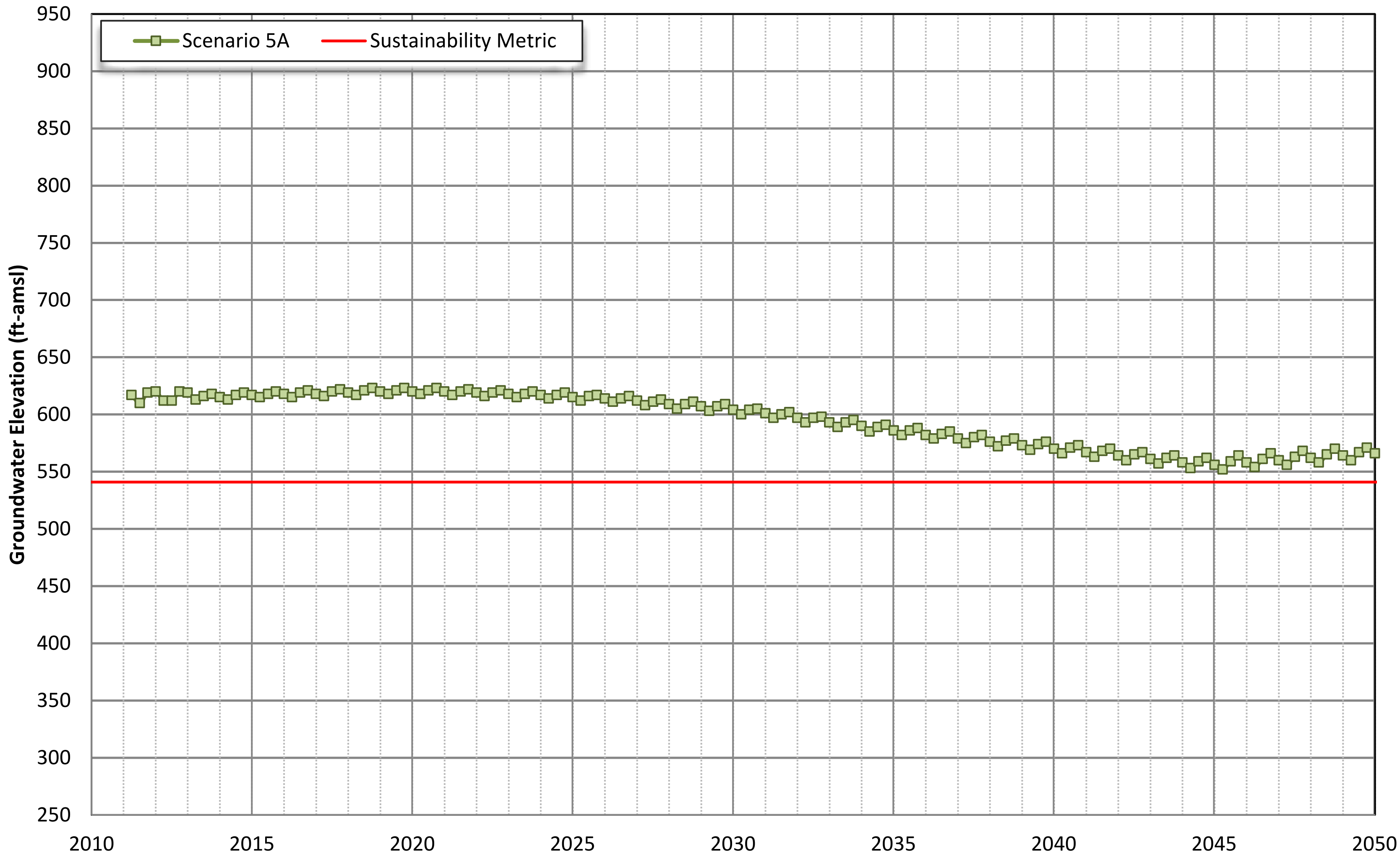

Appendix D_20150916_WellHydrographs_S5A4_Final_LBB2.xlsm
Created: 9/15/15
Printed: 9/16/2015

Figure D-141
Projected Groundwater Elevation for Scenario 5a
City of Ontario Well 47

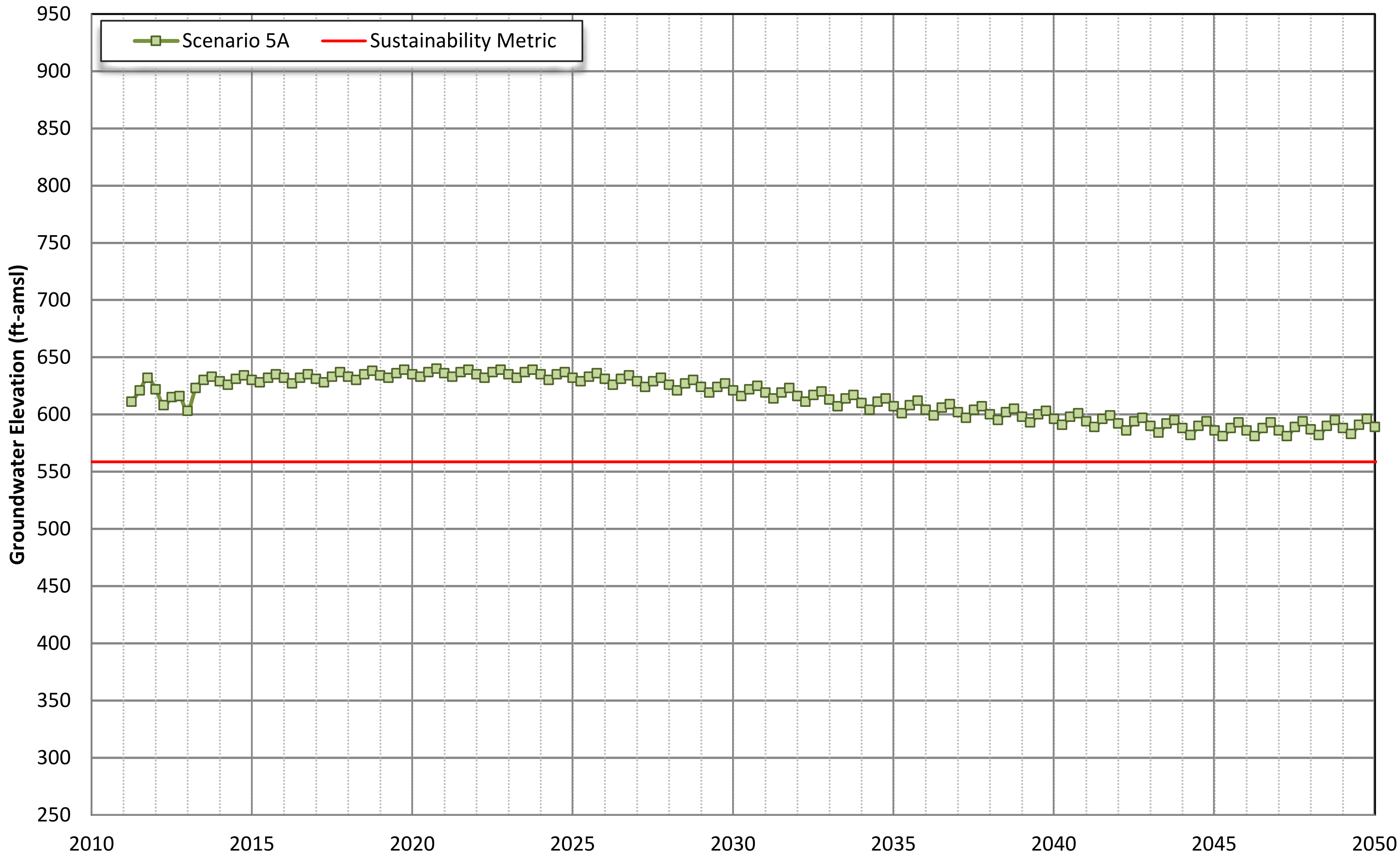

Appendix D_20150916_WellHydrographs_S5A4_Final_LBB2.xlsm
Created: 9/15/15
Printed: 9/16/2015

Figure D-142
Projected Groundwater Elevation for Scenario 5a
City of Ontario Well 48

Appendix D_20150916_WellHydrographs_S5A4_Final_LBB2.xlsm
Created: 9/15/15
Printed: 9/16/2015

Figure D-143
Projected Groundwater Elevation for Scenario 5a
City of Ontario Well 49

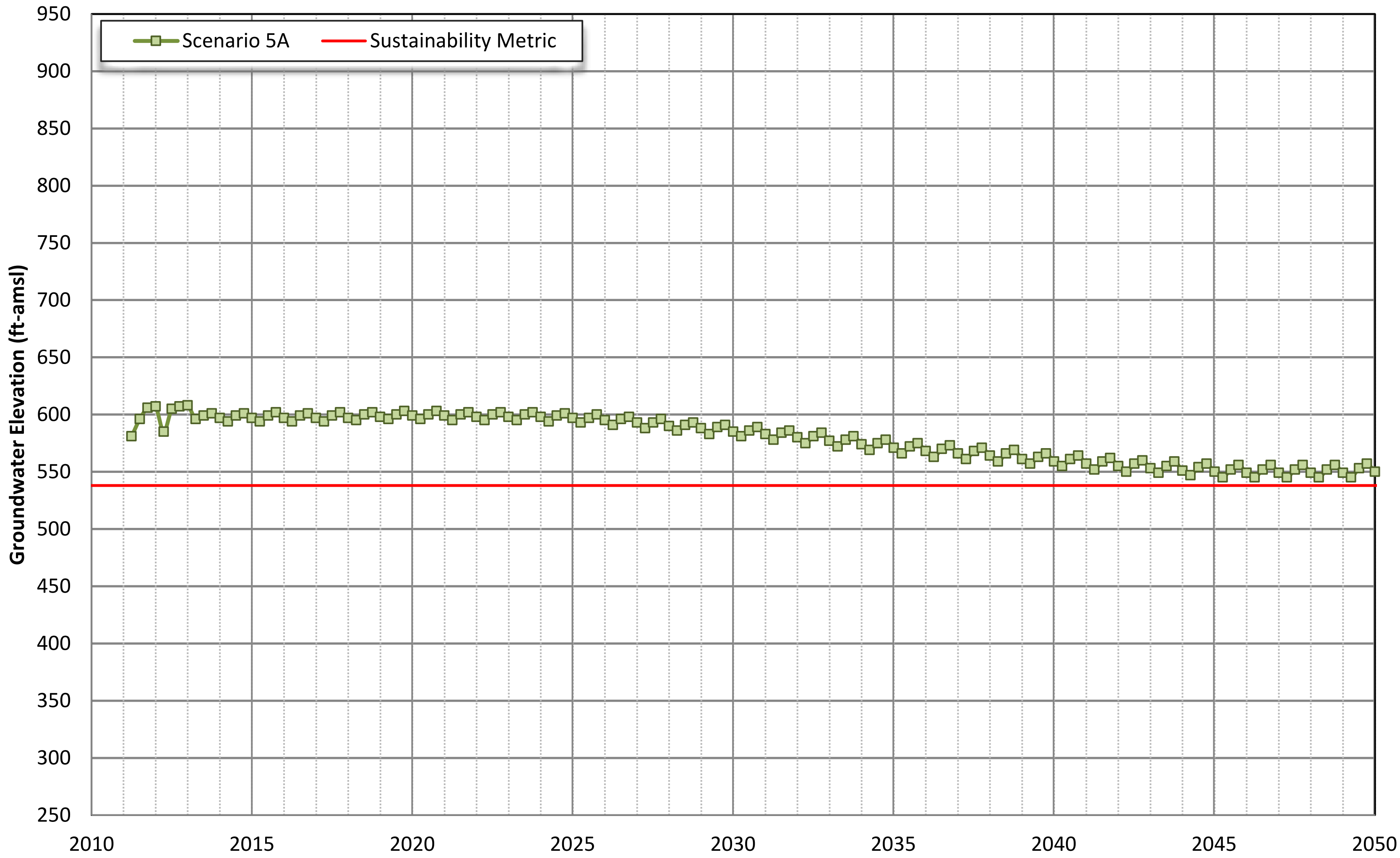

Appendix D_20150916_WellHydrographs_S5A4_Final_LBB2.xlsm
Created: 9/15/15
Printed: 9/16/2015

Figure D-144
Projected Groundwater Elevation for Scenario 5a
City of Ontario Well 50

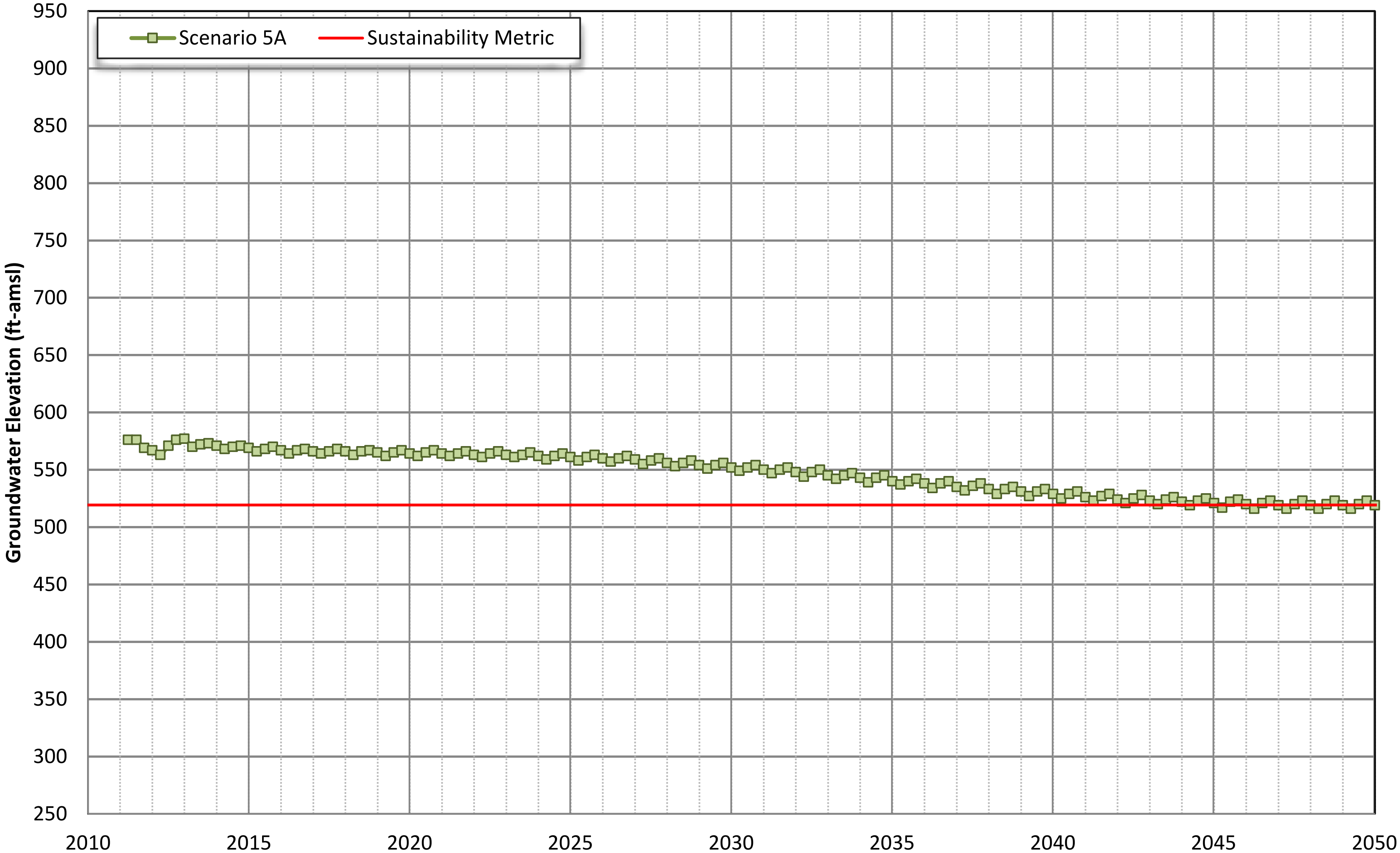

Appendix D_20150916_WellHydrographs_S5A4_Final_LBB2.xlsm
Created: 9/15/15
Printed: 9/16/2015

Figure D-145
Projected Groundwater Elevation for Scenario 5a
City of Ontario Well 51

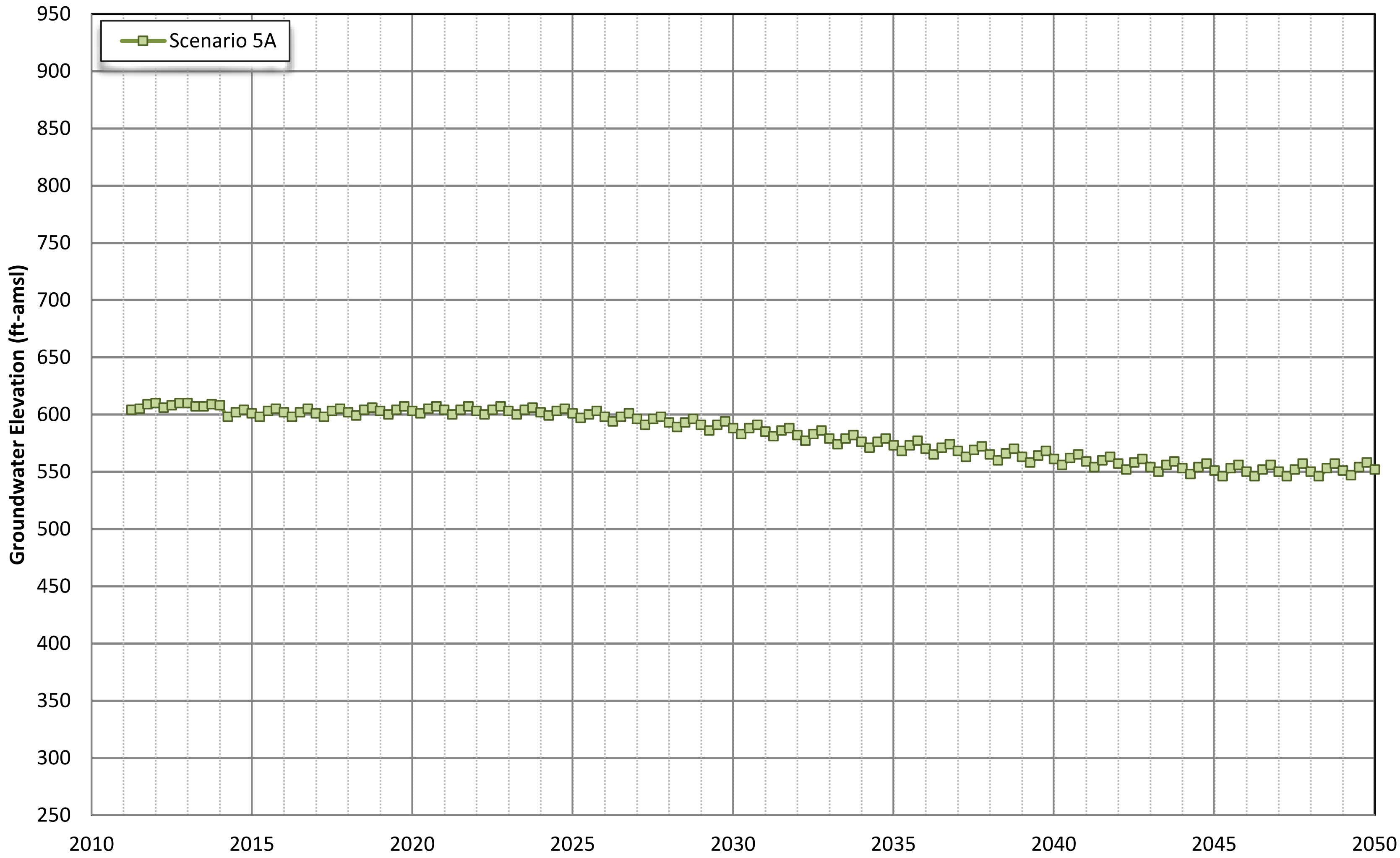

Appendix D_20150916_WellHydrographs_S5A4_Final_LBB2.xlsm
Created: 9/15/15
Printed: 9/16/2015

Figure D-146
Projected Groundwater Elevation for Scenario 5a
City of Ontario Well 52

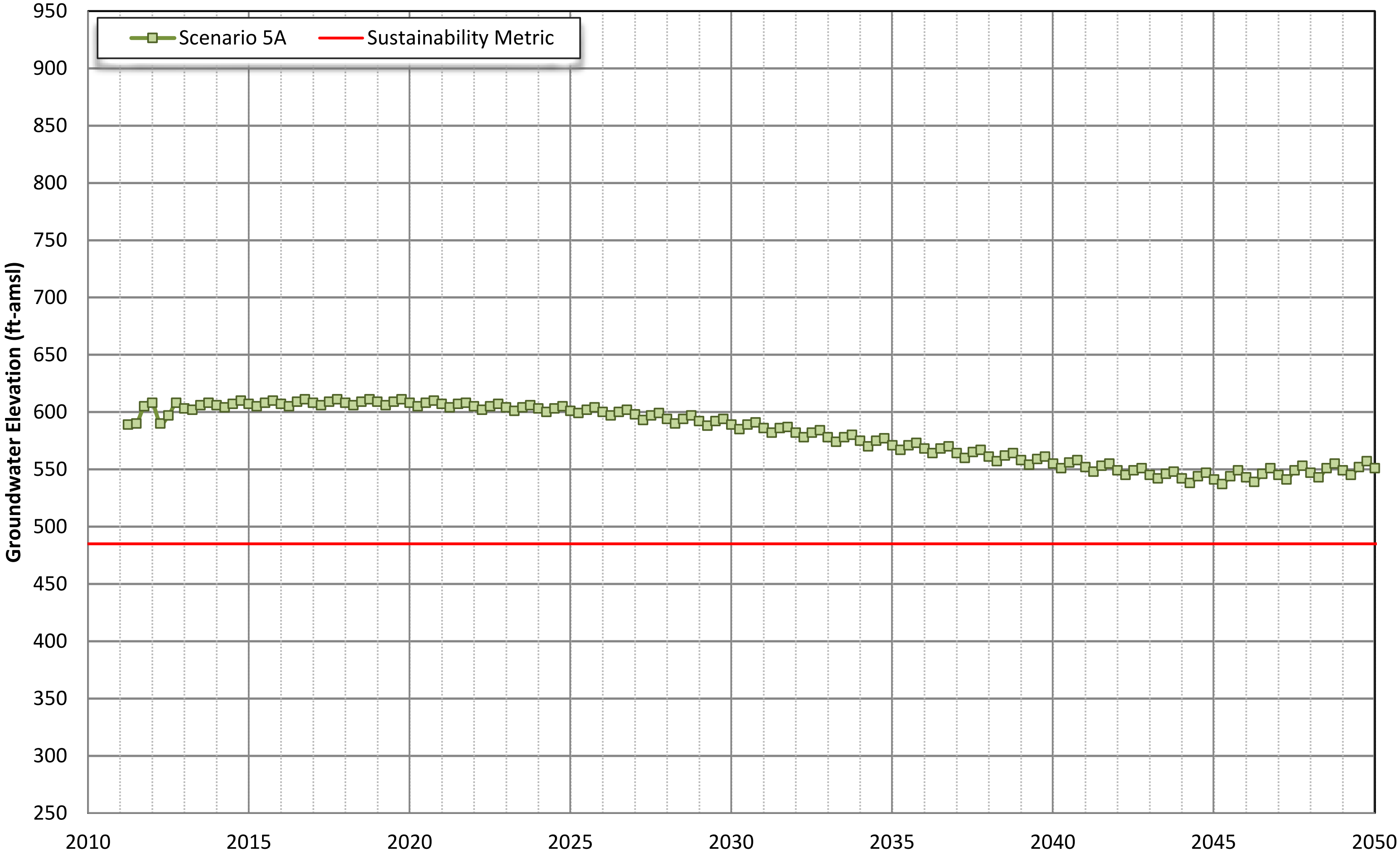

Appendix D_20150916_WellHydrographs_S5A4_Final_LBB2.xlsm
Created: 9/15/15
Printed: 9/16/2015

Figure D-147
Projected Groundwater Elevation for Scenario 5a
City of Ontario Well 100

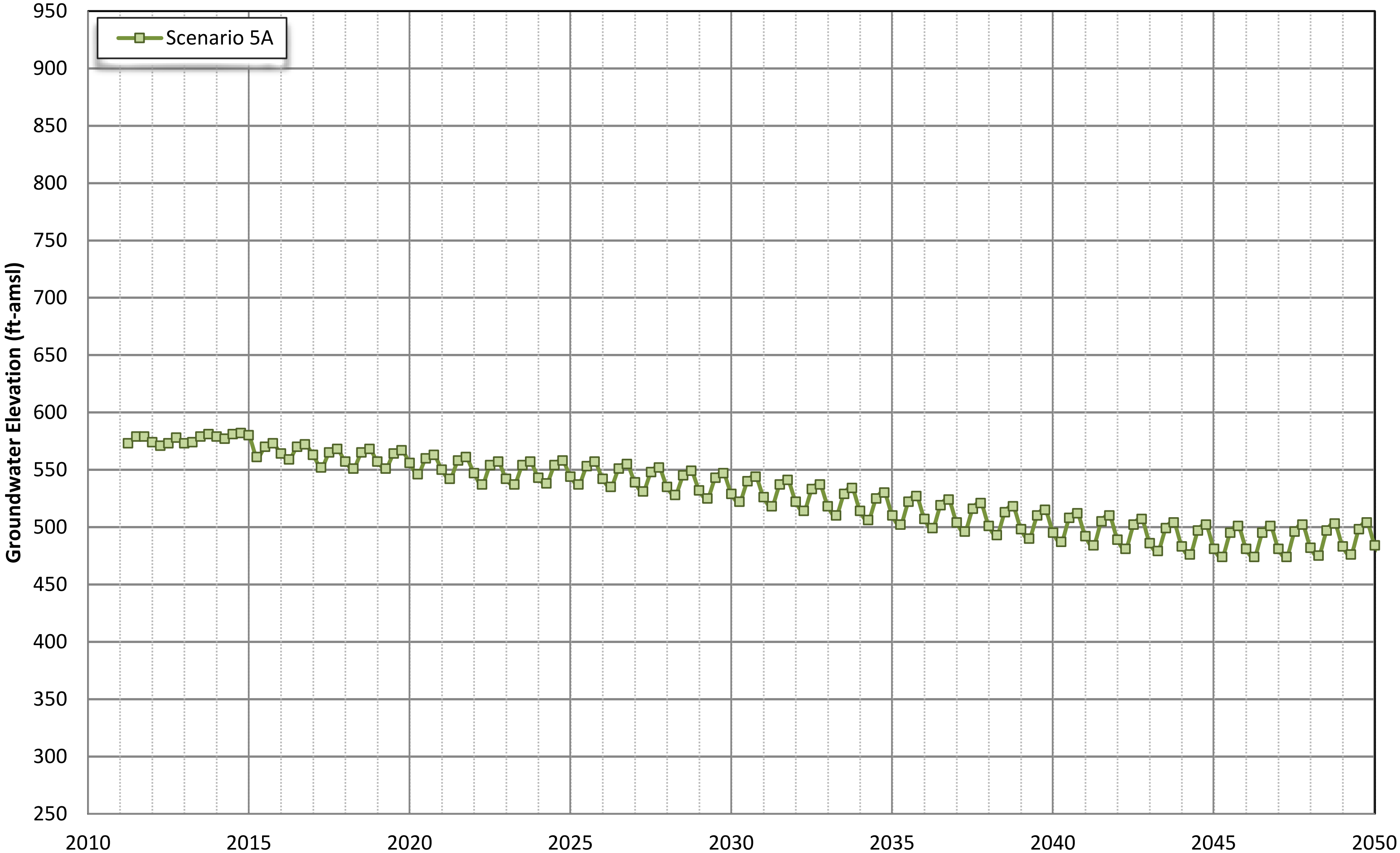

Appendix D_20150916_WellHydrographs_S5A4_Final_LBB2.xlsm
Created: 9/15/15
Printed: 9/16/2015

Figure D-148
Projected Groundwater Elevation for Scenario 5a
City of Ontario Well 101

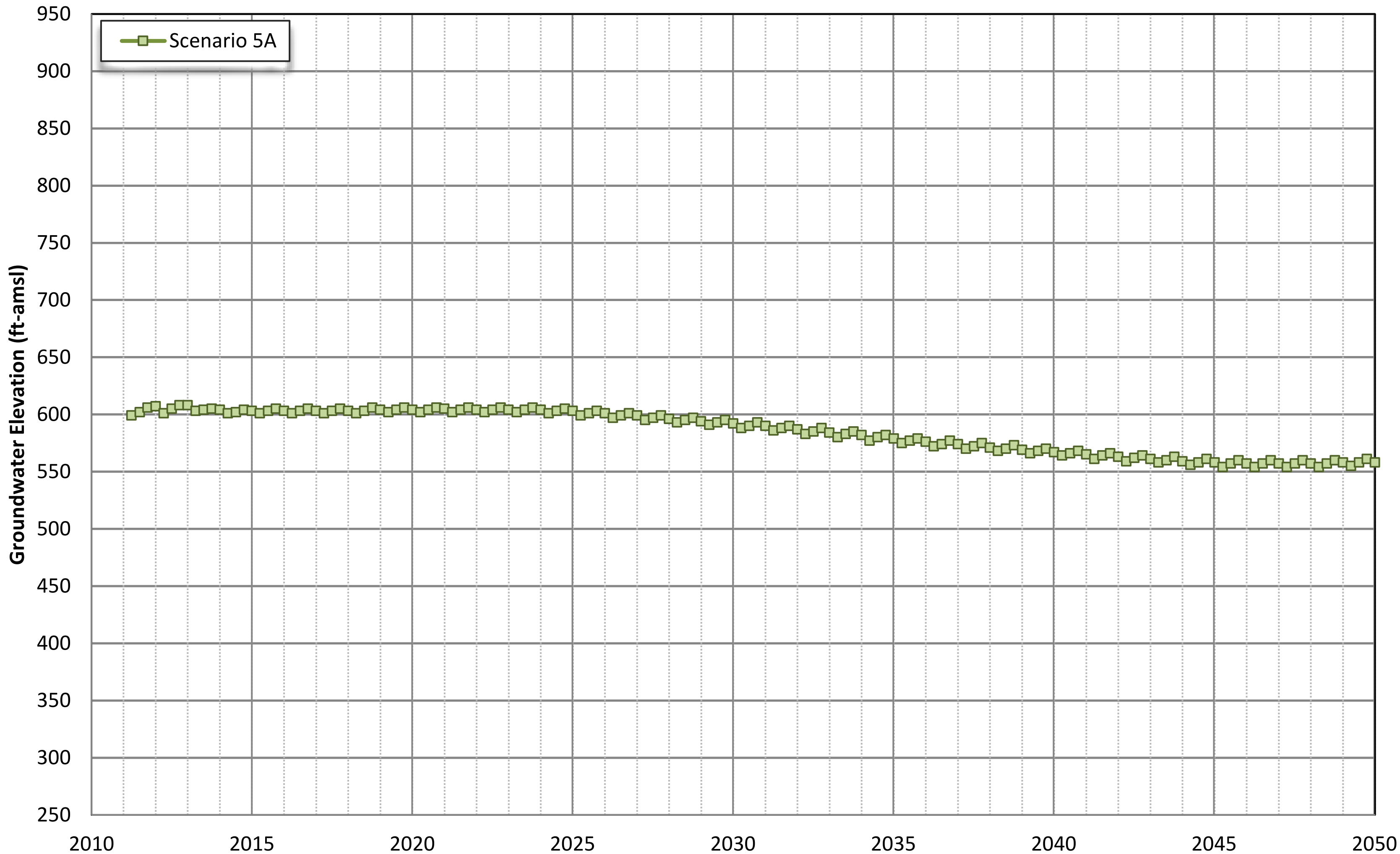

Appendix D_20150916_WellHydrographs_S5A4_Final_LBB2.xlsm
Created: 9/15/15
Printed: 9/16/2015

Figure D-149
Projected Groundwater Elevation for Scenario 5a
City of Ontario Well 103

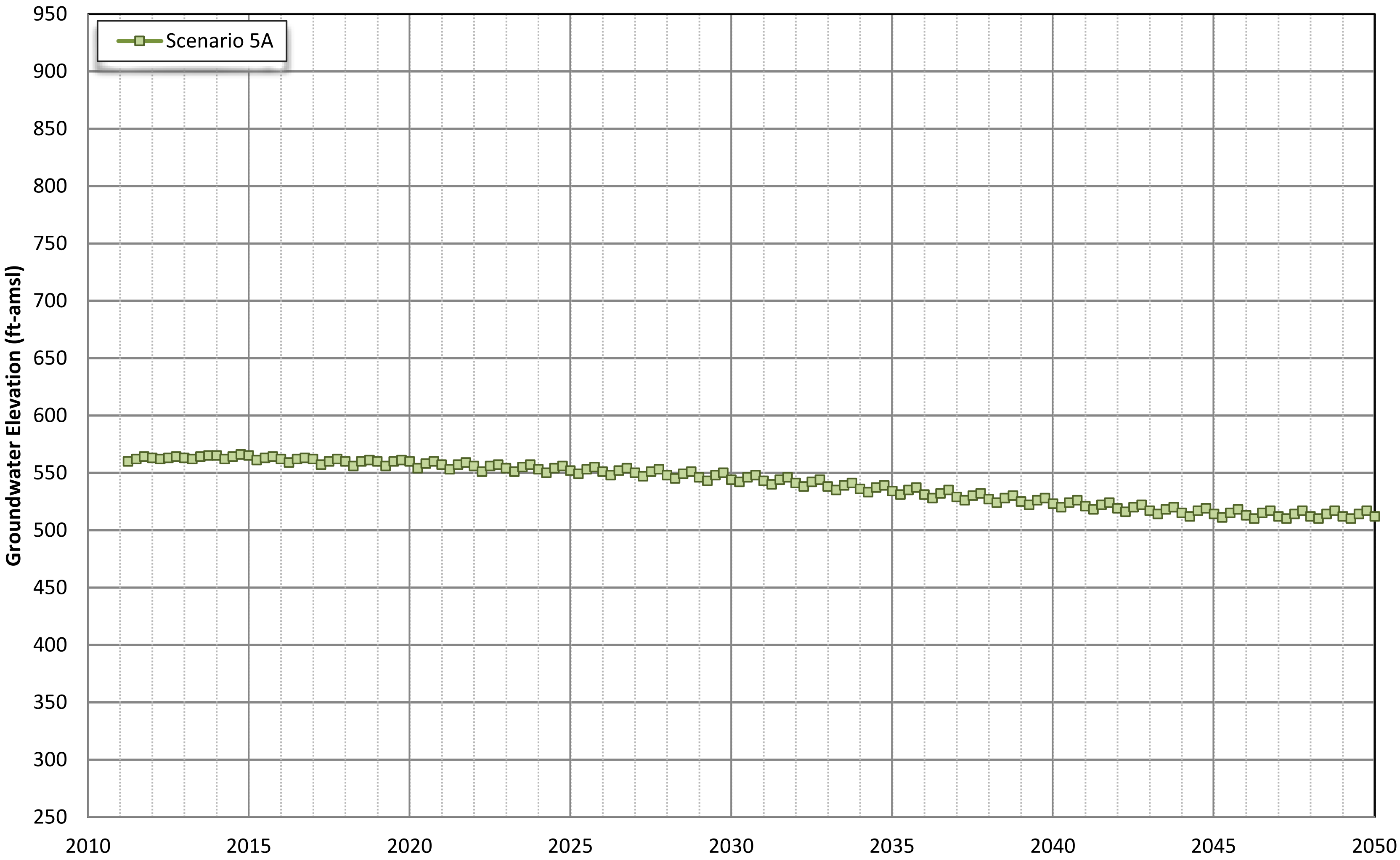

Appendix D_20150916_WellHydrographs_S5A4_Final_LBB2.xlsm
Created: 9/15/15
Printed: 9/16/2015

Figure D-150
Projected Groundwater Elevation for Scenario 5a
City of Ontario Well 104

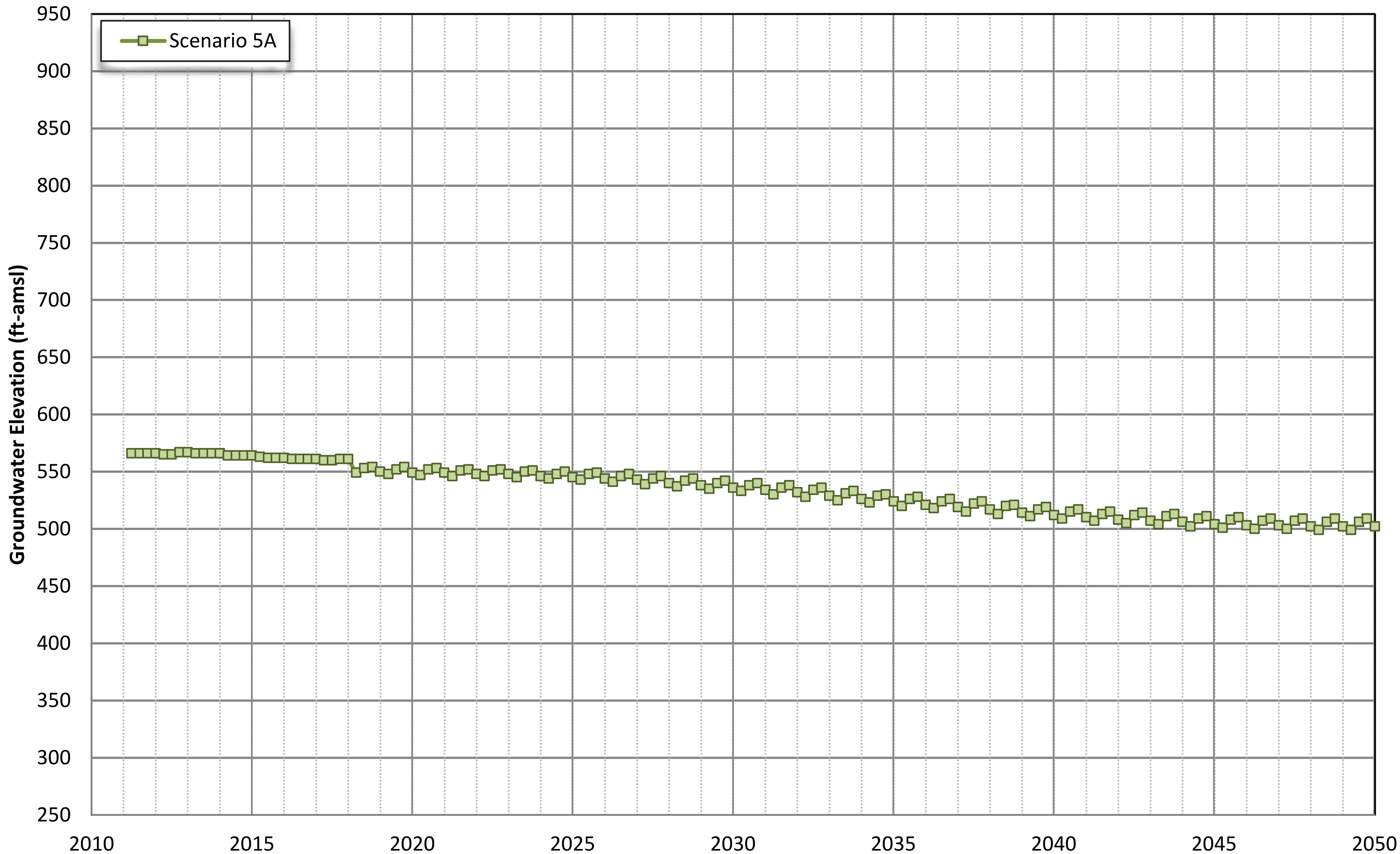

Appendix D_20150916_WellHydrographs_S5A4_Final_LBB2.xlsm
Created: 9/15/15
Printed: 9/16/2015

Figure D-151
Projected Groundwater Elevation for Scenario 5a
City of Ontario Well 105

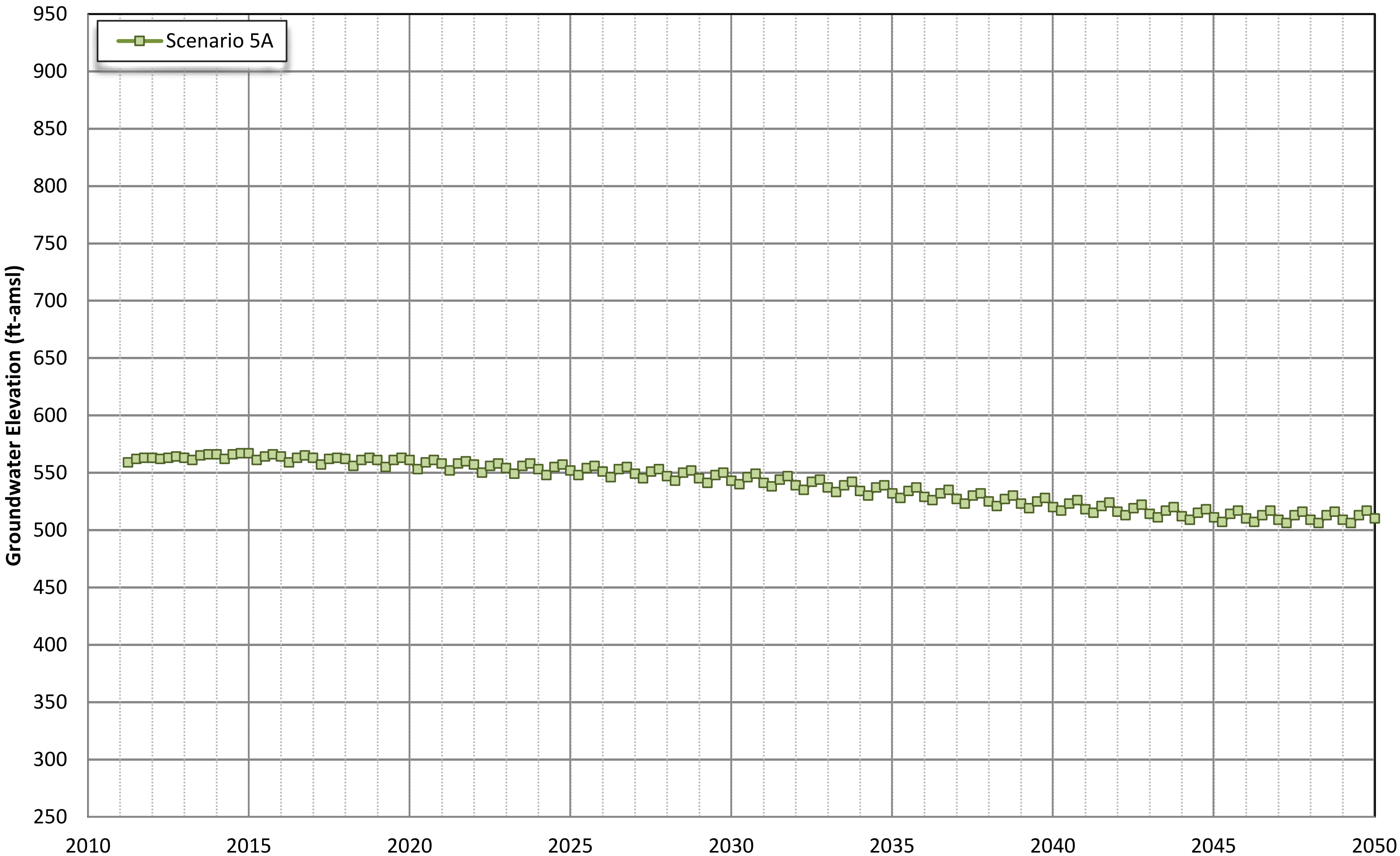

Appendix D_20150916_WellHydrographs_S5A4_Final_LBB2.xlsm
Created: 9/15/15
Printed: 9/16/2015

Figure D-152
Projected Groundwater Elevation for Scenario 5a
City of Ontario Well 106

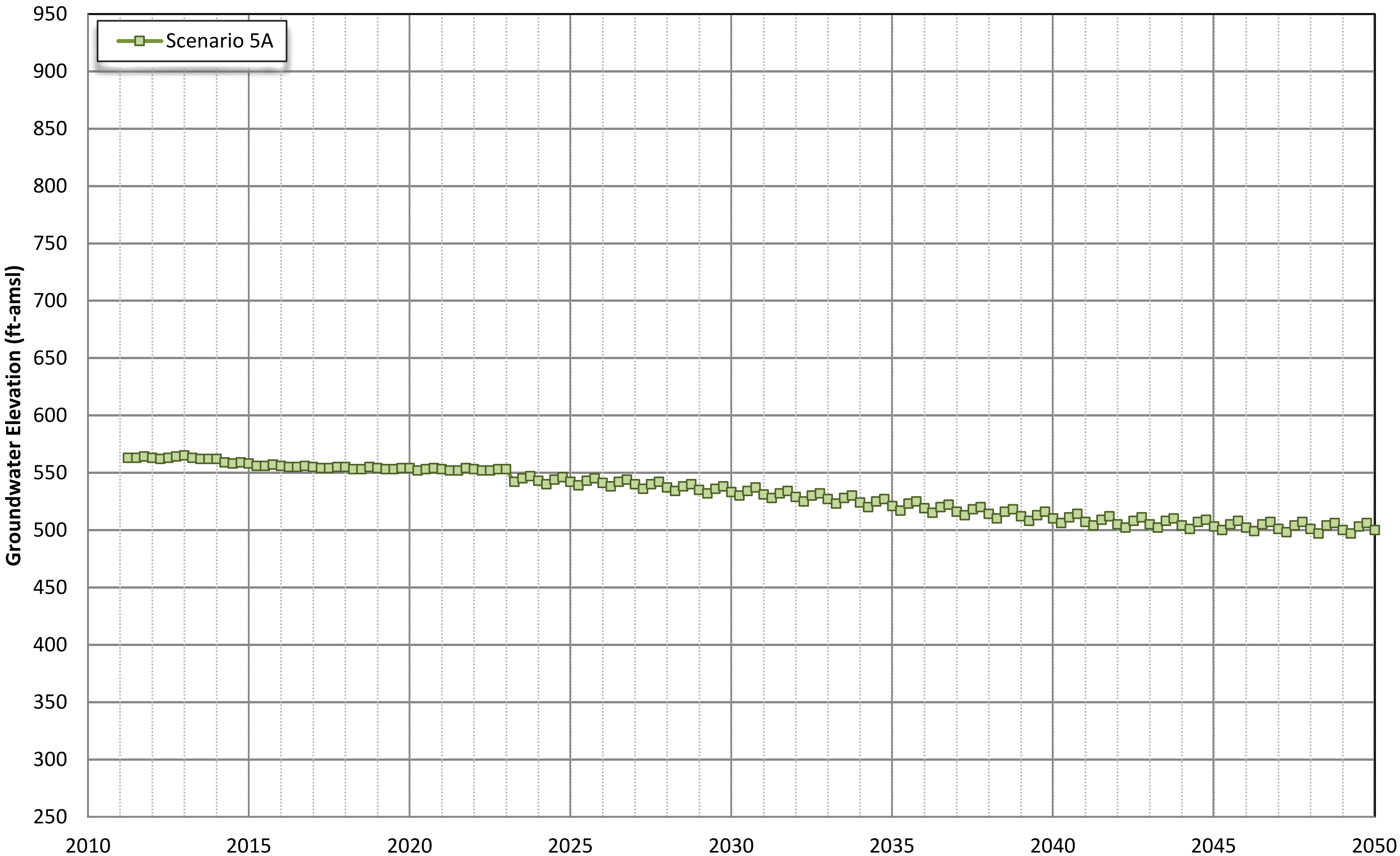

Appendix D_20150916_WellHydrographs_S5A4_Final_LBB2.xlsm
Created: 9/15/15
Printed: 9/16/2015

Figure D-153
Projected Groundwater Elevation for Scenario 5a
City of Ontario Well 109

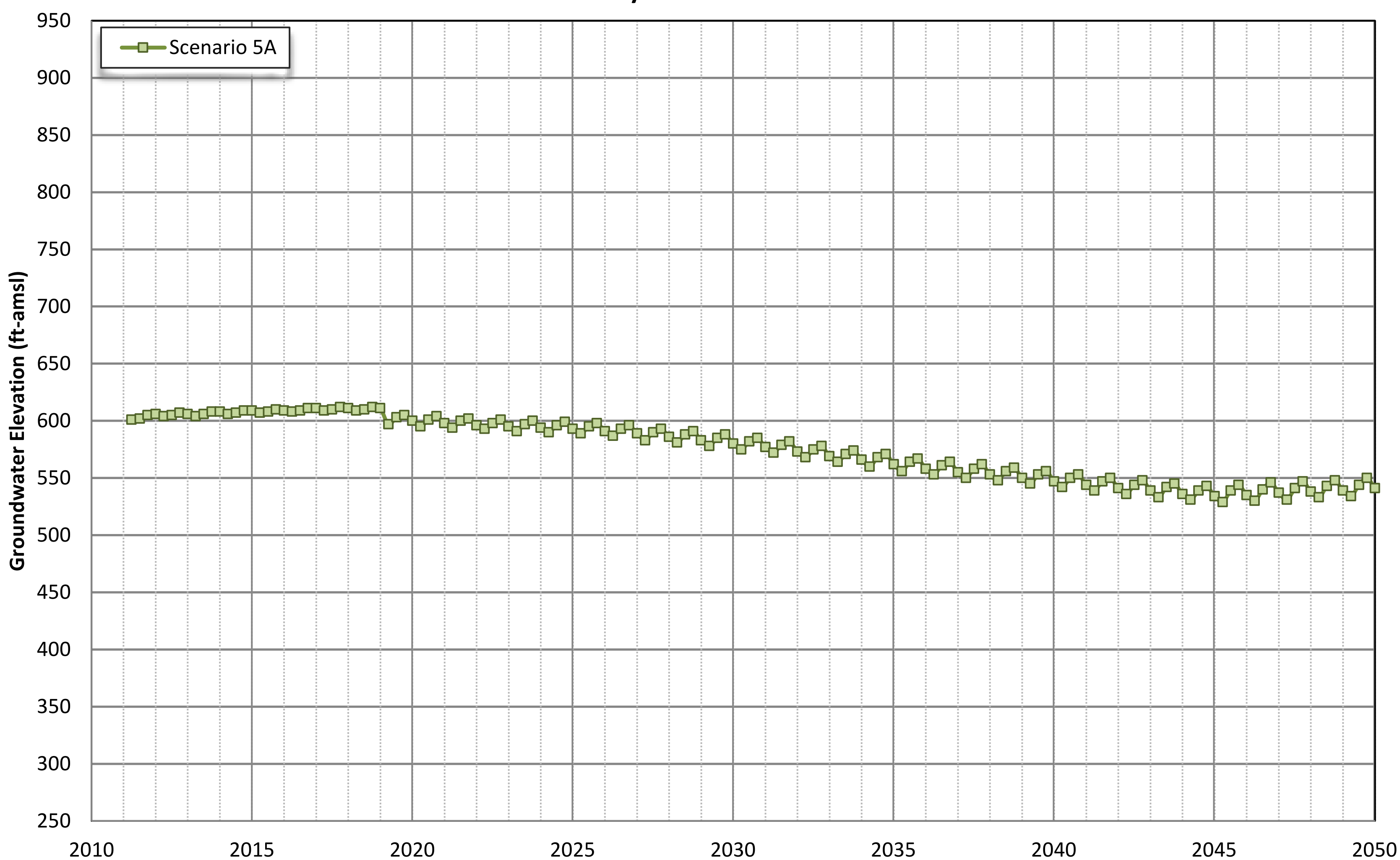

Appendix D_20150916_WellHydrographs_S5A4_Final_LBB2.xlsm
Created: 9/15/15
Printed: 9/16/2015

Figure D-154
Projected Groundwater Elevation for Scenario 5a
City of Ontario Well 111

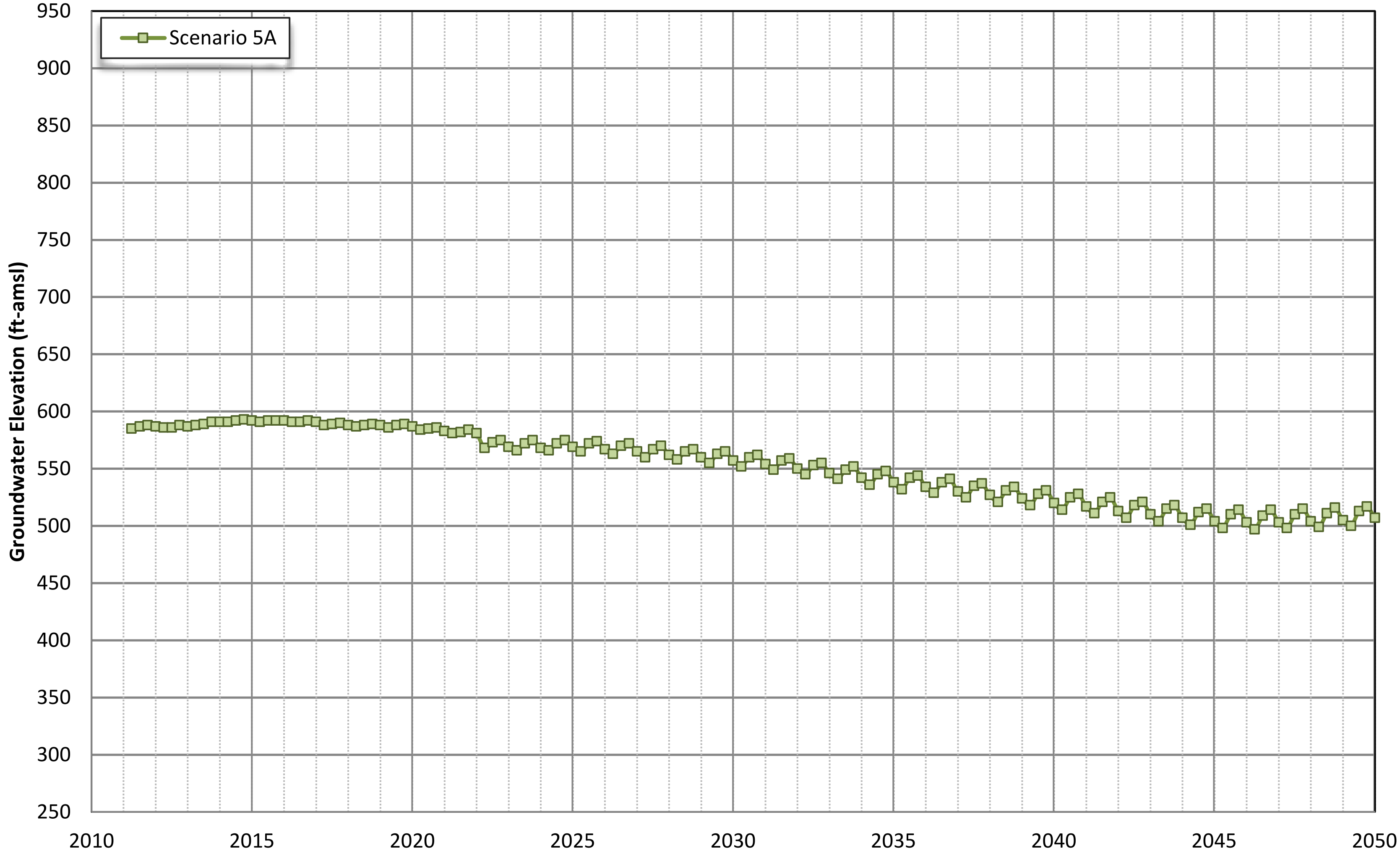

Appendix D_20150916_WellHydrographs_S5A4_Final_LBB2.xlsm
Created: 9/15/15
Printed: 9/16/2015

Figure D-155
Projected Groundwater Elevation for Scenario 5a
City of Ontario Well 115

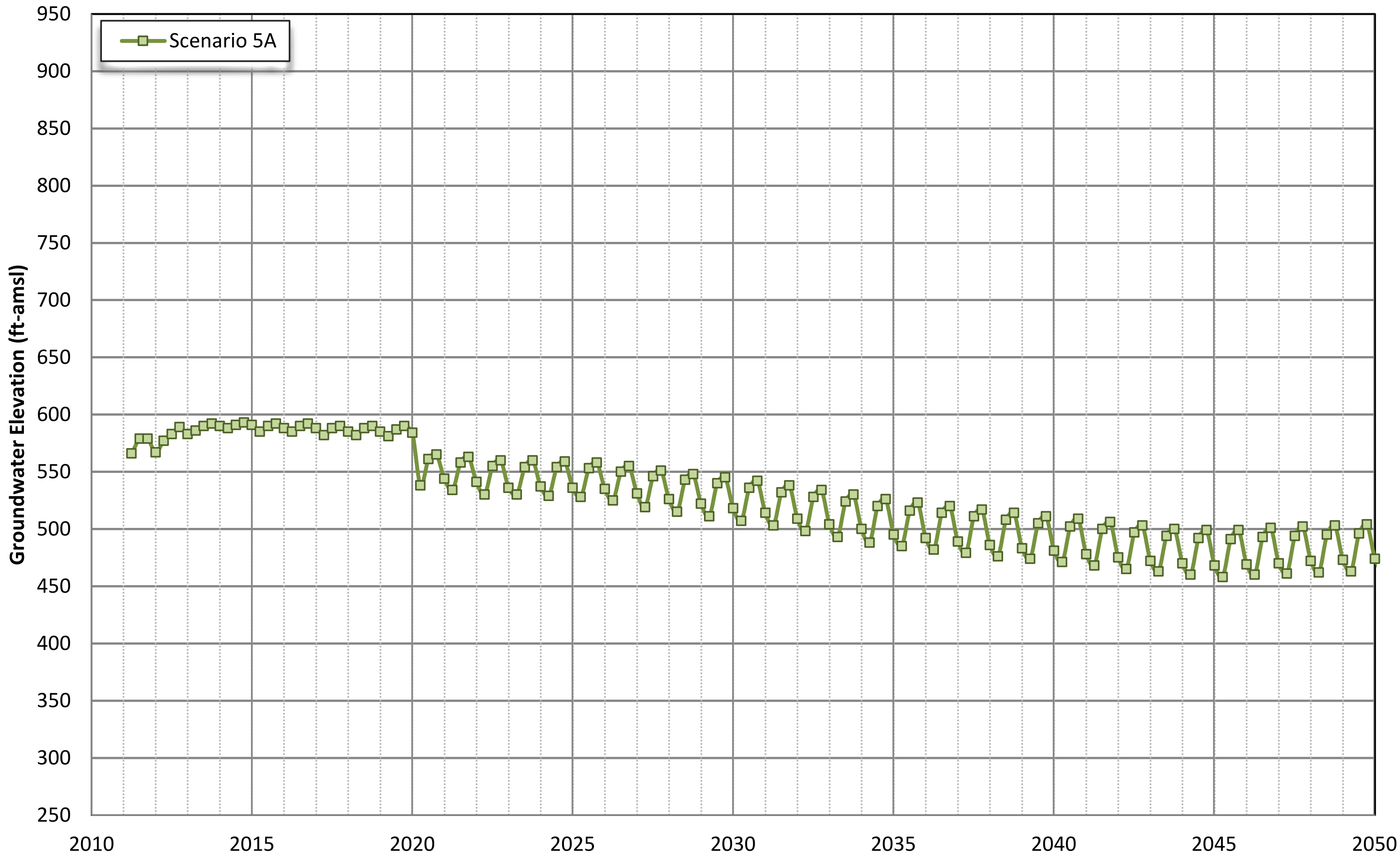

Appendix D_20150916_WellHydrographs_S5A4_Final_LBB2.xlsm
Created: 9/15/15
Printed: 9/16/2015

Figure D-156
Projected Groundwater Elevation for Scenario 5a
City of Ontario Well 119

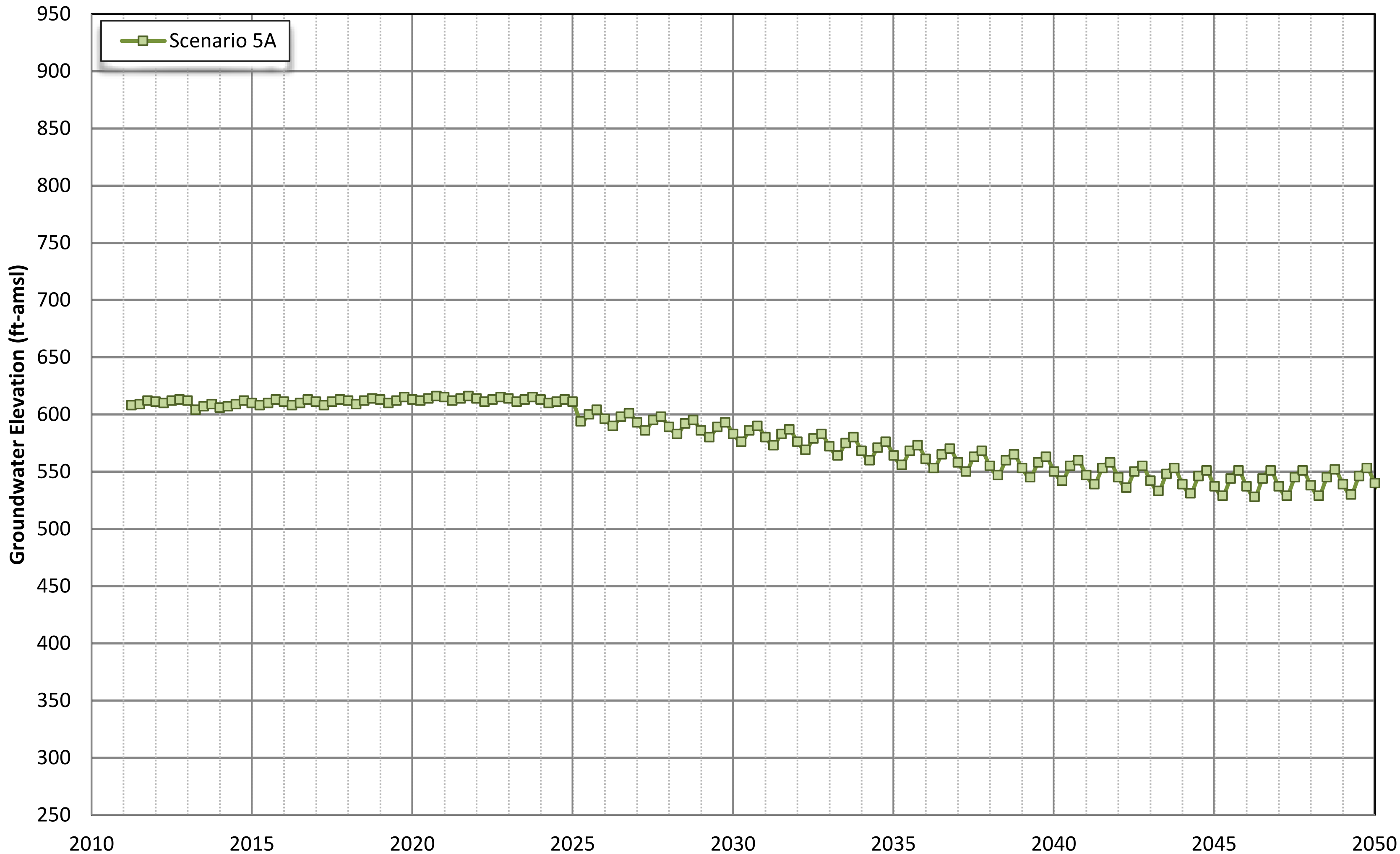

Appendix D_20150916_WellHydrographs_S5A4_Final_LBB2.xlsm
Created: 9/15/15
Printed: 9/16/2015

Figure D-157
Projected Groundwater Elevation for Scenario 5a
City of Ontario Well 120

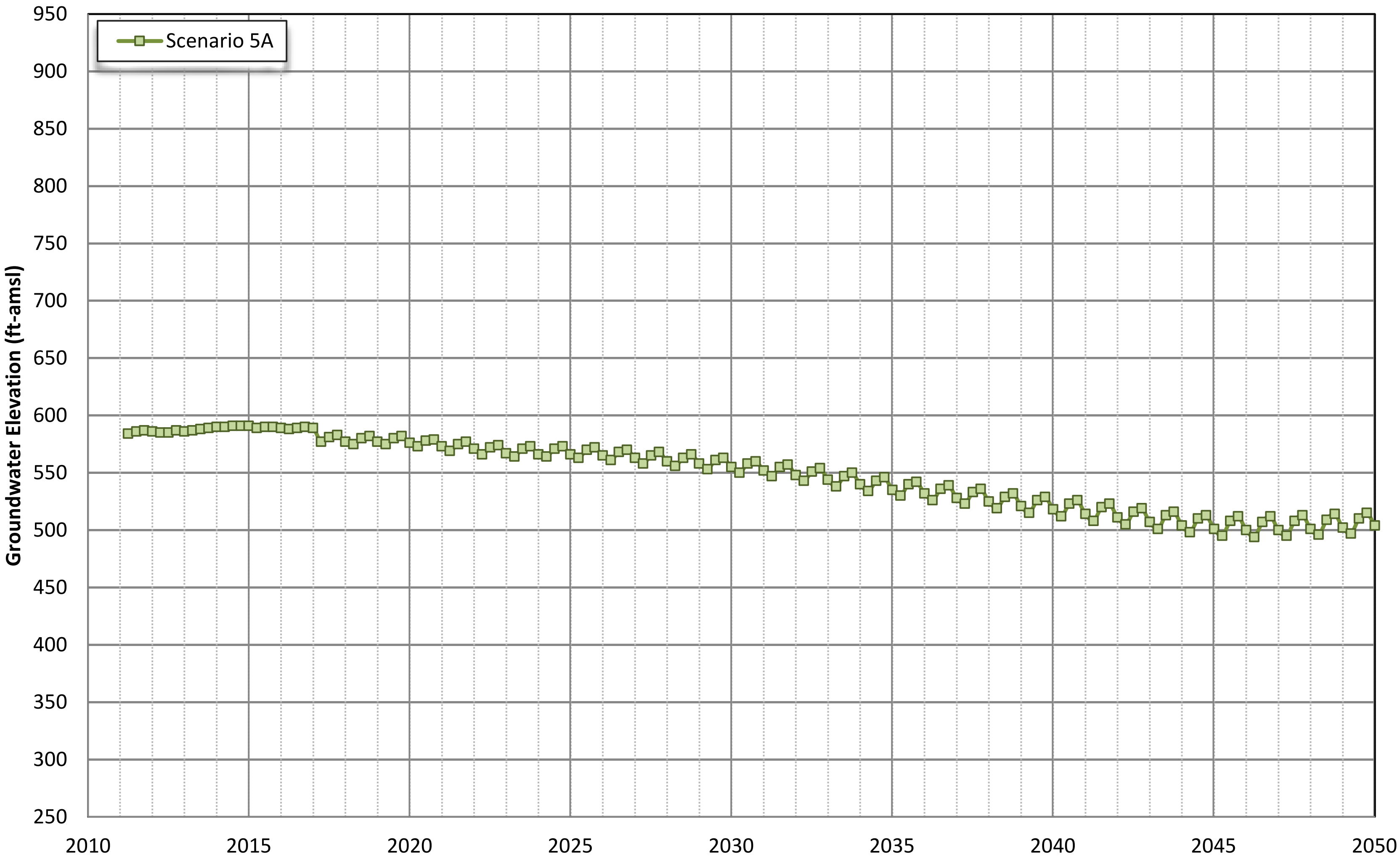

Appendix D_20150916_WellHydrographs_S5A4_Final_LBB2.xlsm
Created: 9/15/15
Printed: 9/16/2015

Figure D-158
Projected Groundwater Elevation for Scenario 5a
City of Ontario Well 126

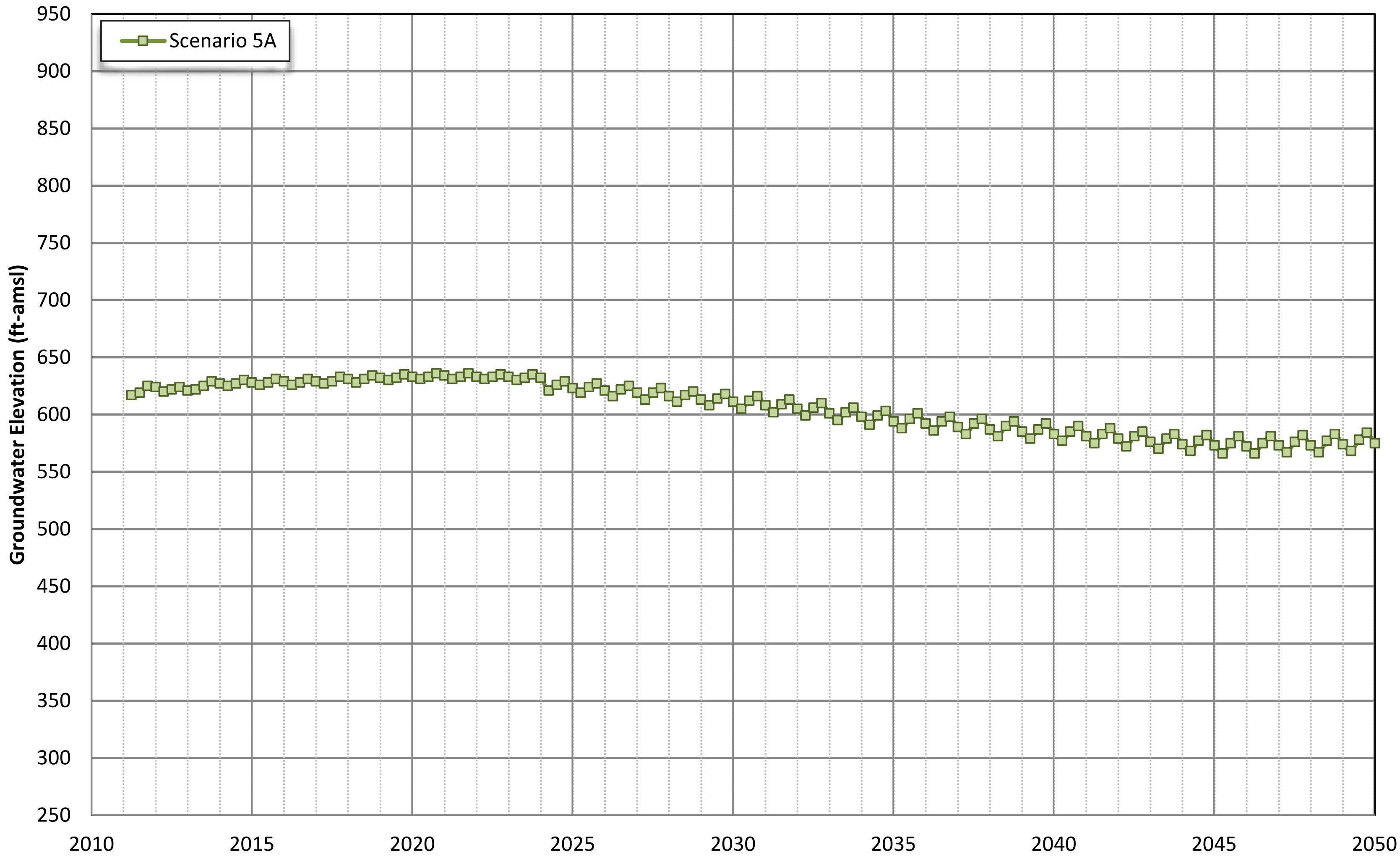

Appendix D_20150916_WellHydrographs_S5A4_Final_LBB2.xlsm
Created: 9/15/15
Printed: 9/16/2015

Figure D-159
Projected Groundwater Elevation for Scenario 5a
City of Ontario Well 134

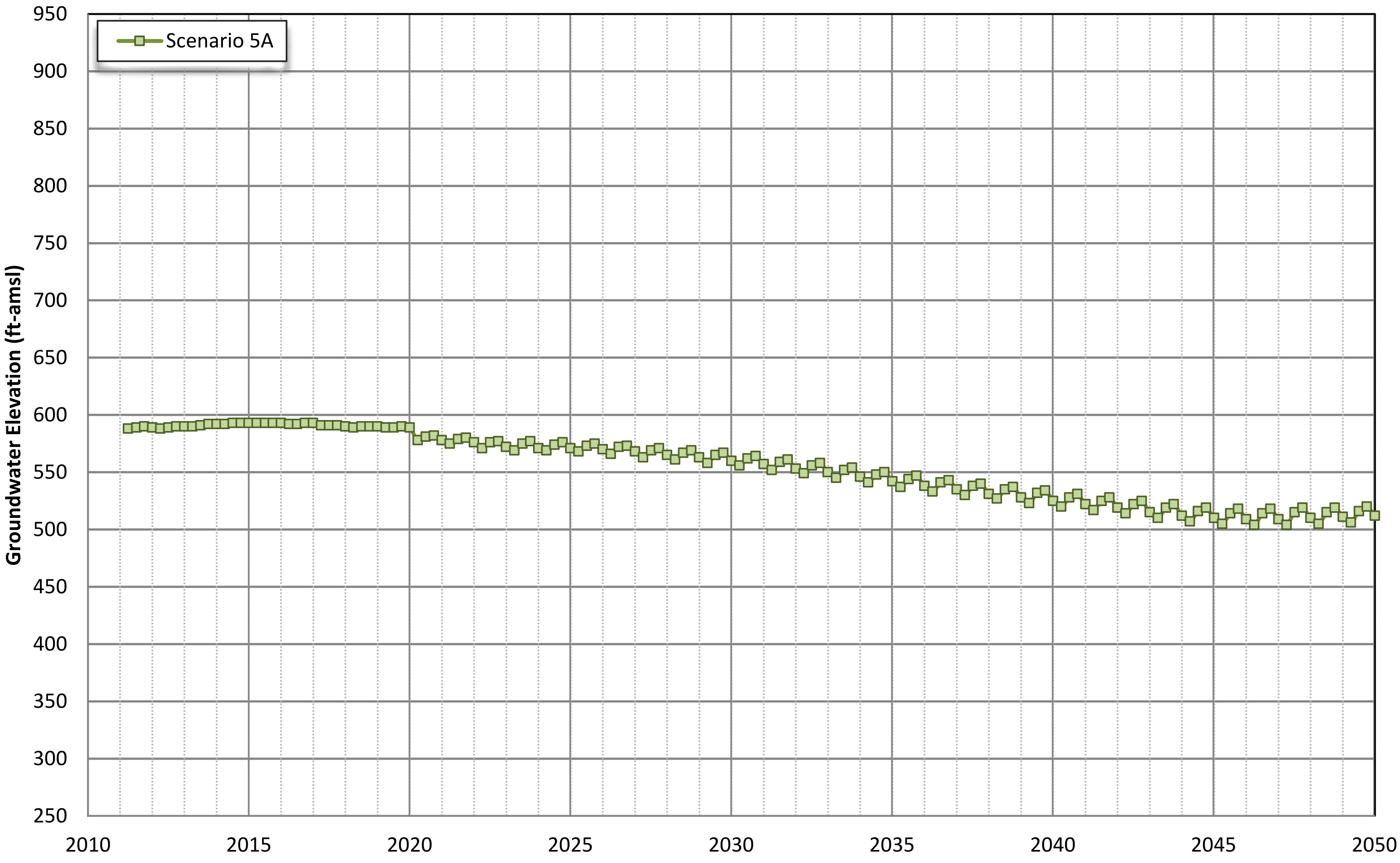

Appendix D_20150916_WellHydrographs_S5A4_Final_LBB2.xlsm
Created: 9/15/15
Printed: 9/16/2015

Figure D-160
Projected Groundwater Elevation for Scenario 5a
City of Ontario Well 136

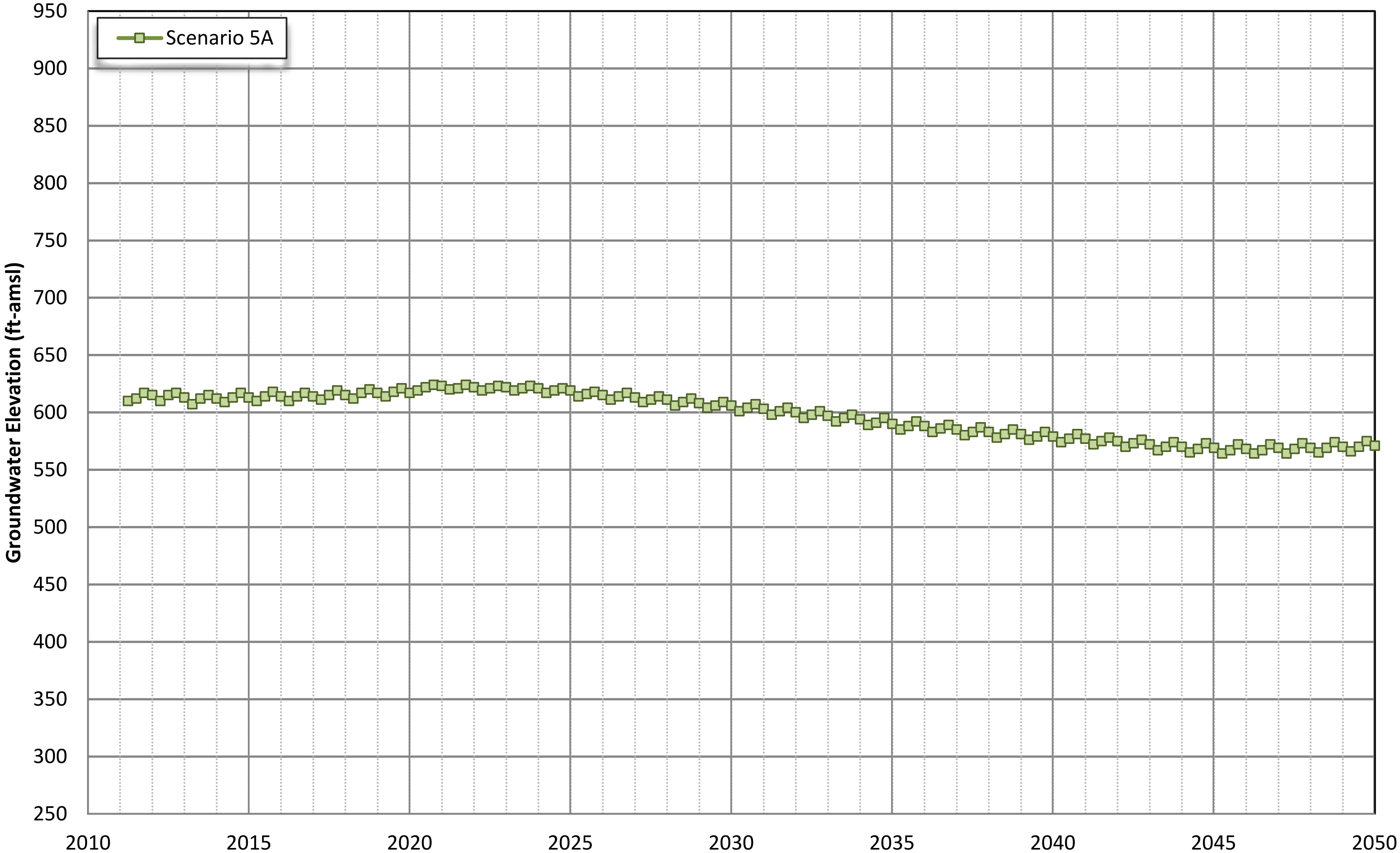

Appendix D_20150916_WellHydrographs_S5A4_Final_LBB2.xlsm
Created: 9/15/15
Printed: 9/16/2015

Figure D-161
Projected Groundwater Elevation for Scenario 5a
City of Ontario Well 138

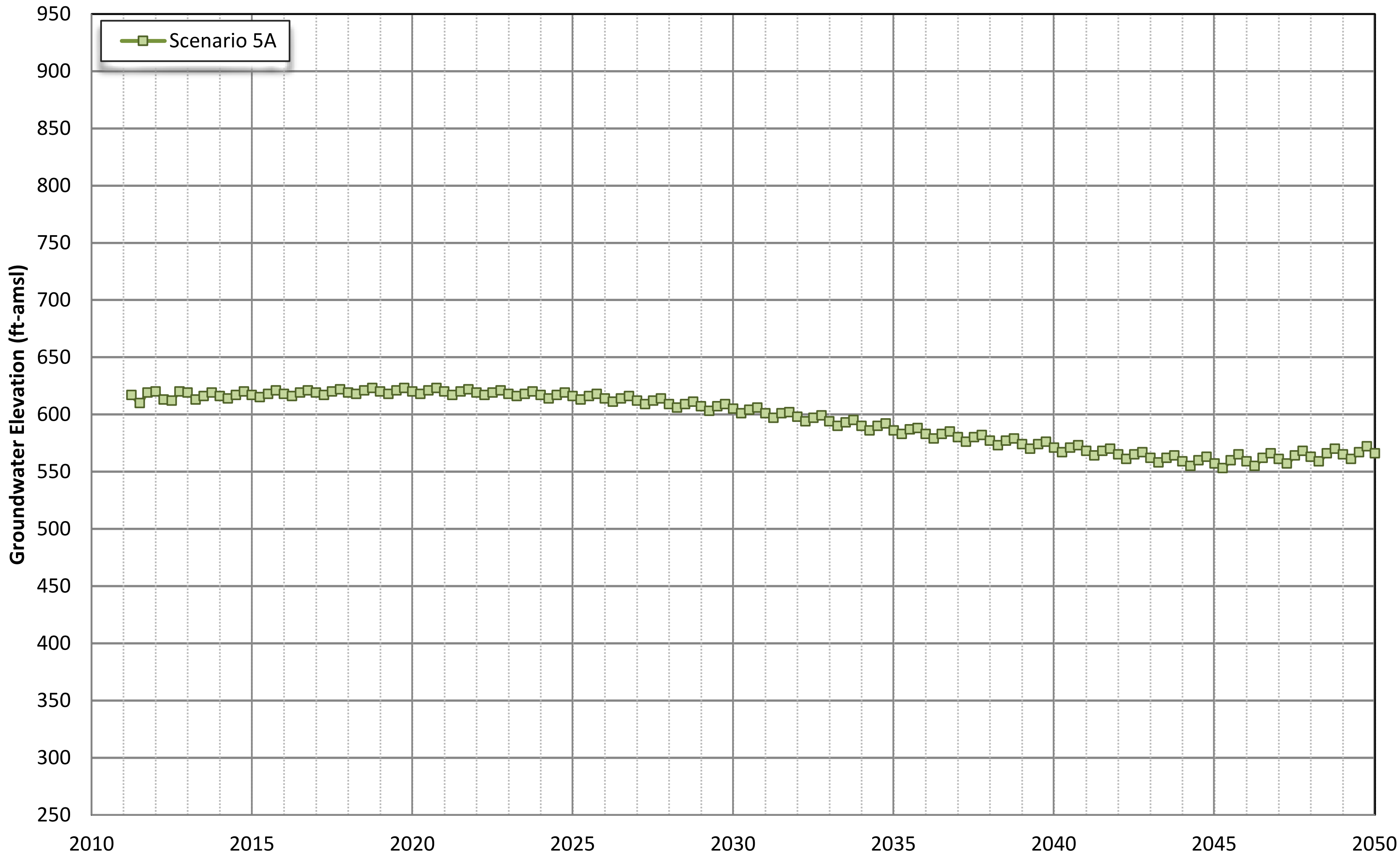

Appendix D_20150916_WellHydrographs_S5A4_Final_LBB2.xlsm
Created: 9/15/15
Printed: 9/16/2015

Figure D-162
Projected Groundwater Elevation for Scenario 5a
City of Pomona Well 2

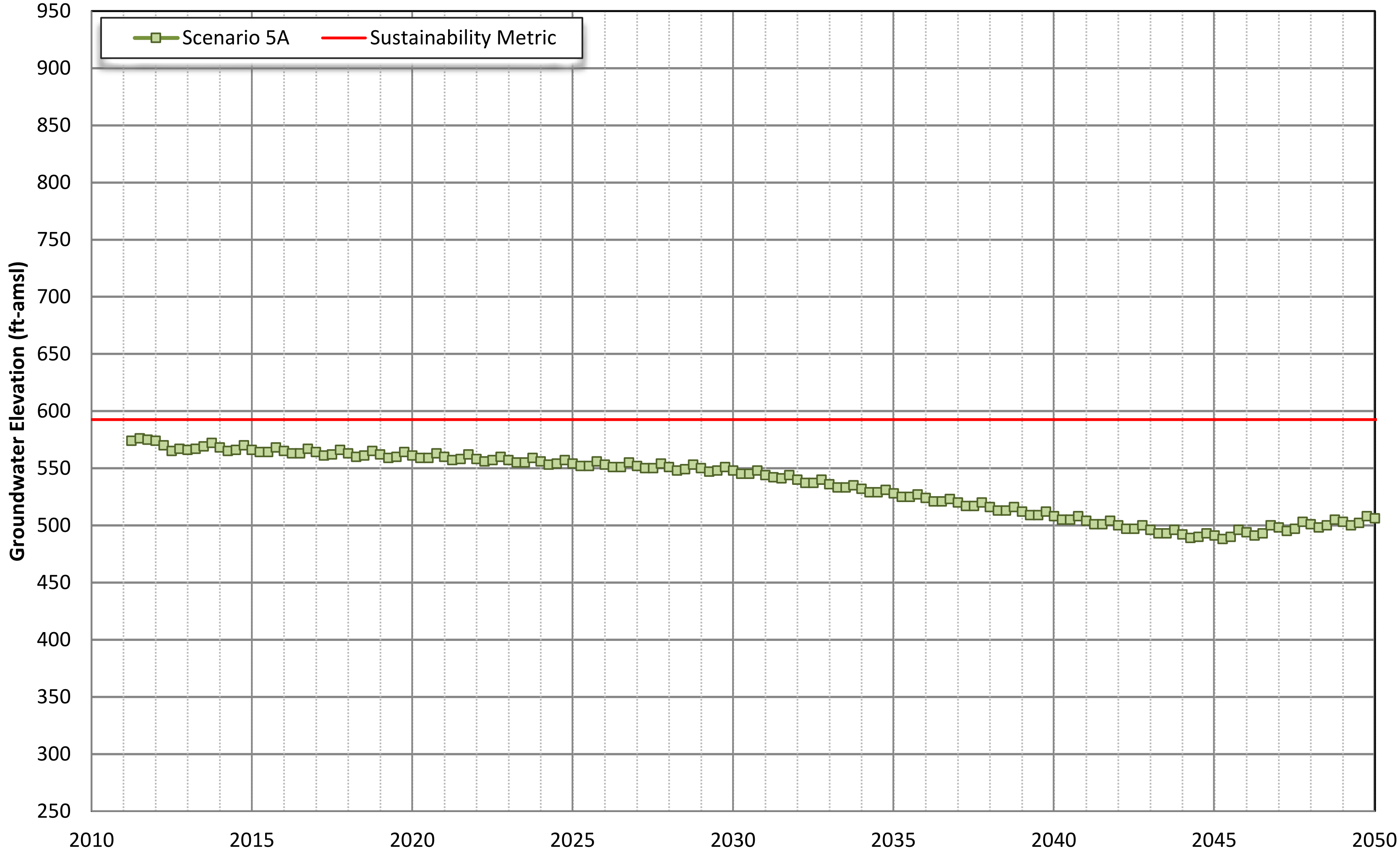

Appendix D_20150916_WellHydrographs_S5A4_Final_LBB2.xlsm
Created: 9/15/15
Printed: 9/16/2015

Figure D-163
Projected Groundwater Elevation for Scenario 5a
City of Pomona Well 6

Appendix D_20150916_WellHydrographs_S5A4_Final_LBB2.xlsm
Created: 9/15/15
Printed: 9/16/2015

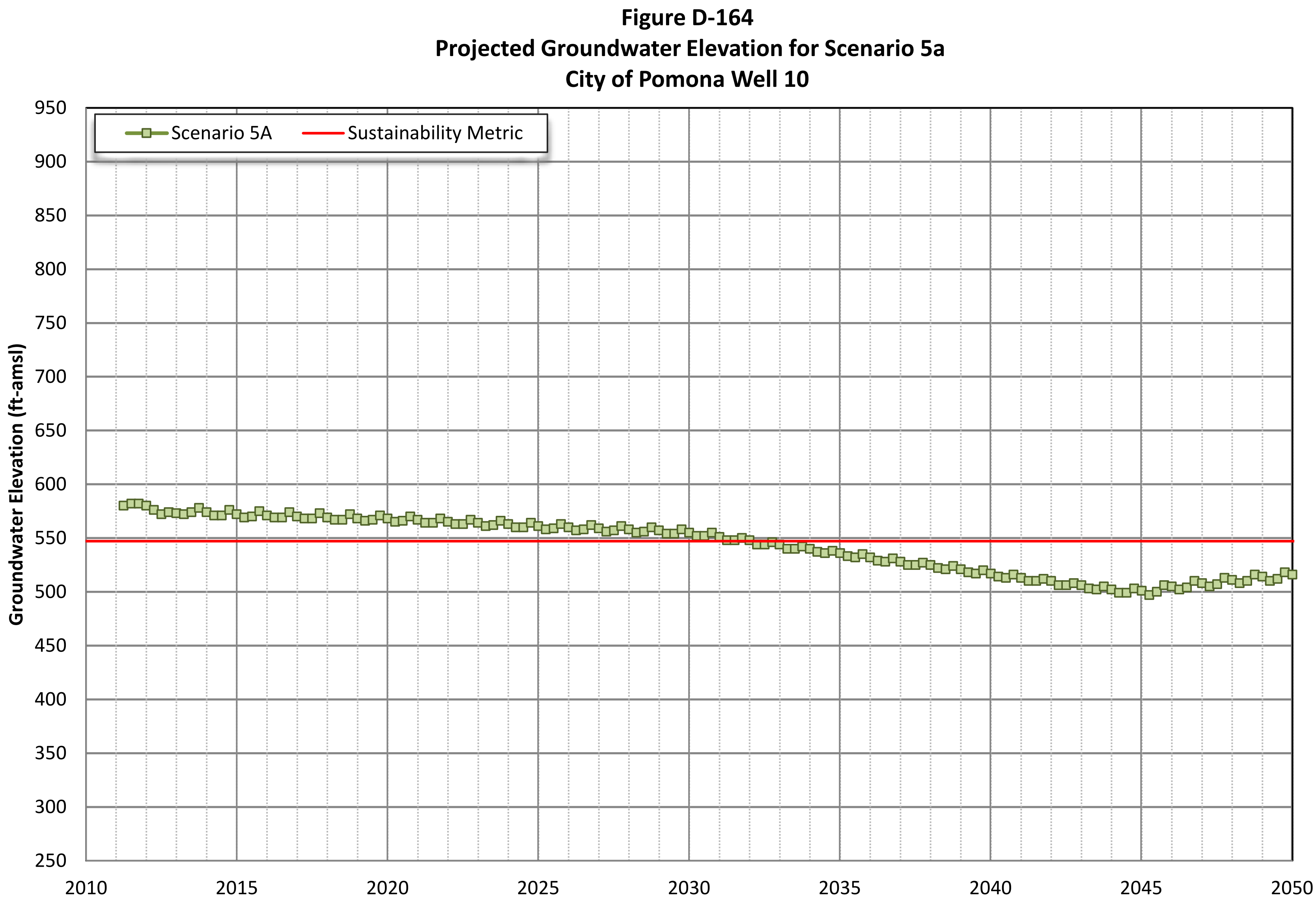

Appendix D_20150916_WellHydrographs_S5A4_Final_LBB2.xlsm
Created: 9/15/15
Printed: 9/16/2015

Figure D-165
Projected Groundwater Elevation for Scenario 5a
City of Pomona Well 11

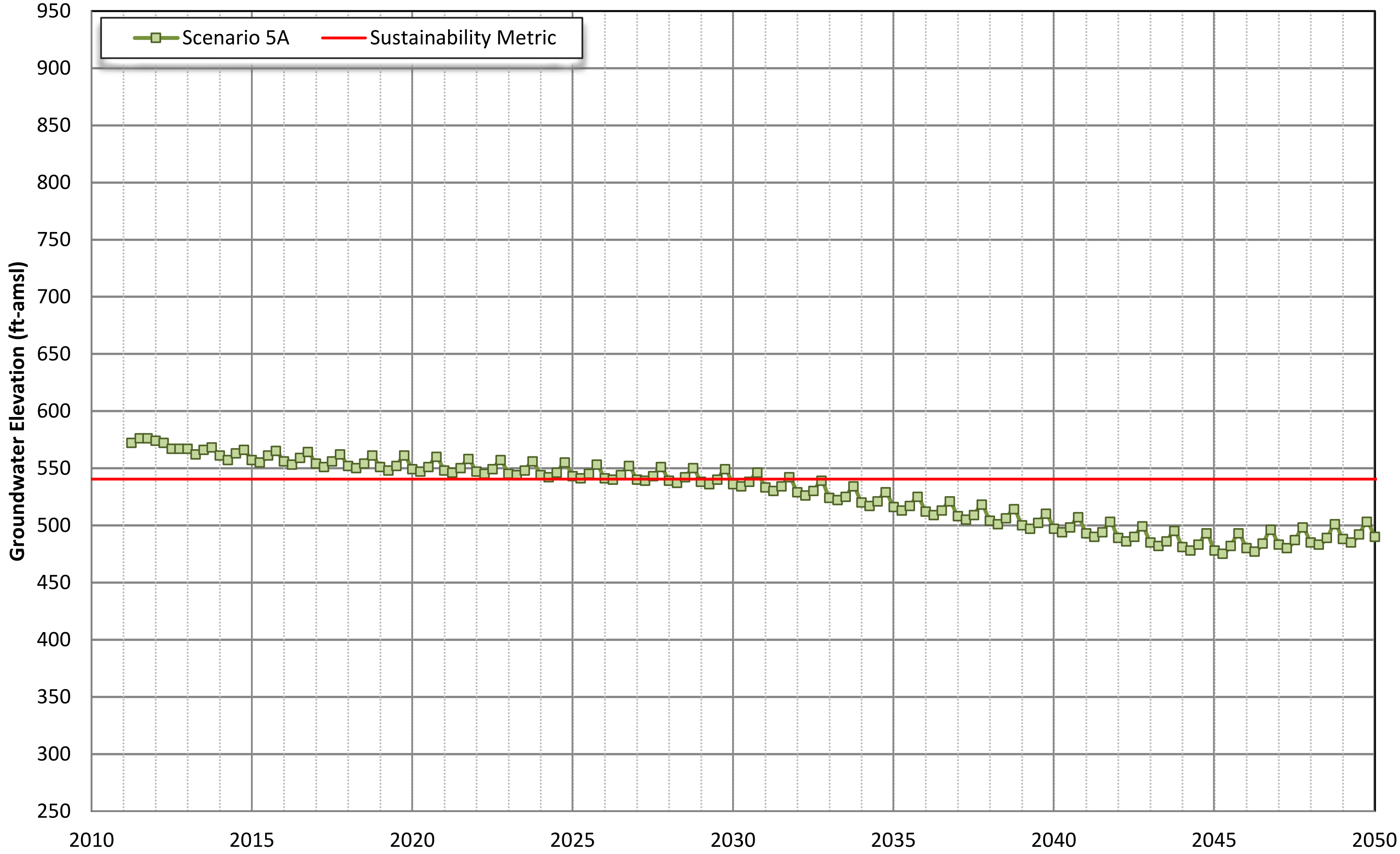

Appendix D_20150916_WellHydrographs_S5A4_Final_LBB2.xlsm
Created: 9/15/15
Printed: 9/16/2015

Figure D-166
Projected Groundwater Elevation for Scenario 5a
City of Pomona Well 12

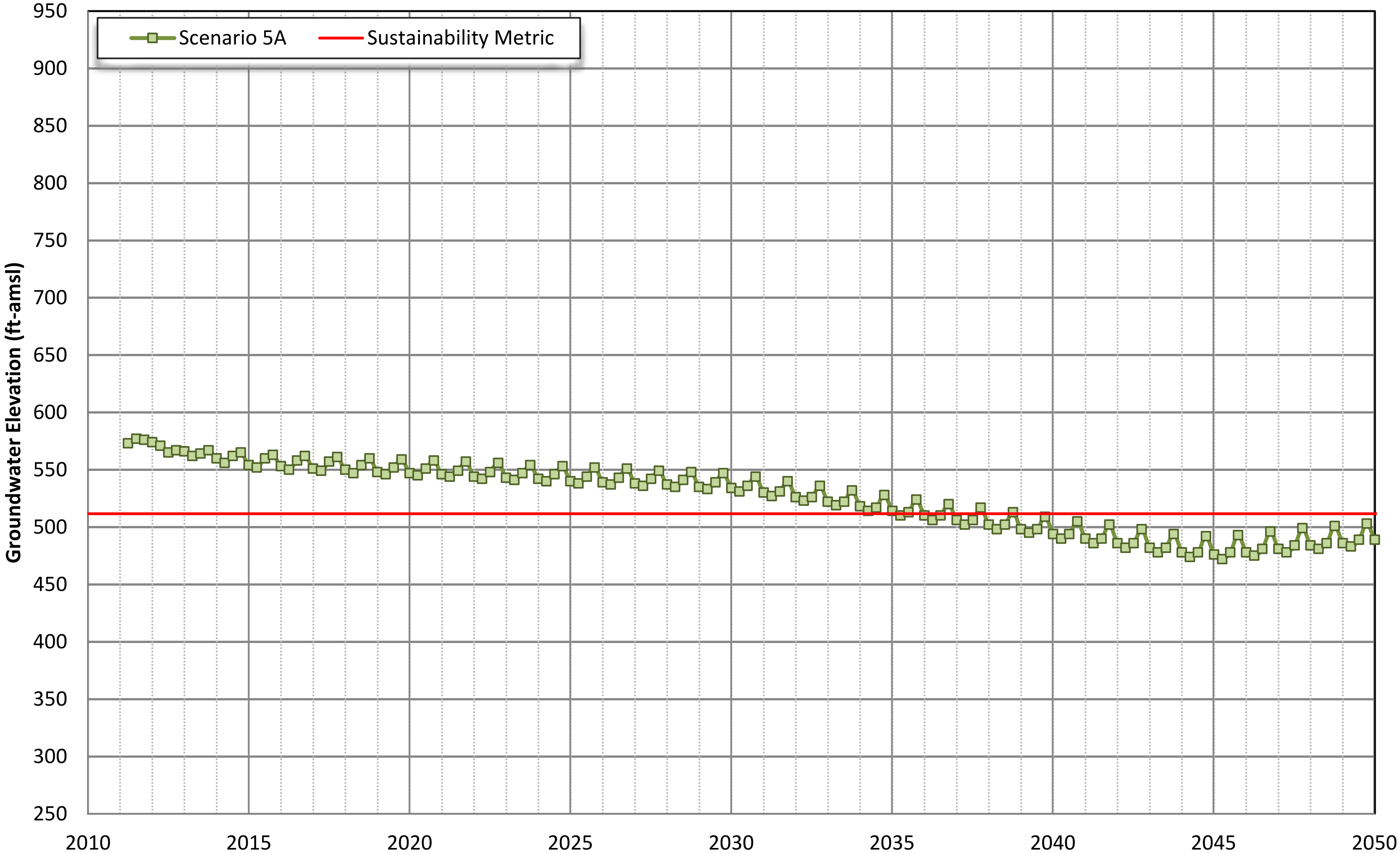

Appendix D_20150916_WellHydrographs_S5A4_Final_LBB2.xlsm
Created: 9/15/15
Printed: 9/16/2015

Figure D-167
Projected Groundwater Elevation for Scenario 5a
City of Pomona Well 14

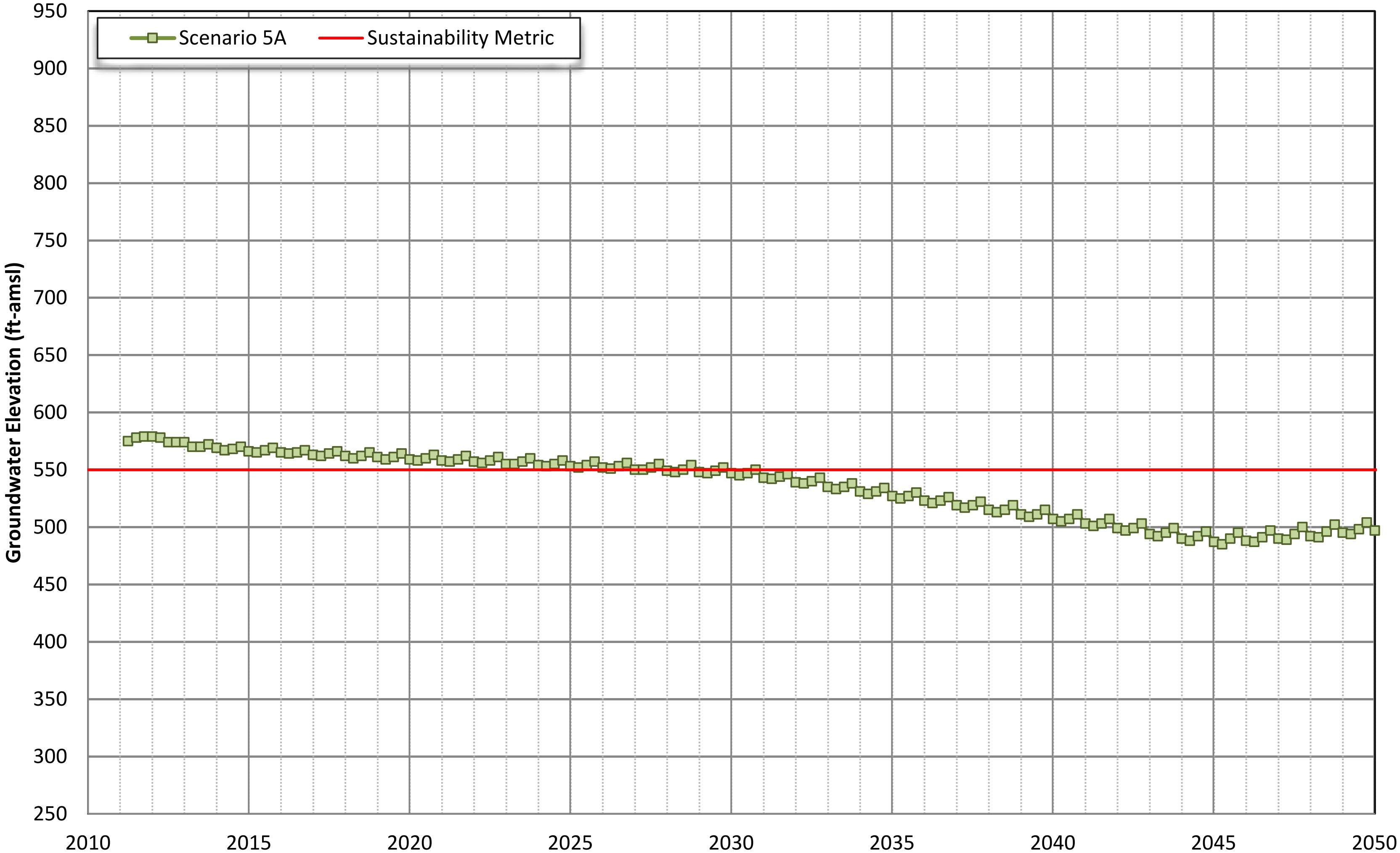

Appendix D_20150916_WellHydrographs_S5A4_Final_LBB2.xlsm
Created: 9/15/15
Printed: 9/16/2015

Figure D-168
Projected Groundwater Elevation for Scenario 5a
City of Pomona Well 15

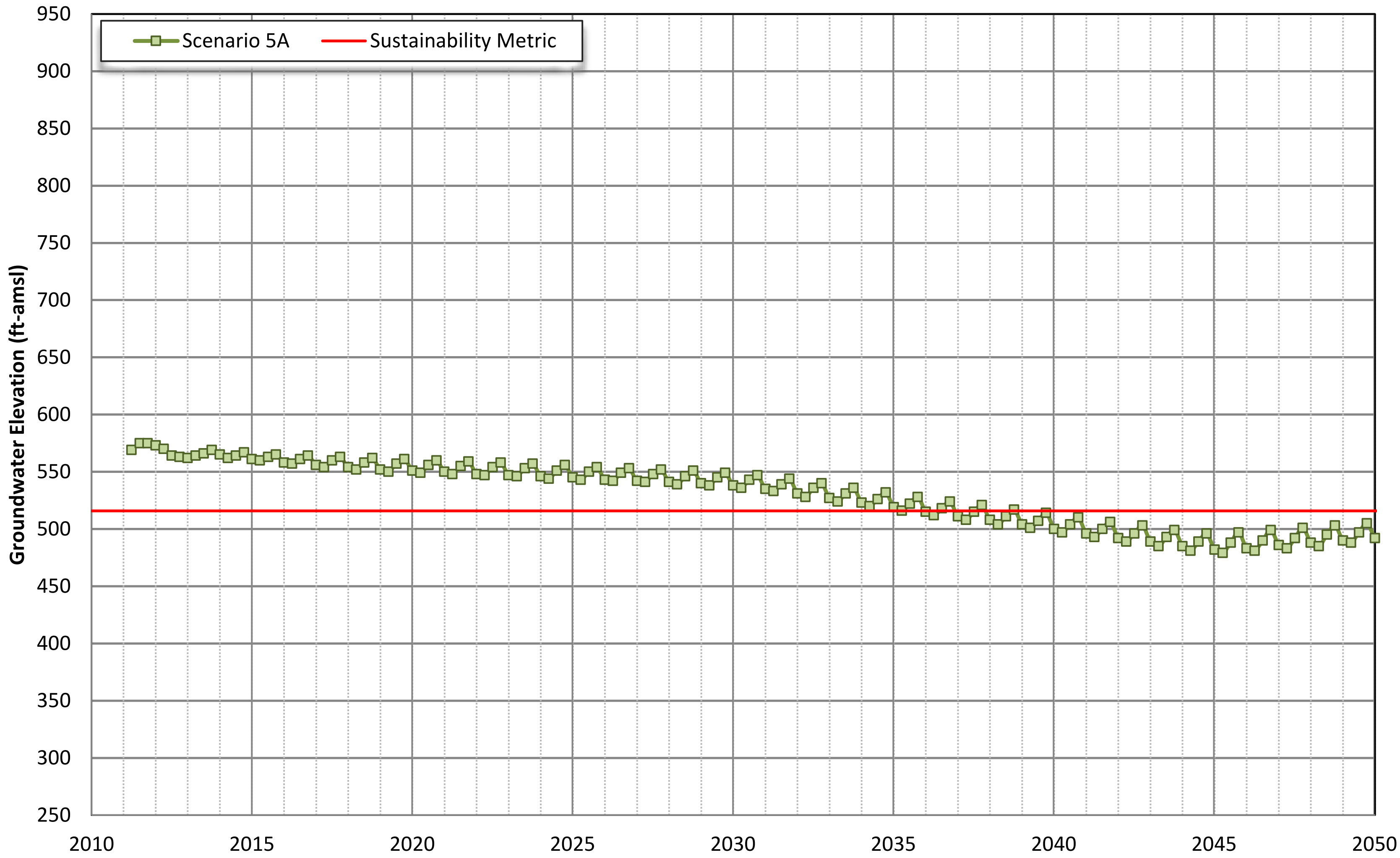

Appendix D_20150916_WellHydrographs_S5A4_Final_LBB2.xlsm
Created: 9/15/15
Printed: 9/16/2015

Figure D-169
Projected Groundwater Elevation for Scenario 5a
City of Pomona Well 16

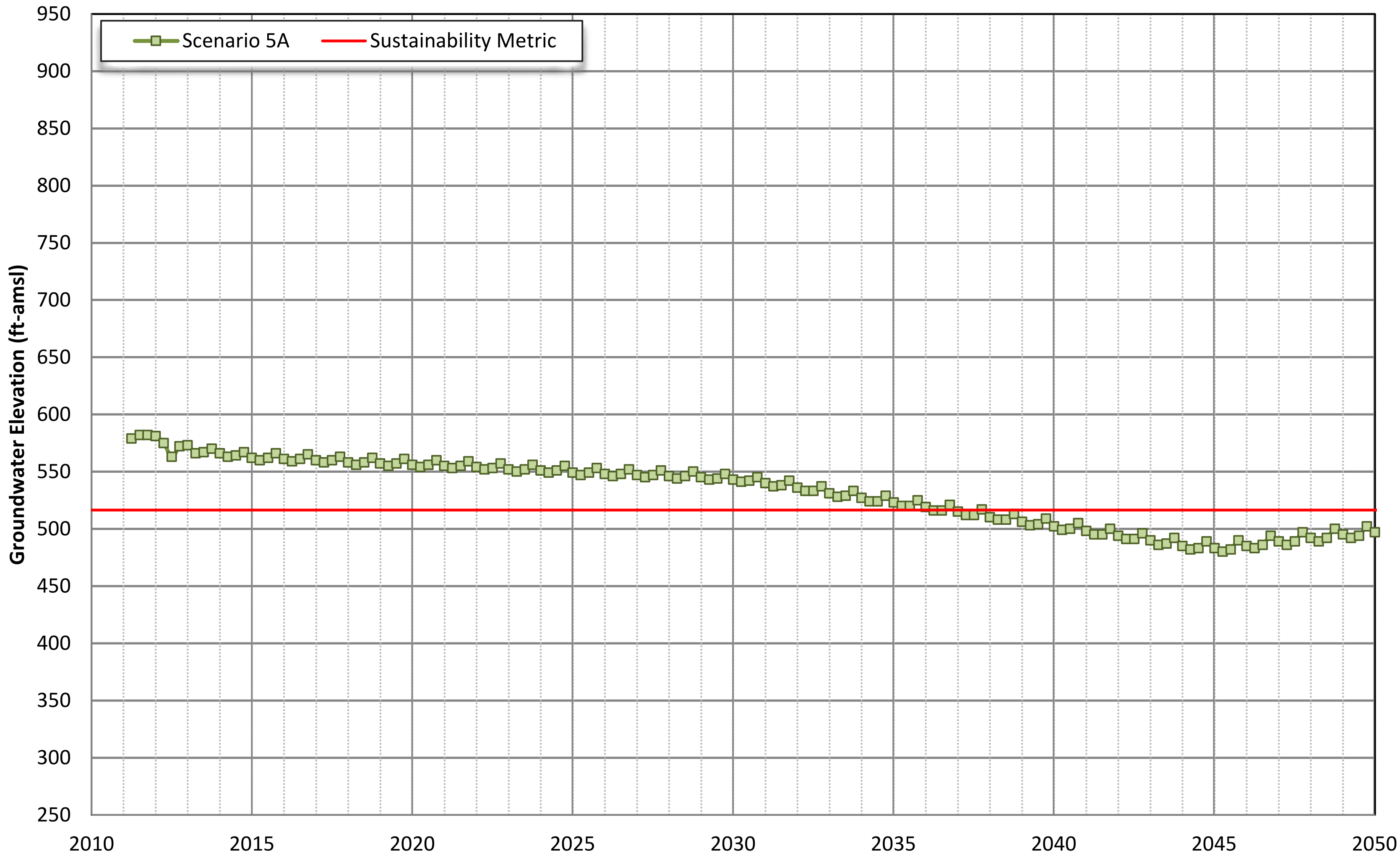

Appendix D_20150916_WellHydrographs_S5A4_Final_LBB2.xlsm
Created: 9/15/15
Printed: 9/16/2015

Figure D-170
Projected Groundwater Elevation for Scenario 5a
City of Pomona Well 17

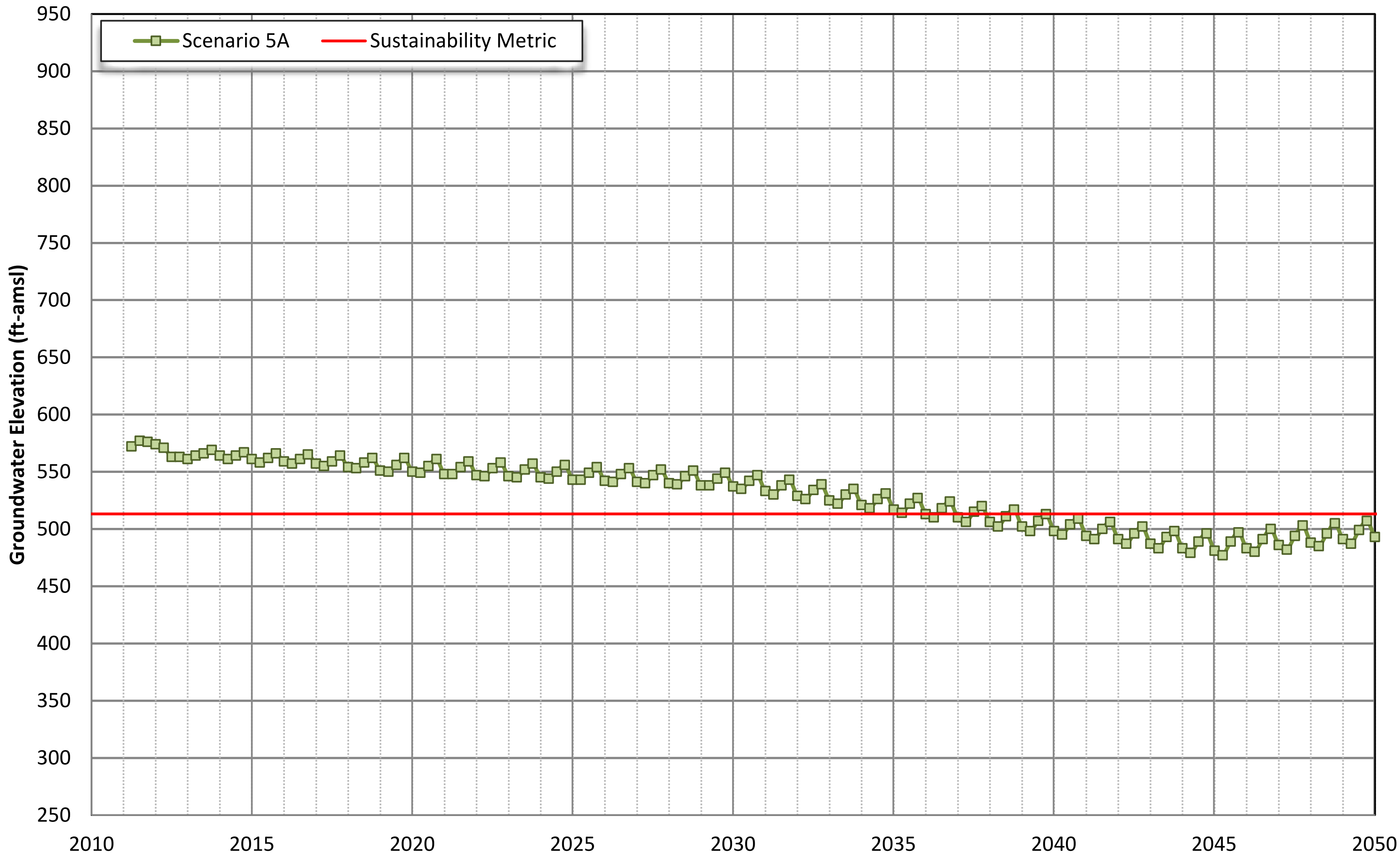

Appendix D_20150916_WellHydrographs_S5A4_Final_LBB2.xlsm
Created: 9/15/15
Printed: 9/16/2015

Figure D-171
Projected Groundwater Elevation for Scenario 5a
City of Pomona Well 18

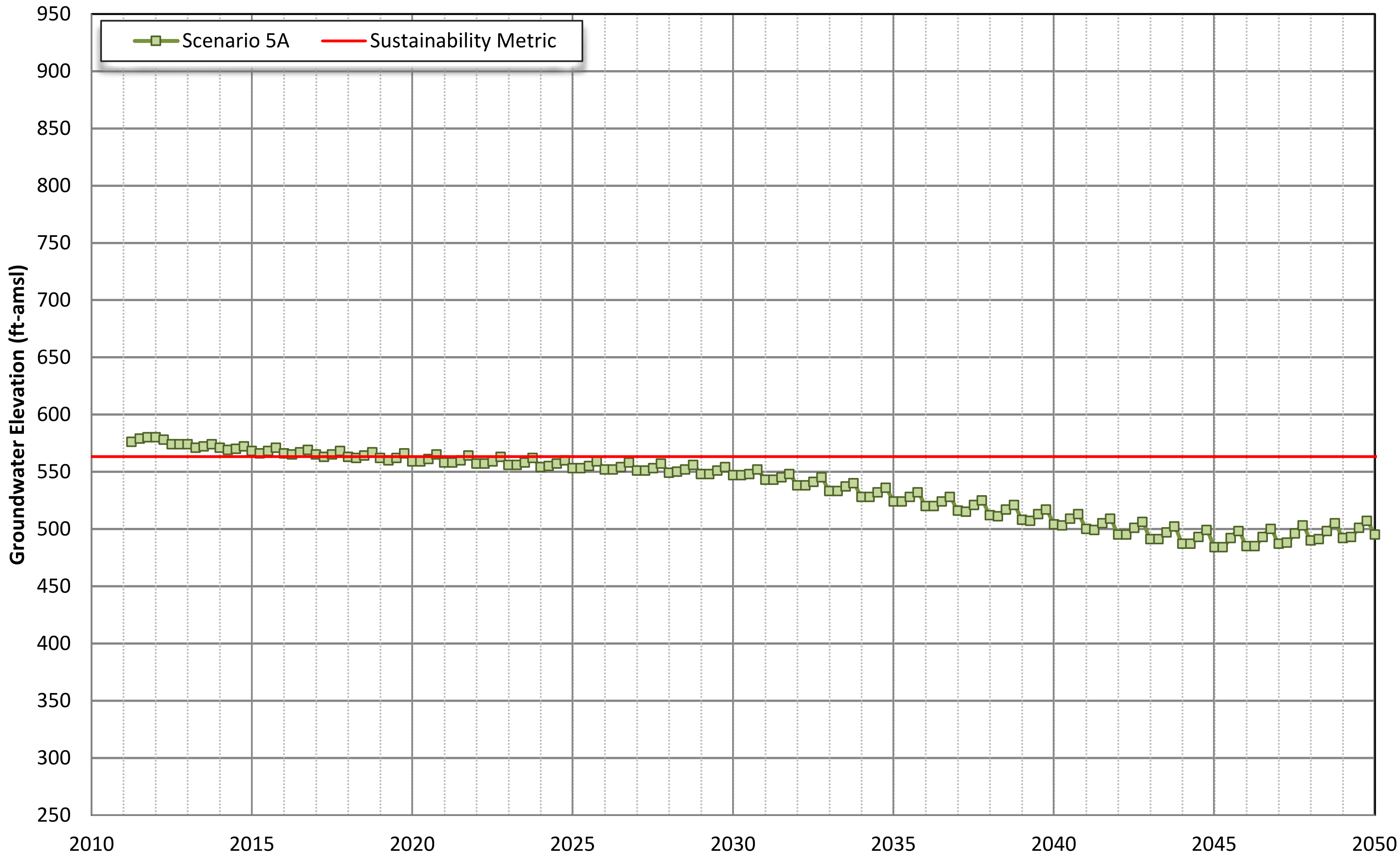

Appendix D_20150916_WellHydrographs_S5A4_Final_LBB2.xlsm
Created: 9/15/15
Printed: 9/16/2015

Figure D-172
Projected Groundwater Elevation for Scenario 5a
City of Pomona Well 21

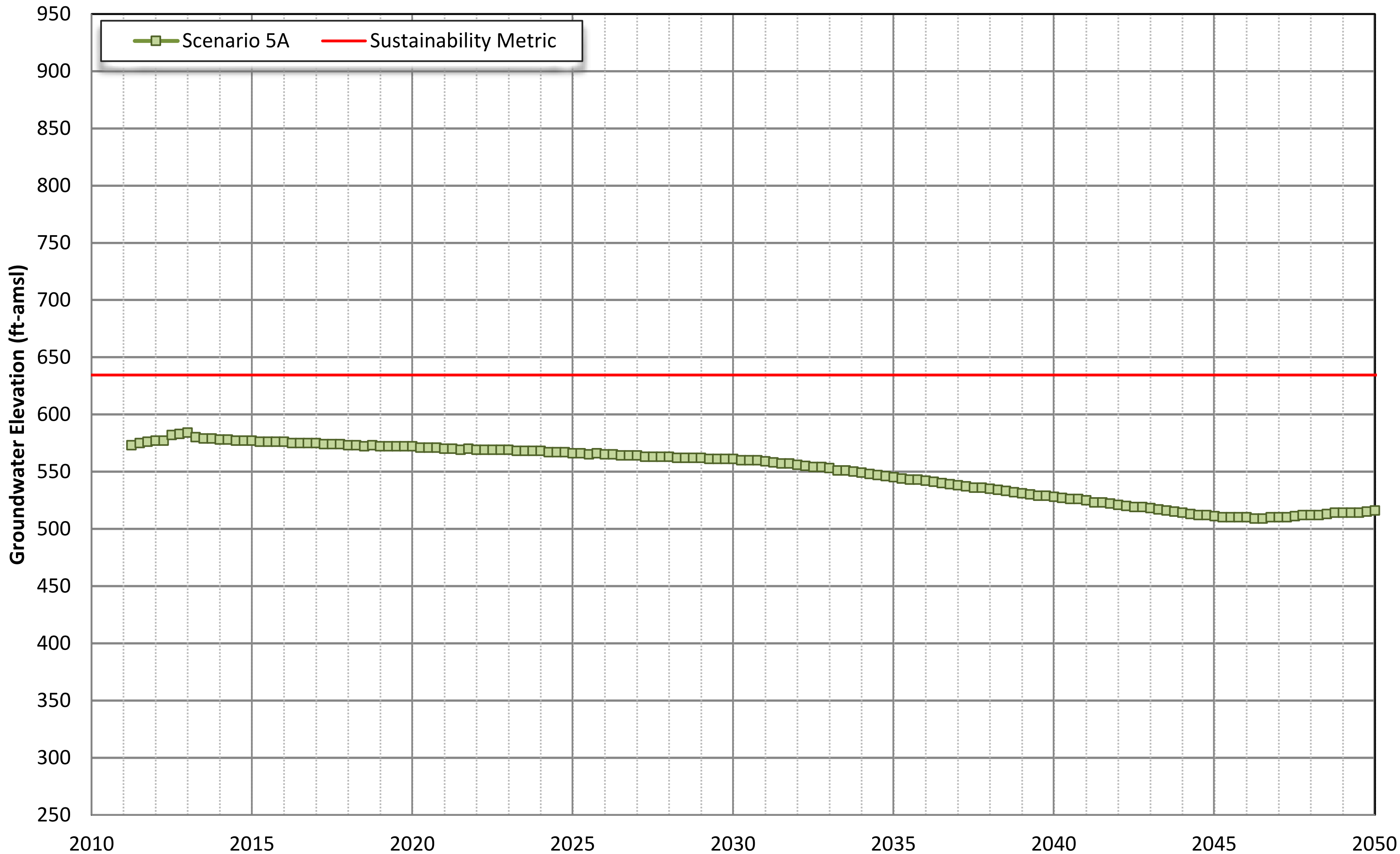

Appendix D_20150916_WellHydrographs_S5A4_Final_LBB2.xlsm
Created: 9/15/15
Printed: 9/16/2015

Figure D-173
Projected Groundwater Elevation for Scenario 5a
City of Pomona Well 23

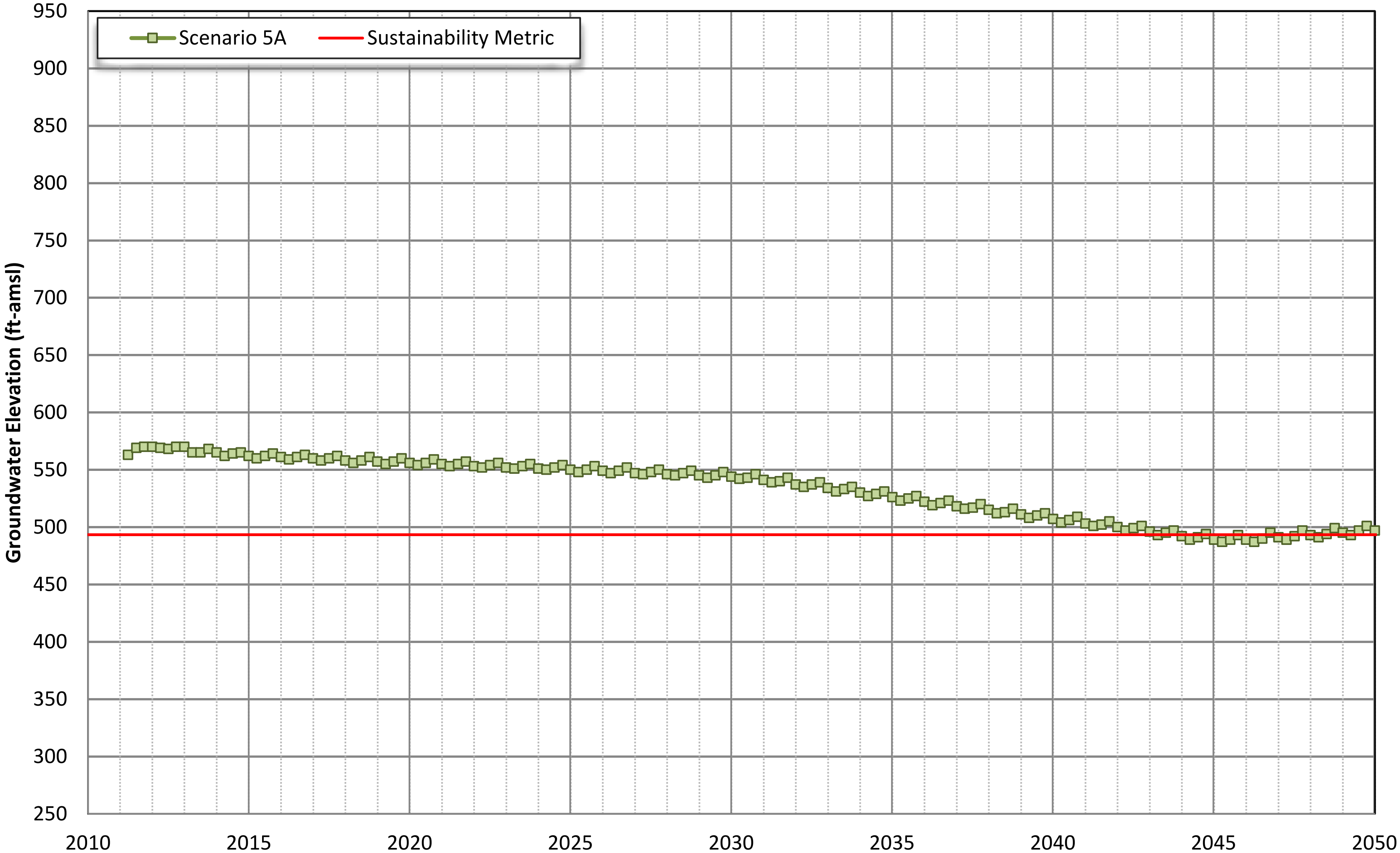

Appendix D_20150916_WellHydrographs_S5A4_Final_LBB2.xlsm
Created: 9/15/15
Printed: 9/16/2015

Figure D-174
Projected Groundwater Elevation for Scenario 5a
City of Pomona Well 25

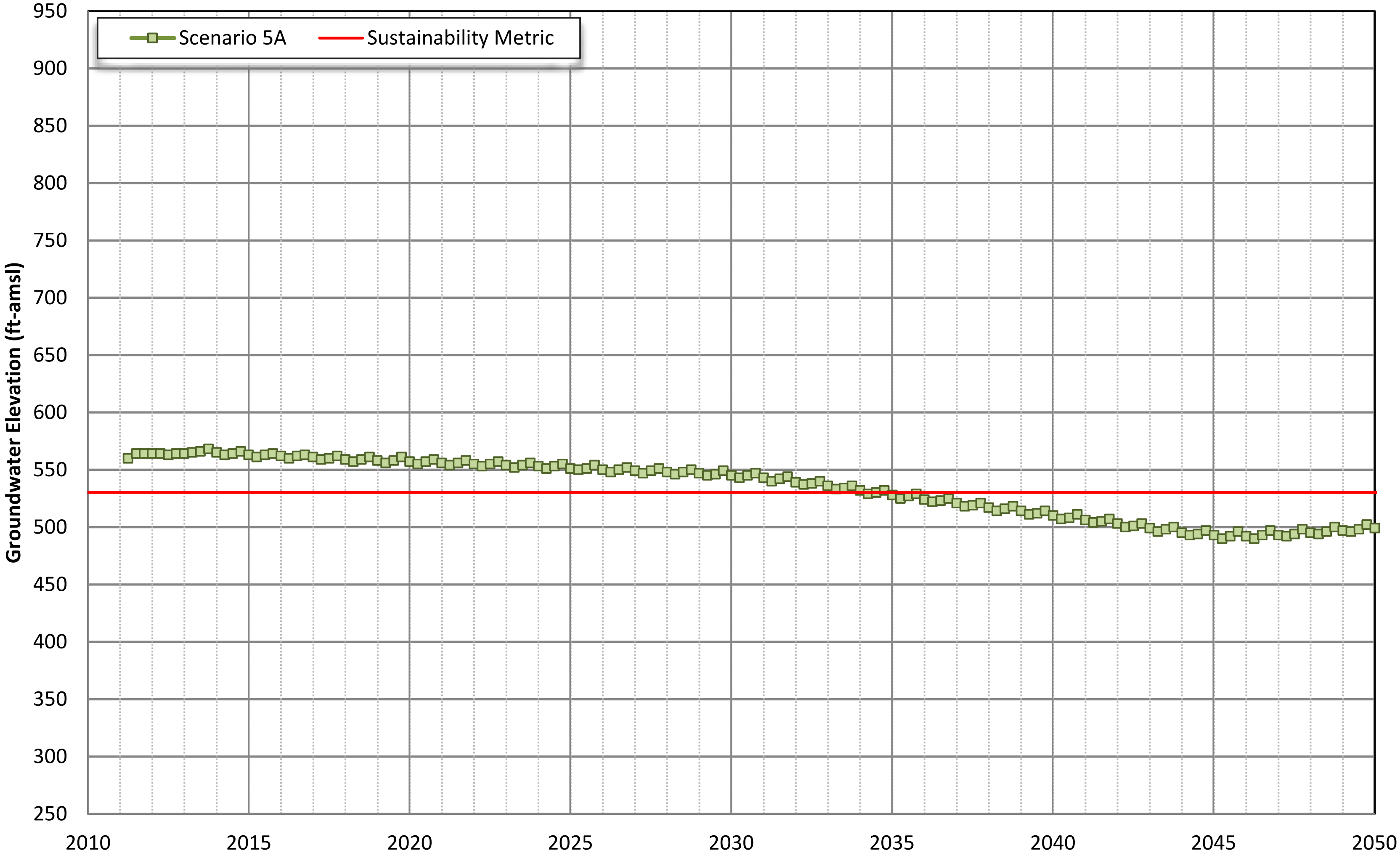

Appendix D_20150916_WellHydrographs_S5A4_Final_LBB2.xlsm
Created: 9/15/15
Printed: 9/16/2015

Figure D-175
Projected Groundwater Elevation for Scenario 5a
City of Pomona Well 26

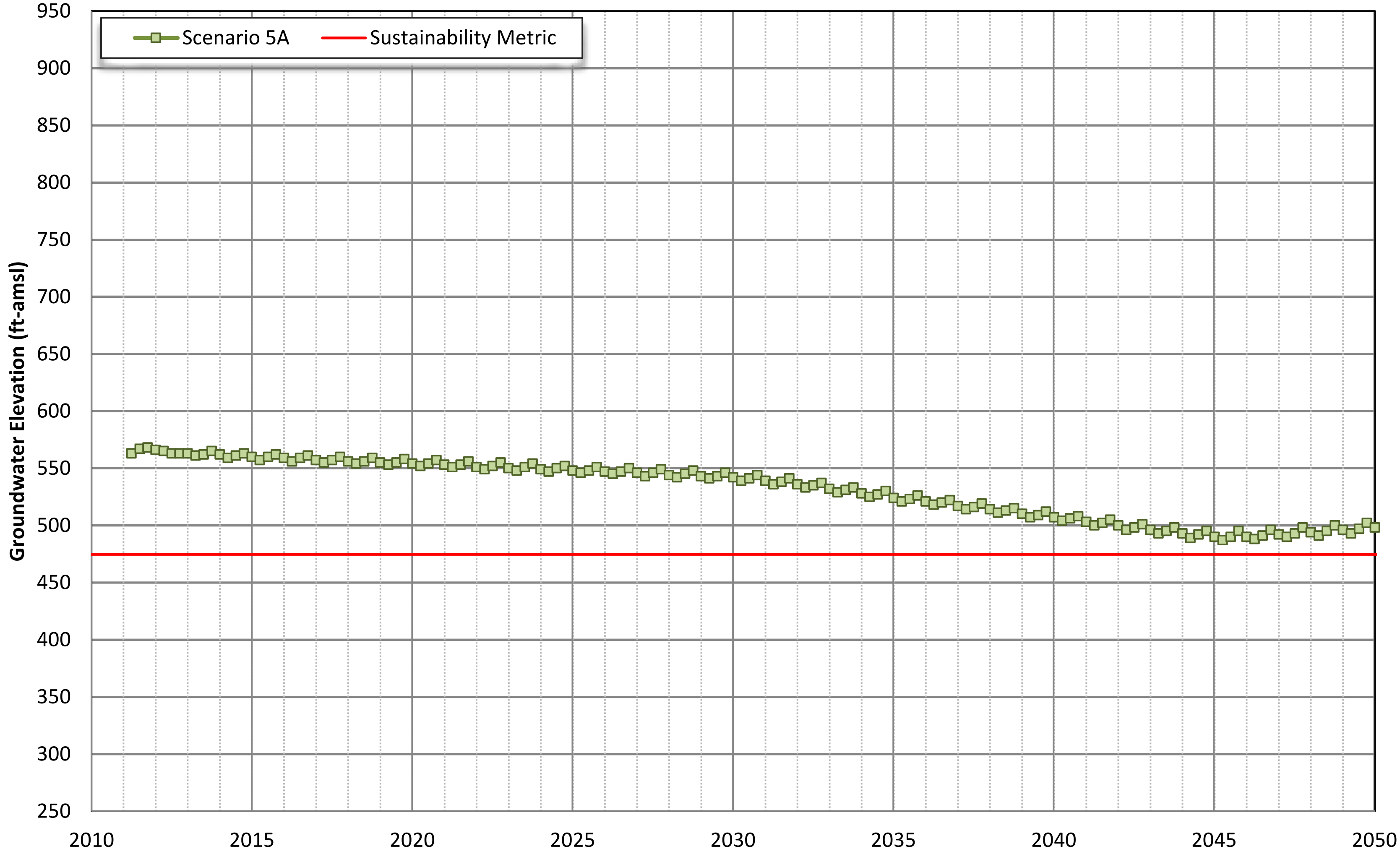

Appendix D_20150916_WellHydrographs_S5A4_Final_LBB2.xlsm
Created: 9/15/15
Printed: 9/16/2015

Figure D-176
Projected Groundwater Elevation for Scenario 5a
City of Pomona Well 27

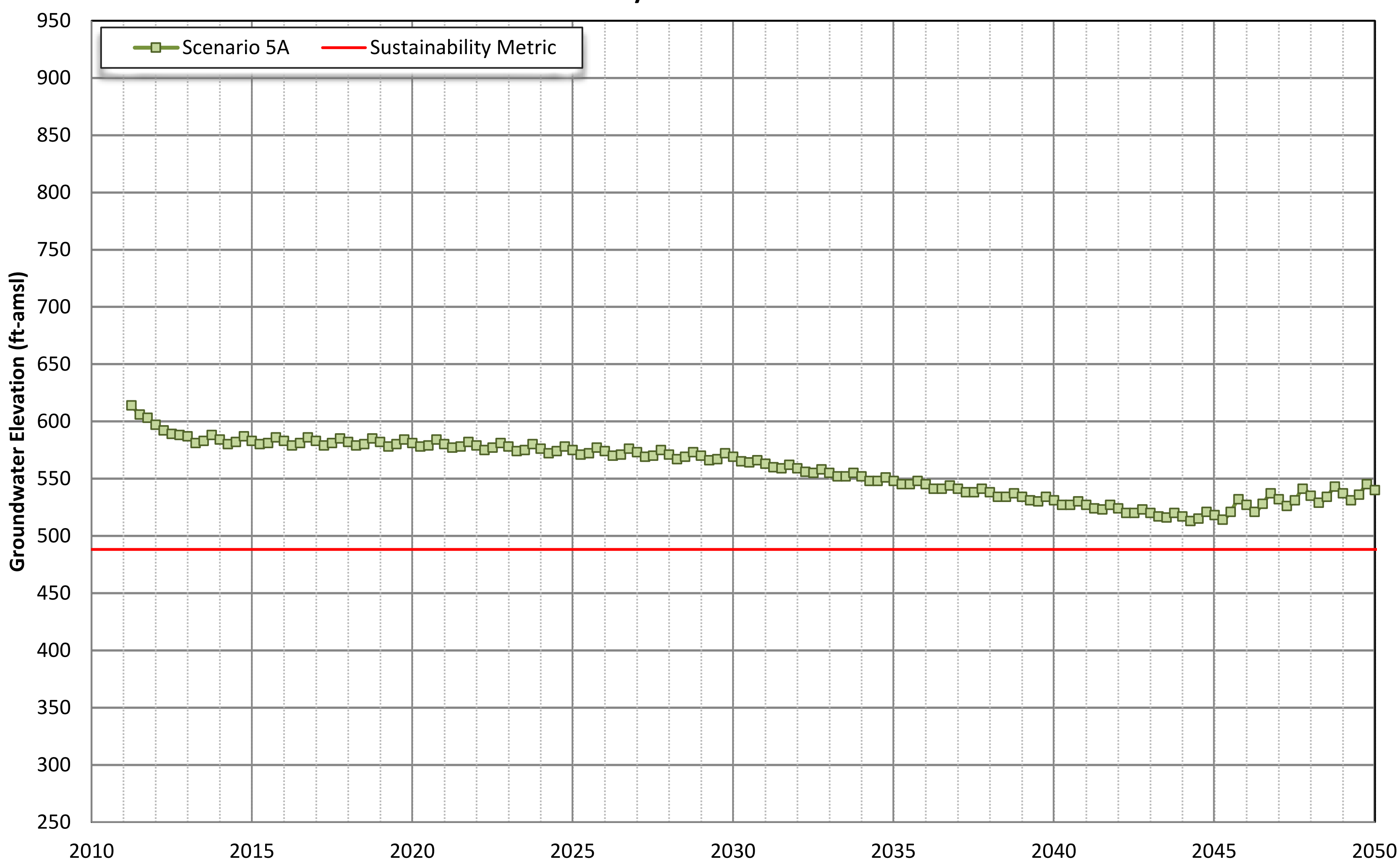

Appendix D_20150916_WellHydrographs_S5A4_Final_LBB2.xlsm
Created: 9/15/15
Printed: 9/16/2015

Figure D-177
Projected Groundwater Elevation for Scenario 5a
City of Pomona Well 29

Appendix D_20150916_WellHydrographs_S5A4_Final_LBB2.xlsm
Created: 9/15/15
Printed: 9/16/2015

Figure D-178
Projected Groundwater Elevation for Scenario 5a
City of Pomona Well 30

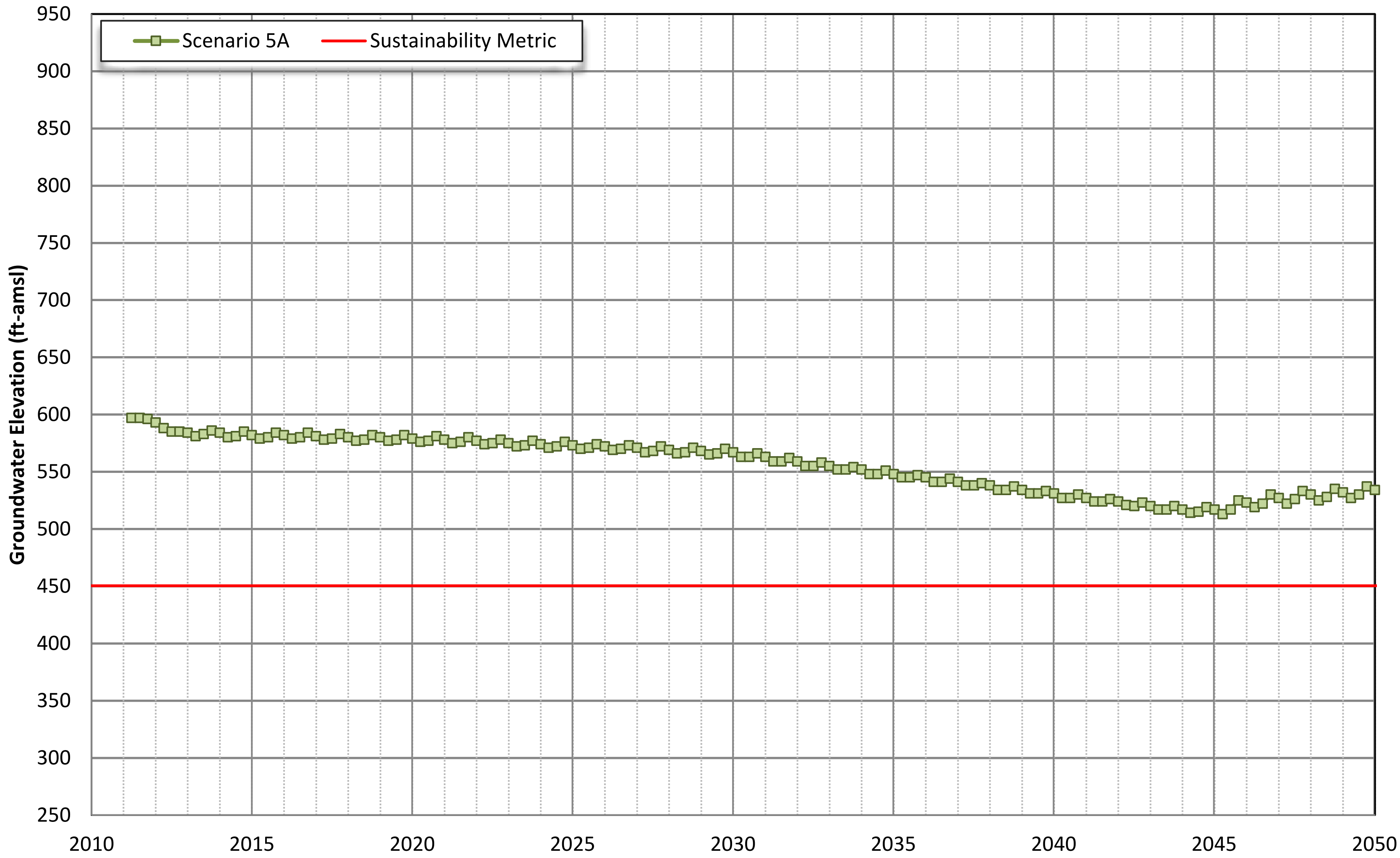

Appendix D_20150916_WellHydrographs_S5A4_Final_LBB2.xlsm
Created: 9/15/15
Printed: 9/16/2015

Figure D-179
Projected Groundwater Elevation for Scenario 5a
City of Pomona Well 34

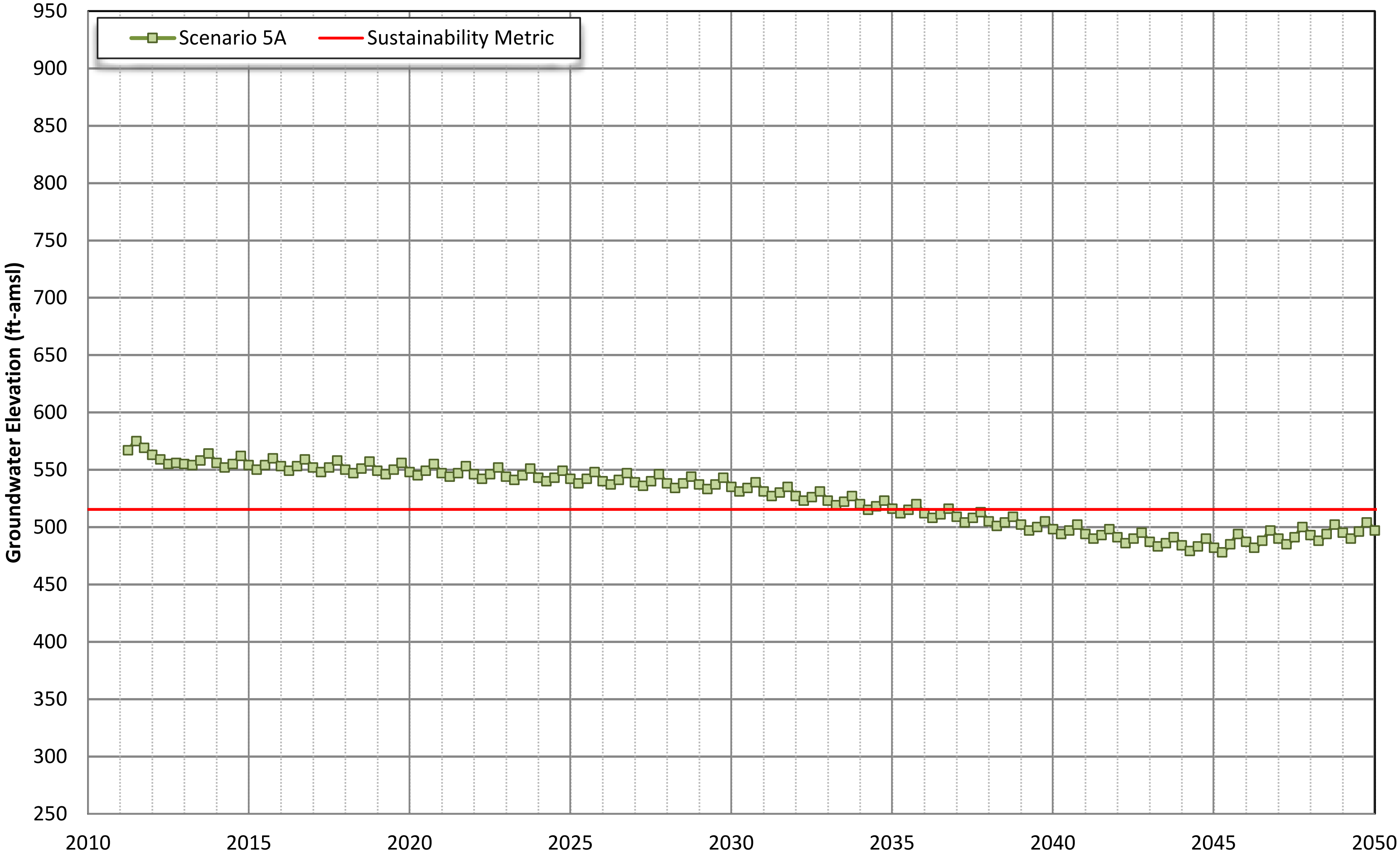

Appendix D_20150916_WellHydrographs_S5A4_Final_LBB2.xlsm
Created: 9/15/15
Printed: 9/16/2015

Figure D-180
Projected Groundwater Elevation for Scenario 5a
City of Pomona Well 35

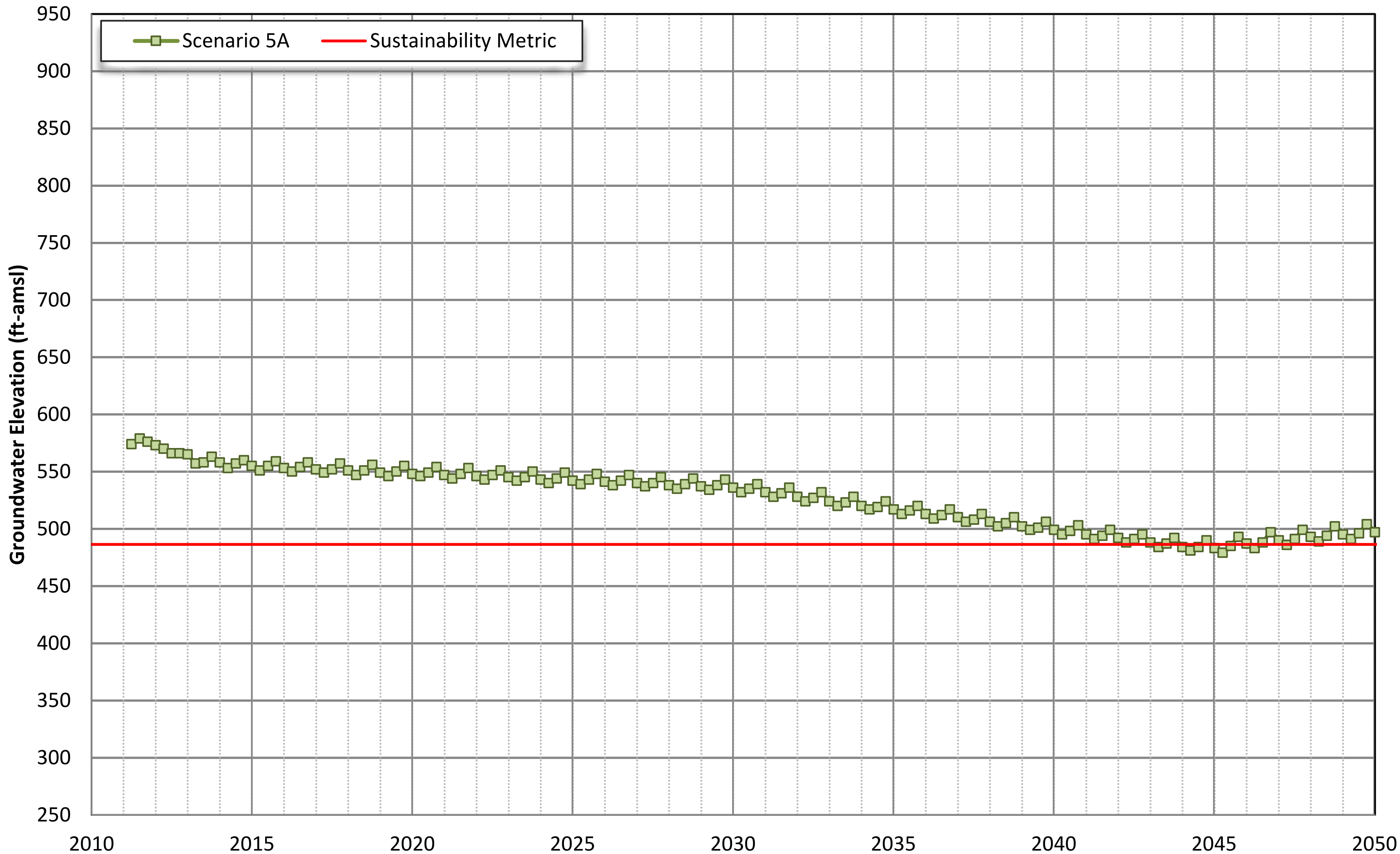

Appendix D_20150916_WellHydrographs_S5A4_Final_LBB2.xlsm
Created: 9/15/15
Printed: 9/16/2015

Figure D-181
Projected Groundwater Elevation for Scenario 5a
City of Pomona Well 36

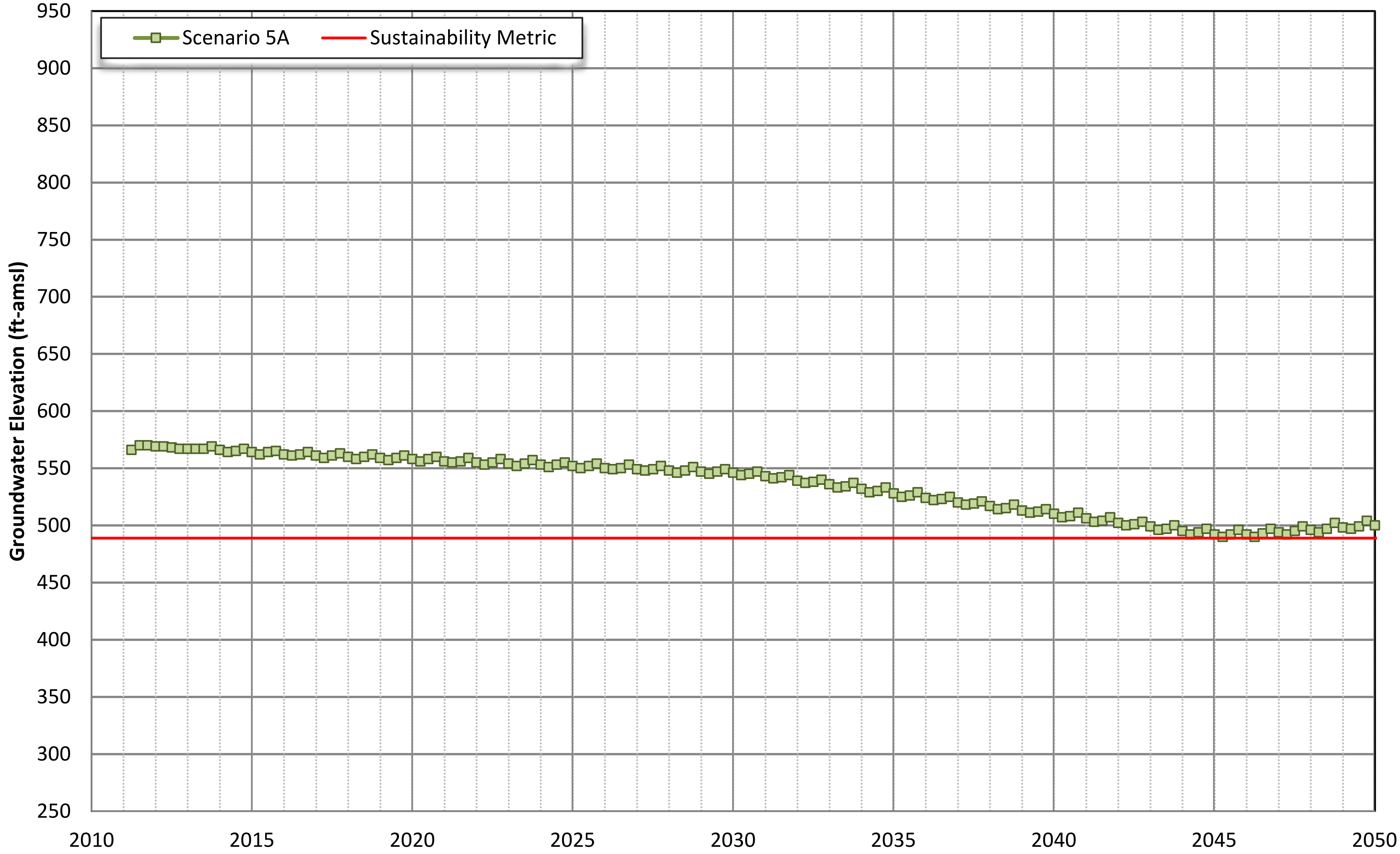

Appendix D_20150916_WellHydrographs_S5A4_Final_LBB2.xlsm
Created: 9/15/15
Printed: 9/16/2015

Figure D-182
Projected Groundwater Elevation for Scenario 5a
City of Pomona Well 5B

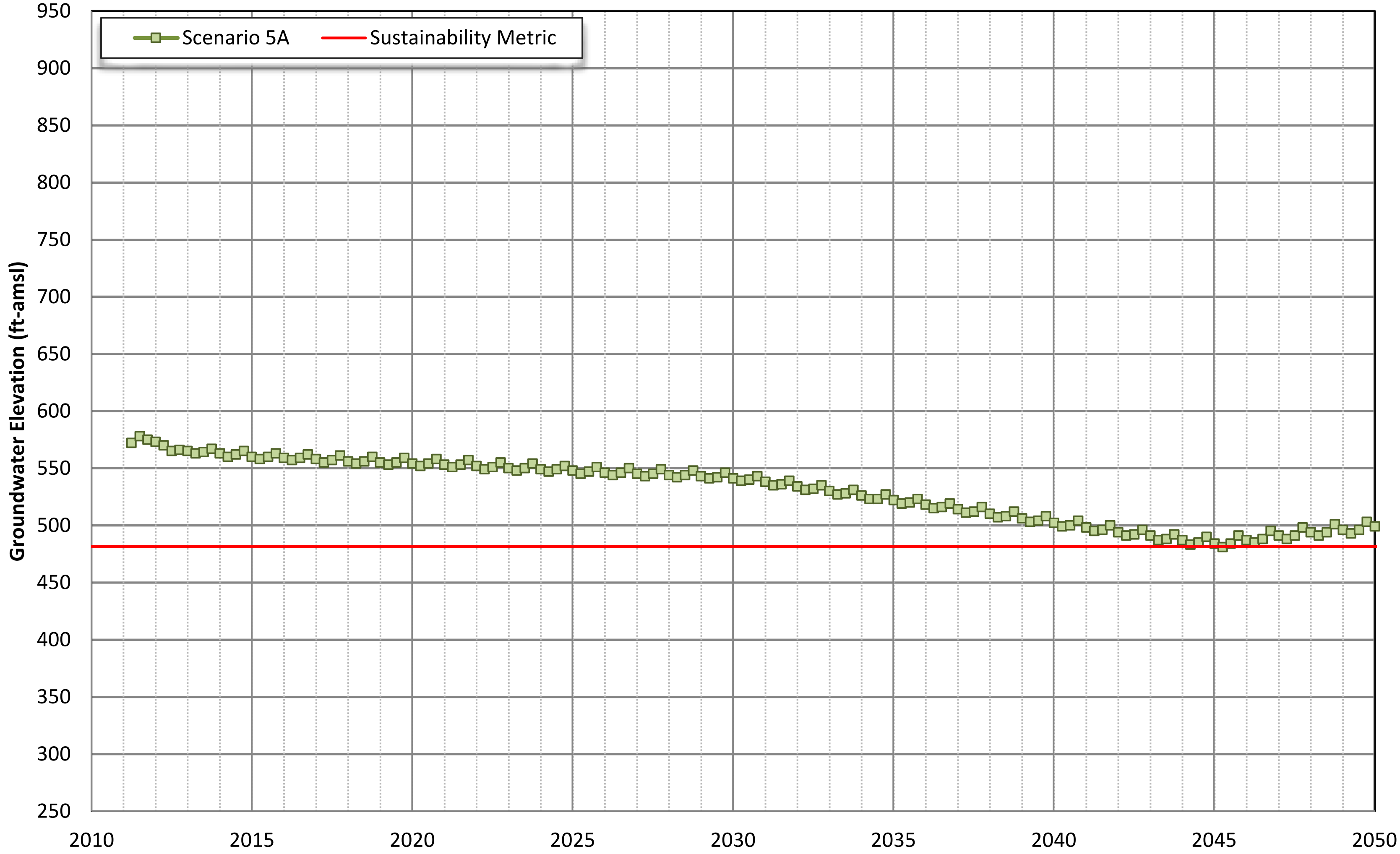

Appendix D_20150916_WellHydrographs_S5A4_Final_LBB2.xlsm
Created: 9/15/15
Printed: 9/16/2015

Figure D-183
Projected Groundwater Elevation for Scenario 5a
San Antonio Water Company Well 01A

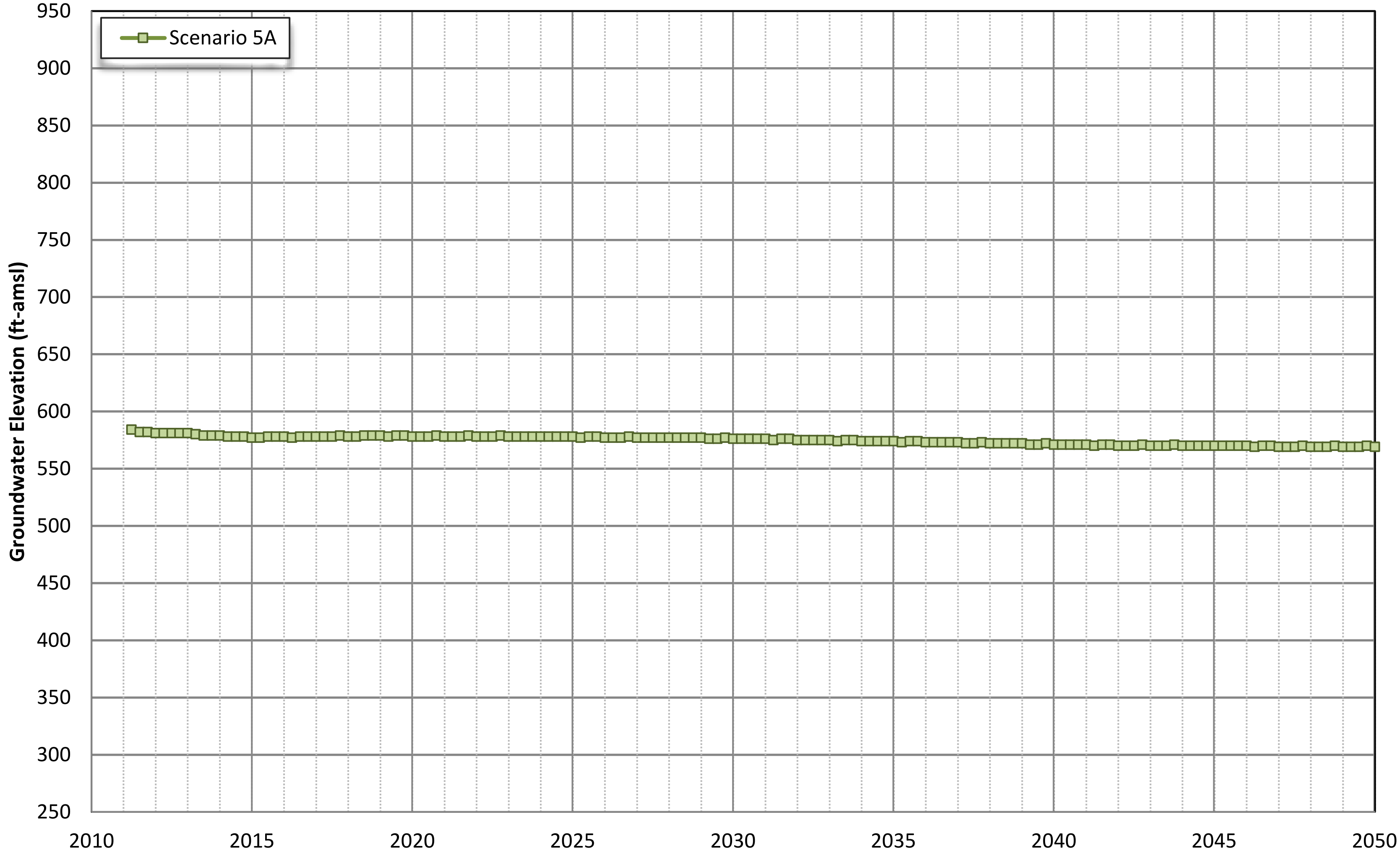

Appendix D_20150916_WellHydrographs_S5A4_Final_LBB2.xlsm
Created: 9/15/15
Printed: 9/16/2015

Figure D-184
Projected Groundwater Elevation for Scenario 5a
San Antonio Water Company Well 03A

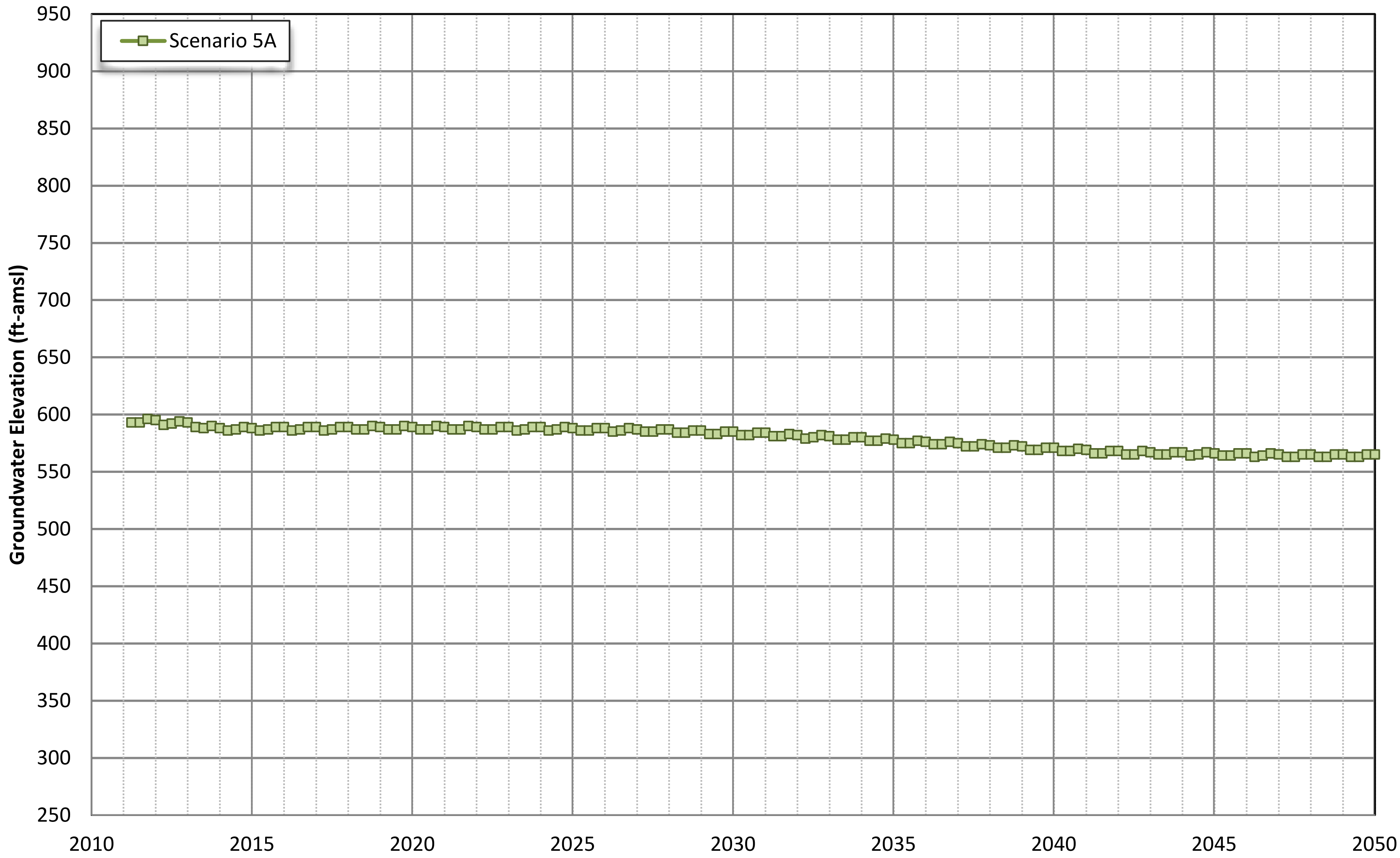

Appendix D_20150916_WellHydrographs_S5A4_Final_LBB2.xlsm
Created: 9/15/15
Printed: 9/16/2015

Figure D-185
Projected Groundwater Elevation for Scenario 5a
City of Upland Well 3

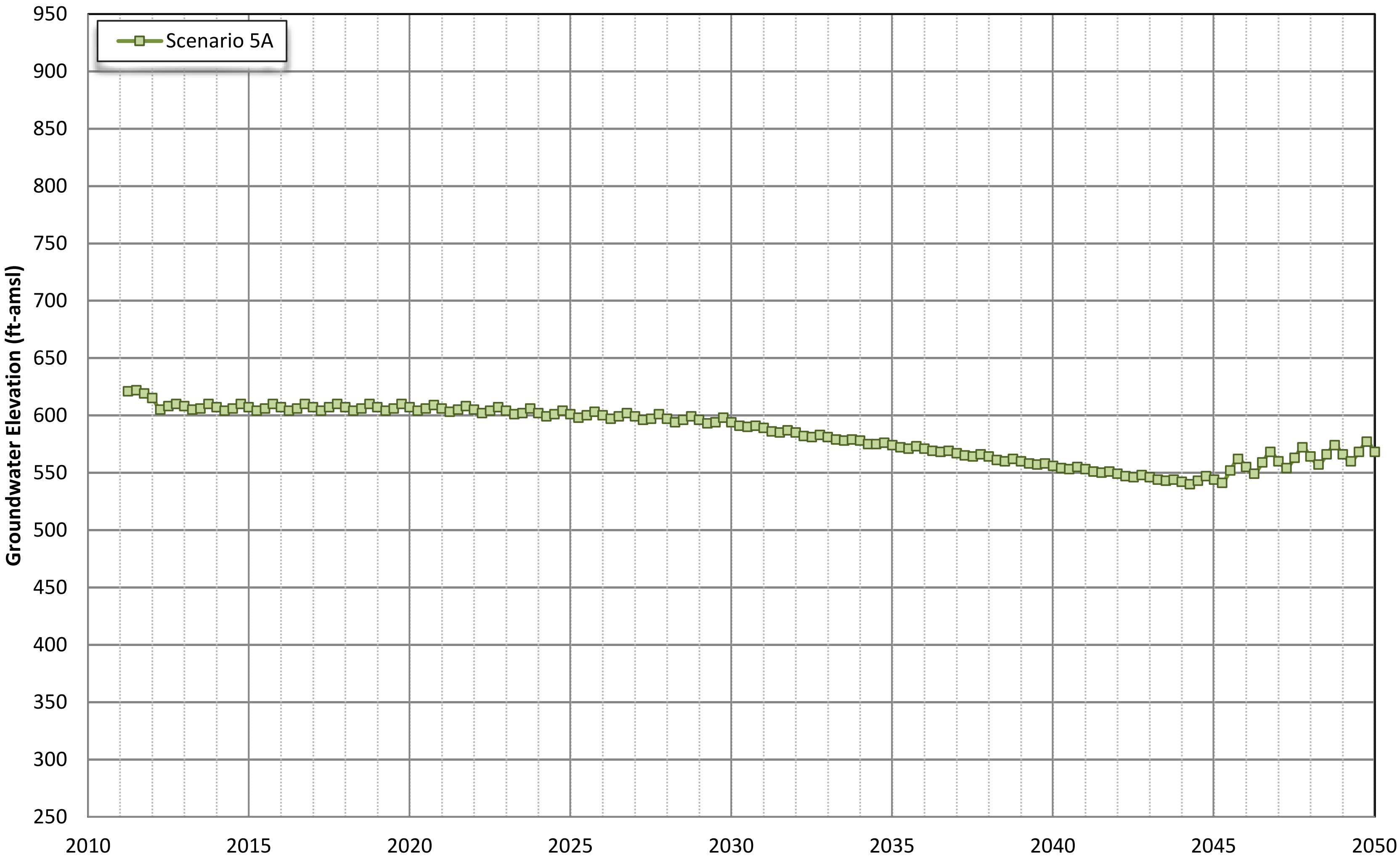

Appendix D_20150916_WellHydrographs_S5A4_Final_LBB2.xlsm
Created: 9/15/15
Printed: 9/16/2015

Figure D-186
Projected Groundwater Elevation for Scenario 5a
City of Upland Well 8

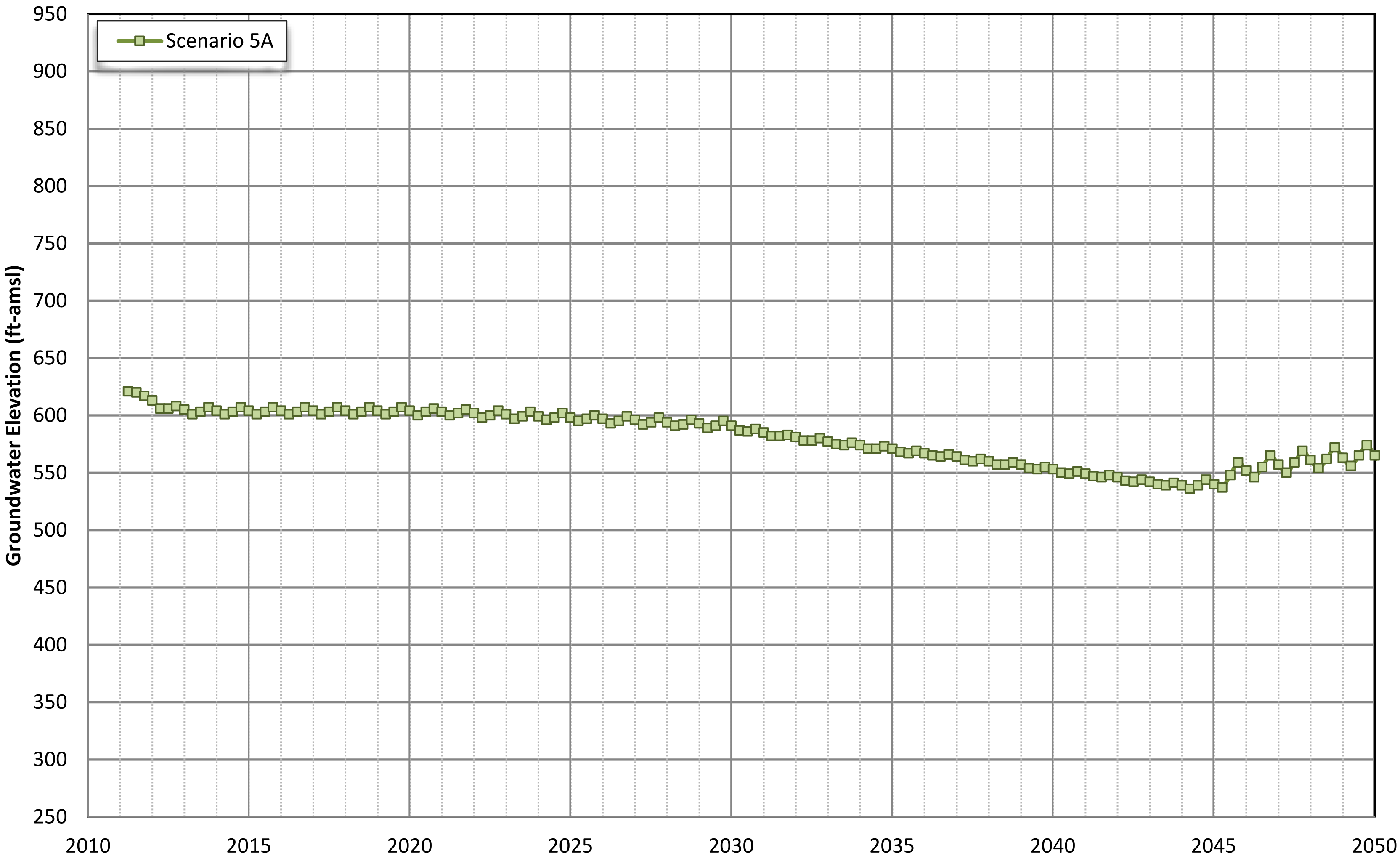

Appendix D_20150916_WellHydrographs_S5A4_Final_LBB2.xlsm
Created: 9/15/15
Printed: 9/16/2015

Figure D-187
Projected Groundwater Elevation for Scenario 5a
City of Upland Well 20

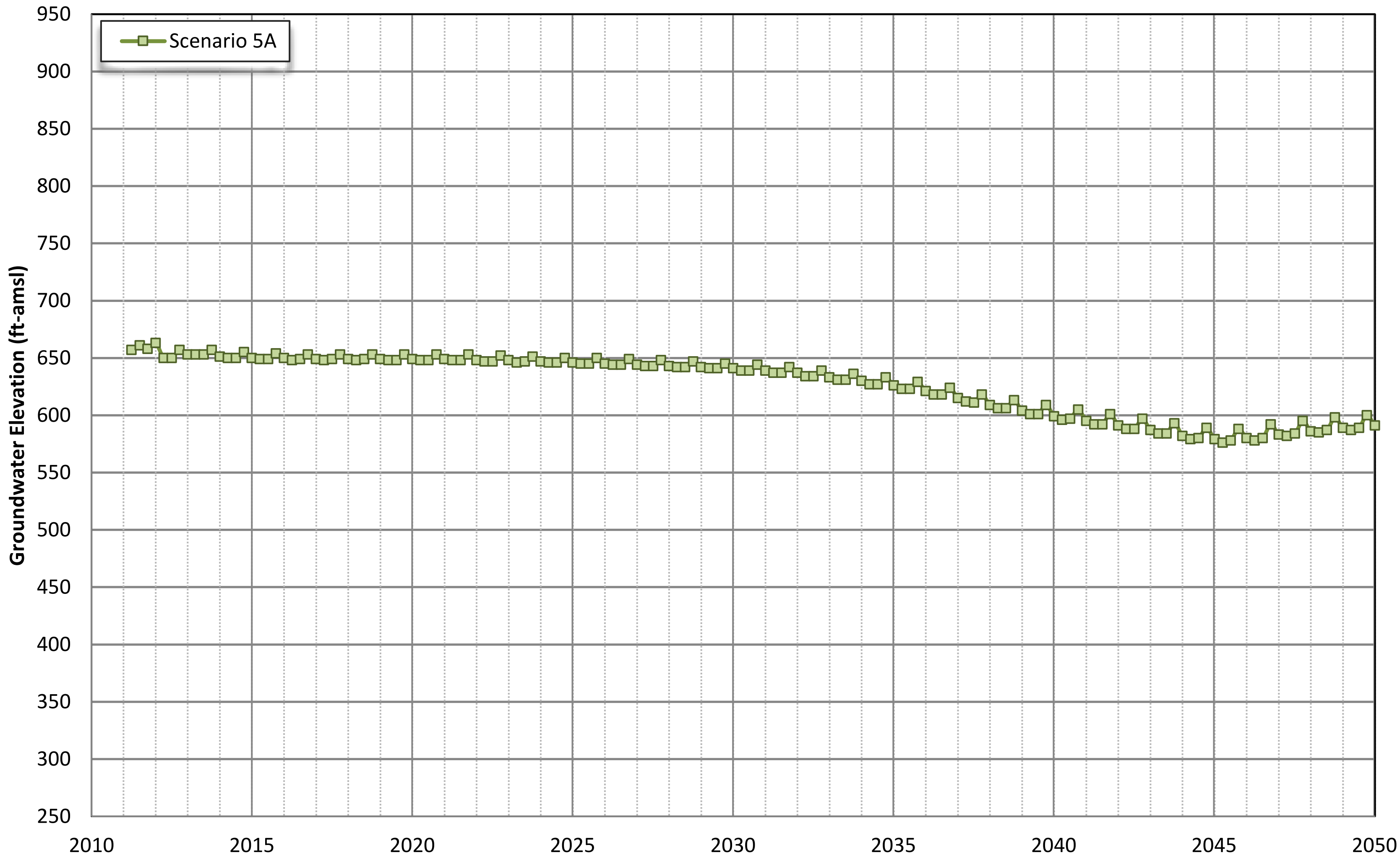

Appendix D_20150916_WellHydrographs_S5A4_Final_LBB2.xlsm
Created: 9/15/15
Printed: 9/16/2015

Figure D-188
Projected Groundwater Elevation for Scenario 5a
City of Upland Well 21A

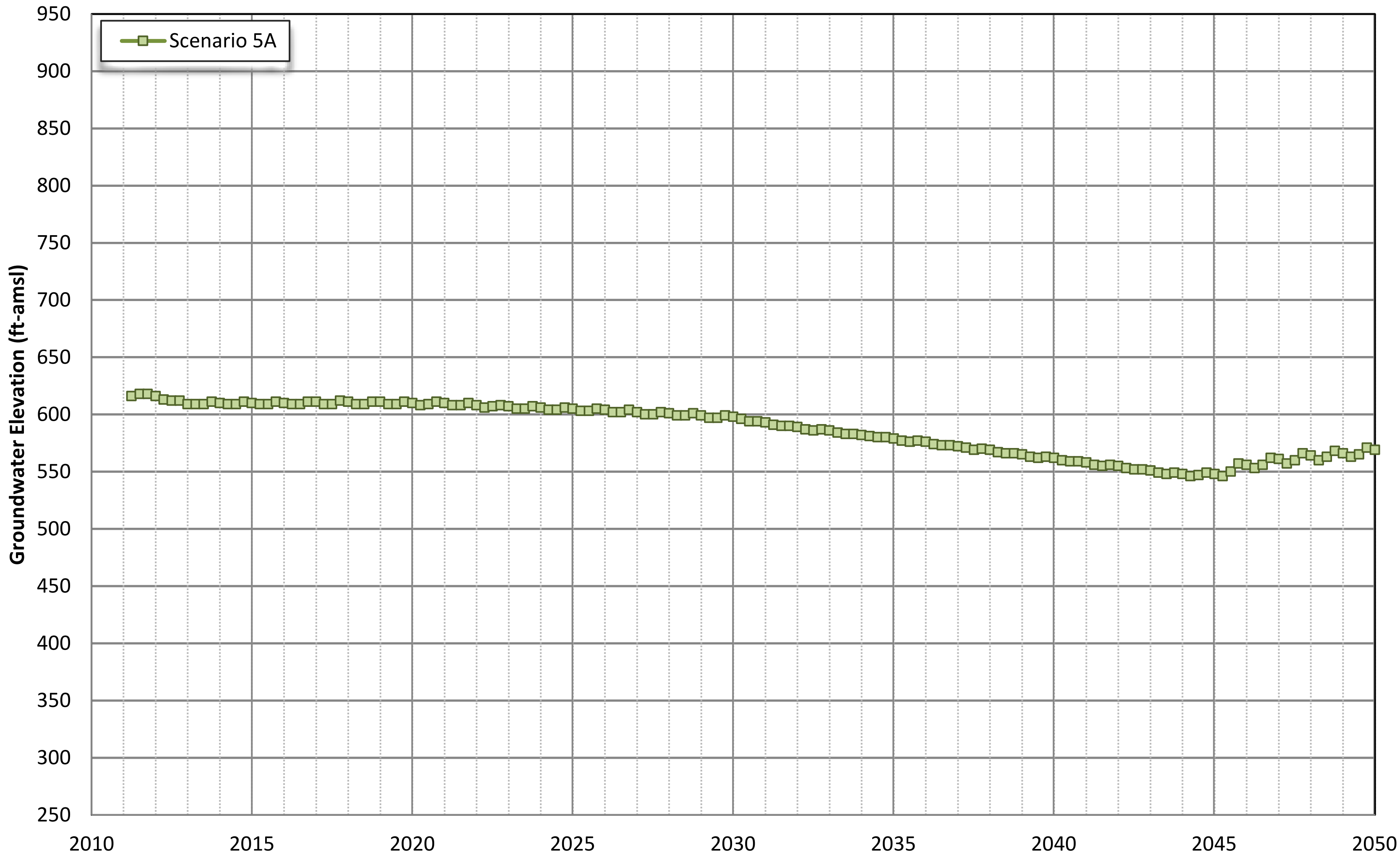

Appendix D_20150916_WellHydrographs_S5A4_Final_LBB2.xlsm
Created: 9/15/15
Printed: 9/16/2015

Figure D-189
Projected Groundwater Elevation for Scenario 5a
City of Upland Well 7A

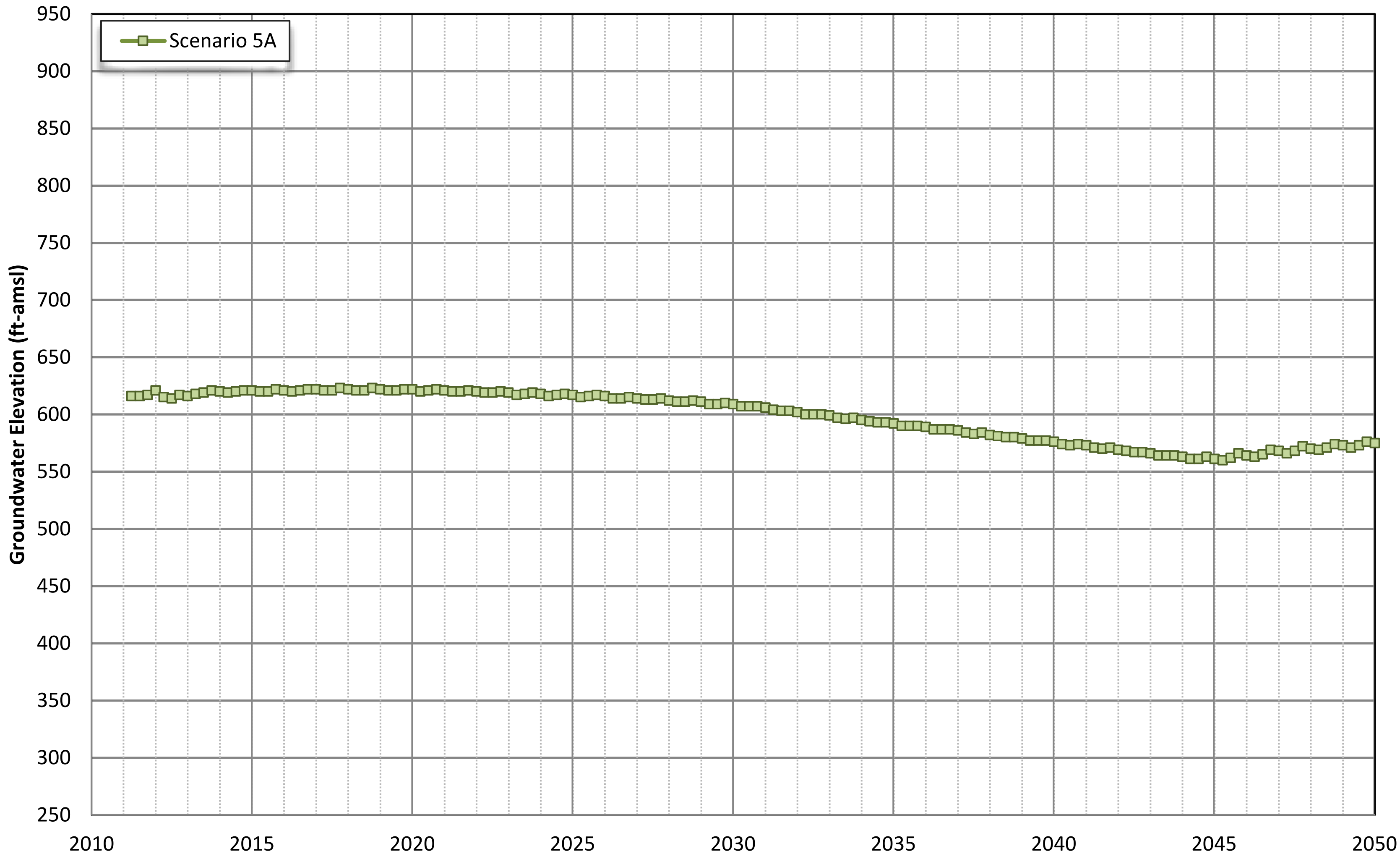

Appendix D_20150916_WellHydrographs_S5A4_Final_LBB2.xlsm
Created: 9/15/15
Printed: 9/16/2015

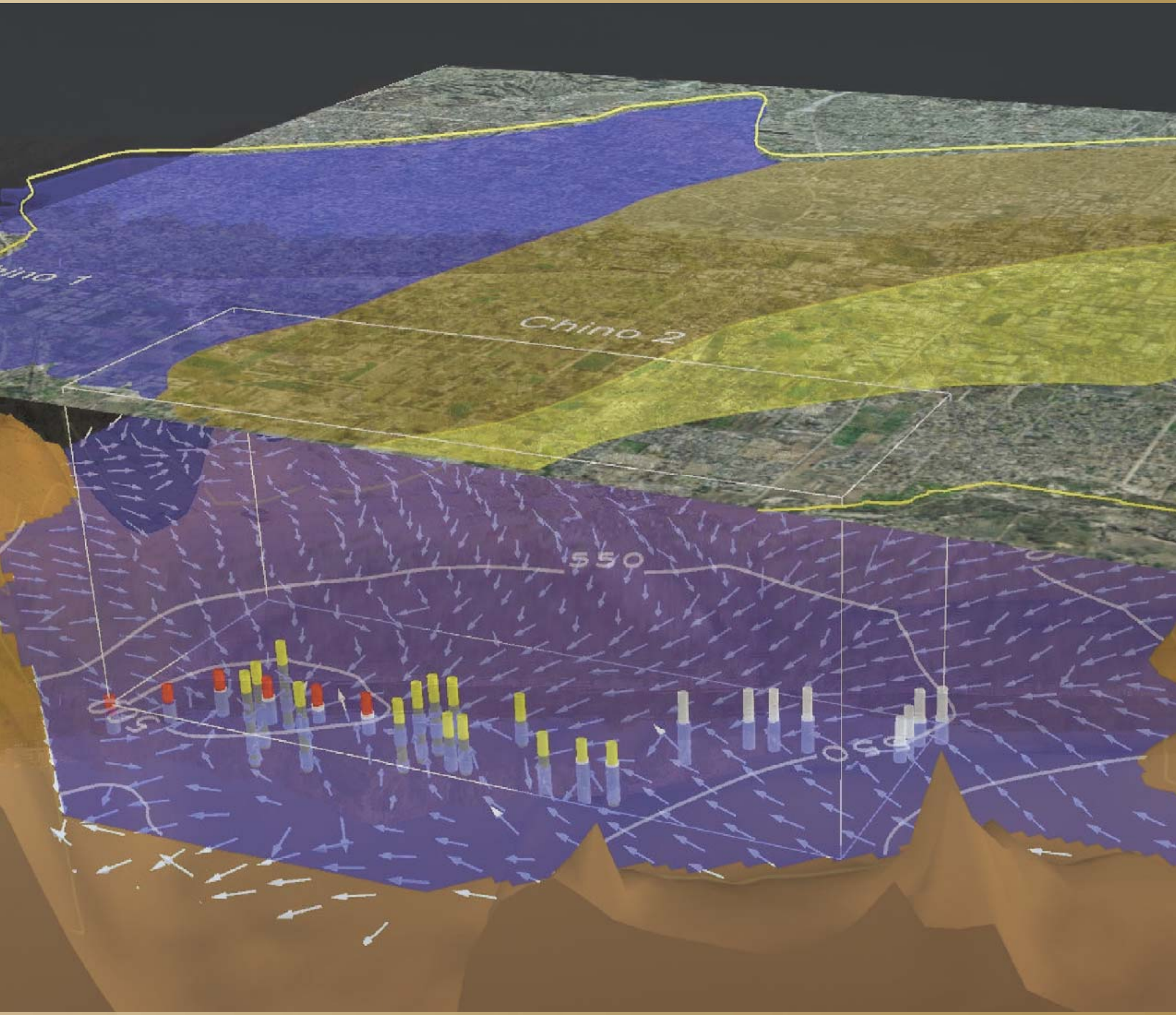

Corporate Office
23692 Birtcher Drive
Lake Forest, California 92630
T: 949.420.3030
F: 949.420.4040

www.WildermuthEnvironmental.com